



STRUCTURE AND DYNAMICS OF MULTIDRUG RESISTANCE ABC TRANSPORTERS

Elucidating the driving force behind ABC transporters

Dissertation

zur Erlangung des Grades

„Doktor der Naturwissenschaften“

im Promotionsfach Chemie

am Fachbereich Chemie, Pharmazie, Geographie und Geowissenschaften

der Johannes Gutenberg-Universität

in Mainz

Dania Rose-Sperling

geb. in Jena

Mainz, 2022

Eingereicht beim Fachbereich Chemie, Pharmazie, Geographie und Geowissenschaften am:

1. Gutachter: Prof. Dr. [REDACTED]

2. Gutachter: Dr. hab. [REDACTED]

Tag der öffentlichen Disputation: _____

ACKNOWLEDGEMENTS

How much this work is based on my family cannot be expressed in words! Luckily, I grew up in a supportive and happy family around me, who was and is always there for me in any enjoyable or problematic situation!

I have to especially honor my best friend for life, my love and since 2016 my husband, [REDACTED]. You are the one who I can always count on! If I have strange and crazy ideas as getting married and then going to a conference, going abroad for a research internship, organizing a life science conference, or going to a conference with our six-month-old daughter you say: "Sure why not, let's do it!". Thank you so much for being always so patient, giving me all the space I need and for being also now such a fantastic father.

For the supportive and challenging environment during my PhD, I am greatly indebted to my supervisor Prof. Dr. [REDACTED]! Without any doubt you made the best scientific researcher out of me! I am honored and grateful that I was chosen to accompany your way and I am looking forward to the next adventures, who have to be tackled.

I further would like to thank the whole [REDACTED] research group and the students who I worked with during this time. With you the time in the lab was an adventure. I would like to thank my longstanding companion Dr. [REDACTED] for becoming a friend for life! She would have said this experiment will take one million hours and when it's over I will die! I guess at the end of the whole PhD this might be almost the truth.

I would also like to acknowledge the research group of Prof. Dr. [REDACTED] of Frankfurt for always helping with recording NMR spectra.

Thanks also to our collaboration partners of the research group of Dr. [REDACTED] from Würzburg and Dr. [REDACTED] for supporting experimental or literature research.

I would like to further acknowledge Prof. Dr. [REDACTED] and Dr. [REDACTED] for giving me the opportunity to do a research internship in their laboratory in Lyon, where I was also trained well on functional assays.

I would also like to express my sincere gratitude to the Hans-Böckler-foundation who provided me with funding for my PhD, funding for my research internship in Lyon, funding for organizing a life science conference and funding for contributing a research conference. Here, I would also like to thank Prof. Dr. [REDACTED] from the westfaelische Hochschule Recklinghausen for being my tutor of the Hans Böckler foundation.

I think in general in this moment now I cannot imagine to be more thankful and grateful again as when I will hand over this thesis.

Thank you to everyone who made this moment to be real happening!

SUMMARY

The ATP binding cassette (ABC) transporter family is a large membrane protein superfamily found in all phyla of life. ABC transporters are essential for the transport of nutrients, ions, peptides, lipids, and also antibiotics and other harmful compounds across the lipid bilayer. Some of these membrane transporters, such as LmrA from *Lactococcus lactis*, MsbA from *Escherichia coli* and BmrA from *Bacillus subtilis* are homologs of the human multidrug resistance (MDR)-related P-glycoprotein. The general architecture of ABC transporters consists of two transmembrane domains (TMDs) and two nucleotide binding domains (NBDs). ATP binding and hydrolysis within the NBDs lead to conformational changes in the TMDs that allow translocation of the substrate. ABC transporters have been studied for more than five decades, and a wealth of structural information is now available. However, it remains unclear how exactly these molecular machines mediate substrate transport across a membrane, how the substrates are recognized in molecular detail and how the TMD and NBD are allosterically coupled to enable progression through the catalytic cycle and the efficient export of substrates. This PhD thesis focuses on the role of the highly conserved ABC transporter NBD and its structure and dynamics during the substrate transport mechanism.

The first part of the thesis deals with the question how nucleotide interaction affects NBD dynamics across timescales, and how this may affect transmission of signals (i.e. nucleotide occupancy within the NBD), from the nucleotide binding side (NBS) to the TMD or across the NBD-NBD interface. The isolated NBDs of the exporters LmrA, MsbA and BmrA could be expressed in *E. coli* in large quantities and showed to be properly folded and able to bind nucleotides via nuclear magnetic resonance (NMR) spectroscopy. Analysis of NMR spectra of LmrA-NBD, MsbA-NBD and BmrA-NBD WT showed that some residues in the apo-state have backbone fluctuations in the μs – ms timescale, which became rigidified in the ADP-bound state. Chemical shift perturbation (CSP), H/D exchange and hetNOE (heteronuclear Overhauser Effect) experiments were carried out with the LmrA-NBD to investigate the dynamics of individual amino acids upon nucleotide binding. For MsbA-NBD WT, photoelectron-transfer fluorescence correlation spectroscopy (PET-FCS), which gives information about global dynamics, was carried out. Nucleotide binding quenches the dynamics of the ATP binding site itself but also affects remote residues thus beginning to shed light on signal propagation pathways through the NBD. Conserved motifs known to be important for ATP-binding and/ or hydrolysis within the NBD, such as the A-loop, the Walker A motif, D-loop, Q-loop or the H-loop and other interesting regions as the coupling helix groove and the C-terminus of the NBD react to nucleotide binding. Overall, the hetNOE measurements showed that the secondary structural elements essentially remain identical on the ps - ns timescale for LmrA-NBD WT in the apo and ADP-bound state, however, while the dynamics of the catalytic subdomain are quenched in the presence of ADP, the α -helical subdomain became more mobile. H/D exchange and CSP experiments also show ADP binding induced rigidification of residues in the catalytic subdomain of LmrA-NBD in the ms - s timescale. These dynamic differences support the role of the α -helical and the catalytic subdomain in transmitting conformational changes between the NBD and the TMD. Considering that the data obtained for the NBD in the ADP-bound state reflect the post-hydrolytic state, the “unique” dynamic profile of this state may have far reaching consequences for substrate unloading and transporter switching from the outward open to the inward open state before a new transport cycle can begin again. Furthermore, backbone dynamic studies revealed differences in dynamics between residues of the D-loop, Q-loop and the C-terminal end of the X-loop, which are flexible in the apo and ADP states, and residues of the N-terminal end of the X-loop and a residue of the Walker B motif, which are rigid in both states. Investigation of the different catalytic states (apo, (Mg)ADP-bound and (Mg)ATP-bound) with the different methods yielded a “dynamic fingerprint” of model ABC transporter NBDs in all physiologically relevant states.

The second part of this PhD thesis examines the structural and dynamic consequences of mutations in the conserved D-loop, Q-loop and H-loop motifs of the LmrA-NBD using NMR spectroscopy. The experiments show that there is crosstalk between the three conserved motifs, with the H-loop as a key team player, and remote NBD regions. Furthermore, D-, Q- and H-loop communicate with other conserved motifs such as the Walker A and Walker B motifs. However, no or only minor effects on the structure and dynamics in A-loop, X-loop and C-loop were observed by the inserted mutations. To identify the role of the D-loop residues in substrate transport and ATP hydrolysis functional assays (i.e. ATPase activity and substrate transport) were carried out using isolated NBDs and the full-length *B. subtilis* transporter BmrA. Substrate transport and ATP hydrolysis were reduced or fully abrogated when mutating the conserved D-loop. The classic ABC transporter D-loop consensus sequence “SALD” is only maintained in MsbA, but slightly modified in LmrA (ASLD) and BmrA (SSLD). Interestingly, when the D-loop mutations ASLD or SALD were introduced into full-length BmrA, substrate transport was still possible. However, for the ASLD mutant, an increase in basal ATP hydrolysis was observed but at the same time, this mutant did not react with an increase of ATP hydrolysis upon substrate addition, i.e.

it lost its ability to carry out “stimulated ATPase activity”, a common feature of ABC multidrug transporters. These observations indicate that the N-terminal serine and conserved aspartic acid residues of the D-loop (⁵⁰⁷S-SLD⁵¹⁰) in BmrA are particularly important for ATP hydrolysis. The functional consequences of the D-loop mutants in combination with CSP experiments lead to the hypothesis that conformational changes and dynamics are incorrectly transmitted to important conserved motifs such as H- and Q-loop and residues in regions important for processing substrate transport, i.e. coupling helix groove and the C-terminus within the NBD.

The third part of this PhD thesis describes the discovery of a novel “communication hinge” linking the Walker A motif to the coupling helix groove and thus connecting NBD and TMD via highly conserved residues in the NBD. NMR spectroscopic studies (i.e. CSP and ¹⁹F NMR) of LmrA-NBD WT, MsbA-NBD WT and BmrA-NBD WT revealed that the C-terminal end of the Walker A helix, which is sequentially highly conserved in type I ABC exporters (type IV), interacts with an opposing bulky hydrophobic/aromatic residue. Mutating the conserved arginine residue at the C-terminal end of the Walker A helix in full-length BmrA was found to disrupt substrate transport for all tested mutants. ATPase activity, on the other hand, showed different results depending on the amino acid inserted at the position of the arginine, thereby showing that substrate transport in the TMD and ATP hydrolysis in the NBD can be selectively decoupled at this site. Furthermore, it was evaluated in this thesis that mutations in this region impact protein stability of type I ABC exporters (type IV). However, none of the NMR experiments conducted in this thesis for the D-, Q- or H-loop motif revealed a link to any residue of our identified allosterically affected region (R-W/L region), suggesting that this is an NBD intradomain signaling pathway independent of these conserved motifs.

The results presented in this thesis for three archetypical bacterial ABC exporters show that the substrate transport and ATP hydrolysis mechanisms are enabled through complex interaction networks.

ZUSAMMENFASSUNG

Die Familie der ATP-bindenden Kassetten-Transporter (ABC-Transporter) ist eine große Superfamilie von Membranproteinen, die in allen Lebewesen vorkommt. ABC-Transporter sind für den Transport von Nährstoffen, Ionen, Peptiden, Lipiden, aber auch von Antibiotika und anderen schädlichen Verbindungen über die Lipiddoppelschicht unerlässlich. Einige dieser Membrantransporter wie LmrA aus *Lactococcus lactis*, MsbA aus *Escherichia coli* und BmrA aus *Bacillus subtilis* sind Homologe des menschlichen *Multidrug Resistance* (MDR)-verwandten P-Glykoproteins. Die allgemeine Architektur von ABC-Transportern besteht aus zwei Transmembrandomänen (TMDs) und zwei Nukleotidbindungsdomänen (NBDs). ATP-Bindung und -Hydrolyse in den NBDs führen zu Konformationsänderungen in den TMDs, die die Translokation des Substrats ermöglichen. ABC-Transporter werden seit mehr als fünf Jahrzehnten erforscht, und inzwischen liegt eine Fülle von Strukturinformationen vor. Es ist jedoch nach wie vor unklar, wie genau diese molekularen Maschinen den Substrattransport durch eine Membran vermitteln, wie die Substrate im molekularen Detail erkannt werden und wie die TMD und NBD allosterisch gekoppelt sind, um das Fortschreiten des katalytischen Zyklus und den effizienten Export der Substrate zu ermöglichen. Diese Dissertation konzentriert sich auf die Rolle der hochkonservierten NBD von ABC-Transportern und deren Struktur und Dynamik während des Substrattransportmechanismus.

Der erste Teil der Arbeit befasst sich mit der Frage, wie die Nukleotidinteraktion die NBD-Dynamik über Zeitskalen hinweg beeinflusst und wie dies die Übertragung von Signalen (ausgelöst durch zum Beispiel Nukleotidbesetzung innerhalb der NBD) von der Nukleotidbindungsseite (NBS) zur TMD oder über die NBD-NBD-Grenzfläche beeinflussen kann. Die isolierten NBDs der Exporter LmrA, MsbA und BmrA konnten in großen Mengen in *E. coli* exprimiert werden und zeigten sich mittels Kernspinresonanzspektroskopie (NMR) als korrekt gefaltet und fähig, Nukleotide zu binden. Die Analyse der NMR-Spektren von LmrA-NBD, MsbA-NBD und BmrA-NBD WT zeigte, dass einige Reste im apo-Zustand Proteinrückrad-Fluktuationen im μ s - ms Zeitbereich aufweisen, die im ADP-gebundenen Zustand gequenchet wurden. Experimente zur chemischen Verschiebung (CV), zum H/D-Austausch und zum heteronuklearen Overhauser-Effekt (hetNOE) wurden mit der LmrA-NBD durchgeführt, um die Dynamik einzelner Aminosäuren bei der Nukleotidbindung zu untersuchen. Für MsbA-NBD WT wurde die *photoinduced electron transfer-fluorescence correlation spectroscopy* (PET-FCS) durchgeführt, die Informationen über die globale Dynamik liefert. Die Nukleotidbindung vermindert die Dynamik der Bindestelle von ATP in der NBD, wirkt sich aber auch auf entfernte Reste aus, was beginnt Aufschluss über die Signalausbreitungswege durch die NBD zu geben. Konservierte Motive, von denen bekannt ist, dass sie für die ATP-Bindung und/oder -Hydrolyse innerhalb der NBD wichtig sind, wie der A-Loop, das Walker-A-Motiv, der D-loop, der Q-loop oder der H-loop, sowie andere interessante Regionen wie die *coupling helix groove* und der C-Terminus der NBD reagieren auf die Nukleotidbindung. Insgesamt zeigten die hetNOE-Messungen, dass die sekundären Strukturelemente auf der ps-ns-Zeitskala für LmrA-NBD WT im apo- und ADP-gebundenen Zustand im Wesentlichen gleichbleiben. Während jedoch die Dynamik der katalytischen Subdomäne in Gegenwart von ADP vermindert wird, wird die α -helikale Subdomäne mobiler. H/D-Austausch- und CV-Experimente zeigen auch, dass die ADP-Bindung eine Versteifung der Reste in der katalytischen Subdomäne von LmrA-NBD im ms-s-Zeitbereich bewirkt. Diese dynamischen Unterschiede unterstützen die Rolle der α -helikalen und der katalytischen Subdomäne bei der Übertragung von Konformationsänderungen zwischen der NBD und der TMD. In Anbetracht der Tatsache, dass die für die NBD im ADP-gebundenen Zustand erhaltenen Daten den post-hydrolytischen Zustand widerspiegeln, könnte das "einzigartige" dynamische Profil dieses Zustands weitreichende Folgen für das Entlassen des Substrates und den Wechsel des Transporters vom nach außen offenen in den nach innen offenen Zustand haben, bevor ein neuer Transportzyklus wieder beginnen kann. Darüber hinaus ergaben Untersuchungen der Proteinrückgratdynamik Unterschiede in der Dynamik zwischen den Resten der D-Loop, der Q-Loop und dem C-terminalen Ende der X-Loop, die im Apo- und ADP-Zustand flexibel sind, und den Resten des N-terminalen Endes der X-Loop und einem Rest des Walker-B-Motivs, die in beiden Zuständen starr sind. Die Untersuchung der verschiedenen katalytischen Zustände (apo, (Mg)ADP-gebunden und (Mg)ATP-gebunden) mit den verschiedenen Methoden ergab einen "dynamischen Fingerabdruck" von Modell-ABC-Transporter-NBDs in allen physiologisch relevanten Zuständen.

Im zweiten Teil dieser Doktorarbeit werden die strukturellen und dynamischen Folgen von Mutationen in den konservierten Motiven D-Loop-, Q-Loop- und H-Loop der LmrA-NBD mittels NMR-Spektroskopie untersucht. Die Experimente zeigen, dass es eine Wechselwirkung zwischen den drei konservierten Motiven, mit dem H-Loop als wichtigen Teamplayer, und mit von diesen Motiven entfernteren NBD-Regionen gibt. Darüber hinaus kommunizieren D-, Q- und H-Loop mit anderen konservierten Motiven wie den Walker-A- und Walker-B-Motiven. Die eingefügten Mutationen hatten jedoch keine oder nur geringe Auswirkungen auf die Struktur und Dynamik des A-Loop, X-Loop und des C-Loop. Um die Rolle der D-Loop-Reste beim Substrattransport und der

ATP-Hydrolyse zu ermitteln, wurden funktionelle Assays (d. h. ATPase-Aktivität und Substrattransport) mit isolierten NBDs und dem Volllänge *B. subtilis*-Transporter BmrA durchgeführt. Der Substrattransport und die ATP-Hydrolyse wurden durch Mutation des Aspartat Restes im D-Loop reduziert oder ganz aufgehoben. Die klassische ABC-Transporter-D-Loop-Konsensussequenz "SALD" ist nur in MsbA enthalten, während sie in LmrA (ASLD) und BmrA (SSLD) leicht verändert ist. Interessanterweise war der Substrattransport immer noch möglich, wenn die D-Loop-Mutationen ASLD oder SALD in BmrA in voller Länge eingeführt wurden. Bei der ASLD-Mutante wurde jedoch ein Anstieg der basalen ATP-Hydrolyse beobachtet, aber gleichzeitig reagierte diese Mutante nicht mit einem Anstieg der ATP-Hydrolyse auf die Zugabe von Substrat, d. h. sie verlor ihre Fähigkeit zur "stimulierten ATPase-Aktivität", ein gemeinsames Merkmal von ABC-*Multidrug*-Transportern. Diese Beobachtungen deuten darauf hin, dass das N-terminale Serin- und der konservierte Asparaginsäurerest des D-Loops (⁵⁰⁷S-SLD⁵¹⁰) in BmrA besonders wichtige Reste für die ATP-Hydrolyse sind. Die Konsequenzen der D-Loop-Mutanten auf die Aktivität des Proteins in Kombination mit den CV-Experimenten führen zu der Hypothese, dass Konformationsänderungen und Dynamik der NBD fehlerhaft auf wichtige konservierte Motive wie H- und Q-Loop und Reste in Regionen übertragen werden, die für die Verarbeitung des Substrattransports wichtig sind, wie die *coupling helix groove* und den C-Terminus innerhalb einer NBD.

Der dritte Teil dieser Dissertation beschreibt die Entdeckung eines neuartigen "Kommunikationsscharniers", das das Walker-A-Motiv mit der *coupling helix groove* verbindet und somit NBD und TMD über hochkonservierte Reste der NBD verbindet. NMR-spektroskopische Untersuchungen (d.h. CV und ¹⁹F NMR) von LmrA-NBD WT, MsbA-NBD WT und BmrA-NBD WT ergaben, dass das C-terminale Ende der Walker A-Helix, das in ABC-Exportern vom Typ I (Typ IV) sequenziell hoch konserviert ist, mit einem gegenüberliegenden sperrigen hydrophoben/ aromatischen Rest interagiert. Die Mutation des konservierten Argininrests am C-terminalen Ende der Walker-A-Helix in BmrA in voller Länge führte bei allen getesteten Mutanten zu einem Verlust des Substrattransports. Die ATPase-Aktivität hingegen zeigte unterschiedliche Ergebnisse in Abhängigkeit von der an der Position des Arginins eingefügten Aminosäure, was zeigt, dass der Substrattransport in der TMD und die ATP-Hydrolyse in der NBD an dieser Stelle selektiv entkoppelt werden können. Darüber hinaus wurde in dieser Arbeit analysiert, wie die Mutationen in dieser Region die Proteinstabilität von ABC-Exporteuren des Typs I (Typ IV) beeinflussen. Keines der NMR-Experimente, die in dieser Arbeit für das D-, Q- oder H-Loop-Motiv durchgeführt wurden, zeigte jedoch eine Verbindung zu irgendeinem Rest der von uns identifizierten allosterisch beeinflussten Region (R-W/L-Region), was darauf hindeutet, dass es sich um einen NBD-Intradomänen-Signalweg handelt, der von diesen konservierten Motiven unabhängig ist.

Die in dieser Arbeit vorgestellten Ergebnisse für drei archetypische bakterielle ABC-Exportere zeigen, dass der Substrattransport und die ATP-Hydrolyse-Mechanismus durch komplexe Interaktionsnetzwerke ermöglicht werden.

"One never notices what has been done; one can only see what remains to be done." Marie Curie

ABBREVIATIONS

| | |
|-----------------------|--|
| Aa | Amino acids |
| ABC transporter | ATP-binding cassette transporter |
| ACF | Autocorrelation function |
| ADP | Adenosine diphosphate |
| APS | Ammonium persulfate |
| ATP | Adenosine triphosphate |
| β -jrs | β -jellyroll-like domains |
| <i>B. subtilis</i> | <i>Bacillus subtilis</i> |
| BisTris-HCl | Bis(2-hydroxyethyl)amino-tris(hydroxymethyl)methane hydrochloride |
| BmrA | Bacillus multidrug resistance ATP |
| bp | base pairs |
| BTFA | 3-bromo-1,1,1-trifluoroacetone |
| CD spectroscopy | Circular dichroism spectroscopy |
| CH | Coupling helix |
| CMC | Critical micelle concentration |
| CRD | C-terminal regulatory domain |
| CSP | Chemical shift perturbations |
| C-terminal | Carboxy-terminal |
| CV | Column volumes |
| dH ₂ O | demineralized water |
| ddH ₂ O | Double-distilled water |
| DDM | n-dodecyl- β -D-1-thiogalactopyranosid |
| DNA | Deoxyribonucleic acid |
| DMSO | Dimethyl sulfoxide |
| DSS | 4,4-dimethyl-4-silapentane-1-sulfonic acid |
| DTT | Dithiothreitol |
| D ₂ O | Deuterium oxide |
| <i>E. coli</i> | <i>Escherichia coli</i> |
| ECF | energy-coupling factor |
| EDTA | Ethylenediaminetetraacetic acid |
| FID | Free induction decay |
| H/D | Hydrogen/ Deuterium |
| HetNOE | Heteronuclear NOE |
| His ₆ -tag | Polyhistidin-tag comprised of 6 histidine |
| HSQC | Heteronuclear single quantum coherence |
| IC ₅₀ | Half maximal inhibitory concentration |
| IPTG | Isopropyl β -D-1-thiogalactopyranoside |
| K-EDTA | Potassium ethylenediaminetetraacetic acid |
| <i>L. lactis</i> | <i>Lactococcus lactis</i> |
| LB-medium | Lysogeny broth medium |
| LDH | Lactate dehydrogenase |
| LMNG | Lauryl maltose neopentyl glycol |
| LmrA | Lactococcus multidrug resistance ATP |
| M9 | Minimal medium |
| MRW | Mean residue weight |
| MsbA | <i>Mannheimia succiniciproducens</i> Lipid A export ATP-binding/permease |
| MSP | Membrane scaffold protein |
| MW | Molecular weight |
| MWCO | Molecular weight Cut-Off |

| | |
|-----------------------|--|
| NBD | Nucleotide binding domain |
| NH | Amine group |
| Ni ²⁺ -NTA | Nickel-Nitrilotriacetic complex |
| NMR | Nuclear magnetic resonance |
| NOE | Nuclear Overhauser effect |
| NTP | Nucleoside triphosphate |
| N-terminal | Amino-terminal |
| OD ₆₀₀ | Optical density measured at wavelength of 600 nm |
| PCR | Polymerase chain reaction |
| PEP | Phosphoenolpyruvate |
| PET-FCS | Photoinduced electron transfer-fluorescence correlation spectroscopy |
| P-gp | P-glycoprotein |
| PK | Pyruvate kinase |
| PLD | Periplasmic domain |
| ppm | parts per million |
| RMSD | Root-mean-square deviation |
| RNA | Ribonucleic acid |
| Rpm | Revolutions per minute |
| RT | Room temperature |
| SBP | Substrate binding protein |
| SDS | Sodium dodecyl sulfate |
| SDS-PAGE | SDS Polyacrylamide gel electrophoresis |
| SEC | Size exclusion chromatography |
| TAE | Tris base -acetate acid-EDTA |
| TEMED | Tetramethylethylenediamine |
| TEV | Tobacco etch Virus |
| TMD | Transmembrane domain |
| Tris-HCl | Tris(hydroxymethyl)-aminomethan hydrochloride |
| TROSY | Transverse relaxation-optimized spectroscopy |
| τ_D | Translational diffusion time constant |
| τ_D | Relaxation time constant |
| v/v | Volume per volume |
| w/v | Weight per volume |
| WT | Wildtype |
| 2XYT | 2x Yeast extract and tryptone |

Table of contents

| | |
|--|------|
| Acknowledgements..... | V |
| Summary | VII |
| Zusammenfassung..... | IX |
| Abbreviations | XIII |
| Table of contents..... | XV |
| Chapter I: Introduction..... | 1 |
| 1. Membrane proteins..... | 1 |
| 2. Multidrug resistance..... | 2 |
| 3. ABC transporters | 4 |
| 3.1. Mammalian ABC proteins | 7 |
| 3.2. ABC transporters in multidrug resistance | 9 |
| 3.3. Structural details of ABC transporters: TMDs and NBDs | 11 |
| 3.4. Transport mechanism of type I ABC exporters: "alternating access" mechanism and its alterations | 22 |
| 3.5. Biophysical methods used to study type I ABC exporter (type IV fold) dynamics | 25 |
| 4. Aim of the thesis..... | 31 |
| Chapter II: Material and methods..... | 33 |
| 1. Chemicals..... | 33 |
| 2. Bacterial Strains, cloning and plasmids for heterologous expression in <i>e. coli</i> | 34 |
| 2.1. Bacterial Strains..... | 34 |
| 2.2. Cloning..... | 34 |
| 2.3. Plasmids..... | 38 |
| 3. Properties of purified proteins | 42 |
| 4. Heterologous/ homologous expression of LmrA-NBD, MsbA-NBD and BmrA-NBD in <i>E. coli</i> | 45 |
| 4.1. Media for protein expression and additives | 45 |
| 4.2. Preparation of competent cells..... | 47 |
| 4.3. Transformation of cells | 47 |
| 4.4. Protein expression conditions..... | 47 |
| 5. Purification of LmrA-NBD, MsbA-NBD and BmrA-NBD | 49 |
| 6. Purification of membrane proteins: full-length ABC transporters MsbA and BmrA..... | 49 |
| 6.1. Preparation of inside out vesicles (IOVs) containing full-length MsbA and BmrA..... | 49 |
| 6.2. Solubilization and purification of full-length MsbA and BmrA | 50 |
| 6.3. Preparation of inside out vesicles (IOVs) containing full-length BmrA..... | 50 |
| 6.4. Solubilization and purification of full-length BmrA..... | 51 |
| 7. Purification of TEV protease..... | 51 |
| 8. Quantitative protein determination..... | 52 |

| | |
|--|-----|
| 9. Reconstitution of membrane proteins into liposomes..... | 53 |
| 10. Biophysical characterization of recombinant proteins..... | 53 |
| 10.1. SDS-Polyacrylamide gel electrophoresis (SDS-PAGE)..... | 53 |
| 10.2. Analytical size exclusion chromatography | 54 |
| 10.3. CD spectroscopy | 55 |
| 10.4. Photoinduced electron transfer – fluorescence correlation spectroscopy (PET-FCS) | 56 |
| 11. Biofunctional characterization of recombinant proteins | 57 |
| 11.1. ATPase activity assay | 57 |
| 11.2. Fluorescence drug transport assay..... | 59 |
| 12. NMR techniques | 60 |
| 12.1. NMR sample preparation | 60 |
| 12.2. NMR experiments: spectrometer, parameters and spectra analysis..... | 60 |
| 12.3. Pulse sequence information of NMR experiments | 61 |
| 12.4. Backbone chemical shift assignments..... | 67 |
| 12.5. ¹ H - ¹⁵ N HSQC protein spectra | 68 |
| 12.6. NMR titration experiments | 68 |
| 12.7. Hydrogen/ Deuterium (H/D) exchange | 69 |
| 12.8. Backbone hetNOE analysis | 69 |
| 12.9. 1D ¹⁹ F - NMR | 70 |
| Chapter III: Results..... | 71 |
| 1. Consequences of nucleotide binding to the NBD of multidrug ABC transporters | 71 |
| 1.1. Introducing the Model System | 71 |
| 1.2. Nucleotide binding to the NBD: Dynamic consequences for conserved motifs and allosteric signal propagation | 74 |
| 1.3. Complementary analysis of protein dynamics across different timescales | 82 |
| 2. Role of conserved motifs in the NBD of multidrug ABC transporters | 92 |
| 2.1. Introduction..... | 92 |
| 2.2. Consequences of mutating D-, Q- and H-loop – a chemical shift analysis | 93 |
| 2.3. Fast Backbone Dynamics of LmrA-NBD D-, Q- or H – loop mutants in the ADP-bound state | 102 |
| 2.4. Molecular crosstalk of the NBD depends on the D-loop motif | 110 |
| 3. Discovery of a novel communication hinge Linking NBS and TMD in multidrug ABC transporters 113 | |
| 3.1. Introduction..... | 113 |
| 3.2. Nucleotide binding is sensed by residues at the C-terminal end of the Walker A helix . | 114 |
| 3.3. The NBD “hinge region” influences full-length Transporter ATPase activity, substrate transport and stability | 117 |
| Chapter IV: Discussion | 121 |

| | |
|---|-----|
| 1. Differences in NBD dynamics of the ABC transporter LmrA induced by nucleotide binding.... | 121 |
| 1.1. Comparison of the apo and ADP-bound state NBD on the ps – ns timescale | 123 |
| 1.2. Relative motions between α -helical and catalytic subdomain | 123 |
| 1.3. Focus on the coupling helix groove – communication about nucleotide occupancy between NBD and TMD..... | 126 |
| 1.4. Consequences of nucleotide binding for residues within conserved motifs | 127 |
| 1.5. Allosteric coupling of nucleotide binding throughout the NBD: focus on the C-terminal region | 130 |
| 1.6. On the physiological relevance of the dynamic and structural differences in nucleotide binding states | 134 |
| 2. NBD intradomain crosstalk: Focus on D-, Q- and H-loops..... | 136 |
| 2.1. Crosstalk of D-, Q- or H-loop with the Walker A and Walker B motifs | 136 |
| 2.2. Communication of the D-, Q- and H-loops with the D-loop helix | 137 |
| 2.3. Crosstalk between coupling helix groove and D-, Q-, H-loops | 137 |
| 2.4. Long-range communication of D-, Q- and H-loops with the C-terminal region..... | 139 |
| 2.5. NBD intradomain crosstalk between D-, Q- and H-loop | 140 |
| 2.6. Crosstalk mediated by LmrA-NBD D-loop variants | 141 |
| 3. “Communication hinges” between the NBS and the TMD of multidrug ABC transporters | 144 |
| 3.1. A potential NBS-TMD signaling pathway Part I – signal propagation via a conserved arginine residue..... | 144 |
| 3.2. A potential NBS-TMD signaling pathway Part II – signal propagation via a conserved tyrosine residue..... | 147 |
| 3.3. Interdomain crosstalk in other ABC transporter classes..... | 148 |
| Outlook..... | 151 |
| Appendix | 153 |
| 1. Chapter I: Introduction | 153 |
| 2. Chapter II: Material and methods | 160 |
| 3. Chapter III: Results..... | 167 |
| 3.1. Consequences of nucleotide binding to the NBD of multidrug ABC transporters..... | 167 |
| 3.2. Role of conserved motifs in the NBD of multidrug ABC transporters..... | 173 |
| 3.3. Discovery of a novel communication hinge Linking NBS and TMD in multidrug ABC transporters..... | 181 |
| 4. Chapter IV: Discussion | 197 |
| 4.1. Differences in NBD dynamics of the ABC transporter LmrA induced by nucleotide binding | 197 |
| 5. List of figures | 198 |
| 6. List of tables..... | 202 |
| Urheberschaftserklärung | 205 |

| | |
|------------------------|-----|
| References..... | 207 |
| Curriculum vitae | 237 |

CHAPTER I: INTRODUCTION

Parts of this chapter are published in:

Rose-Sperling, D., Tran, M. A., Lauth, L. M., Goretzki, B., and Hellmich, U. A. (2019) 19F NMR as a versatile tool to study membrane protein structure and dynamics, *Biological chemistry* 400, 1277–1288. DOI: 10.1515/hsz-2018-0473.

Szöllősi, D., Rose-Sperling, D., Hellmich, U. A., and Stockner, T. (2018) Comparison of mechanistic transport cycle models of ABC exporters, *Biochimica et Biophysica Acta (BBA) - Biomembranes* 1860, 818–832 published online Oct 31, 2017. DOI: 10.1016/j.bbamem.2017.10.028.

Neumann, J., Rose-Sperling, D., and Hellmich, U. A. (2017) Diverse relations between ABC transporters and lipids: An overview, *Biochimica et Biophysica Acta (BBA) - Biomembranes* 1859, 605–618 published online Sep 29, 2016. DOI: 10.1016/j.bbamem.2016.09.023.

1. MEMBRANE PROTEINS

One third of the human genome encodes for integral membrane proteins, and membrane proteins constitute more than 60% of all drug targets^{1,2}. Even though membrane proteins make up a high level of total amount of proteins in cells, only ~1% of the protein entries in the protein data bank³ are membrane proteins. Since the advent of high-resolution cryoEM, the structural information available for membrane protein is growing faster and currently ~10% of entries in the electron microscopy databank⁴ are membrane proteins⁵. Membrane proteins carry out essential functions such as ion, vitamin or metabolite translocation across cellular membranes, cell-cell communication through direct interactions, chemical or electric stimuli and cellular detoxification by extruding antibiotics and toxic compounds^{1,6}.

Regulated transport of molecules across the cell membrane via selective uptake or release mechanisms is essential for cell survival. Many membrane proteins function as gateways, and enable either passive, facilitated or active transport. The transport against a concentration gradient requires energy and is performed by primary active or secondary active transporters. Primary active transporters use the free enthalpy of a high-energy enzymatic reaction, such as ATP hydrolysis, for substrate transport. Transport ATPases, which include the rotary motor F-, A- and V-ATPases, the P-type ATPases and the ATP-binding cassette (ABC) transporters make use of this approach. The large ABC transporter family whose members are ubiquitously expressed in all phyla of life presents an exciting field to study transport mechanisms across cellular membranes. ABC transporters are essential for the transport of many structurally diverse substances across the cellular membranes and thus guarantee cell survival. Substrates include sugars, lipids, peptides but also antibiotics and toxins. The extrusion of toxins, as well as drugs used as chemotherapeutics and antibiotics, is beneficial to protect the cell, but it also leads to emerging problems such as multidrug resistance (MDR).

2. MULTIDRUG RESISTANCE

The extensive and sometimes uncontrolled use of drugs in the past decades led to the increased occurrence of microbial multidrug resistance (MDR)⁷. The phenomenon of MDR is characterized by the fact that such microbial defense mechanisms are not selective to the single drug used during the treatment of a disease, but rather also to other compounds that can even be unrelated in structure and molecular action. In case of pathogenic microorganisms, this can correspond to a resistance to several classes of antimicrobial drugs, resulting in ineffective drug therapy. In cancer cells, MDR manifests as a cross-resistance to a wide variety of anticancer drugs with different structures and mechanisms of action⁸. Hence, in the context of human health, understanding multidrug resistance mechanisms is crucial for chemotherapy as well as for the treatment of bacterial infections with antibiotics⁹⁻¹¹.

The four predominant molecular mechanisms of multidrug resistance⁷ are

(i) *Drug inactivation or modification*

This is the major mechanism of resistance towards β -lactam antibiotics (e.g. penicillin^{12,13}). The enzymatic inactivation of drugs is conducted by e.g. chloramphenicol transferases and aminoglycoside modifying enzymes^{14,15}.

(ii) *Drug target changes or bypass*

The drug target can be altered through mutagenesis, enzymatic alterations (e.g. addition of methyl groups) and/or replacement or bypass of the original target¹⁶. These alterations result in reduced drug binding affinities and drug efficacy. As an example, alterations (i.e. amino acid substitution) of proteins which bind penicillin can lead to the formation of irreversible complexes of protein with penicillin and hence causes an inhibition of their function in cell wall synthesis (i.e. in peptidoglycan synthesis)¹².

(iii) *Diminished drug import*

The cell membrane acts as a physical barrier for drug entry. It also affects resistance as its permeability changes e.g. due to an altered membrane protein composition. For instance, the number of outer membrane porins can be reduced to negatively impact drug uptake of the cell^{7,17,18}.

(iv) *Enhanced active drug export*

Higher expression of protein efflux pumps leads to enhanced drug extrusion, this will be discussed in more details in the following.

The efflux pumps involved in enhanced export of drugs are both primary and secondary active transporters and can be classified in the following groups based on protein sequence homology, energy source for substrate translocation and overall structure (**Figure 1**)¹⁹⁻²³:

(iv1) Primary active transporters

➔ "ATP binding cassette" (ABC) transporter superfamily²⁴⁻²⁶

(iv2) Secondary active transporters

➔ "Major facilitator superfamily" (MFS) family^{27,28}

➔ "Multidrug and toxin compound extrusion" (MATE) family^{22,29}

➔ "Small multidrug resistance" (SMR) family³⁰

(Belonging to the "drug/ metabolite transporter" (DMT) superfamily)

➔ "Resistance-nodulation division" (RND) family^{31,32}

➔ "Proteobacterial antimicrobial compound efflux" (PACE) family²¹

➔ " ρ -aminobenzoyl-glutamate transporter" (AbgT) family³³

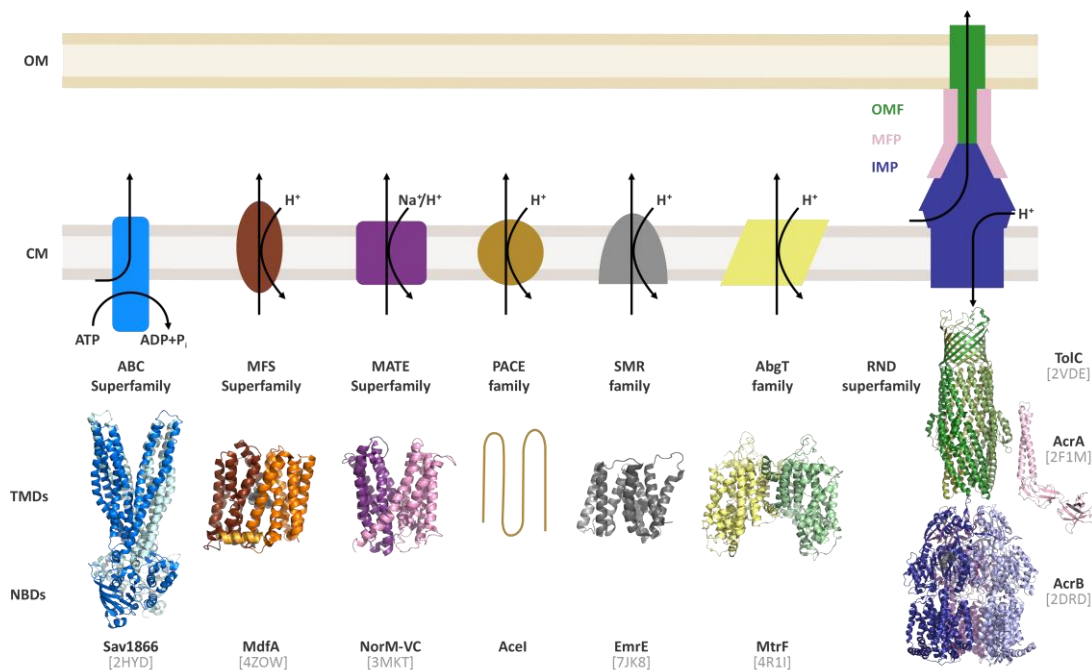


Figure 1: Classification of the seven drug efflux pumps involved in bacterial multidrug resistance (modified from Chitsaz and Brown, 2017²²)

The top scheme represents the seven different efflux pumps within the membrane (inner membrane in case of gram-negative bacteria). Below, the respective known structures are illustrated (not drawn to size). The ABC transporter superfamily (blue, Sav1866, PDB ID: 2HYD³⁴) represents the only primary active transporter family involved in MDR. The MFS superfamily (brown, MdfA, PDB ID: 4ZOW³⁵), the MATE superfamily (dark purple, NorM-VC, PDB ID: 3MKT³⁶), the PACE family (dark yellow, no structure available, shown are the four transmembrane segments as a model), the SMR family (gray, EmrE, PDB ID: 7JK8³⁷), the AbgT family (light green, MtrF, PDB ID: 4R11³⁸) and the RND superfamily (three component scheme for tripartite efflux pump, colored by dark blue - IMP, rose - MFP and green - OMF; AcrB, PDB ID: 2DRD³⁹; AcrA, PDB ID: 2F1M⁴⁰; TolC, PDB ID: 2VDE⁴¹) represent the six secondary active transporters of MDR. EmrE, MdfA and AcrB structures contain a substrate which is shown in gray. The ABC and MFS family form also tripartite efflux pumps with the soluble periplasmic adapter protein AcrA and the β -barrel outer membrane protein TolC or their homologs. NBDs – Nucleotide binding domains. TMDs – Transmembrane domains. OM – Outer membrane in case of gram-negative bacteria. CM - Cytosolic membrane. IMP - Inner membrane protein. OMF - Outer membrane factor family. MFP - Membrane fusion protein family.

Genetic plasticity to adapt to its environment is crucial for organisms from an evolutionary perspective. Especially in microorganisms, in addition to mutation in gene(s) commonly associated with the mechanism of action of a specific compound (see also ii above), incorporation of foreign DNA encoding for resistance determinants via horizontal gene transfer is used¹⁶.

Furthermore, in cancer cells, the inactivation of apoptotic pathways, drug compartmentalization in lysosomes following extrusion, enhanced DNA damage repair, epigenetic alterations and deregulation of mRNAs also result in MDR^{8,42,43}.

The superfamily of ABC transporters is involved both in microbial drug resistance and tumor resistance to chemotherapeutics. This also includes drug resistance in parasites, fungal drug resistance and bacterial multidrug resistance^{44–51}. In human cells ABC transporters are involved in tumor resistance to chemotherapeutics^{52–55}. To efficiently fight cancer, strategies of individualized chemotherapy become more and more important. One interesting novel approach is the search for ABC transporter nonsense mutations, which can be utilized for precision medicine development for individual patients⁵⁶. In summary, this makes ABC transporters one of the most important protein families for human health and disease.

3. ABC TRANSPORTERS

ABC transporters are ubiquitous in all three phyla of life. They mediate the translocation of diverse substrates under ATP consumption^{57,58} and are relevant in diverse physiological processes, such as lipid homeostasis, nutrient import, antigen presentation, antiviral defense, plant development, signal transduction or cellular detoxification^{59–71}. Different classifications can be carried out based on either ABC transporter function or architecture. In general, all ABC transporters consist of a transmembrane domain (TMD), responsible for substrate binding and translocation and a nucleotide binding domain (NBD), responsible for ATP hydrolysis. The structural details of TMD and NBD will be introduced in subchapter 3.3 Structural details of ABC transporters: TMDs and NBDs. In addition, ABC proteins consisting only of soluble NBDs are also present in the superfamily of ABC proteins.

On the functional level, the ABC protein superfamily can be divided into four major groups, of which the first three are membrane proteins:

- (i) Importers (mainly bacterial ABC transporters)
- (ii) ABC proteins that act as ion channels or channel regulators
- (iii) Exporters of diverse compounds including peptides, metabolites or xenobiotics (such as human ABCB family and MDR related ABC transporters)
- (iv) ABC proteins lacking transmembrane domains involved in DNA repair and translation

On a structural level, the TMDs and NBDs can be arranged in different ways, i.e. on a single or on separate polypeptide chains (**Figure 2** modified from Theodoulou & Kerr, 2015⁷²; Lacabanne, 2017⁷³):

- (i) Four separate functional polypeptide chains (can have identical or different NBD and TMD subunits)
- (ii) Three functional polypeptide chains, with two identical separate or fused NBDs and two separate or fused TMDs
- (iii) Two functional polypeptide chains, each with one NBD fused to one TMD, organized as homo- or heterodimers, or
- (iv) A single functional polypeptide chain containing all functional domains.

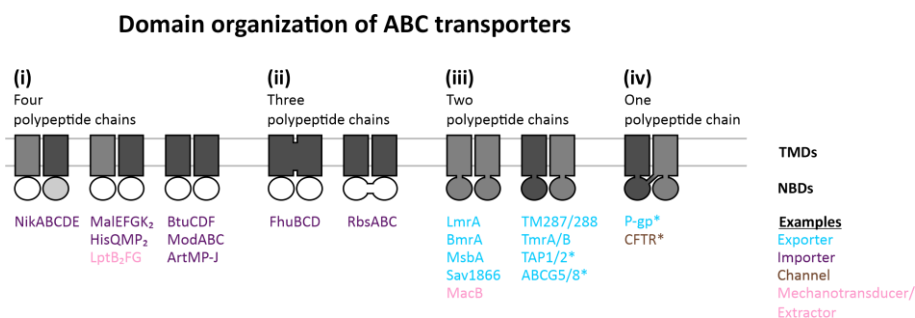


Figure 2: Core domain organization of ABC transporters (modified from Theodoulou & Kerr, 2015⁷²; Lacabanne, 2017⁷³)
Combinations of the two transmembrane domains (TMDs) and two nucleotide binding domains (NBDs). i) Four polypeptide chains, ii) Three polypeptide chains, iii) Two polypeptide chains and iv) One polypeptide chain. Examples for the respective domain organization are given below the respective topology. Colors indicate whether they are exporters, importers, channels or mechanotransducers/ extractors. Asterisks indicate eukaryotic ABC transporters. Not shown are ABC proteins lacking the transmembrane domains.

Furthermore, ABC transporters can contain additional regulatory domains, such as substrate binding domains (SBDs) or C-terminal regulatory domains (CRDs) that are not depicted in **Figure 2**.

Of note, there is currently no clear consensus in the field how to classify ABC transporters and the occurrence of new folds and/or functions may lead to changes in future classification attempts. A summary of currently utilized classifications is shown in **Figure 3**.

Classifications related to ABC transporter architectures and functions

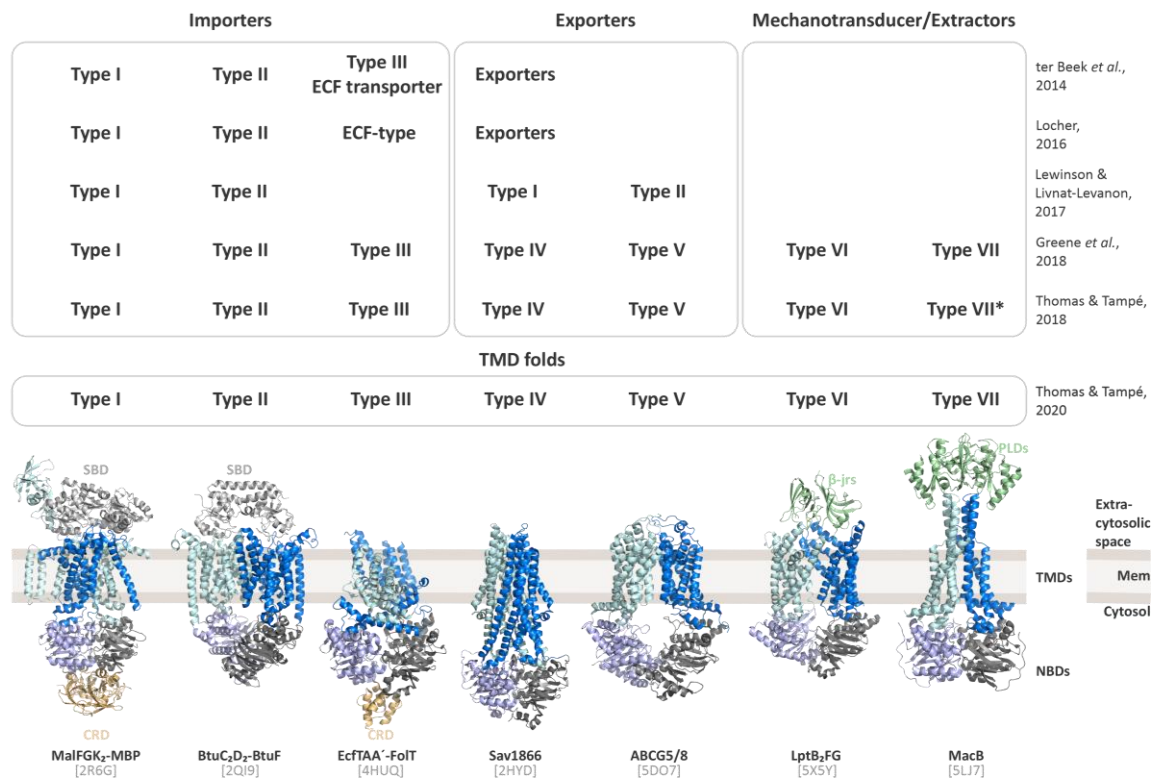


Figure 3: Different proposals for the classification of ABC transporters based on their architecture and function

Seven different structural folds are represented from the current available structural data of ABC transporters. From left to right: maltose transporter (MalFGK₂-MBP, PDB ID: 2R6G⁷⁴), vitamin B12 transporter (BtuC₂D₂-BtuF, PDB ID: 2Q19⁷⁵), folate importer (EcFTSA₂-FolT, PDB ID: 4HUQ⁷⁶), multidrug exporter (PDB ID: Sav1866, 2HYD³⁴), sterol transporter (ABCG5/8, PDB ID: 5D07⁷⁷), lipopolysaccharide extractor (LptB₂FG, PDB ID: 5X5Y⁷⁸) and the enterotoxin and macrolide transporter (MacB, PDB ID: 5LJ7⁷⁹). Different proposals for the classification of ABC transporters are presented. Of note, there is currently no clear consensus in the field how to ultimately classify ABC transporters and the occurrence of new folds and/or functions may lead to changes in future classification attempts. The type VII ABC transporter was originally not specified as type VII mechanotransducer/ extractor in the first paper by Thomas and Tampe, 2018 (asterisks labeled). Domain organization as indicated in **Figure 2** has been neglected within the used color codes. Mem – Membrane. NBDs – Nucleotide binding domains. TMDs – Transmembrane domains. SBD – Substrate binding domain. CRD – C-terminal regulatory domain. PLDs – Periplasmic domains. β -jrs – β -jellyroll-like domains.

ABC transporters can function as exporters (i.e. removing substrates from the cytoplasm), importers (i.e. translocating substrates into the cytoplasm) or mechanotransducers/ extractors (i.e., transduction of mechanical force into the periplasm coupled to movement of substrates across the cell membrane)^{80–82}. Based on these functions, ABC transporters were classified in three types of importers, two types of exporters and were recently extended by the mechanotransducers/ extractors LptB₂FG type and MacB type (**Figure 3**)^{34,74–79,83–88}. 2020 another nomenclature for ABC transporters based on the structural homology of the TMD folds was proposed (**Figure 3**), not predominantly related to the direction of substrate translocation⁸². Accordingly, the classes based on the function in the ABC field were suggested to be renamed from, “type I importers” to “type I” transporters, “type II importers” to “type II” transporters, “type III importers” to “type III”

transporters, “type I exporters” to “type IV” transporters, “type II exporters” to “type V” transporters, “extractor/ mechanotransducer type Lpt_{B2}FG” to “type VI” transporters and “extractor/ mechanotransducer type MacB” to “type VII” (Figure 3 and Figure 4).

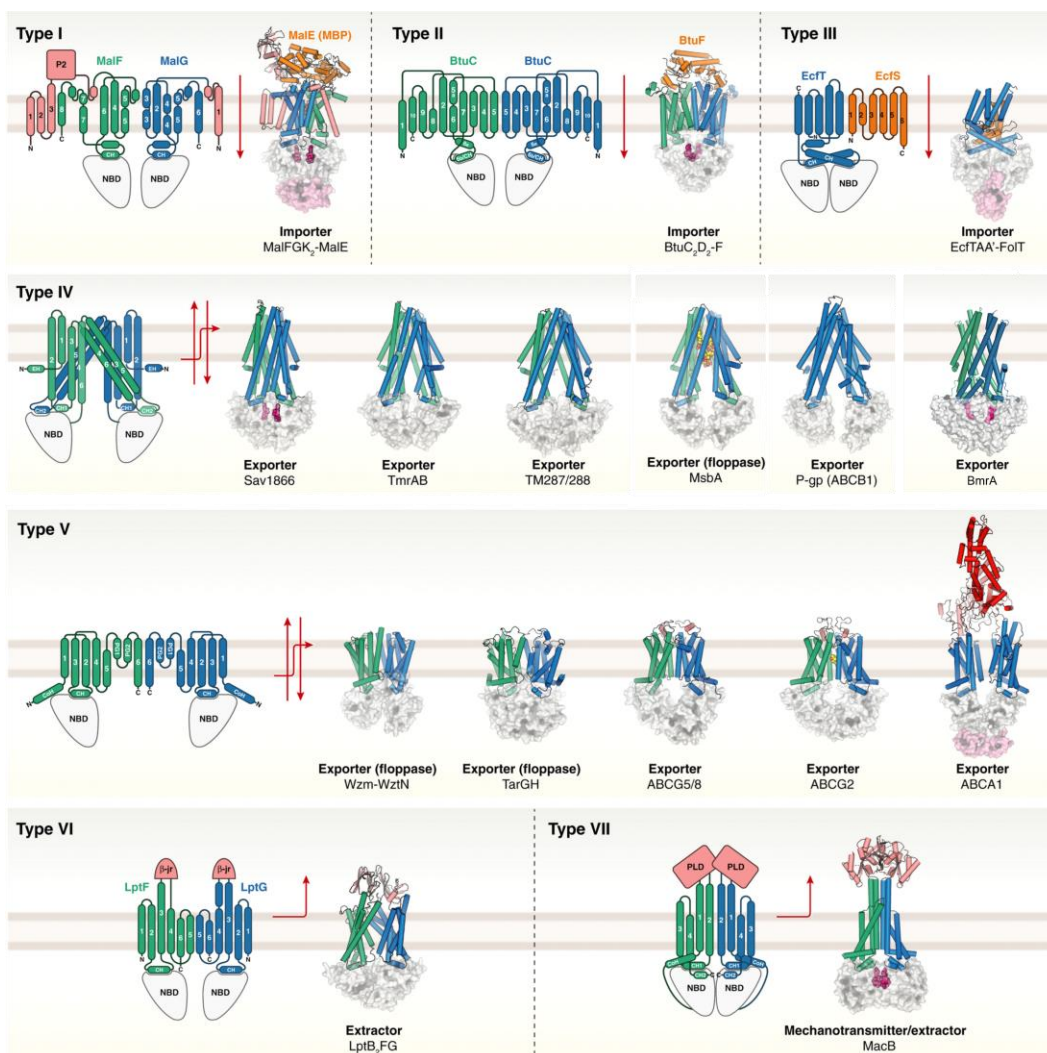


Figure 4: Proposal for a classification of ABC transporter based on the TMD folds (modified from Thomas et al. 2020⁸²)
Of note, there is currently no clear consensus in the field how to ultimately classify ABC transporters and the occurrence of new folds and/or functions may lead to changes in future classification attempts. TMD topologies are illustrated as models, which are based on the first neighboring structure, i.e. type IV model is based on Sav1866. NBDs are shown as surface representations or as simple cartoon. Red arrows indicate possible substrate transport pathways within and across the membrane. The TMDs of each transporter are highlighted in green and blue. When they consist of only one polypeptide chain, they are uniformly highlighted in blue. The substrate binding domains are highlighted in orange for type I – III folds. Additionally, auxiliary TMD helices and auxiliary domains are illustrated in red, light pink and light violet. In the NBDs bound (occluded) nucleotides and magnesium ions are represented as dark pink spheres. Inhibitors and substrates are shown in CPK colors and yellow colors. PDB IDs of shown transporters: MalFGK₂-MalE (2R6G⁷⁴), BtuC₂D₂-BtuF (4F13⁷⁵), EcfTAA'-FoIT (4HUQ⁷⁶), Sav1866 (2HYD³⁴), TmrAB (5MKK⁸⁹), TM287/288 (4Q4H⁹⁰), MsaA (5TV4⁹¹), P-gp (4M1M⁹²), BmrA (6R81⁹³), Wzm-WztN (6OIH⁹⁴), TarGH (6JBH⁹⁵), ABCG5/8 (5DO7⁷⁷), ABCG2 (6HCO⁹⁶), ABCA1 (5XIY⁹⁷), LptB₂FG (5X5Y⁷⁸), MacB (5LJ7⁷⁹). NBD – Nucleotide binding domain. TMD – Transmembrane domain. PLDs – Periplasmic domains. β-jrs – β-jellyroll-like domains. CH – Coupling helix. CoH – Connecting helix. EH – Elbow helix. P2 – Extracytoplasmic loop. PG – Periplasmic gate helix.

3.1. Mammalian ABC proteins

Mammalian ABC proteins belong to seven subfamilies, ABCA-G: Members of the families A-D and G code for membrane transporters (**Table 1**). Members of the ABCE and ABCF families are soluble proteins consisting only of NBDs and are involved in e.g. ribosome recycling or transcription regulation^{98,99}. In members of the ABCA and C families, all four domains are fused in a single polypeptide chain (so-called full transporters), while ABCD and G members (as well as the majority of prokaryotic exporters) are “half-transporters” where one TMD is fused to one NBD (**Figure 2** and **Table 1**). The ABCA transporter subfamily is involved in the regulation of cellular trafficking and cholesterol homeostasis¹⁰⁰. The ABCC subfamily includes ABCC7 (CFTR: cystic fibrosis conductance regulator), which is an ion channel, as well as ABCC8 and ABCC9 that are regulators of the Kir6.2 potassium ion channel¹⁰¹. A unique feature of the ABCG subfamily is their domain topology with an N-terminally leading NBD followed by the TMD (**Table 1**). Four out of five ABCG transporters capable of transporting lipids across a membrane¹⁰². In the ABCB family, both full and half transporters can be found (**Table 1**). Here, two half-transporters will homo- or hetero-dimerize to form a full transporter¹⁰³. In bacteria, many other ABC transporter domain organizations, such as all four domains on separate peptides, exist (**Table 1**). The ABCB subfamily is structurally heterogeneous, as it includes both full length (ABCB1, ABCB4, ABCB5 and ABCB11), as well as hetero- and homodimeric half transporters (ABCB2/B3 and ABCB6-10, respectively).

Across the seven subfamilies, human ABC transporters participate in tasks as versatile as antigen presentation, mitochondrial iron homeostasis, ATP dependent regulation of ion channels or lipid transport. Indeed, twenty out of the 48 human ABC transporter proteins have been implicated in the transport of lipids or lipid-like molecules, such as steroids (including cholesterol and bile acids), phospholipids and sphingolipids (for a detailed description please refer to Vasiliou *et al.*, 2009¹⁰⁴; Tarling *et al.*, 2013¹⁰⁵; Neumann *et al.*, 2017¹⁰⁶). These “lipid translocators” belong to all ABC transporter subfamilies (A, B, C, D, G), thus no subfamily specific trait seems to be responsible for lipid recognition and transport⁸². Mutations in these proteins lead to disruptions in lipid metabolism and distribution. Consequences are lipid-associated diseases such as sitosterolemia¹⁰⁷, Stargardt disease¹⁰⁸ or Tangier disease¹⁰⁹, thus underlining the importance of well-organized cellular lipid translocation. The phenomenon of MDR has been reported to be associated with members of the human ABCB (ABCB1 and ABCB4), ABCC (ABCC1-5, ABCC10) and ABCG (ABCG2 and ABCG4) family and frequently coincides with the ability of a protein to translocate lipids¹¹⁰.

Table 1: Human ABC transporters involved in lipid transport (modified from Neumann et al., 2016¹⁰⁶)
The topology of the different ABC families as well as their substrates and cellular distribution are shown. In parentheses, the subfamily members are given as abbreviations, e.g. A1 stands for ABCA1.

| Human ABC family | ABCA | ABCB | ABCC | ABCD | ABCG |
|---------------------------------|--|--|---|----------------------|--|
| Transporter topology | | | | | |
| Lipophilic substrates | (Phospho) lipids (A1, A3, A4, A7, A12) Sphingomyelin (A1, A3) Cholesterol (A1, A2, A5) | Phospholipids (B1, B4) Sphingolipids (B1) Bile salts (B11) Drugs (B1) | Phospholipids (C1) Bile salts (C1, C2, C3) Steroids (C1, C10) Drugs (C1, C2) | (VLC)FA (D1 - D4) | Lipids (G4) Cholesterol (G1, G4, G5/G8) Steroids (G2, G5/G8) Drugs (G2) |
| Subcellular localization | Plasma membrane (A1, A4, A7) Lysosome (A2, A5) Lamellar bodies (A3, A12) | Plasma membrane (B1, B4, B11) | Plasma membrane (C1, C2, C3, C10) | Peroxisome (D1 - D4) | Plasma membrane (G5/G8) Endosomes (G1, G4) |

3.2. ABC transporters in multidrug resistance

3.2.1. ABCB1 – P-glycoprotein

Members of the human ABCB subfamily exhibit a wide variety of physiological functions. ABCB1 (Multidrug resistance protein 1 (MDR1), P-glycoprotein, or P-gp) is a major player in cellular detoxification and multidrug resistance^{111–113}.

This 170-kDa plasma membrane protein was discovered 1976¹¹⁴. Juliano and Ling isolated mutants of Chinese hamster ovary cells for their cross-resistance to structurally diverse drugs, such as vinblastine, daunomycin and colcemid¹¹⁴. Within these mutants, a correlation between the level of resistance and the presence of the membrane protein P-gp was observed. P-gp is expressed at tissue barriers such as skin, intestine¹¹⁵, blood-brain barrier, placental barrier, and blood testis barrier¹¹¹ to limit the entry of environmental toxins and to keep the level of xenobiotics below a harmful level. Thus, the main role of P-gp seems to be cellular detoxification by expelling a large number of chemically unrelated hydrophobic compounds from the plasma membrane. While normally showing a protective function, P-gp frequently interferes with chemotherapy treatment by actively removing the medication, when cancer cells overexpress the transporter^{116,117}. Besides its problematic role in chemotherapy, P-gp is of further clinical relevance since it regulates bioavailability and pharmacokinetics of many drugs, e.g., by preventing brain penetration, uptake from the intestine or permeation through the placenta¹¹⁸. P-gp transporter activity has also been exploited e.g. in second generation antihistamines to prevent adverse sedative effects by limiting penetration through the blood-brain barrier¹¹⁹.

P-gp structurally belongs to the type I ABC exporters (type IV fold) (**Figure 3** and **Figure 4**). Its two transmembrane domains (TMDs) and nucleotide binding domains (NBDs) are expressed on a single polypeptide chain (**Figure 2**). It has two canonical NBS which per se are capable of conducting ATP hydrolysis, but it was noted that P-gp catalyzes only one ATP per cycle, indicating that asymmetry may occur within P-gp conformations during the substrate transport mechanism¹²⁰. This observation indicates functional analogies with heterodimeric type I ABC exporters (type IV fold).

3.2.2. The bacterial ABC exporters LmrA, BmrA and MsbA

Two decades after the discovery of P-gp, LmrA (Lactococcus multidrug resistance protein ATP) from *Lactococcus lactis* was found as the first prokaryotic multidrug ABC transporter pump¹²¹. Expression of LmrA in human cells complemented P-gp function and hence LmrA was suggested to be a bona fide bacterial homolog of P-gp¹²². Furthermore, hydrophobic drug extrusion from the cell membrane was shown to be mediated by LmrA due to ATP hydrolysis, including various antibiotics. Within the gram-positive strain *L. lactis*, LmrA transports amphiphilic substrates from the inner lipid leaflet of the cytoplasm to the extracytosolic matrix^{121,123}. Other prokaryotic ABC transporters related to drug efflux are BmrA (Bacillus multidrug resistance ATP) in gram-positive bacteria such as *Bacillus subtilis* and MsbA in gram-negative bacteria such as *Escherichia coli*. Gram-negative bacteria possess an inner cytoplasmic membrane and an outer membrane containing phospholipids in its inner leaflet and lipopolysaccharides (LPS) in its outer leaflet. MsbA is found in the cytoplasmic membrane of gram-negative bacteria¹²⁴. MsbA is essential for the translocation of lipid A and LPS from the inner leaflet. Hence, it is important for building and maintaining the outer cell membrane^{125,126}.

The physiological role in lipid transport of LmrA was also supported by the finding that it can functionally substitute MsbA, a lipopolysaccharide (LPS) ABC transporter^{127,128}. As an ABC transporter in gram-positive bacteria that do not contain LPS, LmrA might be involved in flopping of phospholipids¹²⁹. When overexpressing BmrA in *Escherichia coli* membranes, it was competent to transport a high diversity of substrates, such as Hoechst 33342, 7-aminoactinomycin D and

doxorubicin¹³⁰. Similarly, when overexpressing MsbA in *E. coli* or *L. lactis* resistance to multiple drugs was observed^{127,128,131}. Taken these observations, a function as a lipid floppase and multidrug resistance transporter was proposed for MsbA¹³².

In LmrA, BmrA and MsbA, one TMD, (containing 6 transmembrane helices (TMHs)) and one NBD are expressed in a single polypeptide chain with a size of around 65 kDa. A functional transporter forms homodimers (**Figure 2**)^{130,133,134}. The structural similarities between these three bacterial transporters with the mammalian P-gp also support the notion that they potentially share substrate overlap and a similar transport mechanism (**Figure 4 and Table 2**)^{121,127,128}.

The high-resolution crystal structure of MsbA published in 2005 presented the first structure of any ABC transporter but had to be retracted later. Since then, new MsbA structures in different conformations (e.g. Lipid A-bound) have been determined^{135,91}. Recently, three structures of *B. subtilis* BmrA were obtained⁹³. For *L. lactis* LmrA, there is currently no structure available although this transporter has been described extensively with biophysical techniques (**3.5. Biophysical methods used to study type I ABC exporter (type IV fold) dynamics**). For details regarding the details about the architecture of ABC transporters see subchapter 3 ABC transporters.

Table 2: Examples of drugs transported by LmrA, BmrA, MsbA and P-gp (modified from Orelle et al., 2019²⁶)

| Organism | Protein | Transported drug | Selected references |
|---------------------------|--------------------|---|--|
| <i>Lactococcus lactis</i> | LmrA | Ethidium bromide, Hoechst 33342, Daunomycin, Rhodamine 6G, TPP+, macrolides, streptogramins, tetracyclines, chloramphenicol | Van Veen <i>et al.</i> , 1996 ¹²¹ ; Putman <i>et al.</i> , 2000 ¹³⁶ |
| <i>Bacillus subtilis</i> | BmrA | Ethidium bromide, Hoechst 33342, Doxorubicin, 7-amino-actinomycin D, cervimycin, Rhodamine 6G | Steinfels <i>et al.</i> , 2004 ¹³⁷ ; Krugel <i>et al.</i> , 2010 ¹³⁸ ; Chaptal <i>et al.</i> , 2022 ⁹³ |
| <i>Escherichia coli</i> | MsbA | Ethidium, Hoechst 33342 (Binding of drugs: Daunorubicin, Colchicine, Vinblastine) | Reuter <i>et al.</i> , 2003 ¹²⁷ ; Woebking <i>et al.</i> , 2005 ¹²⁸ ; Eckford <i>et al.</i> , 2008 ¹³¹ |
| <i>Homo sapiens</i> | P-gp (ABCB1, MDR1) | Hoechst 33342, Rhodamine 123, Verapamil, cyclosporine A, Azidopine, Diltiazem, FK-506, Daunomycin, Doxorubicin Vinblastine, Vincristine, Colcemid, Actinomycin D, erythromycin, valinomycin | Juliano & Ling, 1976 ¹¹⁴ ; Yusa & Tsuruo, 1989 ¹³⁹ ; Tamai & Safa, 1991 ¹⁴⁰ ; Naito <i>et al.</i> , 1993 ¹⁴¹ ; Saeki <i>et al.</i> , 1993 ¹⁴² ; Germann, 1996 ¹⁴³ ; Shapiro & Ling, 1997 ¹⁴⁴ ; Schinkel & Jonker, 2003 ¹⁴⁵ ; Wang <i>et al.</i> , 2017 ¹⁴⁶ ; Martino <i>et al.</i> , 2018 ¹⁴⁷ |

3.3. Structural details of ABC transporters: TMDs and NBDs

3.3.1. The transmembrane domains and their interactions with the nucleotide binding domains

The TMDs of an ABC transporter form the translocation pathway and determine substrate specificity. The TMDs are very diverse and vary both in sequence and fold (**Figure 3** and **Figure 4**). While the TMDs of most ABC transporter families form dimers with a C2 symmetry axis, the TMDs of the so-called energy-coupling factor (ECF) transporters are an exception. They have a unique transmembrane architecture with only a single TMD and two NBDs. In order to form the transport-competent protein complex, the lone TMD needs to interact with a separate, substrate-binding, integral transmembrane protein that acts as a high-affinity scavenger for low abundance substrates such as vitamins or trace elements. It has been proposed that due to this architecture, ECF transporters have a unique transport mechanism where the substrate binding protein “topples” in the membrane to release the substrate⁸⁰.

Since this thesis investigates ABC transporters of the type I exporters (type IV fold), this domain architecture will be introduced in a bit more detail. Overall, TMDs share a similar basic fold with a core of six transmembrane α -helices. A characteristic feature of the members of this subfamily of ABC transporters is the extensive protrusion of their TMD helices into the cytosol (**Figure 3** and **Figure 4**). This fold was observed in the crystal structure of the multidrug transporter Sav1866 from *Staphylococcus aureus* for the first time³⁴ and since then in many other ABC transporters involved in MDR including MsbA^{91,135}, BmrA⁹³ and P-gp^{92,148,149}. In this fold, the TMD α -helices are connected by loops that are larger in the cytosol than extracytosolic within type I ABC exporters (type IV fold, **Figure 3** and **Figure 4**). Importantly, two of these intracellular loops (ICLs) fold into short α -helices, known as the “coupling helices” and form the non-covalent surface contact with the NBDs (**Figure 4**). One of the two coupling helices from each TMD makes a contact with its own NBD in *cis*, and one reaches over to the opposing NBD to form a contact in *trans* (**Figure 3** and **Figure 4**). Coupling helices are present in all ABC transporters and are crucial for NBD-TMD and TMD-NBD connection (e.g. for transmitting and inducing conformational changes within the domains) during the substrate transport cycle (**Figure 3** and **Figure 4**).

Another interesting feature within the TMDs of the type I ABC exporters (type IV fold) are the elbow helices (**Figure 3** and **Figure 4**). These helices are structural oriented parallel to the membrane has a putative role in anchoring the TMDs to the membrane. Furthermore, an interaction of the elbow helices with substrates was described, which indicates a role at the beginning of the substrate translocation process¹⁵⁰.

3.3.2. Nucleotide binding domains: constitution and function

In ABC transporters, substrate transport is coupled to binding and hydrolysis of ATP by the two NBDs. In contrast to the TMDs, the NBDs are highly conserved within the whole superfamily of ABC transporters, as the name (ATP-binding cassette) also indicates. A similar mechanism for ATP hydrolysis can be proposed across all ABC transporter NBDs as they display sequence identities of 25-30%^{59,151}. A typical NBD has a size of around 250 amino acids (aa). The NBD contains three characteristic conserved motifs: the Walker A motif, the Walker B motif and the ABC motif, which is specific for the ABC protein family (see below).

In general, each NBD contains a nucleotide binding site (NBS). In the ATPase competent NBD dimer, the two NBS from the two subunits are located at the interface between the two NBDs that arrange each other in a “head-to-tail” orientation (**Figure 5A**). The NBS region is the area with the highest sequence conservation (**Figure 5A/B**). An essential feature of the NBS is that an “ATP sandwich” is formed between the conserved motifs A-loop, Walker A, Walker B, Q-loop and the H-loop of one NBD and the D-loop and the ABC signature motif of the opposing NBD (**Figure 5A**, see below for a detailed description of the role of these conserved motifs). In heterodimeric ABC transporter NBDs, one center of hydrolysis can be degenerated due to mutations within the conserved motifs to form a non-canonical NBD. This usually leads to a situation where a nucleotide can still bind but no hydrolysis can be performed within one of the two NBS²⁶.

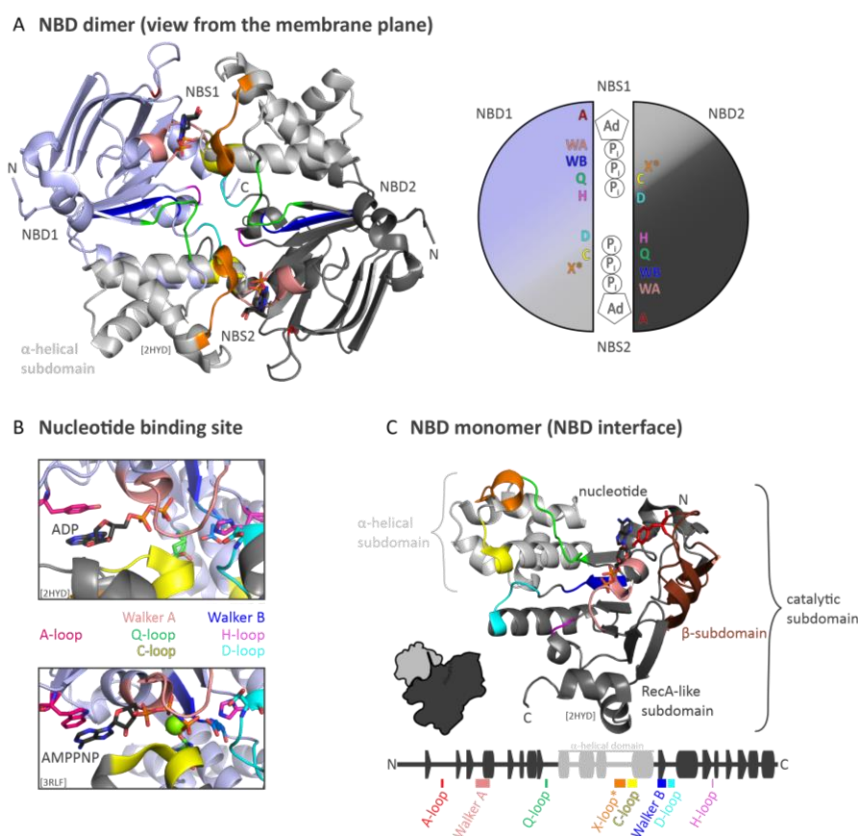


Figure 5: Inter- and intradomain organization of ABC transporter nucleotide binding domains

A) Top view from the membrane plane onto an NBD dimer. Shown is the structure of the NBDs of Sav1866 (PDB ID: 2HYD³⁴, left). The two ADPs in the NBSs are shown as sticks. The arrangement of the conserved residues (color code as in C) around the two nucleotides bound in the interdomain cleft are shown in a schematic on the right. Note the “head to tail” arrangement of the NBD dimer and the resulting NBS symmetry **B)** Close-up view of one NBS, showing nucleotide and magnesium ion interactions within the NBD interface. Upper view represents one NBS of Sav1866 binding ADP. The lower view represents one NBS of Malk (PDB ID: 3RLF¹⁵²) binding the ATP analog AMP-PNP (sticks) and magnesium ion (green ball). Residues of conserved motifs involved in ATP binding and hydrolysis are shown as sticks. **C)** NBD monomer view from the NBD-NBD interface, highlighting the subdomains and the conserved motifs. Below the NBD monomer the according

secondary structure elements of the Sav1866 NBD are displayed, where lighter gray indicates the α -helical subdomain and the conserved motifs are highlighted in different colors (**Appendix 1**). Asterisk marked X-loop motif does only occur within type I ABC exporters (type IV fold). Ad – Adenine. P_i – Phosphate. NBD – Nucleotide binding domain. NBS – Nucleotide binding site.

The NBD monomer can be structurally subdivided into three subdomains, the RecA-like subdomain, a three stranded antiparallel β -sheet forming the β -subdomain, and three to four helices forming an α -helical subdomain (**Figure 5C**)^{80,153}. While the α -helical subdomain only occurs in ABC-transporters, the RecA-like subdomain is also found within other P-loop NTPases. The RecA-like subdomain includes the conserved Walker A (P-loop) and B motifs, as well as the D- and H-loop (**Figure 5** and **Table 3**), while the β -sheet region contains the A-loop. The RecA-like and the β -sheet region together can thus be called “catalytic subdomain”. The α -helical subdomain harbors the C-loop (ABC signature motif) (**Figure 5** and **Table 3**), the X-loop and a region named the structural diverse region¹⁵⁴ (**Appendix 2**). The conserved Q-loop region in the RecA-like subdomain forms the interface between the catalytic and the α -helical subdomain. The conserved motifs are essential for nucleotide binding, hydrolysis and NBD-NBD as well as NBD-TMD communication (**Table 3**). A more detailed description about the function of the conserved motifs is given in the following table and text.

Table 3: Consensus sequence, subdomain localization and function of conserved motifs in the NBDs listed according to their occurrence in the subdomains/ interface between the subdomains (β -subdomain, RecA-like and α -helical subdomain). Asterisk marked motif does only occur within type I ABC exporters (type IV fold). (modified from Szöllösi¹⁵⁵)

| Motif | Consensus sequence | Subdomain localization | Function |
|---|--|--|--|
| A-loop ^{156,157} | Aromatic residue (often Y) | β -subdomain | ATP binding (Base stacking) |
| Q-loop ^{80,158–163} | Stretch of ~ eight aa with a conserved Q | RecA-like subdomain, interface between α -helical and catalytic subdomain | NBD-TMD communication Coordination of the magnesium ion Facilitate NBD closing |
| Walker A (P-loop) ¹⁶⁴ | GxxGxGK(S/T) ¹ | RecA-like subdomain | ATP binding (Phosphate binding) Coordination of the magnesium ion |
| Walker B ^{156,164–167} | $\phi\phi\phi\phi\text{DE}^2$ | RecA-like subdomain | ATP hydrolysis Stabilizing the magnesium ion |
| D-loop ^{168–173,90,174} | SALD | RecA-like subdomain | NBD-NBD communication, NBD-NBD dimerization (Interaction with H-loop and Walker A of the opposing NBD), unidirectional transport |
| H-loop (switch loop) ^{171,175} | ϕAHLR | RecA-like subdomain | ATP hydrolysis Coordination of the magnesium ion NBD-NBD dimerization (Interaction with D-loop of the opposing NBD) |
| ABC motif (Signature motif/ C-loop) ^{60,176} | LSGGQ | α -helical subdomain | ATP binding (Phosphate binding) NBD-NBD communication |
| X-loop* ^{34,177–182} | TxVG(E/D)(R/K)G ¹ | α -helical subdomain | NBD-TMD communication |

1 x = any residue

2 ϕ = hydrophobic residue

Conserved motif in the β -subdomain:

A-loop motif

The A-loop motif is an aromatic amino acid residue (mainly tyrosine, **Table 3** and **Figure 5**)¹⁵⁷. This aromatic amino acid interacts with the adenine ring of ATP or ADP via π - π stacking, hydrogen bonds and van der Waals contacts¹⁵⁷. This relative non-specific interaction led to the idea that it might be responsible for the intrinsic promiscuity of NBDs for various nucleotides¹⁷⁵.

Motifs in the RecA-like subdomain:

Q-loop motif - interface between catalytic and α -helical subdomain

A central conserved motif is the Q-loop, which is named after its conserved glutamine residue (**Table 3** and **Figure 5**). It is located at the interface between the catalytic and the α -helical subdomain⁸⁰. Due to conformational changes of the Q-loop, the glutamine residue can move in and out of the active catalytic center during ATP hydrolysis. In the literature, a role of the Q-loop glutamine in coordinating the magnesium ion for ATP hydrolysis, to communicate ATP binding and hydrolysis at the NBD to the TMDs leading to conformational changes and to facilitate NBD-NBD closing have been discussed^{158-163,183,184}. A structure of P-gp obtained in 2018 showed that the position of the Q-loop glutamine should indeed be able to fulfill all these tasks due to its position in the structure¹⁶³.

In ABC transporters, ATP hydrolysis occurs via the attack of a water molecule on the γ -phosphate. Often the side chain of an amino acid activates the attacking water molecule by deprotonation. In the NBDs of different ABC transporters, the Q-loop glutamine residue, together with the Walker B glutamate, was seen to form hydrogen bonds with a water molecule described to be a candidate for the lytic water during ATP hydrolysis^{156,171}. However, this early observation, that the Q-loop may be potentially important for coordinating the attacking water is not yet fully established. Movements between the catalytic and the RecA-like subdomain may also influence the movements of the Q-loop. On the other hand, flexibility of the Q-loop would be convenient to enable movements between the catalytic and the α -helical subdomain. The coupling helices (**3.3.1** The transmembrane domains and their interactions with the nucleotide binding domains) of the TMDs are also in contact with the Q-loop, which led to the hypothesis that the Q-loop plays a central role in the conformational coupling between NBDs and TMDs and hence the connection of hydrolysis and substrate transport^{34,135,148,163,183,185,186}. Mutating the both Q-loops in the NBDs of P-gp led to loss of ATPase activity, loss of the ability to perform a conformational change within the TMDs and thus transport capability¹⁶¹.

Walker A (P-loop) motif

The best known and one of the earliest motifs described to fulfil an important role in ATP-binding of ATPases is the Walker A motif. Walker *et al.* originally identified this motif in 1982 in different proteins (ATP-utilizing enzymes as RecA, the α and β subunits of F_1 -ATPase and myosin)¹⁶⁴. The Walker A motif (also named P-loop) consists of a loop and a part of the first NBD α -helix. It has the consensus sequence GxxGxGK(S/T), where x is any aa residue (**Table 3** and **Figure 5**)^{164,187}. First insights into the interactions between ATP and the Walker A motif residues came from the crystal structure of HisP, the NBD of the bacterial periplasmic histidine permease HisMQP₂¹⁵⁶. In the structure of HisMQP₂ the Walker A motif wraps around the phosphate groups, which was found to facilitate the formation of hydrogen bonds between the backbone amides of residues of the Walker A (SGSGKST) and the β - and γ -phosphate groups of ATP. Other isolated NBDs (from e.g. MalK¹⁸⁸, GlcV¹⁶⁷, HlyB¹⁸⁹, TAP¹⁹⁰) as well as within full-length (Sav1866^{34,191}, P-gp¹⁶³, MsbA¹³⁵, BmrA⁹³) structures of ABC transporters further

confirmed these interactions. The high content of conserved glycine residues in the Walker A motif may be advantageous for flexibility needed to adopt the loop structure with certain torsion angles which would not be compatible with residues having other sidechains¹⁹². The conserved lysine residue backbone amide and its sidechain can interact with ATP (β - and γ -phosphate of ATP)^{80,93,188,191}. This lysine residue is further thought to neutralize the negative charge of the phosphate groups and to position the nucleotide in a higher-energy conformation¹⁹². Mutations of the lysine residue can result in abolished drug transport (e.g. in P-gp¹⁹³ or BmrA¹³⁷) and to a significant decrease of ATPase activity and/ or impair nucleotide binding^{194–197}. The helix following the Walker A motif also stabilizes the negative phosphate groups of the nucleotides by its electrostatic dipole moment¹⁹⁸. Isolated NBD crystal structures revealed that the serine or threonine residue is involved in directly coordinating the co-factor magnesium (i.e. via their sidechain hydroxyl^{167,171,172,183} or backbone amide groups¹⁵⁶).

Walker B motif

Proteins that contain the P-loop (Walker A motif) also harbor another highly conserved motif, the Walker B motif¹⁶⁴. The Walker B motif consists of hydrophobic residues forming a β -strand and a conserved aspartate and glutamate residue. The consensus sequence is $\phi\phi\phi\phi$ DE (where ϕ is a hydrophobic aa, **Table 3** and **Figure 5**)^{164,187}. The aspartate residue is involved in coordination of the magnesium ion required for catalysis^{156,166,167,171,199}. The catalytic glutamate is responsible for ATP hydrolysis. It presumably acts as a catalytic base^{165,200} responsible for polarizing the attacking water, which induces proton abstraction what consequently forces the nucleophilic attack on the γ -phosphate of the ATP molecule^{152,156,167,169}. However, alternate models beyond the general base model for the glutamate residue exist as for some ABC transporter E/Q mutants reduced but not completely abolished ATPase activity was observed^{74,201–203} (**Appendix table 1** and **Appendix table 2**). These lead to additional models for ATP hydrolysis, i.e., the general acid as well as the substrate-assisted hydrolysis model^{155,171}. Due to the functions of the aspartate and glutamate residue it could be postulated that the Walker B motif is involved in ATP hydrolysis rather than ATP binding.

The E/Q mutation, i.e., substituting the Walker B glutamate by glutamine, is one of the most frequently used mutations in the field to prevent ATP hydrolysis. Based on this mutation and the resulting stabilization of what is believed to be a pre-hydrolysis state in the presence of ATP^{93,163,202} led to numerous ABC transporter protein structures^{93,163,169} (**Appendix table 1** and **Appendix table 2**). Furthermore, E mutants (e.g. E-A) can yield to a defective substrate transport⁹³. Mimicking a pre-hydrolytic state of ABC transporters can also be achieved by trapping with Beryllium fluoride (BeF_x), which stabilizes the tetrahedral geometry of this intermediate state^{204–206}.

D-loop motif

C-terminal of the Walker B motif is the conserved D-loop with the consensus sequence SALD (**Table 3** and **Figure 5**). It is the second hallmark of ABC transporters next to the ABC signature motif. In the NBD dimer interface, the D-loops are located antiparallely between the two NBS. Hence the D-loops are in a prime position to mediate communication between both NBSs. Furthermore, conformational changes of the flexible D-loop can mediate communication between the two NBDs and seem to be important for the formation of the hydrolysis-competent active site^{90,168,173,177,207}. The connection between the two NBDs is mediated by interactions of the D-loop with the H-loop and the Walker A motif of the opposing NBD via a complex hydrogen and electrostatic network^{152,169–172,174}. Thus, the D-loop can stabilize the NBD dimer through multiple interactions in the center of the NBD dimer interface including an extensive cross-interface hydrogen bond network²⁰⁸. Its importance in NBD-NBD dimerization was demonstrated by e.g. mutating the aspartate to an alanine residue, which prevented the formation of a dimer in the presence of ATP¹⁷⁴.

Crystal structures of heterodimeric ABC exporter, TAP revealed that the D-loop aspartate residue can act as a cap for the following C-terminal α -helix and hence represents a key residue to maintain rigidity within the vicinity of the D-loop¹⁷⁴. Mutating the aspartate residue of the D-loop resulted in diverse outcomes for the ATPase activity and substrate transport. When mutating one aspartate residue to an alanine in the heterodimeric sterol transporter ABCG5/8, no impact on sterol transport was reported²⁰⁹. On the other hand, the substitution of the D-loop of the consensus site of other heterodimeric ABC transporters (i.e. TM287/288, LmrCD and EfrCD) was found to be critical for ATPase activity and substrate transport^{90,210}. Furthermore, D-loop mutants were reported to lead to loss of transporter unidirectionality within the heterodimeric ABC exporter TAP¹⁷⁴. Substituting the aspartate residue to a glycine in the homodimeric lipid A exporter MsbA abolished its transport function and yielded enhanced ATPase activity^{211,212}.

H-loop (Switch loop) motif

A conserved histidine residue interacts with the catalytic base from the Walker B motif and the γ -phosphate of ATP¹⁷⁵ (**Table 3** and **Figure 5**). This so-called H-loop is crucial to position the catalytic base, water and magnesium ion correctly for ATP hydrolysis and was hence also named the linchpin of ATP hydrolysis^{171,213}. Furthermore, it undergoes interactions with the D-loop of the opposing NBD^{171,214}. When mutating the H-loop histidine residue in different ABC transporters, such as MsbA or HlyB-NBD^{171,213}, a reduction in ATPase activity and transport efficiency was observed^{171,213,215–217}. For the NBD of HlyB, the deficiency in ATP hydrolysis permitted the stabilization of the NBD dimer arrangement when the H-loop histidine or the Walker B motif glutamate residue were mutated, which resulted in the successful crystallization of NBD dimers in the presence of ATP¹⁷¹.

Motifs in the α -helical subdomain:

ABC signature motif (C-loop)

The ABC signature motif is the first hallmark of ABC transporters^{60,176}. Its presence in the α -helical subdomain of ABC transporters but not in other P-loop NTPases labels a protein as a member of the ABC superfamily. The C-loop is essential for ATP hydrolysis and has the consensus sequence LSGGQ (**Table 3** and **Figure 5**). It is a central part of the NBS in the NBD dimers, where it helps to coordinate ATP^{169,163}. In many crystallographic studies as well as molecular dynamics simulations on isolated NBDs it is suggested that ATP binding induces conformational changes of the α -helical subdomain where the ABC signature motif is localized. This facilitates the coordination of the C-loop and the γ -phosphate of an ATP molecule bound to the opposing NBD subunit^{169,170,189,218–220}. This interaction of ATP via the C-loop across the NBD dimer interface can bring the NBDs close for ATP hydrolysis. The backbone amide groups of the two sequential C-loop glycine residues have been reported to occupy the space between the α - and γ -phosphate. Those glycine residues are able to communicate changes in the active site to the α -helical subdomain^{168,170,221,222}.

X-loop motif

The X-loop motif with the consensus sequence TxVG(E/D)(R/K)G precedes the ABC signature motif and only occurs within type I ABC exporters (type IV fold) (**Table 3** and **Figure 5**)³⁴. It interacts with the coupling helices¹⁷⁸ and was proposed to be important for NBD-TMD communication^{34,177,179–181}. Structural differences have been identified in the X-loop of different transporters upon ATP hydrolysis¹⁷⁹, which might be due to its proximity to the ABC signature motif (C-loop). This would enable the X-loop motif to transmit conformational changes between the ATP binding site and the TMDs^{182,182}. This motif indicates that connection between ATP hydrolysis and substrate transport may be distinct in type I ABC exporters (type IV fold) compared to the other ABC transporters.

3.3.3. Models for the ATPase catalytic cycle in the NBD during the transport mechanism

All models describing the NBDs during the transport cycle of an ABC transporter need to at least consider the following steps: ATP binding, ATP hydrolysis, ADP and P_i release and nucleotide induced conformational consequences in both NBDs. These steps are connected to structural rearrangements within the TMDs, which leads to a potential substrate entry state and a state for substrate release.

Overall, models of the ABC transporter catalytic cycle can be divided into two main categories; either (i) predicting complete NBD separation or (ii) requiring the NBDs to remain in contact throughout the transport cycle. Asymmetric transporter conformations are associated with asymmetric binding states for nucleotides. The best-known models that include NBD separation are the “ATP-switch”²²³, the “tweezers-like” model¹⁷⁰ and the “processive clamp”^{169,224,225} models. In contrast, “constant contact”²²⁶, “alternating sites”²²⁷ and “nucleotide occlusion”^{228–230} models propose continuous NBD-NBD contact of at least one NBS throughout the transport cycle. All models implicitly agree on a tight coupling between NBDs and TMDs, with the closed NBD dimer corresponding to the outward open TMD conformation and the inward facing TMD conformation showing looser NBD association. The catalytic cycle models are summarized in **Figure 6** and **Table 4**. Briefly, the “constant contact” model relies on the relative motions between the α -helical and the catalytic subdomain within the NBDs. This extra flexibility allows nucleotide exchange in the open NBS, while keeping the second NBS closed and ATP-bound in an asymmetric conformation²³¹. Coupling helices of the TMDs are attached to the NBDs at the border between the α -helical and the catalytic subdomain. Subsequently, movements (dynamics) induced by e.g. nucleotide binding between those two subdomains can be transmitted to the TMDs. When considering the different models, it should also be kept in mind that e.g. in *E. coli* the physiological ATP concentrations are in the range of ~1500 - 2600 μ M and physiological ADP concentrations are in the range of ~800 μ M²³². Therefore, transporters may almost always be in the nucleotide bound state, even though the affinity of nucleotides depends on the conformation of the transporter²³⁰.

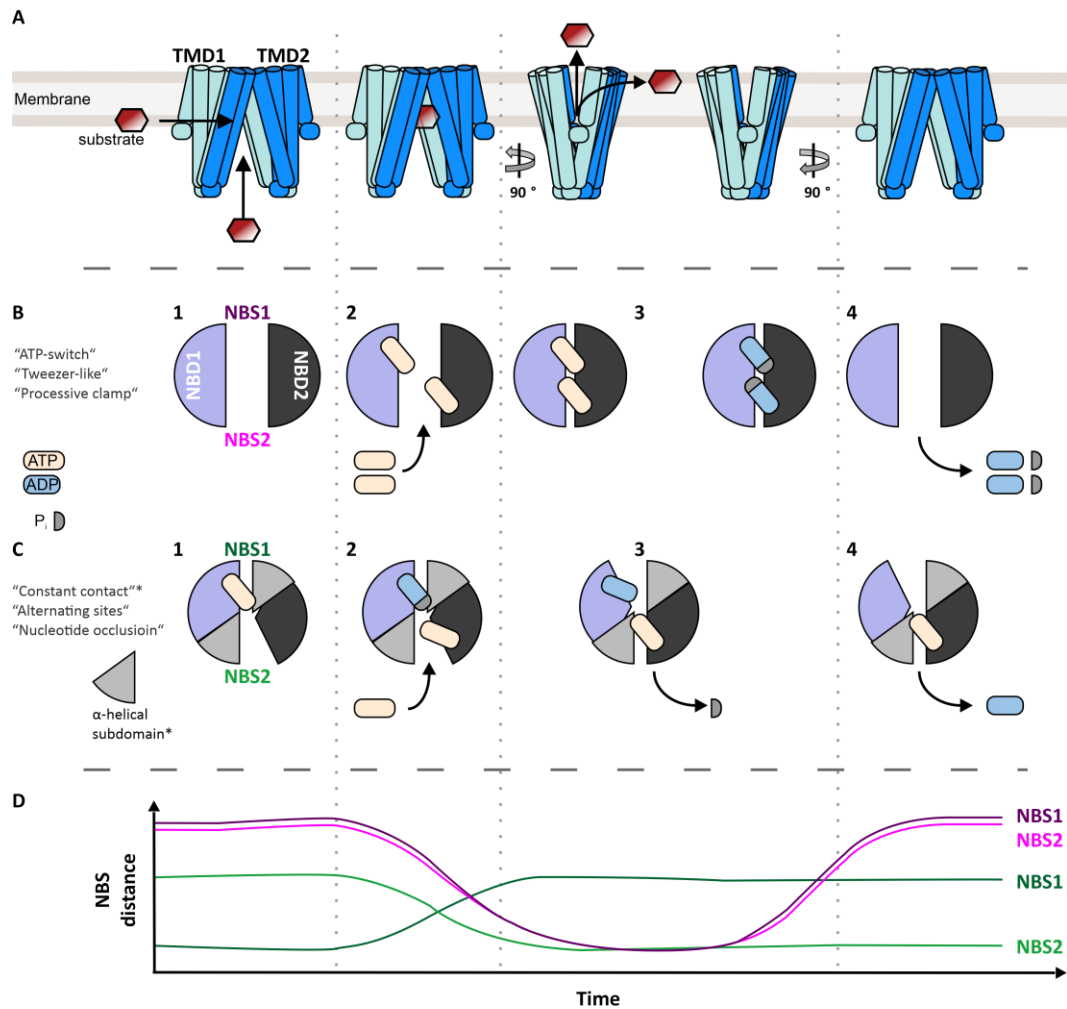


Figure 6: Cartoon summarizing the two main ABC transporter-catalytic cycle models (modified from Szöllösi et al., 2017¹⁵⁵)

A) Motions of the TMDs during the transport cycle of an ABC transporter based on the classic alternating access model. For simplicity, only an inward open state (substrate entry) and an outward facing state (substrate release) are illustrated. The cartoon includes the two possible paths (between membrane sides or membrane leaflets) of substrate binding and release. **B)** Functional models with full NBD separation; "ATP-switch"²²³, "tweezers-like"¹⁷⁰ and "processive clamp"^{169,224,225}. Shown is the top membrane view of the NBD dimers during the transport cycle. **C)** Functional models with constant contact of NBDs; "constant contact"²²⁶, "alternating sites"²²⁷ and "nucleotide occlusion"^{228–230}. **D)** NBS distances change within the functional models shown in B and C during the catalytic cycle. The diagram illustrates the distances between the two NBS (from Walker A to ABC signature motif) during the substrate transport cycle: NBS distances during the models without constant NBD contact (purple); NBS distances during the models with constant NBD contact (green). The asterisk indicates that within the constant contact model alternating NBS separation is induced due to movements between the α-helical subdomain and the catalytic sub domain within the NBD. TMD – transmembrane domain. NBD – Nucleotide binding domain. NBS – Nucleotide binding site.

Table 4: Models of the catalytic cycle of an ABC transporter in four steps.¹⁵⁵ The “tweezer-like” model was originally proposed for the maltose importer and is included for further reference and comparison. Light gray – without constant NBD contact. Dark gray – with constant NBD contact.

| Steps | “Nucleotide occlusion” ^{228–230} | “ATP-switch” ²²³ | “Processive clamp” 169,224,225 | “Alternating sites” ²²⁷ | “Constant contact” ²²⁶ | “Tweezers-like” (in MalFGK ₂) ¹⁷⁰ |
|----------|---|--|---|--|---|--|
| 1 | <u>NBDs:</u> semi-open dimer <u>NBS1:</u> occluded ATP <u>NBS2:</u> loosely ATP binding <u>TMDs:</u> inward open | <u>NBDs:</u> separated, empty <u>TMDs:</u> inward open, substrate binding | <u>NBDs:</u> ATP binding, dimer formation | <u>NBDs:</u> semi-open dimer <u>NBS1:</u> ATP binding <u>NBS2:</u> empty <u>TMDs:</u> inward open, bound substrate | <u>NBDs:</u> semi-open dimer <u>NBS1:</u> occluded, ATP-bound <u>NBS2:</u> occluded, empty | <u>NBDs:</u> semi-open dimer <u>NBSs:</u> empty <u>TMDs:</u> inward open |
| 2 | <u>TMDs:</u> substrate binding | <u>NBDs:</u> ATP binding, dimer <u>TMDs:</u> outward open, substrate release | <u>NBS1#:</u> hydrolysis, maybe release of P _i | <u>NBS2:</u> ATP binding <u>NBS1:</u> hydrolysis → high energy ADP+P _i state <u>TMDs:</u> inward open | <u>NBS1:</u> occluded, hydrolysis <u>NBS2:</u> open | Maltose loaded MBP binds to protein <u>NBSs:</u> ATP binding <u>TMDs:</u> outward open |
| 3 | <u>NBS1:</u> hydrolysis <u>NBS2:</u> occluded <u>TMDs:</u> outward open → substrate release | <u>NBDs:</u> hydrolysis | <u>NBS2#:</u> ATP hydrolysis, release of P _i | <u>NBS1:</u> P _i release <u>TMD:</u> outward open | <u>NBS1:</u> P _i release, open <u>NBS2:</u> binding ATP | <u>NBDs:</u> dimerize MBP: releases maltose |
| 4 | <u>NBS1:</u> ADP, P _i release <u>TMDs:</u> inward open | <u>NBD:</u> ADP, P _i release, separated <u>TMDs:</u> inward open | <u>NBD:</u> separated, ADP release | <u>NBS1:</u> ADP release <u>TMDs:</u> inward open → substrate release | <u>NBS1:</u> ADP release, empty, occluded <u>NBS2:</u> ATP, occluded | <u>NBSs:</u> ATP hydrolysis <u>NBD:</u> separated <u>TMDs:</u> inward open release of maltose and MBP |

MBP - Maltose-binding protein

P_i - Inorganic phosphate or HPO₄²⁻

#Sequential hydrolysis in NBS1 and NBS2 with unknown order.

Interestingly, the “ATP-switch” and “processive clamp” models are mainly supported by measurements on bacterial transporters. In contrast, the “alternating sites”, “constant contact” and “nucleotide occlusion” models are mainly supported by data from mammalian transporters¹⁵⁵. It remains unresolved whether these differences represent a common trend within bacterial and mammalian transporters, are due to experimental under-determination or can be attributed to the particularities of each transporter.

In summary, different models of movements during the catalytic cycle exist for the NBDs. Overall, it seems that NBDs move towards each other when ATP is bound and move apart after hydrolysis (post-hydrolysis), when ADP and P_i are released. Whether this process is a targeted motion remains unclear. Nevertheless, chemical energy from the hydrolysis is converted into conformational changes, which are translocated from the NBD to the second NBD or to the TMDs.

In addition, it remains somewhat unclear whether a transport cycle consumes one or two ATP molecules (and whether the same stoichiometry applies to all ABC transporters). The presence of two centers for hydrolysis would indicate two ATP molecules might be necessary for a functional transport cycle. However, such a hypothesis is somewhat refuted by the existence of ABC transporters with a degenerated NBS. Hence, the stoichiometry may differ between ABC transporters. A lot of effort was invested to shed light on the question of how many ATP molecules are consumed by an ABC transporter to go through a complete transport cycle. Lately a study made use of the slowing down of ATP hydrolysis by the Walker B motif E-Q mutant to examine the ATP consume in a heterodimeric, thermophilic ABC transporter (containing a consensus and a degenerate NBS), TmrAB²³³. In this study it was shown that at least for this transporter, a single ATP can be enough for substrate translocation²³³.

3.4. Transport mechanism of type I ABC exporters: "alternating access" mechanism and its alterations

Due to the different types of available structures and the broad variety of substrates for ABC transporters, a unifying transport mechanism presumably does not exist. In this study, the NBDs and full-length ABC transporters of type I exporters (type IV fold) were used as model systems. Hence, the following chapter will mainly focus on the molecular transport mechanisms related to this class of transporters.

Different ABC transporter structures, with or without nucleotides and/or substrates led to the proposal of different transport mechanisms. The "alternating access" mechanism was first proposed for type I ABC exporters (type IV fold) after crystal structures of MsbA^{91,135} and Sav1866³⁴ had been determined²³⁴. In this mechanism, the ABC transporter alternates between an inward open (apo state) and a nucleotide bound outward facing state (**Figure 7A**). In the NBDs, conformational changes are nucleotide dependent and cause the switch between inward open and outward facing states for the TMDs with two different substrate affinities. The different states of the TMDs allow substrate binding at one and release on the other side of the membrane. Access to the substrate binding site can be blocked by two gates, one of which always needs to be closed to prevent a channel-like function. When a substrate binds from the cytoplasmic side to the TMDs and/or nucleotides bind to the NBDs, a structural rearrangement in the TMDs occurs that allows them to reach the outward facing state via an occluded transition state, with lower substrate affinity leading to substrate release^{235,236}. Nucleotide binding in the NBDs pushes tight association of the NBDs, which causes structural rearrangements of the TMDs that are transmitted via the coupling helices³⁴. During or after ATP hydrolysis, the substrate is released, ADP and P_i are released and the inward open conformation of the transporter is reset.

For drug extrusion by ABC transporters, the "alternating access" mechanism was extended to the "hydrophobic vacuum cleaner" model²³⁷ (**Figure 7A**). This model takes into account that structurally diverse hydrophobic and amphipathic substrates of ABC transporters are enriched in the membrane bilayer²³⁸. Substrates of ABC transporters can be "flopped" from the inner membrane leaflet to the outer leaflet or expelled directly to the extracytosolic space. Importantly, this model may explain how polyspecificity of MDR transporters such as P-gp is possible despite the typically low binding affinity of these substrates when the membrane acts as a concentrator for these molecules. This model implicitly emphasizes the importance of the membrane environment for the transport process. Transport is energized by ATP, which also imposes unidirectionality¹⁷⁴. In addition, substrate binding can stimulate ATPase activity as seen for P-gp, which can trigger enhanced transport activity²³⁹⁻²⁴³.

Other variations of the "alternating access" mechanism have been proposed based on experimental data obtained for the bacterial ABC transporters McjD (antibacterial peptide microcin J25 ABC transporter) and PCAT (peptidase containing ABC transporter)²⁴⁴. Here, crystal structures, electron paramagnetic resonance (EPR) and single-molecule Förster energy transfer (smFRET) measurements indicate that both ATP and substrate binding are needed to reach the outward facing state²⁴⁵⁻²⁴⁸. In comparison, crystal structures of MsbA^{91,135} and Sav1866³⁴ are already in the outward facing state in the presence of nucleotide alone. For the human multidrug resistance related proteins such as P-gp, structures resolved with cryoEM revealed outward facing states for P-gp only in the presence of both nucleotide and substrate²⁴⁹. Nevertheless, in the same study the conformational spectrum of MsbA was identified to have a higher number of conformations in the outward facing state with nucleotide than P-gp in the presence of nucleotides²⁴⁹. Hence, it could be hypothesized that for bacterial multidrug ABC transporters the detail that nucleotide binding already leads to an outward facing state in the transport mechanism may also be related to a varying specificity for substrates²⁵⁰.

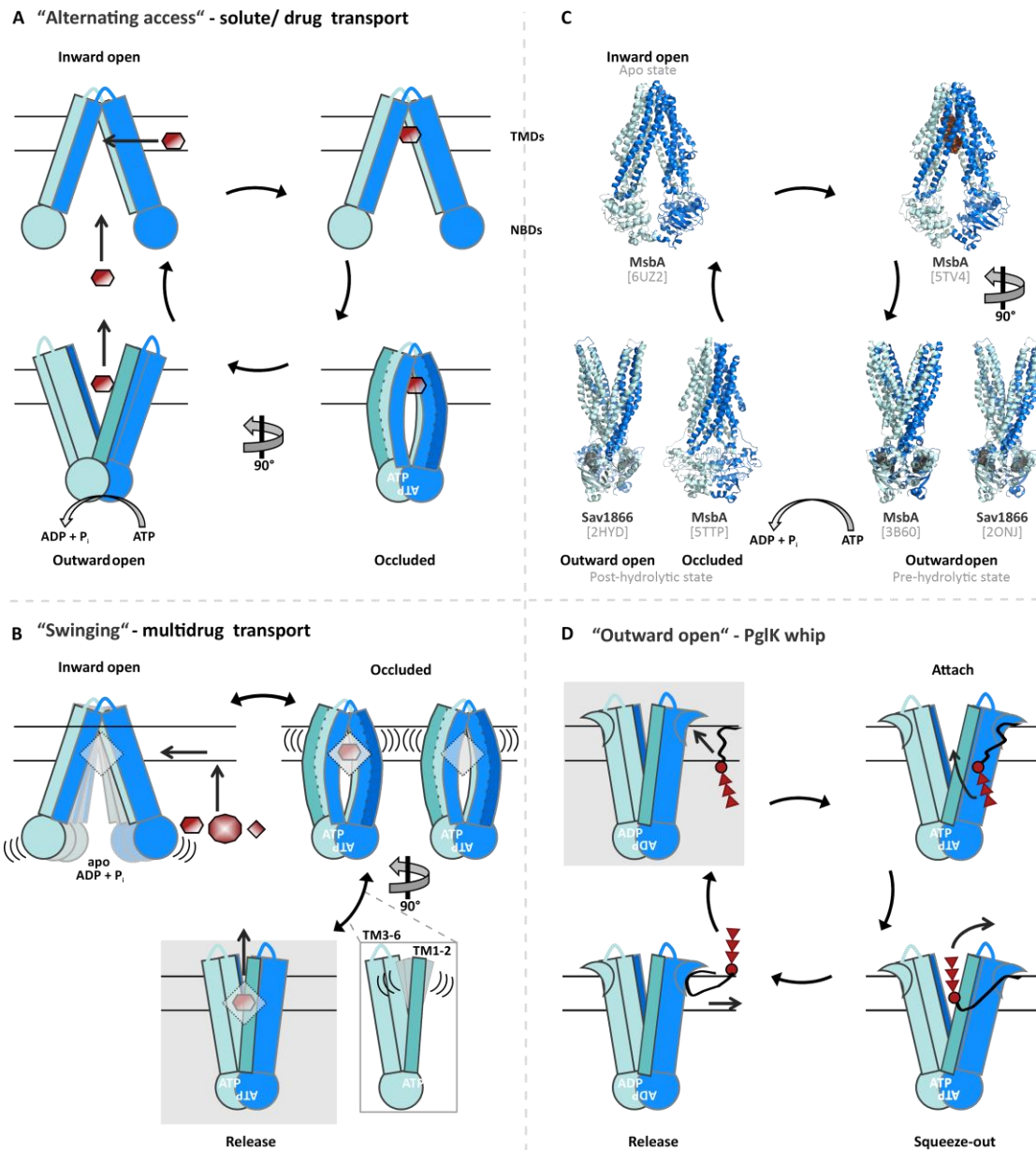


Figure 7: Potential transport mechanisms for type I ABC exporters (type IV fold, modified from Neumann et al., 2017¹⁰⁶) Available crystal structure conformations are indicated by gray backgrounds. **A)** "Alternating access" mechanism including the "vacuum cleaner" model. Solute/drugs can enter from the cytoplasm or the membrane and leave the transporter in the same orientation they have entered the transporter. **B)** "Swinging" mechanism for multidrug transporters such as BmrA following the model by Chaptal et al.⁹³. Different substrates (drugs) may enter the ABC transporter within a dynamic inward open conformation. ATP binding leads to the occluded state, concomitant with dynamics within an outer part within the TMDs (transmembrane helices 1-2 and 3-6), which leads to a drug release. Hydrophobicity of the substrate binding pocket is proposed to subsequently cause the prompt closing after the release of the hydrophobic substrate by motions of the TM1-2, leading to the occluded state. ATP hydrolysis is supposed to be not necessary mechanism but might occur after drug release, leading to the inward facing conformation. **C)** Representative crystal structure snapshots, indicating that details of the classic "alternating access" mechanism are still unclear. Apo state MsbA in peptidiscs (PDB ID: 6UZ2²⁵¹), MsbA with substrate (LPS) (PDB ID: 5TV4⁹¹), pre-hydrolytic states of MsbA with AMP-PNP (PDB ID: 3B60¹³⁵) and of Sav1866 (PDB ID: 2ONJ¹⁹¹) and post-hydrolytic states of MsbA with ADP-vanadate in nanodiscs (PDB ID: 5TTP⁹¹) and Sav1866 with ADP (PDB ID: 2HYD³⁴). **D)** Whipping mechanism for lipid-linked oligosaccharyls (LLO) by PglK following the model by Perez et al. (PDB ID: 5C73²⁵²). The long acyl chain of the LLO attaches to extracytoplasmic helices unique to PglK and transport is proposed to be mediated solely through outward-facing conformations. LLO polar regions are shielded from the lipid bilayer by the transporter cavity, while the acyl chain never leaves the hydrophobic environment. TMDs – Transmembrane domains. NBDs – Nucleotide binding domains.

Recently, another mechanism was proposed based on the first structures of the multidrug ABC transporter BmrA (E/Q mutant) with substrate and ATP-Mg²⁺ in an outward facing conformation, termed the “swinging” mechanism⁹³ (**Figure 7B**). This mechanism is distinct from the classic mechanism where the transporter undergoes a deterministic set of conformations within the transport cycle and finally comes back to its initial state. The proposed “swinging” between states is further supported by hydrogen /deuterium (H/D) exchange and molecular dynamics simulations⁹³. For BmrA, it has been proposed that both the inward and the outward facing conformations are very dynamic and that this is crucial for the substrate binding site to adapt to different types of substrates⁹³. ATP binding leads to the occluded conformation and at the same time to dynamic movements within an outer part of the TMDs, which may enable polyspecificity for multidrug type I ABC exporters (type IV fold). After substrate release, prompt closing of the substrate binding pocket occurs due to its hydrophobicity and dynamics. The transporter then swings back to an occluded conformation, independently of ATP hydrolysis. ATP hydrolysis may occur after releasing the substrate, leading to the inward open conformation²⁵³. The transporter is now ready for another swing. Due to the interplay of transporter intra-dynamics and the substrate binding pocket hydrophobicity, specific defined conformations (steps) within the transport seem to be lacking. Such a mechanism would support the notion that next to the substrate nucleotide binding is required to enable substrate release.

Another possible transport mechanism is the “outward open only” mechanism, which was derived from the proposed whipping mechanism of the lipid-linked oligosaccharide (LLO) ABC transporter PglK^{24,252} (**Figure 7D**). The floppase PglK seems to have developed an intriguing solution how to move long-chain lipid molecules from one side of the membrane to the other by both binding to and translocating the substrate in an outward facing conformation. Crystal structures in two inward open and one ADP bound outward occluded conformation were obtained²⁵². As occlusion of the inward open cavity did not affect transport, Perez *et al.* proposed that only the outward facing states are able to conduct substrate transport. Within the structure of PglK, short external α -helices (EH) at the TMDs and a close hydrophobic groove may be crucial parameters for this type of mechanism. It was proposed that only long-chain LLOs are transported as they are large enough to reach the EH and the hydrophobic groove. In the outward open only mechanism, the polyprenyl tail of LLO interacts with the surface of PglK, and possibly the EH and the hydrophobic region. The pyrophosphate moiety of LLO in the presence of ATP then moves into the outward facing cavity. As ATP is hydrolyzed and the NBDs and successively the TMDs change their conformations, the pyrophosphate group is “squeezed” out of the transporter, released and the hydrophobic tail diffuses off or follows as the polar groups of the LLO are grabbed by subsequent acceptor proteins. Throughout this process, it is suggested that the polyprenyl tail remains outside of the transporter exposed to the lipid bilayer. ATP hydrolysis hence seems to trigger the release of the bound substrate.

Before the proposed “outward open” mechanism, the ADP-bound state had been underappreciated in biophysical studies of ABC transporters, although it is an important transition state within the ATPase catalytic cycle. These ADP bound transition state is generally believed to be either an inward open state with regard to the TMDs. Upon release of P_i, the increase in negative charges at the surface between the NBD interface would move the NBDs apart from each other¹⁶⁹. Despite this negligence of taking the ADP-bound state into account, it is not inconceivable that for some ABC transporters the ADP-bound state could also be an essential part of the substrate translocation cycle, e.g. used to block re-binding of the just released substrate by maintaining the transporter in an outward open state. Indeed, data using EPR spectroscopy have found an ADP-bound outward open state for the ABC exporter LmrA²⁵⁴. Furthermore, cryoEM structures of MsbA showed a small increase in the outward open conformation upon addition of ADP²⁴⁹. The importance of the ADP-bound state within the transport mechanism could hold true regardless of the specific mode of action for substrate

translocation. It might be further relevant if ADP alone, ADP with P_i or ADP with P_i and Mg^{2+} is present in the NBDs during the substrate transport mechanism.

3.5. Biophysical methods used to study type I ABC exporter (type IV fold) dynamics

How many conformations or energetic states ABC transporters populate during their mechanistic cycle remains unclear. ABC transporters are dynamic rather than static membrane proteins. With structural techniques such as X-ray and cryo-EM snapshots of multiple states can be caught (**Appendix table 3**), which leads to important yet somewhat limited information about the dynamics, transition rates and the order of the conformations within the transport cycle. Conformations of ABC transporters with enhanced dynamics, e.g. during NBD closure or opening and events such as substrate release, ATP hydrolysis or phosphate release, are even more difficult to characterize, as they are intrinsically more dynamic²⁵⁵.

To elucidate dynamics of ABC transporters, spectroscopic techniques have been applied (see below). The following section focuses on insights in dynamics obtained with these techniques for the homodimeric type I ABC exporters (type IV fold), LmrA, MsbA and BmrA, as these proteins were often chosen as first candidates to elucidate structural and dynamic details of type I ABC exporters (type IV fold) and are the focus of this thesis. In their catalytic transport cycles, transitions between an inward-facing (IF, dissociated NBDs) to an outward-facing (OF, dimeric close NBDs) state occur but the nature and magnitude of the underlying motions are controversial. Specifically, questions focus for instance on the separation between the two NBDs during the cycle, the extend of opening in the transmembrane domains, the nature of transmembrane helix motion mediating substrate translocation and different conformations of the ABC transporter subdomains.

EPR (Electron paramagnetic resonance) spectroscopy

Pulsed EPR spectroscopic techniques, as DEER (Double electron-electron resonance) also named PELDOR (Pulsed electron-electron double resonance) can be used to capture conformations in a local environment with the protein trapped at cryogenic temperatures. For EPR a site-directed spin label is attached over a cysteine to the protein. It is a complementary method to confirm structural information. It can provide information on dynamics of type I ABC exporters, not only in detergent but also in lipid as in nanodiscs or liposomes and even in its native environment by nanobody-assisted *in situ* EPR²⁵⁶.

The lipid floppase MsbA from *E. coli* has emerged as a popular model system for EPR studies to identify dynamics within type I ABC exporters (type IV fold)^{213,257–264}. Early studies probed local structures as the Walker A motif region²⁵⁸, the ABC signature motif and the H-loop motif²⁶⁰. The study of the Walker A motif region identified an unstructured and a α -helical region in the Walker A motif region²⁵⁸, which fits nicely to the secondary structure observed in crystal structures of MsbA¹³⁵. In this EPR study of MsbA, the pre-, intermediate and post-hydrolysis states were analyzed, revealing two motional components of MsbA in the EPR spectra (i.e. one mobile and one immobilized component)²⁵⁸. ATP binding (pre-hydrolysis) shifted motional conformations to a more immobile conformation within the Walker A motif residues of MsbA (S378-I385). The induction of a transition state immediately following hydrolysis, i.e. with $MgADP V_i$ and $MgADP$, suggest that Walker A motif residues (S378-I385) of MsbA undergo further conformational changes upon hydrolysis of ATP. However, the overall secondary structure of the Walker A motif region analyzed in Buchaklian *et al.* remained intact during ATP binding and hydrolysis, although considerable changes in dynamics occurred²⁵⁸. A follow up study of Buchaklian and Klug determined structure and dynamics of the ABC signature motif (LSGGQ) and the H-loop with the same EPR approach²⁶⁰. In this study they identify the ABC signature motif region to be α -helical, facilitating tertiary contacts during ATP-hydrolysis. The

same pre-, intermediate and post-hydrolysis states were recorded as mentioned above for the Walker A motif residues²⁵⁸ to determine changes during ATP binding and hydrolysis for the ABC signature motif (481-LSGGQ-485) and the H-loop region (540-STI-542) of MsbA. Again, two motional components were identified for residues in these regions. The intermediate state yield to a shift to a more immobilized motional state for all mutations studied in the ABC signature motif, whereas no influence was seen in the presence of only ATP (with one exception S482C). H-loop motif residues also showed no change upon ATP binding and large changes upon vanadate trapping. In conclusion, the studies of Klug^{258,260} showed that amino acid residues can be influenced very differently during ATP-hydrolysis even if they are in proximity to each other.

Complementary structural and dynamic EPR analysis suggest that ATP binding reorients MsbA from an inward- to outward facing conformation in detergent and lipid environment²⁶³ (**Appendix table 3**). Interestingly, reduced dynamics of the backbone on MsbA was reported in the cytoplasmic (i.e. in the NBDs) spin-labeled sides, whereas in contrast the extracellular (i.e. in the TMDs) spin-labeled sides were shown to be more dynamic. Furthermore, this study showed opposite movements at the two sides of the transporter as a result of the transition from the apo state to a high-energy post-hydrolysis intermediate (ADP-V_i) state²⁶³. Another finding in the study of Zou *et al.* was that MsbA reconstituted into liposome compared to detergent showed that the apo state dynamics are more restricted in a lipid environment in the NBD (labeling position at T561) and the intracellular helical (TMD) sides²⁶³. The amplitude of the movement from the TMD and the NBD spin label positions is consistent with expectations based on the static crystal structures of MsbA, suggesting the AMPPNP-bound structure captures the main structural features of the ADP-V_i intermediate. An EPR study on LmrA also revealed a highly dynamic apo state where the protein occupies a large conformational space. This conformational space was significantly reduced upon nucleotide binding²⁵⁴. Another EPR experiment of BmrA analyzing the apo state concluded a possible interaction within the NBD between a glutamine (Q407) and a tyrosine residue (Y408)²⁶⁵. Residue Y408 is found C-terminal of the only tryptophane residue within the NBD of BmrA, assumed to be involved in NBD-TMD communication. Q407 is located in the loop, linking the NBD and TMD. EPR data showed a high flexibility within this linking loop region²⁶⁵. Another study on BmrA used manganese as replacement for the ATP hydrolysis cofactor magnesium for structural and dynamic analysis to combine solid-state NMR with EPR spectroscopy²⁶⁶. The manganese ion has the advantage of being a reporter in both EPR and solid-state NMR experiments. Exploiting of paramagnetic relaxation enhancements (PRE) helped within this study to identify residues within or in the vicinity of the cofactor magnesium, with manganese as reporter²⁶⁷. As a result, some alanine residues (A371, A505, A534, A488 and A218) located within a sphere of 1.5 nm from the metal center could be identified. In the experiments the BmrA MgADP-V_i trapped and BmrA MnADP-V_i trapped state, with VO₄³⁻ mimicking the γ -phosphate of ATP were used. This state mimicks a transition state within the catalytic cycle of ABC transporters, with occupied nucleotide binding sites. Furthermore, DEER experiments could be performed to obtain Mn²⁺-Mn²⁺ distance distributions for the BmrA MgADP-V_i trapped state, yielding to a maximum in the distance distribution of 1.9 nm. This value was shown to be in a good agreement with the Mn²⁺-Mn²⁺ distance in a homology model of BmrA MnADP-V_i with the NBDs closed (1.8 nm)²⁶⁶. In conclusion in this study for BmrA it was possible to exchange Mg²⁺ with Mn²⁺, extract Mn²⁺-Mn²⁺ distances and to determine residues in the surrounding of Mn²⁺.

LRET (Luminescence resonance energy transfer) spectroscopy

Conformational changes of ABC transporters, including MsbA were also followed by LRET experiments. Luminescence resonance energy transfer (LRET) is a spectroscopic technique that allows for measurements of distance changes between a donor and an acceptor attached to a protein while they are functional (i.e. ATPase active)²⁶⁸. Studies of MsbA in detergent and under more physiologic conditions i.e. in liposomes or nanodiscs were performed during ATP hydrolysis^{268–270}. The optical probes attached to single-cysteine mutants in MsbA were placed in the NBDs to follow NBD dissociation and association by measuring interdomain distances. Interestingly, major differences between data of EPR, crystal structures and LRET in the IF conformation of MsbA in detergent micelles could be determined in comparison to the LRET data of MsbA reconstituted in nanodiscs. The authors of the LRET studies claim that they performed the structural/functional analysis of membrane proteins under more native-like conditions that include insertion into a lipid bilayer and “normal” temperature (i.e. 37 °C). Strikingly, reconstitution of MsbA into lipid bilayer yielded conformations with a small separation between NBDs and additionally a large number of molecules that showed conformations with associated NBDs even in the absence of nucleotide²⁷⁰. This indicates that the membrane is sufficient to obtain conformations with closely associated NBDs. remain in contact, or are close to each other, while ATP is hydrolyzed. In detergent micelles, a higher flexibility of MsbA in the apo state was observed as much longer distances between the labels were sampled compared to MsbA in nanodiscs. EPR data with the same positions of the labels within the NBD (i.e. at residue T561) could also confirm that distances between the NBDs are smaller in a lipid environment (i.e. liposomes) than in detergent^{261,263}.

FRET (Fluorescence resonance energy transfer) spectroscopy

Dynamics of ABC transporters were also analyzed by single molecule fluorescence resonance energy transfer (smFRET) experiments, which were performed on variants of MsbA containing a single cysteine residue in each homodimer linked to fluorophores by maleimide chemistry²⁷¹. In this study two individual labeling positions in the NBD (T561C) and the TMD (D277C) were chosen to probe conformational changes of the NBDs and the TMDs during the catalytic cycle, in three environmental conditions (i.e. detergent/DDM, liposomes and nanodiscs). The MsbA variant reflecting the NBD side (cytoplasmic region) revealed three major clusters of conformational states, which were assumed to correspond to inward-facing (cytoplasmic open), intermediate (cytoplasmic-semi-closed) and outward-facing (cytoplasmic-closed) conformations. Read-out from the TMD labeling position showed two such clusters in the periplasmic region, corresponding also to an inward-facing (periplasmic closed; in the apo state, in the presence of ADP or ADP-V_i) and an outward-facing state. This single-molecule FRET study showed that the range of MsbA conformations is constrained in nanodiscs (i.e. NBDs remain close to each other) compared with that measured in detergents and liposomes during the catalytic cycle²⁷¹. Compared to lipid nanodiscs less conformational restrictions in detergent micelles and liposomes were obtained for MsbA. This finding indicated a higher flexibility of MsbA in liposomes and detergent micelles. For example, a wide-open conformation of the NBDs in the apo state was more often present in liposomes and detergents than in nanodiscs. Hence, this state seems to be less populated in nanodiscs, which is in agreement with findings of MsbA from EPR and LRET studies using the same labeling position T561 in the NBD^{263,270}. Furthermore, more restricted conformations with closer NBDs in nanodiscs were also observed. Interestingly, this observation is also in line with a single-particle cryo-EM structure of MsbA in nanodiscs, where the transporter adopts also an inward-facing conformation with closer NBDs⁹¹. The study also indicated that the TMD region of MsbA is less dynamic during the catalytic cycle than NBDs, especially in liposomes and nanodiscs.

Another FRET study was performed earlier on BmrA where cysteine residues for FRET donor or acceptor labeling were introduced in the Walker A (T370C) and the ABC signature motif (G473C), as these regions transiently form the shared NBS across the NBD interface during ATP hydrolysis²⁷². Somewhat surprisingly when taking the swapped domain architecture into account, this study showed that BmrA occurs as a dimer which might be partly monomeric within detergent, which seems to be recovered when reconstituted into inside-out-vesicles. Another conclusion was that the NBDs of most BmrA dimers adopt a closed conformation in the apo state. However, these results need to be taken with a grain of salt, as the introduced cysteine mutations (T370C and G473C) showed an influence on the function of BmrA. Unfortunately, labeling of these positions yield to an abolished ATPase and transport activity, which complicates interpretation of the data. Thus, another mutation (S428C) was introduced. Although mutagenesis and labeling at this position also diminishes ATPase activity (albeit less than the prior mutations), the FRET results obtained with this labeling position seem to overall support the authors conclusions²⁷².

NMR (Nuclear magnetic resonance) spectroscopy

Solution and ssNMR have the advantage to investigate proteins in their near native environments and physiological temperatures. Solid-state NMR (ssNMR) can be used to obtain site-resolved information about structural and dynamic features of reconstituted ABC transporters in different states (open, closed, ligand-bound). Studies on the homodimeric ca. 130 kDa ABC transporters LmrA, MsbA and BmrA demonstrate the feasibility of analyzing the different states of the type I ABC exporters (type IV fold) by ssNMR^{273–276}. LmrA was the first ABC transporter studied by solid-state NMR upon successful selective isotope labeling with ¹³C-glycine in *L. lactis*²⁷³. A follow up study²⁷⁷, used this selective labeling approach with alanine (L-[β-²H₃]-alanine) for deuterium ssNMR to probe the dynamics of reconstituted LmrA in the apo, in a pre- (with AMPPNP) and in a post-hydrolysis (with ADP-V_i) state. Here the authors concluded that the NBDs tumble faster compared to the TMDs (including coupling helix 1 and coupling helix 2), emphasizing that the NBDs are very mobile in the apo state. This mobility of the NBD became restricted in the pre-hydrolytic state whereas the post-hydrolysis state resembled the apo state in term of its motions²⁷⁷. In 2008, a mutant of LmrA, having a low ATPase turnover rate was used to follow ATP hydrolysis by ³¹P real-time solid-state NMR¹⁹⁴. This study allowed to follow the course of the different phosphorylated compounds during an ATP hydrolysis reaction. All three phosphate atoms of ATP (i.e. α-ATP, β-ATP and γ-ATP), two phosphate atoms of ADP (i.e. α-ADP and β-ADP) and free P_i could be monitored¹⁹⁴. This study was the basis for later ³¹P real-time solid-state NMR studies performed on LmrA, MsbA and the heterodimeric type I ABC exporter TmrAB, which showed an unexpected coupling between ATPase and adenylate kinase activity by these proteins²⁷⁶. This study also demonstrated that measuring the ligand can provide important mechanistic insights in the catalytic cycle of type I ABC exporters. A solid-state NMR study on MsbA proposed an additional site for nucleotide binding close to the Q-loop (Q424) in between the known canonical sites²⁷⁶. To probe the additional nucleotide binding side, complementary EPR spectroscopy and MD simulations were carried out. Selective isotope labeling of two unique pairs in the Q-loop and the H-loop of MsbA provided further evidence that an additional nucleotide binding site may exist close to the Q-loop and the H-loop²⁷⁸. Using a combination of liquid-state NMR on the NBD of LmrA and solid-state NMR on selectively labeled full-length LmrA (¹⁵N-lysine and ¹⁵N-tryptophane) showed the possibility to study differences in dynamics upon nucleotide binding on a global and local level (i.e. for specific residues)^{275,279}. It was concluded that the conserved lysine residue of the Walker A and a tryptophane residue C-terminal of the Walker A helix are affected by nucleotide addition²⁷⁵. Furthermore, solid-state NMR experiments of isotope labeled MsbA identified lipid A in complex with MsbA, providing the opportunity to study consequences of lipid- and nucleotide binding in a type I ABC exporter (type IV fold)²⁸⁰. Another solid-state NMR study of MsbA

reconstituted into liposomes used a unique pair labeling approach to study the effect of nucleotide (i.e. trapped with ADP-V_i, post-hydrolysis state) and substrate binding on specific sites in the transmembrane helices 4 and 6²⁸¹, which have been reported to be involved in transmission of conformational changes upon nucleotide binding (TM helix 4²⁸²) and substrate binding (TM helix 6¹⁵⁰). In the solid-state NMR study, both positions in TM helix 4 and TM helix 6 showed a larger conformational space in the apo state compared to the nucleotide trapped post-hydrolytic state. Furthermore, two different substrates of MsbA (Hoechst 33342 and daunorubicin) were shown to influence TM helix 4 and TM helix 6 differently. The unique labeled pair of TM helix 6 was affected by both substrates, whereas the unique pair label of TM helix 4 only by one substrate²⁸¹. These findings fit to the assumption of a large drug binding pocket with distinct, yet overlapping binding sites for different substrates within multidrug ABC transporters. Solid-state NMR was further applied to investigate how NBDs and TMDs are structurally coupled. In BmrA the X-loop, a motif unique for type I ABC exporters (type IV fold), was identified as an important interdomain communication motif¹⁸². A recent solid-state NMR study identified an incomplete switch to the outward-facing conformation in presence of MgATP and V_i in an X-loop mutant (E474R) which might be the cause for the observed defect in transport activity and hence be important for NBD-TMD communication¹⁸².

Conclusively, many NMR spectroscopy studies have shown that ATP-binding triggers an overall rigidification of the homodimeric type I ABC exporters (type IV fold) LmrA^{275,277}, MsbA²⁸¹ and BmrA¹⁸².

Hydrogen/Deuterium exchange (HDX) coupled to mass spectrometry (MS)

The HDX method is routinely used to study the dynamics of soluble proteins and is beginning to emerge as a tool to observe conformational changes in membrane proteins. The technique is not sensitive enough to show high-resolution alterations such as specific side chains that can be seen in crystal structures but robust enough to show local alterations in intra- and extracellular regions of the transporter with respect to binding of ligands, lipids and nucleotides²⁸³.

HDX experiments were performed on BmrA in the two states with (outward-facing conformation) and without ATP (apo state, inward-facing conformation), which showed an unexpected flexibility of the NBDs in the apo state²⁸⁴. Further, it revealed flexibility of the coupling helices, connecting the TMDs to the NBDs, in BmrA depending on the conformation of the transporter.

4. AIM OF THE THESIS

The protein superfamily of ABC transporters present in all phyla of life has been studied extensively, but despite the large knowledge on function, transported compounds and residues involved, several fundamental questions remain at the molecular level. E.g. how are ATP-binding and hydrolysis coupled to substrate transport? What is the underlying mechanism during ATP hydrolysis when ATP-binding, ADP-binding or ADP release, phosphate release occurs within the catalytic cycle? Local events such as ATP binding and hydrolysis at the NBDs are required for the energization of substrate transport across the membrane, which occurs remotely in the TMDs. A fundamental understanding of local conformational changes and their contribution to large-scale conformational transitions in an ABC transporter are crucial as the proteins are not static but rather are highly dynamic in their conformational states. This thesis aims to shed light on the intradomain events that occur upon nucleotide binding in the motor domain, the NBD. The NBD was chosen as it is highly conserved and builds the common structural feature (monophyletic ATPase), which drives the translocation, in the versatile folds of the membrane domains.

Here, nuclear magnetic resonance (NMR) spectroscopy and photoinduced electron transfer-fluorescence correlation spectroscopy (PET-FCS) were combined to provide insights into intramolecular crosstalk and dynamic consequences, e.g. upon nucleotide addition across different time scales. Since studying such intradomain effects within the NBD is not trivial in the context of a full-length transporter, a “divide and conquer” approach, where the NBDs of LmrA from *L. lactis*, MsbA from *E. coli* and BmrA from *B. subtilis* are expressed without the TMDs, was used for many experiments. Working with the selected conserved NBDs can lead to the identification of basic allosteric intradomain NBD effects, in terms of dynamics and structural interacting areas, but also reveal type I ABC exporter specific allosteric effects within the NBD. The experiments on the NBDs were then complemented with functional assays with the full-length transporters focusing on BmrA.

NMR data evaluation confirmed that conserved motifs (i.e. H-, D- and Q-loop motifs) are involved in intradomain events upon nucleotide binding. Possible functions of the D-, Q- and H-loop motifs in intradomain signaling were then investigated by mutation and again studied in detail with NMR spectroscopy. A special focus was put on the D-loop function and further analyzed within functional assays. In addition, a potential novel NBD intradomain signaling pathway identified with the NMR experiments was investigated. Eventually, this thesis provided a foundation for understanding intradomain dynamics and energy transduction in the NBD of ABC transporters, which is essential for understanding the operation of the catalytic mechanism and hence substrate transport across the membrane.

CHAPTER II: MATERIAL AND METHODS

1. CHEMICALS

Unless stated otherwise, chemicals were purchased from Carl Roth GmbH & Co KG, Karlsruhe.

Table 5: Chemicals from other suppliers than Carl Roth GmbH & Co KG, Karlsruhe

| Chemical | Supplier |
|--|---|
| L-Ascorbic acid | Sigma-Aldrich Co.- LLC, Taufkirchen |
| Benzamidine hydrochloride | Sigma-Aldrich Co.- LLC, Taufkirchen |
| BioBeads SM-2 | BioRad, Hercules, USA |
| 3-bromo-1,1,1-trifluoroacetone (BTFA) | Sigma-Aldrich Co.- LLC, Taufkirchen |
| cOmplete™ Protease Inhibitor Cocktail | Roche Diagnostics International AG, Rotkreuz, CHE |
| Dithiothreitol | Sigma-Aldrich Co.- LLC, Taufkirchen |
| n-Dodecyl β-D-maltoside (DDM) | Sigma-Aldrich Co.- LLC, Taufkirchen |
| Doxorubicin (hydrochloride) | Cayman Chemical Co., Ann Arbor, USA |
| <i>E. coli</i> Total lipid extract | Avanti Polar Lipids, Inc., Birmingham USA |
| Ethidium bromide 99.9% | AppliChem, Darmstadt |
| 4-(2-hydroxyethyl)-1-piperazineethanesulfonic acid (HEPES) | Sigma-Aldrich Co.- LLC, Taufkirchen |
| Lauryl maltose neopentyl glycol (LMNG) | Anatrace, Maumee, USA |
| Nickel nitrilotriacetic acid (Ni ²⁺ -NTA) agarose | QIAGEN Monheim GmbH & Co. KG, Monheim |
| Phosphoenolpyruvate (PEP) | Sigma-Aldrich Co.- LLC, Taufkirchen |
| Precision Plus Protein™ Dual Color Standards | BioRad, Hercules, USA |
| SIGMAFAST™ Protease Inhibitor Cocktail tablet, EDTA free | Sigma-Aldrich Co.- LLC, Taufkirchen |

Table 6: Chemicals used for isotope labeling of proteins for NMR studies

| Chemicals for NMR labeling | Supplier |
|---|---|
| L-amino acids (labeled) | α- ¹⁵ N Lysine, ¹⁵ N Phenylalanine, ¹⁵ N Valine, ¹⁵ N Isoleucine, ¹⁵ N Leucine, ¹⁵ N Tyrosine, ¹⁵ N Glycine, ¹⁵ N Serine, ¹⁵ N Tryptophane, ¹⁵ N Arginine, ¹³ C Proline, ¹⁹ F 5-Fluorotryptophane |
| ¹⁵ N ammonium chloride | Cambridge Isotope Laboratories, Inc. (Eurisotop) or CIL Inc., Tewksbury, USA |
| ¹⁹ F 5-Fluoro-DL-tryptophane | Acros Organics B.V.B.A. |

2. BACTERIAL STRAINS, CLONING AND PLASMIDS FOR HETEROLOGOUS EXPRESSION IN *E. COLI*

2.1. Bacterial Strains

Table 7: List of *E. coli* strains used for protein expression and cloning

| Bacterial Strain | Description | Supplier |
|------------------|---|--|
| BL21-Gold (DE3) | B F-ompT hsdS(rB-mB-) dcm+Tetr gal λ(DE3) endA The | Agilent Technologies (Santa Clara, USA); BL21-Gold(DE3) Competent Cells |
| C41(DE3) | F – ompT hsdSB (rB- mB-) gal dcm (DE3) ²⁸⁵ | Sigma-Aldrich Co. LLC (Taufkirchen); OverExpress™ C41(DE3) Competent Cells |
| DH5α | F ϕ80lacZΔM15 Δ(lacZYA-argF) U169 recA 1 endA1 hsdR17(r _k ⁺ , m _k ⁺) phoA supE44 thi-1 gyrA96 relA1 y ⁻ | Thermo Fisher Scientific (Invitrogen/Waltham, USA); DH5 α Competent cells |

2.2. Cloning

Oligonucleotides/ Primers for the mutagenesis of LmrA, MsbA and BmrA were designed by Dania Rose-Sperling (DRS) and purchased by Sigma-Aldrich Co.- LLC (Taufkirchen) unless stated otherwise. Primer numbers are based on the nomenclature of the ██████ group.

Table 8: Oligonucleotides/ Primers used for Quik Change mutagenesis in LmrA

| Primer number | Mutation | Sequence (5'-3') |
|---------------|---------------------------|--|
| P75 | LmrA-NBD A518D (p103) For | CGAGCCTGGATAGCGAGAGCGAAAGCATGGTTC |
| P76 | LmrA-NBD A518D (p103) Rev | CTTTCGCTCTCGCTATCCAGGCTCGCGGTC |
| P117 | LmrA-NBD SALD (p103) For | CTGGATGAGGCGACCAGCGCGCTGGATAGCGAGAGC |
| P118 | LmrA-NBD SALD (p103) Rev | CCATGCTTTCGCTCTCGCTATCCAGCGCGCTGGTCGCC |
| P1051 | LmrA-NBD SSLD (p103) For | GATGAGGCGACCAGCAGCCTGGATAGCGAGAG |
| P1052 | LmrA-NBD SSLD (p103) Rev | GCTTTCGCTCTCGCTATCCAGGCTGCTGGTCGCC |
| P305 | LmrA-NBD W421F (p071) For | GATTCCGTCTCTCGGAAAACCTTCGTAGCCAG |
| P306 | LmrA-NBD W421F (p071) Rev | GAAGCCAATCTGGCTACGAAAGTTTTCCAG |
| P307 | LmrA-NBD W421A (p071) For | GATTCCGTCTCTCGGAAAACGCGCTAGCCAG |
| P308 | LmrA-NBD W421A (p071) Rev | GAAGCCAATCTGGCTACGCGCTTTTTCCAG |
| P309 | LmrA-NBD W457F (p071) For | CTTTACCGACGAAGATCTGTTTCAGGTCCTG |
| P310 | LmrA-NBD W457F (p071) Rev | GCCAGGTCAGGACCTGAAACAGATCTTC |
| P311 | LmrA-NBD R397A (p071) For | CATCTTCTCTGCTGGAAGCGTTCATCAGC |
| P312 | LmrA-NBD R397A (p071) Rev | CTGCAGTCGGCTGATAGAACGCTTCAGC |
| P301 | LmrA-NBD S467C (p071) For | CTGGACCTGGCATTGCGCGTTGTTTCGTGG |
| P302 | LmrA-NBD S467C (p071) Rev | CCGGCATGTTCTCCACGAAACAACGCGCAAATG |
| P502 | LmrA-NBD M524W (p071) For | GACAGCGAATCCGAATCTTGGGTACAGCG |
| P503 | LmrA-NBD M524W (p071) Rev | CAGCGCGCGCTGTACCCAAGATTCGG |
| P688 | LmrA-NBD E512Q (p071) For | CCTGATGCTCGACCAGGCAACCGC |
| P689 | LmrA-NBD E512Q (p071) Rev | CCAGAGAAGCGGTTGCCTGGTCGAG |

Table 9: Primers for cloning of MsbA from *E. coli* BL21-Gold (DE3) into the pET11a vector via Gibson assembly

| Primer number | | Description | Sequence (5'-3') |
|---------------|-----------------------------|--|--|
| P15 | pET11a_For | Primer to amplify pET11a for gibbon assembly | TAAGGATCCGGCTGCTAAC |
| P265 | pET11a_His-TEV_Rev | Primer to amplify pET11a with N-terminal His ₆ -tag and TEV cleavage site for Gibson assembly | GGAGCCTTGAAGTACAGGTTTTTC |
| P362 | MsbA full-length HisTEV For | Primer to amplify full-length MsbA from <i>E. coli</i> BL21-Gold (DE3) for Gibson assembly | GTAAGTCCAAGGCTCCcataacgacaagaatctctctactgtgg |
| P363 | MsbA NBD HisTEV For | Primer to amplify MsbA-NBD from <i>E. coli</i> BL21-Gold (DE3) for Gibson assembly | GTAAGTCCAAGGCTCCgacagtgagcaggagaagaatgaag |
| P365 | MsbA Rev | Primer to amplify MsbA-NBD and full-length MsbA from <i>E. coli</i> BL21-Gold (DE3) for Gibson assembly | GCAGCCGGATCCTTAttggccaaactgcattttgtgaag |

Table 10: Oligonucleotides/ Primers used for Quik Change mutagenesis in MsbA (Primers used on plasmids p236 and p250, Table 12)

| Primer number | Mutation | Sequence (5'-3') |
|---------------|--------------------|-------------------------------------|
| P574 | MsbA-TMD C88S For | GCTATGTCTCCAGCTACTCTATCTCC |
| P575 | MsbA-TMD C88S Rev | CTGATACCCAGGAGATAGAGTAGCTG |
| P576 | MsbA-TMD C315S For | GCGGTATGGCGGCTTCTCAGAC |
| P577 | MsbA-TMD C315S Rev | GGTAAACAGCGTCTGAGAAGCCG |
| P578 | MsbA-NBD D512A For | CTACCTCGGCTCTGGCGACCGAATC |
| P579 | MsbA-NBD D512A Rev | GCACGTTTCGGATTTCGGTCGCCAGAG |
| P584 | MsbA-NBD E506Q For | CTGATTCTGGACCAGGCTACCTCGG |
| P585 | MsbA-NBD E506Q Rev | GCCGAGGTAGCCTGGTCCAGAATC |
| P635 | MsbA-NBD D461C For | GGCCTACGCCATGTGCTTCATCAATAAGATGG |
| P636 | MsbA-NBD D461C Rev | CCGTTATCCATCTTATTGATGAAGCACATGGCG |
| P637 | MsbA-NBD A518W For | GATACCGAATCCGAACGTTGGATTTCAGGCGGCAC |
| P638 | MsbA-NBD A518W Rev | CCAGTGCCGCCTGAATCCAACGTTTCGGATTTCG |

Table 11: Oligonucleotides/Primers used for Quik Change mutagenesis in BmrA (Primers used on plasmids p339, p340 and p427, Table 12)

| Primer number | Mutation | Sequence (5'-3') |
|---------------|---------------------------------|-------------------------------------|
| P700 | BmrA-NBD W413F (p339, p340) For | GATACCTACAGCCTGGAGAGCTTTCGTGAACAC |
| P701 | BmrA-NBD W413F (p339, p340) Rev | CATAACCAATGTGTTCCAGAAAGCTCTCCAGGCTG |
| P704 | BmrA-NBD R389A (p339, p340) For | CTGTTCAAAGTCTGGAGGCGTTTTATAGCCCGAC |
| P705 | BmrA-NBD R389A (p339, p340) Rev | GCGGTTCGGGCTATAAAAACGCCTCCAGCAG |
| P640 | BmrA-NBD N459C (p339, p340) For | CGGAGATGGCGTATGCGCTGTGCTTCATTAAAG |
| P641 | BmrA-NBD N459C (p339, p340) Rev | GTTCCGCGAGTCTTTAATGAAGCACAGCGCATAAC |
| P642 | BmrA-NBD S516W (p339, p340) For | CTGGATAGCCAGAGCGAAAAGTGGGTTTCAGCAAG |
| P643 | BmrA-NBD S516W (p339, p340) Rev | CTCCAGCGCTTGTGTAACCCACTTTTCGCTC |
| P720 | BmrA-NBD R389A (p427) For | CGCTGTTTAAGCTGCTTGAAGCGTTTTATTCTCCG |

| | | |
|------|---------------------------|-------------------------------------|
| P721 | BmrA-NBD R389A (p427) Rev | CTGCAGTCGGAGAATAAAACGCTTCAAGCAGC |
| P966 | BmrA-NBD R389K (p427) For | CGCTGTTTAAGCTGCTTGAAAAATTTTATTCTCCG |
| P967 | BmrA-NBD R389K (p427) Rev | CTGCAGTCGGAGAATAAAATTTTCAAGCAGC |
| P968 | BmrA-NBD R389E (p427) For | CGCTGTTTAAGCTGCTTGAAGAATTTTATTCTCCG |
| P969 | BmrA-NBD R389E (p427) Rev | CTGCAGTCGGAGAATAAAATTTTCAAGCAGC |
| P970 | BmrA-NBD R389M (p427) For | CGCTGTTTAAGCTGCTTGAAATGTTTTATTCTCCG |
| P971 | BmrA-NBD R389M (p427) Rev | CTGCAGTCGGAGAATAAAACATTTCAAGCAGC |
| P972 | BmrA-NBD K380A (p427) For | GCGGCGGGGGAGCGACGACGCTGTTAAG |
| P973 | BmrA-NBD K380A (p427) Rev | CTTAAACAGCGTCGTCGCTCCCCGCCG |
| P767 | BmrA-NBD D510A (p427) For | GCTACCTCAAGTCTCGCGAGCCAATCTG |
| P768 | BmrA-NBD D510A (p427) Rev | GATTTTTAGATTGGCTCGCGAGACTTGAGG |
| P716 | BmrA-NBD ASLD (p427) For | CTTATGCTCGATGAAGCTACGCGAAGTCTCGAC |
| P717 | BmrA-NBD ASLD (p427) Rev | GATTGGCTGTCGAGACTTCGCGTAGCTTC |
| P718 | BmrA-NBD SALD (p427) For | CGATGAAGCTACCTCAGCGCTCGACAGCC |
| P719 | BmrA-NBD SALD (p427) Rev | CAGATTGGCTGTCGAGCGCTGAGGTAGC |
| P791 | BmrA-NBD N459C (p427) For | CGGAGATGGCATATGCGCTCTGCTTTATAAAGG |
| P792 | BmrA-NBD N459C (p427) Rev | GATTCGGCAGCTCCTTTATAAAGCAGAGCGCATAT |
| P793 | BmrA-NBD S516W (p427) For | CGACAGCCAATCTGAAAAATGGGTTTCAGCAGG |
| P794 | BmrA-NBD S516W (p427) Rev | CTCCAGCGCTGCTGAACCCATTTTTCAG |

2.2.1. Polymerase chain reaction (PCR)

Amplification and mutagenesis of DNA fragments were done using the Kapa HiFi HotStart PCR Kit (Kapa Biosystems, Willington) in a Gradient Biometra® PCR machine (analytic Jena GmbH, Jena). The basic PCR protocol is shown in **Table 12**. The annealing temperature was dependent on the used primers. In general, the annealing temperature was set 2-3°C below the melting temperature of the primers. PCR products were digested with DpnI (NEB, Ipswich) for 1 h at 37°C. DpnI recognizes methylated PCR DNA templates. Afterwards, a PCR clean up with the GenepHlow Gel/PCR Kit was performed and DNA eluted in 30 µL of elution buffer or ddH₂O.

Table 12: Kapa HiFi HotStart PCR reaction conditions and DpnI digestion mix composition

| PCR step | T[°C] | Time | DpnI digestion reaction mixture | |
|------------------|-------------------|--------------------|---------------------------------|---------------|
| | | | Component | Volume [50µL] |
| Pre heating | 95 | 3 min | PCR reaction mixture | 23 µL |
| Denaturation | 98 | 20 s | DpnI | 1 µL |
| Annealing | Depend on primers | 15 s | 10x Cut Smart buffer | 5 µL |
| Elongation | 72 | 6 min 30 s/ 7 min* | ddH ₂ O | 21 µL |
| Final elongation | 72 | 7 min/ 7 min 30 s* | | |

* shorter time for NBD constructs and longer time for full-length constructs

2.2.2. Gibson Assembly

Plasmids encoding the MsbA transporter (p236 and p250) were cloned via Gibson assembly²⁸⁶. For this purpose, the MsbA gene fragment was cloned from *E. coli* BL21-Gold (DE3) cells and inserted into pET11a. In **2.2 Cloning a list (Table 9)** of the used primers is shown. DNA fragments (MsbA-NBD WT and full-length MsbA WT) and linearized recipient pET11a plasmid were generated using PCR. Subsequently, the amplified PCR products were digested with DpnI and purified with GenepHlow Gel/PCR Kit. 50 ng (in 5 µL) of the amplified linearized recipient pET11a plasmid and the amplified MsbA fragments were incubated with 15 µL preheated (50°C) assembly master mix (**Table 13**). This mix was incubated for 1 h at 50°C and afterwards transformed into *E. coli* DH5α cells.

Table 13: Composition of the isothermal ligation reaction mix for Gibson assembly

| Recipe for 5x Isothermal Reaction Mix (6 mL) | Assembly master mix (1.2 mL) |
|--|--------------------------------------|
| 3 mL 1 M Tris-HCl (pH7.5), sterile | 320 µL 5x Isothermal Master Mix |
| 300 µL 1 M MgCl ₂ , sterile | 0.64 µL 10 U/ µL T5 exonuclease |
| 600 µL dNTP Mix 10 mM | 20 µL 2 U/ µL Phusion DNA Polymerase |
| 300 µL 1M DTT (50 mM) | 0.16 L 40 U/ µL Taq DNA Ligase |
| 1.5 g PEG-8000 | ddH ₂ O up to 1.2 mL |
| 300 µL 100 mM NAD | |
| ddH ₂ O up to 6 mL | |

To check whether the desired constructs and/or mutants were successfully cloned agarose gel and sequencing (StarSEQ GmbH, Mainz) were used to analyze the quality of the PCR products.

2.2.3. Agarose gel electrophoresis

To separate DNA molecules of various sizes agarose gels of 1-2% (w/c) were prepared with 1x Tris base -acetate acid-EDTA (TAE) buffer. The sample of interest, mixed with DNA sample buffer (NEB, Ipswich), was loaded with a ready to use molecular weight marker (1 kb or 100 bp, from NEB, Ipswich) and run for 1 – 2 h at 80 – 100 V. Visualization of the different DNA plasmids and fragments was achieved by staining with an ethidium bromide solution for 20-40 min. UV light detection of the stained gel bands was performed on a quantum gel documentation system (Peqlab, Erlangen).

Table 14: Composition of 10x TAE buffer for agarose gel electrophoresis

| 10x TAE |
|--------------------------|
| 0.4 M Tris approx. pH8.3 |
| 0.01 M EDTA |

2.2.4. Sequencing

After PCR purification of the desired plasmid, the correct insertion was confirmed by DNA sequencing (StarSEQ GmbH, Mainz). For primers see **Table 15**. Primers S3 and S4 were used to sequence inserts in pET11a and pET23a(+) vectors and were sufficient to check all inserts encoding ABC transporter NBD constructs. For checking the ABC transporter full-length constructs of LmrA, MsbA and BmrA, primers S29, S30, S47, S49 and S50 were used.

Table 15: Sequencing primers

| Primer number | Name | Sequence (5'-3') |
|---------------|---------------------------|------------------------|
| S3 | T7 Promoter | TAATACGACTCACTATAGGG |
| S4 | T7 Terminator | GCTAGTTATTGCTCAGCGG |
| S29 | pET11a-HisTEV-MsbA-full | CAGGTGACCACCAGCG |
| S30 | pET11a-HisTEV-MsbA-full-2 | CACCGATTGTTTCGATTGC |
| S47 | BmrA-full-P427-Seq1_For | GGTGCCGATTGGACGGAAAATG |
| S49 | BmrA-full-P339-Seq1_For | CTGCCGGAGATCCGTC |
| S50 | BmrA-full-P339-Seq2_Rev | GTTCTCACGAATGGTGCC |

2.3. Plasmids

Plasmids encoding variants of LmrA, Msba and BmrA were obtained commercially or cloned in the ██████ group unless stated differently. Plasmid numbers follow the nomenclature of the ██████ group. The plasmids derived from pET11a contain a T7 promoter for the induction of heterologous/homologous protein expression and an N-terminal His₆-tag sequence to purify the protein, followed by a TEV cleavage site sequence for His₆-tag removal during purification. The plasmid pET23a(+) encoding the *B. subtilis* ABC transporter BmrA with a C-terminal His₆ tag sequence for purification (p427) was kindly provided by the Lab of Prof. ██████ and Dr. ██████ from Lyon. The plasmid encoding the MBP-TEV-protease (p081) was a gift by the group of Prof. ██████ from Frankfurt.

Table 16: Plasmids encoding the *L. lactis* ABC transporter LmrA or LmrA variants

| Plasmid number | Insert | Tag/cleavage site | Vector backbone | Resistance | Origin |
|----------------|----------------------------|----------------------------------|-----------------------|------------|---------------------------------|
| p071 | LmrA-NBD wt | N-terminal His ₆ -TEV | pET11a | Ampicillin | Entelechon |
| p429 | LmrA-NBD E512Q | N-terminal His ₆ -TEV | pET11a, based on p071 | Ampicillin | Cloned by Dania Rose-Sperling |
| p073 | LmrA-NBD K388A | N-terminal His ₆ -TEV | pET11a | Ampicillin | Entelechon |
| p074 | LmrA-NBD H543A | N-terminal His ₆ -TEV | pET11a | Ampicillin | Entelechon |
| p085 | LmrA-NBD K486A | N-terminal His ₆ -TEV | pET11a | Ampicillin | Genscript (Piscataway Township) |
| p086 | LmrA-NBD D518A | N-terminal His ₆ -TEV | pET11a | Ampicillin | Genscript (Piscataway Township) |
| P087 | LmrA-NBD Q430A | N-terminal His ₆ -TEV | pET11a | Ampicillin | Genscript (Piscataway Township) |
| p103 | LmrA-NBD wt-opt | N-terminal His ₆ -TEV | pET11a, based on p086 | Ampicillin | Cloned by Dania Rose-Sperling |
| p123 | LmrA-NBD SALD | N-terminal His ₆ -TEV | pET11a, based on p103 | Ampicillin | Cloned by Dania Rose-Sperling |
| p125 | LmrA-NBD SSLD | N-terminal His ₆ -TEV | pET11a, based on p103 | Ampicillin | Cloned by Dania Rose-Sperling |
| p124 | LmrA-NBD W421F | N-terminal His ₆ -TEV | pET11a, based on p071 | Ampicillin | Cloned by Dania Rose-Sperling |
| p207* | LmrA-NBD W421A | N-terminal His ₆ -TEV | pET11a, based on p071 | Ampicillin | Cloned by Dania Rose-Sperling |
| p208 | LmrA-NBD W457F | N-terminal His ₆ -TEV | pET11a, based on p071 | Ampicillin | Cloned by Dania Rose-Sperling |
| p209* | LmrA-NBD R397A | N-terminal His ₆ -TEV | pET11a, based on p071 | Ampicillin | Cloned by Dania Rose-Sperling |
| p306 | LmrA-NBD S467C | N-terminal His ₆ -TEV | pET11a, based on p071 | Ampicillin | Cloned by Dania Rose-Sperling |
| p353 | LmrA-NBD S467C-M524W | N-terminal His ₆ -TEV | pET11a, based on p071 | Ampicillin | Cloned by Dania Rose-Sperling |
| p430 | LmrA-NBD S467C-M524W-E512Q | N-terminal His ₆ -TEV | pET11a, based on p071 | Ampicillin | Cloned by Dania Rose-Sperling |

* constructs successfully cloned but not used for further analysis in this work

Table 17: Plasmids encoding the *E. coli* ABC transporter *MsbA* or *MsbA* variants

| Plasmid number | Insert | Tag/cleavage site | Vector backbone | Resistance | Origin |
|----------------|---|----------------------------------|-----------------------|------------|--|
| p236 | MsbA-NBD | N-terminal His ₆ -TEV | pET11a, based on p061 | Ampicillin | Cloned by ██████████/Dania Rose-Sperling from <i>E. coli</i> BL21-Gold (DE3), ██████████ group |
| p344 | MsbA-NBD E506Q | N-terminal His ₆ -TEV | pET11a, based on p236 | Ampicillin | Cloned by Dania Rose-Sperling, ██████████ |
| p345 | MsbA-NBD D512A | N-terminal His ₆ -TEV | pET11a, based on p236 | Ampicillin | Cloned by Dania Rose-Sperling, ██████████ |
| p397 | MsbA-NBD D461C | N-terminal His ₆ -TEV | pET11a, based on p236 | Ampicillin | Cloned by Dania Rose-Sperling |
| P398 | MsbA-NBD D461C-A518W | N-terminal His ₆ -TEV | pET11a, based on p236 | Ampicillin | Cloned by Dania Rose-Sperling |
| p250* | MsbA-full-length | N-terminal His ₆ -TEV | pET11a, based on p061 | Ampicillin | Cloned by ██████████/Dania Rose-Sperling from <i>E. coli</i> BL21-Gold (DE3), ██████████ group |
| p354* | MsbA-full-length C88S | N-terminal His ₆ -TEV | pET11a, based on p250 | Ampicillin | Cloned by Dania Rose-Sperling, ██████████ |
| p355* | MsbA-full-length C315S | N-terminal His ₆ -TEV | pET11a, based on p250 | Ampicillin | Cloned by Dania Rose-Sperling, ██████████ |
| p378 | MsbA-full-length C88S-C315S | N-terminal His ₆ -TEV | pET11a, based on p250 | Ampicillin | Cloned by Dania Rose-Sperling, ██████████ |
| p492* | MsbA-full-length C88S-C315S-D461C | N-terminal His ₆ -TEV | pET11a, based on p250 | Ampicillin | Cloned by Dania Rose-Sperling, ██████████ |
| p493* | MsbA-full-length C88S-C315S-D461C-A518W | N-terminal His ₆ -TEV | pET11a, based on p250 | Ampicillin | Cloned by Dania Rose-Sperling, ██████████ |
| p490* | MsbA-full-length D461C | N-terminal His ₆ -TEV | pET11a, based on p250 | Ampicillin | Cloned by Dania Rose-Sperling |
| p491* | MsbA-full-length D461C-A518W | N-terminal His ₆ -TEV | pET11a, based on p250 | Ampicillin | Cloned by Dania Rose-Sperling |
| p357* | MsbA-full-length D512A | N-terminal His ₆ -TEV | pET11a, based on p250 | Ampicillin | Cloned by Dania Rose-Sperling, ██████████ |
| p368* | MsbA-full-length E506Q | N-terminal His ₆ -TEV | pET11a, based on p250 | Ampicillin | Cloned by Dania Rose-Sperling, ██████████ |

* constructs successfully cloned but not used for further analysis in this work

Table 18: Plasmids encoding the *B. subtilis* ABC transporter *BmrA* or *BmrA* variants

| Plasmid number | Insert | Tag/cleavage site | Vector backbone | Resistance | Origin |
|----------------|------------------------------|----------------------------------|--------------------------|------------|---------------------------------|
| p340 | BmrA-NBD | N-terminal His ₆ -TEV | pET11a | Ampicillin | Genscript (Piscataway Township) |
| p433* | BmrA-NBD W413F | N-terminal His ₆ -TEV | pET11a, based on p340 | Ampicillin | Cloned by Dania Rose-Sperling |
| p446* | BmrA-NBD R389A | N-terminal His ₆ -TEV | pET11a, based on p340 | Ampicillin | Cloned by Dania Rose-Sperling |
| p404 | BmrA-NBD N459C | N-terminal His ₆ -TEV | pET11a, based on p340 | Ampicillin | Cloned by Dania Rose-Sperling |
| p426 | BmrA-NBD N459C-S516W | N-terminal His ₆ -TEV | pET11a, based on p340 | Ampicillin | Cloned by Dania Rose-Sperling |
| p339 | BmrA-full-length | N-terminal His ₆ -TEV | pET11a | Ampicillin | Genscript (Piscataway Township) |
| p488* | BmrA-full-length N459C | N-terminal His ₆ -TEV | pET11a, based on p339 | Ampicillin | Cloned by Dania Rose-Sperling |
| p489* | BmrA-full-length N459C-S516W | N-terminal His ₆ -TEV | pET11a, based on p339 | Ampicillin | Cloned by Dania Rose-Sperling |
| p427 | BmrA-full-length | C-terminal His ₆ | pET23a(+) | Ampicillin | ████████████████████; Lyon CNRS |
| p440 | BmrA-full-length R389A | C-terminal His ₆ | pET23a(+), based on p427 | Ampicillin | Cloned by Dania Rose-Sperling |
| p565 | BmrA-full-length R389E | C-terminal His ₆ | pET23a(+), based on p427 | Ampicillin | Cloned by Dania Rose-Sperling |
| p566 | BmrA-full-length R389K | C-terminal His ₆ | pET23a(+), based on p427 | Ampicillin | Cloned by Dania Rose-Sperling |
| p567 | BmrA-full-length R389M | C-terminal His ₆ | pET23a(+), based on p427 | Ampicillin | Cloned by Dania Rose-Sperling |
| p568 | BmrA-full-length K380A | C-terminal His ₆ | pET23a(+), based on p427 | Ampicillin | Cloned by Dania Rose-Sperling |
| p441 | BmrA-full-length SALD | C-terminal His ₆ | pET23a(+), based on p427 | Ampicillin | Cloned by Dania Rose-Sperling |
| p450 | BmrA-full-length ASLD | C-terminal His ₆ | pET23a(+), based on p427 | Ampicillin | Cloned by Dania Rose-Sperling |
| p485 | BmrA-full-length D510A | C-terminal His ₆ | pET23a(+), based on p427 | Ampicillin | Cloned by Dania Rose-Sperling |
| p486* | BmrA-full-length N459C | C-terminal His ₆ | pET23a(+), based on p427 | Ampicillin | Cloned by Dania Rose-Sperling |
| p487* | BmrA-full-length N459C-S516W | C-terminal His ₆ | pET23a(+), based on p427 | Ampicillin | Cloned by Dania Rose-Sperling |

* constructs successfully cloned but not used for further analysis in this work

Table 19: Plasmid used for production of TEV protease

| Plasmid number | Insert | Tag/cleavage site | Vector backbone | Resistance | Origin |
|----------------|--------------|----------------------------------|-----------------|------------|---|
| p081 | TEV protease | N-terminal His ₆ -tag | MBP-pMal-c4X | Ampicillin | ██████████ group, Frankfurt university; NEB (Ipswich) |

To amplify a plasmid or during a cloning project (e.g., insertion of a point mutation or insertion of gene sequence), plasmids were transformed in competent *E. coli* DH5 α cells, overnight cultivated in 5 - 10 mL LB and isolated with the E.Z.N.A. Plasmid Miniprep Kit (Omega Bio-Tek, Norcross).

3. PROPERTIES OF PURIFIED PROTEINS

Polyhistidine tags were attached to the proteins of interest for their purification. After binding of the poly-His tag to a resin of chelating Sepharose loaded with Ni²⁺, the bound protein is then eluted with an imidazole gradient from the Ni²⁺ beads. After elution, the tobacco etch virus (TEV) protease was used to cleave off the poly His tag. The TEV protease is a nuclear inclusion protein which recognizes a linear epitope with the consensus sequence E-X_{aa}-X_{aa}-Y-X_{aa}-Q-(G/S). Here ENLYFQG is the sequence used in the proteins.

Physicochemical properties of LmrA (UniProtKB ID: P97046), MsbA (UniProtKB ID: P60752) and BmrA (UniProtKB ID: O06967) constructs were calculated using the ProtParam tool from the ExPasy website (<https://web.expasy.org/protparam/>)²⁸⁷, **Table 20**, **Table 21** and **Table 22**).

Table 20: LmrA ABC transporter protein from *L. lactis* and variants

| Protein | Number of amino acids | | Molecular weight [kDa] | | pI | | Ext. coefficient 280 nm [cm ⁻¹ M ⁻¹] | | Selected Amino acid composition | |
|--------------------------------------|-----------------------|---------|------------------------|---------|----------|---------|---|---------|---------------------------------------|---------------------------------------|
| | with tag | cleaved | with tag | cleaved | with tag | cleaved | with tag | cleaved | with tag | cleaved |
| His ₆ -TEV-LmrA-NBD WT | 279 | 263 | 30.83 | 28.88 | 4.92 | 4.64 | 21430 | 19940 | Cys: 0 Phe: 12 Trp: 2 Tyr: 7 | Cys: 0 Phe: 11 Trp: 2 Tyr: 6 |
| His ₆ -TEV-LmrA-NBD D518A | 279 | 263 | 30.79 | 28.84 | 4.97 | 4.69 | 21430 | 19940 | Cys: 0 Phe: 12 Trp: 2 Tyr: 7 | Cys: 0 Phe: 11 Trp: 2 Tyr: 6 |
| His ₆ -TEV-LmrA-NBD SALD | 279 | 263 | 30.83 | 28.88 | 4.92 | 4.64 | 21430 | 19940 | Cys: 0 Phe: 12 Trp: 2 Tyr: 7 | Cys: 0 Phe: 11 Trp: 2 Tyr: 6 |
| His ₆ -TEV-LmrA-NBD SSLD | 279 | 263 | 30.85 | 28.9 | 4.92 | 4.64 | 21430 | 19940 | Cys: 0 Phe: 12 Trp: 2 Tyr: 7 | Cys: 0 Phe: 11 Trp: 2 Tyr: 6 |
| His ₆ -TEV-LmrA-NBD Q430A | 279 | 263 | 30.77 | 28.82 | 4.92 | 4.64 | 21430 | 19940 | Cys: 0 Phe: 12 Trp: 2 Tyr: 7 | Cys: 0 Phe: 11 Trp: 2 Tyr: 6 |
| His ₆ -TEV-LmrA-NBD H543A | 279 | 263 | 30.76 | 28.81 | 4.86 | 4.60 | 21430 | 19940 | Cys: 0 Phe: 12 Trp: 2 Tyr: 7 | Cys: 0 Phe: 11 Trp: 2 Tyr: 6 |
| His ₆ -TEV-LmrA-NBD K486A | 279 | 263 | 30.77 | 28.82 | 4.86 | 4.59 | 21430 | 19940 | Cys: 0 Phe: 12 Trp: 2 Tyr: 7 | Cys: 0 Phe: 11 Trp: 2 Tyr: 6 |
| His ₆ -TEV-LmrA-NBD K388A | 279 | 263 | 30.72 | 28.82 | 4.8 | 4.55 | 21430 | 19940 | Cys: 0 Phe: 12 Trp: 2 Tyr: 7 | Cys: 0 Phe: 11 Trp: 2 Tyr: 6 |
| His ₆ -TEV-LmrA-NBD R397A | 279 | 263 | 30.74 | 28.79 | 4.86 | 4.59 | 21430 | 19940 | Cys: 0 Phe: 12 Trp: 2 Tyr: 7 | Cys: 0 Phe: 11 Trp: 2 Tyr: 6 |
| His ₆ -TEV-LmrA-NBD W421A | 279 | 263 | 30.71 | 28.76 | 4.92 | 4.64 | 15930 | 14440 | Cys: 0 Phe: 12 Trp: 1 Tyr: 7 | Cys: 0 Phe: 11 Trp: 1 Tyr: 6 |

| | | | | | | | | | | |
|---|-----|-----|-------|-------|------|------|-------|-------|---------------------------------------|---------------------------------------|
| His ₆ -TEV- LmrA-NBD W421F | 279 | 263 | 30.79 | 28.84 | 4.92 | 4.64 | 15930 | 14440 | Cys: 0 Phe: 12 Trp: 1 Tyr: 7 | Cys: 0 Phe: 11 Trp: 1 Tyr: 6 |
| His ₆ -TEV- LmrA-NBD W457F | 279 | 263 | 30.79 | 28.84 | 4.92 | 4.64 | 15930 | 14440 | Cys: 0 Phe: 12 Trp: 1 Tyr: 7 | Cys: 0 Phe: 11 Trp: 1 Tyr: 6 |
| His ₆ -TEV- LmrA-NBD S467C | 279 | 263 | 30.85 | 28.9 | 4.92 | 4.64 | 21430 | 19940 | Cys: 1 Phe: 12 Trp: 2 Tyr: 7 | Cys: 1 Phe: 11 Trp: 2 Tyr: 6 |
| His ₆ -TEV- LmrA-NBD S467C- M524W | 279 | 263 | 30.9 | 28.95 | 4.92 | 4.64 | 26930 | 25440 | Cys: 1 Phe: 12 Trp: 3 Tyr: 7 | Cys: 1 Phe: 11 Trp: 3 Tyr: 6 |
| His ₆ -TEV- LmrA-NBD S467C- M524W- E512Q | 279 | 263 | 30.9 | 28.95 | 4.96 | 4.68 | 26930 | 25440 | Cys: 1 Phe: 12 Trp: 3 Tyr: 7 | Cys: 1 Phe: 11 Trp: 3 Tyr: 6 |

Table 21: MsbA ABC transporter protein from E. coli and variants

| Protein | Number of amino acids | | Molecular weight [kDa] | | pI | | Ext. coefficient 280 nm [cm ⁻¹ M ⁻¹] | | Selected Amino acid composition | |
|--|-----------------------|---------|------------------------|---------|----------|---------|---|---------------------------|--|--|
| | with tag | cleaved | with tag | cleaved | with tag | cleaved | with tag | cleaved | with tag | cleaved |
| His ₆ -TEV- MsbA-NBD WT | 278 | 262 | 31.0 | 29.05 | 5.46 | 5.09 | 11920 | 10430 | Cys: 0 Phe: 7 Trp: 0 Tyr: 8 | Cys: 0 Phe: 6 Trp: 0 Tyr: 7 |
| His ₆ -TEV- MsbA-NBD D512A | 278 | 262 | 30.96 | 29.01 | 5.55 | 5.17 | 11920 | 10430 | Cys: 0 Phe: 7 Trp: 0 Tyr: 8 | Cys: 0 Phe: 6 Trp: 0 Tyr: 7 |
| His ₆ -TEV- MsbA-NBD E506Q | 278 | 262 | 31.00 | 29.05 | 5.54 | 5.16 | 11920 | 10430 | Cys: 0 Phe: 7 Trp: 0 Tyr: 8 | Cys: 0 Phe: 6 Trp: 0 Tyr: 7 |
| His ₆ -TEV- MsbA-NBD D461C | 278 | 262 | 30.99 | 29.04 | 5.55 | 5.17 | 11920 | 10430 | Cys: 1 Phe: 7 Trp: 0 Tyr: 8 | Cys: 1 Phe: 6 Trp: 0 Tyr: 7 |
| His ₆ -TEV- MsbA-NBD D461C- A518W | 278 | 262 | 31.10 | 29.16 | 5.55 | 5.17 | 17420 | 15930 | Cys: 1 Phe: 7 Trp: 1 Tyr: 8 | Cys: 1 Phe: 6 Trp: 1 Tyr: 7 |
| His ₆ -TEV- MsbA-full- length WT | 599 | 583 | 66.42 | 64.47 | 8.32 | 8.63 | 48485 Red.Cys 48360 | 46995 Red.Cys 46870 | Cys: 2 Phe: 24 Trp: 5 Tyr: 14 | Cys: 2 Phe: 23 Trp: 5 Tyr: 13 |
| His ₆ -TEV- MsbA-full- length C88S- C315S | 599 | 583 | 66.39 | 64.44 | 8.48 | 8.78 | 48360 | 46870 | Cys: 0 Phe: 24 Trp: 5 Tyr: 14 | Cys: 0 Phe: 23 Trp: 5 Tyr: 13 |
| His ₆ -TEV- MsbA-full- length E506Q | 599 | 583 | 66.42 | 64.47 | 8.61 | 8.82 | 48485 Red.Cys 48360 | 46995 Red.Cys 46870 | Cys: 2 Phe: 24 Trp: 5 Tyr: 14 | Cys: 2 Phe: 23 Trp: 5 Tyr: 13 |

Table 22: BmrA ABC transporter protein from *B. subtilis* and variants

| Protein | Number of amino acids | | Molecular weight [kDa] | | pI | | Ext. coefficient 280 nm [$\text{cm}^{-1} \text{M}^{-1}$] | | Selected Amino acid composition | |
|--|-----------------------|---------|------------------------|---------|----------|---------|--|----------------------------|--|--|
| | with tag | cleaved | with tag | cleaved | with tag | cleaved | with tag | cleaved | with tag | cleaved |
| His ₆ -TEV-BmrA-NBD WT | 275 | 259 | 30.54 | 28.59 | 5.46 | 5.10 | 17420 | 15930 | Cys: 1 Phe: 8 Trp: 1 Tyr: 8 | Cys: 1 Phe: 7 Trp: 1 Tyr: 7 |
| His ₆ -TEV-BmrA-NBD W413F | 275 | 259 | 30.54 | 28.55 | 5.46 | 5.10 | 11920 | 10430 | Cys: 1 Phe: 9 Trp: 0 Tyr: 8 | Cys: 1 Phe: 8 Trp: 0 Tyr: 7 |
| His ₆ -TEV-BmrA-NBD N459C | 275 | 259 | 30.53 | 28.58 | 5.46 | 5.10 | 17545 Red.Cys 17420 | 16055 Red. Cys 15930 | Cys: 2 Phe: 8 Trp: 1 Tyr: 8 | Cys: 2 Phe: 7 Trp: 1 Tyr: 7 |
| His ₆ -TEV-BmrA-NBD N459C-S516W | 275 | 259 | 30.63 | 28.68 | 5.46 | 5.10 | 23045 Red.Cys 22920 | 21555 Red.Cys 21430 | Cys: 2 Phe: 8 Trp: 2 Tyr: 8 | Cys: 2 Phe: 7 Trp: 2 Tyr: 7 |
| His ₆ -TEV-BmrA-full-length WT p339 | 605 | 589 | 66.4 | 64.45 | 6.53 | 6.49 | 40340 | 38850 | Cys: 1 Phe: 24 Trp: 3 Tyr: 16 | Cys: 1 Phe: 23 Trp: 3 Tyr: 15 |
| BmrA- His ₆ full-length WT p427 | 607 | - | 66.54 | - | 6.53 | - | 38850 | - | Cys: 1 Phe: 23 Trp: 3 Tyr: 15 | - |
| BmrA- His ₆ full-length R389A p427 | 607 | - | 66.46 | - | 6.39 | - | 38850 | - | Cys: 1 Phe: 23 Trp: 3 Tyr: 15 | - |
| BmrA- His ₆ full-length R389E p427 | 607 | - | 66.52 | - | 6.27 | - | 38850 | - | Cys: 1 Phe: 23 Trp: 3 Tyr: 15 | - |
| BmrA- His ₆ full-length R389K p427 | 607 | - | 66.51 | - | 6.53 | - | 38850 | - | Cys: 1 Phe: 23 Trp: 3 Tyr: 15 | - |
| BmrA- His ₆ full-length R389M p427 | 607 | - | 66.52 | - | 6.39 | - | 38850 | - | Cys: 1 Phe: 23 Trp: 3 Tyr: 15 | - |
| BmrA- His ₆ full-length K380A p427 | 607 | - | 66.49 | - | 6.39 | - | 38850 | - | Cys: 1 Phe: 23 Trp: 3 Tyr: 15 | - |
| BmrA- His ₆ full-length D512A p427 | 607 | - | 66.5 | - | 6.70 | - | 38850 | - | Cys: 1 Phe: 23 Trp: 3 Tyr: 15 | - |
| BmrA- His ₆ full-length SALD p427 | 607 | - | 66.53 | - | 6.53 | - | 38850 | - | Cys: 1 Phe: 23 Trp: 3 Tyr: 15 | - |
| BmrA- His ₆ full-length ASLD p427 | 607 | - | 66.53 | - | 6.53 | - | 38850 | - | Cys: 1 Phe: 23 Trp: 3 Tyr: 15 | - |

Table 23: TEV-protease used for purification

| Protein | Number of amino acids | | Molecular weight [kDa] | | pI | | Ext. coefficient 280 nm [$\text{cm}^{-1} \text{M}^{-1}$] | | Selected Amino acid composition | |
|--------------------------------|-----------------------|---------|------------------------|---------|----------|---------|--|---------|---|---------------------------------------|
| | with tag | cleaved | with tag | cleaved | with tag | cleaved | with tag | cleaved | with tag | cleaved |
| His ₆ -TEV-protease | 643 | 248 | 71.9 | 28.6 | 6.82 | 9.59 | 100060 | 32220 | Cys: 4 Phe: 33 Trp: 13 Tyr: 19 | Cys: 4 Phe: 17 Trp: 5 Tyr: 3 |

4. HETEROLOGOUS/ HOMOLOGOUS EXPRESSION OF LMRA-NBD, MSBA-NBD AND BMRA-NBD IN *E. COLI*

4.1. Media for protein expression and additives

Table 24: Composition of protein expression media and additives

| Media or component | Additional information for use/ preparation |
|---|---|
| LB medium 5 g/L yeast extract 10 g/L NaCl 10 g/L tryptone | Freshly autoclaved |
| 2 YT medium/ 2XYT medium 10 g/L yeast extract 16 g/L pepton 5 g/L NaCl | Freshly autoclaved |
| M9 medium 15 g/L KH ₂ PO ₄ 33.9 g/L Na ₂ HPO ₄ 1 g/L NH ₄ Cl* 2.5 g/L NaCl | Freshly autoclaved *leave out NH ₄ Cl and add ¹⁵ NH ₄ Cl 0.75 g/L right before starting main culture for ¹⁵ N isotope labeling |
| Added before used: 4 g/L Glucose% 4 mL/L 1M MgSO ₄ 1 mL/L 10 mM FeCl ₃ 2 mL/L Magic Mix 10 mL/L Trace elements 100 µg/mL Ampicillin | 20% stock solution autoclaved 1M stock solution autoclaved 10 mM stock solution sterile filtered stored at - 20°C See below See below See below |
| Magic mix Centrum® vitamin tablet dissolved in 40 mL ddH ₂ O | Sterile filtered stored at - 20°C |
| Trace elements 0.2 mg/mL CaCl ₂ *2H ₂ O 0.2 mg/mL ZnSO ₄ *7H ₂ O 0.2 mg/mL MnSO ₄ *H ₂ O 5 mg/mL Tryptophane* 5 mg/mL Thiamine 5 mg/mL Niacin 0.1 mg/mL Biotin | Sterile filtered stored at - 20°C *leave out for ¹⁵ N isotope labeling |
| LB-Agar plates 5 g/L yeast extract 10 g/L pepton 10 g/L NaCl 15 g/L agar-agar | Antibiotic added after autoclaving and cooling, LB agar plates were stored at 4°C |
| Ampicillin | 100 mg/mL Stock solution in 20 % EtOH stored at - 20°C |
| IPTG | 1 M IPTG Stock solution in dH ₂ O stored at - 20°C |

Table 25: Defined medium for selective isotope labeling of amino acids

Media for selective labeling of amino acids[#]

| Amino acid | g/L | Additives | g/L | Add before use | |
|--------------|------|---------------------------------|------|-------------------------|-----------|
| Ala | 0.5 | Adenine | 0.5 | 20 % Glucose | 100 mL/L |
| Arg | 0.4 | Guanosine | 0.65 | 1 M MgSO ₄ | 4 mL/L |
| Asn | 0 | Thymine | 0.2 | 10 mM FeCl ₃ | 1 mL/L |
| Asp | 0.4 | Uracil | 0.5 | Magic Mix* | 1 mL/L |
| Cys | 0.05 | Cytosine | 0.2 | Trace elements* | 10 mL/L |
| Gln | 0.4 | | | | |
| Glu | 0.65 | Sodium acetate | 1.5 | | |
| Gly | 0.55 | Succinic acid | 1.5 | Ampicillin | 100 µg/mL |
| His | 0.1 | NH ₄ Cl | 0.5 | | |
| Ile | 0.23 | NaOH | 0.85 | | |
| Leu | 0.23 | K ₂ HPO ₄ | 10.5 | | |
| Lys-hydro-Cl | 0.42 | | | | |
| Met | 0.25 | | | | |
| Phe | 0.13 | | | | |
| Pro | 0.1 | | | | |
| Ser | 2.1 | | | | |
| Thr | 0.23 | | | | |
| Tyr | 0.17 | | | | |
| Val | 0.23 | | | | |

* Composition see **Table 24**

[#] Isotope-labeled amino acids were added instead of unlabeled amino acids

Table 26: Expression media used to produce unlabeled and isotope labeled LmrA, MsbA and BmrA

| Labeling/non labeling for proteins | Media used for expression | Additional information |
|---|---|--|
| Unlabeled protein | LB medium, 2YT medium/ 2XYT medium | |
| Uniform ² H, ¹³ C, ¹⁵ N labeling | <i>E. coli</i> CDN-media OD2 (Silantes GmbH, München) | |
| Uniform ² H, ¹⁵ N labeling | <i>E. coli</i> DN-media OD2 (Silantes GmbH, München) | |
| Uniform ¹⁵ N labeling | M9 medium (Table 24) | Instead of NH ₄ Cl ¹⁵ NH ₄ Cl is added to the media right before growth |
| Selective labeling of specific amino acids | Defined media (Table 25) | Instead of unlabeled amino acids the respective ¹⁵ N amino acid or ¹⁵ N- ¹³ C proline (for unique pair labeling) was added right before growth. |
| Selective ¹⁹ F-Trp labeling | Defined media (Table 25) | Instead of unlabeled ¹⁹ F 5-Fluoro-L-tryptophane or ¹⁹ F 5-Fluoro-DL-tryptophane was added to the media right before growth, unless stated differently 100% ¹⁹ F-Trp was used |

4.2. Preparation of competent cells

To prepare competent *E. coli* cells (DH5 α or BL21-Gold (DE3)), the cells were first grown over night at 37°C in LB media without antibiotics in a shaker at 180 – 200 rpm. The next day, 100 mL fresh LB medium was inoculated with the overnight culture to an OD_{600nm} of 0.5. Subsequently the bacteria suspension was centrifuged in two 50 mL reaction tubes at 3214 xg for 10 minutes. After addition of 20 mL solution I (pre-chilled) to each cell pellet, the pellets were gently resuspended and kept cool on ice (4 – 8 °C) for 1 - 2 h. After another centrifugation step (3214 xg for 10 minutes), each cell pellet was resuspended in 1 – 1.5 mL of solution I and the two solutions then combined. 3 mL of solution II (pre-chilled) was added. The newly competent cells were then aliquoted in 50 - 100 μ L batches in 1.5 mL reaction tubes, frozen immediately with liquid nitrogen and stored at – 80°C until further use.

Table 27: Composition of solutions for the preparation of competent cells

| Solution I | Solution II |
|-------------------------|-------------------------|
| 70 mM CaCl ₂ | 70 mM CaCl ₂ |
| 50 mM MgCl ₂ | 50 mM MgCl ₂ |
| | 30% Glycerol |

4.3. Transformation of cells

15 – 80 ng of plasmid DNA was added to 25 – 50 μ L of competent cells (*E. coli* DH5 α , *E. coli* BL21-Gold (DE3) or *E. coli* C41 (DE3), **Table 7**) and incubated at 4°C for 20 min. After a heat shock (42°C, 45 s), cells were kept cool at 4°C for 2 min. Subsequently, 300 μ L of LB medium were added and the cells grown for 1 - 2 h at 37°C and 180 – 200 rpm. Finally, 100 - 300 μ L of the cell suspension were plated on LB agar plates (containing the antibiotic ampicillin) and incubated overnight at 37°C.

4.4. Protein expression conditions

SDS-PAGE was performed to analyze overexpression the desired proteins. For this a 1 mL sample before (-) and after induction of expression (+) was taken. These samples were centrifuged (2700 xg, 4°C, 1 min) and stored at – 20°C until the SDS-PAGE (**10.1. SDS-Polyacrylamide gel electrophoresis** (SDS-PAGE), 12 - 15% gel) was run.

4.4.1. General conditions for heterologous/ homogenous expression of LmrA-NBD, MsbA-NBD and BmrA-NBD

For expression of LmrA-NBD, MsbA-NBD or BmrA-NBD competent *E. coli* BL21-Gold (DE3) cells were transformed with pET11a plasmids encoding the respective transporters as described above. For the expression of all proteins, a pre-culture (50 - 100mL of LB medium supplemented with 100 μ g/mL ampicillin) was inoculated with some colonies from a LB agar plate. The pre-culture was incubated overnight at 37 °C at 120 - 200 rpm. Depending on the desired expression conditions (specific labeling or no labeling of the proteins) the appropriate medium (**Table 24** and **Table 26**) was inoculated with 5 – 20% (v/v) of pre-culture and cells were grown at 37°C with 180 – 200 rpm to an OD_{600nm} of 0.5 - 0.8. Protein expression was then induced by the addition of 1 mM IPTG and the cells grown overnight at 20 - 21 °C and 180 – 200 rpm. Cells were harvested by centrifugation (4790 xg, 10 min at 4°C), resuspended in lysis buffer (**Table 28**), frozen in liquid nitrogen and stored at – 20°C until further use.

4.4.2. General conditions for heterologous expression of full-length BmrA constructs

The protocol for expression of BmrA is based on the protocol established by the [REDACTED] Laboratory in Lyon²⁸⁸. BmrA encoded on a pET23a(+) plasmid was expressed in *E. coli* C41 (DE3) cells (**Table 22**). A pre-culture (50 – 100 mL of LB medium supplemented with 100 µg/mL ampicillin) was inoculated with some colonies from a LB agar plate. The pre-culture was incubated overnight at 37 °C, 160 rpm. Expression media (2YT or ¹⁹F-Trp defined media, **Table 24** and **Table 25**) was inoculated with pre-culture to obtain an OD_{600nm} value of 0.1 and grown at 37°C, at 120 rpm. When an OD_{600nm} 0.7 – 1.0 was reached, the cells were induced with 700 µM IPTG and grown for 4 h at 25°C 120 rpm. Cells were harvested by centrifugation (2x 6000 xg, 15 min, 4°C), frozen in liquid nitrogen and stored at – 20°C until further use.

The expression medium for ¹⁹F W labeling of full-length BmrA contained 90% ¹⁹F-DL-tryptophane and 10% unlabeled tryptophane. Labeled and unlabeled tryptophane was added to the defined medium right before inoculating the expression culture.

4.4.3. General conditions for heterologous expression of TEV protease

TEV protease was heterologously-expressed in *E. coli* BL21-Gold (DE3) cells. A pre-culture (50 - 100mL of LB medium supplemented with 100 µg/mL ampicillin) was inoculated with some colonies from a LB agar plate. The pre-culture was incubated overnight at 37 °C at 120 - 200 rpm. Then, 1 L of 2XYT medium was inoculated with 5 – 20% (v/v) of pre-culture and the cells were cultivated at 37°C with 180 – 200 rpm. At an OD_{600nm} of 0.6 – 0.8, the expression was induced with 500 µM IPTG and the temperature was reduced to 25°C during expression overnight at 180 – 200 rpm. Cells were harvested with centrifugation (2x 6000 xg, 15 min, 4°C) and frozen with liquid nitrogen in lysis buffer (**Table 31**) and stored until further use. TEV protease contains an N-terminal MBP-tag followed by a TEV cleavage and a His₆-tag. The TEV protease cleaves its own MBP-tag *in vivo*, leaving a His₆ TEV protease ready to use in purifications of LmrA, MsbA and BmrA.

5. PURIFICATION OF LMR A-NBD, MSBA-NBD AND BMR A-NBD

A bacterial cell pellet containing the overexpressed protein of interest was resuspended in lysis buffer (**Table 28**, cells from 0.1 - 0.25 mL culture were dissolved in ~ 25-40 mL lysis buffer with freshly added DNase, RNase and lysozyme, half tablet of protease inhibitor, 1 mM DTT and 1 mM benzamidine), disrupted by sonification (5 – 10 cycles, 45 s – 60 s, 50% - 60% power at 4°C, branson sonifier, Offenbach or bandelin sonifier, Berlin) and cell debris pelleted by centrifugation (20 – 40 min/ 2050 xg/ 4°C). The supernatant containing the soluble NBD protein was added twice to a Ni²⁺-NTA column (**Table 28**), washed extensively with wash buffer A (8 - 10 CV), buffer B (8 - 10 CV) and buffer C (8 – 10 CV). The protein of interest was eluted with buffer D (250 mM imidazole 5 – 6 CV). Eluted protein was combined with TEV protease (25:1 – 40:1 mol/ mol) for His-tag removal and dialyzed (Cut off <12 kDa) overnight at 4°C against dialysis buffer. After centrifugation (4790 xg, 10 min at 4°C), a reverse Ni²⁺-NTA purification step was carried out to remove His-tagged TEV protease and uncleaved protein. The purified NBDs were concentrated (Cut off <10 kDa, Sartorius Vivaspin, Göttingen), centrifuged (4790 xg, 10 min at 4°C) in a fresh reaction tube and run over a Superdex 200/ 16-60 or Superdex 75/ 16-60 (GE Healthcare, Chicago, USA). Protein concentration was determined by absorption at 280 nm (**8. Quantitative protein determination**) and protein purity further analyzed by performing an SDS-PAGE (**10.1. SDS-Polyacrylamide gel electrophoresis (SDS-PAGE)**, 15% gel).

Table 28: Buffer compositions for LmrA-NBD, MsbA-NBD or BmrA-NBD protein purification

| Lysis buffer | Ni ²⁺ -NTA Buffer A | Buffer B | Buffer C | Buffer D | Dialysis/ SEC buffer NMR buffer |
|--------------------------|-----------------------------------|---------------|-----------------|------------------|---------------------------------------|
| 250 mM Sucrose | 50 mM Tris-Cl | 50 mM Tris-Cl | 50 mM Tris-Cl | 50 mM Tris-Cl | 50 mM BisTris |
| 150 mM NaCl | pH8.0 | pH8.0 | pH8.0 | pH8.0 | pH 6.5*/pH 7.0# |
| 10 mM Tris-Cl | 50 mM NaCl | 500 mM NaCl | 50 mM NaCl | 50 mM NaCl | 50mM NaCl |
| pH7.5 | | | 20 mM Imidazole | 250 mM Imidazole | |
| 2.5 mM MgSO ₄ | | | | | |

* in LmrA-NBD purification

in MsbA-NBD and BmrA-NBD purification

6. PURIFICATION OF MEMBRANE PROTEINS: FULL-LENGTH ABC TRANSPORTERS MSBA AND BMR A

Two different membrane protein purification protocols were used.

6.1. Preparation of inside out vesicles (IOVs) containing full-length MsbA and BmrA

The bacterial cell pellet containing the protein of interest was resuspended with lysis buffer (cells from ~1 L culture were dissolved in ~40 - 60 mL lysis buffer **Table 28**) supplemented with DNase, RNase and half a tablet of protease inhibitor (Roche, Basel). After passing the suspension through a cell disruptor three times at 1.24 kbar, 15 mM K-EDTA was added to prevent membrane stacking. Then a low centrifugation step (2050 xg, 10 min, 4°C) was carried out. The supernatant from the low centrifugation step was then subjected to a high spin centrifugation step (18400 xg, 1 h, 4°C). The pellet of the high centrifugation step containing the inside out vesicles (IOVs) were resuspended with solubilization buffer (**Table 29**) and used immediately or frozen with liquid nitrogen and stored at -20°C or -80°C until further use. Before freezing the samples, the protein concentration was quantified with a DCTM protein assay (**8. Quantitative protein determination**). In addition, a SDS-PAGE (**10.1. SDS-Polyacrylamide gel electrophoresis (SDS-PAGE)**, 12% gel) was performed to analyze protein purity.

6.2. Solubilization and purification of full-length MsbA and BmrA

For solubilization of the membrane proteins in the detergent DDM, the IOVs (concentration 5 – 10 mg/mL) were solubilized in solubilization buffer containing 1% DDM for 1 h at 4°C. After an ultracentrifugation step (18400 xg, 1 h, 4°C), the soluble fraction was loaded on a Ni²⁺-NTA column, which was pre-equilibrated with solubilization buffer containing 0.05% DDM. The column was washed with wash buffer A (15 CV), wash buffer B (15 CV), both containing 0.05% DDM. Finally, was the membrane protein eluted with elution buffer containing 150 mM imidazole and 0.05% DDM (8 CV elution buffer/ buffers see **Table 29**). Elution fractions after Ni²⁺-NTA column containing the membrane protein were concentrated (Cut off <30 kDa, sartorius Vivaspin, Göttingen) and run on a Superdex 200/ 16-60 (GE Healthcare, Chicago, USA). Protein concentration was determined by colorimetric DCTM protein assay (**8. Quantitative protein determination**) and a SDS-PAGE (**10.1. SDS-Polyacrylamide gel electrophoresis (SDS-PAGE), 12% gel**) was performed to analyze overexpression of the protein and its purity.

Table 29: Buffer composition for full-length MsbA and BmrA IOV preparation and protein purification

| Solubilization | Ni ²⁺ -NTA | | | Dialysis/ SEC buffer |
|-------------------------|------------------------------|------------------------------|-------------------------------|-------------------------|
| | Wash buffer A | Wash buffer B | Elution buffer | |
| 50 mM Tris-Cl pH 8.0 | 50 mM Tris-Cl pH 8.0 | 50 mM Tris-Cl pH 7.0 | 50 mM Tris-Cl pH 7.0 | 50 mM Tris-Cl pH 7.0 |
| 200 mM NaCl | 100 mM NaCl | 100 mM NaCl | 100 mM NaCl | 50 mM NaCl |
| 10% Glycerol | 10% Glycerol | 10% Glycerol | 10% Glycerol | 10% Glycerol |
| 1% DDM | 20 mM Imidazole 0.05% DDM | 20 mM Imidazole 0.05% DDM | 150 mM Imidazole 0.05% DDM | 0.025% DDM |

6.3. Preparation of inside out vesicles (IOVs) containing full-length BmrA

The protocol for preparing IOVs containing full-length BmrA (constructs based on p427, **Table 22**) is based on the protocol established by the █████ Laboratory (i.e. Dr. █████ and Prof. █████) in Lyon^{288–290}. The bacterial cell pellet containing the protein of interest was resuspended in IOV buffer A (1 liter of culture was dissolved in ~20 - 40 mL IOV buffer, **Table 30**) with freshly added DNase (5 µg/µg) and 1 mM DTT and passed through a cell disruptor three times at 1.24 kbar. The cell debris (unbroken cells) were removed by a low centrifugation step of the samples at 15000 xg for 30 min at 4°C. The supernatant from the low centrifugation step was then spin down by an ultracentrifugation step at 150000 xg for 1 h at 4°C. The membrane pellet (IOVs) after ultracentrifugation was resuspended in IOV buffer B (**Table 30**) and ultracentrifuged (150000 xg, 1 h 30 min, 4°C) again. After homogenization of the membrane pellet in IOV homogenization buffer (**Table 30**) the suspension of membranes was frozen in liquid nitrogen and stored at – 80°C. Protein quantification was carried out with a BCA assay (**8. Quantitative protein determination**). Protein overexpression and purity was checked by SDS-PAGE (**10.1. SDS-Polyacrylamide gel electrophoresis (SDS-PAGE), 12% gel**).

6.4. Solubilization and purification of full-length BmrA

The protocol for solubilizing and purifying full-length BmrA (constructs based on p427, **Table 22**) was kindly provided by Dr. [REDACTED] and Prof. [REDACTED], Lyon^{288–290}. For solubilization of the membrane proteins in the detergent lauryl maltose neopentyl glycol (LMNG), the IOVs were diluted with solubilization buffer (**Table 30**) containing 1% LMNG to 2mg/mL. The solubilization was performed for 1 h at 4°C. Solubilized membrane proteins were collected in the supernatant after ultracentrifugation (150000 xg, 1 h, 4°C). Subsequently, the supernatant was incubated with Ni²⁺-NTA resin for 1 h 30 min at 4°C. The resin was transferred to a column and then washed with wash buffer A (20 CV, **Table 30**) and wash buffer B (2 CV, **Table 30**). Elution was performed with elution buffer (6 – 8 CV, **Table 30**). Samples with high protein concentration were dialyzed (Cut off 12-14 kDa) in dialysis buffer (**Table 30**) at 4°C overnight. For some samples size exclusion runs with SEC buffer (**Table 30**) over a Superdex 200 10/ 300 GL (GE Healthcare, Chicago, USA) were performed after Ni²⁺-NTA column. Proteins were flash frozen in liquid nitrogen and stored in – 80°C after Ni²⁺-NTA column or SEC run. Concentration of the purified membrane protein was determined by measuring absorption at 280 nm and Bradford assay (**8. Quantitative protein determination**). Membrane protein quality control was done by SDS-PAGE (**10.1. SDS-Polyacrylamide gel electrophoresis (SDS-PAGE), 12% gel**).

Table 30: Buffer compositions for BmrA IOV preparation and membrane protein purification

| IOV buffer A | IOV buffer B | IOV Homogenization buffer | | | |
|---|--|--|---|---|---|
| 50 mM Tris-Cl pH 8.0 0.5 mM MgCl ₂ | 50 mM Tris-Cl pH 8.0 1.5 mM K-EDTA | 20 mM Tris-Cl pH 8.0 1 mM K-EDTA 300 mM Sucrose | | | |
| Solubilization Buffer | Ni ²⁺ -NTA Equilibration buffer | Wash buffer A | Wash buffer B | Elution buffer | Dialysis/ SEC buffer/ NMR buffer |
| 100 mM NaPi pH8.0 100 mM NaCl 10 mM Imidazole 15% Glycerol 1% LMNG 1 mM DTT | 50 mM NaPi pH8.0 100 mM NaCl 10 mM Imidazole 15% Glycerol 0.01% LMNG | 50 mM NaPi pH8.0 100 mM NaCl 20 mM Imidazole 15% Glycerol 0.01% LMNG | 50 mM NaPi pH8.0 100 mM NaCl 40 mM Imidazole 15% Glycerol 0.01% LMNG | 50 mM NaPi pH8.0 100 mM NaCl 250 mM Imidazole 15% Glycerol 0.01% LMNG | 50 mM Tris-Cl pH8.0 100 mM NaCl 10% Glycerol 0.01% LMNG |

7. PURIFICATION OF TEV PROTEASE

A bacterial cell pellet containing TEV protease was resuspended in lysis buffer (~1 L culture of was dissolved in ~50 mL of lysis buffer, **Table 31**) with freshly added DNase, RNase and lysozyme, half tablet of protease inhibitor and 10 mM MgCl₂ and incubated at 4°C for 30 min. The cell suspension was then sonified (3 – 4 cycles for 60 s, 60% power, 4°C). After centrifugation (30 min at 7000 xg and 4°C) of the cell suspension, the supernatant containing the soluble His₆-TEV protease was transferred to a Ni²⁺-NTA column, which was pre-equilibrated with buffer A (**Table 31**). Subsequently, the Ni²⁺-NTA column was washed with buffer A (6 CV, **Table 31**) and wash buffer (20 CV, **Table 31**). Finally, the soluble His₆-TEV protease was eluted with 4 CV buffer B, containing 500 mM imidazole (**Table 31**). Elution fractions containing His₆-TEV protease were dialyzed in dialysis buffer (**Table 31**) overnight at 4°C to remove the imidazole. After dialysis, glycerol was added to a final volume of 50% v/v. The protein was aliquoted, frozen in liquid nitrogen and stored at – 80°C. Protein concentration was determined by absorption at 280 nm (**8. Quantitative protein determination**) and protein purity was

analyzed by performing an SDS-PAGE (**10.1. SDS-Polyacrylamide gel electrophoresis (SDS-PAGE), 12 - 15% gel**).

Table 31: Buffer compositions for TEV protease purification

| Lysis buffer | Ni²⁺-NTA Buffer A | Wash buffer | Buffer B | Dialysis/Storage buffer* |
|-------------------------|-------------------------------------|-------------------------|-------------------------|---------------------------------|
| 25 mM Tris-Cl pH 7.8 | See lysis buffer | 25 mM Tris-Cl pH 7.8 | 25 mM Tris-Cl pH 7.8 | 25 mM Tris-Cl pH 8.0 |
| 400 mM NaCl | | 400 mM NaCl | 400 mM NaCl | 400 mM NaCl |
| 25 mM Imidazole | | 70 mM Imidazole | 500 mM Imidazole | 0.5 mM EDTA |
| 1 mM DTT | | 1 mM DTT | 1 mM DTT | 1 mM DTT |

* For storage 50% glycerol were added to the storage buffer

8. QUANTITATIVE PROTEIN DETERMINATION

For protein quantification four different methods were applied.

- Absorption measurement at 280 nm using a NanoDrop 2000c UV-Vis spectrophotometer (Thermo Fisher Scientific, Waltham, USA). To determine the protein concentration via the Lambert-Beer law, the calculated extinction coefficient for each protein construct (3. Properties of purified proteins) has been used.
- Colorimetric detergent compatible (DC)TM assay (BioRad Laboratories GmbH, Hercules, USA). Absorption of 750 nm was measured. This method was applied to the full-length proteins (i.e. MsbA and BmrA) studied in this thesis.
- Colorimetric bicinchoninic Acid (BCA) assay (Thermo Fisher Scientific, Waltham, USA) where absorption of 562 nm was measured to determine the protein concentration.
- Colorimetric Bradford assay (Thermo Fisher Scientific, Waltham, USA). Absorption of 595 nm was measured to determine the protein concentration.

Reactions of DC, BCA and Bradford assay are based on the well documented Lowry assay²⁹¹.

9. RECONSTITUTION OF MEMBRANE PROTEINS INTO LIPOSOMES

The protocol for reconstituting full-length BmrA (constructs based on p427, **Table 22**) into liposomes was kindly provided by Dr. [REDACTED] and Prof. [REDACTED], Lyon²⁸⁹.

Preparation of BioBeads SM-2

BioBeads SM-2 (**Table 5**) were washed with methanol and subsequently washed extensively with water. The hydrated Biobeads were stored in H₂O at 4°C until used for detergent removal.

Reconstitution of membrane proteins into liposomes

Liposomes made from *E. coli* total lipid extract were prepared in a molar ratio of approximately 3300/1 lipid to full-length BmrA. Before mixing the lipids with detergent-solubilized protein, *E. coli* total lipid extract (25 mg/ mL in water) was stirred with 2% DDM (v/v) at RT in a 2 mL reaction tube. After 45 min 100 µg of full-length BmrA solubilized in 0.01% LMNG was added into a total volume of 500 µL. This mixture was incubated in a 2 mL reaction tube and gently stirred for 45 min at RT. The DDM concentration was always kept above the critical micelle concentration (CMC) for the detergent (CMC_{DDM} = 12 mM). Finally, 120 mg of hydrated Biobeads SM-2 were added in three installments of 40 mg each. After addition, the sample was incubated for 1 h at RT (i.e. total incubation time was 3 h). The supernatant containing proteoliposomes was transferred to a fresh reaction tube and used immediately or stored at 4°C.

10. BIOPHYSICAL CHARACTERIZATION OF RECOMBINANT PROTEINS

10.1. SDS-Polyacrylamide gel electrophoresis (SDS-PAGE)

Denaturing protein gel electrophoresis was carried out using the Mini-PROTEAN Tetra cell (BioRad Laboratories GmbH, Hercules, USA) SDS-PAGE system with the Tris-glycine buffer (also known as Laemmli buffer, SDS running buffer, **Table 33**). Samples were mixed with 4 x SDS loading dye (**Table 33**). 5 – 15 µL of the samples were loaded on a chamber of the gel. Gels run (12% or 15%, **Table 32**) at 80 – 180 V for 1 h 30 min – 3 h. Protein bands in the gels were visualized via staining with Coomassie staining solution 1 or 2 (**Table 33**) and destained with destaining solution 1 or 2 (**Table 33**).

Samples containing bacteria cells were resuspended in 100 µl 4 x SDS and incubated for 10 – 15 min at 95°C before loading them on the gel.

Table 32: Composition of the stacking and running gel to perform 4 gels for SDS-PAGE

| Ingredients | Stacking gel | Running gel | |
|-----------------------------|--------------|-------------|--------|
| | | 12% | 15% |
| ddH ₂ O | 4.6 mL | 6.6 mL | 4.6 mL |
| 1.5 mM Tris-Cl pH 8.8 | - | 5 mL | 5 mL |
| 1 mM Tris-Cl pH 6.8 | 0.63 mL | - | - |
| Acrylamid/ Bisacrylamid 30% | 0.83 mL | 8 mL | 10 mL |
| SDS 10% (w/v) | 50 µL | 200 µL | 200 µL |
| APS 10% (w/v) | 50 µL | 200 µL | 200 µL |
| TEMED | 5 µL | 20 µL | 20 µL |

Table 33: Buffers to perform SDS-PAGE

| Buffer | Composition |
|-------------------------------|--|
| SDS loading dye 4x* | 200 mM Tris-Cl pH 6.8, 400 mM DTT, 8% (w/v) SDS, 0.4% (w/v) Bromophenol blue, 40% Glycerol |
| Protein standard | Precision Plus Protein Dual Color Standard (BioRad Laboratories GmbH, Hercules, USA) |
| SDS running buffer 10x | 0.25 M Tris-Cl pH 8.3, 1.92 M Glycerol, 35 mM SDS |
| Coomassie staining solution 1 | 1 g/L Coomassie brilliant blue R250, 10% (v/v) Acetic acid, 40% (v/v) Methanol/ Ethanol |
| Coomassie staining solution 2 | 1 g/L Coomassie brilliant blue R250, 2% (v/v) Phosphoric acid, 40% (v/v) Ethanol |
| Destaining solution 1 | 10% (v/v) Acetic acid |
| Destaining solution 2 | 30% (v/v) Ethanol, 2% (v/v) Phosphoric acid |

* For proteins which build disulfide bridges loading dye with and without DTT was applied.

10.2. Analytical size exclusion chromatography

For analytical size exclusion chromatography, an ENrich™ 70 10 x 300 (BioRad Laboratories GmbH, Hercules, USA) and a Superdex 75 10/300 GL (GE Healthcare, Chicago, USA) column was used. Unless stated differently, NBD constructs (30-40 μ M in 500 μ L) were run isocratically (flow rate 0.8 – 1 mL/min) for 1.1 CV at 4°C over the pre-equilibrated (SEC buffer, **Table 28**) columns. Before loading the constructs on the columns potential aggregates were removed by centrifugation (4790 xg, 10 min at 4°C).

Full-length BmrA constructs (80 μ g) were run over a Superdex 200 10/300 GL, which was pre-equilibrated with SEC buffer containing 0.01% LMNG (**Table 30**).

10.3. CD spectroscopy

Circular dichroism (CD) measurements were carried out on a Jasco-815 CD spectrometer (JASCO EUROPE S.R.L., Pfungstadt). For the measurements, the protein concentration was set to 1.5 – 15 μM in 300 μL and measured in a 1 mm quartz cuvette (Hellma Analytics, Müllheim). Measurements were performed at a spectral range between 190 and 260 nm at 20°C. The scanning interval was set to 1 nm, scanning speed to 50 nm/min, band width to 5 nm and spectra accumulations to 3. From all spectra, the buffer spectral background was subtracted and the measured ellipticity θ (deg) converted to the mean residue ellipticity $\theta_{mrw,\lambda}$ (equation 1).

$$[\theta]_{mrw,\lambda} = \frac{MRW \cdot [\theta]}{10 \cdot c \cdot d} \quad 1$$

θ - Measured ellipticity in deg
 c - concentration in g/mL
 d - pathlength in cm

Mean residue weight (MRW) can be calculated by the following formula: $MRW = \frac{M_w}{N-1}$. M_w corresponds to the molecular weight in Dalton and N to the number of amino acids. For CD spectra analysis and fold recognition, the web program BeStSel^{292,293} (Beta Structure Selection, <http://bestsel.elte.hu/>) was used.

To record melting curves, CD spectra were recorded at wavelengths 208 and 222 nm, where α -helical proteins display two characteristic minima in the CD spectrum. For measurements 1°C/min was set for a heating range from 15°C – 95°C. The melting point T_m is defined as the temperature at which 50% of protein is unfolded. To generate melting temperature curves, the measured ellipticity θ (deg) values for the different temperatures at 208 or 222 nm were plotted against the increasing temperature. In a perfect sigmoidal curve, the inflection point between native state and non-native state then corresponds to the melting temperature (T_m).

10.4. Photoinduced electron transfer – fluorescence correlation spectroscopy (PET-FCS)

Cloning and purification of LmrA, MsbA and BmrA was carried out in the [REDACTED] laboratory, Johannes Gutenberg-university Mainz. PET-FCS labeling, and measurements of the purified constructs were performed by [REDACTED], University of Würzburg^{294,295}. PET-FCS technique allows to study conformational dynamics of biomolecules by recording the quenching of an attached organic fluorophore (AttoOxa11) by an aromatic amino acid (tryptophane) with electron donating properties. A cysteine in the protein is used for fluorophore labeling, typically via a maleimide. PET-FCS uses a single molecule approach, where dynamics between the fluorophore and the quencher (within one nm) in the nanosecond to microsecond timescale can be recorded. The fluorophore enables recording of translational diffusion of the whole molecule and additionally can intra domain diffusions (intra domain dynamics) be recorded due to the quenching of the fluorophore (**Figure 8**).

Briefly information how to analyze the data: Fluorescence fluctuations are analyzed by calculating the autocorrelation function (ACF) i.e. $G(\tau)$ of the recorded fluorescence intensity time trace (equation 2). Under appropriate experimental conditions, constantly emitting fluorescence labels give rise to a stochastic fluctuation of the detector signal as molecules diffuse in and out of the focal volume (detection focus, **Figure 8**). This process results in a decay of the ACF with a characteristic time constant τ_D representing the time constant of molecular diffusion (“Brownian motion”), depending on the size and shape of a molecule as well as its interactions with the environment (**Figure 8**). Equilibrium conformational fluctuations faster than τ_D occur as additional decay in the ACF with the relaxation time constant τ_r (**Figure 8**).

$$G(\tau) = \frac{\langle I(t) \cdot I(t+\tau) \rangle}{I(t)^2} \quad 2$$

$I(t)$ – Fluorescence intensity at time t

$I(t+\tau)$ – Fluorescence intensity after a lag time (τ)

$\langle \rangle$ – denotes the time average over the total observation time

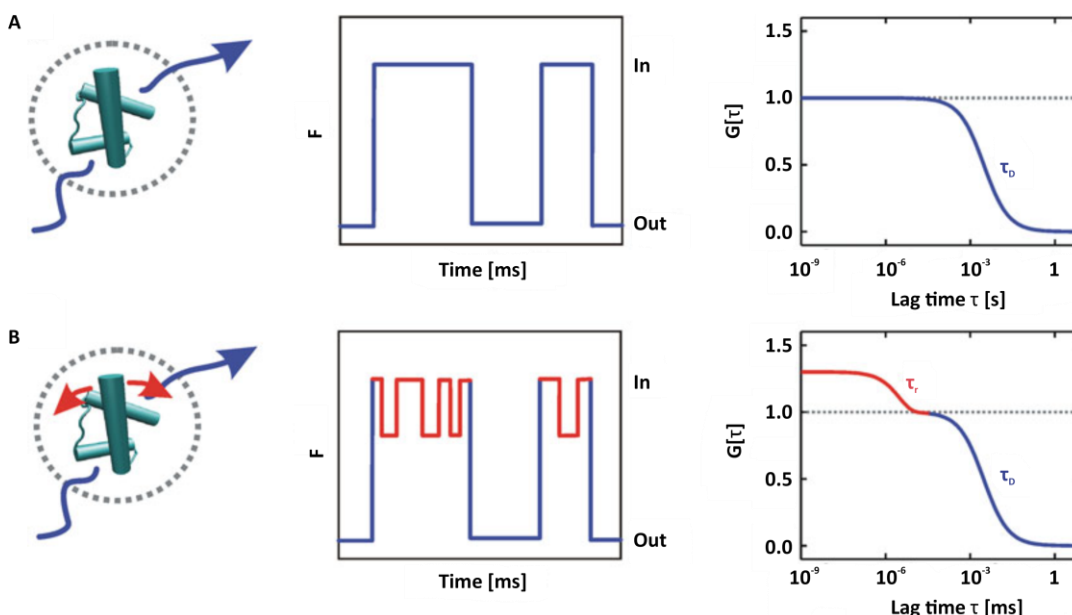


Figure 8: Protein dynamics by PET-FCS measurements (modified from Sauer & Neuweiler, 2014²⁹⁵)

A) Fluorescently labeled protein with constant fluorescence emission. Fluctuations in the fluorescence signal result in a decay of the ACF ($G(\tau)$) with a characteristic time constant of translational diffusion τ_D (blue). **B)** Conformational motions that are faster than τ_D and modulate fluorescence emission result in an additional decay in the ACF with a relaxation time constant τ_r (red). ACF – Autocorrelation function. F – Fluorescence signal. In – Fluorescence signal in the detection focus (focal volume) of the instrument. Out – Fluorescence signal not in the detection focus (focal volume) of the instrument.

11. BIOFUNCTIONAL CHARACTERIZATION OF RECOMBINANT PROTEINS

11.1. ATPase activity assay

The ATPase activities of purified LmrA, MsbA and BmrA constructs were determined by a coupled enzyme assay that uses photometrically NADH^{137,195}. ATPases as LmrA, MsbA or BmrA generate ADP, which is indirectly detected. The first enzyme in this coupled assay, pyruvate kinase, converts ADP back to ATP by transferring phosphoenolpyruvate to pyruvate. Pyruvate is the substrate of the second enzyme, lactate dehydrogenase (LDH), which is converted to lactate by oxidation of NADH to NAD⁺. NADH oxidation by LDH was monitored in the assay by measuring loss of absorbance at 340 nm in an UV-Vis spectrophotometer (Perkin Elmer Lambda 25, Waltham, USA or SAFAS SP2000, Monaco) at 20°C or 37°C over time. Two slightly different ATPase assay protocols were used.

ATPase activity assay protocol 1

Table 34: ATPase activity assay protocol 1 performed in ██████████ laboratory

Buffer components for a total volume of 200 μ L. The assay was carried out in a disposable UV cuvette (BrandTM, Wertheim und Grossostheim).

| Components | Applied for the ATPase assay (200 μ L) |
|---|---|
| 20 mM L-Ascorbic acid | 1 mM |
| 100 mM ATP pH 7.0* ^a | 1 mM |
| 60 mM Phosphoenolpyruvate* ^a | 3 mM |
| 12 mM NADH | 0.21 mM |
| 20 mM MgCl ₂ | 1 mM |
| PK/ LDH mix* ^b | 3.5 μ L |
| Protein or buffer* ^c | as desired for different concentrations LmrA-NBD constructs: 400 μ g MsbA-NBD constructs: 400 μ g BmrA-NBD constructs: 400 μ g Full-length MsbA 3 μ g, 13 – 180 μ g Full-length BmrA 3 μ g |

* *a* - ATP was not added when the positive control was performed. ADP was added instead.

b - 600 – 1000 unit/mL of pyruvate kinase and 900 – 1400 unit/mL of lactate dehydrogenase.

c - Appropriate buffer as negative control for the appropriate protein was used. Buffer control was applied as autozero.

All components except of ATP or ADP were mixed in a disposable UV cuvette (BrandTM, Wertheim und Grossostheim) and absorbance at 340 nm was measured (**Table 34**). After 1 min, ATP was added to the ongoing measurement which was run for another 7 – 240 minutes.

ATPase activity assay protocol 2

This protocol was kindly provided by Dr. [REDACTED] and Prof. [REDACTED] from Lyon¹⁹⁵.

Table 35: ATPase activity assay protocol performed in [REDACTED] laboratory, Lyon
Buffer components for a total volume of 700 μ L. The assay was carried out in an UV cuvette (Hellma Analytics, Müllheim).

| Components | Applied within the ATPase assay (700 μ L) |
|--------------------------------|--|
| 1 M Hepes KOH pH 8.0 | 50 mM |
| 1 M MgCl ₂ | 10 mM |
| 200 mM Phosphoenolpyruvate | 4 mM |
| 10 mg/mL Lactate dehydrogenase | 32 μ g/mL |
| 10 mg/mL Pyruvate kinase | 60 μ g/mL |
| 300 mM NADH | 0.3 mM |
| 10% LMNG | 0.01% LMNG |
| ATP pH 7.0 | 10 mM |
| Protein or buffer* | 3 μ g |

*a - Appropriate buffer as negative control for each protein was used.

All components except LMNG, ATP and purified protein were mixed and added to an UV cuvette (**Table 35**). LMNG and ATP was added to the cuvettes and after incubation of 5 min at RT the purified protein was added and measurement of absorbance at 340 nm initiated. Measurements were performed for 15 minutes. For stimulated ATPase activity measurements 15 μ M Reserpine or 2 μ M Hoechst 33342 were added.

Calculation and representation of ATPase activity assays

$$ATPase\ activity = \frac{(s_{prot} - s_{cont}) \cdot \frac{V}{\epsilon_{NADH} \cdot l}}{m_{prot}} = \frac{s_{cor} \cdot NADH_{const}}{m_{prot}} \quad 3$$

s_{prot} – slope of measurement at 340 nm with protein
 s_{cont} – slope of measurement at 340 nm with buffer
 V_{NADH} – total volume
 ϵ_{NADH} – extinction coefficient of NADH = 6220 1/(M·cm)
 l – optical path length
 m_{prot} – protein mass
 s_{cor} – slope corrected with buffer control

The ATPase activity was calculated as in equation 3. Due to its low activity, the values for the LmrA-NBD ATPase activity are shown in a table where absorption of NADH at 340 nm is compared at specific time points after addition of ATP.

11.2. Fluorescence drug transport assay

Table 36: Fluorescence drug transport assay protocol for the substrate Hoechst 33342 or Doxorubicin performed in [REDACTED] laboratory, Lyon. Buffer components for a total volume of 1 mL. The assay was carried out in an UV Cuvette (Hellma Analytics, Müllheim).

| Components | Amounts applied for the ATPase assay |
|--|--|
| 50 mM Hepes KOH pH 8.0, 8.5 mM NaCl | 50 mM Hepes KOH pH 8.0, 8.5 mM NaCl |
| 200 mM Phosphoenolpyruvate | 4 mM |
| 10 mg/mL Pyruvate kinase | 60 µg |
| 1 M MgCl ₂ | 2 mM |
| IOVs | 100 – 200 µg |
| 1 mM Hoechst 33342 | 2 µM |
| 2 mM Doxorubicin hydrochloride | 10 µM |
| ATP pH 7.0 | 2 mM |

Transport of a fluorescence active drug (Doxorubicin or Hoechst 33342) by an ABC transporter in IOVs was analyzed via fluorescence spectroscopy¹³⁷. In a cuvette (Hellma Analytics, Müllheim) all components (**Table 36**) except the drug and ATP were pre-mixed. After 125 s, the fluorescence active drug was added and after 250 s ATP initiated the transport reaction. Measurements were performed for 600 – 700 s at 25°C. For Doxorubicin excitation wavelength was 480 nm and emission wavelength 590 nm. For Hoechst 33342 excitation wavelength was 355 nm and emission wavelength 457 nm.

12. NMR TECHNIQUES

General information

Influences by ligand interaction and mutations can be analyzed via NMR spectroscopy. In addition to structural information dynamic, kinetic and thermodynamic properties caused by protein-ligand interaction and/ or by protein mutagenesis are observable with NMR.

In this thesis chemical shift perturbation and changes in line widths were measured through ^1H - ^{15}N HSQC spectra. In addition, H/D exchange and $\{^1\text{H}\}$, ^{15}N hetNOE measurements were carried out.

All NMR measurements were carried out with help from Prof. Dr. [REDACTED], Dr. [REDACTED], Dr. [REDACTED], Dr. [REDACTED] or [REDACTED] (members of [REDACTED] laboratory, Goethe university of Frankfurt) and Prof. Dr. [REDACTED].

12.1. NMR sample preparation

All NMR samples were prepared with isotope-labeled proteins and 10 % v/v D_2O as the lock substance. The protein concentration of the samples was between 150 – 450 μM in a 500 μL standard NMR-sample tube for Heteronuclear Single Quantum Coherence (HSQC), H/D exchange or heteronuclear Overhauser effect (hetNOE) spectra. For referencing, 50 μM 4,4-dimethyl-4-silapentane-1-sulfonic acid (DSS) was added to the NMR samples. For 1D ^{19}F NMR measurements, the protein concentration of the sample ranged from 100 to 250 μM . For ^{19}F chemical shift referencing, 3-bromo-1,1,1-trifluoroacetone (BTFA) was used.

12.2. NMR experiments: spectrometer, parameters and spectra analysis

All experiments were carried out on Bruker AVANCE NMR spectrometers with field strengths of 599, 600, 700, 800 and 900 MHz equipped with cryogenic triple resonance probes. Standard Bruker pulse sequences used for recording the spectra are listed from **Table 37** to **Table 43**.

NMR spectra were recorded at 298 K for LmrA, MsbA and BmrA constructs (**Table 37** - **Table 43**). NMR spectra were processed by Bruker TopSpinTM 2.1, 3.2 or 4.0.8 (Bruker, Karlsruhe) and analyzed with CARA²⁹⁶.

12.3. Pulse sequence information of NMR experiments

Standard Bruker pulse sequences were applied. In addition to the mentioned pulse sequences in the following tables `zgpr` was used to record 1D ^1H NMR spectra of LmrA, MsbA and BmrA. All spectra of LmrA-NBD were recorded in 50 mM BisTris pH 6.5, 50 mM NaCl with 10% D_2O . For MsbA-NBD and BmrA-NBD 50 mM BisTris pH 7.0, 50 mM NaCl with 10% D_2O was used. Full-length BmrA spectra were measured in 50 mM Tris pH 7.0, 100 mM NaCl, 0.01% LMNG, 10% glycerol with 10% D_2O . For referencing 50 μM DSS was added to the samples.

Table 37: LmrA-NBD samples used for backbone chemical shift assignment experiments in the ADP-bound state (10 mM ADP)

Conc – concentration, Freq – spectrometer frequency, ns – number of scans, d1 – relaxation delay, TD – size of FID, SW – spectral width

| Sample/ labeling | Conc [μM] | NMR experiment type | Bruker pulse sequence | Freq [MHz] | ns | d1 [s] | ^1H | | | ^{15}N | | | ^{13}C | | |
|--|---------------------------|----------------------------|--------------------------|---------------|----|-----------|--------------|--------------|---------------|-----------------|-----------|--------------|-----------------|-------------|----|
| | | | | | | | TD | off [ppm] | set [ppm] | SW [ppm] | TD | off [ppm] | set [ppm] | SW [ppm] | TD |
| LmrA-NBD D518A/ $^2\text{H}^{15}\text{N}^{13}\text{C}$ | ~ 400 | ^{15}N TROSY-HSQC | trocyf3gppsi19.2 | 800 | 8 | 1.0 - 1.2 | 2048 | 4.698 | 17.95 - 18 | 96, 256 | 117.5 | 37 - 38 | | | |
| | | TROSY-HNCACB | trhncacbgp2h3d | 800 | 16 | 1.0 | 2048 | 4.698 | 17.95 | 64 | 117.5 | 37 | 192 | 38.998 | 71 |
| LmrA-NBD Q430A/ $^2\text{H}^{15}\text{N}^{13}\text{C}$ | ~ 265 | ^{15}N TROSY-HSQC | trocyf3gppsi19.2 | 800 | 4 | 1.2 | 2048 | 4.698 | 17.95 | 192 | 117.5 | 37 | | | |
| | | TROSY-HNCACB | trhncacbgp2h3d | 800 | 16 | 1.0 | 2048 | 4.698 | 17.95 | 64 | 117.5 | 37 | 188 | 38.998 | 71 |
| LmrA-NBD H543A/ $^2\text{H}^{15}\text{N}^{13}\text{C}$ | ~ 300 | ^{15}N TROSY-HSQC | trocyf3gppsi19.2 | 800 | 8 | 1.0 | 2048 | 4.699 | 16 | 256 | 117.5/118 | 38 | | | |
| | | TROSY-HNCACB | trhncacbgp2h3d | 800 | 8 | 1.2 | 2048 | 4.699 | 16 | 96 | 118 | 39 | 204 | 39 | 71 |

Table 38: NMR parameters for LmrA-NBD and MsbA-NBD measurements used for NMR titration experiments (ADP, ATP and addition of magnesium)

Conc – concentration, Freq – spectrometer frequency, ns – number of scans, d1 – relaxation delay, TD – size of FID, SW – spectral width

| Sample/ labeling | Conc [μ M] | NMR experiment type | Bruker pulse sequence | Freq [MHz] | ns | d1 [s] | ^1H | | | ^{15}N | | |
|------------------------------------|--------------------|----------------------------|--------------------------|---------------|----|--------|--------------|--------------|--------------|-----------------|-------|--------------|
| | | | | | | | TD | off [ppm] | set [ppm] | SW [ppm] | TD | off [ppm] |
| LmrA-NBD | ~ 200 | ^{15}N TROSY-HSQC | trocyf3gppsi19.2 | 800 | 8 | 1.2 | 2048 | 4.695 | 17.95 | 256 | 117.5 | 37 |
| D518A/ ^{15}N | ~ 195 | ^{15}N TROSY-HSQC | trocyf3gppsi19.2 | 700 | 4 | 1.0 | 2048 | 4.698 | 16 | 256 | 118 | 40 |
| LmrA-NBD | ~ 180 | ^{15}N TROSY-HSQC | trocyf3gppsi19.2 | 600 | 8 | 1.0 | 2048 | 4.7 | 18 | 200 | 118 | 38 |
| Q430A/ ^{15}N | ~ 195 | ^{15}N TROSY-HSQC | trocyf3gppsi19.2 | 599 | 8 | 1.0 | 2048 | 4.697 | 16 | 200 | 118 | 42 |
| LmrA-NBD H543A/ ^{15}N | ~ 200 | ^{15}N TROSY-HSQC | trocyf3gppsi19.2 | 600 | 8 | 1.0 | 2048 | 4.7 | 16 | 200 | 118 | 39 |
| LmrA-NBD | ~ 180 | ^{15}N TROSY-HSQC | trocyf3gppsi19.2 | 800 | 8 | 1.0 | 2048 | 4.7 | 14 | 200 | 118 | 38 |
| SALD/ ^{15}N | ~ 180 | ^{15}N TROSY-HSQC | trocyf3gppsi19.2 | 800 | 8 | 1.0 | 2048 | 4.7 | 16 | 200 | 118 | 40 |
| LmrA-NBD | ~ 300 | ^{15}N TROSY-HSQC | trocyf3gppsi19.2 | 599 | 4 | 1.0 | 2048 | 4.695 | 18.12 | 200 | 118 | 39 |
| SSLD/ ^{15}N | ~ 300 | ^{15}N TROSY-HSQC | trocyf3gppsi19.2 | 600 | 4 | 1.0 | 2048 | 4.698 | 18 | 200 | 117.5 | 37 |
| LmrA-NBD K486A/ ^{15}N | ~ 195 | ^{15}N TROSY-HSQC | trocyf3gppsi19.2 | 599 | 8 | 1.0 | 2048 | 4.69 | 16 | 200 | 118 | 38 |
| LmrA-NBD K388A/ ^{15}N | ~ 280 | ^{15}N TROSY-HSQC | trocyf3gppsi19.2 | 599 | 4 | 1.0 | 2048 | 4.695 | 18.12 | 200 | 118 | 39 |
| LmrA-NBD | ~ 156 | ^{15}N TROSY-HSQC | trocyf3gppsi19.2 | 600 | 8 | 1.0 | 2048 | 4.696 | 16 | 200 | 118.5 | 37 |
| WT/ $^2\text{H}^{15}\text{N}$ | ~ 156 | ^{15}N TROSY-HSQC | trocyf3gppsi19.2 | 600 | 8 | 1.0 | 2048 | 4.7 | 16 | 256 | 118.5 | 37 |
| MsbA-NBD | ~ 250 | ^{15}N TROSY-HSQC | trocyf3gppsi19.2 | 599 | 8 | 1.0 | 2048 | 4.7 | 16 | 200 | 117 | 36 |
| WT/ ^{15}N | ~ 250 | ^{15}N TROSY-HSQC | trocyf3gppsi19.2 | 599 | 8 | 1.0 | 2048 | 4.7 | 16 | 200 | 117 | 37 |

Table 39: NMR parameters for LmrA-NBD NMR experiments to analyze backbone dynamics

Conc – concentration, Freq – spectrometer frequency, ns – number of scans, d1 – relaxation delay, TD – size of FID, SW – spectral width

| Sample/ labeling | Conc [μ M] | NMR experiment type | Bruker pulse sequence | Freq [MHz] | ns | d1 [s] | ^1H | | | ^{15}N | | |
|--|--------------------|----------------------------|--------------------------|---------------|----|--------|--------------|--------------|--------------|-----------------|-------|--------------|
| | | | | | | | TD | off [ppm] | set [ppm] | SW [ppm] | TD | off [ppm] |
| LmrA-NBD D518A/ $^2\text{H}^{15}\text{N}$ | ~ 210 | ^{15}N HetNOE | 15Nhetnoe7.jf | 600 | 64 | 1.0 | 2048 | 4.699 | 18 | 200 | 118 | 40 |
| LmrA-NBD Q430A/ $^2\text{H}^{15}\text{N}$ | ~ 210 | ^{15}N HetNOE | 15Nhetnoe7.jf | 600 | 64 | 3.0 | 2048 | 4.699 | 18 | 184 | 118 | 40 |
| LmrA-NBD H543A/ $^2\text{H}^{15}\text{N}$ | ~ 220 | ^{15}N HetNOE | 15Nhetnoe7.jf | 599 | 64 | 3.0 | 2048 | 4.699 | 16 | 232 | 118 | 38 |
| LmrA-NBD WT/ $^2\text{H}^{15}\text{N}$ | ~ 210 | ^{15}N HetNOE | 15Nhetnoe7.jf | 600 | 64 | 3.0 | 2048 | 4.7 | 18 | 184 | 118 | 40 |
| LmrA-NBD WT/ $^2\text{H}^{15}\text{N}$ | ~ 300 | ^{15}N HetNOE | trnoetf3gpsi3d.3 | 599 | 32 | 1.0 | 2048 | 4.695 | 18.1 | 200 | 117.5 | 38 |
| NMR measurements performed for H/D exchange experiments | | | | | | | | | | | | |
| LmrA-NBD WT/ $^2\text{H}^{15}\text{N}$ | ~ 200 | ^{15}N TROSY-HSQC | trosyf3gppsi19.2 | 800 | 8 | 1.2 | 2048 | 4.7 | 16 | 200 | 118 | 38 |

Table 40: NMR parameters for MsbA-NBD WT used for backbone chemical shift assignment experiments in the ADP-bound state (10 mM ADP) and to measure the apo state
Conc – concentration, Freq – spectrometer frequency, ns – number of scans, d1 – relaxation delay, TD – size of FID, SW – spectral width

| Sample/ labeling | Conc [μ M] | NMR experiment type | Bruker pulse sequence | Freq [MHz] | ns | d1 [s] | ^1H | | | ^{15}N | | | ^{13}C | | |
|--|--------------------|----------------------------|--------------------------|---------------|-----|--------|--------------|--------------|--------------|-----------------|-------|--------------|-----------------|-------------|----|
| | | | | | | | TD | off [ppm] | set [ppm] | SW [ppm] | TD | off [ppm] | set [ppm] | SW [ppm] | TD |
| $^2\text{H}^{15}\text{N}^{13}\text{C}$ | ~ 240 | ^{15}N TROSY-HSQC | trocyf3gppsi19.2 | 800 | 8 | 1.0 | 2048 | 4.695 | 18. | 256 | 116.5 | 37 | | | |
| | | TROSY-HN(CA)CO | trhncacogp2h3d | 900 | 16 | 1.0 | 2048 | 4.699 | 16.3 | 88 | 116 | 36 | 128 | 175 | 22 |
| | ~ 220 | TROSY-HN(CA)CO | trhncacogp2h3d | 600 | 16 | 1.2 | 2048 | 4.7 | 22 | 80 | 116.5 | 33 | 80 | 175 | 20 |
| | | TROSY-HNCACB | trhncacogp2h3d | 900 | 16 | 1.2 | 2048 | 4.693 | 17.9 | 72 | 115.5 | 35 | 200 | 40 | 70 |
| | | TROSY-HNCO | trhncogp2h3d | 800 | 4 | 1.0 | 2048 | 4.695 | 18 | 96 | 116 | 36 | 96 | 174 | 18 |
| | | TROSY-HNCA | trhncagp2h3d2 | 800 | 8 | 1.0 | 2048 | 4.695 | 18 | 88 | 116 | 36 | 128 | 54 | 40 |
| ^{15}N | ~ 250 | ^{15}N TROSY-HSQC | trocyf3gppsi19.2 | 599 | 8 | 1.0 | 2048 | 4.7 | 16 | 200 | 117.0 | 37 | | | |
| ^{15}N -Tyr | ~ 400 | ^{15}N HSQC | fhsqcf3gpiph | 800 | 4 | 1.0 | 2048 | 4.698 | 16 | 200 | 119 | 28 | | | |
| ^{15}N -Phe | ~ 210 | ^{15}N TROSY-HSQC | trocyf3gppsi19.2 | 800 | 32 | 1.0 | 2048 | 4.703 | 16 | 80 | 121.5 | 19 | | | |
| ^{15}N -Leu | ~ 500 | ^{15}N TROSY-HSQC | trocyf3gppsi19.2 | 800 | 32 | 1.0 | 2048 | 4.703 | 16 | 80 | 117.5 | 35 | | | |
| ^{15}N -Val | ~ 250 | ^{15}N TROSY-HSQC | trocyf3gppsi19.2 | 800 | 32 | 1.0 | 2048 | 4.703 | 16 | 80 | 120 | 30 | | | |
| ^{15}N -Ile | ~ 160 | ^{15}N TROSY-HSQC | trocyf3gppsi19.2 | 800 | 224 | 1.0 | 2048 | 4.703 | 16 | 208 | 117.5 | 35 | | | |
| $^{13}\text{C}^{15}\text{N}$ Pro | ~ 160 | ^{15}N TROSY-HSQC | trocyf3gppsi19.2 | 599 | 128 | 1.0 | 2048 | 4.697 | 19.8 | 200 | 117 | 35 | | | |
| ^{15}N -Lys | ~ 390 | ^{15}N TROSY-HSQC | trocyf3gppsi19.2 | 800 | 8 | 1.0 | 2048 | 4.695 | 18 | 96 | 122.5 | 25 | | | |
| ^{15}N -Arg | ~ 220 | ^{15}N TROSY-HSQC | trocyf3gppsi19.2 | 900 | 8 | 1.0 | 2048 | 4.699 | 16.3 | 200 | 116 | 36 | | | |
| ^{15}N -Ser/Gly | ~ 200 | ^{15}N HSQC | fhsqcf3gpiph | 700 | 8 | 1.0 | 2048 | 4.697 | 15.9 | 96 | 112 | 28 | | | |

Table 41: NMR parameters for BmrA-NBD WT used for backbone chemical shift assignment experiments in the ADP-bound state (10 mM ADP) and to measure the apo state
Conc – concentration, Freq – spectrometer frequency, ns – number of scans, d1 – relaxation delay, TD – size of FID, SW – spectral width

| Sample/ labeling | Conc [μ M] | NMR experiment type | Bruker pulse sequence | Freq [MHz] | ns | d1 [s] | ^1H | | | ^{15}N | | | ^{13}C | | |
|--|--------------------|----------------------------|--------------------------|---------------|----|--------|--------------|--------------|--------------|-----------------|-------|--------------|-----------------|-------------|----|
| | | | | | | | TD | off [ppm] | set [ppm] | SW [ppm] | TD | off [ppm] | set [ppm] | SW [ppm] | TD |
| $^2\text{H}^{15}\text{N}^{13}\text{C}$ | ~ 250 | ^{15}N TROSY-HSQC | trocyf3gppsi19.2 | 599 | 4 | 1.0 | 2048 | 4.697 | 18 | 200 | 118 | 32 | | | |
| | | TROSY HNCO | b_trhncogp3d.2 | 599 | 8 | 0.2 | 1024 | 4.697 | 16 | 128 | 118 | 32 | 130 | 174 | 14 |
| | | TROSY HNCO | trhncogp3d | 599 | 8 | 1.0 | 2048 | 4.697 | 18 | 84 | 118 | 32 | 96 | 173.5 | 14 |
| | | TROSY HNCACO | trhncacogp3d | 599 | 8 | 1.0 | 2048 | 4.697 | 18 | 84 | 118 | 32 | 72 | 173.5 | 14 |
| | | TROSY HNCA | trhncagp2h3d2 | 900 | 8 | 1.0 | 2048 | 4.699 | 17.9 | 88 | 118 | 30 | 128 | 53.2 | 40 |
| | | TROSY HNCOCACB | trhncocacbgp2h3d | 900 | 8 | 1.0 | 2048 | 4.699 | 17.9 | 84 | 118 | 30 | 160 | 43 | 74 |
| | | TROSY HNCACB | trhncacbgp2h3d | 900 | 8 | 1.0 | 2048 | 4.699 | 17.9 | 96 | 118 | 30 | 164 | 43 | 74 |
| ^{15}N -Arg | ~ 225 | ^{15}N TROSY-HSQC | b_trocyetf3gpsi.2 | 800 | 4 | 0.2 | 2048 | 4.698 | 15 | 256 | 116.5 | 33 | | | |
| ^{15}N -Trp | ~ 220 | ^{15}N TROSY-HSQC | b_trocyetf3gpsi.2 | 800 | 4 | 0.2 | 2048 | 4.698 | 15 | 256 | 116.5 | 33 | | | |
| ^{15}N -Tyr | ~ 380 | ^{15}N TROSY-HSQC | b_trocyetf3gpsi.2 | 800 | 4 | 0.2 | 2048 | 4.7 | 15 | 256 | 116.5 | 33 | | | |
| ^{15}N -Phe | ~ 440 | ^{15}N TROSY-HSQC | b_trocyetf3gpsi.2 | 800 | 4 | 0.2 | 2048 | 4.7 | 15 | 256 | 116.5 | 33 | | | |
| ^{15}N -Val | ~ 440 | ^{15}N TROSY-HSQC | b_trocyetf3gpsi.2 | 800 | 4 | 0.2 | 2048 | 4.7 | 15 | 256 | 116.5 | 33 | | | |
| ^{15}N -Lys | ~ 225 | ^{15}N TROSY-HSQC | b_trocyetf3gpsi.2 | 800 | 4 | 0.2 | 2048 | 4.697 | 15 | 256 | 116.5 | 33 | | | |
| ^{15}N -Ile | | | | | | | | | | | | | | | |
| $^{13}\text{C}^{15}\text{N}$ -Pro | ~275 | ^{15}N TROSY-HSQC | trocyf3gppsi19.2 | 599 | 48 | 1.0 | 2048 | 4.698 | 16 | 96 | 124 | 22 | | | |
| ^{15}N -Leu | ~487 | ^{15}N TROSY-HSQC | trocyf3gppsi19.2 | 599 | 8 | 1.0 | 2048 | 4.698 | 16 | 96 | 123 | 18 | | | |
| ^{15}N -Ser/Gly | ~420 | ^{15}N HSQC | hsqcfpf3gpiphwg | 600 | 8 | 1.0 | 2048 | 4.699 | 16 | 256 | 118 | 36 | | | |
| ^{15}N -Gly | ~486 | ^{15}N HSQC | hsqcfpf3gpiphwg | 600 | 8 | 1.0 | 2048 | 4.699 | 16 | 256 | 118 | 36 | | | |

Table 42: NMR parameters for LmrA-NBD 1D ¹⁹F NMR experiments

| Sample/ labeling | Conc [μM] | NMR experiment type | Bruker pulse sequence | Freq [MHz] | ns | d1 [s] | ¹⁹ F | | |
|---|--------------|---------------------|--------------------------|---------------|------|--------|-----------------|--------------|--------------|
| | | | | | | | TD | off [ppm] | set [ppm] |
| LmrA-NBD W421F/ ¹⁹ F Trp | ~ 100 | 1D NMR | zgT2.ed | 564.7 | 1024 | 1.0 | 4096 | -110 | 100.62 |
| LmrA-NBD W457F/ ¹⁹ F Trp | ~ 120 | 1D NMR | zgT2.ed | 564.7 | 1024 | 1.0 | 4096 | -110 | 100.62 |
| LmrA-NBD WT/ ¹⁹ F Trp | ~ 240 | 1D NMR | zgT2.ed | 564.7 | 512 | 1.0 | 32768 | -120 | 100.62 |
| LmrA-NBD WT/ ¹⁹ F Trp | ~ 270 | 1D NMR | zgT2.ed | 564.7 | 128 | 1.0 | 4096 | -110 | 245.97 |

Table 43: NMR parameters for BmrA 1D ¹⁹F NMR experiments

| Sample/ labeling | Conc [μM] | NMR experiment type | Bruker pulse sequence | Freq [MHz] | ns | d1 [s] | ¹⁹ F | | |
|---|--------------|---------------------|--------------------------|---------------|---------------|--------|-----------------|--------------|--------------|
| | | | | | | | TD | off [ppm] | set [ppm] |
| BmrA-NBD/ ¹⁹ F Trp | ~ 210 | 1D NMR | zgT2.ed | 564.7 | 1024 | 1.0 | 32768 | -120 | 201.25 |
| | | 1D NMR | zgT2.ed | 564.7 | 1024 | 1.0 | 32768 | -120 | 201.25 |
| | | 1D NMR | zgT2.ed | 564.7 | 512, 32768 | 1.0 | 4096 | -110 | 246 |
| | | 1D NMR | zgT2.ed | 564.7 | 512 | 1.0 | 4096 | -110 | 246 |
| Full-length BmrA/ ¹⁹ F Trp | ~ 80 | 1D NMR | zgT2.ed | 564.7 | 32768 | 1.0 | 4096 | -110 | 246 |

12.4. Backbone chemical shift assignments

12.4.1. LmrA-NBD D518A (D-loop), LmrA-NBD Q430A (Q-loop) and LmrA-NBD H543A (H-loop) backbone chemical shift assignments

A large number of backbone chemical shifts of LmrA-NBD WT²⁷⁹ (261 aa, ~97%) in the ADP-bound state (10 mM ADP) were transferable to the ¹H-¹⁵N TROSY-HSQC spectra of the mutants LmrA-NBD D518A, LmrA-NBD Q430A and LmrA-NBD H543A in the ADP-bound state. To verify the transferred backbone assignments and to identify aa which were shifted in the spectra 3D HNCACB spectra of ²H¹⁵N¹³C labeled sample were recorded²⁹⁷ (Table 37).

12.4.2. MsbA-NBD WT backbone chemical shift assignment

A nearly complete backbone chemical shift assignment of MsbA-NBD WT (260 aa, ~78%) in the ADP-bound state (10 mM ADP) was obtained via standard triple resonance TROSY based NMR experiments of a ²H¹⁵N¹³C labeled sample: ¹⁵N TROSY-HSQC, TROSY-HNCO, TROSY-HNCA, TROSY-HN(CA)CO and TROSY HNCACB spectra were recorded²⁹⁷. For the backbone chemical shift assignment, amino acids were selectively labeled (¹⁵N-Arg, ¹⁵N-Lys, ¹⁵N-Phe, ¹⁵N-Leu, ¹⁵N-Val, ¹⁵N-Ile, ¹⁵N-Ser/¹⁵N-Gly and ¹⁵N-Tyr) within MsbA-NBD WT and ¹⁵N TROSY HSQC spectra were recorded for identification of those aa in the spectra. Information about pulse sequences and NMR experiments for MsbA-NBD are listed in Table 40.

12.4.3. BmrA-NBD WT backbone chemical shift assignment

For a nearly complete backbone chemical shift assignment of BmrA-NBD WT²⁹⁸ (259 aa, ~97.2% of all non-proline residues, referring to NH) in the ADP-bound state (10 mM ADP) standard triple resonance TROSY based NMR experiments²⁹⁷ of a ²H¹⁵N¹³C labeled sample were recorded: ¹⁵N TROSY-HSQC, TROSY-HNCO, TROSY-HNCA, TROSY-HN(CA)CO, TROSY HNCACB, TROSY HN(CO)CACB. ¹⁵N TROSY-HSQC spectra of the selectively labeled amino acids ¹⁵N-Arg, ¹⁵N-Lys, ¹⁵N-Leu, ¹⁵N-Ile, ¹⁵N-Ser/¹⁵N-Gly, ¹⁵N-Val, ¹⁵N-Phe, ¹⁵N-Tyr, ¹⁵N-Trp of BmrA-NBD WT in the ADP-bound state were also recorded for the assignment. Information about pulse sequences and NMR experiments for BmrA-NBD are listed in Table 41.

12.5. ^1H - ^{15}N HSQC protein spectra

^1H - ^{15}N HSQC spectra show correlations between ^1H and ^{15}N -nuclei of the amide groups in a protein. In addition to the backbone amide groups, NH/NH₂ containing side chains can yield peaks in the spectrum (**Figure 9**).

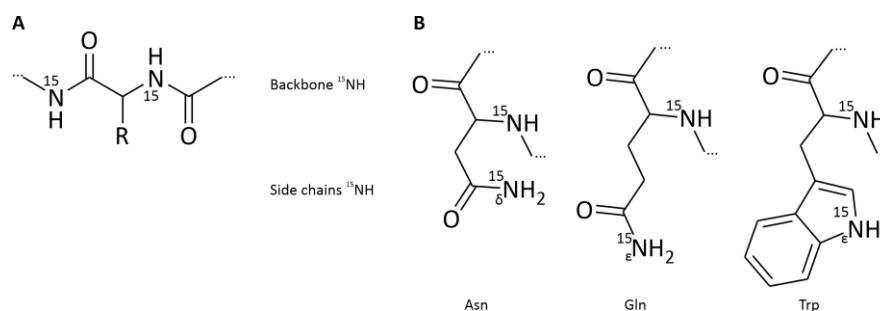


Figure 9: NH correlations seen in a ^1H - ^{15}N HSQC spectra

A) Backbone amide group NH correlation is mainly seen in a ^1H - ^{15}N HSQC spectra. **B)** Mainly backbone amide group NH correlations are visible, but tryptophane side chain and asparagine and glutamine side chains do also occur. Dots indicate continuing protein sequence. R – Amino acid residue side chain.

Chemical shift differences $\Delta\delta$ of HSQC NMR titration experiments and HSQC experiments for comparing WT against mutants were calculated with equation 4^{299,300}.

$$\Delta\delta_{comp} = \sqrt{\Delta\delta_H^2 + (\Delta\delta_N/6.5)^2} \quad 4$$

12.6. NMR titration experiments

If a ligand binds to a protein, this influences the chemical shift of the nuclei of the aa in the ligand binding side. Furthermore, structural changes can be induced by the interaction with a ligand and these effects are also visible through chemical shift changes. Finally, long-range effects of ligands or mutations can be probed via chemical shift perturbation experiments. Binding, which also affects the chemical shift in a spectrum, whereby those can be also long-range effects far away from the binding side. It is not possible to know the proportion of these parameters because their impact occurs at the same time.

When the chemical shift of a given peak changes upon addition of a ligand, the dissociation constant can be calculated, by plotting the ligand concentration against the chemical shift difference of the apo state. The k_{off} rate is much larger than the chemical shift difference for weak complexes ($K_D > \text{nM}$), which leads to one signal in the NMR spectra for each titration step. The signal corresponds to the average of free and bound state. This condition is called fast exchange on the NMR timescale^{300,301}. When the k_{off} rate of the complex is lower than the chemical shift difference a strong complex ($K_D < \mu\text{M}$) formation occurs. This leads to dis- and reappearing of the signal in the spectra during titration steps. This would be called slow exchange on the NMR time scale. For the monomeric NBDs the one site binding model was applied to calculate the K_D values (equation 5).

$$y = \frac{B_{max} \cdot x}{(k_1 + x)} \quad 5$$

B_{max} – maximum binding capacity
 k_1 – initial slope of the binding curve (= K_D)
 y – chemical shift difference
 x – concentration of the added ligand

For our calculations of K_D values from ^1H - ^{15}N TROSY HSQC experiments, 10% of the total amino acid residues, which had significant chemical shift differences, have been used to calculate the K_D values for binding of ADP or ATP to LmrA-NBD WT or its variants (D518A, Q430A and H543A). Concentrations of the proteins ranged from $\sim 150 - 200 \mu\text{M}$ for titration experiments.

For LmrA-NBD and MsbA-NBD, ^{15}N TROSY-HSQC experiments were recorded while titrating nucleotide (ADP, ATP) or magnesium (**Table 44**).

Table 44: Concentrations used for titrations of ADP, ATP and addition of magnesium for ^1H - ^{15}N HSQC or ^1H - ^{15}N TROSY HSQC experiments

| Compound and concentration |
|----------------------------|
| 0 (apo state) |
| 150 μM ADP/ATP |
| 300 μM ADP/ATP |
| 500 μM ADP/ATP |
| 750 μM ADP/ATP |
| 1 mM ADP/ATP |
| 2.5 mM ADP/ATP |
| 5 mM ADP/ATP |
| 7.5 mM ADP/ATP |
| 10 mM ADP/ATP |
| 15 mM ATP |
| 20 mM ATP |
| 10 mM Mg^{2+} |

12.7. Hydrogen/ Deuterium (H/D) exchange

H/D exchange experiments were performed by [REDACTED] (**Table 39**). ^2H , ^{15}N -labeled LmrA-NBD WT was lyophilized and dissolved in D_2O NMR buffer (**Table 28**). ^{15}N TROSY HSQC spectra for LmrA-NBD in the apo state were recorded after ~ 25 min, ~ 45 min, 80 min, 116 min, 152 min, 188 min, 224 min, 260 min, 296 min, 332 min, 368 min, 404 min and 440 minutes. The ^{15}N TROSY HSQC spectra for the ADP-bound state (with 10 mM ADP) were recorded after ~ 25 and the recorded every ~ 25 minutes until 450 minutes were reached.

12.8. Backbone hetNOE analysis

The heteronuclear Overhauser effect (hetNOE) is a relaxation parameter. It describes the NOE buildup between a proton and its attached heteronucleus. Information over flexible and rigid amide groups are given by $\{^1\text{H}\}$, ^{15}N hetNOE. Two encapsulated spectra were recorded to obtain hetNOE datasets, one with proton saturation (NOE) and one without proton saturation (no NOE).

Obtained signals were integrated with TopSpin 4.0.8. Integral ratio of datasets with proton and no proton saturation (NOE/no NOE) were plotted into a table against the amino acid residues. ^2H , ^{15}N labeled LmrA-NBD constructs were used for these experiments (**Table 39**) and measured in the apo or ADP-bound state (10 mM ADP).

12.9. 1D ¹⁹F - NMR

¹⁹F NMR measurements were carried out on a Bruker AVANCE 3 600 MHz spectrometer with a Prodigy TCI cryoprobe (Bruker, Karlsruhe) using a standard pulse sequence (**Table 42** and **Table 43**). ¹H and ¹⁹F are measured in the same coil (and thus without proton decoupling during the ¹⁹F acquisition). ¹⁹F chemical shift was referenced to BTFA (signal at -5.7 ppm)³⁰². One method of titrating was to add 100 mM ADP or ATP (pH 7) and subsequently 1 M MgCl₂ stock solutions. Another method was to titrate with 90 mM MgADP (pH 7) or 90 mM MgATP (pH 7) stock solutions (**Table 45**).

Table 45: Concentrations used for titrations of (Mg)ADP, (Mg)ATP and magnesium addition for 1D ¹⁹F NMR experiments

| Compound and concentration | |
|----------------------------|---------------------------|
| 0 (apo) | |
| 75 μM | ADP/ ATP/ MgADP/ MgATP |
| 150 μM | ADP/ ATP/ MgADP/ MgATP |
| 300 μM | ADP/ ATP/ MgADP/ MgATP |
| 500 μM | ADP/ ATP/ MgADP/ MgATP |
| 750 μM | ADP/ ATP/ MgADP/ MgATP |
| 1 mM | ADP/ ATP/ MgADP/ MgATP |
| 2.5 mM | ADP/ ATP/ MgADP/ MgATP |
| 5 mM | ADP/ ATP/ MgADP/ MgATP |
| 7.5 mM | ADP/ ATP/ MgADP/ MgATP |
| 10 mM | ADP/ ATP/ MgADP/ MgATP |
| 10 mM | Mg ²⁺ |

CHAPTER III: RESULTS

1. CONSEQUENCES OF NUCLEOTIDE BINDING TO THE NBD OF MULTIDRUG ABC TRANSPORTERS

1.1. Introducing the Model System

For ABC transporters, nucleotide binding to the NBDs initiates the catalytic cycle. ATP binding leads to NBD dimerization and NBS closure, which is followed by ATP hydrolysis, TMD reorganization and ultimately substrate release/ translocation across the membrane. However, studying NBD-NBD, NBD-TMD or TMD-NBD interactions and the consequences of nucleotide binding in the context of the full-length ABC transporter is difficult, as the individual contributions of interdomain interactions are difficult to separate. Thus, trying to gain deeper insights into the direct structural and dynamic effects of nucleotide binding within the NBD of ABC transporters, we took advantage of the well-behaved soluble NBDs of the ABC exporters LmrA from *L. lactis*, MsbA from *E. coli* and BmrA from *B. subtilis*. Those NBDs serve as optimal model systems to study intradomain dynamics and structural consequences of nucleotide binding and to make comparisons across highly conserved proteins. This should allow to obtain insights into the (dis)similarities of ABC transporter motor domain dynamics.

To obtain complementary views on the protein dynamics across different timescales, solution NMR spectroscopy was combined with photoinduced electron transfer-fluorescence correlation spectroscopy (PET-FCS) in collaboration with the ██████████ group (University of Würzburg). NMR experiments yielding information on peak linewidths, H/D exchange as well as $\{^1\text{H}\}$, ^{15}N hetNOE measurements allow to derive protein dynamic information in the slow (μs - s) and fast (ps - ns) timescale while PET-FCS fills the dynamic gap in the intermediate timescale (ns - ms).

The isolated NBDs of the exporters LmrA, MsbA and BmrA can be expressed in *E. coli* in large quantities. The structural integrity, oligomerization state and secondary structure of the three NBDs were analyzed by CD spectroscopy and SEC (**Figure 10**). The NBD monomers have a molecular weight of around 30 kDa and are thus amenable for solution NMR spectroscopy. The purified protein can be concentrated up to 500 - 600 μM without aggregating. Importantly, LmrA-NBD and BmrA-NBD monomers showed no interactions (dimerization) as apparent from SEC runs (**Figure 10D**). To carry out NMR experiments, beginning with backbone assignments, the NBDs were labeled with ^2H , ^{13}C and ^{15}N . All three proteins yielded well-dispersed spectra thus showing that the proteins are properly folded (**Figure 12**, **Figure 13** and **Figure 14**).

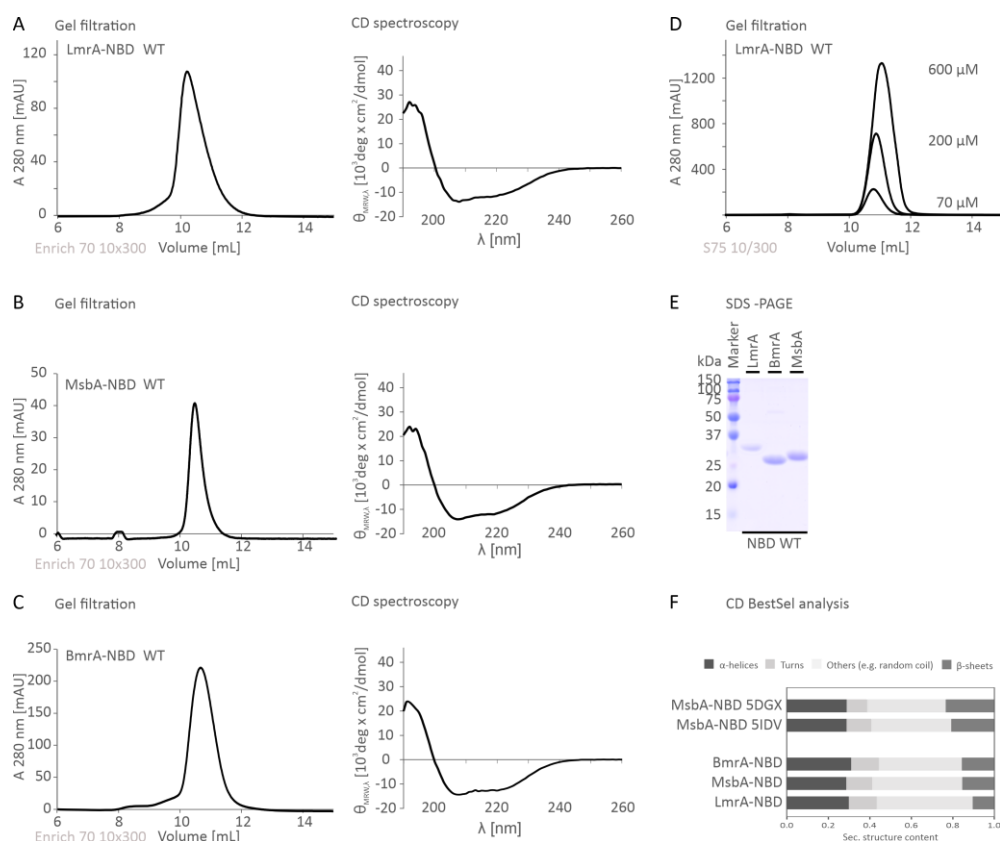


Figure 10: Protein characterization/ Structural integrity of LmrA-NBD WT (~28.9 kDa), MsbA-NBD WT (~29.1 kDa) and BmrA-NBD WT (~28.6 kDa)

A) Gel filtration profile and CD spectrum of LmrA-NBD WT. **B)** Gel filtration profile and CD spectrum of MsbA-NBD WT. **C)** Gel filtration profile and CD spectrum of BmrA-NBD WT. **D)** Probing different concentrations of LmrA-NBD WT with gel filtration to analyze whether LmrA-NBD WT forms aggregates or oligomers. LmrA-NBD WT is a monomer as it runs at elution volumes characteristic for a protein around 30 kDa. **E)** SDS-PAGE of purified LmrA-NBD, BmrA-NBD and MsbA-NBD from *E. coli* BL21-Gold (DE3) cells. 5 μ g protein were loaded onto a 15% SDS-PAGE and stained with Coomassie blue after the final purification step (SEC run). LmrA-NBD, BmrA-NBD and MsbA-NBD WT constructs differ in their gel running behaviour although they are similar in molecular weight. **F)** Analysis of the respective NBD's secondary structure content based on their respective CD spectra using the BestSel secondary structure analysis (<http://bestsel.elte.hu/index.php>^{292,293}). The data were compared to the secondary structure content of the NBD crystal structures of other type I ABC exporters (type IV fold). The predicted α -helical/turn/other like random coil/ β -sheet content of the purified constructs is 29.9/13.5/46.2/10.4% for LmrA-NBD WT, 28.7/12.5/43.4/15.5% for MsbA-NBD WT and 31.0/13.3/40.1/15.6% for BmrA-NBD WT. The predicted α -helical/turn/other like random coil/ β -sheet content of the NBD crystal structures 28.8/11.9/38.5/20.9% for MsbA-NBD WT (PDB ID: 5IDV³⁰³) and 28.9/9.8/37.9/23.5% for MsbA-NBD WT (PDB ID: 5DGX³⁰⁴).

LmrA-NBD, MsbA-NBD and BmrA-NBD were all able to properly bind to nucleotides as shown by ^1H - ^{15}N TROSY HSQC chemical shift perturbation experiments (**Figure 16**, **Figure 17**, **Appendix 11** and **Appendix 12**). The respective affinities for ADP and ATP were calculated for LmrA-NBD WT based on chemical shift perturbations with the nucleotides across the physiologically relevant concentration range²³² (**Figure 11**). Magnesium was added in excess (~10 mM) compared to the cytosolic concentration range of 1 – 2 mM ADP showed a higher affinity ($K_D = 268 \pm 32 \mu\text{M}$) compared to ATP ($K_D = 3000 \pm 295 \mu\text{M}$) for the LmrA-NBD. These values are in the range of previously described values of homologous ABC transporters¹³² (**Appendix table 4**).

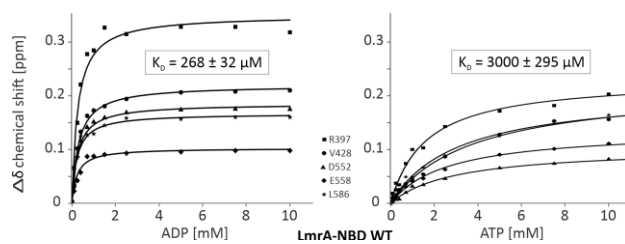


Figure 11: Affinity of ADP and ATP for ^{15}N -LmrA-NBD determined by ^1H - ^{15}N TROSY HSQC NMR titration experiments
ADP has a higher affinity than ATP to LmrA-NBD WT. Each curve presents the chemical shift values through the titration for the amide resonance of one amino acid residue in an ^1H - ^{15}N TROSY HSQC NMR spectrum (12.6. NMR titration experiments).

1.2. Nucleotide binding to the NBD: Dynamic consequences for conserved motifs and allosteric signal propagation

In ^1H - ^{15}N HSQC or ^1H - ^{15}N TROSY HSQC spectra, the correlation of non-exchanging NH bonds of the protein backbone (as well as sidechains) are recorded. This leads to characteristic fingerprint spectra for every protein. For LmrA-NBD, MsbA-NBD and BmrA-NBD WT well-dispersed ^1H - ^{15}N TROSY HSQC spectra in the ADP-bound state could be obtained (**Figure 12**, **Figure 13** and **Figure 14**).

Taking advantage of the previously assigned ^1H - ^{15}N TROSY HSQC spectra of LmrA-NBD in the ADP-bound state, (~95% of backbone resonances, 246 amino acids out of the total number of 261 amino acids²⁷⁹), backbone assignments of the protein in the apo (no nucleotides, ~87%, 226/261aa, **Appendix 13**), ATP- (~83%, 215/261, **Appendix 13**), MgADP- (~68%, 178/261, **Appendix 14**) and MgATP (~71%, 185/261aa, **Appendix 15**)-bound states could be determined by chemical shift perturbation mapping in the course of this thesis.

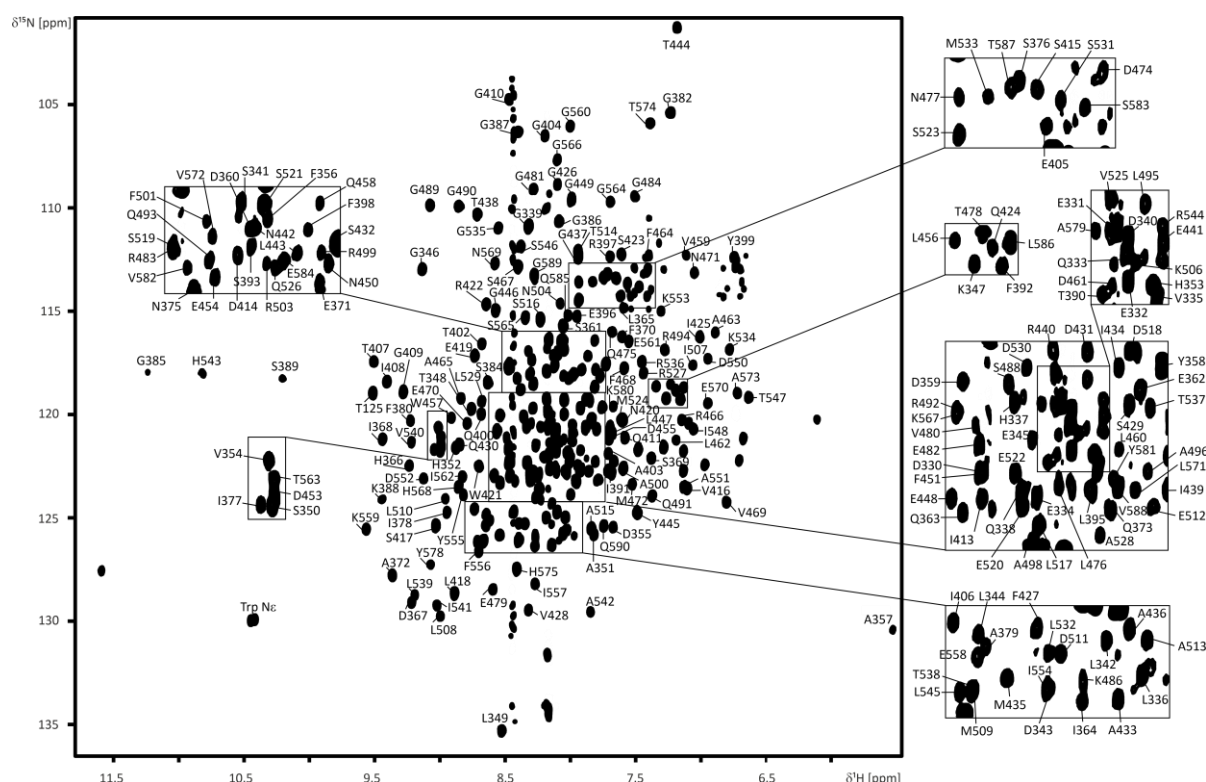


Figure 12: Backbone chemical shift assignment of LmrA-NBD in the ADP-bound state (modified from Hellmich et al., 2012²⁷⁹)

2D ^1H - ^{15}N TROSY HSQC spectrum recorded with a 400 μM sample of ^2H , ^{13}C , ^{15}N -labeled LmrA-NBD WT in the ADP-bound state (10 mM ADP) at 298 K. Assigned residues are labeled with their residue name (single letter code, number according to full-length LmrA). Crowded regions are shown as close-up views indicated by boxes.

To complement the backbone NMR assignment of the LmrA-NBD, ^2H , ^{13}C , ^{15}N labeled MsbA-NBD and BmrA-NBD WT were prepared and measured with the same set of standard triple resonance pulse sequence (12. NMR techniques). The *de novo* NMR backbone assignments of the isolated NBDs of MsbA (~78%) and BmrA (~97.2%)²⁹⁸ in the ADP-bound state could be obtained in collaboration with [REDACTED] (AG [REDACTED], Figure 13 MsbA-NBD assignment ongoing and Figure 14).

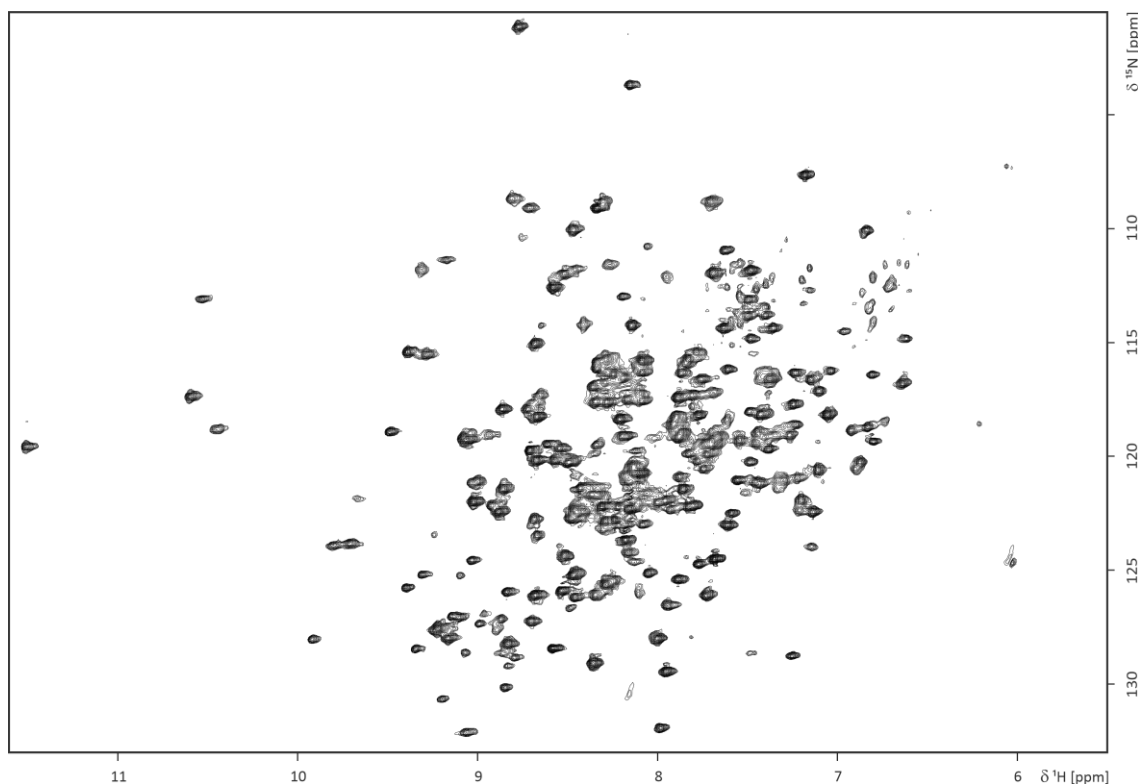


Figure 13: 2D ^1H - ^{15}N TROSY HSQC spectrum of MsbA-NBD

Spectrum was recorded with a $\sim 240\ \mu\text{M}$ sample of ^2H , ^{13}C , ^{15}N -labeled MsbA-NBD WT in the ADP-bound state (10 mM ADP) at 298 K (assignment currently ongoing).

The NH assignment of the NBD's lysine, phenylalanine, tyrosine, arginine, valine, leucine, isoleucine, serine, glycine and tryptophane are verified by using amino acid specific ^{15}N -Lys, ^{15}N -Phe, ^{15}N -Tyr, ^{15}N -Arg, ^{15}N -Val, ^{15}N -Leu, ^{15}N -Ile, ^{15}N -Ser/ ^{15}N -Gly or ^{15}N -Trp labeled MsbA-NBD or BmrA-NBD, respectively (12.4.2. MsbA-NBD WT backbone chemical shift assignment and 12.4.3. BmrA-NBD WT backbone chemical shift assignment). For all three NBDs, the ADP-bound state was chosen to represent the "nucleotide-bound state" for additional NMR-based experiments, because it yields the most complete set of peaks.

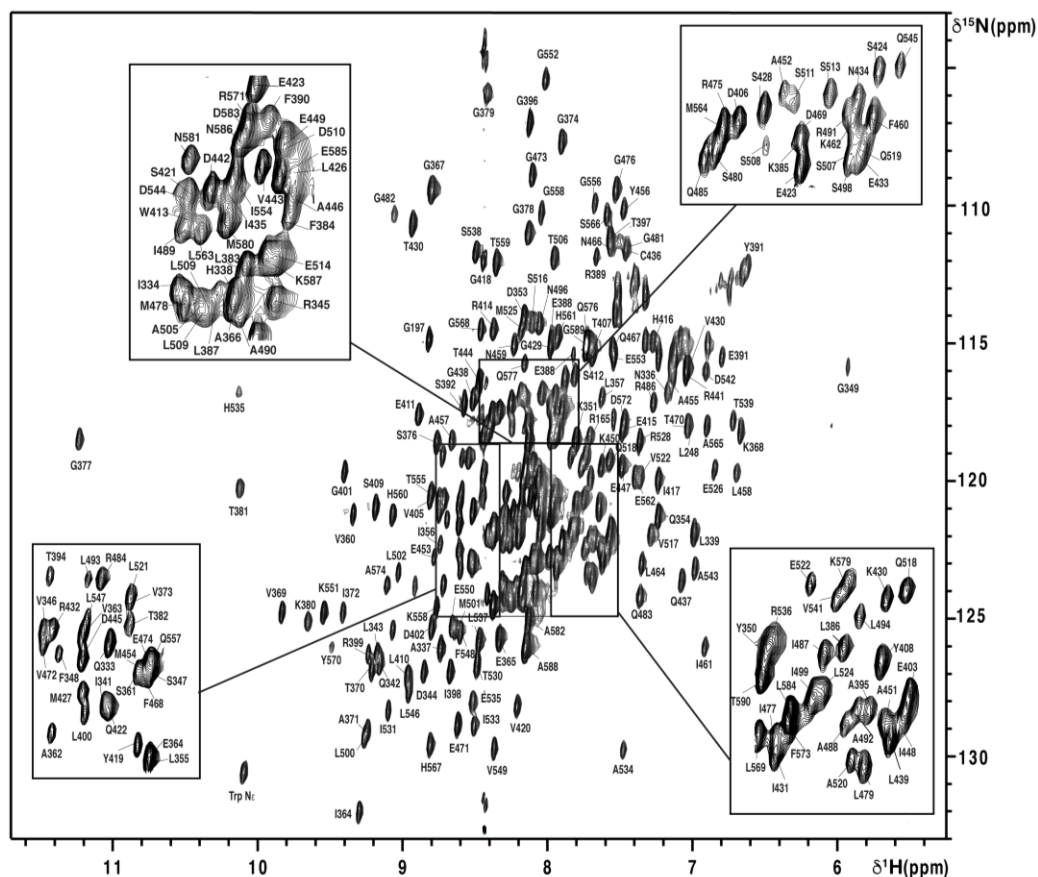


Figure 14: Backbone chemical shift assignment of BmrA-NBD in the ADP-bound state²⁹⁸

2D ^1H - ^{15}N TROSY HSQC spectrum recorded with a 280 μM sample of ^2H , ^{13}C , ^{15}N -labeled BmrA-NBD WT in the ADP-bound state (10 mM ADP) at 298 K. Assigned residues are labeled with their residue name (single letter code, numbering according to full-length BmrA). Crowded regions are shown as close-up views indicated by boxes.

In NMR spectra, both linewidth and peak position yield important information about local dynamics and structural changes within a protein. A change in the chemical environment of an amino acid residue will lead to a shift in the position of the corresponding resonance. Causes for this can be direct ligand interaction or allosteric propagation of binding sensed by this residue, i.e. the residue is distant from the binding site. In the case of LmrA-NBD, MsbA-NBD and BmrA-NBD WT, fewer peaks are present in the ^1H - ^{15}N TROSY HSQC in the apo compared to the ADP-bound state, i.e. that the linewidths of some resonances decrease upon addition of ADP (**Figure 15A/B, Appendix 17**). This indicates that these residues are in intermediate exchange in the absence of a nucleotide, thus implying protein backbone fluctuations in the μs – ms timescale. However, even in the presence of ADP, not all resonances become visible thus indicating that further residues are always in a dynamic state leading to line broadening in the NMR spectrum.

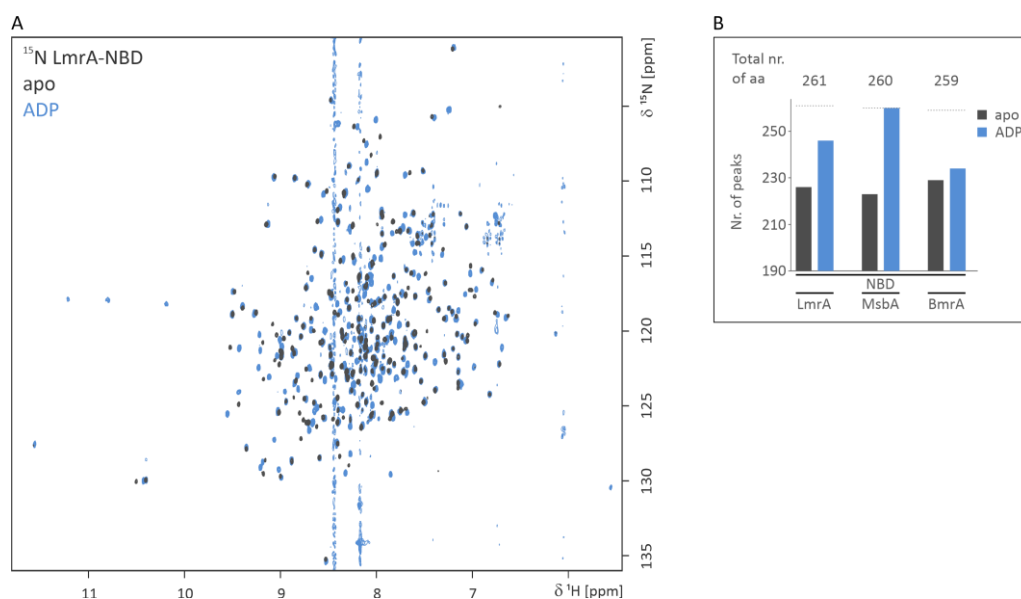


Figure 15: Effects of ADP binding to isolated ABC transporter NBDs

A) Overlay of ^1H - ^{15}N TROSY HSQC spectra of ^{15}N -labeled LmrA-NBD in the apo (gray) and ADP-bound states (10 mM ADP, blue). **B)** Number of peaks observed in the ^1H - ^{15}N TROSY HSQC spectra of ^{15}N -labeled LmrA-NBD, MsbA-NBD and BmrA-NBD in ADP-bound (blue) and in apo states (gray) differs from total number of amino acids in each NBD. LmrA: NBD: total - 261, apo - 226, ADP - 246; MsbA-NBD: 260/223/260; BmrA-NBD: 259/229/234 (**Appendix 11 and Appendix 12**).

Here, a detailed analysis of amino acids whose resonances are affected by ADP binding was carried out for LmrA-NBD WT. In the following, three ways of effects are discussed within this subchapter (**Figure 16A and Figure 17A**): (i) line sharpening and chemical shift changes (“appearance of peaks upon ADP addition”) (ii) major chemical shift changes ($>1\sigma$); (iii) minor ($<1\sigma$) or no linewidth and chemical shift changes. Here (i) corresponds to the detected line sharpening of peaks by adding ADP to ^{15}N -labeled LmrA-NBD, which reflects the quenching effect upon addition of ADP (blue spheres in **Figure 17A**).

All residues in the first category, i.e. those with severely line broadened peaks in the apo state are found in or in close proximity to the NBS (Y358, S384, G385, G387-S393, Y399 and H543) and belong to the A-loop (Y358), the Walker A motif (S384, G385, G387-T390) and the H-loop (H543A) (**Figure 17A**). Most but not all “missing peaks” appear when titrating ADP to the LmrA-NBD (**Figure 16A**). Once ADP is bound, the motions these amino acids experience in the apo state are quenched and thus the peaks become visible in the resulting ^1H - ^{15}N TROSY HSQC spectrum. “Missing resonances” and chemical shift differences between apo and ADP-bound state of LmrA-NBD are represented in **Figure 17A** with a bar graph diagram and plotted on a homology model of LmrA-NBD based on Sav1866 (PDB ID: 2HYD³⁴) for better visualization of the regions of the NBD whose dynamics are presumably quenched upon nucleotide binding (blue spheres in **Figure 17A**).

Residues in the second category, i.e. those displaying significant chemical shift changes, can be found for example in the conserved Q-loop (S429, Q430, D431 and S432), Walker B motif (I507, M509-E512) and D-loop (S516, L517) (**Figure 16A** (ii) and **Figure 17A**). For residues in the X-loop and the ABC motif (C-loop) no changes in their chemical shifts were detected upon ADP addition, so they belong to the third category.

In summary, the residues whose resonances were affected strongly by ADP addition can be found in the conserved motifs A-loop, Walker A motif, Q-loop, Walker B motif and H-loop, which are part of the NBS (**3.3.2. Nucleotide binding domains: constitution and function, Figure 16A** and **Figure 17A**). These residues thus “sense” ADP binding. The D-loop, which is responsible for NBD-NBD communication and sits C-terminal to the Walker B motif, also “senses” ADP binding.

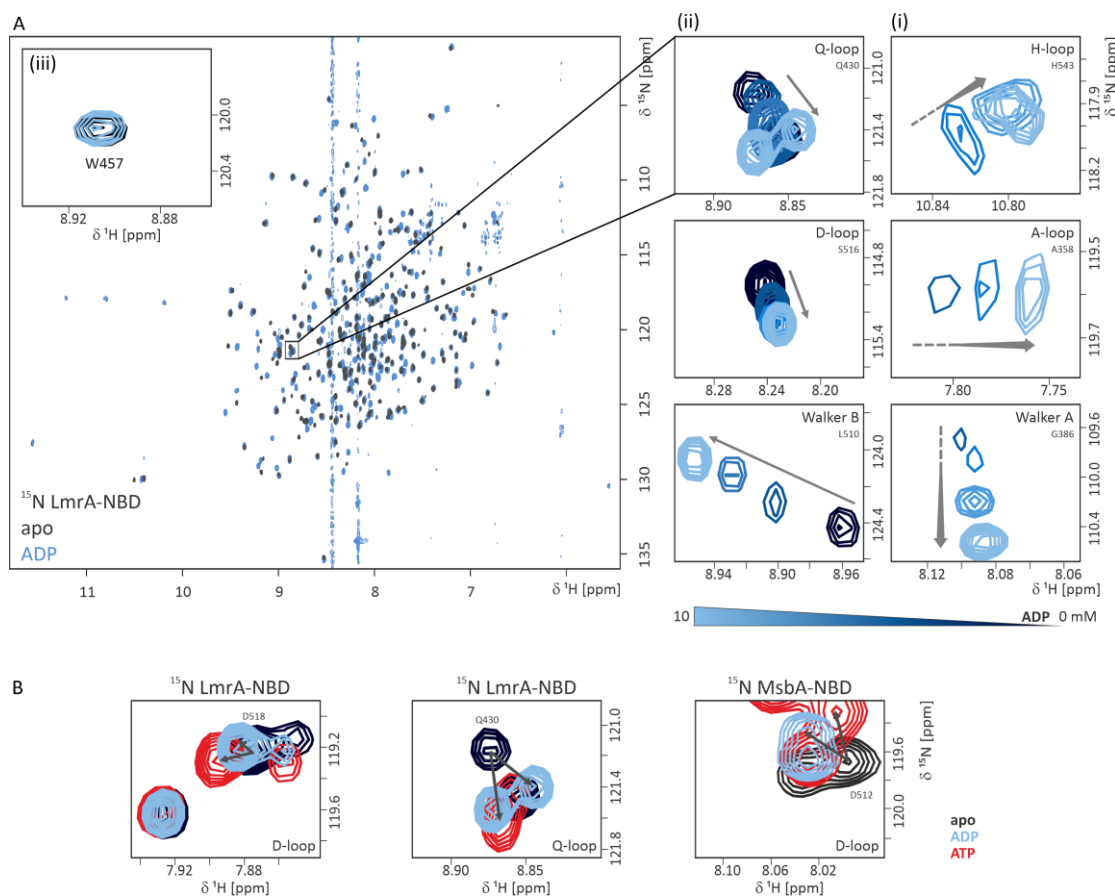


Figure 16: Conserved motifs sense nucleotide binding and can distinguish between ATP and ADP

A) Overlay of ^1H - ^{15}N TROSY HSQC spectra of ^{15}N -labeled LmrA-NBD WT in the apo (gray) and ADP-bound states (10 mM ADP, blue). Close-up views of the ^1H - ^{15}N TROSY HSQC spectra, showing selected chemical shift changes of conserved motifs during ADP titration (0 – 10 mM, color key is represented below the close-up views). Direction of peak shifts are indicated by arrows. Resonances which are not present in apo state are marked with dashed gray lines. **B)** Close-up views of selected residues from ^1H - ^{15}N TROSY HSQC spectra of conserved motifs (D-loop or Q-loop) in LmrA-NBD and MsbA-NBD WT that were found to distinguish between ADP (blue) and ATP (red) binding. The Q-loop glutamine residue for MsbA-NBD WT could only be assigned within the ADP-bound state, hence no analysis could be performed. For BmrA-NBD WT titration experiments are not complete, hence no more information for the residues is currently available.

In addition, residues which sense ADP binding are not only located in the NBS but found also remotely from the NBS (**Figure 17A**), e.g. in the C-terminal region (N569 and E570 in $\alpha 10$; H575, Y578, A579, V582, S583 and Q585 in $\alpha 11$ and L586-G589) and the coupling helix groove (I425-S432), where the NBDs connect to the TMDs. This indicates the presence of a long-range allosteric communication network within the NBD which reacts to nucleotide (or at least ADP) binding.

Since the ADP-bound state reflects the post-hydrolysis state, but the conformational cycle of an ABC transporter begins with ATP binding, the effect of the triphosphate nucleotide was also probed. Addition of ATP to the ^{15}N -labeled LmrA-NBD showed similar but not identical effects to ADP (**Figure 17B**). In contrast to what was observed upon ADP addition, the resonances for the H-loop (H543), A-loop (Y358) and Walker A motif (S384, G385, G387-T390) residues did not appear as the ATP titration progressed. ATP (Mg^{2+}) addition did also not result in line sharpening of the residues in the NBS (**Appendix 14**, **Appendix 15** and **Appendix 16**).

Those observations indicate that the residues in the NBS are less dynamic in the ADP-bound state than the apo state or ATP-bound state. A lower affinity for ATP ($K_D = 3000 \pm 295 \mu\text{M}$) was noted in comparison to ADP ($K_D = 268 \pm 32 \mu\text{M}$). Moreover, upon ATP binding, significant chemical shift perturbations were found for residues in the conserved motifs Walker A motif (G382, G386), Q-loop (S429-S432), Walker B motif (I507, M509-E512) and the D-loop (A515-D518) (**Figure 17B**). Besides the conserved motifs, residues in the coupling helix groove (I425-S432) and the C-terminal region (H568, N569 and V572 in $\alpha 10$; Y578, A579, Y581-Q585 in $\alpha 11$ and L586-G589) also showed chemical shift perturbations upon ATP binding (**Figure 17B**). Furthermore, the C-loop residue G489 was affected by addition of ATP whereas the X-loop residues showed no significant chemical shift change.

Intriguingly, specific NBD residues in the Walker A motif (G382 and G386), the Q-loop (S429 and Q430), the C-loop (S488 and G489), the Walker B motif (M509-E512), the D-loop (A515-D518), the coupling helix groove (I425, G426, V428-Q430) and the C-terminal region (in $\alpha 10$ E570, in $\alpha 11$ A579, Y581 and S583 and in the disordered C-terminal region L586-G589) were found to have distinct chemical shifts depending on whether ADP or ATP was added to the NBD (**Figure 16B** and **Figure 17C**). This observation indicates that those regions can distinguish between ADP and ATP binding, which may have important implications for the role the NBD plays in the progression of the ABC transporter's catalytic cycle that go beyond merely mediating ATP hydrolysis.

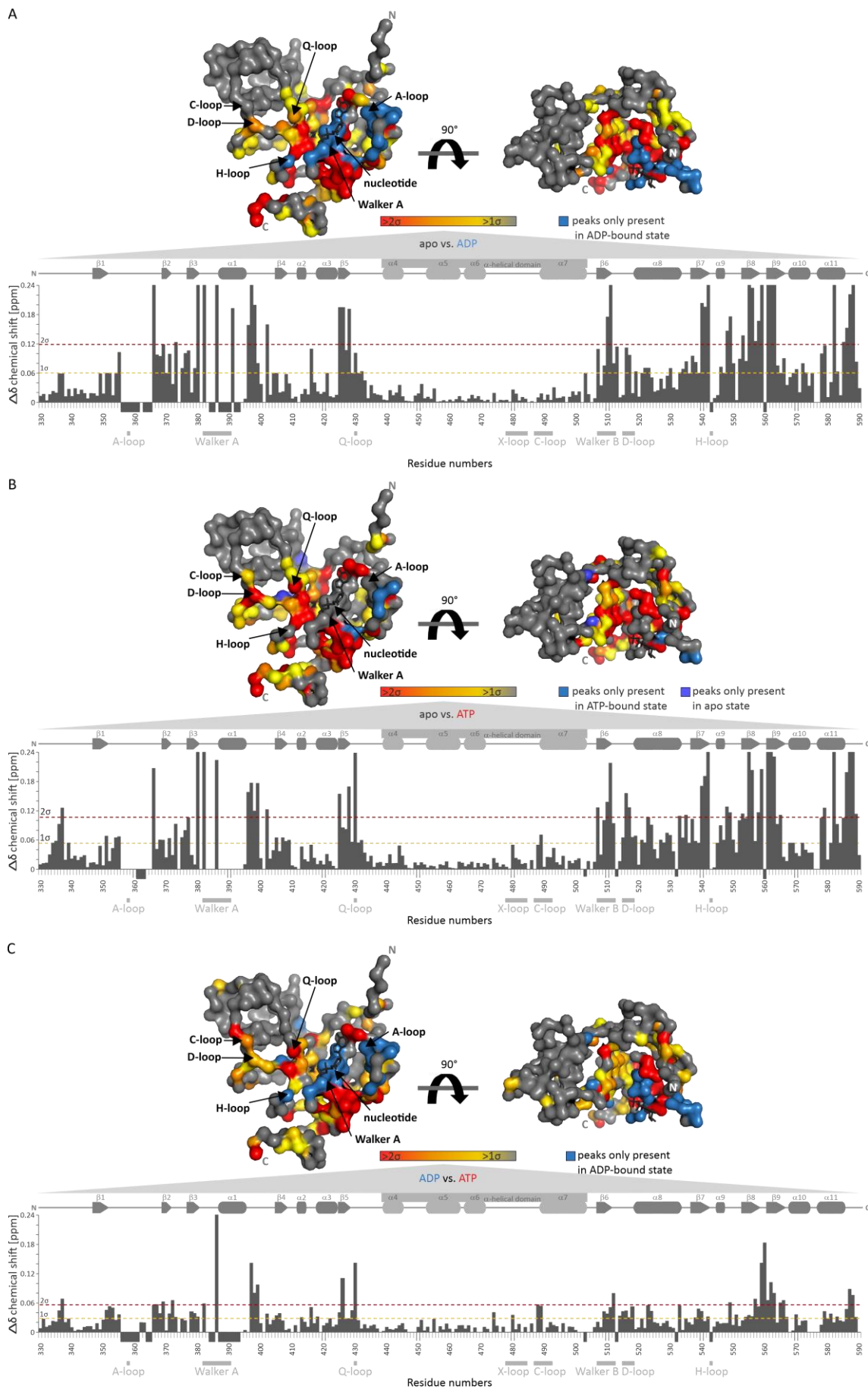


Figure 17: Effect of nucleotide binding to the isolated ABC transporter LmrA-NBD

Effect of nucleotide binding to the isolated ABC transporter LmrA-NBD

A) Effect of ADP binding monitored through chemical shift changes. Bar graph showing chemical shift differences between apo and ADP-bound state for LmrA-NBD WT. Blue indicates residues whose peaks are only present in the ^1H - ^{15}N TROSY HSQC spectra of the ADP-bound state. **B)** Effect of ATP binding. Blue or violet indicate residues whose peaks are only present in the ATP-bound or apo state. **C)** Residues capable of distinguishing between ADP and ATP binding. Bar graph showing the comparison of chemical shift differences between ATP and ADP-bound state for LmrA-NBD. In all plots (A, B and C), amino acid numbering is based on the full-length transporter. Above the bar graphs of A, B and C, the corresponding secondary structure elements of LmrA-NBD are displayed. Lighter gray indicates the α -helical subdomain. Gray boxes represent residues of conserved motifs of the NBD. Yellow and red dotted lines indicate 1σ and 2σ standard deviation. Downward orientated bars represent peaks only present in the apo, ADP-bound or ATP-bound state. Above the bar graphs (A, B and C), chemical shift changes are shown plotted on a ribbon surface representation of a LmrA-NBD homology model based on Sav1866 (PDB ID: 2HYD³⁴). View on the NBD-NBD interface (left) and view on the coupling helix groove (right) are shown. Color gradient from yellow to red represents increasing chemical shift differences from $>1\sigma$ (yellow) to $>2\sigma$ (red). C-terminal LmrA-NBD homology model ends at residue T587. Residues with $\Delta\delta$ values below 1σ , residues whose $\Delta\delta$ values could not be determined reliably (missing in plots of A, B and C) or remain unassigned (missing in plots of A, B and C) are shown in gray in the ribbons surface representations of A, B and C.

1.3. Complementary analysis of protein dynamics across different timescales

The observations made in the 2D ^1H - ^{15}N TROSY HSQC spectra for the LmrA-NBD shown above suggest that the apo state NBD has intrinsic flexibility that is quenched by ADP binding. These NMR experiments give information about slow NBD backbone dynamics in the ms – s timescale. To gain more insights into the NBD's dynamic behavior on complementary timescales, additional hydrogen/deuterium exchange, $\{^1\text{H}\}$, ^{15}N hetNOE and PET-FCS experiments (in the latter case for MsbA-NBD) were carried out. Since the ADP-bound state gave rise to the largest number of resonances in the ^1H - ^{15}N TROSY HSQC spectrum, this state was treated as the representative nucleotide bound state for further NMR experiments.

1.3.1. Slow NBD dynamics of LmrA-NBD on the ms - s timescale are quenched by ADP

NH bonds can be strongly polarized because of their difference in electronegativity, this leads to the effect that protons exchange with the solvent (buffer). In aqueous solutions this exchange is acid (H_3O^+) and base (OH^-) catalyzed, whereas base catalysis is much more efficient. This leads to a strong pH-dependence of the H/D exchange. Additionally, exchange is dependent on temperature. In unfolded peptides and proteins exchange occurs within the ms - s timescale. When amide hydrogens as part of hydrogen bonds are protected from the solvent, exchange is drastically slowed down (up to hours or weeks)³⁰⁵. Thus, in folded proteins H/D exchange is mainly observed in transiently unfolded regions or partly folded conformations and the speed of exchange depends on the presence of such H/D exchangeable conformations.

In agreement with the dynamic quenching observed through the decrease in line width upon ADP addition (**Figure 16A** (i) and **Figure 17A**), a reduction in H/D exchange (**Figure 18**) was observed for ^{15}N -labeled LmrA-NBD in the presence of ADP compared to the apo state. This may be another indication of NBD stabilization in the post-hydrolysis state. In the H/D exchange experiments of the LmrA-NBD, H/D exchange for the apo and ADP-bound state were compared (**Figure 18**). ^{15}N -labeled, protonated protein was lyophilized and taken up in deuterated buffer for the recording of consecutive ^1H - ^{15}N TROSY HSQC spectra. Temporal resolution for those experiments was limited to the time which one 2D spectrum could be recorded (~ 20 - 25 min). Within the first ~ 25 min, mainly NH protons of solvent-exposed residues in flexible regions as loops and the N- and C-termini exchanged in either the apo or ADP-bound states (**Figure 18**). An exception were residues in the loop between β -sheet 1 and 2 (V354-F356 and F364-S369) and residues in the loop at the C-terminal end of the Walker A helix (L395-Y399, $\alpha 1$), which were stabilized by ADP binding.

Other regions with quick exchange rates ($\leq \sim 25$ min) include the Q-loop, which indicates flexibility in this hinge region between the α -helical and the catalytic subdomain. Another region that showed exchange after $\leq \sim 25$ min in both the apo and the ADP state were the amide protons of the N-terminal end of the D-loop helix ($\alpha 8$, S519-A528). In contrast, the residues on the C-terminal end of the D-loop helix (L529, D530, L532 and M533) showed slower deuteration in both states, with the ADP-bound state exchanging slightly more slowly than the apo state.

The differences in H/D exchange between apo and ADP-bound state are particularly pronounced for residues in the core β -sheets of the catalytic subdomain close to the NBS ($\beta 5$, I425/G426; $\beta 6$, I507-L510; $\beta 7$, T537-A542; $\beta 8$, K553-F556 and $\beta 9$, E561/I562/G564). All of these residues show significantly decreased exchange in the presence of ADP. Notably, $\beta 5$ is located in the coupling helix groove, which builds a structural connection from the NBD to the TMDs.

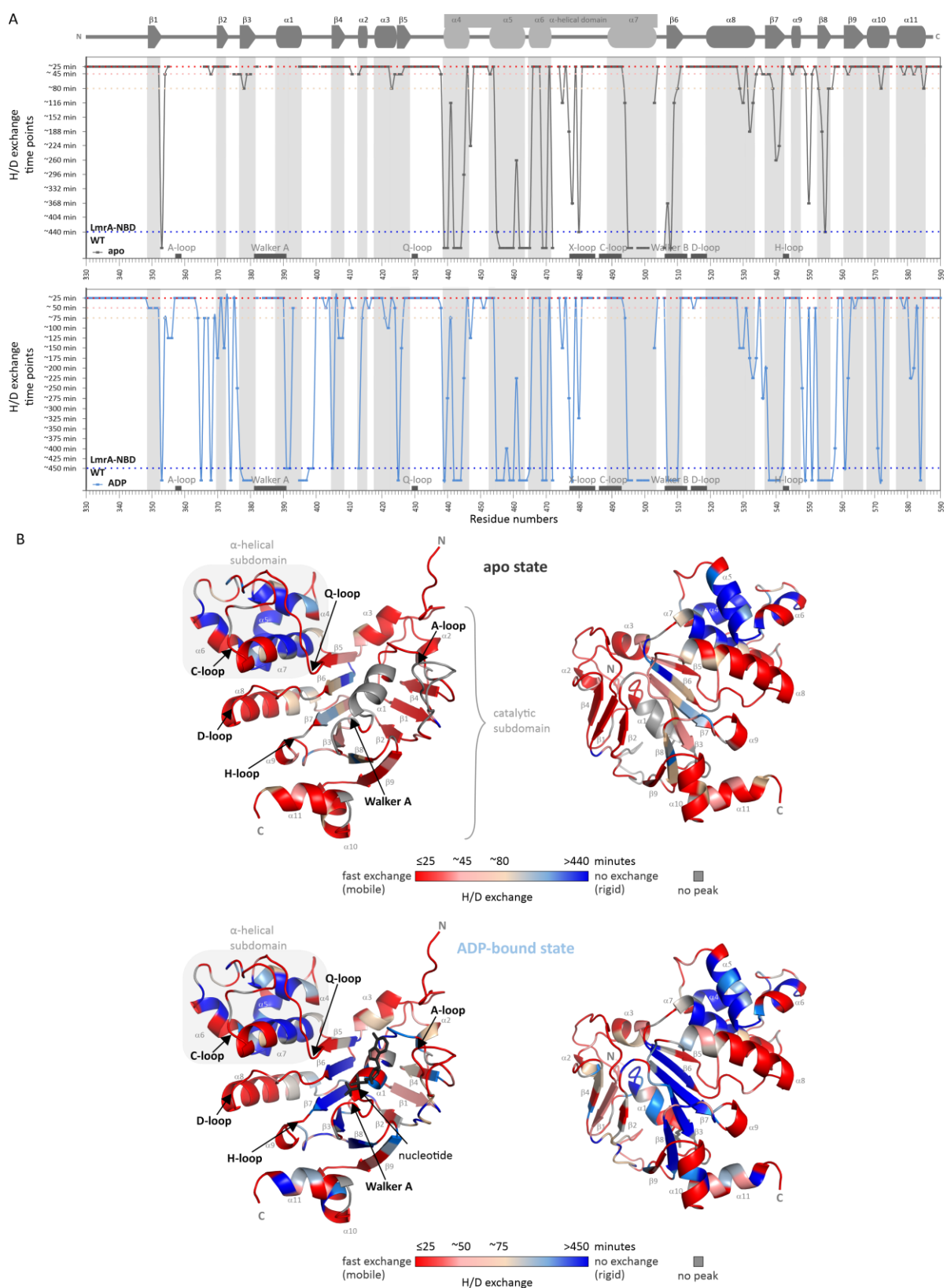


Figure 18: H/D exchange for LmrA-NBD in the apo and ADP-bound state

A) NMR-based H/D exchange experiments with ^2H - ^{15}N -labeled LmrA-NBD in the apo (top) and ADP-bound (10 mM ADP bottom) state. Plotted are the time points when no peak signal intensity (integral) within ^1H - ^{15}N TROSY HSQC spectra was seen anymore, against the residue numbers. Amino acid numbering is based on the full-length transporter. **B)** Data from H/D exchange as shown in A are plotted on a homology model of LmrA-NBD based on Sav1866 (PDB ID: 2HYD³⁴). C-terminal LmrA-NBD homology model ends at residue T587. Views on the NBD-NBD interface (left) and view on the NBD surface (right) are shown. “Missing” data points in the plots of A indicate either prolines, chemical shifts which could not be determined reliably or unassigned residues. Those residues are colored in gray in the plots in B. Above the diagrams in A, the corresponding

secondary structure elements of LmrA-NBD are displayed. Lighter gray indicates the α -helical subdomain. Gray boxes represent residues of conserved motifs of the NBD.

With regard to the conserved motifs, a stabilizing effect (i.e. reduction of H/D exchange) could also be observed for residues within the X-loop (T478 and V480), the D-loop (A516) and the Walker B motif (I507, M509 and L510) upon ADP addition. The Walker B residues I507, M509 and L510 showed no exchange throughout the entire analyzed time frame of 450 min in the presence of ADP. A slow exchange for these residues is not surprising because they are located in a β -sheet ($\beta 6$). However, this also means that in the apo state, this region, despite presenting the structural core of the NBD is somewhat dynamic. An exception presents residue L508 of the Walker B motif, which shows exchange in neither apo nor ADP-bound state throughout the measured time frame of ~ 450 min. The conserved aspartate residue (D511) of the Walker B motif remained flexible in both the apo and the ADP-bound states (i.e. fast exchange in either case). The resonance for the conserved catalytic glutamate of the Walker B motif (E512) could only be determined in the ADP-bound state, where it had a fast H/D exchange. In the D-loop (SALD motif), the stabilization of the alanine residue upon ADP binding was minor, here the amide proton exchanged after ~ 50 min. Other residues for which ADP slowed deuteration are found in the helix $\alpha 3$ (R422) and in the C-terminal helices $\alpha 10$ (L571 and V572) and $\alpha 11$ (Y581-E584). Intriguingly, the α -helical subdomain showed a reduced H/D exchange for residues in both the apo and ADP bound states (R440, L443, Y445, D455-L460, L462, A463, V469, E470, M472, L495, A496, A498-F501) compared to the catalytic subdomain.

Together, the data show that there are regions that are strongly affected by nucleotide binding and that the presence of the ADP in general seems to stabilize the LmrA-NBD.

1.3.2. LmrA-NBD backbone dynamics in the apo and ADP-bound state in the ps - ns timescale probed by $\{^1\text{H}\}$, ^{15}N hetNOE experiments

In addition to the NMR-based linewidth analysis and H/D exchange measurements that “look” at NBD motions in the “slower” ms – s regime, $\{^1\text{H}\}$, ^{15}N hetNOE experiments can be used to study very fast motions in the ps – ns timescale. This technique is based on detecting fluctuations of the NH bond vector and thus completes insights in the residue specific NBD backbone dynamics on multiple timescales³⁰⁶.

For the LmrA-NBD WT, $\{^1\text{H}\}$, ^{15}N hetNOE experiments were carried out with and without nucleotide (**Figure 19A/B**). Rigid regions within the protein, which are mostly folded domains, display $\{^1\text{H}\}$, ^{15}N hetNOE values close to 1.0. Here, the resonance intensity between the hetNOE experiment value is similar to the hetNOE experiment without NOE (**12.8**. Backbone hetNOE analysis). Very flexible protein backbone regions show hetNOE values close to 0. The hetNOE data for the LmrA-NBD in the apo and ADP-bound states (**Figure 19A/B**) specify structured regions (α -helical and β -sheet regions) to be rigid as indicated by $\{^1\text{H}\}$, ^{15}N hetNOE values $> \sim 0.6$ ³⁰⁷ (**Figure 19A/B**). Hence $\{^1\text{H}\}$, ^{15}N hetNOE values are reflective of the secondary structure elements in the NBD. To visualize the backbone dynamics with and without nucleotide, $\{^1\text{H}\}$, ^{15}N hetNOE values were mapped on a LmrA-NBD homology model based on Sav1866 (PDB ID: 2HYD³⁴, **Figure 19C/D**).

In both the apo and ADP-bound states (**Figure 19**), three very flexible regions can be noted, the disordered N-terminus (D330-G346), residue G449 within the α -helical subdomain between helices α_4 and α_5 and the disordered C-terminus (T587-Q590). With regard to interpretations of the flexibility of the N-terminus, one must consider that in the context of the full-length transporter the transmembrane domains are attached here. Nevertheless, as there is a long connecting loop region between NBD and TMD, it is possible that this region is highly flexible also in the full-length transporter. Further flexible residues were found in the loop between β -sheet 2 and 3 (Q373-S376), the C-terminal end of the Walker A helix (L395) and in the loop between helix α_7 and β -sheet 6 (K506). Flexibility of residues in both recorded states were further obtained in or in vicinity of the conserved motifs Q-loop (S429, D431, A433 and G437), X-loop (G481-G484) and D-loop (S516-D518).

Interestingly, when examining the hetNOE values of LmrA-NBD in the apo state (**Figure 19A/C**) residues of the secondary structure elements β_1 (A351), β_4 (E405), α_5 (D461), α_8 (E520) and the C-terminal helices α_{10} (E570) and α_{11} (Y581) could be identified to be flexible.

More peaks are visible in the HSQC spectrum of the ADP-bound compared to the apo state NBD. Thus, more residues were accessible to evaluate their $\{^1\text{H}\}$, ^{15}N hetNOE values in the ADP-bound state (**Figure 19B/D**). This means that residues between β -sheets 1 and 2, where the A-loop residue (Y358) resides, could also be investigated. While some of them were dynamic (D360-E362) others were found to be rather rigid (A357 and Y358). Residues of the Walker A helix (α_1) in general appeared to be rigid. An exception is residue Y399 in the C-terminal loop of α_1 .

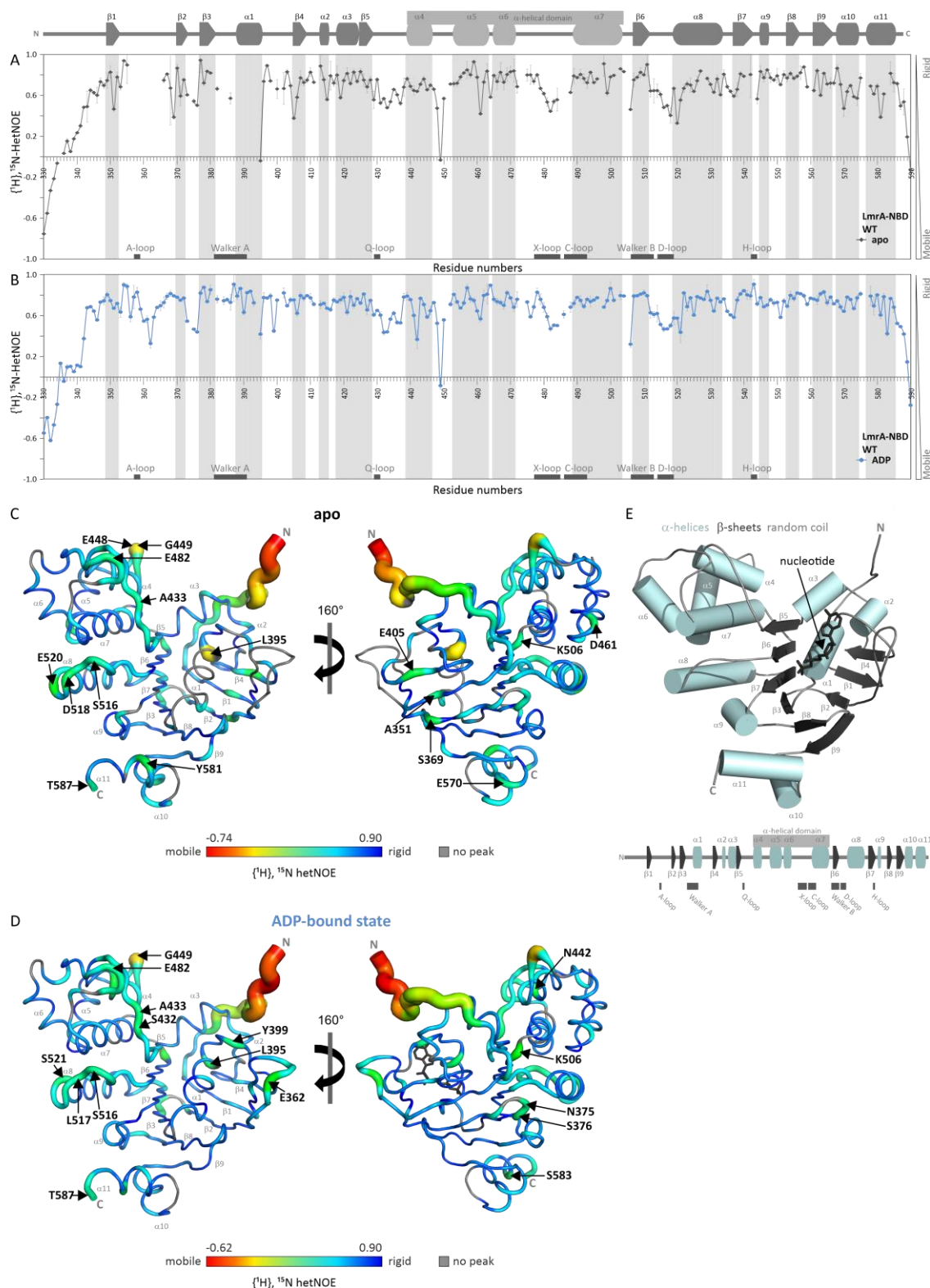


Figure 19: Backbone dynamics of LmrA-NBD in the apo and ADP-bound state determined via $\{^1\text{H}\}$, ^{15}N hetNOE measurements

A, B $\{^1\text{H}\}$, ^{15}N hetNOE values of the backbone amides for the apo (gray) and ADP-bound state (10 mM ADP, blue) of LmrA-NBD WT plotted versus the residue numbers. The error bars represent the standard deviation of the mean from two consecutive hetNOE measurements. Gray boxes represent residues of the conserved motifs of the NBD. The corresponding secondary structure elements of LmrA-NBD are displayed in a topology model on top of the graphs (A and B). Lighter gray indicates the α -helical subdomain. **C, D** $\{^1\text{H}\}$, ^{15}N hetNOE values of the backbone amides of LmrA-NBD WT in the apo state (C) or the ADP-bound state (D) are plotted onto the LmrA-NBD homology model based on Sav1866 (PDB ID: 2HYD³⁴). C-terminal LmrA-NBD homology model ends at residue T587. NBD-NBD interface (left). Color key is shown below the NBD structures. Thicker tubes indicate mobile amino acids and thinner tubes rigid amino acids. Missing data points in the structure

are shown in thin gray tubes and indicate prolines, residues which were not assigned or $\{^1\text{H}\}$, ^{15}N hetNOE values which could not be determined reliably. Amino acid numbering is based on the full-length transporter. E) Ribbon representation of the NBD monomer, view from the NBD-NBD interface (LmrA-NBD model based on Sav1866, PDB ID: 2HYD³⁴), showing the secondary structure elements. Below the NBD monomer the according secondary structure elements of the NBD are displayed, where lighter gray indicates the α -helical subdomain and the conserved motifs are highlighted in dark gray.

For a detailed view which regions of the NBD become more/less mobile in the apo compared to the ADP-bound state, the Δ hetNOE values were plotted on a cartoon representation of a LmrA-NBD homology model based on Sav1866 (PDB ID: 2HYD³⁴, **Figure 20A/B**). 95 amino acids showed strong differences ($>1\sigma$) in dynamics upon addition of ADP (**Figure 20C**), with 45 residues displaying a higher and 50 residues lower rigidity compared to the apo state.

Interestingly, a high number of the residues that become more rigid upon ADP binding are found within the catalytic subdomain, especially in β -sheets β 1 (A351), β 2 (E371), β 3 (I378), β 4 (E405) and β 9 (T563 and S566). As seen in the ^1H - ^{15}N TROSY HSQC and H/D exchange NMR experiments, these residues are localized in and around the NBS. ADP binding also induced rigidity in residues of the C-terminal helices α 10 (E570-T474) and α 11 (Y578-V582). In contrast, more residues between α 2 and β 6 exhibited a higher rigidity in apo than in the ADP-bound state, which is indicated in yellow in the plots of **Figure 20A** and **B**. This finding indicates that the α -helical subdomain is more rigid in the apo state. Exceptions of residues that became rigidified in this subdomain upon ADP are residues L462 in helix α 5, F464 in the kink between helices α 5 and α 6 and, in a minor fashion, residues V480 and G481 of the X-loop.

When looking at other conserved motifs, it was seen that the Q-loop residue Q430 became more rigid upon nucleotide binding. In the D-loop and the C-terminal D-loop helix (α 8), nucleotide induced rigidity (D518, E520, E522, M524, L529 and M533) as well as mobility (A515, S519, S521 and R527) were observed. Furthermore, residues of the C-terminal end of the Walker A helix (α 1) were also found to display contrary dynamic effects, with L395 becoming more rigid, and R397 more mobile upon nucleotide addition.

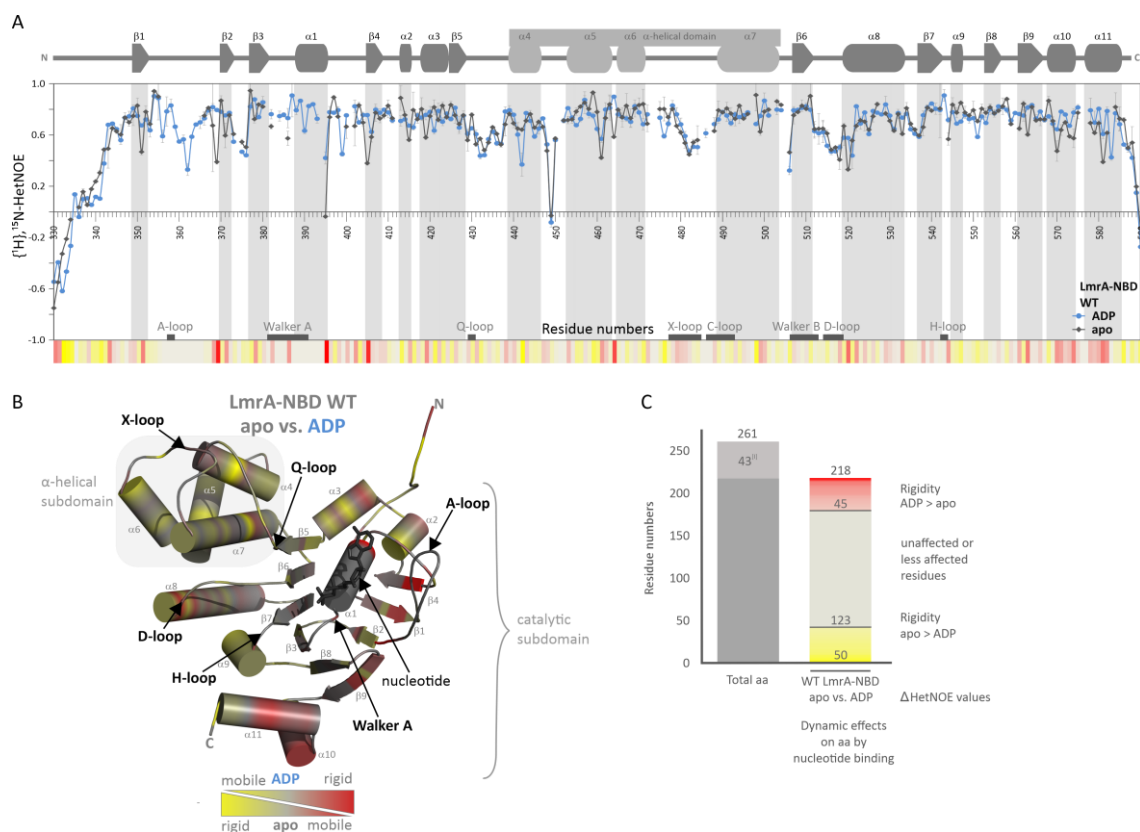


Figure 20: Differences in backbone dynamics on the ps – ns timescale of LmrA-NBD WT between apo and ADP-bound states

A) Overlay of the $\{^1\text{H}\}$, ^{15}N hetNOE values of the backbone amides of LmrA-NBD WT in the apo state (gray) compared to the ADP-bound state (blue) plotted versus the residue numbers (Figure 10). **B)** Difference in $\{^1\text{H}\}$, ^{15}N hetNOE values between LmrA-NBD WT in the apo and ADP-bound state plotted on a LmrA-NBD homology model based on Sav1866 (PDB ID: 2HYD³⁴, nucleotide shown as black sticks). Red indicates $\{^1\text{H}\}$, ^{15}N hetNOE values of LmrA-NBD WT in the ADP-bound state to be higher than in the apo state, i.e. the ADP-bound state is more rigid at this position in the protein than in the apo state. Yellow indicates $\{^1\text{H}\}$, ^{15}N hetNOE values of LmrA-NBD WT in the apo state to be higher than the $\{^1\text{H}\}$, ^{15}N hetNOE values of LmrA-NBD WT in the ADP-bound state, i.e. the apo state is more rigid at this position in the protein than in the ADP-bound state. C-terminal LmrA-NBD homology model ends at residue T587. **C)** Number of amino acids that become either more rigid (red) or more flexible (yellow) in the ADP-bound state compared to the apo state of LmrA-NBD WT. Out of the 218 amino acids, for which the amide resonance could be assigned in both the apo and the ADP-bound states, 45 residues are more rigid in the ADP-bound state, and 50 are more rigid in the apo state. [1] 43 aa residues cannot be evaluated as they remain unassigned in either apo state, ADP-bound state, or both states. 123 aa are either completely unaffected or have low ($<1\sigma$) differences in hetNOE values between the two states.

Unfortunately, only the PET reporter pair in the MsbA-NBD D416C, A518W yielded usable PET-FCS results. Autocorrelation functions (ACFs) of fluorophore-labeled MsbA-NBD D461C-A518W were recorded under various conditions, without nucleotide (apo state), with nucleotide (ADP, MgADP, ATP or MgATP) or with magnesium ions (Mg^{2+}) (**Figure 22**). All ACFs exhibit decays at a lag time (τ_D) of ~ 1.69 to 1.89 ms that arose from translational diffusion (Brownian motion) of the MsbA-NBD molecules through the detection volume of the PET-FCS instrument (**Figure 22, 10.4**. Photoinduced electron transfer – fluorescence correlation spectroscopy (PET-FCS)). These values are appropriate for a protein of the size of MsbA-NBD (~ 29.1 kDa). Additional exponential relaxations (τ_1, τ_2, τ_3) on the nanosecond to microsecond (ns - μ s) time scale have been obtained and potentially arose from the dynamic interaction of the two PET reporters (C461 labeled with AttoOxa11 and W518) in MsbA-NBD (**Figure 22**). Thus, control samples which lacked the engineered tryptophane residue (MsbA-NBD D461C labeled with AttoOxa11) were prepared and measured without nucleotide (apo state), with nucleotide (ADP, MgADP, ATP or MgATP) or magnesium (Mg^{2+}) (**Figure 22**). In these controls, the previously observed additional decays were absent, thus showing that the observed decays in the presence of the tryptophane residue indeed resulted from PET quenching. Residual decays observed in the μ s time scale for some of the control samples can be explained by the fact that the AttoOxa11 is an environmentally sensitive fluorophore that translates structural fluctuations associated with changes in polarity of its microenvironment into minor modulations of fluorescence intensity²⁹⁴. It can be concluded that the decays in the ns - μ s timescale result from intramolecular PET-induced fluorescence fluctuations caused by conformational switching of W418, of C461 labeled with AttoOxa11 or of both W418 and C461 labeled with AttoOxa11. Hence, this position can be used to observe relative, global motions between the α -helical and the catalytic subdomain in the NBD of MsbA. The obtained sub-millisecond decays for the measured samples of MsbA-NBD D461C-A418W are dominated by a single kinetic phase with a relaxation time constant τ_1 . A second, and for two conditions (MgADP and MgATP, **Figure 22B/D**) even a third kinetic phase with τ_2 and τ_3 is underlying the dominant kinetic phase (τ_1). We observed different PET-FCS values for MsbA-NBD D461C-A518W in the different states (apo; Mg^{2+} ; ADP; ATP; MgADP; MgADP). There are no differences between the relaxation time constants of the dominating kinetic phases or the underlying second kinetic phases when comparing the apo state ($\tau_1 = 12.0 \pm 5 \mu$ s, $\tau_2 = 0.9 \pm 0.009 \mu$ s) with the ADP-bound ($\tau_1 = 27 \pm 13 \mu$ s, $\tau_2 = 1.4 \pm 0.5 \mu$ s) or the ATP-bound state ($\tau_1 = 17 \pm 7 \mu$ s, $\tau_2 = 1.1 \pm 0.5 \mu$ s) (**Figure 22A/C**). However, τ_1 of the dominating phase in the presence of MgADP ($\tau_1 = 255 \pm 82 \mu$ s) or MgATP ($\tau_1 = 62 \pm 21 \mu$ s) show significant differences compared to the apo state ($\tau_1 = 12 \pm 5 \mu$ s) and Mg^{2+} ($\tau_1 = 20 \pm 5 \mu$ s) state. Those differences in kinetic phase values are highlighted in blue and light orange in the tables in **Figure 22A/B/C/D** and indicate a decrease in dynamics between α -helical and catalytic subdomain in the presence of MgADP and MgATP compared to the apo state or with magnesium. The PET-FCS experiments on the MsbA-NBD thus lead to two observations: (i) addition of MgADP and MgATP is translated to changes in dynamics between α -helical and catalytic subdomain. Nucleotide binding is thus propagated to regions distant from the NBS. (ii) α -helical and the catalytic subdomain undergo changes in dynamics, specifically a reduction in subdomain dynamics (rigidification) upon addition of MgADP or MgATP.

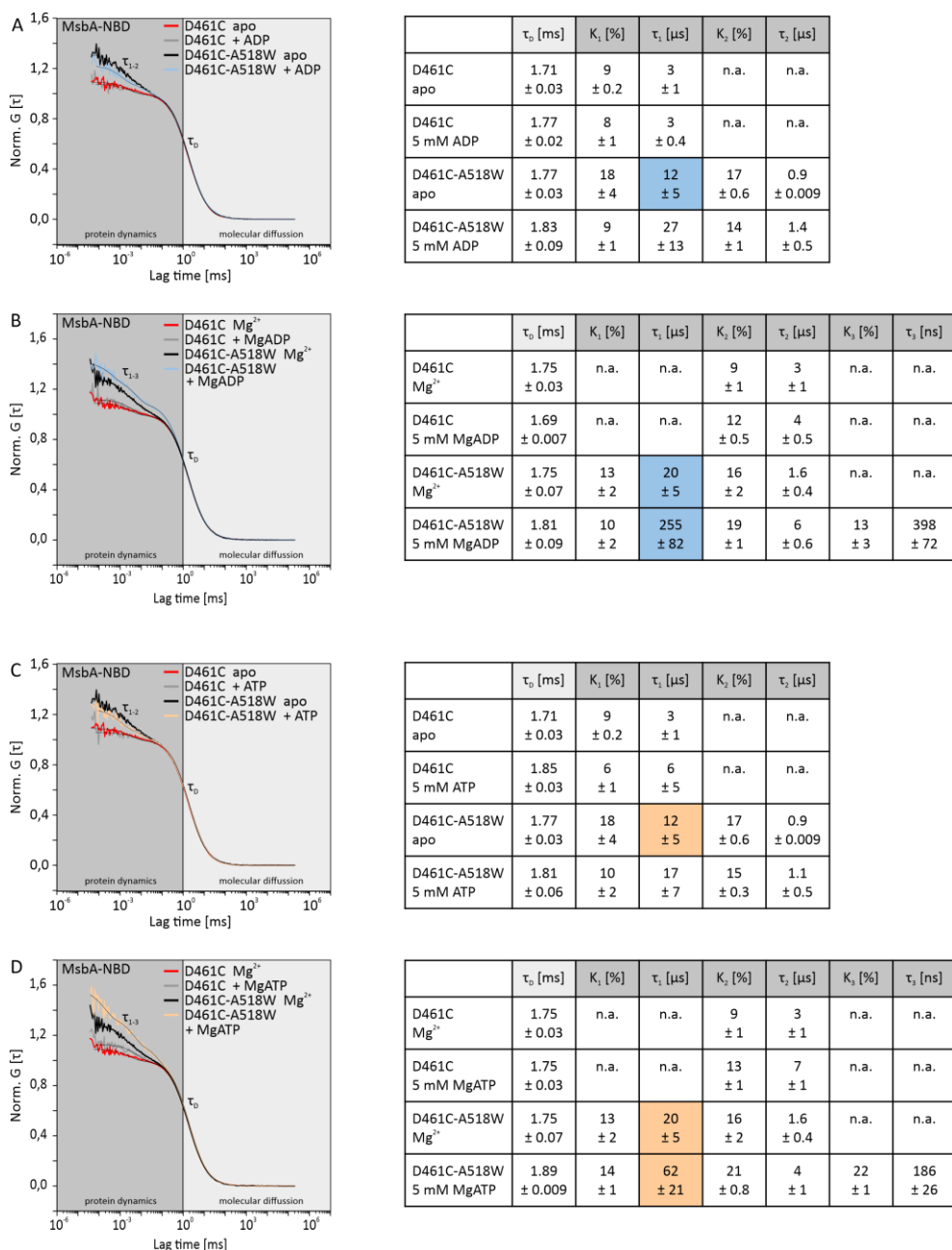


Figure 22: PET-FCS analysis of nucleotide binding within the NBD of MsbA

A, B, C, D) PET-FCS autocorrelation functions $G[\tau]$ (left) recorded from MsbA-NBD D461C-A518W mutant labeled with AttoOxa11 under different conditions in the apo state (black, **A, C**), with Mg^{2+} (black, **B, D**), in the ADP-bound (blue, **A**), MgADP-bound (blue, **B**), the ATP-bound (light orange, **C**) and MgATP-bound state (light orange, **D**). MsbA-NBD D461C labeled with AttoOxa11 was used as a control and measured also under different conditions in the apo state (red, **A, C**), with magnesium (red, **B, D**), in the ADP-bound (gray, **A**), MgADP-bound (gray, **B**), ATP-bound (gray, **C**) and MgATP-bound state (gray, **D**). Due to the lack of a quenching Trp residue in the vicinity, the autocorrelation functions observed for AttoOxa11-labeled MsbA-NBD should not decay due to PET but only due to molecular diffusion. Next to the autocorrelation functions in **A, B, C** and **D** are the tables with kinetic parameters determined for MsbA-NBD D461C-A518W and MsbA-NBD D461C labeled with AttoOxa11 from the PET-FCS measurements under different conditions (apo state, with magnesium, ADP-bound state, MgADP-bound state, ATP-bound state and MgATP-bound state) shown. Errors are standard deviations of three measurements (technical replicates). n.a. – not available. Blue and light orange highlight the observed differences in PET kinetics with and without nucleotide.

2. ROLE OF CONSERVED MOTIFS IN THE NBD OF MULTIDRUG ABC TRANSPORTERS

2.1. Introduction

Almost five decades of research have been carried out to elucidate the molecular details of ABC transporters functional mechanism. However, it remains unclear how exactly ATP hydrolysis leads to substrate transport across a membrane. The role of many highly conserved motifs within the NBD that are involved in ATP binding and hydrolysis, are not yet fully understood. Carrying out solution NMR spectroscopy on the monomeric LmrA-NBD WT revealed that conserved motif residues including in the Walker A motif, D-loop, Q-loop and H-loop can “sense” nucleotide binding (1.2. Nucleotide binding to the NBD: Dynamic consequences for conserved motifs and allosteric signal propagation). However, the crosstalk between these conserved motifs within the NBD remains partially unexplored. Thus, in the course of this thesis, the structural and dynamic consequences of mutating residues within these motifs in the D-, Q- and H-loop were investigated. NMR backbone resonance assignments of the LmrA-NBD mutants D518A (D-loop), Q430A (Q-loop) and H543A (H-loop) in the ADP-bound states were carried out and information about NBD intradomain crosstalk mediated by those conserved residues could be obtained. In addition, the dynamics of the D-loop, Q-loop and H-loop mutants were probed with $\{^1\text{H}\}$, ^{15}N hetNOE measurements and compared to the LmrA-NBD WT.

To gain more information about function of the D-loop motif and its role in the structural dynamics of the NBD, ATP hydrolysis and substrate transport experiments with LmrA from *L. lactis*, BmrA from *B. subtilis* and MsbA from *E. coli* were performed.

2.2. Consequences of mutating D-, Q- and H-loop – a chemical shift analysis

The WT LmrA-NBD as well as its mutants K388A (Walker A motif), D518A (D-loop), Q430A (Q-loop) and H543A (H-loop) can be expressed in high amounts in *E. coli* and purified as soluble proteins. Gel filtration chromatograms, SDS-PAGE, CD spectra and melting curves for the LmrA-NBD variants are similar to the LmrA-NBD WT, which indicates that the overall fold and stability of the NBD is not altered by the mutations (**Figure 23**).

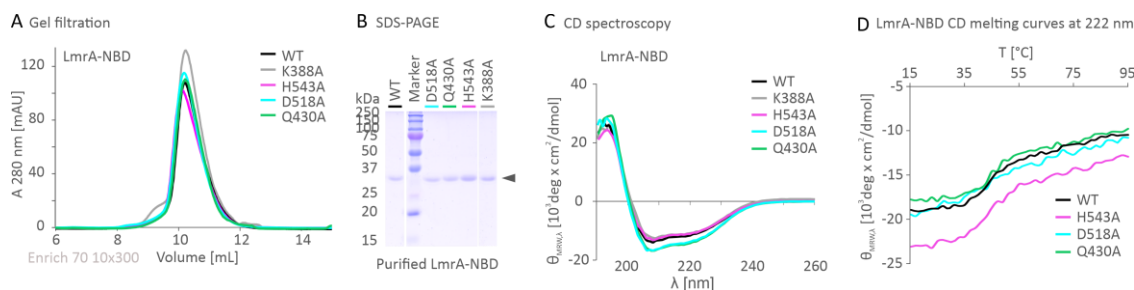


Figure 23: Characterization of WT LmrA-NBD and its variants **A)** Gel filtration profiles for WT LmrA-NBD (black) and LmrA-NBD variants (K388A - gray, D518A - cyan, Q430A - green and H543A - violet). **B)** Purified LmrA-NBD proteins from *E. coli* BL21-Gold (DE3) cells. After the final purification step (SEC run) 5 μ g protein was loaded onto a 15% SDS-PAGE and stained with Coomassie blue. **C)** CD spectra of WT LmrA-NBD (black) and its variants. **D)** CD melting curves recorded for LmrA-NBD WT and its variants. The melting temperature of the purified constructs is $\sim 47^\circ\text{C}$ for WT LmrA-NBD, $\sim 43^\circ\text{C}$ for LmrA-NBD D518A, $\sim 48^\circ\text{C}$ for LmrA-NBD Q430A and 47°C for LmrA-NBD H543A. Amino acid numbering is based on the full-length transporter.

The recorded 2D ^1H - ^{15}N HSQC spectra of the ^{15}N -labeled LmrA-NBD variants yield well-dispersed spectra and showed that the proteins are folded (**Figure 24**, **Figure 25**, **Figure 26** and **Appendix 19**).

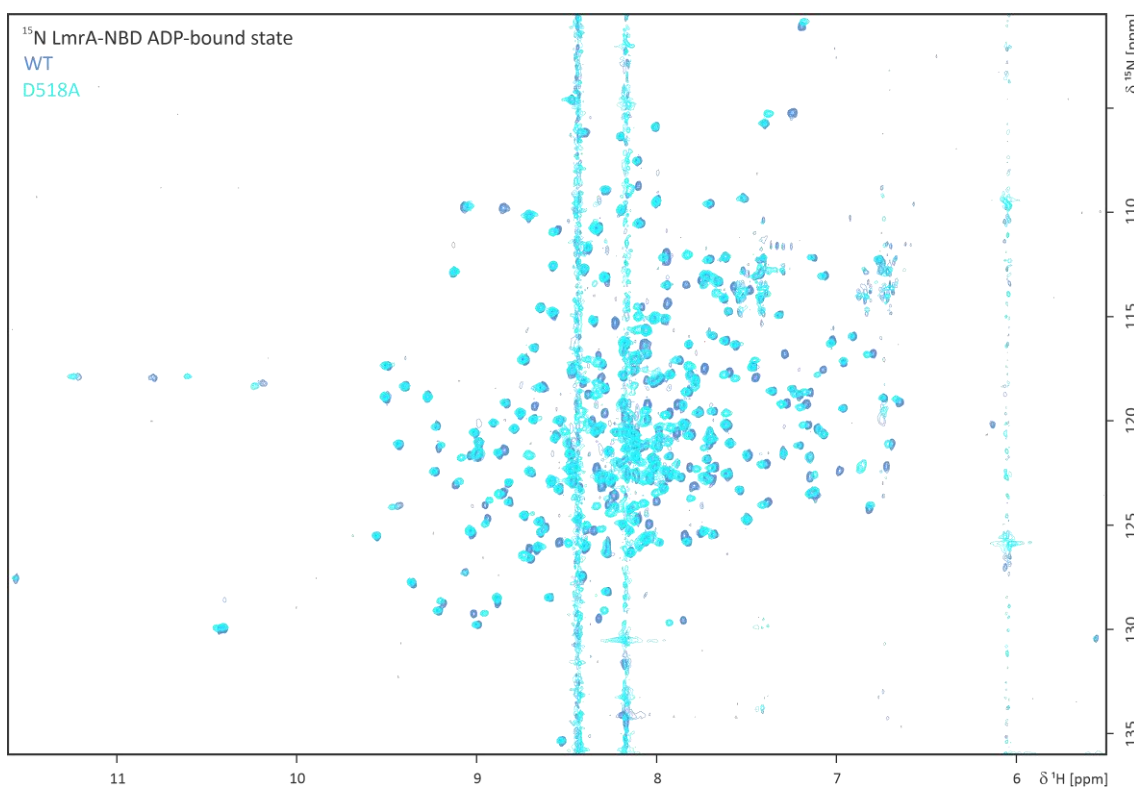


Figure 24: Spectral differences between WT LmrA-NBD and the the D-loop mutant (D518) in the ADP-bound state (10 mM ADP) Overlay of ^1H - ^{15}N TROSY HSQC spectra of ^{15}N -labeled LmrA-NBD WT (blue) and D518A (cyan). See subchapter Material and methods (12. NMR techniques) for exact experimental conditions.

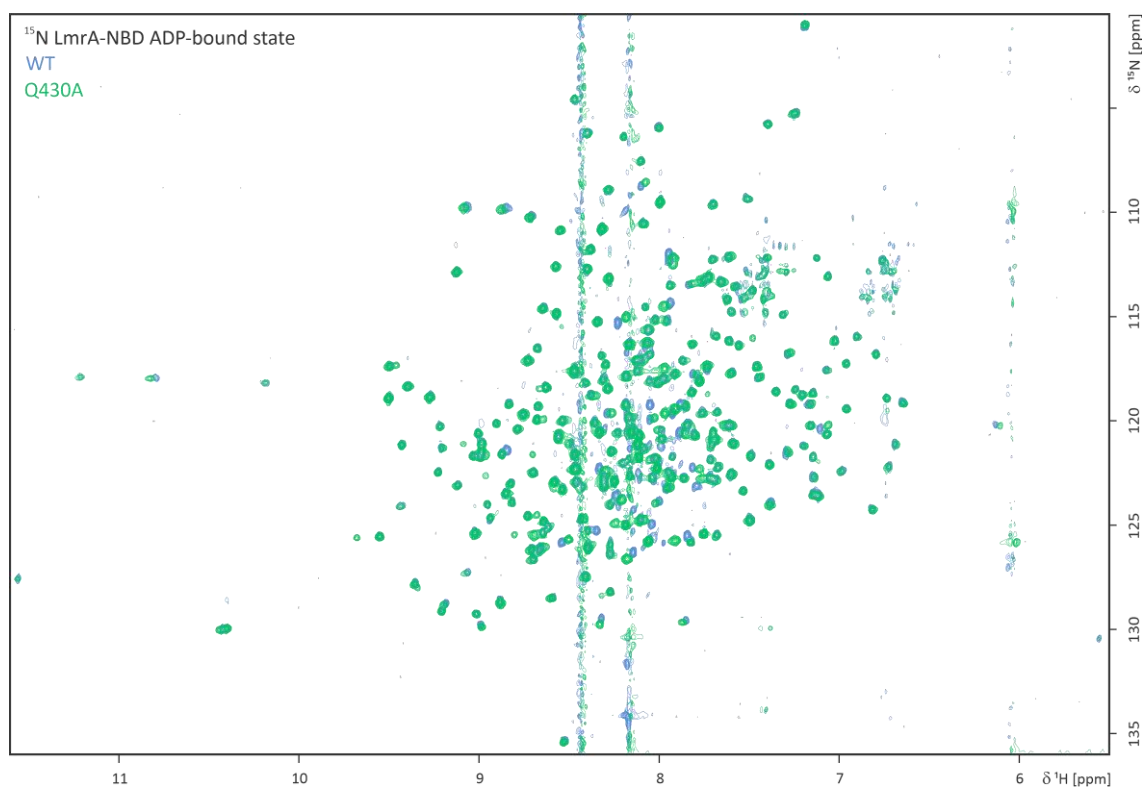


Figure 25: Spectral differences between WT LmrA-NBD and the the Q-loop mutant (Q430A) in the ADP-bound state (10 mM ADP) Overlay of ^1H - ^{15}N TROSY HSQC spectra of ^{15}N -labeled LmrA-NBD WT (blue) and Q430A (green). See subchapter Material and methods (12. NMR techniques) for exact experimental conditions.

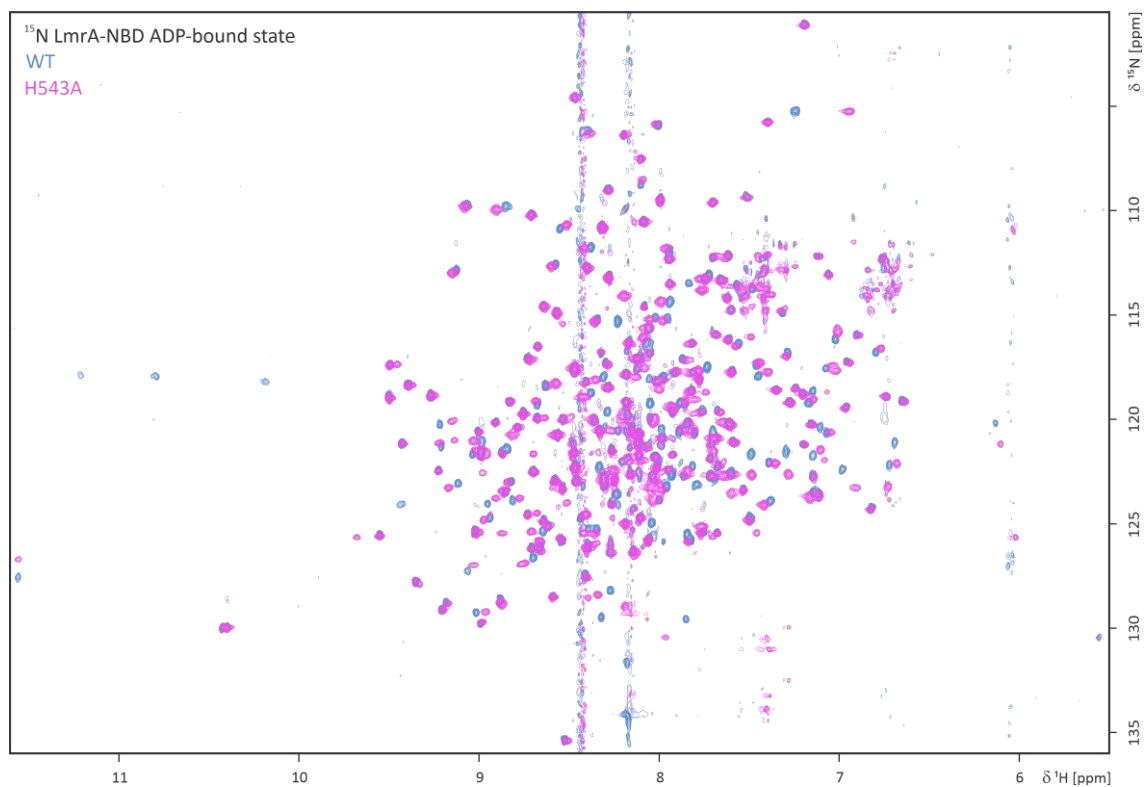


Figure 26: Spectral differences between WT LmrA-NBD and the the H-loop mutant (H543A) in the ADP-bound state (10 mM ADP) Overlay of ^1H - ^{15}N TROSY HSQC spectra of ^{15}N -labeled LmrA-NBD WT (blue) and H543A (violet). See subchapter Material and methods (12. NMR techniques) for exact experimental conditions.

Upon addition of nucleotides, peaks in the ^1H - ^{15}N TROSY HSQC spectra of the LmrA-NBD D518A, Q430A and H543A mutants showed shifts, indicating that these mutants have not lost their ability to interact with nucleotides (**Figure 27A**). In addition, the LmrA-NBD D-, Q- and H-loop mutants showed nucleotide binding affinities for ATP and ADP in the same range as the WT K_D values (**Figure 27B/C**). As described in chapter III results **1.1**. Introducing the Model System for the WT LmrA-NBD, affinity for ADP was always higher than for ATP. Using the NMR chemical shift assignments for the three mutants (see below for more details), it was further possible to determine that the nucleotide indeed interacts with the protein variants at the expected site (**Figure 27A**).

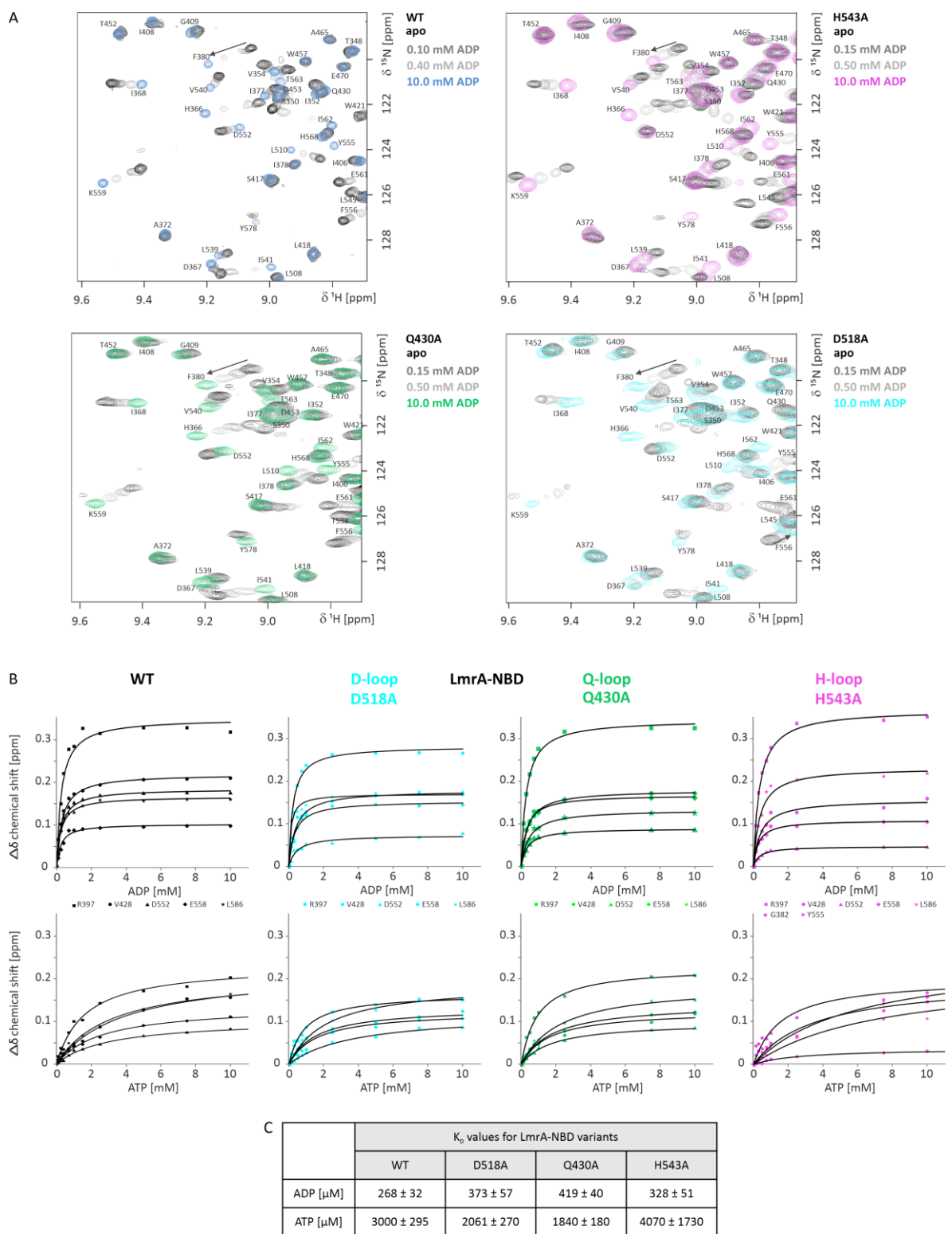


Figure 27: Nucleotide binding ability and affinity is maintained upon mutating the D-, Q- or H-loop residues in LmrA-NBD
A) ^1H - ^{15}N TROSY HSQC spectra of ^{15}N -labeled LmrA-NBD WT and its variants (D518A, Q430A and H543A) titrated with different concentrations of ADP. **B)** Chemical shift differences ($\Delta\delta$) of NH resonances of residues, R397, V428, D552, E558 and L586 in the background of LmrA-NBD WT (black), LmrA-NBD D518A (cyan), LmrA-NBD Q430A (green), are plotted versus ADP or ATP concentration. The same residues were used to obtain the plot for LmrA-NBD H543A (violet) with ADP, while residues G382, R397, Y555, E558 and L586 were plotted upon addition of ATP. **C)** K_D values of ADP and ATP binding to LmrA-NBD variants \pm standard deviation.

Taking advantage of the well-resolved HSQC spectra of the D-loop (D518A), Q-loop (Q430A) and H-loop (H543A) mutants in the ADP-bound state, a combination of de novo backbone assignments and chemical shift transfers using the available assignment of the WT LmrA-NBD²⁷⁹ was used to obtain near-complete amide chemical shift assignments for the three mutant proteins (~89% for LmrA-NBD D518A, ~94% for Q430A and ~91% for H543A, respectively). These assignments then allowed a detailed comparison which amino acids within the NBD “sense” the mutation and how this affects the conserved motifs (**Figure 28**, **Figure 24**, **Figure 25** and **Figure 26**).

It is noteworthy, that several NH resonances that are present and unambiguously assigned in the LmrA-NBD WT could not be observed within the D-, Q- and H-loop mutants (**Figure 28**). This might indicate that the respective residues are in intermediate exchange (μs – ms timescale) within the mutants and consequently, that the D-, Q- or H-loop are important for stabilizing those regions within LmrA-NBD WT. Peaks which could not be assigned in the ADP-bound state of LmrA-NBD WT did also not show up in the ^1H - ^{15}N TROSY HSQC spectra of the three LmrA-NBD mutants. For the D-loop mutant (D518A), most residues whose resonances showed line broadening compared to the WT protein were indeed located within or in the vicinity of the D-loop (A515 and S519) and the D-loop helix $\alpha 8$ (E522-Q526, D530 and S531). Furthermore, additional NH resonances in the Walker A motif (T390), in the loop between helices $\alpha 6$ and $\alpha 7$ (L476), in the C-loop (G490) as well as residues of β -sheet 8 (K506, I554) were not present in the D-loop mutant. In the Q-loop mutant (Q430A) the resonance for the neighboring residue D431 next to the mutation also disappeared. The H-loop mutant led to missing NH resonances of residues which are located in (G385, K388-T390) or near (I391) the Walker A motif, as well as for residue A513, which is between Walker B motif and D-loop.

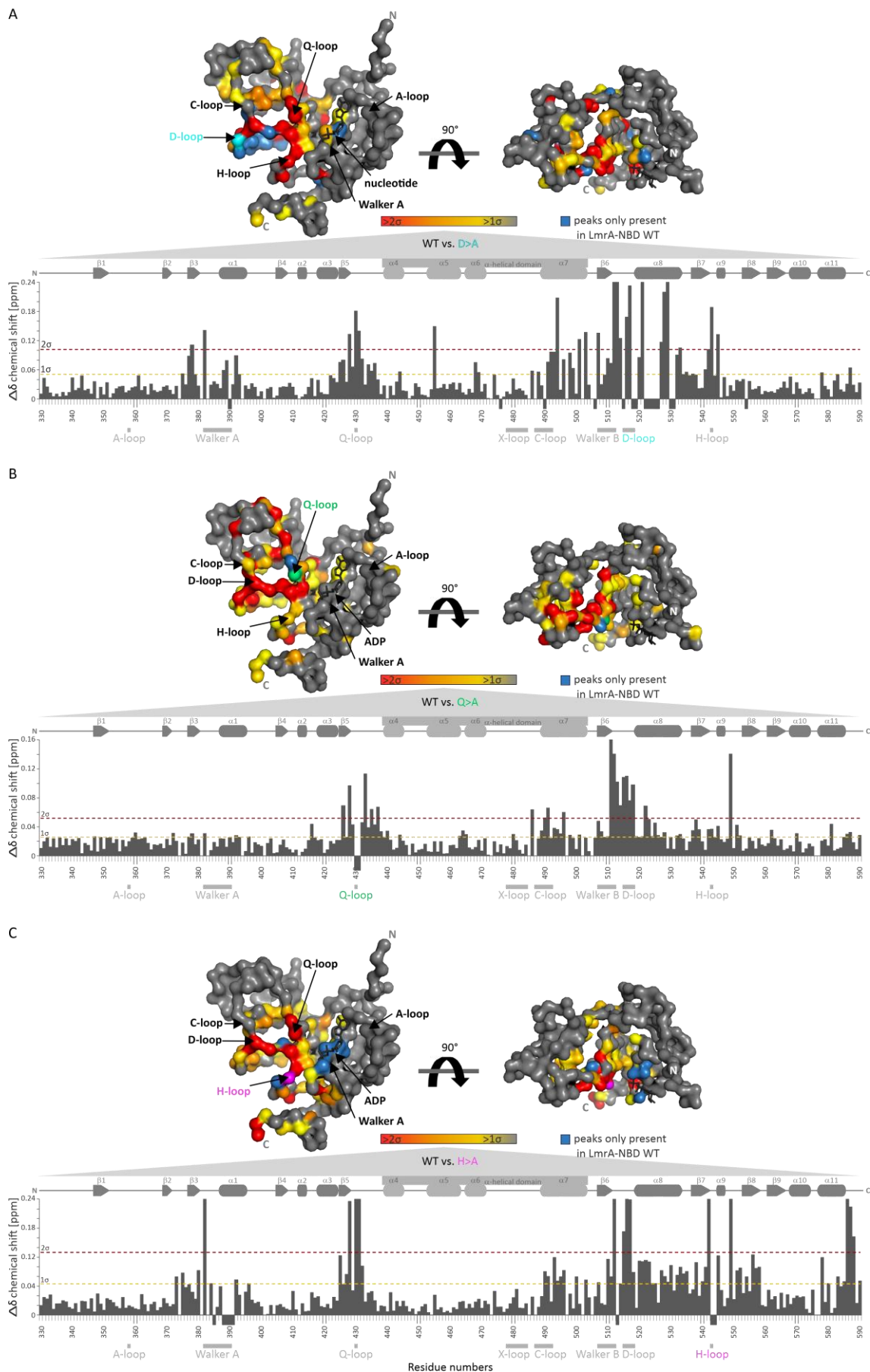


Figure 28: Chemical shift differences between LmrA-NBD WT and the D-loop (D518A), Q-loop (Q430A) or H-loop (H543A) mutants in the ADP-bound state

Chemical shift differences between LmrA-NBD WT and the D-loop (D518A), Q-loop (Q430A) or H-loop (H543A) mutants in the ADP-bound state

A) Chemical shift differences between LmrA-NBD WT and D518A mutant. **B)** Chemical shift differences between LmrA-NBD WT and Q430A mutant. **C)** Chemical shift differences between LmrA-NBD WT and H543A mutant. In all plots (A, B and C), amino acid numbering is based on the full-length transporter, the yellow and red dotted lines indicate 1 σ and 2 σ standard deviation. Above the bar graphs of A, B and C, the corresponding secondary structure elements of LmrA-NBD are displayed. Lighter gray indicates the α -helical subdomain. Gray boxes represent residues of the conserved motifs of the NBD. Downward orientated bars represent peaks not present in the ADP-bound state of the LmrA-NBD variants (D518A, Q430A or H543A) but in the WT. Above the bar graphs of A, B and C, chemical shift changes are shown plotted on a ribbon surface representation of a LmrA-NBD homology model based on Sav1866 (PDB ID: 2HYD³⁴). View on the NBD-NBD interface (left) and view on the coupling helix groove (right) are shown. Color gradient from yellow to red represents increasing chemical shift differences from $>1 \sigma$ (yellow) to $>2 \sigma$ (red). C-terminal LmrA-NBD homology model ends at residue T587. Residues with $\Delta\delta$ values below 1 σ , residues whose $\Delta\delta$ values could not be determined reliably (missing in plots of A, B and C) or remain unassigned (missing in plots of A, B and C) are shown in gray in the ribbons surface representations of A, B and C.

In addition to resonances fully disappearing, the chemical shift of many NH resonances of residues in different conserved motifs including the Walker A motif, the Walker B motif, the D-loop and H-loop as well as the D-loop helix and the α -helical subdomain showed perturbations compared to the corresponding WT resonances upon the introduction of the D-, Q- or H-loop mutations.

In both the D-loop and H-loop mutants, chemical shift changes in the Walker A motif could be observed (D-loop mutant G382, K388 and S389; H-loop G382) in addition to peaks showing significant line broadening as pointed out above. Although the Walker A motif is known to be important for nucleotide binding¹⁶⁴, apparently the observed changes in its chemical environment by the H-loop mutant and D-loop mutant yield not to a loss of nucleotide binding within the NBD, as it was seen that the K_D values of the LmrA-NBD mutants for ADP (H/A: $328 \pm 51 \mu\text{M}$, D/A: $373 \pm 57 \mu\text{M}$) and ATP (H/A: $4070 \pm 1730 \mu\text{M}$, D/A: $2061 \pm 270 \mu\text{M}$) were in the same range as the WT LmrA-NBD (K_D ADP = $268 \pm 32 \mu\text{M}$ and K_D ATP = $3000 \pm 295 \mu\text{M}$). In contrast to the D-loop and H-loop mutations, the Q-loop mutation did not result in chemical shift changes of NH resonances from Walker A motif residues. As a control, a mutant in the Walker A motif (K388A) with decreased ATPase activity was used^{194,195,309}. The spectra of this variant did not show chemical shift differences between the apo state and the nucleotide bound states. This may indicate that nucleotide binding is either abolished or that the binding affinity of this mutant is significantly decreased. The latter explanation seems more likely as this Walker A mutant does show ATP hydrolysis, although at a much slower rate than the WT protein (**Appendix 20**).

Chemical shift differences between D-, Q- or H-loop mutants and WT LmrA-NBD were also observed for the NH resonances of Walker B motif residues. When mutating the Q-loop, the chemical shifts of all six Walker B motif residues (⁵⁰⁷ILMLDE⁵¹²) were perturbed. When mutating the H- or the D-loop, residues I507 and L510-E512 were affected.

Interestingly, mutation of the D-loop aspartate (D518A), Q-loop glutamine (Q430A) or the H-loop histidine (H543A) residues also affects the chemical shift of resonances of residues within the coupling helix groove compared to the NBD WT (**Figure 28** and **Figure 29**). This groove connects the NBD to the TMD and thus plays an important role in transmitting interdomain information. Mutation of the D-loop led to chemical shift differences for coupling helix groove residues I425, G426, V428-S431 and I434-A436 in comparison to the LmrA-NBD WT (**Figure 28** and **Figure 29**). Mutating the Q-loop led to chemical shift differences for coupling helix groove residues G426-S429 and D431-R440 and mutating the H-loop coupling helix groove residues I425, F427, V428 and Q430-S432 showed chemical shift differences compared to the WT (**Figure 28** and **Figure 29**). Notably, V428, which is part of the flexible Q-loop as well as the coupling helix groove, was affected by both the addition of nucleotide within the LmrA-NBD WT and upon introduction of mutations in the D-, Q- or H-loop motifs (**Figure 29**). In summary, the fact that the residues in the coupling helix groove are affected both by nucleotide addition and mutation of the conserved motifs supports the notion that the three

conserved motifs, D-, Q- and H-loop, are involved in communication between the NBD and TMD within an ABC transporter.

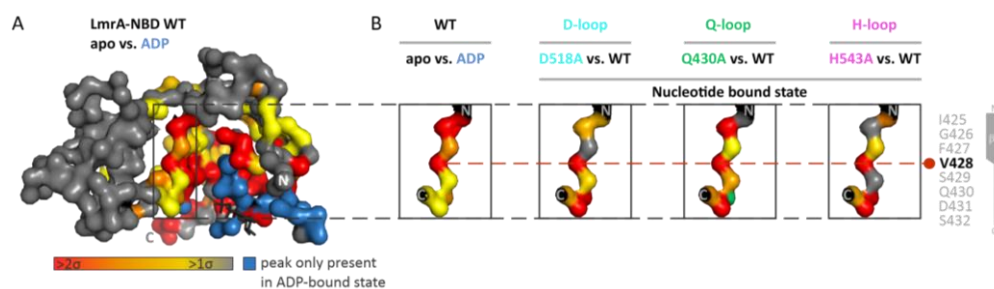


Figure 29: Nucleotide binding and mutation of conserved motifs affect residues within the coupling helix groove
A) Chemical shift differences ($\Delta\delta$) from ^1H - ^{15}N TROSY HSQC experiments of ^{15}N -labeled LmrA-NBD in the apo and ADP-bound state plotted on a ribbon surface representation of a LmrA-NBD homology model based on Sav1866 (PDB ID: 2HYD³⁴, **Figure 17**). View on the coupling helix groove within the NBD, which contacts the TMD. **B)** Zoom-ins of the coupling helix region of residues I425 – S432, which show significant $\Delta\delta$ CS between the LmrA-NBD WT in the apo and ADP-bound state and the LmrA-NBD WT and the D-loop, Q-loop, and H-loop mutants in the ADP-bound state. Amino acid numbering is based on the full-length transporter, yellow and red spheres indicate significant chemical shift differences ($>1\sigma$ and $>2\sigma$ standard deviation). Blue spheres indicate residues whose peaks are only present in the ^1H - ^{15}N HSQC spectra of the ADP-bound state of the WT LmrA-NBD. Residues with chemical shift differences below 1σ , residues whose $\Delta\delta$ values could not be determined reliably or remain unassigned are shown in gray.

For the LmrA-NBD WT, chemical shift changes of some resonances of residues in the C-terminal region (residues L568-Q590 with H568-T574 forming helix α_{10} and L577-Q585 forming helix α_{11}) were observed when adding nucleotide (**Figure 17**). Residues in this region were also affected when mutating the D-, Q- or H-loop motifs (**Figure 28**), albeit to very different degrees. In particular, the mutation of the H-loop led to large chemical shift differences in the C-terminal unstructured region (residues L586-V588, Q590). In addition, the H543A mutation also induced minor chemical shift differences for residues Y578, K580, S583 and Q585, which are located in the C-terminal helix α_{11} . The mutation of the Q-loop and D-loop led to only a few small chemical shift differences. In the case of the Q-loop mutant, residues E570 within helix α_{10} , Y581 of helix α_{11} and L586, T587 and Q590 within the unstructured region of the C-terminal region were affected. The D-loop mutant showed chemical shift differences for residues Y578 and S583 in helix α_{11} and residue T587 in the unstructured C-terminal end.

Finally, a strong influence of the D-, Q- and H-loop residues on each other was observed indicating a crosstalk between these three motifs (**Figure 30**). This did not only affect the resonances for amino acids D518, Q430 and H543 in the respective mutants, but also additional residues in the D-loop helix (8α). These either vanished (see above) or showed distinct chemical shift changes. In particular, NH resonances for residues S519-A528, D530, L532 and M533 were affected by the Q-loop mutation, while NH resonances of residues E520-V524 and R527-M533 showed chemical shift changes when the H-loop was mutated.

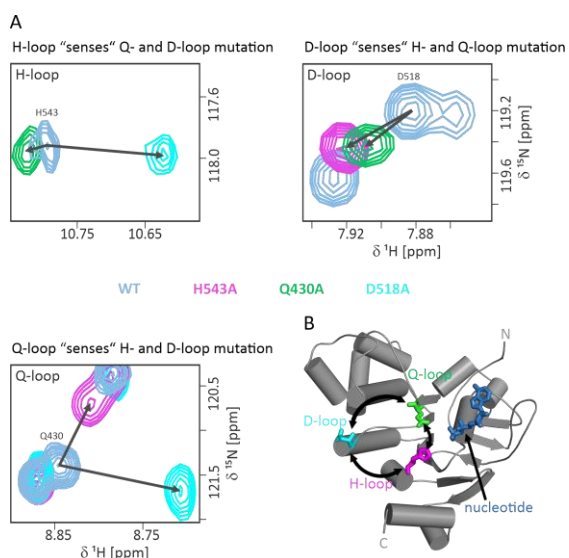


Figure 30: Crosstalk between the conserved D-, Q- and H-loop motifs

A) Close-up views of the ^1H - ^{15}N TROSY HSQC spectra of ^{15}N -labeled LmrA-NBD WT and its variants (D518A, Q430A and H543A), showing selected chemical shift changes by mutagenesis of D- (cyan), Q- (green) and H-loop (violet) in the ADP-bound state (**Figure 24**, **Figure 25** and **Figure 26**). **B)** Homology model of LmrA-NBD based on Sav1866 (PDB ID: 2HYD³⁴) illustrating the intradomain crosstalk between D-, Q- and H-loop. The nucleotide is colored blue. Amino acid numbering is based on the full-length transporter.

In chapter III results **1**. Consequences of nucleotide binding to the NBD of multidrug ABC transporters, titration of ^{15}N -labeled LmrA-NBD WT with nucleotides and the recording of ^1H - ^{15}N TROSY HSQC experiments indicated that conserved motifs including the Q-loop and D-loop “sense” nucleotide binding and can distinguish between ATP and ADP (**Figure 16B**, **Figure 31A**). Strikingly, the D-loop aspartate in the H543A background did not show chemical shift differences between the apo and either nucleotide bound state (**Figure 31B**, **Appendix 21** and **Appendix 22**). As the H-loop mutant had a similar affinity to nucleotides as the WT LmrA-NBD (**Figure 27**), this presumably shows that the D-loop aspartate residue lost the ability to sense and distinguish between nucleotides when the H-loop histidine residue is mutated. In contrast, the other D-loop motif residues, $^{515}\text{ASL}^{517}$, were still able to “sense” and distinguish nucleotide binding in the mutated H-loop background (**Appendix 23**, **2.4**. Molecular crosstalk of the NBD depends on the D-loop motif). Hence, the H-loop might be crucial for transmitting the information of nucleotide occupancy to the D-loop. The analysis of the resonance of the H-loop histidine residue other than in the ADP-bound state was not possible because the peak for H543 was only present in the ADP-bound state.

In the Q430A background, residue D518 of the D-loop was still able to “sense” nucleotide binding (**Figure 31C**, **Appendix 24** and **Appendix 25**) although the direction of the chemical shift changed when nucleotides were added compared to the NBD WT (**Figure 31A/C**). Thus, it indicates that information of nucleotide occupancy still reaches the D-loop.

Similar observations as for the D-loop aspartate residue could also be made for the Q-loop glutamine. The NH resonance of the Q-loop glutamine residue “sensed” nucleotides, when the H-loop (H543A) or D-loop (D518A) motifs were mutated (**Figure 31D/E**, **Appendix 21**, **Appendix 22**, **Appendix 24** and **Appendix 25**). However, it was noted that the direction of the chemical shifts changed for the Q-loop glutamine residue when mutating H543A or D518A in LmrA-NBD compared to the WT (**Figure 31A/D/E**).

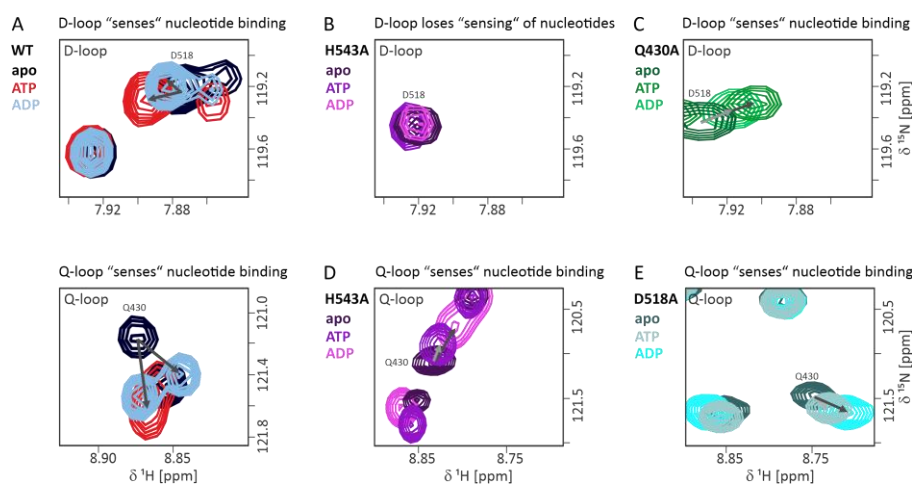


Figure 31: Effect of nucleotide addition to the NH resonances of residues within the conserved D-loop and Q-loop motifs
A) Close-up views of ^1H - ^{15}N TROSY HSQC spectra of ^{15}N -labeled LmrA-NBD WT showing the resonance for the D-loop aspartate residue (top) and the Q-loop glutamine residue (bottom). Overlays of the apo (black), ATP-bound (red) and ADP-bound (blue) states are shown (**Appendix 13** and **Appendix 26**). **B)** Close-up views of ^1H - ^{15}N TROSY HSQC spectra of ^{15}N -labeled LmrA-NBD H543A showing the resonance for the D-loop aspartate residue. Overlays of the apo (dark purple), ATP-bound (purple) and ADP-bound (violet) states are shown (**Appendix 21** and **Appendix 22**). **C)** Close-up views of ^1H - ^{15}N TROSY HSQC spectra of ^{15}N -labeled LmrA-NBD Q430A showing the D-loop aspartate residue. Overlays show the apo (dark green), ATP-bound (olive green) and ADP-bound (green) states (**Appendix 24** and **Appendix 25**). **D)** Close-up views of ^1H - ^{15}N TROSY HSQC spectra of ^{15}N -labeled LmrA-NBD H543A showing the Q-loop glutamine residue. Overlays show the apo (dark purple), ATP-bound (purple) and ADP-bound (violet) states (**Appendix 21** and **Appendix 22**). **E)** Close-up views of ^1H - ^{15}N TROSY HSQC spectra of ^{15}N -labeled LmrA-NBD D518A showing the Q-loop glutamine residue. Overlays show the apo (dark turquoise), ATP-bound (light turquoise) and ADP-bound (cyan) states (**Appendix 27** and **Appendix 28**). For the ADP-bound and ATP-bound states 10 mM nucleotide was added. Amino acid numbering is based on the full-length transporter.

2.3. Fast Backbone Dynamics of LmrA-NBD D-, Q- or H – loop mutants in the ADP-bound state

To complement the ^1H - ^{15}N TROSY HSQC chemical shift perturbation experiments, residue specific backbone dynamics of the ^2H - ^{15}N -labeled D-, Q- or H-loop variants of LmrA-NBD in the ADP-bound state were probed on the ps - ns timescale via $\{^1\text{H}\}$, ^{15}N hetNOE experiments. The resulting hetNOE values of each mutant in comparison to the results for the LmrA-NBD WT were plotted against the amino acid residue numbers (**Figure 32**). HetNOE values close to 1.0 are indicative of rigid regions within the protein, which mostly coincide with folded domains (**12.8**. Backbone hetNOE analysis). Very flexible protein backbone regions show hetNOE values close to or below 0. As expected, both in the WT and the D-, Q- and H-loop variants of LmrA-NBD in the ADP-bound state, the N- and C-termini are very flexible while the majority of the residues have hetNOE values $> \sim 0.6$ ³⁰⁷ indicative of stable secondary structure (**Figure 32**). For a better visualization of the the NBD backbone dynamics the hetNOE values were plotted on a LmrA-NBD homology model based on Sav1866 (PDB ID: 2HYD³⁴, **Figure 33A/B/C/D**).

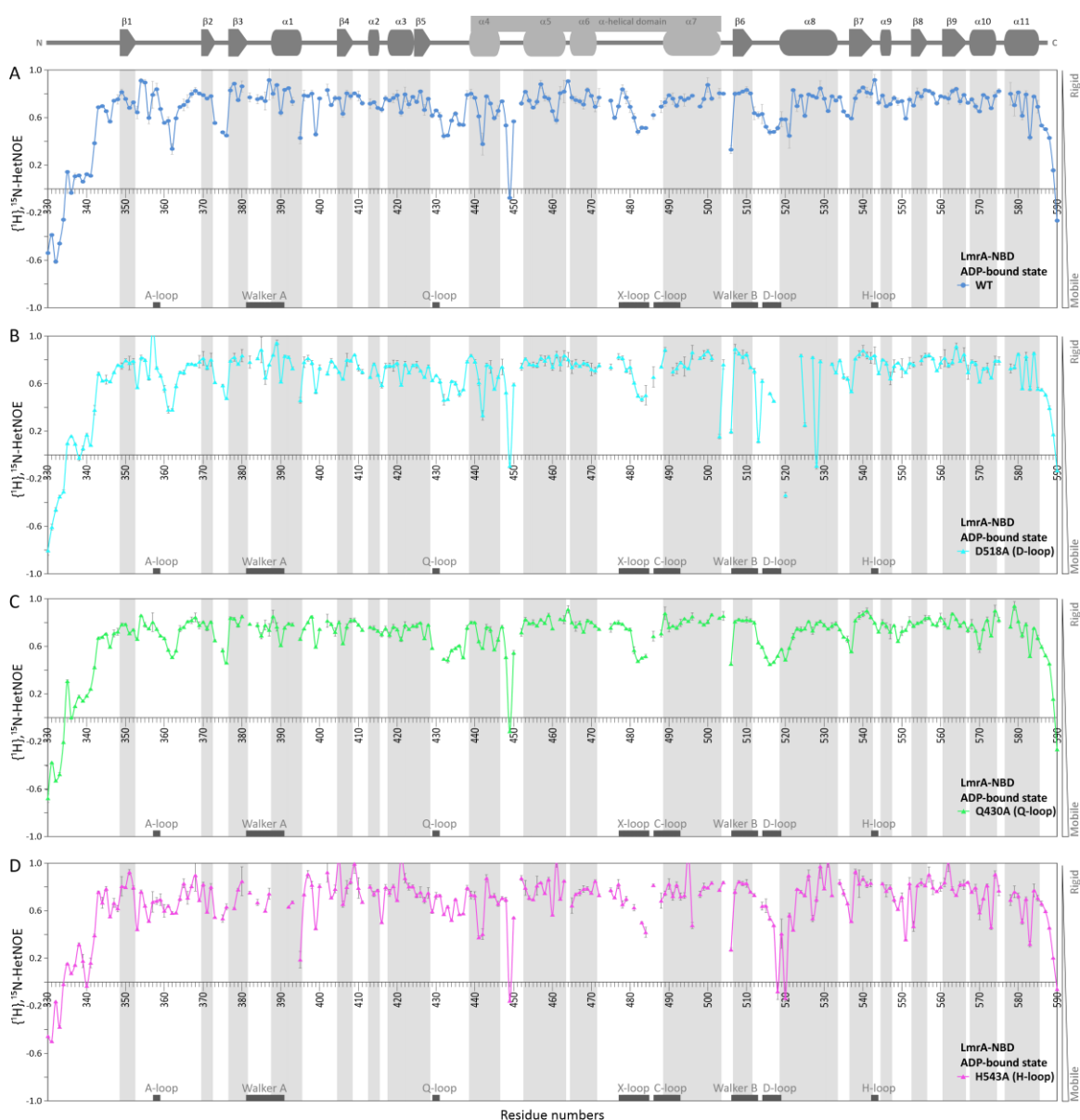


Figure 32: Backbone dynamics of LmrA-NBD WT and the D-, Q- and H-loop variants in the ADP-bound state

A) $\{^1\text{H}\}$, ^{15}N hetNOE values of the backbone amides within the ADP-bound state of LmrA-NBD WT (blue) plotted versus residue numbers. **B)** $\{^1\text{H}\}$, ^{15}N hetNOE values of the backbone amides within the ADP-bound state of LmrA-NBD D518A (D-loop, cyan) plotted versus residue numbers. **C)** $\{^1\text{H}\}$, ^{15}N hetNOE values of the backbone amides within the ADP-bound state of LmrA-NBD Q430A (Q-loop, green) plotted versus residue numbers. **D)** $\{^1\text{H}\}$, ^{15}N hetNOE values of the backbone amides within the ADP-bound state of LmrA-NBD H543A (H-loop, violet) plotted versus residue numbers. Above all diagrams (A, B, C and D) the corresponding secondary structure elements of LmrA-NBD are displayed. Lighter gray indicates the α -helical subdomain. "Missing" data points indicate either prolines, unassigned residues or $\{^1\text{H}\}$, ^{15}N hetNOE values that could not be determined reliably. The error bars represent the standard deviation of the mean from two consecutive hetNOE measurements. Gray boxes represent residues of the conserved motifs of the NBD. Amino acid numbering is based on the full-length transporter.

Both the WT LmrA-NBD and the D-, Q- and H-loop mutants have four regions with very high backbone flexibility, the N-terminus (D330-L342, G346), the C-terminus (D330-L342), the region between the α -helical and the catalytic (including RecA-like subdomain) subdomain (specifically residue K506 between helix $\alpha 7$ and β -sheet 6) and within the α -helical subdomain (G449) between helices $\alpha 4$ and $\alpha 5$ (Figure 32 and Figure 33). Flexibility can be also noted for residues in or in vicinity of key functional motifs of ABC transporters in all four NBD constructs. This includes residues H353 and D360-Q363 in the loop between β -sheets 1 and 2 near the conserved A-loop (Y358) and residues S429, S432-I434, A436 and G437 (between β -sheet 5 and helix $\alpha 4$) which are flanking the Q-loop glutamine residue.

As the Q-loop is located at the interface between the α -helical and the catalytic subdomain, this result is not unexpected. The X-loop is located between helices $\alpha 6$ and $\alpha 7$. Here, residues R483 and G484 show increased flexibility. Other residues which showed to be dynamic in all four constructs were residues N375 and S376 in the loop between β -sheets 2 and 3, residue Y399 at the end of the Walker A helix (between $\alpha 1$ and $\beta 4$), residue N442 in the helix $\alpha 4$ and N450 in the loop between helices $\alpha 4$ and $\alpha 5$.

The region in and around the D-loop is also dynamic and shows similarities and differences with the inserted mutations. So, residues 516SL517 of the D-loop ($A^{516}SL^{517}D$) flexibility when the D-loop aspartate (D518A), Q-loop glutamine or the H-loop (H543A) were mutated. The H-loop mutant yield to a decrease in flexibility for the D-loop residue A515, whereas the other two mutation did not decrease its flexibility. In addition, in the H543A mutant, high flexibility was observed for the D-loop residue D518 (**Figure 32A/C** and **Figure 33B/D**). Residues in the D-loop helix $\alpha 8$ ($^{519}SESES^{523}$, $^{525}VQRAL^{529}$ and S531) following the D-loop also showed high backbone dynamics in the D-loop and/or H-loop mutant. Specifically, residues E520, V525, A528 were affected upon mutating the D-loop and residues S519-S523, V525-L529 and S531 when mutating the H-loop (**Figure 32A/C** and **Figure 33B/D**). Furthermore, drastic dynamics were observed for the D-loop vicinal residue A513 in the background of the D-loop mutant but not the H-loop mutant. Intriguingly, mutagenesis of the Q-loop did not lead to significant changes in the dynamics of the D-loop region in comparison to the WT NBD (**Figure 32A/C** and **Figure 33A/C**).

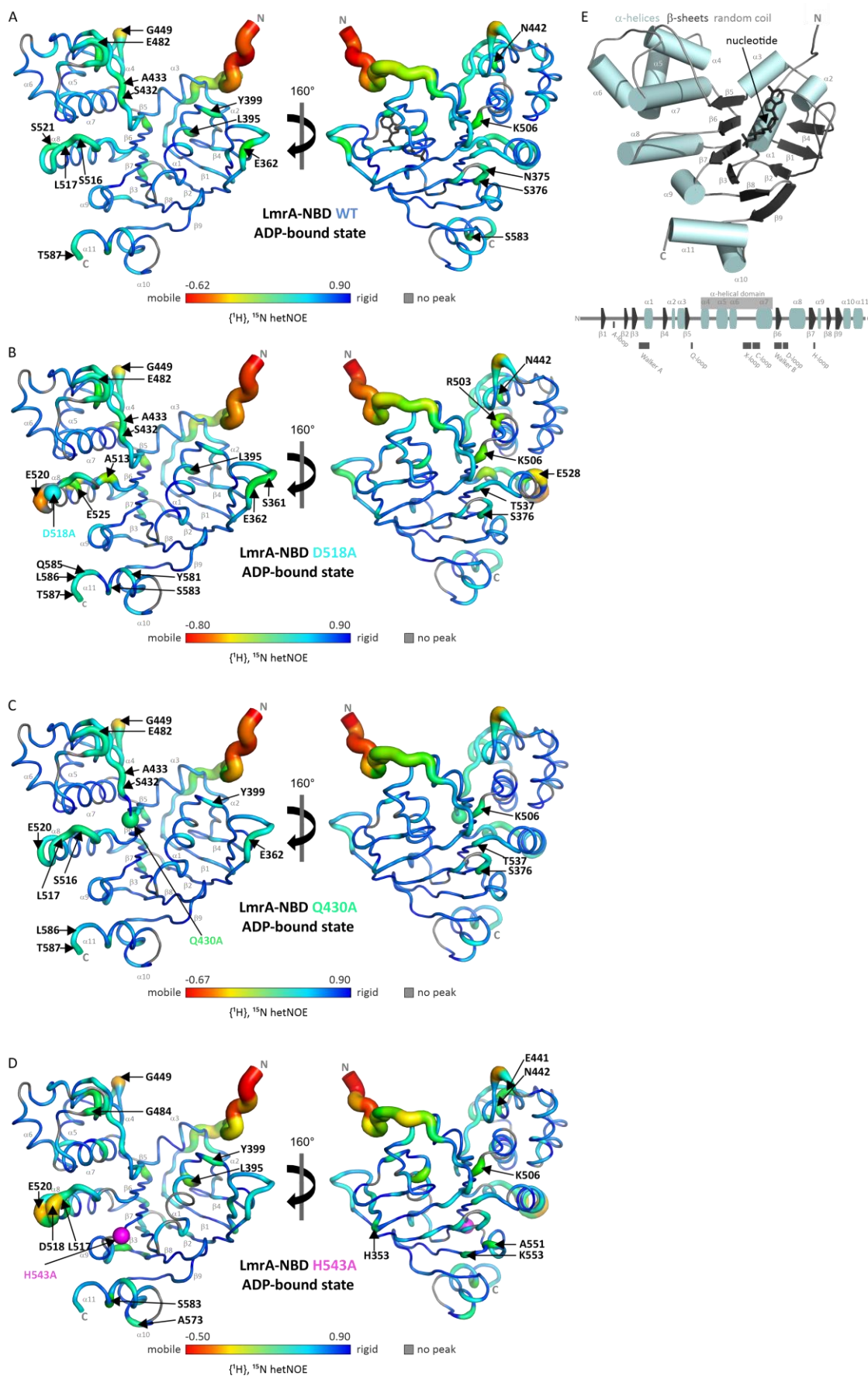


Figure 33: Backbone dynamics of LmrA-NBD WT and the D-, Q- and H-loop variants in the ADP-bound state

Backbone dynamics of LmrA-NBD WT and the D-, Q- and H-loop variants in the ADP-bound state

A) $\{^1\text{H}\}$, ^{15}N hetNOE values of the backbone amides of LmrA-NBD WT in the ADP-bound state are plotted onto the LmrA-NBD homology model based on Sav1866 (PDB ID: 2HYD³⁴). **B)** $\{^1\text{H}\}$, ^{15}N hetNOE values for the D-loop mutant (D518A). **C)** $\{^1\text{H}\}$, ^{15}N hetNOE values for the Q-loop mutant (Q430A). **D)** $\{^1\text{H}\}$, ^{15}N hetNOE values for the H-loop mutant (H543A). Color code see below the structures. Thicker tubes indicate mobile amino acids and thinner tubes rigid amino acids. Missing data points in the structure are shown in thin gray tubes and indicate prolines, residues which were not assigned or $\{^1\text{H}\}$, ^{15}N hetNOE values that could not be determined reliably. Amino acid numbering is based on the full-length transporter. C-terminal LmrA-NBD homology model ends at residue T587. **E)** Cartoon representation of secondary structure elements of the LmrA-NBD homology model based on Sav1866 (PDB ID: 2HYD³⁴).

Comparison of backbone dynamics between WT and the D-, Q- and H-loop variants of LmrA-NBD in the ADP-bound state

Comparing the $\{^1\text{H}\}$, ^{15}N hetNOE values of the LmrA-NBD WT with the D-, Q- or H-loop mutants, an overall similar trend and subsequently a similar behavior in dynamics can be observed (**Figure 32** and **Figure 33**). To pinpoint differences between the constructs in more detail, the differences in $\{^1\text{H}\}$, ^{15}N hetNOE values between the WT and the respective mutant were also plotted against the protein sequence (**Figure 34A/B/C**). In addition, these differences were also plotted on the LmrA-NBD homology model based on Sav1866 (PDB ID: 2HYD³⁴) (**Figure 34D**). To specify how many residues are overall dynamically affected, a bar graph displaying the overall numbers of residues strongly affected ($>1\sigma$) is shown in **Figure 35**. When the D-loop was mutated, 92 residues showed dynamic differences compared to the WT, with 52 residues displaying higher and 40 residues lower rigidity within LmrA-NBD D518A. The Q-loop mutation also affected 92 residues, with 77 residues displaying higher and 15 residues lower rigidity within LmrA-NBD Q430A. Furthermore, in the H-loop mutant, the highest number of residues (118 total) was affected, with 73 residues displaying a higher and 45 residues a lower rigidity compared to the NBD WT. In general, more residues within the NBD became rigid when the mutations within the D-, Q- or H-loop were introduced and the H-loop mutant had the most noticeable affects. An ABC transporter NBD contains two large β -sheet regions, one of which is formed by $\beta 1$, $\beta 4$ and $\beta 2$ and the other by the remaining β -strands (**Figure 34D**). In these β -sheets, mutation of the H-loop residue H543 leads to the rigidification of residues within $\beta 1$ (S350-H352), $\beta 2$ (E371), $\beta 4$ (E405) and $\beta 9$ (E561 and I562). This was not observed for either the D-loop or the Q-loop mutations (**Figure 34A/B/D**). Thus, the H-loop seems to play a role in enabling long-range dynamics in highly conserved structural elements of an ABC transporter NBD.

In the following, a closer look will be taken at residues that with altered rigidity in the context of the single point mutations in the D-, Q- and H-loop compared to the WT. A particular focus of interest are the conserved motifs (e.g. A-loop, Walker A motif, Walker B motif, Q-loop and D-loop), the secondary structure element following the D-loop the helix $\alpha 8$ (D-loop helix), the C-terminal region (residues H568-T574 belonging to $\alpha 10$, L577-Q585 belonging to $\alpha 11$ and L586-Q590 belonging to the unstructured C-terminal end) and the α -helical subdomain.

One conserved motif whose stability was affected when mutating the H- or the D-loop but not the Q-loop was the A-loop (Y358). In either case, residue Y358 was more mobile compared to the WT (**Figure 34A/B/D**). This indicates that the A-loop residue Y358 becomes stabilized by the H-loop histidine residue and the D-loop aspartate residue. For the H543A mutation, the residues H353-A357, which are N-terminal from residue Y358, also showed higher mobility compared to the WT. The D518A mutation showed a similar effect for residues H353-D355, but residue A357 showed a decrease in flexibility. Mutation Q430A showed an increase in flexibility for D355 and a decrease in flexibility for the following residue F356. Residues 360DSE362 C-terminal of the A-loop residue Y358 showed also differences in flexibility upon inserting of one of the three mutations (D518A, Q430A or H543A) in the LmrA-NBD. Specifically, mutation H543A showed a decrease in flexibility for residues 360DSE362.

Mutation Q430A showed also a decrease in flexibility for residues D360 and E362 and no difference for residue S361. In contrast, mutation D518A led to an increase in flexibility for S361 and no difference in dynamics in comparison to the WT for residues D360 and E362.

Residues in the Walker A motif (³⁸⁴SGGGKS³⁸⁹) also show significant differences in {¹H}, ¹⁵N hetNOE values between LmrA-NBD WT and the mutants (D518A, Q430A or H543A) (**Figure 34A/B/C/D**). The dynamic of residue S384 was only affected by the H543A mutation which led to increased mobility compared to the NBD WT. G385 was not affected by the H543A mutation while the Q-loop and D-loop mutants affected it differently, leading to increased and decreased mobility, respectively. The opposite was observed for G386, where both the D-loop and the H-loop mutation led to increased mobility while the Q430A mutant led to a decreased dynamic. Residue G387 is the only residue in the Walker A motif that is affected by all three mutations similarly with increased dynamics compared to the WT. K388 is only affected by the Q430A mutation, which leads to a stabilization of this residue. Finally, residue S389 is more mobile in the Q430A background, less mobile in the D518A mutant and not affected by the H543A mutation.

In the other Walker motif, the Walker B motif (⁵⁰⁷ILMLDE⁵¹²), only the catalytic glutamine residue (E512) showed to become more rigid, when inserting one of the mutations, D518A, Q430A or H543A. The other residues (⁵⁰⁷ILMLD⁵¹¹) of the Walker B motif remained on a similar level to be rigid in the NBD WT and the mutated NBDs.

In the H543A background, the Q-loop glutamine residue (Q430) and two vicinal residues (D431-A433) were found to be more rigid. Interestingly, the H-loop histidine (H543) was also found to be more rigid in the Q430A background (**Figure 34B/C/D**) compared to the WT. These findings show that H- and Q-loop may be dynamically coupled. In addition, the mobility of the H-loop seems to be further connected to the D-loop, because we also observed the H-loop histidine residue H543 to be more rigid in the D518A background compared to the WT (**Figure 34A/D**). In return, the first two amino acids of the D-loop (⁵¹⁵AS⁵¹⁶LD) are more mobile in the WT compared to the H543A mutant (**Figure 34C**). In contrast, the aspartate residue (ASLD⁵¹⁸) of the D-loop is more rigid within the WT compared to H543A (**Figure 34C/D**), hence different amino acids within the same conserved motif can react differently to the mutation of a second conserved motif. Nevertheless, these observations indicate that D-loop and H-loop are also dynamically connected. In addition, no influence on the dynamics of the observable D-loop residues ⁵¹⁶SL⁵¹⁷ was noted when mutating the D-loop aspartate (D518A).

A position which shows one of the most drastic differences in dynamics between LmrA-NBD WT and the D-loop (**Figure 34A/D**) and H-loop mutants (**Figure 34C/D**) is the D-loop helix (S519-M533). Residues E520, V525 and A528 show significantly increased mobility compared to the WT NBD when the D-loop aspartic acid (**Figure 34A/D**) was mutated. In contrast, mutation of the H-loop (**Figure 34C/D**) led to both decreased (S519, E520, E522 and R527) and increased (S521, S523, V525, Q526, L529 and S531) rigidification compared to the WT. For the Q-loop mutation (**Figure 34B/D**), only minor differences could be observed, but here again residues with increased (E520, E522) as well as decreased mobility (S521, S523, V525, S531 and M533) were detected. In conclusion, this seems to indicate that the Q-loop plays only a minor role in stabilizing the D-loop helix, while the H- and D-loops both strongly influence D-loop helix dynamics.

Within the C-terminal region (residues H568-T574 belonging to α 10, L577-Q585 belonging to α 11 and L586-Q590 belonging to the unstructured C-terminal end, **Figure 34**), all three mutants showed different yet pronounced effects. In the D518A mutant, residues L571, Y578, Y581 and Q585 became less and residues N569, S583, E584 and Q590 more rigid compared to the WT (**Figure 34A/D**). The H543A mutation increased the mobility for many residues within the C-terminal region (L571, A573 and K580-S583) but led to more rigid residues (L586, T587 and Q590) within the unstructured C-

terminal region (L586-Q590) (**Figure 34C/D**). Mutation of residue Q430 in the Q-loop led to changes in mobility for a number of residues (N569, V572, T574, A579, Y581 and S583) within the C-terminal region (**Figure 34B/D**). Together, these results for the C-terminal region may indicate that structural and/or dynamic changes in the D-, Q- and H-loop, potentially upon nucleotide binding and hydrolysis, might be associated to dynamic changes in the C-terminal region (especially for helix $\alpha 11$). The H-loop seems to be of particular importance for this effect because mutating it led to the highest differences in dynamics compared to the WT. Furthermore, the conserved motifs may even be important to maintain a dynamic equilibrium within the C-terminal helix $\alpha 11$ of LmrA-NBD WT in the ADP-bound state, whereas the H-loop might be important for rigidity and the D- and Q-loop for mobility.

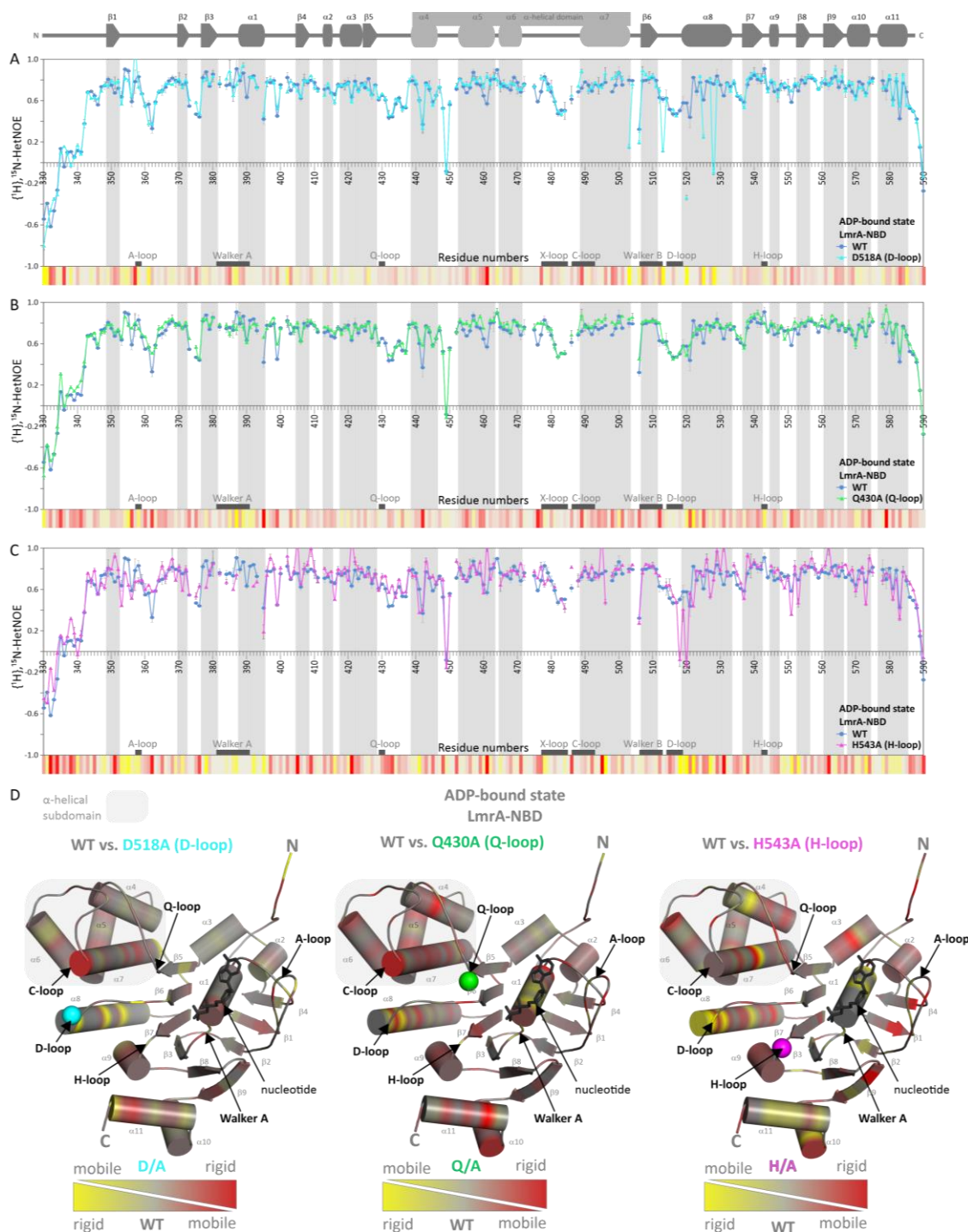


Figure 34: Differences in backbone dynamics between LmrA-NBD WT and its D-, Q- or H-loop mutant

Differences in backbone dynamics between LmrA-NBD WT and its D-, Q- or H-loop mutant

A) $\{^1\text{H}\}$, ^{15}N hetNOE values of the backbone amides within the ADP-bound state of LmrA-NBD WT (blue) compared to the D-loop variant D518A (cyan) plotted versus residue numbers. **B)** $\{^1\text{H}\}$, ^{15}N hetNOE values of the backbone amides within the ADP-bound state of LmrA-NBD WT (blue) compared to the Q-loop variant Q430A (green) plotted versus residue numbers. **C)** $\{^1\text{H}\}$, ^{15}N hetNOE values of the backbone amides within the ADP-bound state of LmrA-NBD WT (blue) compared to the H-loop variant H543A (violet) plotted versus residue numbers. **D)** Differences in the $\{^1\text{H}\}$, ^{15}N hetNOE values for LmrA-NBD WT and the respective mutant are mapped on a LmrA-NBD homology model based on Sav1866 (PDB ID: 2HYD³⁴). C-terminal LmrA-NBD homology model ends at residue T587. Yellow indicates $\{^1\text{H}\}$, ^{15}N hetNOE values of LmrA-NBD WT in the ADP-bound state to be higher than for the respective mutant, i.e. this residue in the LmrA-NBD WT is more rigid than in the respective mutant. Red indicates $\{^1\text{H}\}$, ^{15}N hetNOE values of the respective mutant in the ADP-bound state to be higher than the LmrA-NBD WT, i.e. this residue in the mutant is more rigid than in the LmrA-NBD WT. Above the diagrams (A/B/C), the corresponding secondary structure elements of LmrA-NBD are displayed. Lighter gray indicates the α -helical subdomain. "Missing" data points in the diagrams of A, B or C indicate either prolines, unassigned residues or $\{^1\text{H}\}$, ^{15}N hetNOE values that could not be determined reliably. The error bars in the diagrams of A, B and C represent the standard deviation of the mean from two consecutive hetNOE measurements. Gray boxes represent residues of the conserved motifs of the NBD. Amino acid numbering is based on the full-length transporter.

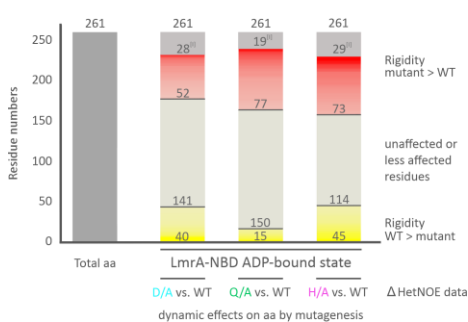


Figure 35: Differences in backbone dynamics caused by mutations in D-, Q- or H-loop

Number of amino acid residues that became more (red) or less (yellow) rigid within the 261 aa of LmrA-NBD variants (D518A - cyan, Q430A - green and H543A - violet) compared to the LmrA-NBD WT. In all three mutants, 141, 150 or 114 aa residues, respectively, remain unaffected or have non-significant ($<1\sigma$) differences in hetNOE values between WT and mutant. [1] 28, 19 and 29 aa residues, respectively, cannot be evaluated as they remain unassigned in either WT, mutant, or both.

Mutations of D-, Q- or H-loop also affected residues in the α -helical subdomain. The majority of residues in the D-loop mutant (D455, V459-D461, F468, N477, V480, S488, G489, A496, A498, R499 and F501), Q-loop mutant (N442, E454-L456, V459, L460, S467, N471, L476, N477, V480, K486, G489, R492, R494-A496, A498 and F501) and H-loop mutant (L443, Y445, E448, T452, L456, V459, D461, F468, N471, L476, N477, K486, R492, L495, F501) showed decreased mobility compared to LmrA-NBD WT (Figure 34A/B/C/D). Less residues in the D-loop mutant (W457, F464, V469, E470, E479, Q491, R503), Q-loop mutant (W457 and A500) and H-loop mutant (E441, G449, L460, L462, A465, T478, G484, A496, A500) displayed increased mobility compared to LmrA-NBD WT. The H-loop mutant led to drastic differences in dynamics for residues D461, K486, L495 and A49. Thus, D-, Q- and H-loop seem to play a major role for mobility within the α -helical subdomain in the LmrA-NBD WT.

2.4. Molecular crosstalk of the NBD depends on the D-loop motif

The D-loop consensus sequence is SALD. While MsbA indeed contains this consensus sequence, it is slightly varied in LmrA (ASLD) and BmrA (SSLD) (**Figure 37A**). Thus, the D-loop alterations ASLD and SALD were generated in BmrA and the D-loop alterations SSLD and SALD in LmrA to study effects on structure and dynamics on the NBD. Furthermore, in full-length BmrA, either the conserved aspartate (D510A) or the entire D-loop (SSLD → SALD and SSLD → ASLD) was mutated. These constructs were used to investigate the role of the D-loop on ATPase and transport activity.

First, it was analyzed whether the D-loop mutations had any influence on the overall structural integrity, oligomerization state or secondary structure of the proteins. Therefore, size exclusion (SEC) chromatography profiles, SDS-PAGE and, in the case of the isolated NBDs, also CD spectra were compared to the respective WT constructs. No differences in SEC or SDS-PAGE running behavior or within the CD spectra could be observed (**Figure 36**). This indicates that the D-loop variants did not perturb the overall fold and secondary structure of the proteins. Furthermore, the effects on the chemical shifts in the ^1H - ^{15}N -HSQCs of the NBD were mapped to probe how mutagenesis of the D-loop affects the remainder of the protein (**Appendix 29**).

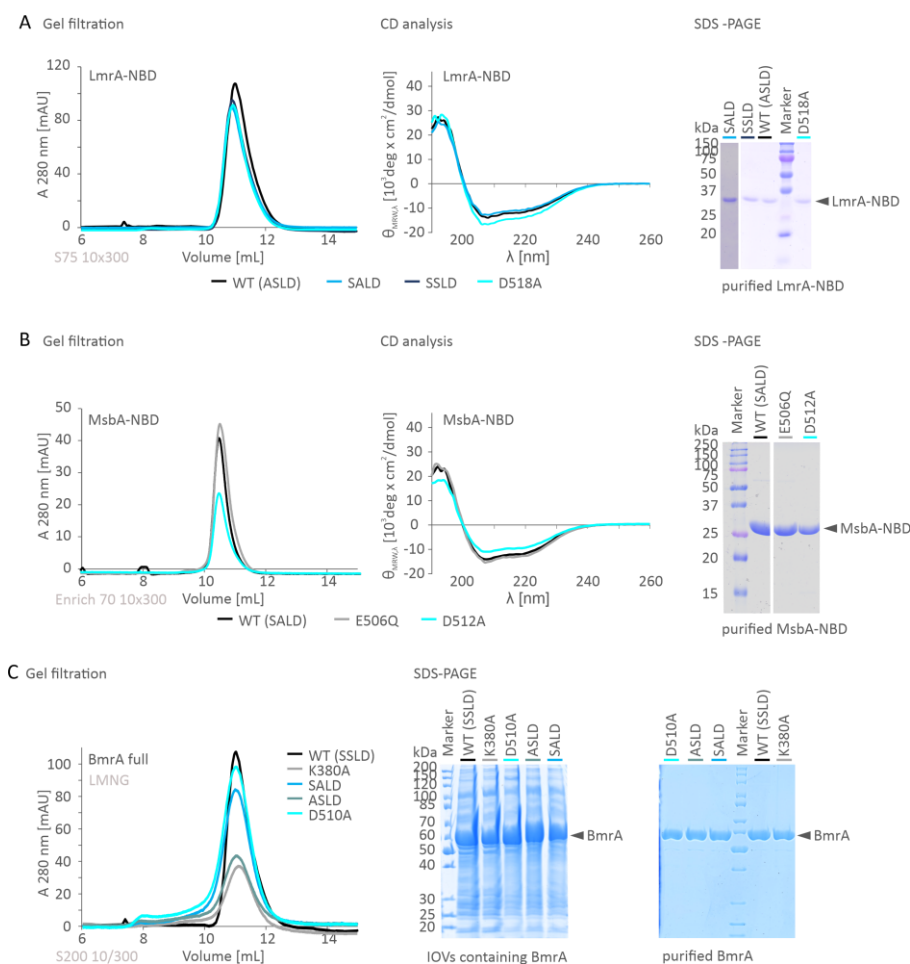


Figure 36: Structural integrity of the D-loop variants of LmrA-NBD, MsbA-NBD and full-length BmrA

A) Structural integrity of LmrA-NBD WT and its D-loop variants (SALD - light blue, SSLD - dark blue and D518A - cyan) analyzed by gel filtration, CD spectroscopy and SDS-PAGE (15% gel and stained with Coomassie blue). **B)** Structural integrity of MsbA-NBD WT and its variants (E506Q - gray and D512A - cyan) analyzed by gel filtration, CD spectroscopy and SDS-PAGE (15% gel and stained with Coomassie blue). **C)** Gel filtration of full-length BmrA WT and its variants (K380A - gray, SALD - light blue, ASLD - dark cyan and D510A - cyan) in LMNG. (left) SDS-PAGE (12% gel) stained with Coomassie blue showing the overexpression of full-length BmrA WT and its variants (K380A - gray, SALD - light blue, ASLD - dark cyan and D510A - cyan) in IOVs of *E. coli* C41 (DE3) cells. (middle) SDS-PAGE (12% gel) stained with Coomassie blue showing full-length BmrA WT and its variants (K380A - gray, SALD - light blue, ASLD - dark cyan and D510A - cyan) after purification in LMNG (right). IOV - Inside out vesicles. LMNG - Lauryl maltose neopentyl glycol.

To analyze the consequences of D-loop variations on substrate transport, full-length BmrA was heterologously expressed in *E. coli* and inside out vesicles (IOVs) were prepared. Similar to the WT with its SSLD D-loop sequence, the variants introducing the consensus sequence (SALD) or that from LmrA (ASLD) were still able to transport substrates in an ATP-dependent manner. (**Figure 37B**). In contrast, the D510A mutant behaved as the negative control in which the Walker A lysine was mutated (K380A). Both variants are transport inactive. Next, the ATPase activity of all full-length constructs was determined in the detergent lauryl maltose neopentyl glycol (LMNG) as well as with protein reconstituted into liposomes (**Figure 37C**). As reported in the literature, the lipid environment led to an increase in ATP hydrolysis for WT full-length BmrA^{137,195} (**Figure 37C**). Similarly, BmrA SALD and BmrA ASLD showed ATPase activity both in detergent and in liposomes. Interestingly, the ATPase activity for BmrA ASLD is significantly higher in lipids compared to what was observed for the WT (SSLD) and the SALD variant. In contrast, both the BmrA D510A mutant and the negative control, BmrA K380A, are inactive. Many ABC exporters are known to display “stimulated ATPase activity”, i.e. the ability of a substrate to increase the ATPase activity. In the case of BmrA WT, a slight stimulation with reserpine or Hoechst 33342 could be observed. The SALD mutant could also be stimulated with reserpine but not Hoechst 33342. For the ASLD mutant neither compound showed a stimulation of ATPase activity. However, importantly, this mutant showed by far the highest basal ATPase activity (Values of BmrA WT = 2.79 ± 0.16 and ASLD = 5.44 ± 0.34 reconstituted in liposomes normalized to full-length BmrA WT in LMNG). This may indicate that BmrA ASLD has already reached its maximal ATP turnover capacity and can thus not be stimulated further. However, and equally importantly, this enhanced ATPase activity does not come with an increase in transport activity (**Figure 37B**) indicating that ATPase activity and substrate transport may not be optimally coupled in this mutant. The K380A and D510A mutants showed no ATPase activity in the presence of either drug (**Figure 37C**).

In addition to these experiments with the full-length BmrA transporter, the ATPase activity was also determined for the isolated NBDs of LmrA and MsbA. For MsbA-NBD WT, ATPase activity could be measured, which was abrogated when the D512A mutant was introduced. A mutation in the Walker B motif (E506Q) served as the negative control (**Figure 37D** and **Appendix 30**). In contrast, none of the tested LmrA-NBD constructs showed any ATPase activity (**Appendix 31**).

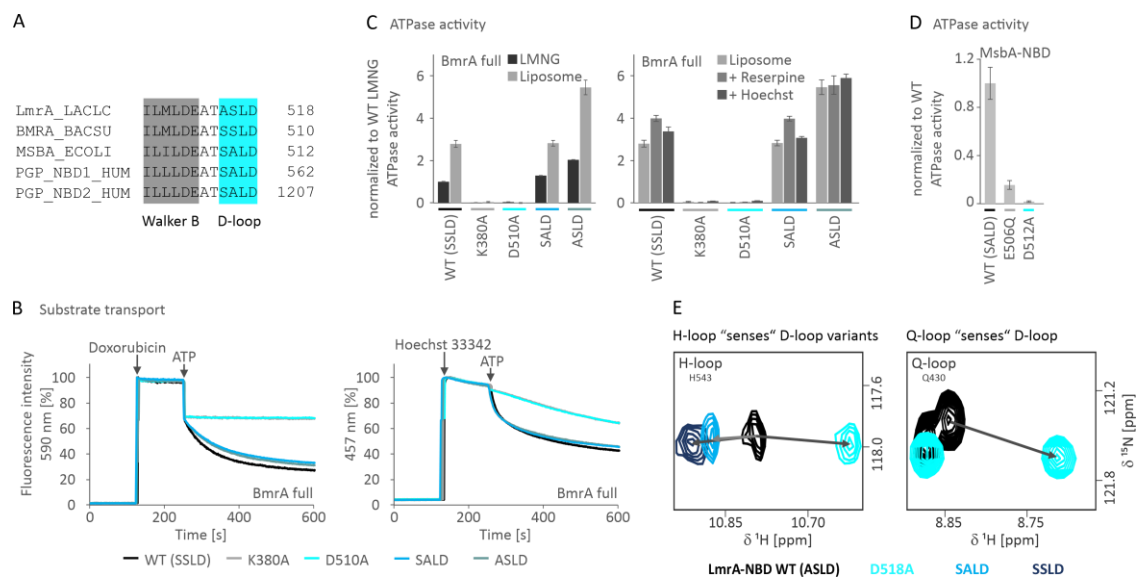


Figure 37: Molecular crosstalk within the NBD is connected to the D-loop

A) Amino acid sequence alignment of LmrA from *L. lactis*, BmrA from *B. subtilis*, MsbA from *E. coli* and human P-glycoprotein (P-gp/MDR1/ABCB1) NBD1 and NBD2 of the D-loop region (cyan) within the NBD (www.ebi.ac.uk/Tools/msa/clustalo/³¹⁰).

B) Doxorubicin or Hoechst 33342 transported by full-length BmrA WT (black) and its variants (K380A - gray, D510A - cyan, SALD - light blue, and ASLD - dark cyan) in inside out vesicles. (100–200 μg total membrane protein) After ~ 2 min, the substrate (2 μM of Hoechst 33342 or 10 μM Doxorubicin) was added. After an additional ~ 2 min, ATP (2 mM) was added and fluorescence intensity monitored for ~ 6 min. **C)** Basal and substrate stimulated ATPase activities of BmrA WT (black) and its variants (K380A - gray, D510A - cyan, SALD - light blue, and ASLD - dark cyan). ATPase activities of BmrA (3 μg) in LMNG and BmrA reconstituted in liposomes were recorded at 37 $^{\circ}\text{C}$. For stimulated ATPase activities, 15 μM Reserpine or 2 μM Hoechst 33342 were used. Data of B and C are normalized to full-length BmrA WT in LMNG and presented as means \pm s.d. ($n=3$). **D)** Basal ATPase activities of MsbA-NBD WT (black, ~ 400 μg) and its variants E506Q (gray) and D512A (cyan) were recorded in buffer (50 mM BisTris pH 7.0, 50 mM NaCl) at 37 $^{\circ}\text{C}$. **E)** Close-up views of ^1H - ^{15}N TROSY HSQC spectra of the D-loop variants of ^{15}N -labeled LmrA-NBD in the ADP-bound state, showing the chemical shift differences of the H-loop and the Q-loop. Amino acid numbering is based on the full-length transporter. LMNG - Lauryl maltose neopentyl glycol.

However, due to the availability of the near complete backbone NMR assignments in the ADP-bound state, the effect of the D-loop mutations (D518A, SALD or SSLD) on the chemical shifts of other conserved motifs were explored. Importantly, the 2D ^1H - ^{15}N TROSY HSQC spectra for all three the LmrA-NBD D-loop mutations in the ADP-bound state showed that they are properly folded (**Appendix 29**). Interestingly, the resonance for the H-loop H543 residue is affected differently depending on how the D-loop is mutated (**Figure 37E**, **Figure 24** and **Appendix 29**). In the D518A background, the H-loop histidine residue shifts to lower ^1H frequencies compared to the LmrA-NBD WT. For the peak of the H-loop histidine, a chemical shift to higher ^1H frequencies were observed within the D-loop variants SALD and SSLD. The SALD and SSLD mutations thus seem to affect the H-loop in a similar manner. As described in subchapter 2.2. Consequences of mutating D-, Q- and H-loop – a chemical shift analysis, introducing the D518A mutant resulted in a chemical shift to lower ^1H frequencies compared to the LmrA-NBD WT for the Q-loop glutamine residue. Here no information about NH resonances of the Q-loop glutamine residue was available within the other D-loop variants SALD or SSLD as it could not be assigned. The observed changes in chemical shifts in different directions for the H-loop histidine residue and the Q-loop glutamine residue due to the D-loop mutations (D518A, SSLD or SALD) in LmrA-NBD might be associated with the obtained differences for the D-loop variants of full-length BmrA and MsbA-NBD in ATP hydrolysis and substrate transport (**Figure 37B/C/D/E**). Thus, it can be noted that the D-loop residues seem to have very distinct roles in function (ATP hydrolysis and substrate transport) and dynamics (subchapter 2.3 Fast Backbone Dynamics of LmrA-NBD D-, Q- or H-loop mutants in the ADP-bound state) within ABC transporters.

3. DISCOVERY OF A NOVEL COMMUNICATION HINGE LINKING NBS AND TMD IN MULTIDRUG ABC TRANSPORTERS

3.1. Introduction

To properly function as a substrate translocator, ABC transporters need to efficiently couple nucleotide binding and ATP hydrolysis in the NBDs to large-scale motions of the TMDs. Within the NBD, several conserved motifs, including Walker A, A-loop, Q-loop, Walker B and H-loop, are involved in ATP binding and hydrolysis as well as transmitting information between the NBDs and/or to the TMDs. The Walker A motif is an integral part of the ABC transporter's nucleotide binding site (NBS) and structurally consists of a loop and the beginning of an α -helix (chapter I: introduction see **Figure 5**). Its conserved signature sequence is GxxGxGK(S/T), where x can be any amino acid. Previous studies showed that this conserved motif coordinates Mg^{2+} , interacts with the terminal phosphates of the bound nucleotide and places them at the right position for the nucleophilic reaction with water^{164,187}.

From recent structures of ABC transporters with and without nucleotides and even with and without substrates/ inhibitors, a lot of information about the different states within the catalytic transport cycle could be obtained^{93,135,183,186,311–315}. However, despite the advances in understanding details of the ABC transporter catalytic cycle, many aspects of the dynamic consequences and long-range effects introduced by nucleotide binding within the NBD remain unclear. One major challenge is to elucidate how the nucleotide binding site in the NBD and the substrate-binding site in the TMDs are structurally and functionally coupled, because it is still not fully understood how the information of a bound nucleotide within the NBS is transmitted to the TMD (or vice versa).

Here, a novel "communication hinge" linking the Walker A motif to the coupling helix groove and thus to the TMD via two highly conserved residues in the NBD has been discovered. Although they are not part of the NBS, both residues R397 and W421 in the LmrA-NBD show nucleotide dependent chemical shifts in solution NMR experiments. These two residues are conserved in type I ABC exporters (type IV fold, **Figure 38**) including BmrA and MsbA although in the latter case the tryptophane residue is replaced by a bulky leucine residue. Mutagenesis studies in the transporter NBDs and functional assays on full-length BmrA support the notion that these residues are important for ATPase activity, substrate transport and protein stability.

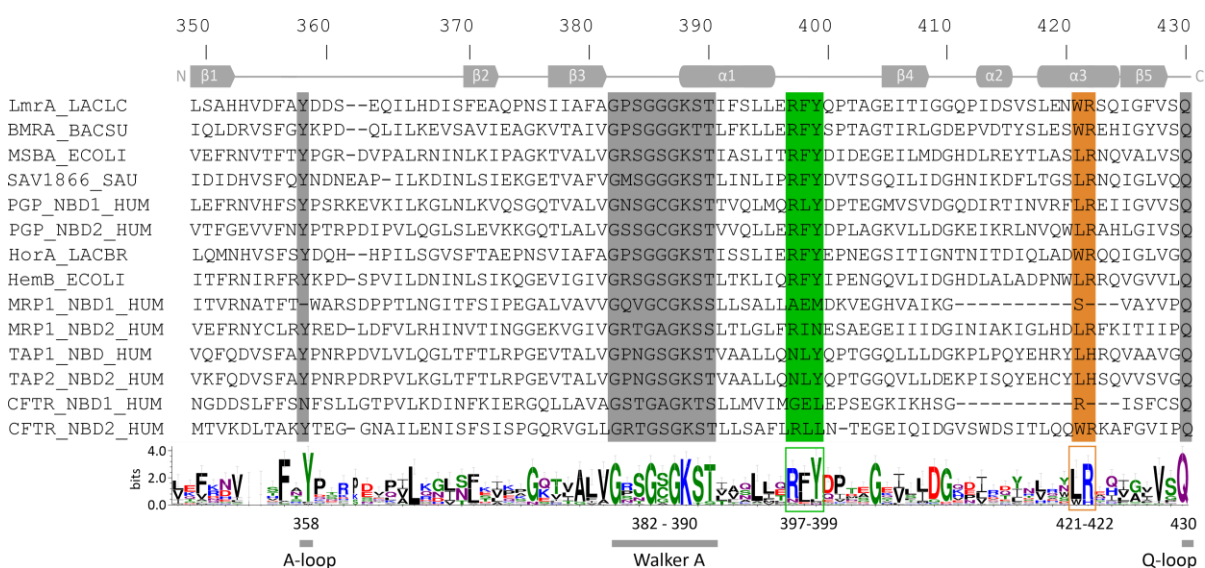


Figure 38: Sequence alignment and sequence logo of the NBDs of different type I ABC exporters

Sequence alignment (www.ebi.ac.uk/Tools/msa/clustalo/³¹⁰) for the NBD region from the A-loop to the Q-loop, which includes the highly conserved arginine residue on the C-terminal end of the Walker A helix ($\alpha 1$ helix in the NBD, green) and the $\alpha 3$ helix that contains a bulky hydrophobic or aromatic residue (orange, for details see text). Uniprot KB accession numbers of the proteins used for the sequence alignment are P97046, O06967, Q99T13, P60752, Q9HUG8, Q99T13, O32748, P08716, Q03518, Q03519, P13569, P08183 and P33527. The secondary structure is displayed on top of the sequence alignment (all numbers according to LmrA sequence). The sequence logo was generated by WebLogo 3 (<http://weblogo.threeplusone.com/create.cgi>^{316,317}) from 34 ABC exporter sequences (type IV fold, Appendix 3.3) for the displayed region. Within the sequence logo amino acids are colored green for polar residues, purple for neutral residues, blue for basic residues, red for acidic residues and black for hydrophobic residues.

3.2. Nucleotide binding is sensed by residues at the C-terminal end of the Walker A helix

At the N-terminus of the Walker A helix resides a conserved lysine residue (K388 in LmrA) which is responsible for the interaction with the β - and γ -phosphate of ATP. On the C-terminal end of the Walker A helix, a highly conserved arginine (R397 in LmrA) faces an equally conserved bulky hydrophobic/ aromatic residue (W421 in LmrA). In 2D ^1H - ^{15}N TROSY HSQC spectra of the LmrA-NBD, the resonances for residues W421 and R397 showed strong chemical shift changes upon nucleotide addition despite not making direct contact with the bound nucleotide²⁷⁵ (**Figure 39A** and **Figure 17**). In addition, residues in the vicinity of R397 are also affected by nucleotide addition including the conserved aromatic residues F398 and Y399 (**Figure 39D**). Similarly, chemical shift changes for the resonances of the corresponding residues in the ^1H - ^{15}N TROSY HSQC spectra of MsbA- and BmrA-NBD were observed upon nucleotide addition (**Figure 39D** and **Appendix 32**). In contrast, no changes in chemical shift were observed for residues at the surface of the NBDs of LmrA, BmrA and MsbA, distant from the NBS (**Figure 39A/B/C/D**, W457 in LmrA-NBD, E451 in MsbA-NBD and K450 in BmrA-NBD, **Appendix 32**).

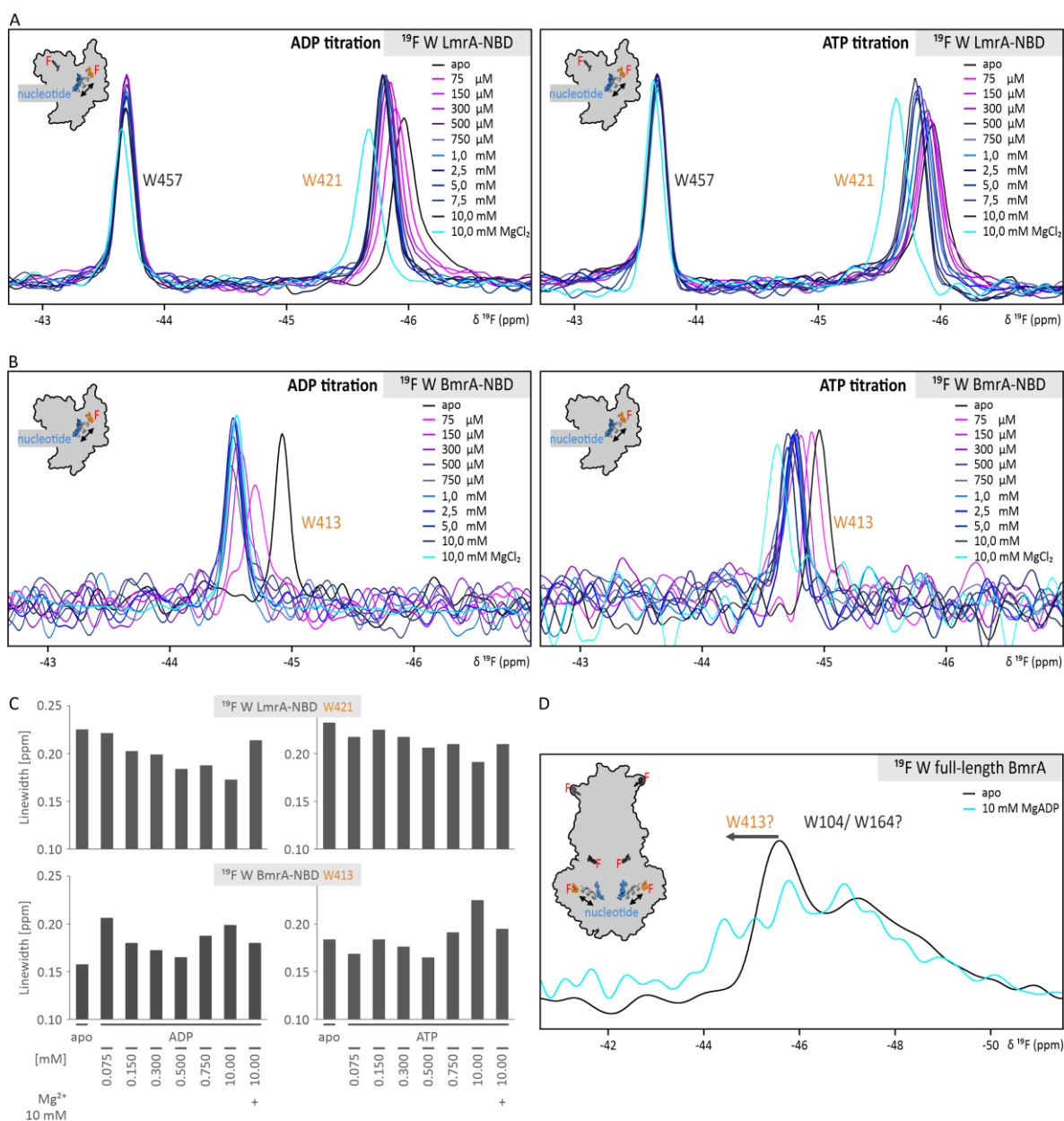


Figure 40: ^{19}F NMR on LmrA and BmrA confirms involvement of W421/W413 in nucleotide sensing

A) ^{19}F solution NMR spectra of 5- ^{19}F -Trp-labeled LmrA-NBD WT. Two peaks for the two native tryptophane residues, W457 on the protein surface and W421 in the C-terminal part of the Walker A helix could be observed. Upon addition of nucleotides only W421 showed chemical shift changes. Magnesium (10 mM final conc.) was added at the end of each titration. **B)** ^{19}F solution NMR spectra of 5- ^{19}F -Trp-labeled BmrA-NBD WT. BmrA contains only one native tryptophane residue (W413) on the C-terminal end of the Walker A helix which senses nucleotide binding. **C)** Linewidth of the ^{19}F resonances observed for W421 in LmrA and W413 in BmrA in A and B. **D)** ^{19}F solution NMR spectra of full-length 5- ^{19}F -Trp-labeled BmrA which contains three tryptophane residues (W104, W164 and W413). The apo spectrum (black) gives rise to broad peaks. Upon addition of 10 mM MgADP (cyan) ^{19}F resonances change in the spectrum, indicating nucleotide binding.

In agreement with what was observed in the ^1H - ^{15}N TROSY HSQC experiments, titration of both LmrA and BmrA-NBD with either ADP or ATP led to ^{19}F peak shifts for residues W421 in LmrA and W413 in BmrA, respectively (Figure 39C, Figure 40A/B and Appendix 35A/B). The peak of the second tryptophane residue in LmrA-NBD, W457, did not react to nucleotide addition. Also, in agreement with our earlier observations for LmrA-NBD (Figure 11), ADP and MgADP has a higher affinity for the NBD (Appendix 35C/D/E). Here, lower nucleotide concentrations are required to obtain the maximum chemical shift change compared to ATP or MgATP (Appendix 35C/D/E). The addition of

magnesium ions lead to further chemical shift changes for the ^{19}F resonance of the hydrophobic residue of interest (W421 LmrA-NBD or W413 BmrA-NBD, **Figure 40A/B**) as well as changes in linewidth (**Figure 40C**) for BmrA-NBD and LmrA-NBD. In contrast, subsequent addition of magnesium ions after ADP titration to BmrA-NBD did not lead to additional chemical shift changes and changes in linewidth (**Figure 40B/C**). This demonstrates that the metal ion plays an important role in nucleotide binding and how this is “sensed” in regions remote of the NBS. When titrations were performed in the presence of ADP and Mg^{2+} (MgADP) or ATP and Mg^{2+} (MgATP) simultaneously, chemical shift changes and changes in linewidth were also observed (compare **Appendix 35A/B** and **Appendix 36**). The observations of the ^{19}F solution NMR data for LmrA- and BmrA-NBD gives another indication that the identified residues of the novel interdomain communication hinge, in spatial proximity to the coupling helix groove, are structurally and dynamically coupled to nucleotide occupancy in the NBS and can potentially build an information hub between NBD and TMD.

To assess whether the conserved aromatic/hydrophobic residue indeed plays an important role for NBD-TMD communication also in the context of the full-length transporter, full-length BmrA, which contains three native tryptophane residues, was labeled with 5- ^{19}F -Trp (**Figure 40D**). The ^{19}F NMR spectrum of the transporter in detergent was recorded and led to the observation of broad lines in the same frequency range as within the isolated 5- ^{19}F -Trp-labeled BmrA-NBD. After addition of MgADP, the ^{19}F resonances changed to lower frequencies also in agreement to what was observed for the isolated NBD (**Figure 40B**). While sample optimization and a resonance assignment of the tryptophane peaks in the full-length transporter are needed, this is a promising result. It indicates that it should be possible to obtain interesting insights into the behavior of the important tryptophane residue within the ABC transporter NBD and its role in nucleotide binding, ATP hydrolysis and/ or long-range sensing of substrate or inhibitor binding to the TMD.

3.3. The NBD “hinge region” influences full-length Transporter ATPase activity, substrate transport and stability

3.3.1. Influence on protein stability

To explore the potential interaction of the newly identified “hinge-region” composed of a highly conserved arginine and a bulky aromatic or hydrophobic residue within the NBD on protein stability, ATP hydrolysis as well as substrate transport, different mutants were generated in BmrA from *B. subtilis*. The conserved arginine (R389) in the BmrA-NBD was mutated to alanine, lysine, glutamate or methionine. The motivation was to replace the R389 by a residue without a charged large sidechain (R/A), to maintain a basic character of an amino acid at this position (R/K), to invert the charge of the residue (R/E) or to neutralize the charge at this position while still retaining the bulkiness of the amino acid (R/M). Further, the second amino acid in the “hinge”, W413, was mutated to phenylalanine, to maintain an aromatic residue in this position, to leucine, to mimic the amino acid found at this position in MsbA and to introduce a bulky hydrophobic residue, as well as alanine. As a control for functional assays, the conserved lysine residue in the Walker A motif, K380 in BmrA, was mutated to alanine.

Full-length BmrA was purified in the detergent LMNG (**Figure 41**). With size exclusion chromatography, both BmrA WT and the K380A mutant showed the expected running behavior, but for full-length BmrA R389A, a large amount of protein aggregate was observed (**Figure 41A**). However, a small fraction of the protein variant also elutes at the same volume as the WT and Walker A mutant proteins. This indicates that the R/A mutant is more prone to aggregate, but, when folded, can presumably adopt the correct structure. Similarly, mutating the arginine residue to glutamate also led to the formation of aggregates, whereas full-length BmrA R389K and R389M behaved similar

as full-length BmrA WT (**Figure 41A**). Interestingly, it was possible to obtain at least a small amount of purified BmrA R389A and BmrA R389E in the context of the full-length transporter. In contrast, it was not possible to purify these constructs within the context of the isolated NBD. BmrA-NBD R389K failed to express properly, while BmrA-NBD R389A and R389E led to fully aggregated protein. BmrA-NBD R389M and W413F eluting at the expected volume on SEC could be obtained in small amounts, although these mutants, too, displayed aggregates.

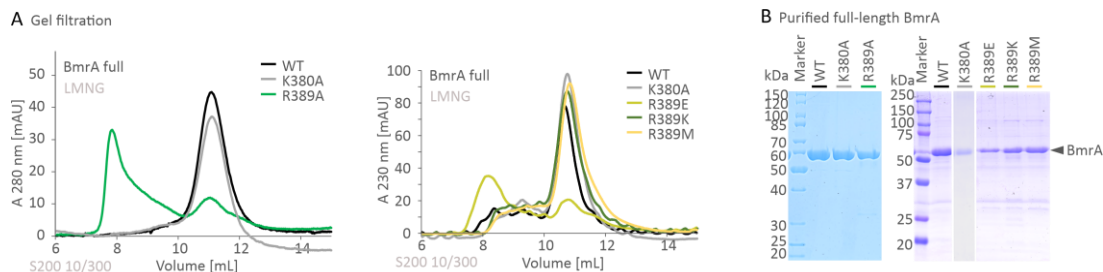


Figure 41: Characterization of full-length BmrA WT and “communication hinge” mutants

A) Gel filtration profiles for full-length BmrA WT (black) and its variants (K380A - gray, R389A - green, R389E - light green, R389K - dark green and R389M - yellow) in LMNG. **B)** LMNG-solubilized full-length BmrA purified from *E. coli* C41 (DE3) cells. 2.5 μ g protein were loaded onto a 12% gel to perform an SDS-PAGE after the final purification step staining was performed with Coomassie blue. LMNG - Lauryl maltose neopentyl glycol.

In striking contrast to the behavior of the BmrA-NBD point mutants, LmrA-NBD mutants in this region (R397A, W421F, W421A) can be purified and show proper SEC elution profiles (**Figure 42A/B**). Nonetheless, the two alanine mutants were also accompanied by a higher amount of aggregates on SEC (**Figure 42A**). Furthermore, the LmrA-NBD mutants elute earlier than the WT NBD. Comparing the LmrA-NBD mutants to the wildtype protein, no or only minor differences in the CD spectra are observed (**Figure 42C**) and no changes within the respective secondary structure content was predicted using the BestSel tool^{292,293}. All LmrA-NBD constructs including the WT and the K388A (Walker A lysine mutant) showed no or negligible ATPase activity (**Figure 42D**).

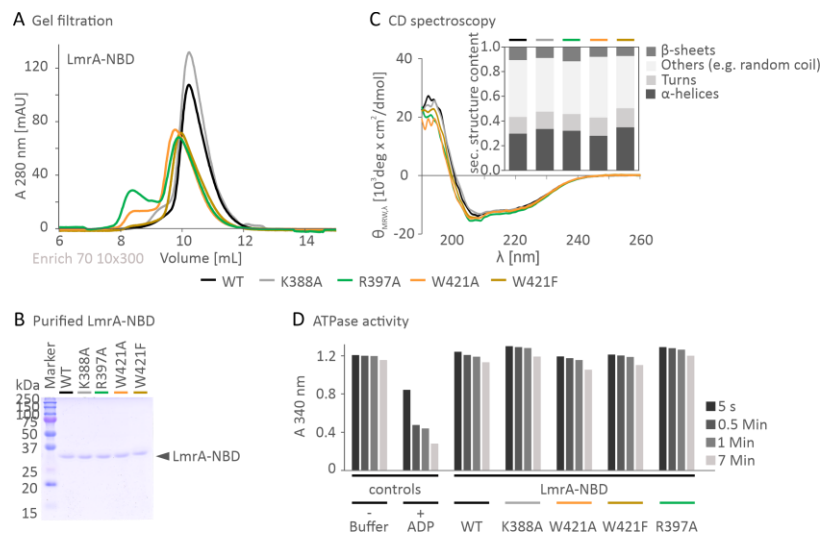


Figure 42: Characterization of LmrA-NBD WT and its mutations in the “communication hinge”

A) Gel filtration profiles for LmrA-NBD WT (black) and its variants (K388A - gray, R397A - green, W421A - orange and W421F - dark yellow). **B)** SDS-PAGE (15%, 5 μ g protein/lane) of purified LmrA-NBD variants. Staining was performed with Coomassie blue **C)** CD spectra of LmrA-NBD WT (black) and its variants (K388A - gray, R397A - green, W421A - orange and W421F - dark yellow). Inlet shows the analysis of the respective NBD’s secondary structure content based on the CD spectra using the BestSel secondary structure analysis (<http://bestsel.elte.hu/index.php>^{292,293}). The predicted α -helical/turn/other like random coil/ β -sheet content of the purified constructs is 29.9/13.5/46.2/10.4% for LmrA-NBD WT, 33.7/14.0/43.6/8.6% for LmrA-NBD K388A, 32.2/13.5/42.9/11.5% for LmrA-NBD R397A, 28.2/14.8/49.2/7.8% for LmrA-NBD W421A and 35.0/15.5/42.4/7.1% for LmrA-NBD W421F. **D)** Basal ATPase activities of LmrA-NBD WT and its variants (K388A - gray, R397A - green, W421A - orange and W421F - dark yellow) recorded with \sim 400 μ g purified NBD in buffer (50 mM BisTrisPH6.5, 50 mM NaCl) at 37 $^{\circ}$ C for the indicated time. As LmrA-NBD shows no ATPase activity, ADP was added as a positive control and buffer was used as a negative control.

3.3.2. Role of the conserved arginine residue in the NBD of BmrA on ATPase activity and substrate transport

Purified full-length BmrA in the detergent lauryl maltose neopentyl glycol (LMNG) or reconstituted in liposomes (*E. coli* total lipid extract) was used to measure the ATPase activity of the transporter (**Figure 43**). BmrA WT and a mutant of the Walker A motif, BmrA K380A, which is known to be ATPase and transport inactive, served as positive and negative controls, respectively (**Figure 43B/D**).

In agreement with previous studies, the BmrA K380A mutant showed a significant decrease in ATPase activity compared to the full-length BmrA WT both in detergent and proteoliposomes¹⁹⁵. An increased ATPase activity for reconstituted full-length BmrA WT compared to detergent-solubilized protein was observed^{137,195}. This activity could be further stimulated by addition of reserpine or Hoechst 33342¹³⁷. As expected, BmrA K380A’s ATPase activity could not be stimulated with substrates.

In LMNG, the basal ATPase activity of both BmrA R389E and R389A mutants dropped to the level of the K380A mutant rendering these proteins essentially ATPase inactive (**Figure 43A/B**). In contrast, both BmrA R389M and BmrA R389K still showed residual ATPase activity (**Figure 43A/B**). Only the BmrA R389A mutant was tested in proteoliposomes, where it intriguingly showed a slightly higher activity compared to LMNG, although it could be not stimulated by reserpine and Hoechst 33342. Together, these results imply that the ATPase activity of BmrA is strongly dependent on the transporter environment and that residue R389 is important for ATPase activity.

Especially interesting is the loss of stimulation by substrate/inhibitor in R389A, which indicates a potential loss of connection between substrate/inhibitor recognition and ATPase activity, i.e. between TMD and NBD. The ATPase activity of the tryptophane mutants performed by our collaboration partner in Lyon will be discussed in chapter IV: discussion subchapter 3.1. A potential NBS-TMD signaling pathway Part I – signal propagation via a conserved arginine residue³¹⁸.

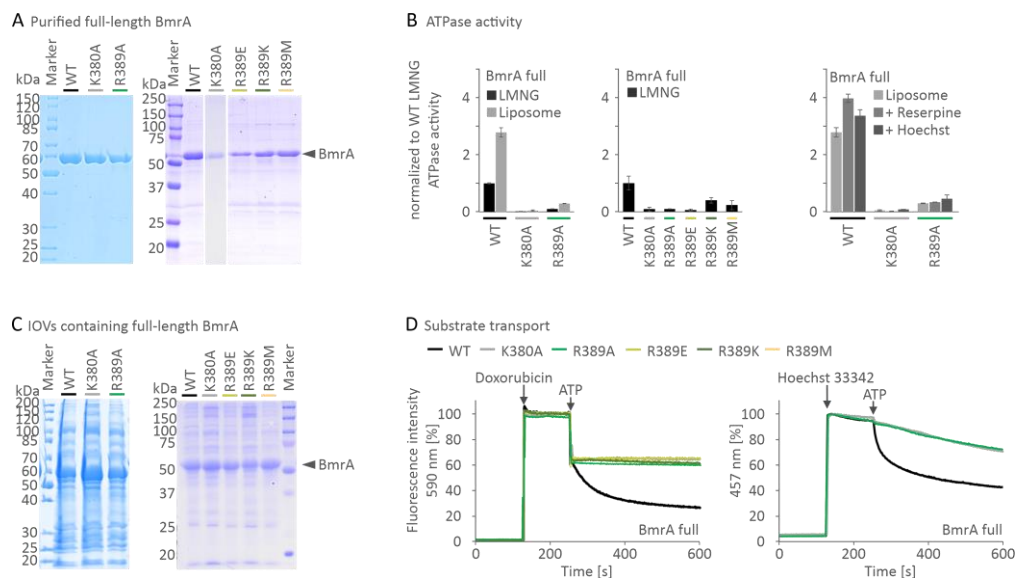


Figure 43: Role of conserved residue R389 in the NBD of BmrA on ATPase activity and substrate transport

A) LMNG-solubilized full-length BmrA purified from *E. coli* C41 (DE3) cells. 2.5 μ g protein were loaded onto a 12% gel to perform an SDS-PAGE after the final purification step and stained with Coomassie blue. **B)** Basal and substrate stimulated ATPase activities of full-length BmrA WT (black) and its variants (K380A - gray, R389A - green, R389E - light green, R389K - dark green and R389M - yellow). ATPase activities of BmrA (3 μ g) in LMNG and reconstituted in liposomes (*E. coli* total lipid extract) were recorded at 37 $^{\circ}$ C. For stimulated ATPase activities, 15 μ M Reserpine or 2 μ M Hoechst 33342 were used. **C)** IOVs prepared from *E. coli* C41 (DE3) cells overexpressing different BmrA variants. IOVs (20 μ g total membrane protein) were analyzed by SDS-PAGE (12% gel). **D)** Doxorubicin or Hoechst 33342 transport by BmrA WT (black) and its variants (K380A-grey, R389A-green, R389E-light green, R389K-dark green and R389M-yellow) in inside out vesicles (100 – 200 μ g total membrane protein). After \sim 2 min at 37 $^{\circ}$ C the substrate (2 μ M of Hoechst 33342 or 10 μ M Doxorubicin) was added. After an additional \sim 2 min, ATP (2 mM) was added and the fluorescence intensity monitored for \sim 6 min. Data of B and D are normalized to BmrA WT LMNG for the ATPase activity assay and presented as means \pm s.d. (n=3). LMNG - Lauryl maltose neopentyl glycol.

Next, the influence of the mutations on the transport activity was tested. Here, inside out vesicles were used (Figure 43C/D). Hoechst 33342 and Doxorubicin were used as fluorescent substrates. Although reserpine leads to ATPase stimulation, it cannot be used in these assays as it is not fluorescent. BmrA WT, the ATPase inactive control mutant K380A, as well as the four arginine mutants were tested. Only BmrA WT was able to translocate the two fluorescent substrates across the membrane. In the case of BmrA K380A and R389E, the most likely explanation is that the lack of ATPase activity translates to an inability of the transporter to translocate substrates. For the R389E in LMNG, no ATPase activity was measured. If this variant has a residual ATPase activity in liposomes needs to be analyzed further. No ATPase activity for R389A was obtained in LMNG. Finally, a small but significant ATPase activity was detected for R389A in liposomes and for R389M and R389K in LMNG (Figure 43B). However, but none of these mutants were able to translocate the two substrates in the fluorescence assay. This indicates that in these mutants, not only ATP hydrolysis, but also interdomain coupling may be negatively affected. Therefore, substrate transport is disrupted in the alanine, lysine and methionine mutants. These findings further support the hypothesis that the conserved R389/W413 pair (BmrA residue numbering) present a novel allosteric interaction site that couples ATP binding and hydrolysis within the NBD to substrate translocation via the TMD.

CHAPTER IV: DISCUSSION

1. DIFFERENCES IN NBD DYNAMICS OF THE ABC TRANSPORTER LMR A INDUCED BY NUCLEOTIDE BINDING

It is challenging to gain detailed insights into the structural and dynamic consequences of nucleotide binding to the NBD of an ABC transporter. In particular the identification of signal propagation pathways that communicate nucleotide-binding and/ or hydrolysis to the TMD and vice versa, i.e. the elucidation of mechanisms how the NBD receives information about substrate binding from the TMDs remain difficult tasks. In this study, detailed information about the allosteric consequences and the dynamic landscape of an NBD monomer upon nucleotide binding could be obtained. For this, the NBDs of the homologous ABC exporters LmrA from *L. lactis*, MsbA from *E. coli* and BmrA from *B. subtilis* were expressed and purified²⁷⁵ (Chapter III: results subchapter 1. see **Figure 10**).

Importantly, to draw conclusions about protein dynamics, one must also consider the technique used. Biophysical methods such as EPR¹, FRET², LRET³ or also PET-FCS⁴, which was used here on the MsbA-NBD (Chapter III: results subchapter 1. see **Figure 21** and **Figure 22**), rely on the placement of reporters at defined positions of the protein of interest. They can then yield valuable information about the local protein dynamics caused by the labels or about the distance between the labels bound to the protein^{254,258,260,263,265}. This way, long-range conformational changes can be derived. In comparison, NMR experiments are powerful tools to obtain information about the dynamics of every residue at atomic resolution but cannot easily deliver long-range information. In this thesis, NMR spectroscopy has been used to study the effects of nucleotide binding to the LmrA-NBD (Chapter III: results subchapter 1. see **Figure 11**, **Figure 15**, **Figure 16**, **Figure 17**, **Figure 18**, **Figure 19** and **Figure 20**). Investigating protein structure and dynamics at an atomic resolution with NMR spectroscopy and global dynamics by PET-FCS are thus complementary approaches and greatly add to the picture derived from other techniques, such as X-ray crystallography or cryogenic electron microscopy (cryo-EM).

Based on the NMR experiments on LmrA-NBD, it can be concluded that the interaction with ADP quenches backbone amide bond fluctuations on the ps - ns timescale (Chapter III: results subchapter 1. see **Figure 20**, **Figure 44B**) and secondary structure rearrangements on the ms – s timescale (**Figure 44B**, chapter III: results subchapter 1. see **Figure 17** and **Figure 18**), particularly in the nucleotide binding site (NBS). LmrA-NBD, MsbA-NBD and BmrA-NBD showed less peaks in the apo compared to the ADP-bound state in the ¹H-¹⁵N TROSY HSQC (Chapter III: results subchapter 1. see **Figure 15**), implying protein backbone fluctuations in the μ s – ms timescale in the absence of ADP. PET-FCS experiments on MsbA-NBD demonstrate interdomain movements between the α -helical and catalytic subdomains in the μ s timescale (**Figure 44B**, chapter III: results subchapter 1. see **Figure 21** and **Figure 22**).

Analysis of NMR chemical shift differences (Chapter III: results subchapter 1. see **Figure 15**, **Figure 16**, **Figure 17**, **Appendix 11** and **Appendix 12**) showed that addition of nucleotide altered peak position and linewidth throughout the HSQC spectra of the three studied NBDs, thus demonstrating that the presence of the nucleotide has far reaching consequences. Of note, ADP was used in most of the experiments described, as it yielded the highest number of peaks in the HSQC spectra of the ABC

¹ EPR – Electron paramagnetic resonance

² FRET – Fluorescence resonance energy transfer

³ LRET – Luminescence resonance energy transfer

⁴ PET-FCS – Photoinduced electron transfer-fluorescence correlation spectroscopy

transporter NBDs. In the case of LmrA-NBD, where a complete backbone NMR assignment is available²⁷⁹, it was possible to pinpoint these structural and dynamic changes to specific residues. Importantly, the majority of the peaks “missing” from the spectra of the apo and ATP-bound states derive from residues in the NBS, thus underscoring that there are important dynamic differences between the two nucleotide-bound states. However, the elucidation of these differences requires further experiments in the future. Below, the consequences of ADP binding to an NBD across different timescales as dissected in this thesis are discussed in more detail.

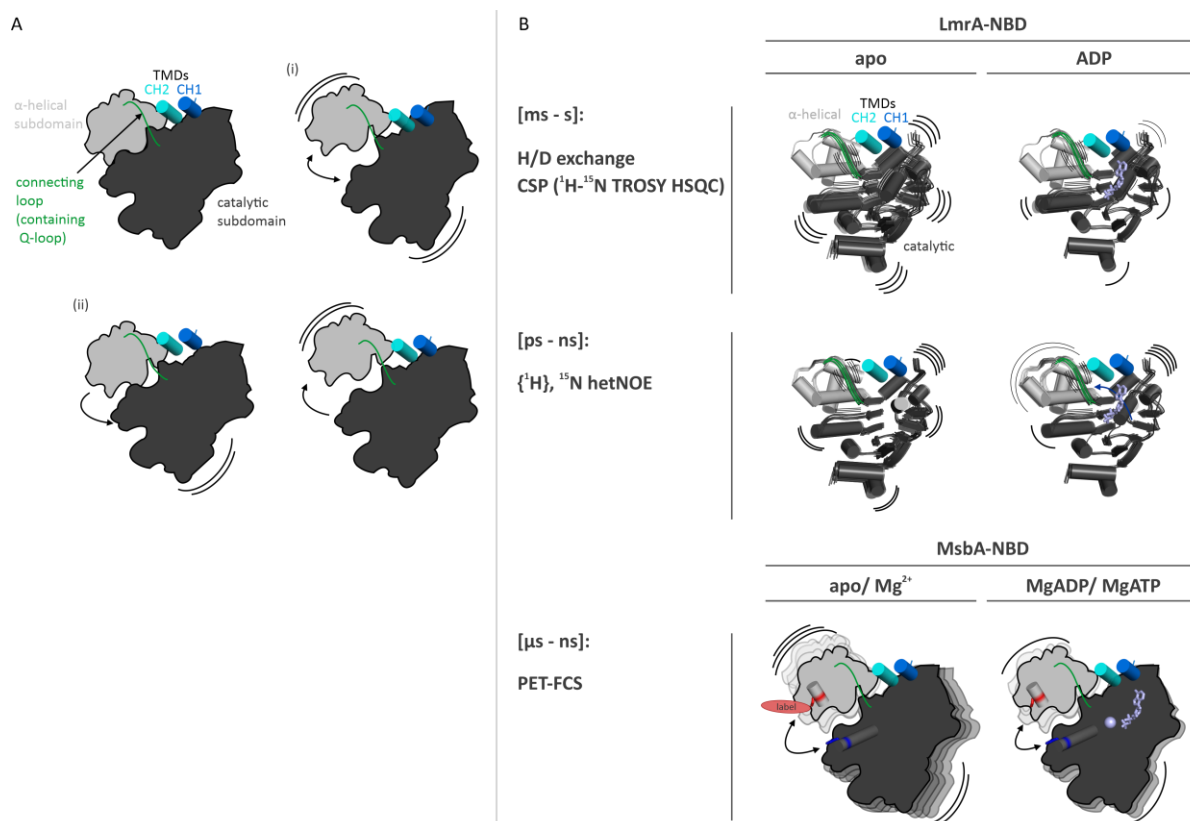


Figure 44: Schematic illustration of NBD dynamics obtained from techniques used in this thesis for LmrA-NBD and MsbA-NBD, focusing on relative motions of α -helical and catalytic subdomain

A) Schematic representation of the possible relative motions between α -helical (light gray) and catalytic (dark gray) subdomain, with (i) both subdomains moving/rotating or (ii) only one of the two subdomains moving/rotating. **B)** Cartoon representation of dynamics for LmrA-NBD obtained from NMR experiments (chemical shift perturbation, H/D exchange and ¹H, ¹⁵N hetNOE) in the apo and ADP-bound state (top). Cartoon representation of dynamics for MsbA-NBD obtained from PET-FCS (bottom). Nucleotide (ADP or MgADP) is shown in light violet. Red indicates the position of the fluorophore within the NBD for the PET-FCS measurements. NBD – Nucleotide binding domain. CH – Coupling helix (blue/cyan). TMDs – Transmembrane domains. Connecting loop of the α -helical and catalytic subdomain (including Q-loop) is shown in green.

1.1. Comparison of the apo and ADP-bound state NBD on the ps – ns timescale

Overall, the dynamic hetNOE analysis of LmrA-NBD in the apo and ADP-bound states showed that the secondary structural elements essentially remain identical on the ps - ns timescale (**Figure 44B** and chapter III: results subchapter 1. see **Figure 19**). However, quenching of intramolecular NBD dynamics for residues in the catalytic (including the NBS) subdomain was observed in the presence of ADP (**Figure 44B**, chapter III: results subchapter 1. see **Figure 19** and **Figure 20**). At the same time, residues of the α -helical subdomain became more mobile upon ADP binding. Thus, it can be hypothesized, that rigidification upon nucleotide binding in the catalytic subdomain of the NBD induces mobility within the α -helical subdomain of the NBD. The intrinsic dynamic equilibrium within the NBD seems to become reorganized by ADP binding and thus may cause intramolecular rearrangements that could have implications on NBD-NBD and NBD-TMD crosstalk via the coupling helix groove (**Figure 44B**, chapter III: results subchapter 1. see **Figure 20**). These intramolecular rearrangements are reversible during the catalytic cycle when resetting to the apo state, hence these reversible deformations can be considered as an elastic deformation within the NBD in the fast timescale, affecting both the α -helical and the catalytic subdomain (**Figure 44B**).

In the ps – ns timescale previous solution NMR studies (based on ^{15}N R_1 , R_2 , and $\{^1\text{H}\}$, ^{15}N hetNOE experiments) on the MJ1267 ABC from the branched-chain amino acid transporter from *Methanococcus janaschii*, reported that a sequence element termed “LivG” (Leu-Iso-Val), which is unique to Liv transporters²¹⁸, is the most dynamic part of the NBD in the apo state and that its flexibility increased in the presence of MgADP³¹⁹. MJ1267 is 29% identical to LivG and LivF, NBDs from the branched-chain amino acid transporter of *E. coli*. In MJ1267 a helical LivG sequence insert is found in the α -helical subdomain. This sequence insert is not found in the NBD from LmrA studied in this thesis. The NMR study of Wang *et al.*, analyzing MJ1267 in the ps - ns timescale described no other residue of the α -helical subdomain to be flexible in the apo or MgADP-bound state³¹⁹. In comparison, it should be noted that in our study, the hetNOE data on LmrA-NBD indicate differences between apo and ADP-bound state in the α -helical subdomain within the ps - ns timescale. The experimental outcome may have been different because of the presence/absence of Mg^{2+} in the two studies and potentially the unique LivG insertion in MJ1267.

1.2. Relative motions between α -helical and catalytic subdomain

Nucleotide binding has been described to be crucial for triggering large conformational changes within ABC transporters^{34,90,169,183,191,202,249,252,254,261,284,308,320–323}. Previous NMR and EPR studies concluded that the apo state of type I ABC exporters (type IV fold) is highly dynamic (literature examples for LmrA^{254,275,277}, BmrA²⁸⁴, MsbA^{261,321,324}, BmrCD³²⁴, Pgp^{320,322}). For the type I ABC exporter LmrA, a global decrease of its conformational space upon nucleotide binding was observed²⁵⁴. Hence, nucleotides seem to induce huge conformational changes and changes dynamics in ABC transporters.

In the NBDs, the movements between the α -helical and catalytic subdomain within the NBD of ABC transporters were identified to play an important role for both the catalytic and the transport cycle^{226,308,325}. During ATP binding and hydrolysis, a rotation of the α -helical relative to the catalytic subdomain within the NBD was observed in several crystal structures^{169,170,189,218,220,326}. ATP binding yielded an inward movement of the α -helical subdomain towards the catalytic subdomain^{170,169,189,218,308}, whereas the post-hydrolysis stage induced a rotation of the α -helical subdomain away from the catalytic subdomain^{218,308,327}. Motions between the α -helical and the catalytic subdomain were predicted to be important for NBD-NBD communication during the catalytic cycle and led to one of the models where NBD contact is required for the catalytic cycle, the constant contact model^{171,218,226,328} (**Figure 45**, chapter I: introduction subchapter 3.3.3. see **Figure 6**

and **Table 4**). Briefly, in this model the NBDs remain partially associated during the catalytic cycle (**Figure 45**). ATP hydrolysis occurs alternately at each NBS²²⁶. In the beginning, ATP is bound to NBS1, while NBS2 is empty (step 1). Upon or after ATP hydrolysis in NBS1, rotation between the catalytic and the α -helical subdomain allows ATP binding to the second, free NBS (NBS2). NBS1 is maintained closed and in the ADP P_i -bound state³²⁹ (**Figure 45** step 2). ATP binding to NBS2 induces an inward rotation of the catalytic subdomain (**Figure 45** step 3), leading to an occlusion of ATP. At the same time, NBS1 is opened and the hydrolysis products (ADP and P_i) are subsequently released (**Figure 45** step 3 and step 4). Now the cycle repeats with NBS2 leading the conformational changes (steps 5-7) until the original state (step 1) is reached again.

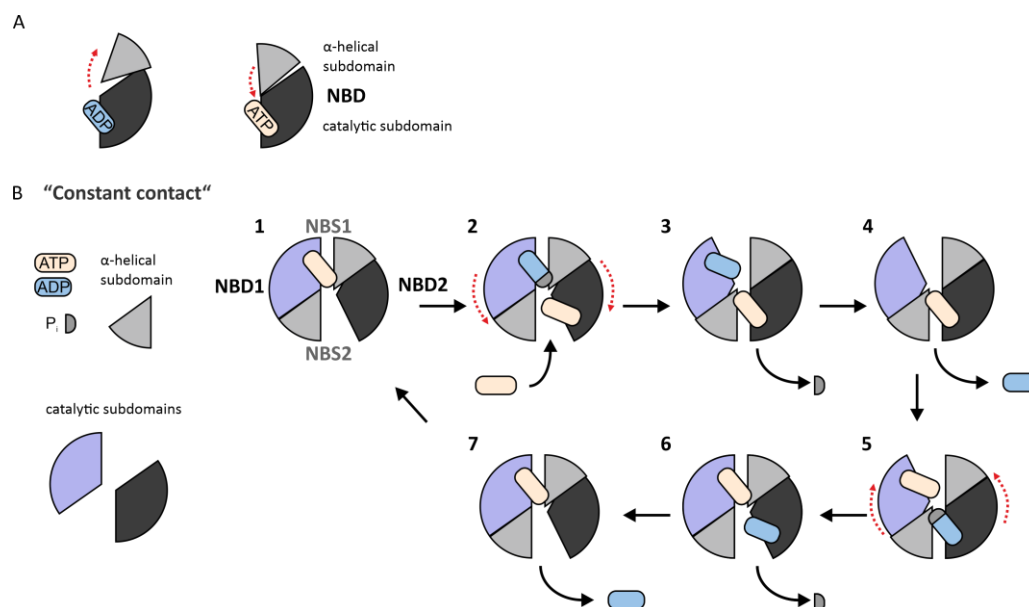


Figure 45: Schematic representation of relative movements of the catalytic and the α -helical NBD subdomains. **A)** Inward movement of the α -helical subdomain towards the catalytic subdomain upon ATP binding and outward movement of the α -helical subdomain against the catalytic subdomain in the post-hydrolysis state (ADP-bound). **B)** The constant contact model for the catalytic cycle of ABC transporters (modified from Gerorge & Jones et al., 2013³²⁹ and Szöllösi et al., 2017¹⁵⁵). NBD dimers are illustrated schematically with their larger catalytic subdomains and smaller α -helical subdomains as a top view. Step 1: ATP is occluded in NBS1. NBS2 is empty and open due to an outward rotation of the catalytic subdomain. Step 2: ATP hydrolysis in NBS1 induces a switch to high affinity for ATP in the outward orientated catalytic subdomain of NBS2, allowing ATP binding in NBS2. Steps 3 & 4: ATP binding to the empty open catalytic subdomain in NBS2 induces its inward rotation and subsequent occlusion of ATP. This induces opening of NBS1 and release of the hydrolysis products P_i and ADP. Steps 5-7: Repetition of steps 1-4 in the opposite manner with respect to the two active sites (NBS1 and NBS2) to complete the cycle. NBD – Nucleotide binding domain. NBS – Nucleotide binding site.

The global NBD subdomain conformational changes in the μ s timescale between the α -helical and the catalytic subdomains in different states of the catalytic cycle could be detected on MsbA-NBD using PET-FCS (**Figure 44B** and chapter III: results subchapter 1. see **Figure 22**). To the best of our knowledge, this is the first time the precise fluctuation rates of this motion have been described in an ABC transporter NBD. The ATP-bound state yielded fluctuations in the μ s timescale (ATP-bound state $\tau_1 = 17 \pm 7 \mu$ s), which were similar time to those observed in the apo and ADP-bound states (apo $\tau_1 = 12 \pm 5 \mu$ s and ADP-bound state $\tau_1 = 27 \pm 13 \mu$ s). However, we find that the interdomain fluctuations between α -helical and catalytic subdomain observed by PET-FCS are slowed down upon binding of nucleotide with magnesium, i.e. in the presence of MgATP ($\tau_1 = 62 \pm 21 \mu$ s) or MgADP ($\tau_1 = 255 \pm 82 \mu$ s) (**Figure 44B** and chapter III: results subchapter 1. see **Figure 22**). This falls in line with the overall interpretation that nucleotide binding leads to NBD rigidification, although there seem to be important differences between ATP (Mg) and ADP (Mg) on certain timescales accessible with our NMR studies. Overall, several options which potentially cause altered global dynamics between the two subdomains in different catalytic states are conceivable: (i) motion of both

subdomains is slowed down or is increased or (ii) one of the two subdomain motion changes (**Figure 44A**). While this cannot be answered satisfactorily based on the available PET-FCS data on MsbA-NBD, taking the hetNOE and H/D exchange data on LmrA-NBD into account, a slowing down of global fluctuations between the two subdomains might be based on the nucleotide-induced increase in rigidity within the catalytic subdomain (**Figure 44B**). Nonetheless, it is important to note that two different ABC transporter NBDs were used in PET-FCS and NMR experiments. In addition, only for MsbA-NBD, but not for LmrA-NBD, an ATPase activity of the purified domain was observed which may also indicate that there are differences between the two transporter NBDs. Interestingly, the NMR H/D exchange experiments (**Figure 44B** and chapter III: results subchapter 1. see **Figure 18**) with LmrA-NBD also showed notable differences for the two subdomains when comparing the apo and the ADP-bound states. In the apo state, the α -helical subdomain showed a certain “stability”, i.e. overall very slow H/D exchange (**Figure 44B**). One could conceive that a bound TMD at this site may affect this identified “stability” within the α -helical subdomain. The catalytic subdomain on the other hand was found to be much more stable upon ADP binding (**Figure 44B**). The data from the chemical shift perturbation analysis showed no or very low effects within the α -helical subdomain between apo and ADP-bound states (**Figure 44B**, chapter III: results subchapter 1. see **Figure 17** and **Appendix 16**). A prior NMR study on the MJ1267 ABC studied the apo and MgADP-bound state and identified the α -helical subdomain as the most dynamic part on the μ s – ms timescale (based on TROSY spin-echo experiment for backbone NH resonances^{155,330,331}). When MgADP was present within our chemical shift perturbation analysis, only a few residues in the α -helical subdomain had different chemical shifts in comparison to the apo state (**Appendix 16**). Interestingly, adding magnesium and ADP yield to disappearing resonances in the region where magnesium is assumed to be positioned within the NBS, i.e. close to the Walker A and the Walker B motifs. However, within our study further dynamic analysis with magnesium would be needed in the future for more information about differences in dynamics in the presence or absence of magnesium and/or nucleotide.

Together, these observations may indicate that ADP binding affects very fast (ps - ns) and rather slow (ms - s) motions (**Figure 44B** and chapter III: results subchapter 1. see **Figure 18** and **Figure 20**) but not motions on the intermediate timescale (**Figure 44B** and chapter III: results subchapter 1. see **Figure 22**).

In summary, ADP binding in LmrA-NBD induces rigidification of residues in the catalytic subdomain in the ms - s and the ps – ns timescale. Rigidification in the ps - ns timescale in the catalytic subdomain is hypothesized to simultaneously induce local mobility in the α -helical subdomain (**Figure 44B**). These dynamic differences are possibly sensed by the TMD and might be important for transmitting conformational changes back and forth between the NBD and the TMD. Considering that the data obtained for the NBD in the ADP-bound state reflect the post-hydrolytic state, the “unique” dynamic profile of this state may have far reaching consequences for substrate unloading and transporter switching from the outward open to the inward open state before a new transport cycle can begin again (Chapter I: introduction subchapter 3.4. see **Figure 7**).

1.3. Focus on the coupling helix groove – communication about nucleotide occupancy between NBD and TMD

The TMDs of an ABC transporter interact via their so-called coupling helices with the NBDs. These helices bind in the interface between the α -helical and the catalytic subdomain of the NBD in the so-called “coupling helix groove”^{154,308,332–337} (**Figure 46A**). Movements induced by nucleotide binding between the two NBD subdomains can be transmitted from the NBDs to the TMDs via the coupling helix groove.

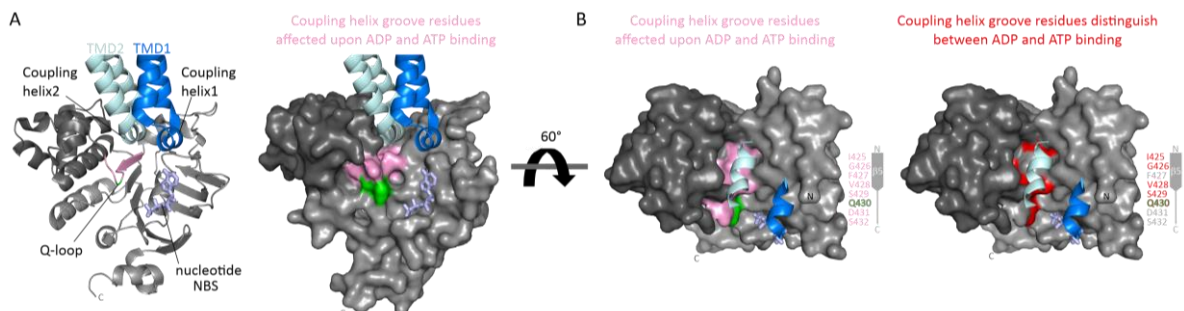


Figure 46: Residues in the coupling helix groove affected by nucleotide binding

A) NBD monomer viewed from the NBD-NBD interface. **B)** Top view (from the membrane) of one NBD monomer with coupling helix 1 and coupling helix 2 in the coupling helix groove. The coupling helix groove is in the interface between the α -helical (light gray) and the catalytic subdomain (dark gray). Residues of the coupling helix groove affected by ADP or ATP binding identified with NMR experiments (chapter III: results subchapter 1. see **Figure 17**) in this thesis are colored in rose. Residues which could further distinguish between ADP or ATP binding are colored in red. NBS – Nucleotide binding site. PDB ID: 2HYD³⁴.

The coupling helices and the coupling helix groove thus play a pivotal role in transmitting conformational changes between NBDs and TMDs during substrate transport and ATP binding/hydrolysis^{34,338–340}. NMR data in this thesis (Chapter III: results subchapter 1. see **Figure 17**) revealed that residues in the coupling helix groove are indeed affected by nucleotide binding (**Figure 46**). Interestingly, some residues are even capable to distinguish between binding of ADP or ATP (**Figure 46B**). These different signals transmitted from NBD to TMD might be related to the observed different conformations (inward open, occluded or outward open) for type I ABC exporters (type IV fold) in the presence of different types of nucleotides^{34,90,91,93,135,163,201,202,233,314,341}.

The observed nucleotide-induced dynamics in our measurements may provide important clues about the dynamic details of how signals are transmitted between NBD and TMDs via the coupling helix groove. As described above, nucleotide binding induces mobility within the α -helical subdomain and rigidity within the catalytic subdomain on the ps - ns timescale (**Figure 44B** and chapter III: results subchapter 1. see **Figure 20**). Local changes in the dynamic landscape of these two subdomains presumably influences overall NBD dynamics and thus global movements between the α -helical and the catalytic subdomain and ultimately between NBD and TMD. Notably, the α -helical subdomain has a structural diverse region (LmrA⁴⁶⁰LDLAFARSFVENMPDQLNTEVGERGVK⁴⁸⁶, **Appendix 2**), which might have evolved to fit to the structural diverse TMDs in ABC transporters^{61,154}. For LmrA-NBD no significant influence in the ms – s timescale has been observed within this region in the different states i.e. apo, ADP-bound and ATP-bound states (Chapter III: results subchapter 1. see **Figure 17** and **Figure 18**). Interestingly, in the presence of magnesium and nucleotide a few residues (MgADP-bound state: A463, A465, V469, G481 and MgATP-bound state: V469, G481) showed differences in their resonances within the spectra compared to the apo state (**Appendix 16**). The ps – ns experiments for LmrA-NBD within this thesis (Chapter III: results subchapter 1. see **Figure 19** and **Figure 20**) revealed overall similar dynamics in the apo and ADP-bound state but some residues became more stable (D461 and F464) or more flexible (L460, S467, N471 and L476) due to ADP binding. If these dynamics

in the ps – ns timescale might be able to induce further dynamics within the TMDs remains unresolved with our experimental approach as the TMDs are missing.

One requirement for movements between the two NBD subdomains is a certain degree of flexibility in their interface. At the interface between α -helical and the catalytic subdomain the important Q-loop is located^{168,218,334} (**Figure 46A**). As the Q-loop has a primary role in interdomain signal communication between NBD and TMD^{158,161}, the obtained Q-loop flexibility seems to be important for transmitting nucleotide occupancy. Indeed, this region was found to be very flexible on the ps - ns timescale and on the ms – s timescale in both the apo and the ADP-bound state based on the hetNOE and H/D exchange data (**Figure 44A** and chapter III: results subchapter 1. see **Figure 18** and **Figure 19**). This indicates that intramolecular subdomain motions can occur both with and without nucleotide. Furthermore, the observed significant chemical shift differences between the apo and nucleotide bound states for the Q-loop itself (Chapter III: results subchapter 1. see **Figure 16** and **Figure 17**) suggest that the Q-loop can sense and distinguish nucleotide binding, which will be discussed later in more detail.

1.4. Consequences of nucleotide binding for residues within conserved motifs

Similar to a previously published NMR-based dynamic study on MJ1267³¹⁹, the results for the nucleotide binding site (NBS) of LmrA-NBD indicate a “selected fit” model³⁴² (**Appendix 37**) for binding of ADP. In this model, the ligand binding site is inherently flexible and able to sample multiple conformations. When the ligand binds, a specific set of binding-competent states is stabilized favoring protein ligand interaction. The absence of resonances in the HSQC spectrum of LmrA-NBD for the Walker A motif residues which are part of the NBS (e.g. K388 and G385)^{275,279} (Chapter III: results subchapter 1. see **Figure 17**) in the apo state, indicates interconversion between different conformations and consequently flexibility. These motions are quenched upon ADP binding hence leading the resonances to “appear”. It is known that the Walker A motif is responsible for the direct interaction of the nucleotide with the NBD¹⁶⁴. Interestingly, the corresponding residue to the aforementioned glycine residue (G385) was also reported to be affected by nucleotide binding (MgADP) in NMR studies on MJ1267 and the NBD of the ABC transporter and ABCB6^{319,343}. Furthermore, in crystal structures of ABC transporter NBDs in the apo state, different conformations for the Walker A motif residues have been observed^{154,167}. Previously, an increase in flexibility in the ps - ns timescale was reported for the Walker A motif and its vicinity in MJ1267 upon addition of MgADP³¹⁹. In contrast, within our observed hetNOE values for residues in and vicinity of the Walker A motif, we obtain a rigidification in the ps - ns timescale upon nucleotide binding (ADP) in the NBD of LmrA. When Mg²⁺ was included, this also led to an increase of resonances that were significantly broadened and complicated the analysis. Similar to what we observed for MsbA-NBD in the PET-FCS measurements, Mg²⁺ may decisively affect the dynamics of nucleotide binding.

Other residues of conserved motifs showing sharpening of broadened lines upon ADP addition, are the conserved residues of the H-loop (H543) and the A-loop (Y358). For the A-loop, this has also been observed for the NBD of ABCB6 with MgADP³⁴³. The A-loop is known to stabilize the adenine ring of the nucleotide and thus interacts with both ATP and ADP¹⁵⁷. Our NMR data indicates that in the ADP-bound state, the A-loop and H-loop become stabilized (Chapter III: results subchapter 1. see **Figure 16**). The H-loop is known to coordinate the γ -phosphate of ATP, the magnesium ion, the attacking water and the catalytic glutamate¹⁷¹. Hence stabilization upon ADP binding for the H-loop in our NMR data (Chapter III: results subchapter 1. see **Figure 16**) might be not related to a direct interaction of the H-loop with ADP, but rather the overall stabilization of the catalytic subdomain when ADP was added.

Since most resonances for the residues in the NBS could only be assigned in the ADP-bound state, it was not possible to retrieve more information about their dynamics, in particular in a state-dependent manner. Fortunately, the resonances for the residues of the Walker B motif, D-loop and Q-loop could be assigned within the apo, ADP-bound and ATP-bound states. Here, the respective resonances showed significant chemical shift differences between the apo and the nucleotide bound states indicating sensing of nucleotide binding (Chapter III: results subchapter 1. see **Figure 16** and **Figure 17**). Intriguingly, in many cases the chemical shifts differed depending on whether ADP or ATP were added to the sample, indicating that these residues not only sense binding but can also distinguish between nucleotides. In addition, more detailed dynamic insights into Walker B motif, D-loop and Q-loop could be drawn using H/D exchange and hetNOE experiments which were carried out in the apo and ADP bound states.

The N-terminal residues I507, M509 and L510 of the Walker B motif (⁵⁰⁷ILMLDE⁵¹²) had a lower solvent accessibility (i.e. H/D exchange) in the nucleotide-bound state, interpreted as nucleotide-induced stability in the ms - s timescale (Chapter III: results subchapter 1. see **Figure 18**). This finding, indicative of a destabilization in the apo state compared to the ADP-bound state, is interesting because these residues are located in a β -sheet, which in general is very stable. Backbone dynamics in the ps - ns timescale as gauged by hetNOE experiments of the Walker B motif residues I507-D511 showed an overall rigidity regardless of the absence and presence of ADP (Chapter III: results subchapter 1. see **Figure 19**). However, when adding nucleotide, the aspartate residue (D511) of the Walker B motif residues in the ps – ns timescale (i.e. hetNOE experiments) remained rigid but nonetheless became slightly more flexible. This aspartate residue is known to be involved in coordinating the magnesium ion¹⁶⁵. In contrast, on the ms – s timescale (i.e. H/D exchange) the Walker B aspartate residue was very flexible in the apo and the ADP-bound state. As we did not include magnesium in the hetNOE and H/D exchange measurements, the Walker B motif or at least presumably the aspartate residue dynamics might be different in its presence. The catalytic glutamate residue (E512) was found to be the most dynamic residue within the Walker B motif in the ps – ns timescale (i.e. hetNOE experiments) in the two recorded states. H/D exchange data, which could only be obtained in the ADP-bound state for the catalytic glutamate residue of the Walker B motif, also revealed the glutamate to be flexible. An intrinsic flexibility of the catalytic glutamate might be of relevance for ATP hydrolysis within ABC transporters as this residue is known to be crucial for effective ATP hydrolysis^{152,165,289,344}. The ¹⁵N-HSQC spectra of LmrA-NBD recorded with MgADP showed that the resonances of the Walker B motif residues D511 and E512 are not present anymore. This may be caused by line broadening of these resonances.

Overall, the D-loop (⁵¹⁵ASLD⁵¹⁸) residues are flexible within the ps – ns (hetNOE experiments) and the ms – s (H/D exchange) timescale in both the apo and the ADP-bound state (Chapter III: results subchapter 1. see **Figure 18**, **Figure 19** and **Figure 20**). Nevertheless, small differences between the apo and the ADP-bound state were observed. The hetNOE experiments showed slightly more mobility (compared to the average mobility) for the alanine residue while the aspartate residue showed slightly more rigidity (but still maintaining an overall relatively high mobility) upon ADP binding. In contrast, H/D exchange experiments revealed less solvent accessibility of the D-loop alanine residue upon nucleotide binding, which was interpreted as nucleotide-induced stability (Chapter III: results subchapter 1. see **Figure 18**). The D-loop has been reported to interact with the H-loop and Walker A motif of the opposing NBD^{90,168,173,177,207}, thus the described differences in the dynamics of the D-loop residues between the apo and ADP-bound state may be transmitted across the NBD-NBD interface. Furthermore, the D-loop was reported to be crucial for unidirectionality within a heterodimeric type I ABC exporter (type IV fold), which might be connected to a certain inducible rigidity within the D-loop aspartate residue¹⁷⁴.

The Q-loop, which connects the catalytic subdomain and the α -helical subdomain, overall remains flexible upon nucleotide addition, which is in line with observations for other ABC transporters (i.e. HisP³³⁴, MJ0796³²⁷ and MJ1267³¹⁹). By comparing the nucleotide-free and nucleotide bound state, our data reveal the Q-loop to be mobile within the ms – s and the ps - ns timescale, with a small increase in the already existing flexibility in the ps – ns timescale upon ADP addition (Chapter III: results subchapter 1. see **Figure 18** and **Figure 20**). A flexible Q-loop fits to the assumption in the literature that the α -helical subdomain is loosely associated to the catalytic subdomain^{218,345}. As the Q-loop has a primary role in interdomain NBD/TMD signal communication, Q-loop flexibility seems to be important for transmitting nucleotide occupancy^{158,161}. Indeed flexibility between the Q-loop and the coupling helix (CH1 of the opposing TMD) was reported to be essential for ATPase activity and substrate transport of the type I ABC exporter (type IV fold), BmrA¹⁸⁵.

The X-loop is a unique motif within type I ABC exporters (type IV fold) and can transmit conformational changes of the NBS, via the C-loop (ABC signature motif), to the TMDs^{177–179,181,182}. When NBDs dimerize in a ‘head-to-tail’ manner, the C-loop comes in contact with the Walker A motif within the catalytic subdomain of the opposing NBD^{34,120,168,169,171,346,347} (Chapter I: introduction subchapter 3.3.2. Nucleotide binding domains: constitution and function). That the majority of the residues of the X-loop and C-loop showed no chemical shift and dynamic differences between the apo and ADP-bound states, might be explained by the absence of an opposing NBD in our experiments. In general, residues at the N-terminal end of the X-loop (G481-G484) were rigid and residues at the C-terminal end mobile (T478 and V480) in both recorded states (apo and ADP-bound) on the ps – ns (i.e. hetNOE, Chapter III: results subchapter 1. see **Figure 19** and **Figure 20**) and ms – s (i.e. H/D exchange, Chapter III: results subchapter 1. see **Figure 18**) timescale. An exception presents residue E479 in the X-loop, which seems to be dynamic within the ms – s timescale but not on the ps – ns timescale.

On the ps – ns timescale, all C-loop residues had intrinsic rigidity independent of nucleotide presence. However, the H/D exchange experiments revealed a very fast exchange in both recorded states, indicative of motions within the C-loop on the ms – s timescale.

In summary, chemical shift perturbation experiments of LmrA-NBD (Chapter III: results subchapter 1. see **Figure 17**) revealed that all conserved motifs located in the catalytic subdomain (Walker A motif, A-loop, H-loop, Walker B motif, D-loop and Q-loop) “sense” nucleotide binding. NH resonances of residues of the Walker A motif, A-loop (Y358) and H-loop (H543) “missing” in the apo state were present in the ADP-bound state. This was interpreted as mobility of these residues in the apo state and quenching of these motions in the presence of ADP. NH resonances of residues of the Walker B motif, D-loop and Q-loop could be obtained in the apo, ADP-bound and ATP-bound states. Thus, it was possible to observe that residues in these motifs (Walker B motif, D-loop and Q-loop) were able to “sense” and distinguish nucleotide binding. Residues of the conserved motifs of the α -helical subdomain (X-loop and C-loop) showed no effect upon nucleotide addition.

1.5. Allosteric coupling of nucleotide binding throughout the NBD: focus on the C-terminal region

In LmrA-NBD, the residues in and around the NBS are the most affected upon nucleotide binding. Nonetheless, differences in NBD dynamics upon nucleotide binding seem not only to be important in the NBS but are rather “felt” throughout the NBD. Transition between rigidity and flexibility within conserved motifs in the NBD of ABC transporters has already been described to be possibly important for mechanochemical energy transduction³¹⁹. In the same study it has been noted that restriction of correlated protein motions is a central mechanism for allosteric communications. Dynamic coupling is thus probably the basis of nucleotide-dependent allosteric reorganization processes within the TMDs to facilitate substrate transport mechanisms and may also enable the transmission of feedback signals to the NBD due to substrate binding in the TMD. On the other hand, dynamic coupling may also facilitate NBD-NBD interactions to fine-tune the steps of the catalytic cycle (i.e. nucleotide binding, ATP hydrolysis, nucleotide release, P_i release), across the two NBS in an ABC transporter dimer. A region of particular interest for NBD crosstalk are the C-terminal helices, α 10 and α 11 in LmrA-NBD (**Figure 47**). Some residues in these helices were responsive to nucleotide addition (Chapter III: results subchapter 1. see **Figure 17**). Furthermore, chemical shift perturbations could be observed that differed depending on whether ADP or ATP were added to LmrA-NBD (Chapter III: results subchapter 1. see **Figure 17** and **Appendix 16**).

In the ms – s timescale (Chapter III: results subchapter 1. see **Figure 18**) and the ps - ns timescale (Chapter III: results subchapter 1. see **Figure 20**), the two C-terminal helices were more flexible within the apo state compared to the ADP-bound state.

Interestingly, in a solution NMR study of the NBD of ABCB6, ~15 residues at the C-terminal end were predicted to be unfolded from a secondary structure analysis^{343,348} (chemical shift index-CSI). This C-terminal loop region (~15 residues) in ABCB6-NBD showed broadened peaks in apo state but distinct peaks in the MgADP-bound state³⁴³. Due to this observation and a modelled structure for ABCB6-NBD, which showed that these C-terminal residues can be close to either of the nucleotide binding motifs; Walker A, H-loop or D-loop; the authors assumed a C-terminal interaction with one of the mentioned nucleotide binding motifs in the absence of nucleotide but no or weak interaction in the MgADP-bound state. Similarly, the crystal structure of LptB (the NBD of the lipopolysaccharide ABC transporter LptB₂FG) revealed that the C-terminal loop of LptB₂FG has intramonomer interactions with the Walker A motif and the H-loop³⁴⁹. It remains unclear if a similar model could be true for our LmrA-NBD. The secondary structure predictions of LmrA-NBD in the ADP-bound state²⁷⁹ indicated that there are some unfolded residues (~5 residues) at the C-terminal end but not as many as were predicted for the ABCB6-NBD (~15 residues). Whether the secondary structure differs in the C-terminus depending on the catalytic state (apo, ADP-bound or ATP-bound) in LmrA-NBD requires further analyses in the future.

More recently, a molecular dynamic simulation study assumed a possible exit pathway for the inorganic phosphate after ATP hydrolysis through a hydrated channel from the NBS towards the C-terminal helices²⁰². However, it can only be speculated about the exact P_i release pathway as only a picture (**Appendix 38**) is available of the simulation without further description in the manuscript. Based on the available figure it seems that P_i would be released between the C-terminal helices of one NBD and the catalytic subdomain of the second NBD. Release of inorganic phosphate might be important for resetting the transporter to the inward open conformation (Chapter I: introduction subchapter 3.4. Transport mechanism of type I ABC exporters: “alternating access” mechanism and its alterations) of ABC transporters²⁰². One could assume that the observed rigidification of the C-terminal helices for LmrA-NBD in the ADP-bound state (Chapter III: results subchapter 1. see **Figure 17**) could facilitate P_i release via this pathway. In our work, ADP as the ATP hydrolysis product was seen to be important for stabilizing the residues in the C-terminal helix. Hence, this may be favorable

Over the years, many inward open apo state structures with separated NBDs have been reported, thus somewhat contradicting the idea that the “zipper helices” always loosely associate the two NBDs. The majority of the type I ABC exporter (type IV fold) structures (**Figure 47**, PglK²⁵², ABCB10¹⁸³, CmABCB1³⁵¹, MRP1³¹¹ and CFTR³⁵²) confirm the finding for P-gp^{148,186,353–355} and its ortholog, MsbA^{135,350} that in the absence of nucleotides, the NBDs are widely separated and hence also their C-termini do not interact. Interesting in this context is the fact that in the structure of ABCB10 16 amino acid residues of the C-terminus are not resolved in the shown structure, hence the C-termini of the NBDs might be able to interact, but it cannot be seen in the ABCB10 structures (**Figure 47**). Another observation is that the complete resolved C-termini of PglK do not have the C-terminal helices, which might promote that NBDs are separated in the apo state (**Figure 47**). However, there are also numerous structures reported, even before TmrAB⁸⁹, where the C-termini are involved in contacts to the opposing NBD in the apo state, e.g. in MsbA¹³⁵ and TM287/288⁹⁰ (**Figure 47**). Indeed, the number of ABC transporter structures showing NBD interaction via its C-terminus seems to grow steadily^{251,356,357}.

However, it should be noted that X-ray crystallography can only reveal snapshots of proteins that may have many, potentially quite dynamic conformations. Cryo-EM is capable to capture different conformations of proteins^{358–360}, but studies still often focus on a single 3D class with the best final resolution, thus other conformations might be neglected. Nevertheless, cryo-EM studies of P-gp³⁶¹, MsbA²⁴⁹ and TmrAB²⁰² discovered more than one state in one catalytic step of type I ABC exporters (type IV fold). P-gp was observed in both an inward (NBDs apart) and an outward facing (NBDs close) conformation without nucleotide³⁶¹. A population of a conformation in closer contact between the C-terminal helices in the apo state might also occur in other type I ABC exporters (type IV fold), which may have not resolved yet because of its dynamics, which may lead to lower resolution in cryo-EM studies and no crystals in X-ray crystallography.

Type I ABC importers (type I fold) and ECF transporters (type III fold, **Figure 48**) have large C-terminal domains attached to their NBDs. These C-terminal domains are responsible for keeping NBDs in close contact^{74,76} or have other regulatory functions. For example, the C-terminal domain of the type I ABC importer (type I fold), ModBC regulates substrate uptake by binding the substrate, resulting in inhibition of substrate import^{362,363}. Thus, a role of the C-terminal region of type I ABC exporters might also play a role for NBD organization as well as substrate transport. In the literature a connection of substrate transport with the C-terminal region has been described^{89,349}. Interestingly, the recorded NMR experiments within this thesis showed that nucleotide binding leads to changes within the C-terminal region in the LmrA-NBD (Chapter III: results subchapter 1. see **Figure 17**), which might be important for allosteric effects resulting to a functional substrate transport. For further studies it will be interesting to analyze whether and how the C-terminal region is affected when a substrate or both substrate and nucleotide are bound to a type I ABC exporter (type IV fold).

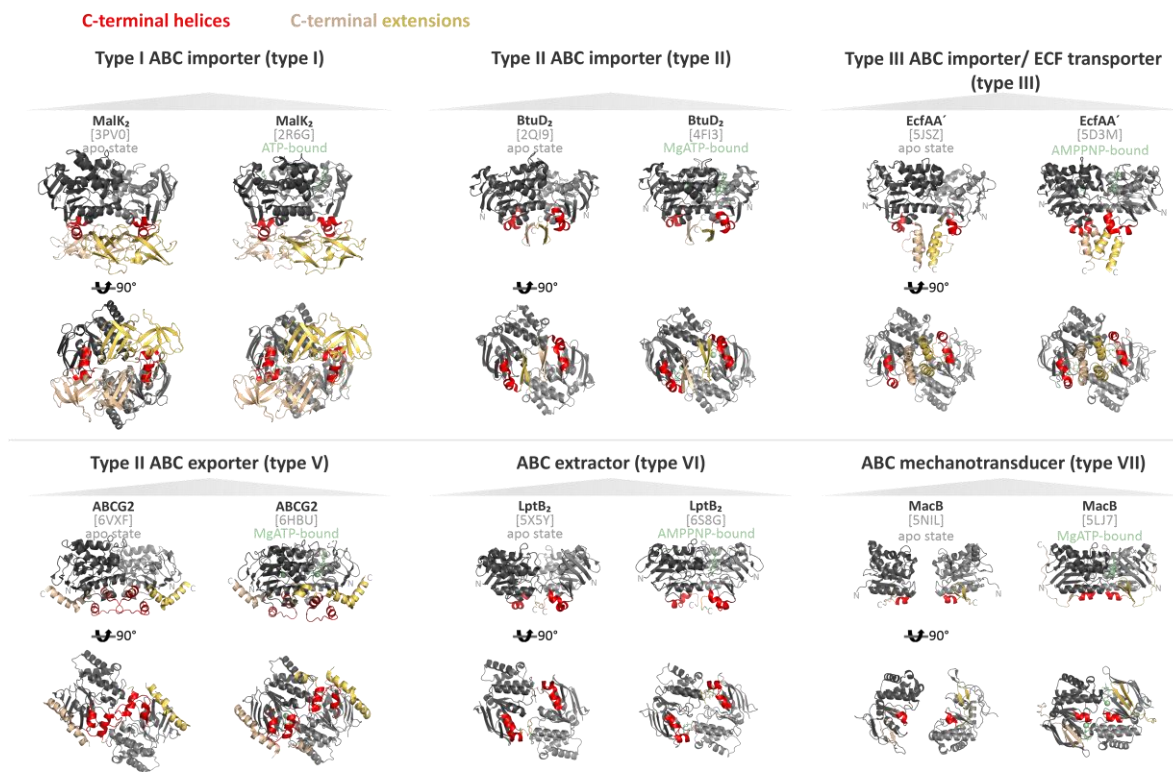


Figure 48: C-terminal helices and C-terminal extensions of NBDs of ABC transporters. The transporter structures are shown in apo and nucleotide bound state in a side view and a view from cytoplasm. PDB IDs of shown transporters: MalFGK₂-MalE (3PVO²¹⁴, 2R6G⁷⁴), BtuC₂D₂-BtuF (2QI9³⁶⁴, 4FI3³⁶⁵), EcfTAA'-FolT (5JSZ³⁶⁶, 5D3M³⁶⁶), ABCG2 (6VXF³⁶⁷, 6HBU³⁶⁸), LptB₂FG (5X5Y⁷⁸, 6S8G³⁶⁹), MacB (5NIL⁸⁶, 5LJ7⁷⁹).

“Static” structural X-ray and cryo-EM studies of ABC transporters have been complemented with spectroscopic data to obtain important insights into the dynamics of e.g. the C-termini of an ABC transporter. Different modes of binding were identified for substrate and inhibitors within P-gp^{315,322}. In that study, EPR labeling positions within one C-terminal helix in P-gp were demonstrated to be highly dynamic in the apo, substrate-bound, AMP-PNP-substrate-bound and ATP-substrate-bound states. Only in the substrate-bound post-hydrolysis state (ADP-V_i substrate) a rigidification and a closer distance for the C-terminal helix area was noted. In the case of LmrA, EPR studies with a label attached to the C-terminal helix α 10 showed a high degree of flexibility in this region in all catalytic stages of the ATPase cycle²⁵⁴. Considering that the C-terminal region of one NBD come in close contact to the second NBD in the catalytic cycle, the C-terminal region (C-terminal helices) may play an important role for transmitting conformational changes between the NBDs upon nucleotide binding (as hypothesized also from the data of the presented study). A transient contact between the C-terminal regions could also be possible within the native (membrane) environment as the degree of opening between the NBDs seems to depend on the lipid environment^{91,251,263,268,370,371}.

1.6. On the physiological relevance of the dynamic and structural differences in nucleotide binding states

Differences obtained within our data between the chemical shifts in (Mg)ADP- and (Mg)ATP-bound states of the LmrA-NBD reflect the difference in structural dynamics between the pre- or post-hydrolysis states within the catalytic cycle of an ABC transporter (Chapter I: introduction subchapter 3.3.3. Models for the ATPase catalytic cycle in the NBD during the transport mechanism and 3.4. Transport mechanism of type ABC exporters: “alternating access” mechanism and its alterations). The observed differences indicate that pre- and post-hydrolysis states are characterized by the propagation of distinct allosteric intramolecular signals from the NBS throughout the NBD and possibly beyond. For example, it was shown in this thesis that in particular the Q-loop and the coupling helix groove are affected by nucleotide binding. These intramolecular signals might induce different conformational changes within the TMDs, leading to occluded- or outward-facing conformations within the ABC transport mechanisms (Chapter I: introduction subchapter 3.4. Transport mechanism of type ABC exporters: “alternating access” mechanism and its alterations).

In addition, it was shown that specific residues react differently to ATP and ADP. This could lead to different intradomain signals in each NBD of the NBD dimer, especially when the nucleotide occupancy is asymmetric, i.e. when in one NBS ADP is bound and in the second NBS ATP. For the interpretations made here, it should be kept in mind that distinct recognition of ATP analogues has been suggested for homodimeric and heterodimeric NBDs²⁵⁵. Thus, dynamic details may differ between different ABC transporters also depending on whether they form homo- or heterodimers.

Finally, in the data presented here for the LmrA-NBD WT, magnesium ions seem to destabilize the NBD monomer as less resonances were observed in the TROSY ¹H-¹⁵N HSQC spectra (**Appendix 17**). This could play a role for resetting the catalytic mechanism. Notably, in previous studies for P-gp a lower nucleotide binding affinity was recorded in the presence of magnesium ions³⁷². Comparing the affinity of ADP and ATP to the NBD of LmrA, ADP was identified to have the higher affinity. The role of the ADP-bound state within the transport cycle may potentially be underestimated, although it is an important transition state within the catalytic cycle of ABC transporters^{106,252}. For instance, the structures of the type I ABC exporter (type IV fold), PglK revealed two inward open apo conformations and an outward occluded ADP-bound conformation. Since occluding the inward open cavity did not affect the transport activity of PglK, it was concluded that only the outward open (nucleotide-bound) states are able to perform substrate transport. If this is also true for other type I ABC exporters (type IV fold) remains elusive, as PglK has some unusual structural features for substrate recognition, which are not found in other proteins with a type I ABC exporter (type IV) fold. There is currently no indication that the ABC transporters investigated here are able to conduct the same substrate translocation mechanism as PglK. In MsbA a similar mechanism to transport Lipid A across the membrane may occur as structures for MsbA showed potential lipid A binding sites within a cavity between the TMDs but also on an outer surface cleft³⁷³. This surface cleft seems to be at a similar position as the unusual structural feature in PglK, which has been described to be involved in lipid (i.e. lipid-linked oligosaccharides) transport, indicating that lipid A could follow a similar mechanism in MsbA. Nevertheless, more details about the mechanism in MsbA would be needed to provide evidence for a similar lipid transport mechanism as in PglK. However, it may be speculated for ABC transporters in general, that the ADP-bound state is not just a product of ATP hydrolysis, but rather an essential part of the substrate translocation cycle, used for example to block the re-binding of a just released substrate by maintaining the ABC transporter in an outward occluded state for longer. Our data also reveal that dynamically, the ADP-bound (post-hydrolytic) state seem to be the most stable state for the LmrA-NBD within the catalytic cycle. In the cell, millimolar concentrations of ATP and micromolar concentrations of ADP are present^{232,374}, which argues for the presence of either an

ADP- or an ATP-bound state in the transport cycle at all times, while an apo state (inward-facing conformation) might occur only transiently and be lowly populated. The higher affinity for ADP could enhance the probability for an ABC transporter to occupy the outward open state. Only when the local concentration of ATP is high enough, ATP replaces ADP for a new transport cycle. A high ADP affinity may also be favorable in the context of the reported coupling of ATP hydrolysis with a putative adenylate kinase activity for ABC exporters (MsbA, LmrA and TmrAB)²⁷⁶. For different type I ABC exporters (type IV fold), a broad range of affinity values for ATP and ADP have been measured (**Appendix table 4**). Many studies that determine nucleotide affinities to type I ABC exporters (type IV fold) show very different results, which might be related to the used techniques and the specific ABC protein investigated. However, the previously obtained affinities for MsbA for binding ATP or ADP¹³² (with fluorescence quenching experiments) seem to be in the same range as the affinities we observe for LmrA-NBD with NMR experiments and agree on a higher binding affinity for ADP over ATP¹³². In this context it has to be considered that for several ABC transporters, such as P-gp³⁷⁵ or MalFGK₂³⁷⁶, an increase in ATP affinity by substrate binding has been described, which cannot be assessed when studying isolated NBDs.

In this chapter, detailed allosteric and dynamic consequences upon nucleotide binding on the most conserved region within ABC transporters, the NBD, were described. The observations how nucleotide interaction affects NBD dynamics across timescales lead to hypotheses how the transmission of nucleotide occupancy within the NBD, from the NBS to the TMD or between the NBD-NBD interface may occur during the substrate transport mechanism.

2. NBD INTRADOMAIN CROSSTALK: FOCUS ON D-, Q- AND H-LOOPS

NBDs contain several conserved sequence motifs that are pivotal for the catalytic cycle of ABC transporter such as the D-loop, Q-loop and H-loop. Monitoring structural and dynamic intradomain interactions in regions in and around these conserved motifs is difficult in the context of the full-length transporter but can be carried out on isolated NBDs in a relatively straight-forward manner. Combining mutagenesis studies and NMR spectroscopy on the ADP-bound LmrA-NBD, it was possible to reveal which NBD regions are structurally and dynamically connected to the D-, Q- or H-loops (Chapter III: results subchapter 2. see **Figure 28**, **Figure 32**, **Figure 33** and **Figure 34**).

The data from chapter III results subchapter 2. Role of conserved motifs in the NBD of multidrug ABC transporters show that the residues forming the D-, Q- and H-loops sense nucleotide binding and can also distinguish between ATP and ADP. Upon mutation of either D-, Q- or H-loop residues, regions in the proximity of the mutation were affected, but intriguingly also remote regions, e.g. residues in the coupling helix groove and the C-terminal region showed chemical shift differences (Chapter III: results subchapter 2. See **Figure 28** and **Figure 34**). These results indicate a crosstalk between the conserved motifs and remote NBD regions. Furthermore, D-, Q- and H-loop communicate with other conserved motifs such as the Walker A and Walker B motifs. No or minor effects on structure and dynamics in A-loop, X-loop and C-loop were observed by the inserted mutations.

2.1. Crosstalk of D-, Q- or H-loop with the Walker A and Walker B motifs

The resonances of the conserved Walker A motif, which is known to be involved in nucleotide binding¹⁶⁴ could be shown to change in ¹⁵N-labeled LmrA-NBD when either the H-loop histidine and D-loop aspartate residues were mutated (Chapter III: results subchapter 2. See **Figure 28**). This is despite the fact that crystal structures of NBDs with mutated H-loop (e.g. HlyB) show no difference in the arrangement of the Walker A residues compared to the wildtype protein¹⁷¹, thus highlighting the importance of complementary, spectroscopic studies. In contrast to H- and D-loop mutants, no chemical shift perturbation for the Walker A motif was noted when the Q-loop glutamine residue was mutated, indicating that these conserved motifs do not undergo crosstalk (Chapter III: results subchapter 2. see **Figure 28**). In a second step, the backbone dynamics of WT and D-, Q- or H-loop point mutants in LmrA-NBD were compared using HetNOE experiments (Chapter III: results subchapter 2. see **Figure 34**). These experiments reveal that H-loop, D-loop and Q-loop residues can influence the dynamics of the Walker A motif. More specifically, these NMR experiments indicate that in LmrA-NBD WT, the D-loop and Q-loop play a role in mobility and stability of the Walker A motif. The H-loop histidine residue in the LmrA-NBD shows to be relevant for rigidity within the Walker A motif (Chapter III: results subchapter 2. see **Figure 34C/D**). However, despite the dynamic differences in the Walker A motif, the D-, Q- and H-loop mutants had no effect on the affinity of LmrA-NBD to nucleotides, as K_D -values were found to be in the same range as for LmrA-NBD WT (Chapter III: results subchapter 2. see **Figure 27B/C**). This finding is in line with data from the literature where nucleotide binding still occurred when the D-loop aspartate, Q-loop glutamine or the H-loop histidine residue was mutated, even if ATP hydrolysis abolished¹⁷¹ or decreased^{158,161} in the respective ABC transporter.

In addition to the Walker A motif, the Walker B motif is the second hallmark of ABC transporters. The NMR experiments (Chapter III: results subchapter 2. see **Figure 28**, **Figure 32**, **Figure 33** and **Figure 34**) in this thesis show that Walker B motif residues also senses when the D-, Q- or H-loop residues are replaced by alanine (D518A, Q430A and H543A). These results indicate a communication between

the Walker B and the D-, Q- and H-loop. Dynamics obtained by HetNOE experiments for the NBD WT in the ADP-bound state showed that the Walker B motif residues ⁵⁰⁷ILMLD⁵¹¹ are rigid and only the catalytic E512 is mobile (Chapter III: results subchapter 1. see **Figure 20**). Comparison of the dynamics of the three ADP-bound LmrA-NBD mutants (D518A, Q430A or H543A) showed that only the catalytic glutamine (E512) decreased in flexibility in the mutants (Chapter III: results subchapter 2. see **Figure 32**, **Figure 33** and **Figure 34**) Conversely, this means that the D-, Q- and H-loop in the WT LmrA-NBD contribute to stabilization of the glutamine residue. H-loop histidine has been described to promote ATP hydrolysis by forming a stabilizing hydrogen bond to the transition states of the catalytic cycle, where the glutamine residue was described to support this stabilization¹⁷².

2.2. Communication of the D-, Q- and H-loops with the D-loop helix

The NBD-NBD interaction within the catalytic cycle of type I ABC exporter (type IV fold) is in part mediated via the D-loop of one NBD and the Walker A motif of the opposing NBD. Those interactions have been reported to be abrogated in the absence of nucleotides in e.g. the heterodimeric type I ABC exporter, TM287/288⁹⁰. Major rearrangements occur between nucleotide-bound and apo states within the D-loop and the D-loop helix. This led to the hypothesis that D-loop helix dynamics and intra-NBD-domain interaction of the D-loop helix with the D-loop play an important supportive role for the opening and closing of the NBD dimer⁹⁰. Vakkasoglu *et al.* reported that the non-homodimerizing NBD of the human type I ABC exporter TAP was able to form NBD dimers when D-loop helix residues from the homodimerization competent rat TAP1 NBD were introduced³⁷⁷. These findings support the notion that D-loop helix residues play an important role in the NBD-NBD interaction. Another study on the TAP D-loop showed that a D-loop aspartate to alanine mutation destabilizes the beginning N-terminal residues of the D-loop helix¹⁷⁴. The NMR data on LmrA-NBD show that the D-loop aspartate and the H-loop histidine residues are important for stabilizing the D-loop helix. Upon mutation of the conserved D- and H-loop aspartate and histidine, the D-loop helix residues showed strong dynamic differences (i.e. D-loop mutant lead to an increase in flexibility and the H-loop mutant lead both increase and decrease in flexibility in the D-loop helix) compared to the LmrA-NBD WT in the HetNOE data (Chapter III: results subchapter 2. see **Figure 32A/B/D**, **Figure 33A/B/D** and **Figure 34A/C**). The effects of mutating the Q-loop glutamine on the D-loop helix dynamics were less pronounced but nonetheless indicate a role for the Q-loop in the flexibility of this NBD region (Chapter III: results subchapter 2. see **Figure 32C**, **Figure 33C** and **Figure 34B**).

2.3. Crosstalk between coupling helix groove and D-, Q-, H-loops

In ABC transporters, the NBD structurally connects to the TMD via the coupling helix groove, into which the TMD coupling helix locks like a ball in a socket^{34,135,148,183,186,332,333,335,336} (**Figure 49**). The groove is comprised of residues I425-S432 (LmrA). These residues form part of the β 5-strand of the NBD and are located in the vicinity of the Q-loop glutamine residue. Upon mutation of the D-, Q- or H-loops, large chemical shift perturbations were observed for the residues in the coupling helix groove (**Figure 49**, Chapter III: results subchapter 2. see **Figure 28** and **Figure 29**).

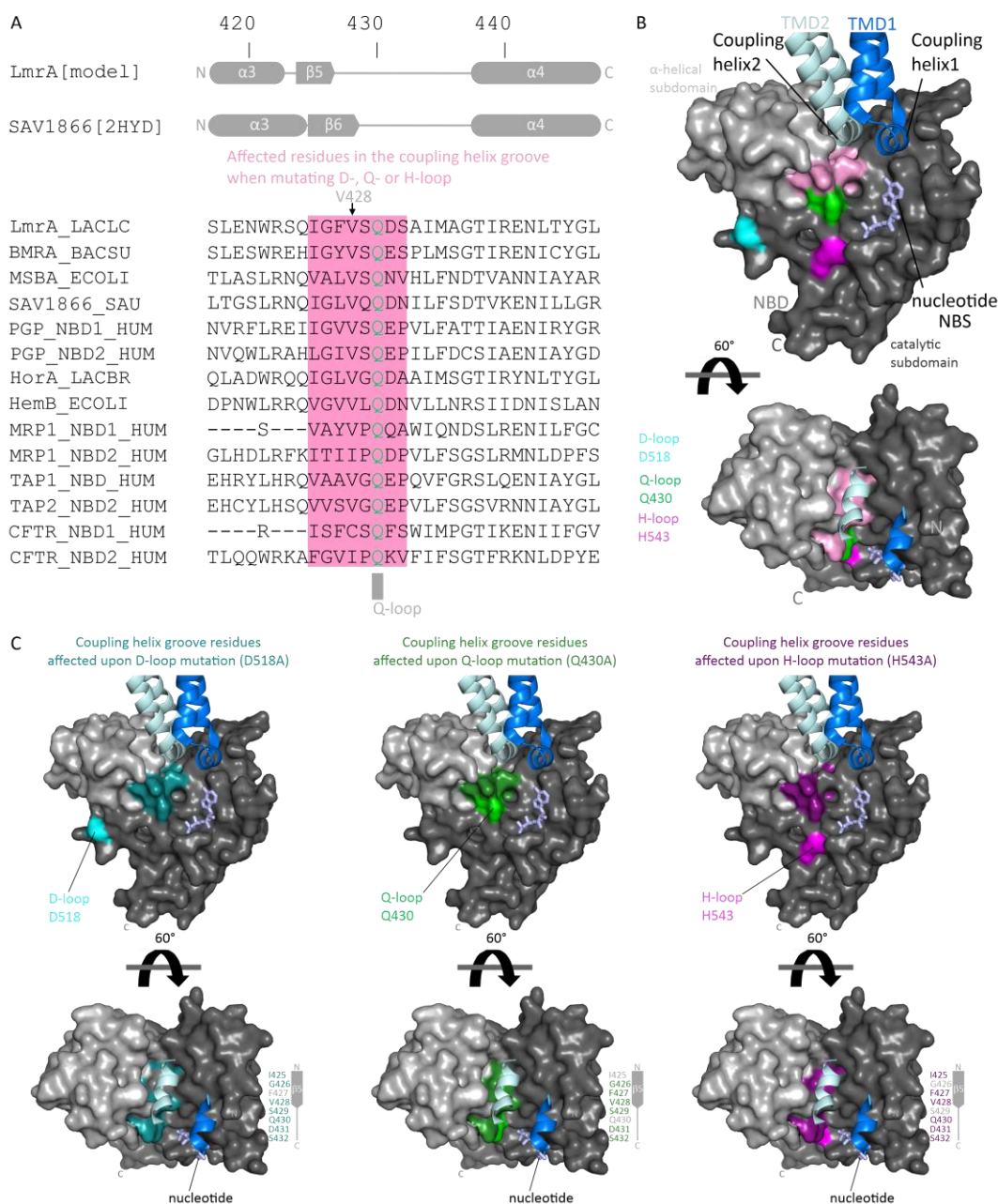


Figure 49: Coupling helix groove residues affected by mutation of D-, Q- or H-loop in the NBD of LmrA

A) Sequence alignment (www.ebi.ac.uk/Tools/msa/clustalo/310) for the NBD region of the coupling helix groove of type I ABC exporters (type IV fold). The corresponding secondary structure elements of LmrA-NBD (modeled on Sav1866 PDB ID: 2HYD³⁴) are displayed. Numbering based on LmrA. Residues “crosstalking” with D-, Q- or H-loop of the coupling helix groove are highlighted in rose. The conserved Q-loop glutamine residue is displayed in green. Residues that show chemical shift perturbation compared to the WT upon introduction of point mutants in the D-, Q- or H-loop are highlighted in pink. Of note, residue V428 in the LmrA coupling helix groove was one coupling groove residue affected by the introduction of all mutants and is highly conserved among type I ABC transporters. **B)** Interface between TMDs and the NBD (coupling helix groove) in the type I ABC exporter Sav1866 (PDB ID: 2HYD³⁴) highlighting the region which is interacting with the D-, Q- or H-loop (pink). D-, Q-, and H-loop are indicated in cyan, green, and violet, the nucleotide in light purple. **C)** Residues in the coupling helix groove affected by mutating the D-loop, Q-loop or H-loop identified by chemical shift perturbation analysis with NMR experiments are colored in dark cyan (in D518A mutant), dark green (Q430A) or dark purple (H543A), respectively. The coupling helix groove is in the interface between the α-helical (light gray) and the catalytic subdomain (dark gray). NBS – Nucleotide binding site. NBD – Nucleotide binding domain. TMD – Transmembrane domain.

The resonances for residues V428, D431 and S432 in the LmrA-NBD coupling helix groove, reacted to mutations in all three conserved motifs, H-loop (H543A), D-loop (D518A) and Q-loop (Q430A) with

shift changes compare to the WT. Interestingly, V428 seems to be conserved across type I ABC exporters (**Figure 49**, Chapter III: results subchapter 2. see **Figure 29**) and therefore may be crucial for crosstalk between the NBD and TMD. In summary, D-, Q- and H-loop motifs are able to communicate with the coupling helix groove. It is known that the coupling helix groove translocates signals such as nucleotide occupancy from the NBD to the TMD and is thus important for substrate transport. Inactivity in substrate transport has been described in the literature when the D-loop of type I ABC exporters (i.e. MsbA²¹¹ and TM287/288⁹⁰) were mutated due to defective NBD-TMD^{90,211}. Likewise, due to the chemical shift perturbation observed for resonances of coupling helix groove residues upon mutation of the D-, Q- and H-loop, it may be speculated that these mutations also have transport defects in LmrA due to faulty NBD-TMD crosstalk. When the Q-loop was mutated in both NBDs of the type I ABC exporter P-gp, this resulted in the loss of ATPase activity and the ability to perform a conformational change within the TMDs, and thus transport capability¹⁶¹. In contrast, the single Q-loop mutants of P-gp were still able to maintain an almost P-gp WT like transport function and substrate binding, thus showing that such mutations in one NBD can at least be partially compensated.

Also, the H-loop motif (switch loop) with its invariant histidine residue, was described to be essential for transport and ATP hydrolysis, but not for ATP binding in ABC transporters^{215,217,378–382}. It has been proposed that the H-loop histidine participates in conformational changes of the NBD after ATP binding¹⁸⁹. Considering the observation that mutagenesis of the H-loop also led to chemical shift changes for coupling helix groove residues in LmrA-NBD (i.e. CSP data H-A mutant, **Figure 49C**, Chapter III: results subchapter 2. see **Figure 28** indicates that the H-loop may be involved in structural coupling to the TMDs and subsequently affect substrate transport. However, it should be noted that this observation was made with ADP-bound protein. Whether the crosstalk between coupling helix groove and the D-, Q- or H-loops is similar or different in other catalytic states requires further investigation.

2.4. Long-range communication of D-, Q- and H-loops with the C-terminal region

In this study, it could be shown that mutations of the D-, Q- and H-loop affect residues in the C-terminal region of LmrA-NBD, as these residues showed notable chemical shift differences compared to the WT. Thus, the C-terminus might be able to sense conformational and dynamical changes of D-, Q- or H-loop invoked by nucleotide binding or hydrolysis. Interestingly, the mutation of the H-loop seemed to affect the C-terminal region the most, here the strongest chemical shift perturbations and differences in dynamics (i.e. in hetNOE experiments, chapter III: results subchapter 2. see **Figure 28C** and **Figure 34C/D**, see below) compared to the WT were observed. It remains to be shown whether the opposite is also true, i.e. whether mutations in the C-terminal regions of the NBDs also affect the conserved residues in the NBD. In chapter IV: discussion 1.4. (see also Chapter III: results subchapter 1. **Figure 16** and **Figure 17**) it was described that D-, Q- and H-loops “sense” nucleotide binding. Therefore, their “reaction” to nucleotide addition could also be recognized by residues of the C-terminal region. Whether the C-terminal region also affects the conserved motifs is not yet known.

Interestingly, mutations in all three conserved motifs show differences in NBD dynamics of the C-terminal helices ($\alpha 10$ and $\alpha 11$) of the NBD in HetNOE experiments (Chapter III: results subchapter 2. see **Figure 34**). This is particularly pronounced for α -helix 11. As the C-terminal helix has been described to influence substrate transport of the type I ABC exporter (type IV fold) TmrAB⁸⁹ by interacting with the opposing NBD, dynamics in this helix might be crucial for proper substrate transport and NBD interaction. Interestingly, this would indicate that D-, Q- and H-loop are indirectly involved in this process, too.

In a solution NMR study by Kurashima *et al.* on the NBD of the type I ABC exporter ABCB6³⁴³, it was hypothesized that the C-terminal loop region interacts directly with the conserved D-loop and H-loop motifs in the apo state. In addition, it was suggested that there is no or only a weak interaction in the MgADP-bound state³⁴³, as the authors reported broad peaks in the C-terminal loop region in the apo state but distinct peaks in the MgADP-bound state. Another study of the NBD of the LptB ABC transporter identified a unique C-terminal loop in an NBD crystal structure, which also showed an intradomain interaction with the H-loop³⁴⁹. At the moment, it cannot be concluded whether a direct interaction of D- and H-loop residues with the C-terminus of LmrA-NBD can lead to the observed chemical shift and dynamic changes in the C-terminal helices, but the data (i.e. from CSP and hetNOE experiments, Chapter III: results subchapter 2. see **Figure 28** and **Figure 34**) strongly suggests that there is crosstalk between these regions within the monomeric NBD.

2.5. NBD intradomain crosstalk between D-, Q- and H-loop

Mutagenesis studies of the D-, Q- or H-loop residues (D518A, Q430A and H543A) in ¹⁵N-labeled LmrA-NBD revealed an influence on each other's chemical shifts, which indicates intra-domain communication between these conserved motifs (Chapter III: results subchapter 2. see **Figure 28** and **Figure 30**). In addition, the D-loop aspartate can "sense" and distinguish nucleotides, but this ability requires an intact H-loop. In contrast, mutation of the Q-loop glutamine did not interfere with the ability of the D-loop. However, regardless of whether D- or H-loop were mutated, the Q-loop was always able to "sense" nucleotide occupancy (although without distinguishing between pre- and post-hydrolysis state). Nevertheless, long range transmission of the information whether a nucleotide is bound may be defunct in all NBDs with mutated D-, Q- or H-loops, since NMR peak positions were shifted compared to LmrA-NBD WT in all cases (Chapter III: results subchapter 2. see **Figure 28** and **Figure 30**). These observations could thus be one cause for observed defects in ATPase activity and/or substrate transport reported in literature when mutating the conserved D-loop aspartate^{90,174,211,276}, Q-loop glutamine¹⁶¹ or H-loop histidine residue^{171,215-217}.

Analysis of backbone dynamics within the ps – ns timescale (Chapter III: results subchapter 2. see **Figure 32**, **Figure 33** and **Figure 34**) showed that the H-loop dynamics are connected to the integrity of the D-loop and Q-loop and vice versa, whereas the respective D-loop and Q-loop mutations had no effect on each other's dynamics. For the ABC transporter haemolysin B (HylB), an interaction of the Q-loop residue with the extended D-loop region in the ADP-bound state has been described¹⁸⁹. The results from this thesis confirm such a crosstalk for LmrA-NBD, indicating that it may be a general feature of ABC transporter NBDs (Chapter III: results subchapter 2. see **Figure 28**). In the HylB study, the α -helical subdomain is described to rotate outward after ATP hydrolysis (P_i release) and then is pinned in this position caused an interaction of the Q-loop and the extended D-loop region. The authors conclude that the D-loop might be important to hold a non-productive position of the NBD in the absence of ATP, because of that pinning. The described pinning between those two regions (Q-loop and this extended D-loop region) might be an explanation that no dynamic interaction between the Q-loop and the D-loop (Chapter III: results subchapter 2. see **Figure 32**, **Figure 33** and **Figure 34**) were noted within this thesis in the ADP-bound state.

As mentioned above, the dynamics of the H-loop histidine residue were found to be dependent on the integrity of the Q-loop and the D-loop region (Chapter III: results subchapter 2. see **Figure 34**). Specifically, it was shown that the histidine residue is associated with mobility of the Q-loop and the D-loop. Furthermore here (Chapter III: results subchapter 2. see **Figure 34**), it was found that the H-loop histidine is a major player in stabilizing the D-loop aspartate residue and the C-terminal residues of the D-loop (i.e. D-loop helix α 8 in LmrA-NBD, chapter III: results subchapter 2. see **Figure 34A** and

Appendix 23). Molecular dynamic simulations of the ABC transporter, Sav1866 reported that both D-loop and D-loop helix movements occur in concert with movements of the α -helical subdomain¹⁷³. Similarly, because we observed coupling between H-loop and D-loop structural dynamics, the H-loop might be indirectly involved in the movements of the α -helical subdomain of the LmrA-NBD. We also found that all three conserved motifs seem to play an important role for mobility in the ps – ns timescale within the α -helical subdomain (Chapter III: results subchapter 2. see **Figure 34**). As described before, mobility of the α -helical subdomain may be important for the substrate transport mechanism within ABC transporters (Chapter IV: discussion subchapter 1.1. and 1.2.). Reduced ATPase activity in H-loop mutants may also potentially be explained via a change in the observed network of the H-loop residue in this thesis. Specifically, cross-linking to the flexibility of the Q-loop and the D-loops has been proposed to be important for the formation of a hydrolysis competent active site in ABC transporter NBDs^{171,173,215–217,380,382,383}.

Finally, interdomain crosstalk of the H-loop with the D-loop of the opposing NBD has been described to be crucial for NBD-NBD communication¹⁷¹. However, but the results presented in this thesis (Chapter III: results subchapter 2. see **Figure 28** and **Figure 30**) indicate that the H-loop histidine residue is already a key “team player” for NBD intradomain crosstalk.

2.6. Crosstalk mediated by LmrA-NBD D-loop variants

2.6.1. Role of the D-loop aspartate residue for substrate transport and ATPase activity

As outlined in chapter III: results subchapter 2. Role of conserved motifs in the NBD of multidrug ABC transporters, the role of the D-loop aspartate in substrate transport and ATP hydrolysis in different bacterial ABC transporters was investigated with biophysical methods and functional assays (Chapter III: results subchapter 2. see **Figure 28A**, **Figure 32A/B**, **Figure 33A/B**, **Figure 34A/D** and **Figure 37**). When mutating the aspartate residue to an alanine, substrate transport and ATP hydrolysis were reduced or fully abrogated (within full-length BmrA and MsbA-NBD, Chapter III: results subchapter 2. see **Figure 37**), but nucleotide binding was still possible within the NBD of the studied transporters (LmrA-NBD, MsbA-NBD and BmrA-NBD, Chapter III: results subchapter 2. see **Figure 27** here nucleotide binding shown for LmrA-NBD-D518A). In a study on heterodimeric TAP¹⁷⁴, mutation of both D-loops led to inactive substrate transport. Strikingly, when mutating only one D-loop (NBD consensus site D-A) substrate translocation (i.e. for TAP peptide translocation) still occurred in the presence of different nucleotide variants (ADP, ATP, AMPPNP) but ATP hydrolysis was disrupted. Thus, the D-loop is important for the transporter “knowing” whether and which nucleotide is bound. Our chemical shift perturbation data of the LmrA-NBD WT monomer supports the notion that the D-loop can indeed “sense” and distinguish between nucleotides (Chapter III: results subchapter 1. see **Figure 16** and **Figure 17**). Flexibility of the D-loop was reported to be important for ATP hydrolysis and substrate transport for numerous type I ABC exporters (type IV fold) such as, MRP1³⁸⁴, TM287/288⁹⁰ and Sav1866¹⁷³. Our data (Chapter III: results subchapter 2.3. Fast Backbone Dynamics of LmrA-NBD D-, Q- or H – loop mutants in the ADP-bound state) on an isolated NBD also support a key role for D-loop flexibility and an alteration in NBD flexibility, when the conserved aspartate is mutated to alanine. In this mutant (in LmrA-NBD), no increase in flexibility in the ps-ns timescales was observed within the other conserved D-loop residues (Chapter III: results subchapter 2. see **Figure 32A/B**, **Figure 33A/B** and **Figure 34A/D**), however neighboring residues, in particular the D-loop helix ($\alpha 8$ based on LmrA-NBD, Chapter III: results subchapter 2. see **Figure 32A/B**, **Figure 33A/B** and **Figure 34A/D**), showed major increase in flexibility. Notably, when comparing LmrA-NBD WT and LmrA D518A, an increased number of resonances showed severe line broadening in the mutant (Chapter III: results subchapter 2. see **Figure 28A**), further supporting the notion that the D-loop mutation

alters NBD dynamics (i.e. increase in flexibility for these NBD regions) across different timescales. As described above, D-loop and D-helix movements occur in concert with movements of the α -helical subdomain¹⁷³, hence the observed change in dynamics in the D-loop helix may alter α -helical subdomain movements. Consequently, a D/A mutation in the D-loop may induce different conformational changes within the TMD and hence lead to inactive or passive transport as observed in TAP¹⁷⁴. Differences in transmission of intradomain conformational changes upon D-loop mutation which lead to deficient substrate transport might be further supported by a study of Schultz *et al.*, where they report an increased instead of a decreased ATP hydrolysis for a D-loop aspartate mutant (D/G) in MsbA, which also led to a deficient substrate transport²¹¹. In contrast, for a D/A mutant in MsbA no ATP hydrolysis was reported²⁷⁶, in agreement with our observations for D-loop alanine substitutions. It remains to be seen whether a glycine mutation in the D-loop leads to increased flexibility and can thus explain the observed differences.

2.6.2. Role of D-loop sequence organization - ASLD/ SALD/ SSLD

The consensus sequence for the D-loop is SALD. However, when comparing the NBDs studied in this thesis, sequence differences were noted. Only MsbA (⁵⁰⁹SALD⁵¹²) adheres to the “classic” sequence, while both LmrA (⁵¹⁵ASLD⁵¹⁸) as well as BmrA (⁵⁰⁷SSLD⁵¹⁰) diverge from the consensus sequence. This prompted us to investigate what the functional consequences of a sequence exchange would entail for three ABC transporters. Herein, the mutants of full-length BmrA D-loop SSLD to SALD or ASLD showed that they could still perform substrate transport (Chapter III: results subchapter 2. see **Figure 37**). Intriguingly, basal ATP hydrolysis was increased for the ASLD mutant. However, stimulated ATPase activity through substrate addition, a common observation for ABC multidrug transporters, was abrogated in this mutant. These observations indicate that the N-terminal serine residue of the D-loop (⁵⁰⁷S-SLD) in BmrA is important for ATP hydrolysis. The fact that substrate transport was not changed by a higher ATP turnover rate in the ASLD mutant thus indicates that ATPase activity and substrate transport may not be optimally coupled in this mutant. Moreover, these observations may argue for a “capping” of ATP hydrolysis by the D-loop in BmrA WT (SSLD). Increased ATP hydrolysis has been described for the D-loop aspartate mutant within TM287/288 and has been assumed to be caused by loss of intradomain interactions between the C-loop (ABC signature motif) and the D-loop aspartate⁹⁰. Whether something similar is also the case within BmrA ASLD will require further investigation. Interestingly, another study for MsbA²⁶² with its consensus SALD D-loop sequence also described very diverse effects on ATP hydrolysis by mutating the different D-loop residues. An S to C mutation (⁵⁰⁹C-ALD) resulted in similar ATPase activity as the WT²⁶². When mutating A to C (S-⁵¹⁰C-LD) the protein was not expressed whereas mutation of the terminal L and D to C (SA-⁵¹¹CD and SALC⁵¹²) lead to 4% and 10% of ATP hydrolysis, respectively. Together, all results indicate that the amino acids of the D-loop can fulfill very different functions within the NBD, which are important for regulation of ATP hydrolysis, but the structural details remain to be elucidated.

The differences in ATPase activity observed in this thesis for the full-length D-loop variants of BmrA (BmrA SSLD (WT), BmrA ASLD and BmrA SALD, Chapter III: results subchapter 2. see **Figure 37**) appear to correlate with the different peak positions for the H-loop residue in the NMR experiments of the D-loop variants of LmrA-NBD, i.e. LmrA-NBD ASLD (WT), LmrA SSLD and LmrA SALD (Chapter III: results subchapter 2. see **Figure 30** and **Figure 37**). Here, the NH resonances of the H-loop histidine residue were found to shift relative to the WT protein in the HSQC spectra of LmrA-NBD SALD and LmrA-NBD SSLD (Chapter III: results subchapter 2. see **Figure 30** and **Figure 37**). In either case the H-loop resonance shifted to a similar position indicating that both D-loop mutations have a similar effect on the chemical environment of the H-loop. In full-length BmrA, the variants with the two corresponding D-loop sequences (SALD and SSLD (WT)) were both ATPase- and substrate transport-

active. In contrast, the ASLD variant in full-length BmrA showed normal substrate transport but increased basal ATPase activity that could not be stimulated further with the tested substrates (Chapter III: results subchapter 2. see **Figure 37**).

Finally, the D-loop aspartate mutation in LmrA-NBD led to a third peak position of the NH resonance for the H-loop histidine residue, which showed neither ATPase activity nor transport activity in full-length BmrA. (Chapter III: results subchapter 2. see **Figure 37**). Additionally, as described above backbone amide dynamics for the H-loop mutant in LmrA-NBD (H543A) illustrate that the H-loop has different influence on dynamics on the N-terminal part of the D-loop ($^{515}\text{AS}^{516}$ -LD in LmrA-NBD, less effected in the hetNOE data) than on the aspartate residue of the D-loop (ASLD⁵¹⁸ in LmrA-NBD, more pronounced effect in hetNOE data, chapter III: results subchapter 2. see **Figure 32A/D**, **Figure 33A/D** and **Figure 34C/D**). This observation may be another reason for the differences in ATPase activity and substrate transport among the D-loop variants (D518A, SALD, SSLD and ASLD; chapter III: results subchapter 2. see **Figure 37**). It indicates again that fine-tuned intradomain crosstalk between D-loop and H-loop is essential for the catalytic mechanism in ABC transporters.

Overall, we found that conformations and dynamics of all amino acids of the D-loop are crucial for ATP hydrolysis and substrate transport (aspartate residue). The NBD intradomain effects of the D-loop reported in this thesis extend previous experimental observations which showed that overall flexibility of the D-loop is important for NBD-NBD interaction, with the D-loop of one NBD, for example, described to interact with the Walker A motif and the H-loop of the opposite NBD⁹⁰.

3. “COMMUNICATION HINGES” BETWEEN THE NBS AND THE TMD OF MULTIDRUG ABC TRANSPORTERS

The solution NMR studies²⁷⁵ (i.e. ¹H-¹⁵N HSQC, chapter III: results subchapter 3. see **Figure 39**, **Appendix 32** and ¹⁹F spectra, chapter III: results subchapter 3. see **Figure 40**) within this work identified an until now uncharacterized allosterically affected region at the C-terminal end of the Walker A helix consisting of residues RFY and W or L (**Figure 50**). These residues appear to be highly conserved within type I ABC exporters (Chapter III: results subchapter 3. see **Figure 38**), which may support a role of these residues in signal propagation, e.g. from nucleotide binding, throughout the NBD. These residues may play an essential role in coupling of ATP binding and/ or hydrolysis to substrate transport. Furthermore, it was evaluated in this thesis that mutations in this region impact protein stability of type I ABC exporters (type IV fold).

3.1. A potential NBS-TMD signaling pathway Part I – signal propagation via a conserved arginine residue

Our NMR studies in chapter III: results subchapter 1. provide insights into the nucleotide-dependent dynamics of an allosterically affected region (residues RFY – W or L, **Figure 50**) within the NBD (Chapter III: results subchapter 1. see **Figure 18**, **Figure 19** and **Figure 20**). Upon nucleotide addition, the H/D exchange for this region is suppressed (Chapter III: results subchapter 1. see **Figure 18**), indicating protein rigidification or compaction. However, the backbone dynamics on the ps – ns timescale paint a more complex picture. While residues R397 and W421 in LmrA-NBD became more mobile with the addition of nucleotide, residue L395 in the vicinity of the arginine residue was rigidified (Chapter III: results subchapter 1. see **Figure 19** and **Figure 20**). In the Walker A helix (α 1 in LmrA-NBD) residue L395 is one out of two residues (i.e. I391 and L395) for which NH resonances in both the apo and nucleotide-bound states could be detected. The resonances for the other residues of the Walker A helix (³⁸⁸KST³⁹⁰ and ³⁹²FSL³⁹⁴) appear only when adding ADP. As pointed out in chapter III: results subchapter 1., the appearance of peaks by nucleotide addition is indicative for quenching of dynamics. The observed rigidification of the Walker A helix (α 1) in the ps – ns timescale could play a role for the observed mobility of the arginine residue R397 in α 1 as well as tryptophane residue W421 within α 3, which is opposite of the C-terminal end of the Walker A helix (**Figure 50**). Residues of this helix exhibit an increase in flexibility upon nucleotide addition in the ps – ns timescale but seems to undergo stabilization at slower timescales accessed by H/D exchange experiments and inferred from line broadening. These complex changes in dynamics may be the basis of communicating nucleotide binding from the NBS to the TMD since the allosterically affected region contacts the coupling helix of the TMDs (**Figure 50**). In addition, the short α -helix 3 (based on LmrA-NBD, **Figure 50**), containing the conserved tryptophane residue, is located N-terminal to the Q-loop motif, which is known to be involved in interdomain signal communication between NBD and TMD^{158,161}. Thus, an interaction of the Q-loop with the tryptophane residue of α -helix 3 would be conceivable. However, none of the NMR experiments conducted in this thesis for the Q-, D- or H-loop motif (Chapter III: results subchapter 2. see **Figure 28**) revealed a link to any residue of our identified allosterically affected region (R-W/L region), suggesting that this is an NBD intradomain signaling pathway independent of these conserved motifs. Strikingly, members of the ABCC subfamily as CFTR and MRP1 have a conserved “deletion” of amino acid residues within the NBD1 at the position equivalent to α -helix 3 in LmrA-NBD^{311,352} (Chapter III: results subchapter 3. see **Figure 38**). Insertion of a helix at this position in NBD1 of MRP1 reduced substrate transport to around 30%³⁸⁵. Previous studies have shown that proteins of the ABCC family have non-equivalent NBDs during the catalytic cycle^{52,385–387} and it seems likely that the missing α -helix as well as the lacking catalytic glutamine is relevant for this³⁸⁴. Hence, fine-tuned structure and dynamics in the motor domain (i.e. NBD) of the

protein instability or incorrect folding. The fact that a tryptophane to tyrosine mutant³¹⁸ (■■■■ laboratory) showed residual substrate transport and ATPase activity is maintained points to reliability of the data within the IOVs.

Interestingly, when the conserved arginine and tryptophane residues in BmrA-NBD were mutated, the mutants could not be purified due to extensive protein aggregation. In contrast, the same mutations within the LmrA-NBD could be purified. The differences in the stability of the mutants in two closely related and functionally homologous ABC transporter NBDs suggest that there are subtle differences in the interaction network stabilizing the NBDs. Interestingly, in the context of the full-length transporter, the same mutations were much more stable and correctly folded protein (as judged by their SEC elution profiles) could be obtained. This may be due to enhanced stabilization of the NBD through the TMDs, e.g. the interaction of the coupling helices with the coupling helix groove. Nonetheless, mutating the arginine residue at the C-terminal end of the Walker A helix in full-length BmrA was found to disrupt substrate transport for all tested mutants (Chapter III: results subchapter 3. see **Figure 43D**). ATPase activity, on the other hand, showed different results depending on the amino acid inserted at the position of the arginine. Mutation of the arginine residue to alanine or glutamate yield to no ATP hydrolysis in full-length BmrA, whereas insertion of lysine or methionine partially maintained ATP hydrolysis (Chapter III: results subchapter 3. see **Figure 43B**). This suggests that the chemical nature of residues present at this position is important for a proper functioning of ATP hydrolysis. Considering the influence of arginine mutation on substrate transport and ATP hydrolysis, the arginine residue seems to be crucial for substrate transport and plays an important yet secondary role for ATP hydrolysis. Potentially the connection between NBS and TMDs is disrupted when mutating the arginine. This hypothesis is further supported by the observation that substrate stimulation vanished within our R389A mutant of BmrA (Chapter III: results subchapter 3. see **Figure 43B**).

In a complementary approach, the effect of mutating the conserved tryptophane residue opposing the arginine residue, on substrate transport and ATP hydrolysis of full-length BmrA was studied by our collaborators in the ■■■■ laboratory in Lyon³¹⁸. Transport activity of BmrA was differently affected by mutations of the tryptophane residue to alanine, leucine, phenylalanine or tyrosine. W413A resulted in no substrate transport, while W413L and W413F reduced substrate transport to almost the control levels. Substrate transport was also reduced when the tryptophane residue was mutated to tyrosine but not as pronounced as in the other two mutants (W413L and W413F). An interesting observation in this analysis was also that substrate transport differed among the mutations depending on which substrate was used. Examination of the effects of the tryptophane mutations on ATP hydrolysis also revealed very interesting differences³¹⁸ (■■■■ laboratory). W413A again showed no ATP hydrolysis, whereas W413L, W413F and W413Y showed diminished ATP hydrolysis rates with varying degrees. W413Y retained ATP hydrolysis best, presumably in agreement with the transport assay where it showed residual activity. As described above, the tryptophane residue belonging to an α -helix (α -helix 3 in LmrA-NBD, **Figure 50**) might be able to detect changes within the TMD. In this context, it seems conceivable that tryptophane mutants may react differently in substrate transport depending on which type of substrate binds at which site in the TMDs. On the other hand, the arginine variants in this thesis were not able to discriminate between the substrates used in the substrate transport assay (i.e. no difference in substrate transport activity). This seems reasonable regarding its position at the end of the Walker A helix, which has no direct contact with the TMDs. Nevertheless, more results to emphasize the importance of this interaction region are needed, as performing ATPase activity assays in a lipid environment with more diverse substrates in background of the full-length BmrA variants (i.e. Arg to Glu, Arg to Lys, Arg to Met, Trp to Ala, Trp to Tyr, Trp to Phe and Trp to Leu). Furthermore, NMR experiments with the full-length ¹⁹F-Trp labeled BmrA offer the possibility of visualizing effects of the tryptophane residue by the addition of nucleotide or substrate. By

performing H/D exchange of BmrA with and without substrate or nucleotide, the collaboration partners of the █████ laboratory were able to further substantiate our findings of the novel “hinge” region between NBDs and TMDs. When aligning sequences of type I ABC exporters (type IV fold, Chapter III: results subchapter 3. see **Figure 38**), a leucine residue, for example in MsbA, was also often observed at the position of the tryptophane residue. If the leucine residue fulfills similar tasks in that region would also need further investigations, even if first data of BmrA indicate that no functional exchange is possible (█████ laboratory). Ultimately, substrate transport and ATP hydrolysis were perturbed by mutating the arginine or the tryptophane residue, leading to the hypothesis that an interrupted connection between ATP binding and/ or hydrolysis (NBS) and the TMDs (substrate binding site) occurs. Consequently, it can be proposed that the identified allosterically affected region is one important interaction site for a correct NBS-TMD and/ or TMD-NBS crosstalk.

3.2. A potential NBS-TMD signaling pathway Part II – signal propagation via a conserved tyrosine residue

Interestingly, one of the first crystal structures of an ABC transporter, the type I ABC exporter (type IV fold) Sav1866 described a conserved tyrosine residue (Y391) at the C-terminal end of the Walker A helix, which seemed to interact with the TMD³⁴. During this thesis, this conserved tyrosine residue (Y399 in LmrA-NBD, **Figure 50**) came into focus because it exhibited nucleotide-induced changes in its chemical shift (Chapter III: results subchapter 1. see **Figure 17**). In line with the structural information available from Sav1866³⁴, it is possible that this conserved tyrosine residue constitutes a potential communication point to transfer conformational changes, e.g. induced by nucleotide binding, from the NBD to the TMD. Thus, in addition to the presumed nucleotide communication “hinge” between the arginine and tryptophane residues and potential subsequent transmission from α -helix 3 to the coupling helices of the TMDs discussed above, there may be a second interdomain pathway. Looking at the sequences and structures of other type I ABC exporters (type IV fold), such as human P-glycoprotein^{186,201}, *Bacillus subtilis* BmrA⁹³, *Salmonella typhimurium* MsbA, human ABCB10¹⁸³ and *Thermus thermophilus* TmrAB⁸⁹, showed that there is always a tyrosine residue at the same position that can contact the TMDs (**Figure 51**). Specifically, the conserved tyrosine residue in the NBD connects to an arginine/lysine residue (in one coupling helix of the TMDs) and an aspartate residue (in the second coupling helix of the TMDs) thus creating a tight connection across the NBD-TMD interface. Interestingly, the heterodimeric ABC transporter TmrAB has the conserved tyrosine only in the NBD of TmrA (⁴⁰⁸RFY⁴¹⁰). In TmrB, the position of the tyrosine residue is replaced by a leucine (³⁸⁶RLL³⁸⁸). Whether these findings lead to differences in interdomain communication would require further investigation.

In summary, there are two conceivable communication pathways from the NBS to the TMD upon binding of a nucleotide. The signal that a nucleotide has bound is mediated to the C-terminus of the Walker A helix and then transferred either (i) from Arg to Trp (in the α -helix 3 in LmrA and Sav1866, **Figure 50**) to the coupling helices (coupling helix 2 from the other homodimer might be favored since α -helix 3 is nearby, **Figure 50**) or (ii) from Arg over Phe to a Tyr and subsequently to the coupling helices. For the pathway from tyrosine to the coupling helices, coupling helix 1 might be favored since the loop of the conserved tyrosine residue is somewhat closer to it (**Figure 50** and **Figure 51**).

Intriguingly, the identified tyrosine residue is in proximity of the tyrosine residue of the A-loop³⁴ (**Figure 50**). Thus, the allosterically affected tyrosine residue potentially senses conformational changes of the A-loop, which is known to interact with the adenine ring of the nucleotide¹⁵⁷ and vice versa.

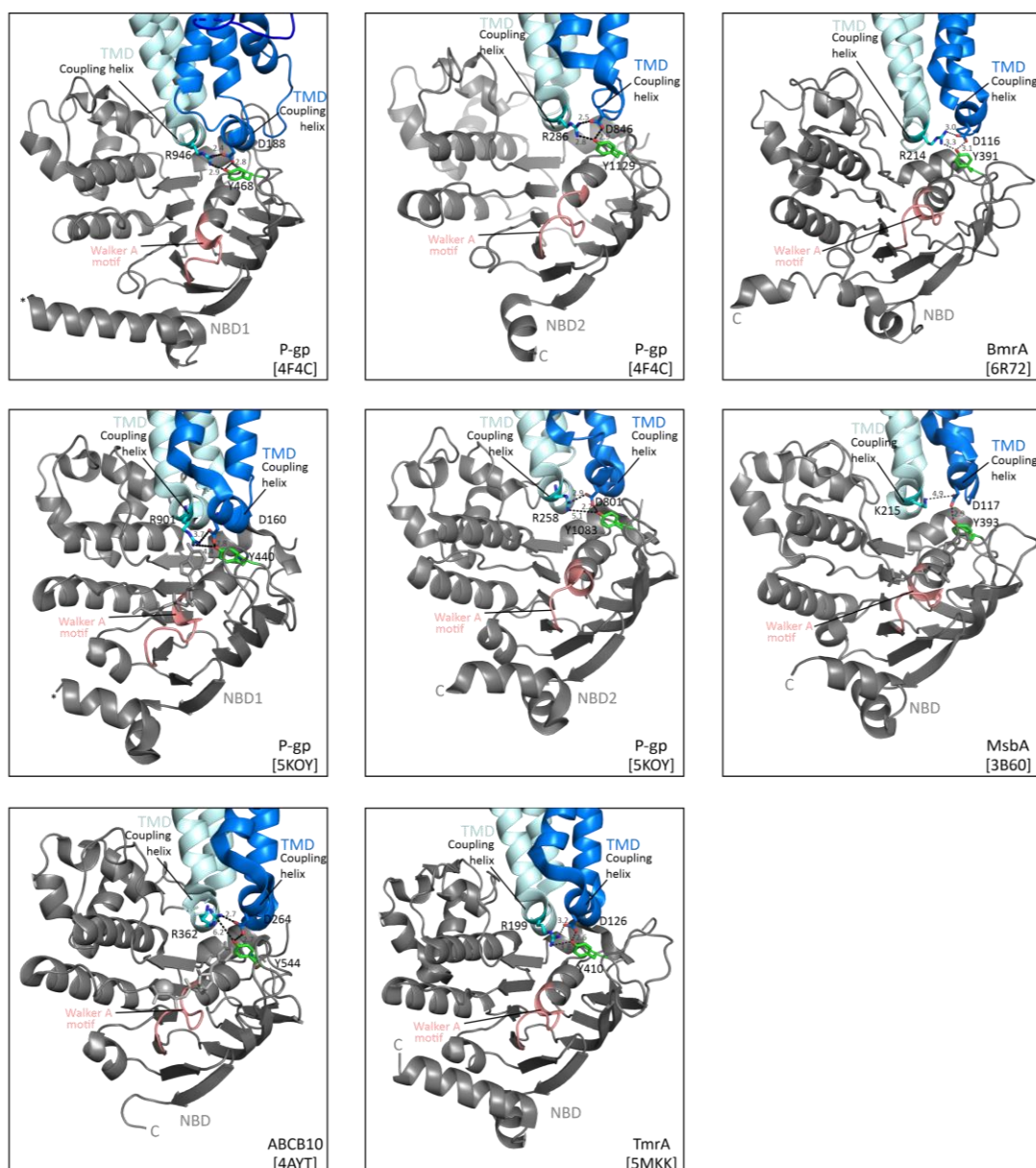


Figure 51: Polar interactions of a tyrosine at the C-terminus of the Walker A helix may mediate allosteric crosstalk within type I ABC exporter (type IV fold)

Contacts between residues of the P-glycoprotein (P-gp, *Mus musculus*, PDB ID: 5KOY²⁰¹, *C. elegans* PDB ID: 4F4C¹⁸⁶), BmrA (*B. subtilis*, PDB ID: 6R72⁹³), MsbA (*S. typhimurium*, PDB ID: 3B60¹³⁵), ABCB10 (*Homo sapiens*, PDB ID: 4AYT¹⁸³) and TmrA (*T. thermophilus*, PDB ID: 5MKK⁸⁹) TMD-NBD coupling helices. In all proteins, a tyrosine residue (green) in the NBDs is seen to interact with an aspartate and/or an arginine residue of each coupling helix from the TMDs. Asterisks mark unresolved parts in the protein structure. Distances (in Angstrom) were measured between the nitrogen's of the arginine residue and the oxygens of the aspartate or the tyrosine residue. Furthermore, distances between the oxygen of the aspartate and the oxygen of the tyrosine were measured. In MsbA distances were measured between the nitrogen of the lysine residue and the oxygen of the aspartate residue and between the oxygen of the tyrosine and the oxygen of the aspartate residue.

3.3. Interdomain crosstalk in other ABC transporter classes

Looking at seven structures of the seven currently available ABC transporter architectures reveals that an α -helix is frequently located at the opposing site of the C-terminal end of the Walker A helix (**Figure 52**). This α -helix appears to be crucial to transmit nucleotide-induced conformational changes from the NBS to the TMDs, as it is in vicinity to the coupling helices. As in type I ABC exporters (type

IV fold), the available structures of the type II exporters (type V fold) ABCG5/8⁷⁷ and ABCG2^{367,388} feature an arginine residue at the end of the Walker A helix (**Figure 52A/B**, R121 in ABCG8). This arginine residue may transmit conformational changes to the coupling helix of the TMD via an opposite α -helix (**Figure 52B**). Nevertheless, the arginine residue (R121 in ABCG8) could even form contacts to the coupling helix directly since the arginine residue is vicinal in the structure of ABCG5/8.

Inspection of the protein structures of type I (MalFGK₂), type II (BtuC₂D₂) and type III (ECFSA⁺) ABC importers revealed that a leucine residue is present at the C-terminus of the Walker A helix for type I and type III importers (**Figure 52C/D/E**). In those transporters, an arginine residue was found in the opposing α -helices (**Figure 52C/D/E**). However, it seems that only the arginine residue R75 of MalFGK₂ can make contacts to residues at the C-terminus of the Walker A helix (**Figure 52C**). In ECFSA⁺ another arginine residue (R80) points in the direction of the coupling helices and hence may make contacts to the TMD (**Figure 52E**).

A charged and a bulky amino acid are also found in the C-terminal tip of the Walker A helix and the opposing α -helix within the extractor/mechanotransducer LptB₂FG and MacB. As seen for other ABC transporter architectures, these residues may make contacts with residues of the coupling helix (L52 and R77 in LptB₂FG **Figure 52F**; L56 and R83 in MacB **Figure 52G**) of the TMD or may form connections between the C-terminal end of the Walker A helix and an α -helix at the opposing side (R75 in LptB₂FG **Figure 52F**; L82 in MacB **Figure 52G**).

Overall, conserved arginine and leucine residues in the identified region (C-terminal end of the Walker A helix and the opposing α -helix) seem to be important in forming contacts between the NBS and the TMD. It seems that depending on the precise position of arginine or leucine residues they could potentially form i) contacts to the TMDs via the coupling helices or ii) contacts between the C-terminal end of the Walker A helix and the opposing α -helix. Interestingly, type I ABC exporters (type IV fold) seem to be an exception. Here, the interaction of two coupling helices with one NBD is unique (**Figure 52A**), thus the residues of interest (RFY and W or L) presumably interact differently with the TMDs compared to other ABC transporter structure types (**Figure 50** and **Figure 52A**). Importantly, the identified conserved residues triad RFY within type I ABC exporters (type IV fold) seem to occur only in this ABC transporter architecture. The fact that in type I ABC exporters two coupling helices from each TMD dock into one NBD might be an explanation for different passages of signal transduction from the NBD to the TMD compared to the other ABC transporter architectures.

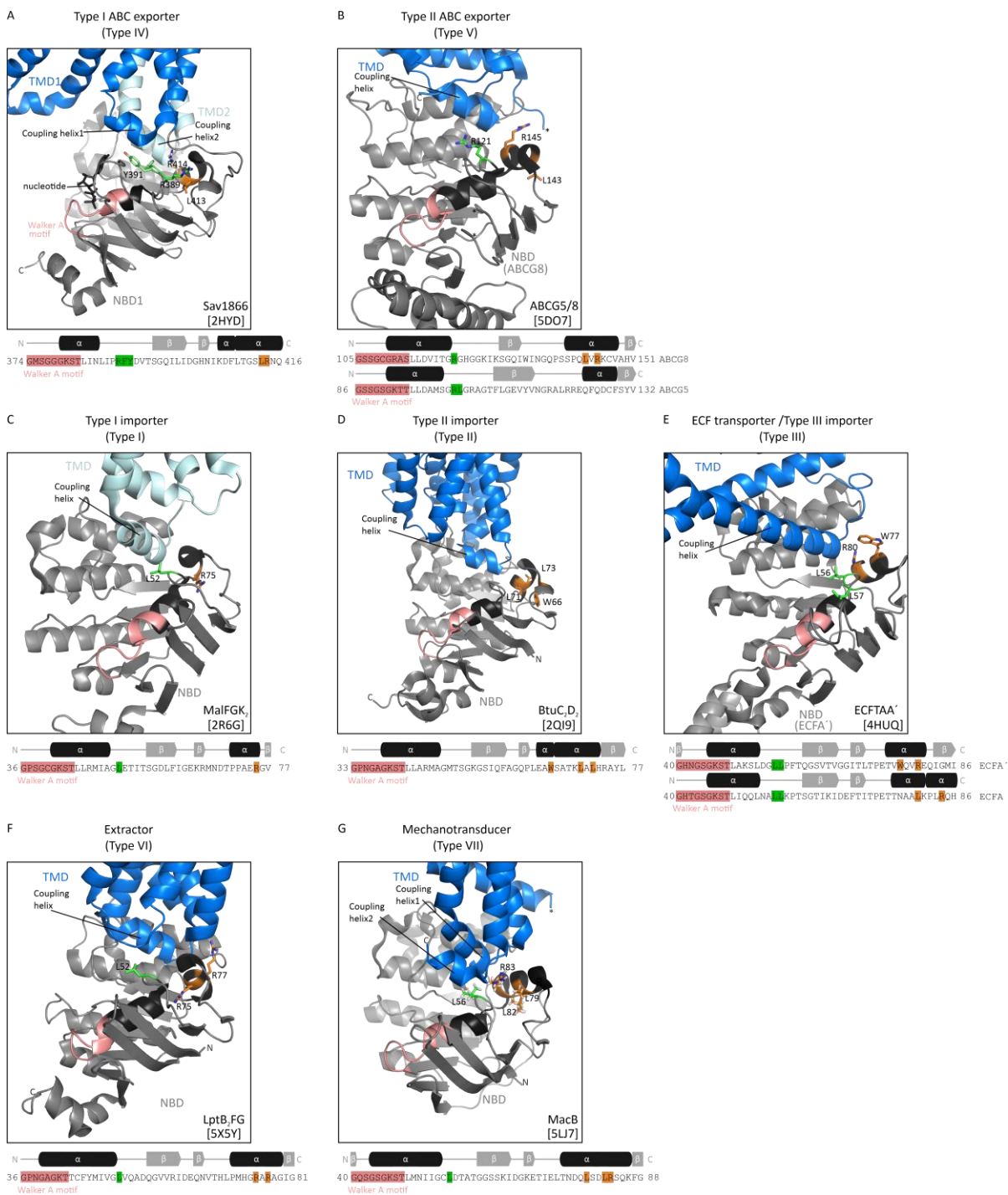


Figure 52: Potential connection between the C-terminal end of the Walker A helix and the opposing α -helix with the TMD across different ABC transporter architectures

A) Type I ABC exporter (type IV fold) Sav1866 (PDB ID: 2HYD³⁴) **B)** Type II ABC exporter (type V) ABCG5/8 (PDB ID: 5D07⁷⁷) **C)** Type I ABC importer (type I) MalFGK₂ (PDB ID: 2R6G⁷⁴) **D)** Type II ABC importer (type II) BtuC₂D₂ (PDB ID: 2QI9⁷⁵) **E)** Type III ABC importer (type III) ECFTAA' (PDB ID: 4HUQ⁷⁶) **F)** ABC extractor (type VI) LptB₂FG (PDB ID: 5X5Y⁷⁸) **G)** ABC mechanotransducer (type VII) MacB (PDB ID: 5LJ7⁷⁹) Sequence and topology for the NBD region from the Walker A motif to the α -helix potentially interacting with the end of the C-terminal end of Walker A helix are shown under the boxes in A, B, C, D, E and F. Arginine/leucine residues on the C-terminal end of the Walker A helix ($\alpha 1$ in the NBDs, black) are highlighted in green. Arginine, tryptophane or leucine residues in the opposing α -helix ($\alpha 2$ or $\alpha 3$ in the NBDs, black) are highlighted in orange. The secondary structure is displayed on top of the sequences in A, B, C, D, E, F and G. Asterisks mark not resolved parts in the protein structure.

OUTLOOK

In this thesis the main focus are structure and dynamics of the highly conserved NBD of ABC transporters. The assignments of LmrA-NBD in different catalytic states and of LmrA-NBD mutants in conserved motifs (D-, Q- and H-loop) helped to investigate in detail intradomain effects on specific amino acid residues²⁷⁹ (chapter III: results subchapter 1. and 2.). Now that assignments for BmrA-NBD²⁹⁸ (chapter III: results subchapter 1.) and MsbA-NBD (ongoing) are also available, the effects found in the NMR experiments for LmrA-NBD due to nucleotide binding or mutation of a conserved motif can be compared with these two homologous NBDs in the future. In the ¹⁵N HSQC NMR data, numerous resonances of amino acids residues showed line broadening in the apo state and sharpening after addition of nucleotide (Chapter III: results subchapter 1. see **Figure 16**). Resonances of residues also showed line broadening when a mutation in one of the conserved motifs, D-, Q- or H-loop, was performed (Chapter III: results subchapter 2.). Additional NMR relaxation dispersion experiments could be performed that would provide more information on the chemical shift exchanging states, which could be used for further structural interpretations^{306,389,390}. In addition to the intradomain NBD results obtained for the very fast dynamics (ps - ns timescale) with NMR using {¹H}, ¹⁵N hetNOE (Chapter III: results subchapter 1. see **Figure 19**, **Figure 20**, **Figure 32**, **Figure 33** and **Figure 34**), NMR experiments can be performed to determine relaxation times (T_1 and T_2). With these NMR experiments, local correlation times of backbone amide NH bond vectors can be determined, providing further insight into local dynamics in the NBD^{306,391}. Moreover, the ¹⁵N HSQC NMR data of LmrA-NBD showed that remote residues from the NBS, such as the C-terminus, can sense and distinguish nucleotide binding (Chapter III: results subchapter 1. see **Figure 16** and **Figure 17**). These results lead to the assumption that the C-terminal region may have important implications for the role of the NBD in the catalytic cycle of the ABC transporter, beyond simply mediating ATP hydrolysis. A link between the C-terminal region and substrate translocation within ABC exporters has been reported, which may support a key role of the C-terminal region within the transport mechanism^{89,349}. Thus, the question arises as to what happens to the C-terminal region of the NBDs when a substrate or inhibitor is bound to the TMDs. It could make a difference whether a substrate or an inhibitor is bound, as different binding modes for a substrate and inhibitors have been identified within P-gp^{315,322}. It would also be interesting to investigate whether the coupling helix groove is affected by modulation of the C-terminal region. In addition to ¹⁵N HSQC NMR experiments on mutants of amino acid residues in the C-terminal region of the NBD, photosensitive unnatural amino acids could also be introduced into the C-terminal region to perform excitation of the C-terminal region and analyze its consequences³⁹².

To investigate whether the obtained global dynamics in the NBD of ABC type I exporter between the α -helical and the RecA-like subdomains (Chapter III: results subchapter 1. see **Figure 22**) are similar in the full-length ABC protein, the identified PET reporter pair (Chapter III: results subchapter 1. see **Figure 21**) was also introduced in full-length MsbA. It would be very interesting to see if PET-FCS measurements of full-length MsbA in detergent or in a native like environment, i.e. lipid mimetics, yield similar timescales as MsbA-NBD. Furthermore, it would be of interest to analyze dynamic consequences on the α -helical and the RecA-like subdomain and their relaxation time constants in MsbA-NBD and/ or full-length MsbA if a conserved motif is mutated, such as the lysine residue from the Walker A motif, which is known to be important for ATP hydrolysis and substrate transport^{137,193-197}.

To gain more information about the function of the conserved D-loop motif and its role in the structural dynamics of the NBD, ATP hydrolysis and substrate transport experiments with LmrA from *L. lactis*, BmrA from *B. subtilis* and MsbA from *E. coli* were performed (Chapter III: results subchapter **2.4**. Molecular crosstalk of the NBD depends on the D-loop motif). For further D-loop analyses, variants (ASLD and SSLD) of the consensus sequence (SALD) were also generated within the MsbA-NBD and full-length MsbA, the influence of which on ATP hydrolysis would still need to be investigated. Furthermore, would it be interesting to record ^1H - ^{15}N HSQC spectra of the MsbA-NBD D-loop variants and the BmrA-NBD D-loop variants, which could provide information on whether the peak shifts will show similar effects to those in LmrA-NBD (Chapter III: results subchapter **2.4**. see **Figure 37**). Future studies may also address the ATP hydrolysis and substrate transport of the mutants within the conserved motifs, H-loop and Q-loop, in full-length MsbA and/ or BmrA to complement these data.

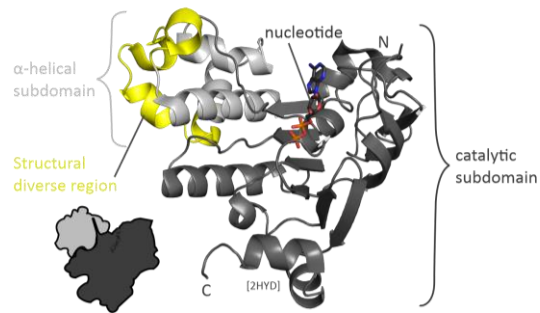
In this thesis, the solution NMR studies (Chapter III: results subchapter **3**. see **Figure 39**, **Figure 40**, **Appendix 32** and **Appendix 35**) further^{275,279} revealed a novel “communication hinge” linking the Walker A motif to the coupling helix groove, and thus to the TMD, via two highly conserved residues (i.e. R397 and W421 in LmrA-NBD) in the NBD. These two residues are conserved in type I ABC exporters (type IV fold, **Figure 38**) including BmrA and MsbA although in the latter case the tryptophane residue is replaced by a bulky leucine residue. To investigate the effect of nucleotide binding on the conserved tryptophane, solution ^{19}F W NMR experiments were performed on the NBDs. Interestingly, it was possible to obtain also ^{19}F W spectra of ^{19}F -Trp labeled full-length BmrA in detergent, which showed broad lines in the same frequency range as within ^{19}F -Trp labeled BmrA-NBD (Chapter III: results subchapter **3**. see **Figure 40**). For further analysis a resonance assignment would be needed as full-length BmrA contains three tryptophane residues. Nevertheless, this observation opens the door for further investigation of the novel communication hinge region. To support the idea of a communication hinge of R and W residues, a full-length BmrA R/X (X = K or M) mutant labeled with ^{19}F W could be generated and measured with substrate to see whether the tryptophane is affected or not. To gain insight into the identified region and its effects in a native environment, it would also be interesting to record full-length ^{19}F W NMR spectra of BmrA in membrane mimetics, such as nanodiscs and SMALPs (styrene maleic acid lipid particles). Mutagenesis studies in the transporter NBDs and functional assays on full-length BmrA support the notion that the identified residues are important for ATPase activity, substrate transport and protein stability (Chapter III: results subchapter **3**. see **Figure 41**, **Figure 42** and **Figure 43**). To further verify the role of the conserved arginine, further stimulated ATPase activities and substrate transport assays of the R/X (X = A, M, K, and E) mutants would need to be performed.

APPENDIX

1. CHAPTER I: INTRODUCTION

| | | |
|---|---|------|
| LmrA_L.lactis | -----MERGPQ-----MANRIEGKAVDKTSIKHF | 24 |
| BmrA_B.subtilis | -----MPTKKQKSKSLKPF | 15 |
| MsbA_E.coli | -----MHNDKDLST | 9 |
| P-gp_human1 | -----MDLEGDRNGGAKKKN-----FFKLNNKSEKDKKPKTQVSV | 36 |
| P-gp_human2 | AADESKSEIDALEMSSNDRSSLRKRSTRRSVVRGSAQDRKLS--TKEALDESI PPVVF | 697 |
| . | | |
| LmrA_L.lactis | VKLIRA-AKPRVLFVIGIV---AGIIGTLIQLQVPMVQPLI----- | 63 |
| BmrA_B.subtilis | FALVRR-TNPSYGLAFALA---LSVVTTLVSLLIPLLTQQLV----- | 54 |
| MsbA_E.coli | WQTFRR-LWPTIAPFKAGLIVAGVALILNAASDTFMLSLLK----- | 50 |
| P-gp_human1 | FSMFRYSNWLDKLYMVVGTL---AAIIGHAGLPLMLVFGEQMDIFANAGNLEDLMSNI | 92 |
| P-gp_human2 | WRIMK-LNLTEWPFYVGVF---CAIINGGLQPAFAIIFSKIIGVFTRIIDDPETKRON- | 751 |
| .: : : | | |
| LmrA_L.lactis | -----NSFGHGV-NGGKVALVIALYIGSAVAIAA---IVLGIFGESVVKNLTR | 110 |
| BmrA_B.subtilis | -----DGFMSNLSGTQIGLIALVFFVQAGLSAYAT---YALNYNGQKII SGLREL | 102 |
| MsbA_E.coli | -----LLDDGFGKTD---RSVLVWMPLVVIGLMLRGTISYVSSYCSISWVGKVVMTMRRR | 103 |
| P-gp_human1 | TNRSDINDTGFFMNL---EEDMTRYAYYYSGIGAGVLAAYIQVSWFLCAGRQIHKIRKQ | 150 |
| P-gp_human2 | -----S-----NLSLLFLALGIIISFITFFLQGFTEFGKAGEILT KRLRYM | 791 |
| : : * | | |
| LmrA_L.lactis | VWDKMIHLPVKYFDEV--KTGEMSSRLANDTTQVKNLIANSIQAFTSILLVGSII FML | 168 |
| BmrA_B.subtilis | LWKLIKLPVSYFDTN--ASGETVSRVNTDMVKELITTHISGFITGII SVIGSLTILF | 160 |
| MsbA_E.coli | LFGHMMGMPVSVFFDKQ--STGTLRSRTYDSEQVASSSSGALITVVRREGASII GLFIMMF | 161 |
| P-gp_human1 | FPHAIMRQEIWFVDVH--DVGELNTRLTDVDSKINEGIGDKI GMFQSMATFTTFGVVGF | 208 |
| P-gp_human2 | VFRSMLRQDVSWFDDPKNTTGALTTRLANDAQAQVKGAI GSRVAITQNIANLGTGII ISF | 851 |
| .: : : : * * * : * : * : : : : | | |
| LmrA_L.lactis | QMQRWLTAMI IAVPIVMLIMFPIMTFGQKIGWTRQDSLAFQGIASELSEIRLVKSSN | 228 |
| BmrA_B.subtilis | INNWKLTLLVLVVPLAALIIVPIGRKMFISRETDQETARFTGLNQLPEIRLVKASN | 220 |
| MsbA_E.coli | YYSQWLSIILIVLAPVSI IARVVSXRFNISKMNQMTQMGGVTSAEQMLKHKEVLIFG | 221 |
| P-gp_human1 | TRGWKLTLLVLAISPVLGLSAAVNAKILSSFTDKELAYAKAGAAVEVLAIRTVIAFG | 268 |
| P-gp_human2 | IYGWQLTLLLLAIVPIIATAGVEMKMLSGQALKDKKELEGSGKIATEAIENFRTVVSLT | 911 |
| * : * : * : * : : : * | | |
| LmrA_L.lactis | AEQASKKAENDVNALYKIGVKEAVFDGLMSPVMMLS-----MMLMIFGLLAYGIYLIST | 283 |
| BmrA_B.subtilis | AEDVYGRGKMGISSLFKLGVREAKVQSLVGLISLV-----LMAALVAVIYGGMQVSS | 275 |
| MsbA_E.coli | GQEVTKRFDKVSNRMLQGMKMSASSISDPIIQLIASLALAVLYAASF-----SVM | 276 |
| P-gp_human1 | GQKELERYNKMLEAKRIGIKKAITANISIGA-----AFLLIYASYALAFWYGTFLVLS | 323 |
| P-gp_human2 | QEQKFEMYAQSLQVPYRNLSRKAHIFGITFSF-----TQAMMYFSYAGCFRFGAVLVAH | 966 |
| .: : : : : : : | | |
| LmrA_L.lactis | GVMSLGTLLGMMYLMNLIGVPTVATFFTELAKASGSTGRLELLEDEQEVLH---QGD | 340 |
| BmrA_B.subtilis | GELTAGALVAFILYLFQIIMPQGQITFFFTLQKSI GATERMIEILAEEDDTV---TGK | 332 |
| MsbA_E.coli | DSLTAGTITVVFSSMALMRPLKSLTNVNAQFQRGMAACQTLFTILDSEQKDE---GKR | 333 |
| P-gp_human1 | GEYSIGQVLTVFVSLVIGAFVQVQAQSPSIEAFANARGAAYEIFKIIDNKPSISYSGKSH | 383 |
| P-gp_human2 | KLMSFEDVLLVFSAVVFGAMAVGQVSSFPADYAKAKISAAHII MIIEKTPILDSYSTEGL | 1026 |
| : : : : : : : | | |
| LmrA_L.lactis | SLDLEGKTL SAHHDVFAID--DSEQLHDISFEAQPNSSII IAFAGPSGGGKSTIFSLLERF | 398 |
| BmrA_B.subtilis | QENAHLPQLDRVDFGK--PDQLLKEVSAVIEAGKVTVAIVGPGSGGKSTLFKLLERF | 390 |
| MsbA_E.coli | VIERATGDVEFRNVFTFVGR-DVPALRNINLKI PAKGTVALVCRSGSGKSTIASLITRF | 392 |
| P-gp_human1 | KPDNIKGNLEFRNVHFS--FSRKEVKILKGLNKLKQVQGTVALVNSCGGKSTVQQLMQR | 443 |
| P-gp_human2 | MPNTLEGNVTFGEVVFN--PTRPDIPVQLGLSLEVKGQTLALVSSCGGKSTVQQLLERF | 1086 |
| .: : : : * * * * * : : : * : * : * | | |
| LmrA_L.lactis | YQPTAGEITIGGQPIDSVSLNWRSQIGFVSSSAIMAGTIRENLTYGLEGN-FTDEDLW | 457 |
| BmrA_B.subtilis | YSPTAGTIRLGDPEVDYTSLESWREHIGYVSESPLMSGTIRENICYGLERD-VTDAAIE | 449 |
| MsbA_E.coli | YDIDEGEILMDGHDLDREYTLASLRNQVALVSNVHLFNDTVANNIAYARTEQ-YSREQIE | 451 |
| P-gp_human1 | YDPTEGMVSDGQDIRTINVRFLREIIGVVSSEPVLFATTIAENIRYGRENV--TMDEIE | 501 |
| P-gp_human2 | YDPLAGKVLDDGKEIKRNLVQWLRHLGIVSEEPILFDCSIAENIAYGDNRSRVVQSEIIV | 1146 |
| * . * : : : : : * : * : * : : : : : * : : : : * | | |
| LmrA_L.lactis | QVLDLAFARSFVENMPDQLNTEVGERGVKISGGGQRORIAIARAFLRNPHITLMLDEATASL | 517 |
| BmrA_B.subtilis | KAAEMAYALNFIKELPNQFDTEVGERGIMLSSGGQRORIAIARALLRNPHITLMLDEATSSL | 509 |
| MsbA_E.coli | EAARMAYALDFINKMDNGLDTEVGENGVLSGGQRORIAIARALLRDSHITLMLDEATASL | 511 |
| P-gp_human1 | KAVKEANAYDFIMKLPKFDTEVGERGACLSGGQRORIAIARALVRNPHITLMLDEATASL | 561 |
| P-gp_human2 | RAAKENIHAFIESLPNKYSFVGVGDKGTQLSSGGQRORIAIARALVRPHITLMLDEATASL | 1206 |
| : : * * * * * : : * * * * * : : * * * * * : : * * * * * : : * | | |
| LmrA_L.lactis | QSESESMVQRALDSLMKGRITLVIA--RLSTIVDADKIYFIEKGEITGSGKHNLVATHPL | 577 |
| BmrA_B.subtilis | DSQSEKSVQQALEVLMEGRITLVIA--RLSTIVDADQLLFVEKGEITGRGTHHELMASHGL | 569 |
| MsbA_E.coli | QTESERAIQAALDELQKNRTSLVIA--RLSTIEKADEIVVVDGVI VERGTHNDLLEHRGV | 571 |
| P-gp_human1 | QTESAVVQVALDKARKGRTTIVIA--RLSTVNRADVIAGFDDGVI VEKGNHDELMKKEGI | 621 |
| P-gp_human2 | QTESKVVQEAALDKAREGRTTIVIA--RLSTIQNADLIVVFQNGRVEKHEGTHQQLLAQKGI | 1266 |
| * : * * * * * : * * * * * : * * * * * : * * * * * : * * * * * : * * * * * : * | | |
| LmrA_L.lactis | YAKYVSEQLTVGQ-----590 | |
| BmrA_B.subtilis | YRDFAEQQLKMNAD-LENKAG589 | |
| MsbA_E.coli | YAQLHKMQFGQ-----582 | |
| P-gp_human1 | YFKLVMTQTAGNEVELEN---639 | |
| P-gp_human2 | YFSMVSVAQAGTKRQ-----1280 | |
| * . * * | | |

Appendix 1: Sequence alignment (www.ebi.ac.uk/Tools/msa/clustalo³¹⁰) of type I ABC exporters (type IV according to a new classification system⁸²), LmrA from *L. lactis*, BmrA from *B. subtilis*, MsbA from *E. coli* and human P-glycoprotein (P-gp/MDR1/ABC1) 1 and 2. Residues of the conserved motifs are highlighted in different colors: A-loop – red, Walker A motif – rose, Q-loop glutamine – green, X-loop – orange, ABC signature motif (C-loop) – yellow, Walker B motif – blue, D-loop – cyan and H-loop – violet. The structurally diverse region (SDR) is highlighted by a gray frame.



Appendix 2: Crystal structure of the NBD of Sav1866 (PDB ID: 2HYD³⁴), highlighting two subdomains and the structural diverse region¹⁵⁴

Appendix table 1: Structures of E-Q mutants in NBDs of ABC transporters

| ABC transporter (Organism) | Remarks | Ligand | ATP hydrolysis | Res. Å | PDB | Literature |
|---|-------------|--------------------|--------------------------|--------|------|--|
| Type I exporter (type IV fold) HylB-NBD E631Q (<i>Escherichia coli</i>) | NBD monomer | ADP | Defective ATP hydrolysis | 1.9 | 2FFB | Zaitseva <i>et al.</i> , 2006 ¹⁸⁹ X-ray |
| Type I exporter (type IV fold) HylB-NBD E631Q (<i>Escherichia coli</i>) | NBD monomer | ATP | Defective ATP hydrolysis | 2.7 | 2FGK | Zaitseva <i>et al.</i> , 2006 ¹⁸⁹ X-ray |
| MJ0796 E171Q (<i>Methanocaldococcus jannaschii</i>) | NBD dimer | MgADP | Abolished ATP hydrolysis | 2.7 | 1F3O | Yuan <i>et al.</i> , 2001 ³²⁷ ; Moody <i>et al.</i> , 2002 ³⁴⁴ X-ray |
| MJ0796 E171Q (<i>Methanocaldococcus jannaschii</i>) | NBD dimer | ATP | Abolished ATP hydrolysis | 1.9 | 1L2T | Smith <i>et al.</i> , 2002 ¹⁶⁹ ; Moody <i>et al.</i> , 2002 ³⁴⁴ X-ray |
| MJ0796 E171Q (<i>Methanocaldococcus jannaschii</i>) | NBD dimer | ADP P _i | Abolished ATP hydrolysis | 2.7 | 3TIF | Zoghbi <i>et al.</i> , 2012 ³⁹³ ; Moody <i>et al.</i> , 2002 ³⁴⁴ X-ray |

Appendix table 2: Structures of E-Q mutants in full-length ABC transporters

| ABC transporter (Organism) | Remarks | Ligand | ATP hydrolysis | Res. in Å | PDB | Literature |
|---|--|---------------------|----------------------------------|-----------|------|---|
| Type I importer (type I fold) MalFGK ₂ -MBP maltose uptake transporter MalK E159Q (<i>Escherichia coli</i>) | Outward-facing conformation, NBD closure | Maltose, ATP | Defective rate of ATP hydrolysis | 2.8 | 2R6G | Oldham <i>et al.</i> , 2007 ⁷⁴ X-ray |
| Type II importer (type II fold) BtuC ₂ D ₂ F complex E159Q (<i>Escherichia coli</i>) | BtuC in asymmetric conformation Closed translocation pore from both sites | - | Abolished ATP hydrolysis | 3.5 | 4DBL | Korkhov <i>et al.</i> , 2012a ³⁶⁵ X-ray |
| MlaFEDB E170Q (<i>Escherichia coli</i>) | NBDs and TMDs close but NBDs and TMDs closed | ATP | Reduced rate of ATP hydrolysis | 3.7 | 7CHO | Chi <i>et al.</i> , 2020 ²⁰³ Cryo-EM |
| Type I exporter (type IV fold) TmrA E523Q/B (<i>Thermus thermophilus</i>) | Outward facing open | MgATP | Reduced rate of ATP hydrolysis | 2.8 | 6RAH | Hofmann <i>et al.</i> , 2019 ²⁰² Cryo-EM |
| Type I exporter (type IV fold) TmrA E523Q/B (<i>Thermus thermophilus</i>) | Inward facing open (wide) | - | Reduced rate of ATP hydrolysis | 4.2 | 6RAN | Hofmann <i>et al.</i> , 2019 ²⁰² Cryo-EM |
| Type I exporter (type IV fold) TmrA E523Q/B (<i>Thermus thermophilus</i>) | Outward facing occluded | MgATP | Reduced rate of ATP hydrolysis | 2.9 | 6RAI | Hofmann <i>et al.</i> , 2019 ²⁰² Cryo-EM |
| Type I exporter (type IV fold) BmrA E504A (<i>Bacillus subtilis</i>) | Outward facing | MgATP | Abolished ATP hydrolysis | 3.9 | 6R81 | Chaptal <i>et al.</i> , 2022 ⁹³ ; Orelle <i>et al.</i> , 2003 ²⁸⁹ Cryo-EM |
| Type I exporter (type IV fold) BmrA E504A (<i>Bacillus subtilis</i>) | Outward facing | MgATP | Abolished ATP hydrolysis | 3.9 | 6R72 | Chaptal <i>et al.</i> , 2022 ⁹³ ; Orelle <i>et al.</i> , 2003 ²⁸⁹ X-ray |
| Type I exporter (type IV fold) BmrA E504A (<i>Bacillus subtilis</i>) | Outward facing | MgATP, Rhodamine 6G | Abolished ATP hydrolysis | 4.2 | 7BG4 | Chaptal <i>et al.</i> , 2022 ⁹³ ; Orelle <i>et al.</i> , 2003 ²⁸⁹ Cryo-EM |
| Type I exporter (type IV fold) P-glycoprotein/ ABCB1 E556Q, E1201Q (<i>Homo sapiens</i>) | Outward facing conformation | MgATP | Abolished ATP hydrolysis | 3.4 | 6C0V | Kim & Chen, 2018 ⁴⁶³ Cryo-EM |
| Type I exporter (type IV fold) P-glycoprotein/ ABCB1 E552Q, E1197Q (<i>Mus musculus</i>) | Inward facing open | - | Reduced rate of ATP hydrolysis | 3.35 | 5KPD | Esser <i>et al.</i> , 2017 ²⁰¹ ; Tomblin <i>et al.</i> , 2004 ³⁹⁴ X-ray |

| ABC transporter (Organism) | Remarks | Ligand | ATP hydrolysis | Res. in Å | PDB | Literature |
|--|---|---------------------|--------------------------------|-----------|------|---|
| Type I exporter (type IV fold) P-glycoprotein/ ABCB1 E552Q (<i>Mus musculus</i>) | Inward facing open | ATP | Reduced rate of ATP hydrolysis | 3.85 | 5KOY | Esser <i>et al.</i> , 2017 ²⁰¹ ; Tomblin <i>et al.</i> , 2004 ³⁹⁵ X-ray |
| Type I exporter (type IV fold) P-glycoprotein/ ABCB1 (<i>Homo sapiens-mus musculus</i> chimeric ABCB1) | Occluded conformation with a distinct degree of NBD opening | Zosuquidar | Not available | 3.9 | 6QEE | Alam <i>et al.</i> , 2019 ³¹² Cryo-EM |
| Type I exporter (type IV fold) MRP1/ ABCC1 E1454Q (<i>Bos taurus</i>) | Outward facing | MgATP | Abolished ATP hydrolysis | 3.1 | 6BHU | Johnson <i>et al.</i> , 2018 ²⁵³ Cryo-EM |
| Type I exporter (type IV fold) PCAT1 E648Q (<i>Clostridium thermocellum</i>) | Occluded conformation | ATPyS | Reduced rate of ATP hydrolysis | 5.5 | 4S0F | Lin <i>et al.</i> , 2015 ²⁴⁶ X-ray |
| Type I exporter (type IV fold) Atm1 E523Q (<i>Novosphingobium aromaticivorans</i>) | Occluded conformation | ATP | Reduced rate of ATP hydrolysis | 3.3 | 6PAQ | Fan <i>et al.</i> , 2020 ³⁹⁶ X-ray |
| Type I exporter (type IV fold) ABCC7/CFTR E1372Q (<i>zebrafish-Danio rerio</i>) | Inward close NBD conformation | ATP, phosphorylated | Abolished ATP hydrolysis | 3.4 | 5W81 | Zhang <i>et al.</i> , 2017 ³⁹⁷ Cryo-EM |
| Importer (type V fold) ABCA4 E1087Q (<i>Homo sapiens</i>) | Outward closed conformation | MgATP, lipids | Abolished ATP hydrolysis | 3.3 | 7LKZ | Liu <i>et al.</i> , 2021 ³⁹⁸ Cryo-EM |

Appendix table 3: Available full-length structures of the type I ABC exporters (type IV according to a new classification system⁸²) MsbA and BmrA
 OF – Outward (extracellular) facing, Inward (cytoplasmic) facing, DDM - dodecyl-D-maltoside, UDM - undecyl-D-maltoside. BP-1 - β -sheet peptides.

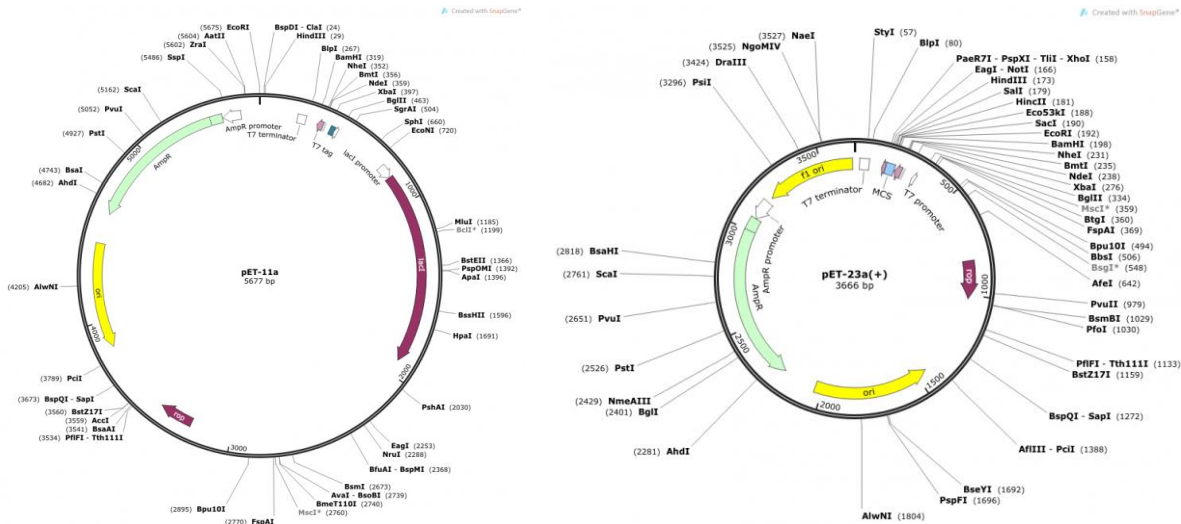
| ABC transporter (Organism) | Environment | NBDs | Conformation | Ligand | Res. In Å | PDB | Literature |
|--|--|--|---|--|-----------|-----------|--|
| MsbA (<i>Escherichia coli</i>) | Detergent: DDM | Open | Inward-facing | Apo (no ligand) | 5.3 | 3B5W | Ward <i>et al.</i> , 2007 ¹³⁵ X-ray |
| MsbA (<i>Vibrio cholera</i>) | Detergent: DDM | Closer to each other, but no dimer formation | Inward-facing | Apo (no ligand) | 5.5 | 3B5X | Ward <i>et al.</i> , 2007 ¹³⁵ X-ray |
| MsbA (<i>Salmonella typhimurium</i>) | Detergent: UDM | Closed | Outward-facing | AMPNP | 4.5 | 3B5Y | Ward <i>et al.</i> , 2007 ¹³⁵ X-ray |
| MsbA (<i>Salmonella typhimurium</i>) | Detergent: UDM | Closed | Outward-facing | ADP-V _i | 4.2 | 3B5Z | Ward <i>et al.</i> , 2007 ¹³⁵ X-ray |
| MsbA (<i>Salmonella typhimurium</i>) | Detergent: UDM | Closed | Outward-facing | AMPPNP | 3.7 | 3B60 | Ward <i>et al.</i> , 2007 ¹³⁵ X-ray |
| MsbA (<i>Escherichia coli</i>) | Lipid-bilayer mimicking environment (<i>E. coli</i> polar lipids and amphiphile BP) | Closed to open | Both outward- and inward-facing in different states | Different ligands: Apo (no ligand) MgATP MgAMPPNP ATP MgATP-V _i MgADP-V _i MgADP (nucleotide addition yield to an increase of OF conformations) | 30.0 | 6025-6033 | Moeller <i>et al.</i> , 2015 ²⁴⁹ Cryo-EM |
| MsbA (<i>Staphylococcus aureus</i>) | Nanodisc | Closed | Closed TMDs | ADP-V _i | 4.8 | 5TTP | Mi <i>et al.</i> , 2017 ⁹¹ Cryo-EM |
| MsbA (<i>Staphylococcus aureus</i>) | Nanodisc | Open with C-terminus close to each other | Inward-facing | LPS | 4.2 | 5TV4 | Mi <i>et al.</i> , 2017 ⁹¹ Cryo-EM |

| ABC transporter (Organism) | Environment | NBDs | Conformation | Ligand | Res. In Å | PDB | Literature |
|---|--------------------------------------|--|---|-----------------|-----------|---------|---|
| MsbA (<i>Salmonella typhimurium</i>) | Detergent: UDM | Open | Inward-facing | Lipid A | 2.8 | 6BL6 | Padayatti <i>et al.</i> , 2019 ³⁷³ X-ray |
| MsbA (<i>Salmonella typhimurium</i>) | Detergent: UDM | Open | Inward-facing | Apo (no ligand) | 4.5 | 6O30 | Padayatti <i>et al.</i> , 2019 ³⁷³ X-ray |
| MsbA (<i>Escherichia coli</i>) | Peptidisc | Open | Inward-facing | Apo (no ligand) | 4.4 | 6UZL | Angiulli <i>et al.</i> , 2020 ²⁵¹ Cryo-EM |
| MsbA (<i>Escherichia coli</i>) | Peptidisc | Open with C-terminus close to each other | Inward-facing | Apo (no ligand) | 4.2 | 6UZ2 | Angiulli <i>et al.</i> , 2020 ²⁵¹ Cryo-EM |
| MsbA (<i>Acinetobacter baumannii</i>) | Nanodisc | Open | Inward-facing | Apo (no ligand) | 5.2 | 7RIT | Thélot <i>et al.</i> , 2021 ³⁵⁰ Cryo-EM |
| MsbA (<i>Acinetobacter baumannii</i>) | Nanodisc | Open (driving closure) | Inward-facing | TBT1 | 4.0 | 7MET | Thélot <i>et al.</i> , 2021 ³⁵⁰ Cryo-EM |
| MsbA (<i>Acinetobacter baumannii</i>) | Nanodisc | Open | Inward-facing | G247 | 3.9 | 7MEW | Thélot <i>et al.</i> , 2021 ³⁵⁰ Cryo-EM |
| MsbA (<i>Acinetobacter baumannii</i>) | Detergent: DDM | Open | Inward-facing | G247 | 3.9 | Not yet | Thélot <i>et al.</i> , 2021 ³⁵⁰ Cryo-EM |
| MsbA (<i>Escherichia coli</i>) | Sposin-lipid nanoparticles(Salipro) | Closed | Occluded conformation (similar to 5TTP) | ADP vanadate | 3.5 | 7BCW | Kehlenbeck <i>et al.</i> , 2021 ³⁹⁹ Cryo-EM |
| MsbA (<i>Escherichia coli</i>) | Detergent-solubilized: | Open with C-terminus close to each other | Inward-facing | LPS, G7090 | 2.98 | 7SEL | Verma <i>et al.</i> , 2022 ⁴⁰⁰ X-ray |

| ABC transporter (Organism) | Environment | NBDs | Conformation | Ligand | Res. In Å | PDB | Literature |
|--|---------------------------------|--------|----------------|---------------------|-----------|------|---|
| BmrA E504A (<i>Bacillus subtilis</i>) | Detergent: DDM:cholate (1:1) | Closed | Outward-facing | MgATP | 3.9 | 6R81 | Chaptal <i>et al.</i> , 2022 ⁹³ Cryo-EM |
| BmrA E504A (<i>Bacillus subtilis</i>) | DDM:cholate (1:1) | Closed | Outward-facing | MgATP | 3.95 | 6R72 | Chaptal <i>et al.</i> , 2022 ⁹³ Cryo-EM |
| BmrA E504A (<i>Bacillus subtilis</i>) | DDM:cholate (1:1) | Closed | Outward-facing | MgATP, Rhodamine 6G | 4.2 | 7BG4 | Chaptal <i>et al.</i> , 2022 ⁹³ Cryo-EM |

2. CHAPTER II: MATERIAL AND METHODS

I supervised the Bachelor theses of [REDACTED], as well as the internships of [REDACTED] and [REDACTED], who contributed in part to this thesis.



Appendix 3: Bacterial expression vectors pET11a and pET23a+ (GSL Biotech; available at snapgene.com)



Appendix 4: DNA and protein sequence of LmrA-NBD WT with N-terminal HisTEV tag (commercially obtained from Genscript). Pink boxes indicate amino acids that have been exchanged in LmrA-NBD WT.

TEV cleavage

His₆-Tag TEV recognition sequence

330

atg ggt cat cac cac cat cat cac ggc tcc gaa aac ctg tac ttc cag ggc tct /gat gag
M G H H H H H H G S E N L Y F Q G S / D E

gaa cag gaa gtt ctg cac cag ggt gat tct ctg gac ctc gaa ggc aaa acc ctc tct gcg
E Q E V L H Q G D S L D L E G K T L S A

cat cac gtt gat ttc gcg tac gac gac tcc gaa cag atc ctg cac gac atc agc ttc gaa
H H V D F A Y D D S E Q I L H D I S F E

gcc cag ccg aac tct att atc gcg ttt gct ggt cca agc ggt ggc ggt aaa agc acc atc
A Q P N S I I A F A G P S G G G K S T I

gcg A K388A

ttc tct ctg ctg gaa cgc ttc tat cag ccg act gca ggc gaa att acc att ggt ggt cag
F S L L E R F Y Q P T A G E I T I G G Q

gcg A R397A

ccg atc gat tcc gtc tct ctg gaa aac tgg cgt agc cag att ggc ttc gtt agc cag gat
P I D S V S L E N W R S Q I G F V S Q D

ttt F W421F

gcg A W421A

tcc gct att atg gct ggc acg atc cgt gag aac ctg act tat ggt ctg gaa ggt aac ttt
S A I M A G T I R E N L T Y G L E G N F

acc gac gaa gat ctg tgg cag gtc ctg gac ctg gca ttt gcg cgt tcc ttc gtg gag aac
T D E D L W Q V L D L A F A R S F V E N

ttt F W457F

tgt C S467C

atg ccg gat cag ctg aac acc gaa gta ggt gag cgt ggt gtg aaa atc tct ggc ggt cag
M P D Q L N T E V G E R G V K I S G G Q

cgt cag cgt ctg gcc att gct cgc gcc ttc ctg cgt aac ccg aaa atc ctg atg ctc gac
R Q R L A I A R A F L R N P K I L M L D

gaa gca acc gct tct ctg gac agc gaa tcc gaa tct atg gta cag cgc gcg ctg gac tct
E A T A S L D S E S E S M V Q R A L D S

cag Q E512Q

tgg W M524W

ctg atg aaa ggt cgt acc acg ctg gtt atc gct cac cgt ctg agc acg att gtg gat gcg
L M K G R T T L V I A H R L S T I V D A

gcg A H543A

gac aaa atc tac ttc atc gag aaa ggc gaa atc act ggc tct ggc aaa cac aac gaa ctg
D K I Y F I E K G E I T G S G K H N E L

gta gca acc cac ccg ctg tac gca aaa tac gtt tcc gag cag ctg act gtg ggt cag taa
V A T H P L Y A K Y V S E Q L T V G Q -

590

Appendix 5: DNA and protein sequence of LmrA-NBD WT with N-terminal HisTEV tag (commercially obtained from Entelechon). Pink boxes indicate amino acids that have been exchanged in LmrA-NBD WT.

| | | His ₆ -Tag | | | | | | TEV recognition sequence | | | | | | TEV cleavage | 323 | | | | |
|-------|-----|-----------------------|-----|-----|-----|-----|-----|--------------------------|-----|-----|-----|-----|-----|--------------|-----|-----|-----|-----|-------|
| atg | ggt | cat | cat | cat | cat | cat | cac | ggt | agc | gaa | aac | ctg | tac | ttc | caa | ggc | tcc | gac | agt |
| M | G | H | H | H | H | H | H | G | S | E | N | L | Y | F | Q | G | S | D | S |
| gag | cag | gag | aaa | gat | gaa | ggt | aag | cgc | gtg | atc | gag | cgt | gcg | act | ggc | gac | gtg | gaa | ttc |
| E | Q | E | K | D | E | G | K | R | V | I | E | R | A | T | G | D | V | E | F |
| cgc | aat | gtc | acc | ttt | act | tat | ccg | gga | cgt | gac | gta | cct | gca | ttg | cgt | aac | atc | aac | ctg |
| R | N | V | T | F | T | Y | P | G | R | D | V | P | A | L | R | N | I | N | L |
| aaa | att | ccg | gca | ggg | aag | acg | gtt | gct | ctg | gtt | gga | cgc | tct | ggt | tcg | ggt | aaa | tca | acc |
| K | I | P | A | G | K | T | V | A | L | V | G | R | S | G | S | G | K | S | T |
| atc | gcc | agc | ctg | atc | acg | cgt | ttt | tac | gat | att | gat | gaa | ggc | gaa | atc | ctg | atg | gat | ggt |
| I | A | S | L | I | T | R | F | Y | D | I | D | E | G | E | I | L | M | D | G |
| cac | gat | ctg | cgc | gag | tat | acc | ctg | gcg | tcg | tta | cgt | aac | cag | gtt | gct | ctg | gtg | tcg | cag |
| H | D | L | R | E | Y | T | L | A | S | L | R | N | Q | V | A | L | V | S | Q |
| aat | gtc | cat | ctg | ttt | aac | gat | acg | ggt | gct | aac | aac | att | gct | tac | gca | cgg | act | gaa | cag |
| N | V | H | L | F | N | D | T | V | A | N | N | I | A | Y | A | R | T | E | Q |
| tac | agc | cgt | gag | caa | att | gaa | gaa | gcg | gcg | cgt | atg | gcc | tac | gcc | atg | gac | ttc | atc | aat |
| Y | S | R | E | Q | I | E | E | A | A | R | M | A | Y | A | M | D | F | I | N |
| | | | | | | | | | | | | | | | | tgc | | | |
| | | | | | | | | | | | | | | | | C | | | D461C |
| aag | atg | gat | aac | ggt | ctc | gat | aca | gtg | att | ggt | gaa | aac | ggc | gtg | ctg | ctc | tct | ggc | ggt |
| K | M | D | N | G | L | D | T | V | I | G | E | N | G | V | L | L | S | G | G |
| cag | cgt | cag | cgt | att | gct | atc | gct | cga | gcc | ttg | ttg | cgt | gat | agc | ccg | att | ctg | att | ctg |
| Q | R | Q | R | I | A | I | A | R | A | L | L | R | D | S | P | I | L | I | L |
| gac | gaa | gct | acc | tcg | gct | ctg | gat | acc | gaa | tcc | gaa | cgt | gcg | att | cag | gca | ctg | gat | |
| D | E | A | T | S | A | L | D | T | E | S | E | R | A | I | Q | A | A | L | D |
| | cag | | | | | | gcg | | | | | | tgg | | | | | | |
| | Q | | | | | | A | | | | | | W | | | | | | A518W |
| E506Q | | | | | | | | D512A | | | | | | | | | | | |
| gag | ttg | cag | aaa | aac | cgt | acc | tct | ctg | gtg | att | gcc | cac | cgc | ttg | tct | acc | att | gaa | aag |
| E | L | Q | K | N | R | T | S | L | V | I | A | H | R | L | S | T | I | E | K |
| gca | gac | gaa | atc | gtg | gtc | gtc | gag | gat | ggt | gtc | att | gtg | gaa | cgc | ggt | acg | cat | aac | gat |
| A | D | E | I | V | V | V | E | D | G | V | I | V | E | R | G | T | H | N | D |
| ttg | ctt | gag | cac | cgc | ggc | ggt | tac | gcg | caa | ctt | cac | aaa | atg | cag | ttt | ggc | caa | taa | |
| L | L | E | H | R | G | V | Y | A | Q | L | H | K | M | Q | F | G | Q | - | |

Appendix 6: DNA and protein sequence of MsbA-NBD WT cloned from E. coli BL21-Gold (DE3) with N-terminal HisTEV tag. Pink boxes indicate amino acids that have been exchanged in MsbA-NBD WT.


```

                                     His-Tag                               TEV recognition sequence          TEV cleavage
atg ggt   cat cat cat cat cat cac   ggt agc   gaa aac ctg tac ttc caa   ggc tcc / cat aac
M  G     H  H  H  H  H  H           G  S     E  N  L  Y  F  Q           G  S / H  N
gac aaa gat ctc tct acg tgg cag aca ttc   cgc cga ctg tgg cca acc att gcg cct ttc
D  K     D  L  S  T  W  Q           T  F  R  R  L  W  P  T  I  A  P  F
aaa gcg ggt ctg atc gtg gcg ggc gta gcg   tta atc ctc aac gca gcc agc gat acc ttc
K  A     G  L  I  V  A  G  V  A           L  I  L  N  A  A  S  D  T  F
atg tta tcg ctc ctt aag cca ctt ctt gat   gat ggc ttt ggt aaa aca gat cgc tcc gtg
M  L     S  L  L  K  P  L  L  D  D           G  F  G  K  T  D  R  S  V
ctg gtg tgg atg ccg ctg gtg gtg atc ggg   ctg atg att tta cgt ggt atc acc agc tat
L  V     W  M  P           L  V  V  I  G  L  M  I  L  R  G  I  T  S  Y
gtc tcc agc tac   tgt   atc tcc tgg gta tca   gga aag gtg gta atg acc atg cgt cgc cgc
V  S     S  Y   C   I  S  W  V  S  G           K  V  V  M  T  M  R  R  R
                                     C88S
ctg ttt ggt cac atg atg gga atg cca gtt   tca ttc ttt gac aaa cag tca acg ggt acg
L  F     G  H  M  M  G  M  P  V  S           F  F  D  K  Q  S  T  G  T
ctg ttg tca cgt att acc tac gat tcc gaa   cag gtt gct tct tct tcc ggc gca ctg
L  L     S  R  I  T  Y  D  S  E  Q  V  A  S  S  S  S  S  G  A  L
att act gtt gtg cgt gaa ggt gcg tcc atc   atc ggc ctg ttc atc atg atg ttt tac
I  T     V  V  R  E  G  A  S  I  I  G  L  F  I  M  M  F  Y  Y
agt tgg caa ctg tcg atc att ttg att gtg   ctg gca ccg att gtt tcg att gcg att cgc
S  W     Q  L  S  I  I  L  I  V  L  A  P  I  V  S  I  A  I  R
gtt gta tcg aag cgt ttt cgc aac atc agt   aaa aac atg cag aac acc atg ggg cag gtg
V  V     S  K  R  F  R  N  I  S  K  N  M  Q  N  T  M  G  Q  V
acc acc agc gca gaa caa atg ctg aag ggc   cac aaa gaa gta ttg att ttc ggt cag
T  T     S  A  E  Q  M  L  K  G  H  K  E  V  L  I  F  G  G  Q
gaa gtg gaa acg aaa cgc ttt gat aaa gtc   agc aac cga atg cgt ctt cag ggg atg aaa
E  V     E  T  K  R  F  D  K  V  S  N  R  M  R  L  Q  G  M  K
atg gtt tca gcc tct tcc atc tct gat   ccg atc att cag ctg atc gcc tct ttt gcg ctg
M  V     S  A  S  S  I  S  D  P  I  I  Q  L  I  A  S  L  A  L
gcg ttt gtt ctg tat gcg gcg agc ttc   cca agt gtc atg gat agc ctg act gcc ggt acg
A  F     V  L  Y  A  A  S  F  P  S  V  M  D  S  L  T  A  G  T
att acc gtt gtt ttc tct tca atg att gca   ctg atg cgt ccg ctg aaa tcg ctg acc aac
I  T     V  V  F  S  S  M  I  A  L  M  R  P  L  K  S  L  T  N
gtt aac gcc cag ttc cag cgc ggt atg gcg   gct   tgt   cag acg ctg ttt acc att ctg gac
V  N     A  Q  F  Q  R  G  M  A  A   C   Q  T  L  F  T  I  L  D
                                     C315S
agt gag cag gag aaa gat gaa ggt aag cgc   gtg atc gag cgt gcg act ggc gac gtg gaa
S  E     Q  E  K  D  E  G  K  R  V  I  E  R  A  T  G  D  V  E
ttc cgc aat gtc acc ttt act tat ccg gga   cgt gat gta cct gca ttg cgt aac atc aac
F  R     N  V  T  F  T  Y  P  G  R  D  V  P  A  L  R  N  I  N
ctg aaa att ccg gca ggg aag acg gtt gct   ctg gtt gga cgc tct ggt tcg ggt aaa tca
L  K     I  P  A  G  K  T  V  A  L  V  G  R  S  G  S  G  K  S
acc atc gcc agc ctg atc acg cgt ttt tac   gat att gat gaa ggc gaa atc ctg atg gat
T  I     A  S  L  I  T  R  F  Y  D  I  D  E  G  E  I  L  M  D
ggt cac gat ctg cgc gag tat acc ctg gcg   tcg tta cgt aac cag gtt gct ctg gtg tcg
G  H     D  L  R  E  Y  T  L  A  S  L  R  N  Q  V  A  L  V  S
cag aat gtc cat ctg ttt aac gat acg gtt   gct aac aac att gct tac gca cgg act gaa
Q  N     V  H  L  F  N  D  T  V  A  N  N  I  A  Y  A  R  T  E
cag tac agc cgt gag caa att gaa gaa gcg   gcg cgt atg gcc tac gcc atg   gac   ttc atc
Q  Y     S  R  E  Q  I  E  E  A  A  R  M  A  Y  A  M   D   F  I
                                     D461C
aat aag atg gat aac ggt ctc gat aca gtg   att ggt gaa aac ggc gtg ctg ctc tct ggc
N  K     M  D  N  G  L  D  T  V  I  G  E  N  G  V  L  L  S  G
ggt cag cgt cag cgt att gct atc gct cga   gcc ttg ttg cgt gat agc ccg att ctg att
G  Q     R  Q  R  I  A  I  A  R  A  L  L  R  D  S  P  I  L  I
ctg gac   gaa   gct acc tcg gct ctg   gat   acc gaa tcc gaa cgt   gcg   att cag gcg gca ctg
L  D     E  A  T  S  A  L  D  T  E  S  E  R  A  I  Q  A  A  L
                                     E506Q
                                     D512A
                                     A518W
gat gag ttg cag aaa aac cgt acc tct ctg   gtg att gcc cac cgc ttg tct acc att gaa
D  E     L  Q  K  N  R  T  S  L  V  I  A  H  R  L  S  T  I  E
aag gca gac gaa atc gtg gtc gtc gat ggt   gtc att gtg gaa cgc ggt acg cat aac
K  A     D  E  I  V  V  V  E  D  G  V  I  V  E  R  G  T  H  N
gat ttg ctt gag cac cgc ggc gtt tac gcg   caa ctt cac aaa atg cag ttt ggc caa tga
D  L     L  E  H  R  G  V  Y  A  Q  L  H  K  M  Q  F  G  Q  -
                                                                                                                                 582

```

Appendix 7: DNA and protein sequence of full-length MsbA WT cloned from of E. coli BL21-Gold (DE3) with N-terminal HisTEV tag. Pink boxes indicate amino acids that have been exchanged in MsbA WT.

1

```

atg gct agc /atg cca acc aag aaa caa aaa tct aaa agt aaa ttg aaa ccc ttt ttt gcc
M A S / M P T K K Q K S K S K L K P F F A
tta gta aga cgg acc aat cct tct tat gga aag ctc gcc ttt gcg ctt gcc ctc agt gta
L V R R R T N P S Y G K L A F A L A L S V
gta acc acg ctg gtc agc ctg ctc att cca tta tta acg aag cag ctt gtc gat ggt ttt
V T T L V S L L I P L L T K Q L V D G F
tct atg tca aat ctg tca ggc acg caa atc ggt ttg atc gcg ctg gtg ttt ttc gtt cag
S M S N L S G T Q I G L I A L V F F V Q
gcg ggt tta agc gct tat gcc acc tat gcg ctt aac tat aat gga caa aaa atc att tcc
A G L S A Y A T Y A L N Y N G Q K I I S
ggg ctg cgg gag tta tta tgg aag aaa tta att aag ctg cct gtc tct tat ttc gat aca
G L R E L L W K K L I K L P V S Y F D T
aat gct tcc gga gaa atc gtc agc cgt gta acg aac gat acg atg gtg gtc aaa gaa ttg
N A S G E T V S R V T N D T M V V K E L
att aca acc cat atc agc gga ttt att aca ggc atc att tct gtc att gga tca ttg aca
I T T H I S G F I A T G I I S V I G S L T
atc ttg ttt att atg aac tgg aag ctg act ctg ctt gtg tta gtg gtc gtt ccg ctg gcc
I L F I M N W K L T L L V L V V V P L A
gct ctt att ttg gtg ccg att gga cgg aaa atg ttc tcc att tca cgg gaa acg caa gat
A L I L V P I G R K M F S I S R E T Q D
gaa acg gct cgt ttt aca ggc ctg ctt aat caa att ctc ccg gaa atc aga ctt gtt aag
E T A R F T G L L N Q I L P E I R L V K
gct tca aat gcg gag gat gtc gaa tat ggg cgc ggg aag atg ggg att tcc tca tta ttt
A S N A E D V E Y G R G K M G I S S L F
aag ctt ggc gtt cgt gaa gcc aag gtt caa tcg ctt gtc ggc ccg ctt att tca ctc gtg
K L G V R E A K V Q S L V G P L I S L V
tta atg gca gcg ctt gtc gca gtg atc gga tat ggc ggc atg cag gtc tca tca ggc gag
L M A A A L V A V I G Y G G M Q V S S G E
ctc aca gcc gga gcg ctc gtg gct ttt att tta tat ttg ttt caa att att atg ccg atg
L T A G A L V A F I L Y L F Q I I M P M
ggc cag att aca acg ttt ttc aca cag ctg caa aaa tca atc ggt gca aca gaa cga atg
G Q I T T F F T Q L Q K S I G A T E R M
att gag att ttg gca gag gaa gag gaa gat aca gtg aca gga aaa caa att gaa aat gca
I E I L A E E E E D T V T G K Q I E N A
cat ctg cct atc cag ctt gat cgc gtg tct ttt gga tat aag cct gat cag ctg atc tta
H L P I Q L D R V S F G Y K P D Q L I L
aaa gag gtc agc gcc gtc att gaa gca ggg aaa gtg aca gcg atc gtc ggt ccg agc gcc
K E V S A V I E A G K V T A I V G P S G
ggg gga /aaa acg acg ctg ttt aag ctg ctt gaa /cgc ttt tat tct ccg act gca ggg acc
G G K T T L F K L L E R F Y S P T A G T
gcg A K380A
gcg A R389A
aaa K R389K
gaa E R389E
atg M R389M

att cgg ctg ggg gac gag ccg gtc gat act tac tcg ctt gaa tcg tgg agg gag cat atc
I R L G D E P V D T Y S L E S W R E H I
ggg tat gta tca cag gaa agc ccg tta atg tcc ggg aca atc aga gaa aat att tgc tac
G Y V S Q E S P L M S G T I R E N I C Y
ggg tta gaa cga gat gtg acg gat gct gag atc gaa aaa gcc gcg gag atg gca tat gcg
G L E R D V T D A E I E K A A E M A Y A
ctc /aat ttt ata aag gag ctg ccg aat cag ttt gat aca gaa gtg ggc gaa cgc ggc att
L N F I K E L P N Q F D T E V G E R G I
tgC C N459C

atg ctg tca ggc gga caa agg caa aga atc gcg att gcg aga gcg ctt ctc cgt aac cca
M L S G G Q R R I A I A R A L L R N P
agc att ctt atg ctc gat gaa gct acc /tca /agt ctc /gac agc caa tct gaa aaa /tca gtt
S I L M L D E A T S S L D S Q S E K S V
S507A A A S508A A D510A W S516W

cag cag gcg ctg gag gtg ctg atg gag ggc cgc aca acg att gtt atc gct cac cgc cta
Q Q A L E V L M E G R T T I V I A H R L
tct acc gtt gta gat gcg gac cag ctt ttg ttt gtt gaa aaa ggg gaa att acc ggt cgt
S T V V D A D Q L L F V E K G E I T G R
gga aca cac cat gag tta atg gct tcc cat ggc ctt tac ccg gat ttt gct gaa cag cag
G T H H E L M A S H G L Y R D F A E Q Q
ctg aaa atg aat gcg gac tta gaa aac aaa gcc ggg /gtc gac aag ctt gcg gcc gca ctc
L K M N A D L E N K A G V D K L A A A L
gag /cac cac cac cac cac cac /tga 589
E H H H H H H -
His6-Tag

```

Appendix 8: DNA and protein sequence of full-length BmrA WT with C-terminal His₆ tag (BmrA WT provided by Prof. [redacted] Lyon). Pink boxes indicate amino acids that have been exchanged in BmrA WT.

```

                                           TEV cleavage
                                           331
                    His-Tag                    TEV recognition sequence
atg ggg cat cat cac cac cac cac gga tca gaa aat cta tat ttt caa ggc aaa cag att
M  G  H  H  H  H  H  H  G  S  E  N  L  Y  F  Q  G  K  Q  I
gaa aac gcg cac ctg ccg atc caa ctg gac cgt gtg agc ttt ggt tac aag ccg gat cag
E  N  A  H  L  P  I  Q  L  D  R  V  S  F  G  Y  K  P  D  Q
ctg att ctg aaa gag gtt agc gcg gtg atc gaa gcg ggc aaa gtt acc gcg att gtg ggt
L  I  L  K  E  V  S  A  V  I  E  A  G  K  V  T  A  I  V  G
ccg agc ggt ggc ggt aaa acc acc ctg ttc aaa ctg ctg gag cgt ttt tat agc ccg acc
P  S  G  G  G  K  T  T  L  F  K  L  L  E  R  F  Y  S  P  T
                                           gcg
                                           A  R389A

gcg ggt acc atc cgt ctg ggt gac gaa ccg gtt gat acc tac agc ctg gag agc tgg cgt
A  G  T  I  R  L  G  D  E  P  V  D  T  Y  S  L  E  S  W  R
                                           ttt
                                           F  W413F

gaa cac att ggt tat gtg agc cag gag agc ccg ctg atg agc ggc acc att cgt gag aac
E  H  I  G  Y  V  S  Q  E  S  P  L  M  S  G  T  I  R  E  N
atc tgc tac ggt ctg gaa cgt gac gtt acc gat gcg gag atc gaa aag gcg gcg gag atg
I  C  Y  G  L  E  R  D  V  T  D  A  E  I  E  K  A  A  E  M
gcg tat gcg ctg aac ttc att aaa gaa ctg ccg aac cag ttt gat acc gag gtg ggt gag
A  Y  A  L  N  F  I  K  E  L  P  N  Q  F  D  T  E  V  G  E
                                           tgc
                                           C  N459C

cgt ggt atc atg ctg agc ggc ggt cag cgt caa cgt atc gcg att gcg cgt gcg ctg ctg
R  G  I  M  L  S  G  G  Q  R  Q  R  I  A  I  A  R  A  L  L
cgt aac ccg agc att ctg atg ctg gac gag gcg acc agc agc ctg gat agc cag agc gaa
R  N  P  S  I  L  M  L  D  E  A  T  S  S  L  D  S  Q  S  E
aag agc gtt cag caa gcg ctg gaa gtg ctg atg gaa ggt cgt acc acc atc gtt att gcg
K  S  V  Q  Q  A  L  E  V  L  M  E  G  R  T  T  I  V  I  A
                                           tgg
                                           W  S516W

cac cgt ctg agc acc gtt gtg gac gcg gat caa ctg ctg ttc gtg gag aaa ggc gaa atc
H  R  L  S  T  V  V  D  A  D  Q  L  L  F  V  E  K  G  E  I
acc gcc cgt ggt acc cac cac gaa ctg atg gcg agc cac ggt ctg tac cgt gat ttt gcg
T  G  R  G  T  H  H  E  L  M  A  S  H  G  L  Y  R  D  F  A
gaa caa caa ctg aag atg aat gcg gac ctg gag aat aag gcg ggc taa
E  Q  Q  L  K  M  N  A  D  L  E  N  K  A  G  -
                                           589

```

Appendix 9: DNA and protein sequence of BmrA-NBD WT with N-terminal HisTEV tag (commercially obtained from Genscript). Pink boxes indicate amino acids that have been exchanged in BmrA-NBD WT.

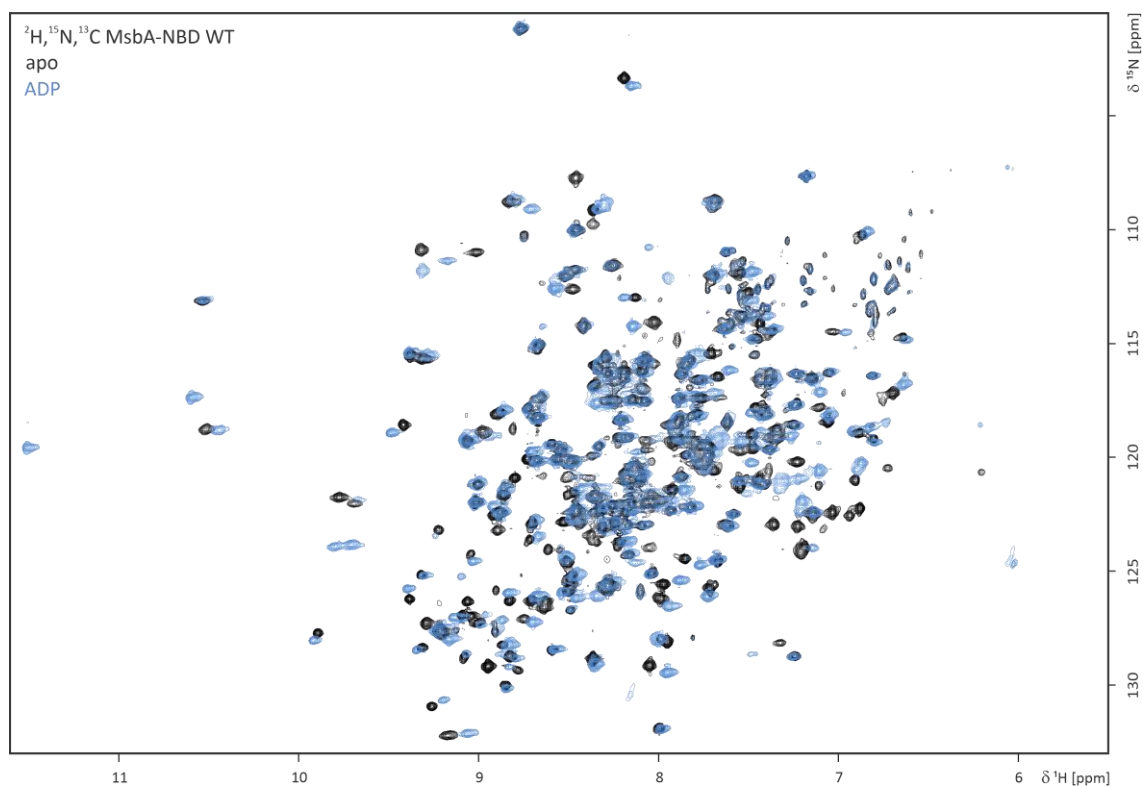
TEV cleavage

| | | | |
|---|---|--------------------------|---|
| | His-Tag | TEV recognition sequence | 2 |
| <p>atg ggg cat cat cac cac cac cac gga tca gaa aat cta tat ttt caa ggg ccc acc aag M G H H H H H H G S E N L Y F Q G P T K aag cag aaa agc aag agc aag ctg aaa ccg ttt ttt gcg ctg gtt cgt cgt acc aac ccg K Q K S K S K L K P F F A L V R R T N P agc tac ggt aaa ctg gcg ttt gcg ctg gcg ctg agc gtg gtt acc acc ctg gtt agc ctg S Y G K L A F A L A L S V V T T L V S L ctg atc ccg ctg ctg acc aaa cag ctg gtt gac ggc ttt agc atg agc aac ctg agc ggc L I P L L T K Q L V D G F S M S N L S G acc cag atc ggt ctg att gcg ctg gtt ttc ttt gtg caa gcg ggt ctg agc gcg tac gcg T Q I G L I A L V F F V Q A G L S A Y A acc tat gcg ctg aac tac aac ggc caa aag atc att agc ggt ctg cgt gag ctg ctg tgg T Y A L N Y N G Q K I I S G L R E L L W aag aaa ctg atc aaa ctg ccg gtt agc tat ttc gac acc aac gcg agc ggc gaa acc gtg K K L I K L P V S Y F D T N A S G E T V agc cgt gtg acc aac gat acc atg vtg gtt aag gaa ctg atc acc acc cac att agc ggc S R V T N D T M G V V K E L I T T H I S G ttc atc acc ggt atc att agc gtg atc ggt agc ctg acc atc ctg ttt att atg aac tgg F I T G I I S V I G S L T I L F I M N W aag ctg acc ctg ctg gtt ctg gtg gtt gtt ccg ctg gcg gcg ctg att ctg gtg ccg att K L T L L V L V V P L A A L I L V P I ggt cgt aaa atg ttc agc att agc cgt gaa acc cag gac gaa acc gcg cgt ttt acc ggt G R K M F S I S R E T Q D E T A R F T G ctg ctg aac caa att ctg ccg gag atc cgt ctg gtt aag gcg agc aac gcg gag gat gtg L L N Q I L P E I R L V K A S N A E D V gaa tat ggc cgt ggt aaa atg ggc atc agc agc ctg ttc aag ctg ggt gtt cgt gaa gcg E Y G R G K M G I S S L F K L G V R E A aaa gtt cag agc ctg gtg ggc ccg ctg atc agc ctg gtg ctg atg gcg gcg ctg ggt gtt K V Q S L V G P L I S L V L M A A L G V gcg gtg att ggt tac ggt ggc atg caa gtt agc agc ggt gaa ctg acc gcg ggt gcg ctg A V I G Y G G M Q V S S G E L T A G A L gtt gcg ttc atc ctg tac ctg ttc cag atc att atg ccg atg ggc caa atc acc acc ttc V A F I L Y L F Q I I M P M G Q I T T F ttt acc cag ctg caa aag agc att ggt gcg acc gag cgt atg atc gaa att ctg gcg gag F T Q L Q K S I G A T E R M I E I L A E gaa gag gaa gac acc gtt acc ggc aaa cag att gaa aac gcg cac ctg ccg atc caa ctg E E E D T V T G K Q I E N A H L P I Q L gac cgt vtg agc ttt ggt tac aag ccg gat cag ctg att ctg aaa gag gtt agc A G V D R V S F G Y K P D Q L I L K E V S A V atc gaa gcg ggc aaa gtt acc gcg att gtg ggt ccg agc ggt ggc ggt aaa acc acc ctg I E A G K V T A I V G P S G G K T T L ttc aaa ctg ctg gag cgt ttt tat agc ccg acc gcg ggt acc atc cgt ctg ggt gac gaa F K L L E R F Y S P T A G T I R L G D E gcg R389A A</p> | <p>ccg gtt gat acc tac agc ctg gag agc tgg cgt gaa cac att ggt tat gtg agc cag gag P V D T Y S L E S W R E H I G Y V S Q E ttt W413F F</p> <p>agc ccg ctg atg agc ggc acc att cgt gag aac atc tgc tac ggt ctg gaa cgt gac gtt S P L M S G T I R E N I C Y G L E R D V acc gat gcg gag atc gaa aag gcg gcg gag atg gcg tat gcg ctg aat ttc att aaa gaa T D A E I E K A A E M A Y A L N F I K E tgc N459C C</p> <p>ctg ccg aac cag ttt gat acc gag gtg ggt gag cgt ggt atc atg ctg agc ggc ggt cag L P N Q F D T E V G E R G I M L S G G Q cgt caa cgt atc gcg att gcg cgt gcg ctg cgt aac ccg agc att ctg atg ctg gac R Q R I A I A R A L L R N P S I L M L D gag gcg acc agc agc ctg gat agc cag agc gaa aag agc gtt cag caa gcg ctg gaa gtg E A T S S L D S P S E K A G S V Q Q A L E V tgg S516W w</p> <p>ctg atg gaa ggt cgt acc acc atc gtt att gcg cac cgt ctg agc acc gtt gtg gac gcg L M E G R T T I V I A H R L S T V V D A gat caa ctg ctg ttc gtg gag aaa ggc gaa atc acc ggc cgt ggt acc cac cac gaa ctg D Q L L F V E K G E I T G R G T H H E L atg gcg agc cac ggt ctg tac cgt gat ttt gcg gaa caa caa ctg aag atg aat gcg gac M A S H G L Y R D F A E Q Q L K M N A D ctg gag aat aag gcg ggc taa L E N K A G -</p> | <p>589</p> | |

Appendix 10: DNA and protein sequence of full-length BmrA with N-terminal HisTEV tag (BmrA WT commercially obtained from Genscript, numbering based on). Pink boxes indicate amino acids that have been exchanged in BmrA WT.

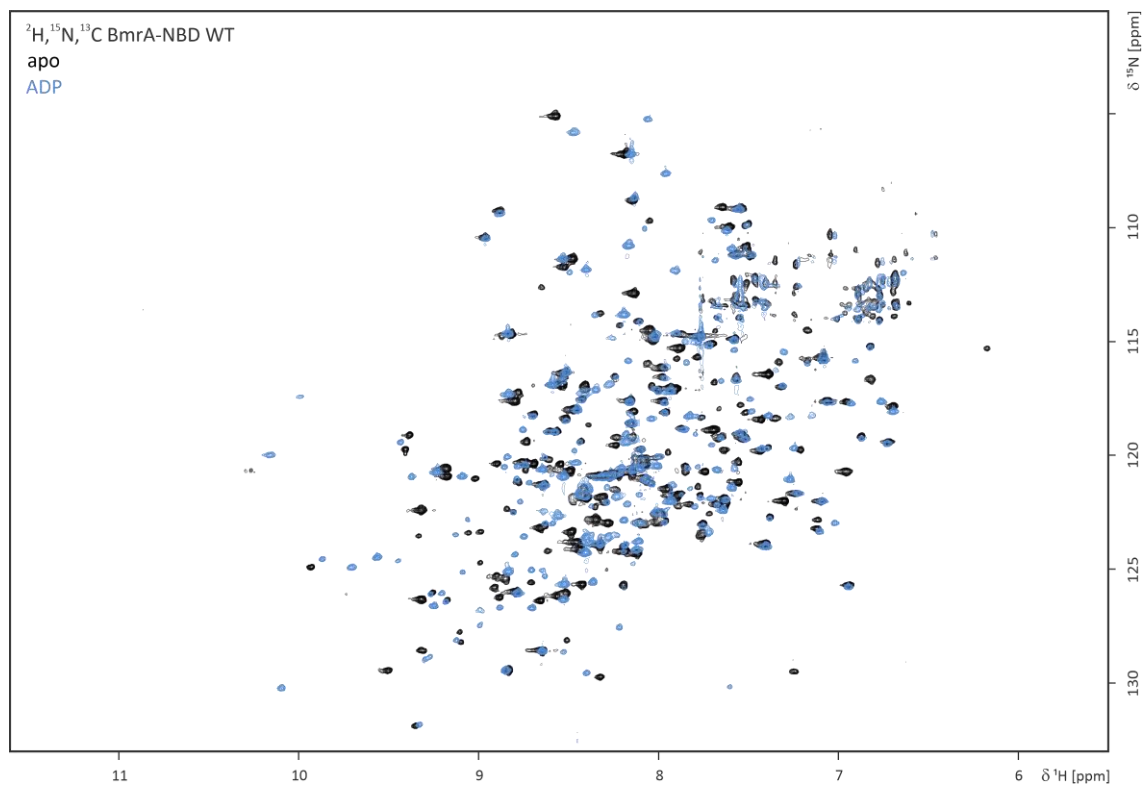
3. CHAPTER III: RESULTS

3.1. Consequences of nucleotide binding to the NBD of multidrug ABC transporters



Appendix 11: Effect of ADP binding to the isolated ABC transporter NBD of MsbA

Overlay of ^1H - ^{15}N TROSY HSQC spectra of $^2\text{H}, ^{15}\text{N}, ^{13}\text{C}$ -labeled MsbA-NBD in the apo (black) and ADP-bound state (blue – 10 mM ADP).

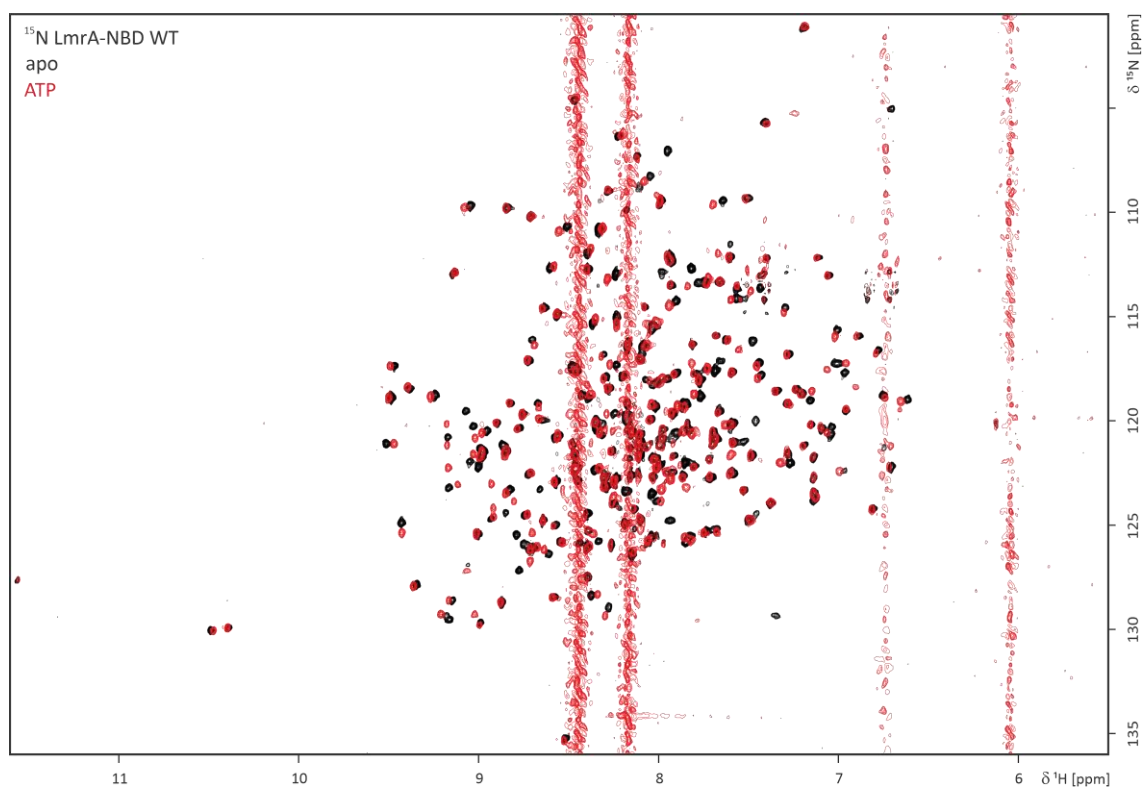


Appendix 12: Effect of ADP binding to the isolated ABC transporter NBD of BmrA

Overlay of ^1H - ^{15}N TROSY HSQC spectra of $^2\text{H}, ^{15}\text{N}, ^{13}\text{C}$ -labeled BmrA-NBD in the apo (black) and ADP-bound state (blue – 10 mM ADP).

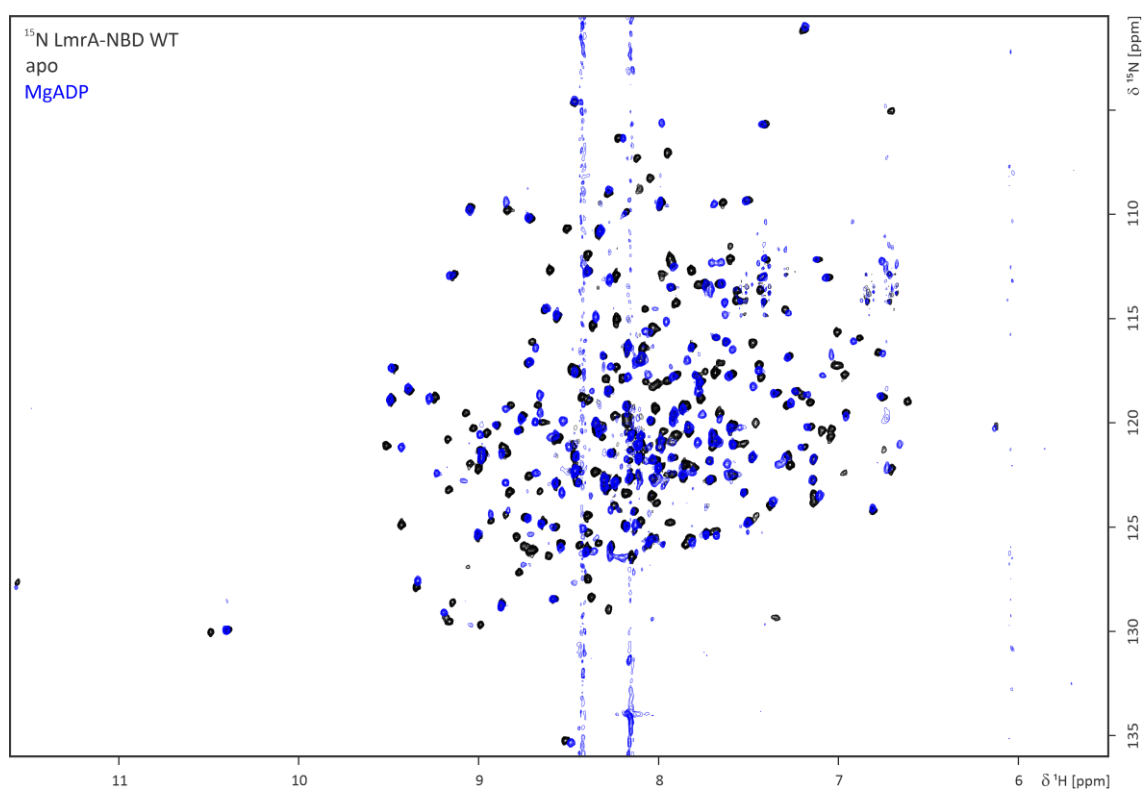
Appendix table 4: Comparison of reported K_D values for different ABC transporters for ADP and ATP

| ABC transporter | K _D value | K _D value | Reference |
|-----------------------------|--------------------------------|--------------------------|--|
| | ATP [μ M] | ADP [μ M] | |
| Atm1 (C-NBD) | 97 | 43 | Chen & Cowan, 2003 ⁴⁰¹ |
| Mdl1p (NBD) | 2 (+Mg ²⁺) | 64 (+Mg ²⁺) | Janas <i>et al.</i> , 2003 ²²⁴ |
| MRP1 (N-NBD) | 118 (+Mg ²⁺) | 139 (+Mg ²⁺) | Ramaen <i>et al.</i> , 2003 ⁴⁰² |
| MRP1 | 32.3 \pm 10.9 | - | Buyse <i>et al.</i> , 2006 ⁴⁰³ |
| P-gp (chin. Hamster) | 870 \pm 120 | 330 | Siarheyeva <i>et al.</i> , 2010 ²³⁰ |
| P-gp (chin. Hamster) | 404 \pm 42 | 407 \pm 33 | Qu <i>et al.</i> , 2003 ⁴⁰⁴ |
| P-gp (chin hamster) | 280 | 330 | Liu <i>et al.</i> , 2000 ⁴⁰⁵ |
| | 50.6 (TNP-ATP) | 43.9 (TNP-ADP) | |
| P-gp | 2200 (TNP-ATP) | | Dayan <i>et al.</i> , 1996 ⁴⁰⁶ |
| | 6300 (ATP displacement) | | |
| P-gp | 1200-1800 | 2300 | Baubichon-Cortay <i>et al.</i> , 1994 ⁴⁰⁷ |
| | (TNP-ATP) | (TNP-ADP) | |
| | 2500 – 3000 (ATP displacement) | | |
| MsbA (<i>E. coli</i>) | 3050 \pm 430 | 130 \pm 60 | Siarheyeva & Sharom, 2009 ¹³² |
| BmrA (<i>B. subtilis</i>) | 1550 | - | Steinfels <i>et al.</i> , 2004 ¹³⁷ |
| | TNP ATP 850 \pm 60 | | |



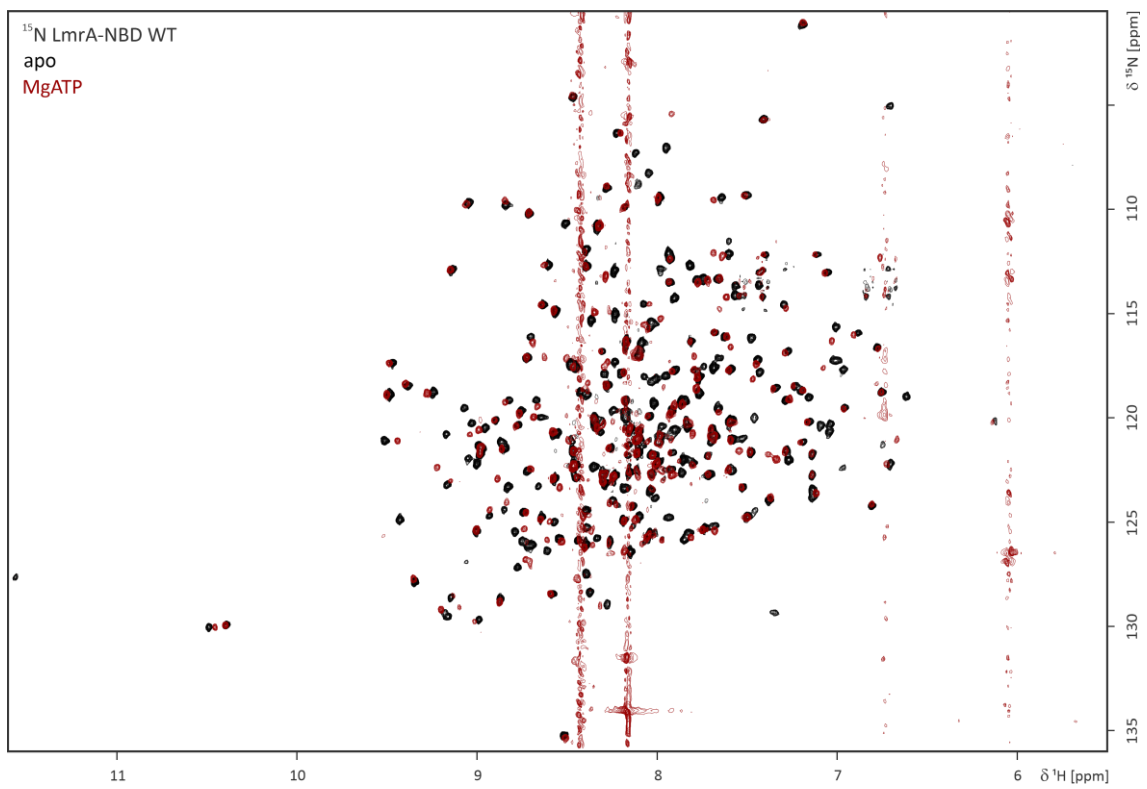
Appendix 13: Effect of ATP binding to the isolated ABC transporter NBD of LmrA

Overlay of ¹H-¹⁵N TROSY HSQC spectra of ¹⁵N-labeled LmrA-NBD in the apo (black) and ATP-bound state (red-10 mM ATP).

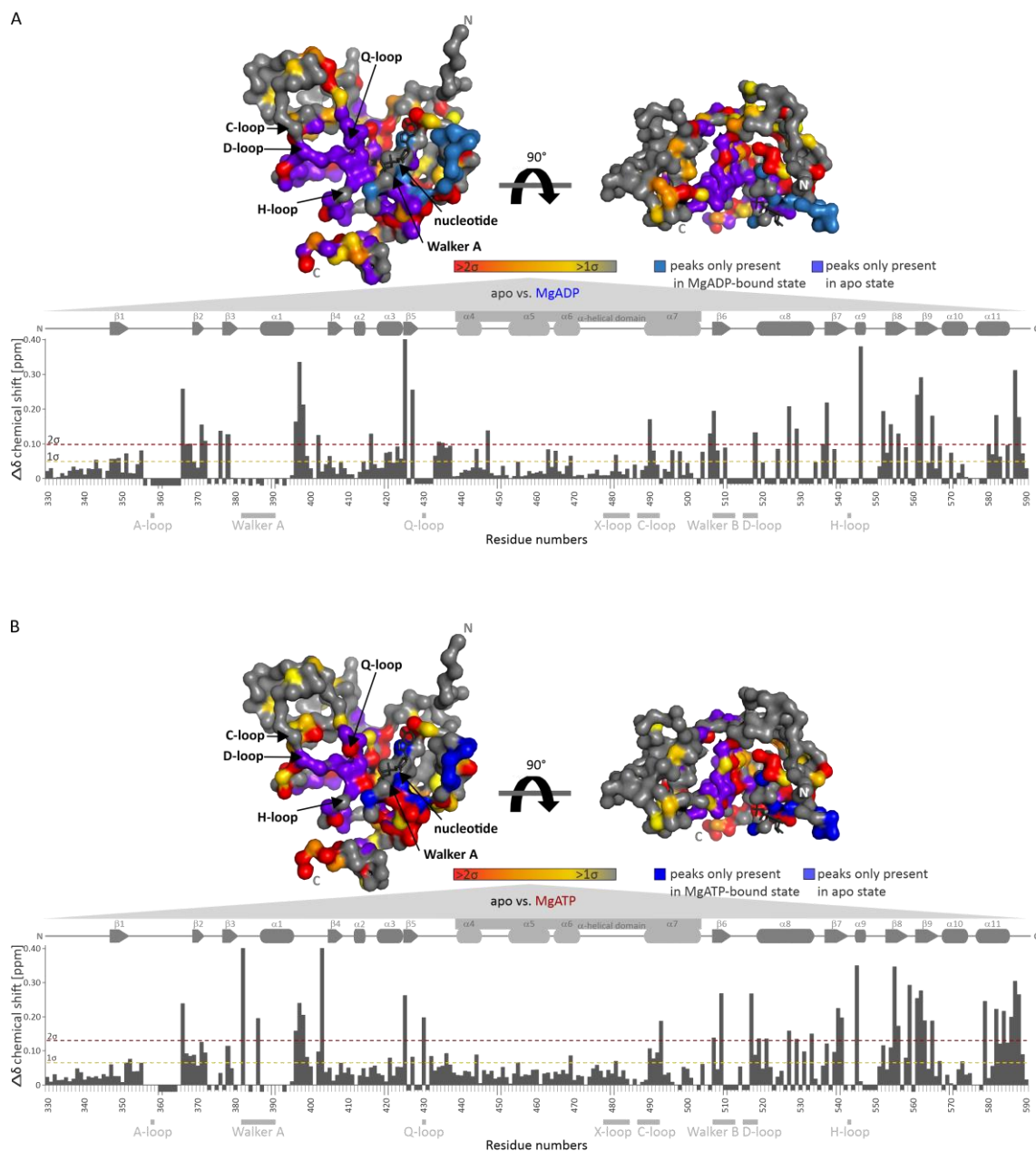


Appendix 14: Effect of MgADP binding to the isolated ABC transporter NBD of LmrA

Overlay of ¹H-¹⁵N TROSY HSQC spectra of ¹⁵N-labeled LmrA-NBD in the apo (black) and MgADP-bound state (blue-10 mM MgADP).

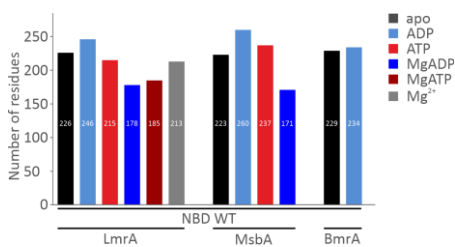


Appendix 15: Effect of MgATP binding to the isolated ABC transporter NBD of LmrA
Overlay of ^1H - ^{15}N TROSY HSQC spectra of ^{15}N -labeled LmrA-NBD in the apo (black) and MgATP-bound state (brown-10 mM MgATP).

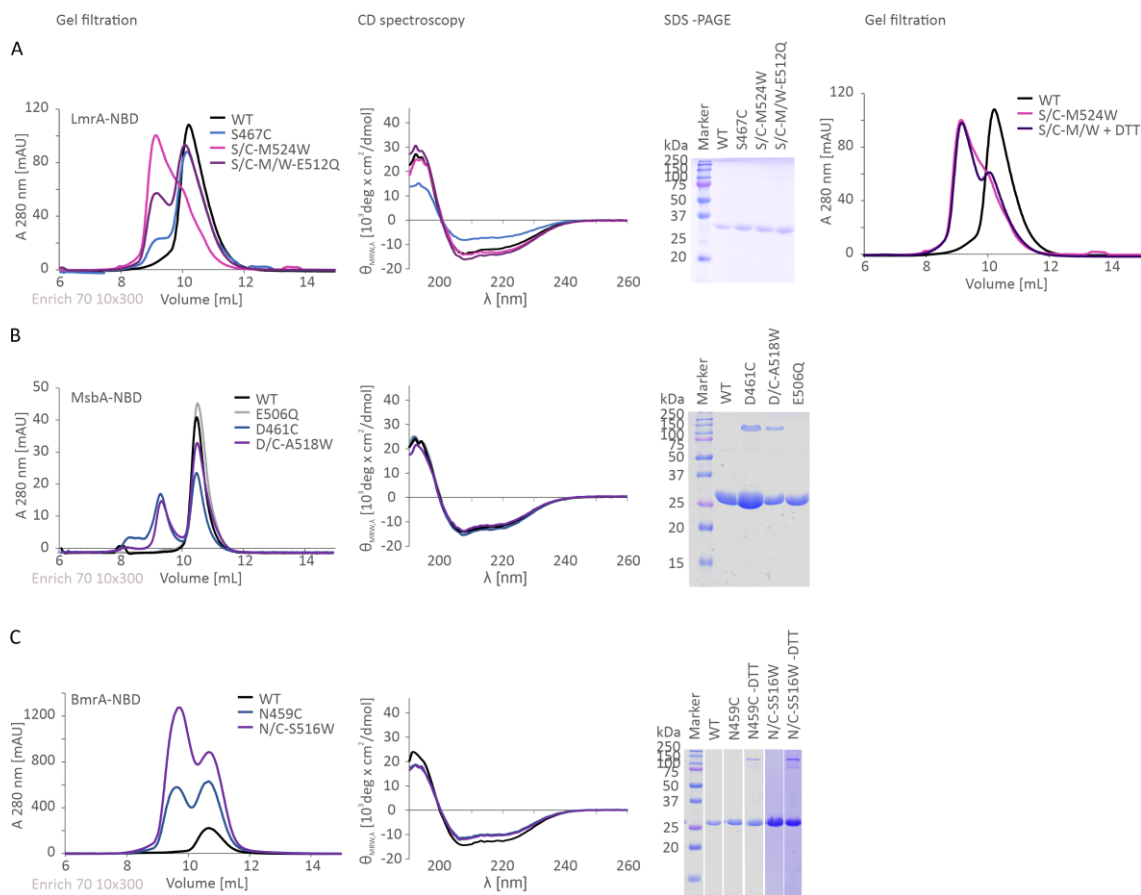


Appendix 16: Effect of nucleotide binding with magnesium to the isolated ABC transporter LmrA-NBD

A) Effect of MgADP binding Bar graph showing the comparison of chemical shift differences between apo and MgADP-bound state for LmrA-NBD. Above the bar graph chemical shift changes are shown plotted on a ribbon surface representation of a LmrA-NBD homology model based on Sav1866 (PDB ID: 2HYD³⁴). View on the NBD-NBD interface (left) and view on the coupling helix groove (right) are shown. Blue or violet indicate residues whose peaks are only present in the ¹H-¹⁵N HSQC spectra of the MgADP-bound state or the apo state, respectively. **B) Effect of MgATP binding.** Bar graph showing the comparison of chemical shift differences between apo and ATP-bound state for LmrA-NBD. Above the bar graph chemical shift changes are shown plotted on a ribbon surface representation of a LmrA-NBD homology model based on Sav1866 (PDB ID: 2HYD³⁴). View on the NBD-NBD interface (left) and view on the coupling helix groove (right) are shown. Dark blue or violet indicate peaks whose peaks are only present in the ¹H-¹⁵N TROSY HSQC spectra of the MgATP-bound state or the apo state, respectively. Amino acid numbering is based on the full-length transporter, yellow and red dotted lines indicate 1 σ and 2 σ standard deviation. Color gradient from yellow to red represents increasing chemical shift differences from >2 σ (red) to 1 σ (yellow). Residues with chemical shift differences below 1 σ or those that could not be traced reliably or remain unassigned are shown in gray. Downward orientated bars represent peaks not present in the apo but in the ADP-bound state. Missing data points indicate either prolines, unassigned residues or negligible $\Delta\delta$ values. Above the bar graph, the corresponding secondary structure elements of LmrA-NBD are displayed. Lighter gray indicates the α -helical subdomain.



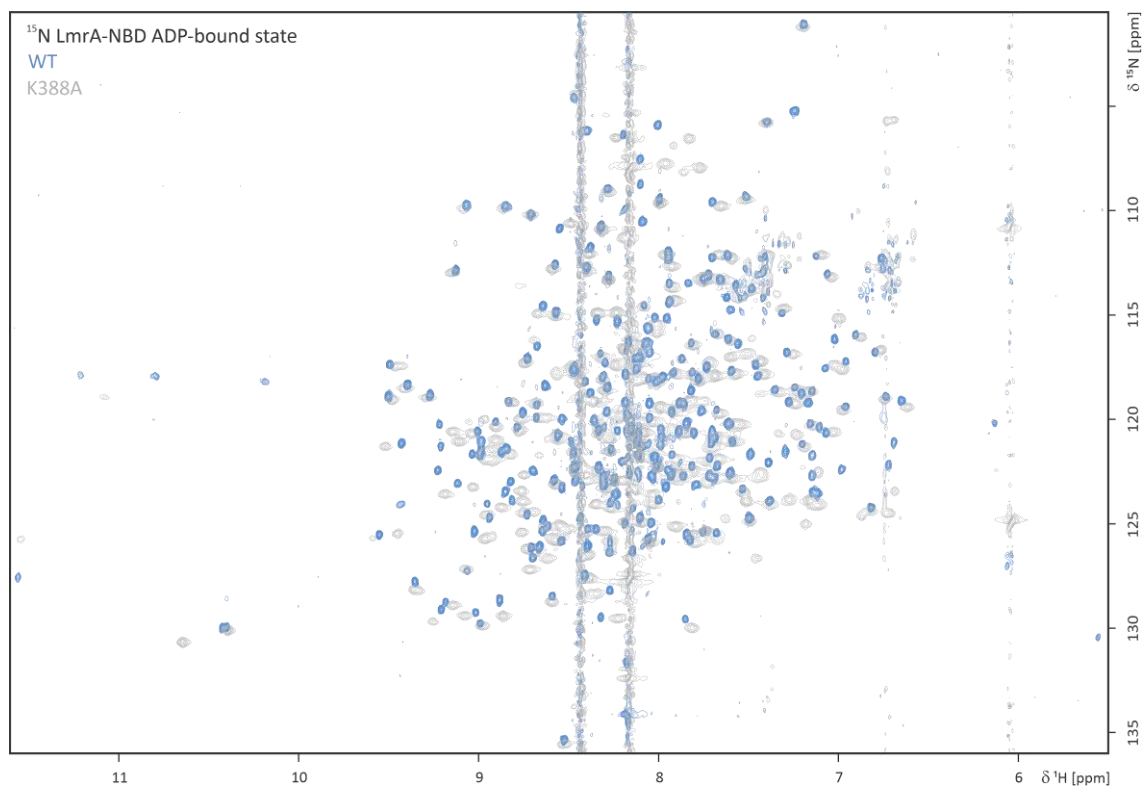
Appendix 17: Bar graph representation of the amino acid residue numbers (total number of peaks) of ¹H-¹⁵N TROSY HSQC spectra of WT LmrA-NBD, MsbA-NBD and BmrA-NBD with and without ligand.



Appendix 18: Characterization of protein constructs used in PET-FCS

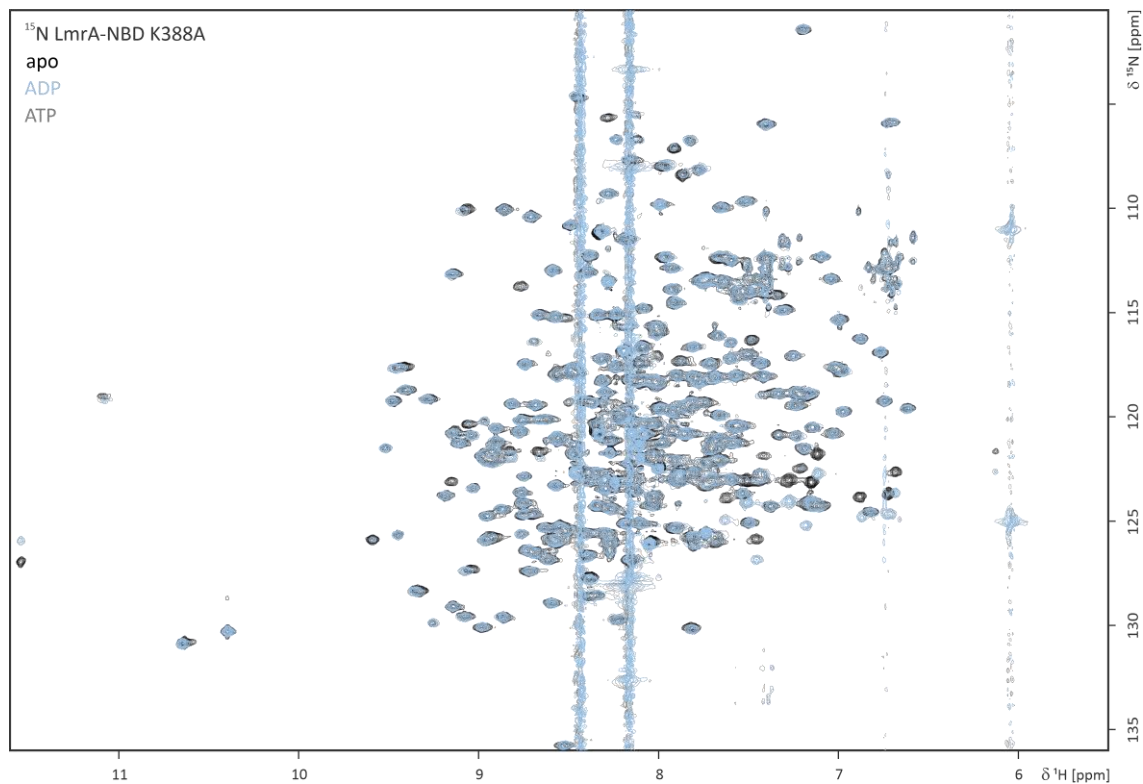
A) Structural integrity and oligomerization state of WT LmrA-NBD and constructs (S467C – blue, S467C-M524W – pink and S467C-M524W-E512Q – dark purple) used in PET-FCS analyzed by gel filtration, CD spectroscopy and SDS-PAGE. **B)** Structural integrity and oligomerization state of WT MsbA-NBD, E506Q mutant and constructs used for PET-FCS (E506Q – gray, D461C – blue, D461C-A518W – dark purple) analyzed by gel filtration, CD spectroscopy and SDS-PAGE. **C)** Structural integrity and oligomerization state of WT BmrA-NBD and constructs used for PET-FCS (N459C – blue, N459C-S516W – dark purple) analyzed by gel filtration, CD spectroscopy and SDS-PAGE.

3.2. Role of conserved motifs in the NBD of multidrug ABC transporters



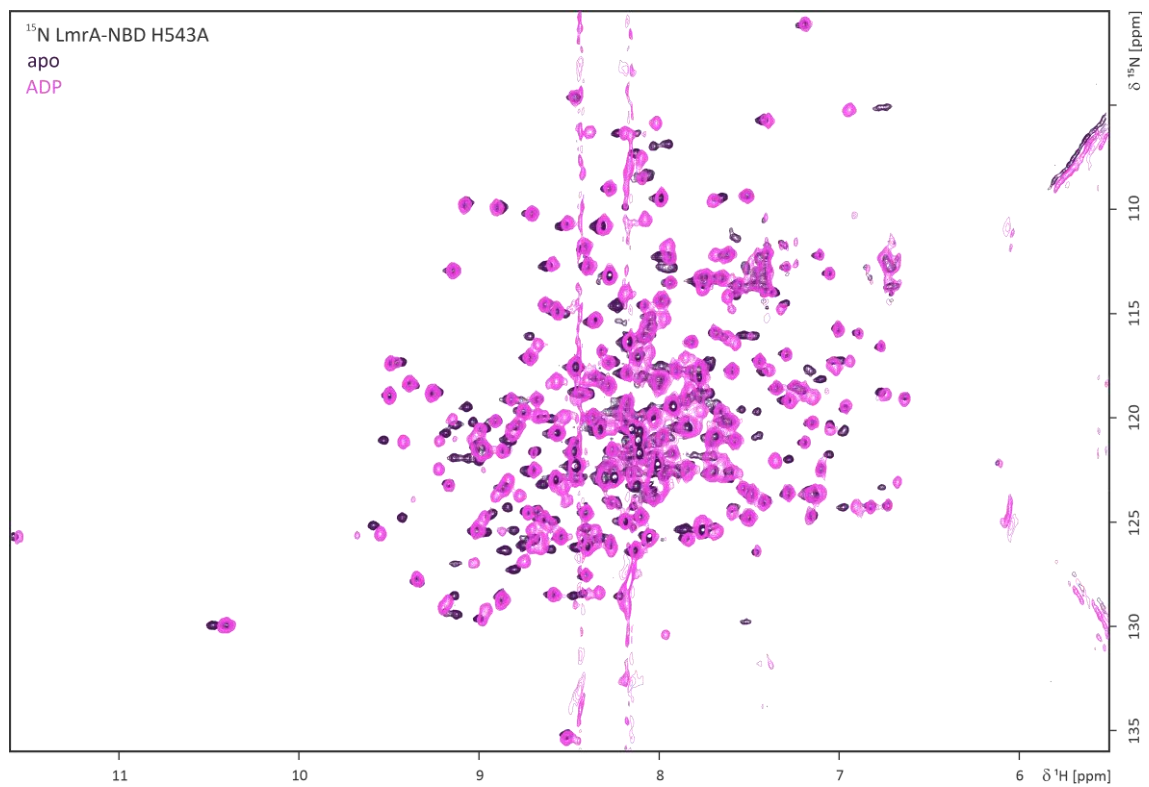
Appendix 19: Spectral differences between WT LmrA-NBD and the Walker A motif mutant (K388A) in the ADP-bound state (10 mM ADP)

Overlay of ^1H - ^{15}N TROSY HSQC spectra of ^{15}N -labeled LmrA-NBD WT (blue) and K388A (light gray).



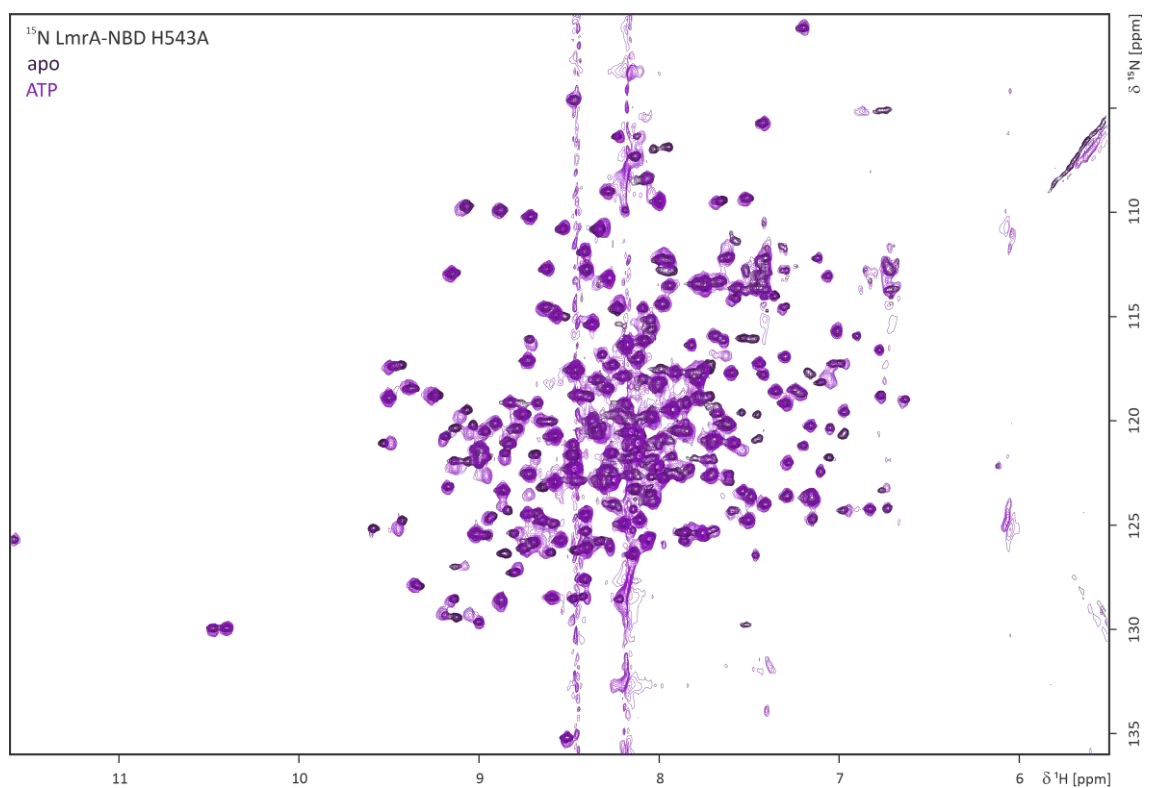
Appendix 20: Spectral differences between LmrA-NBD Walker A motif mutant (K388A) in the apo, ADP-bound state (10 mM ADP) and ATP-bound state (10 mM ATP)

Overlay of ^1H - ^{15}N TROSY HSQC spectra of ^{15}N -labeled LmrA-NBD K388A in the apo (black), ADP-bound state (blue-10 mM ADP) and ATP-bound state (dark gray-10 mM ATP).



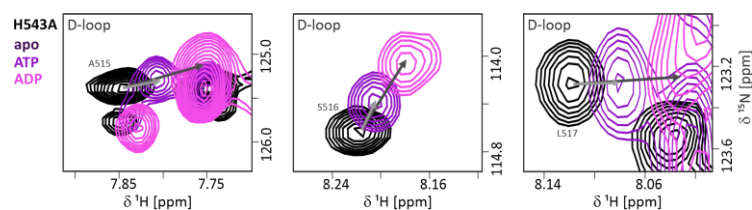
Appendix 21: ADP binding to the H-loop mutant (H543A) of LmrA-NBD

Overlay of ^1H - ^{15}N TROSY HSQC spectra of ^{15}N -labeled LmrA-NBD H543A in the apo (dark purple) and ADP-bound state (violet-10 mM ADP).



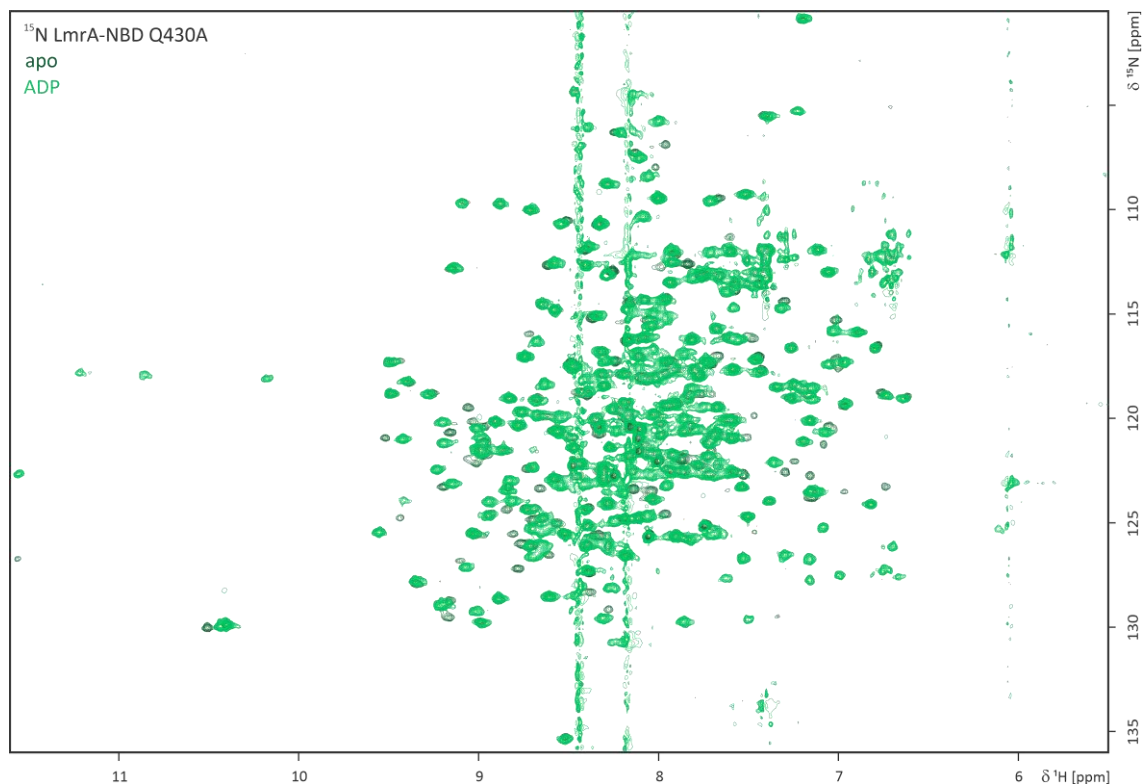
Appendix 22: ATP binding to the H-loop mutant (H543A) of LmrA-NBD

Overlay of ^1H - ^{15}N TROSY HSQC spectra of ^{15}N -labeled LmrA-NBD H543A in the apo (dark purple) and ATP-bound state (purple-10 mM ATP).



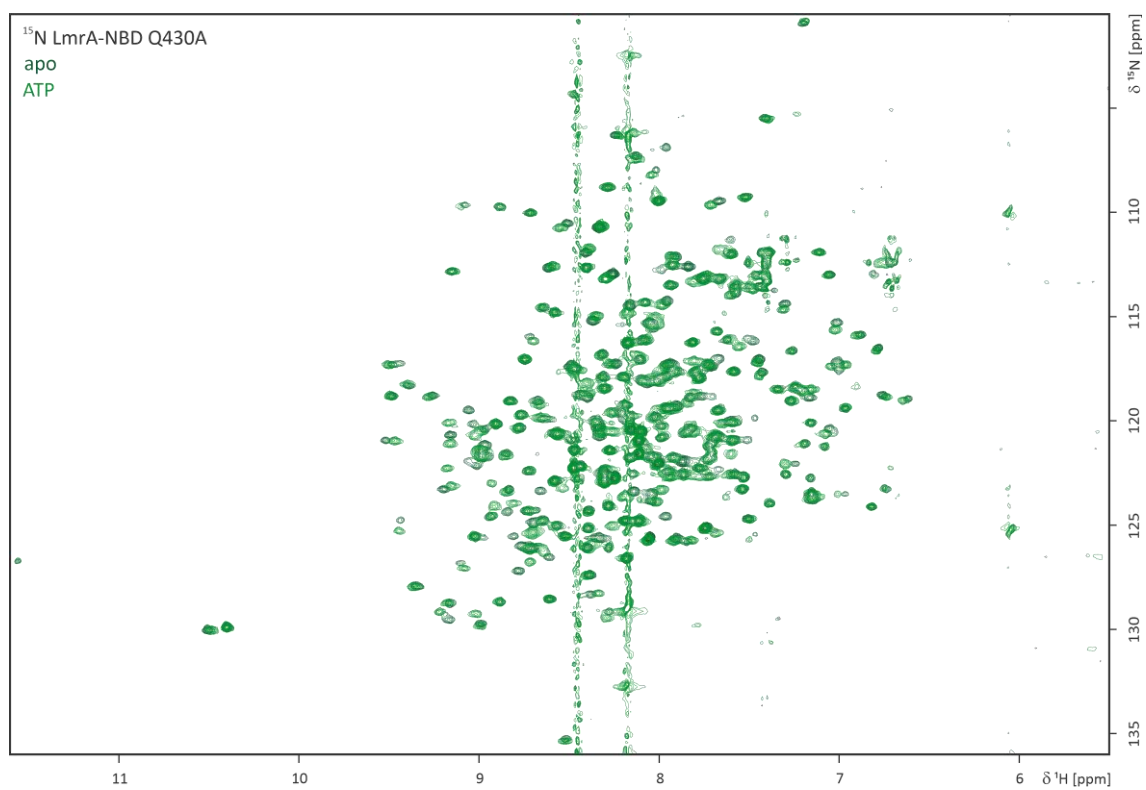
Appendix 23: NH resonances of the D-loop residues A515-L517 “sense” nucleotide binding

Close-up views of ^1H - ^{15}N TROSY HSQC spectra of ^{15}N -labeled LmrA-NBD H543A showing the NH resonances for the D-loop residues A515, S516 and L517 in the apo, ADP-bound (10 mM). Overlays of the apo (black), ATP-bound (purple) and ADP-bound (violet) states are shown (**Appendix 21** and **Appendix 22**).



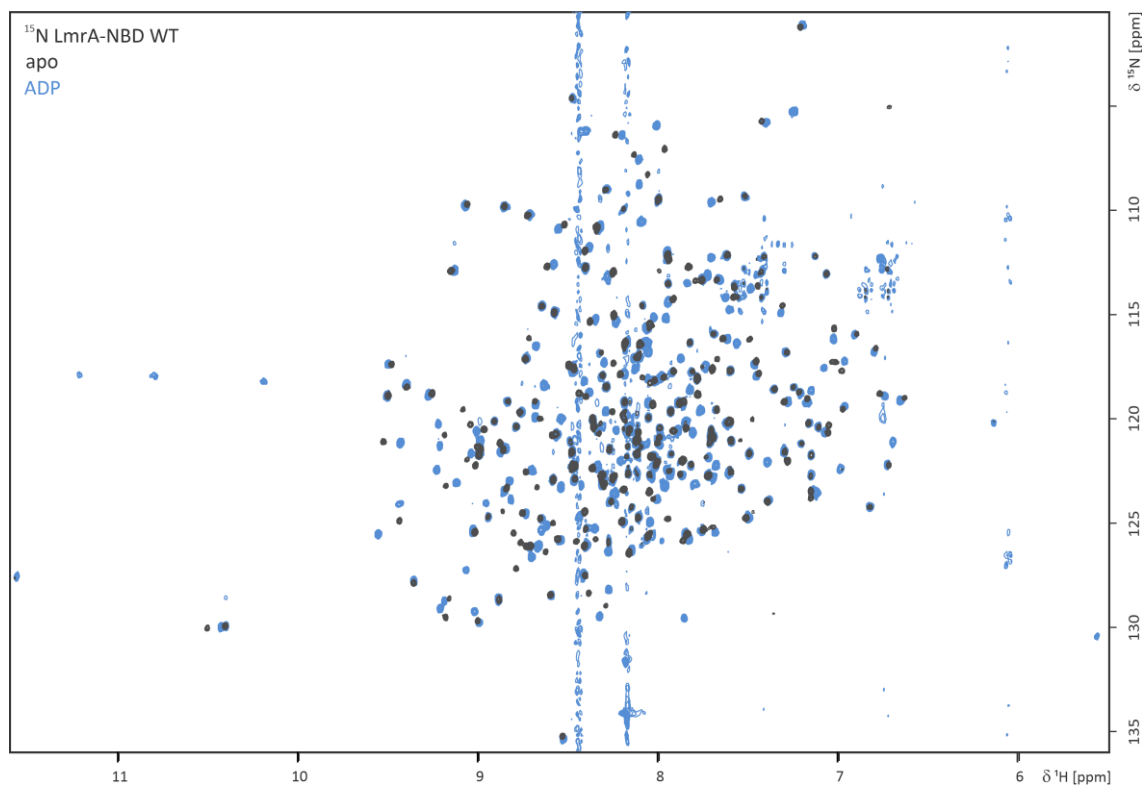
Appendix 24: ADP binding to the Q-loop mutant (Q430A) of LmrA-NBD

Overlay of ^1H - ^{15}N TROSY HSQC spectra of ^{15}N -labeled LmrA-NBD Q430A in the apo (dark green) and ADP-bound state (green-10 mM ADP).



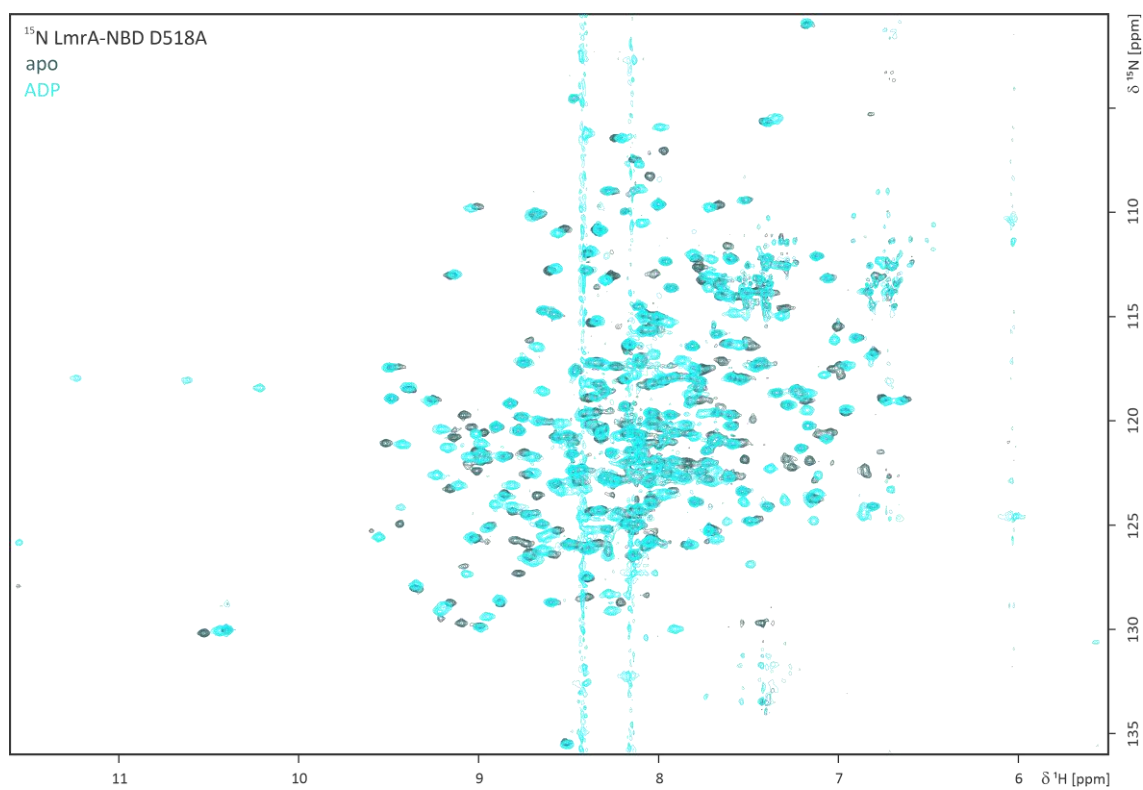
Appendix 25: ATP binding to the Q-loop mutant (Q430A) of LmrA-NBD

Overlay of ^1H - ^{15}N TROSY HSQC spectra of ^{15}N -labeled LmrA-NBD Q430A in the apo (dark green) and ATP-bound state (olive green-10 mM ATP).



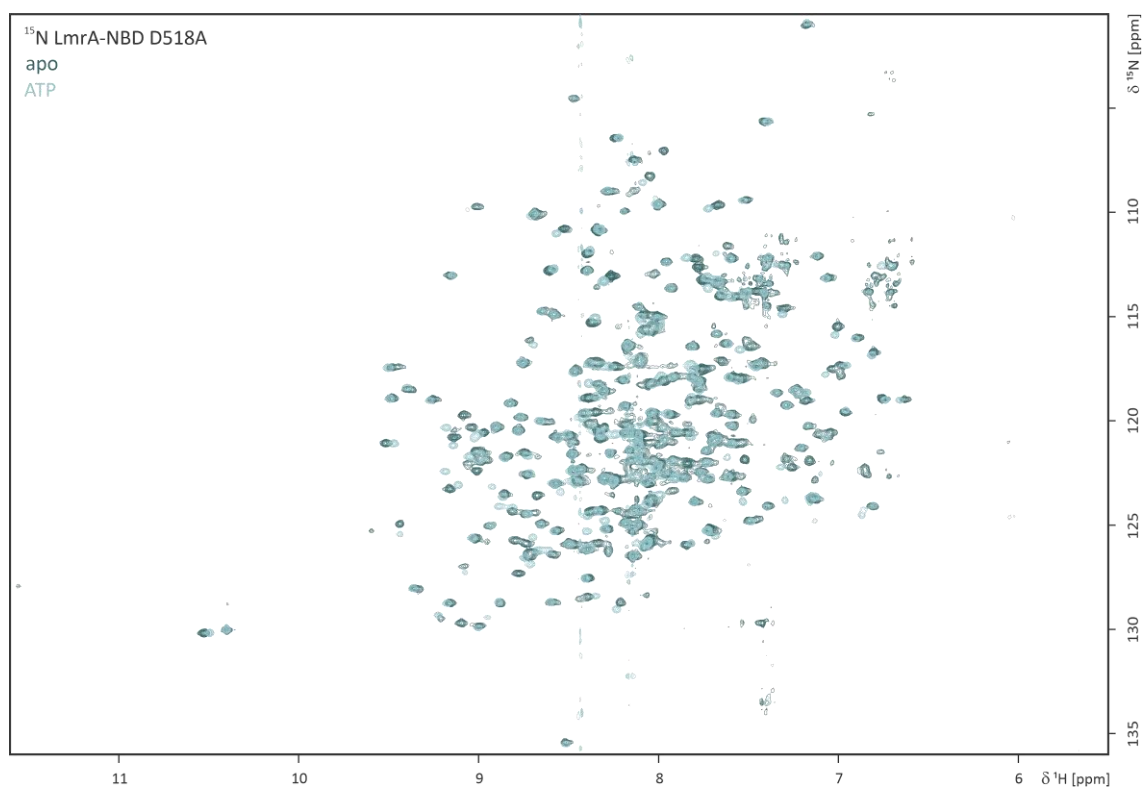
Appendix 26: Effect of ADP binding to the isolated ABC transporter NBD of LmrA

Overlay of ^1H - ^{15}N TROSY HSQC spectra of ^{15}N -labeled LmrA-NBD in the apo (black) and ADP-bound state (blue-10 mM ADP).



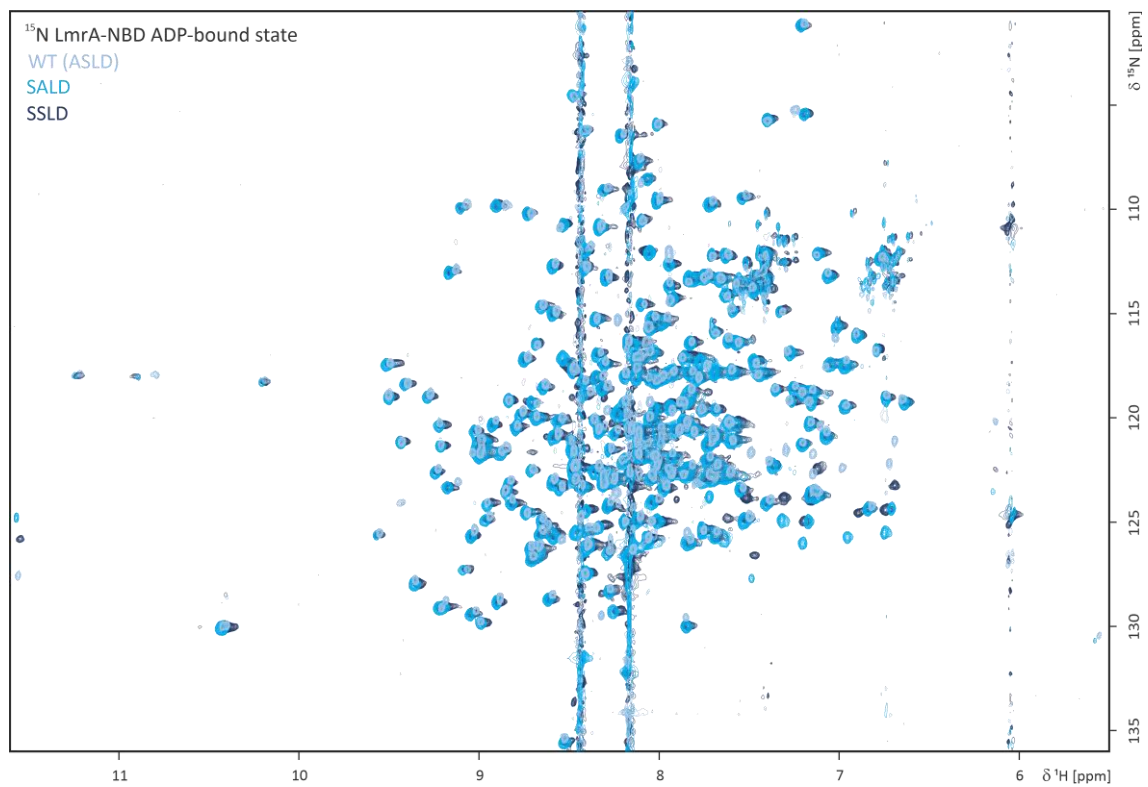
Appendix 27: ADP binding to the D-loop mutant (D518A) of LmrA-NBD

Overlay of ^1H - ^{15}N TROSY HSQC spectra of ^{15}N -labeled LmrA-NBD D518A in the apo (dark cyan) and ADP-bound state (cyan-10 mM ADP).



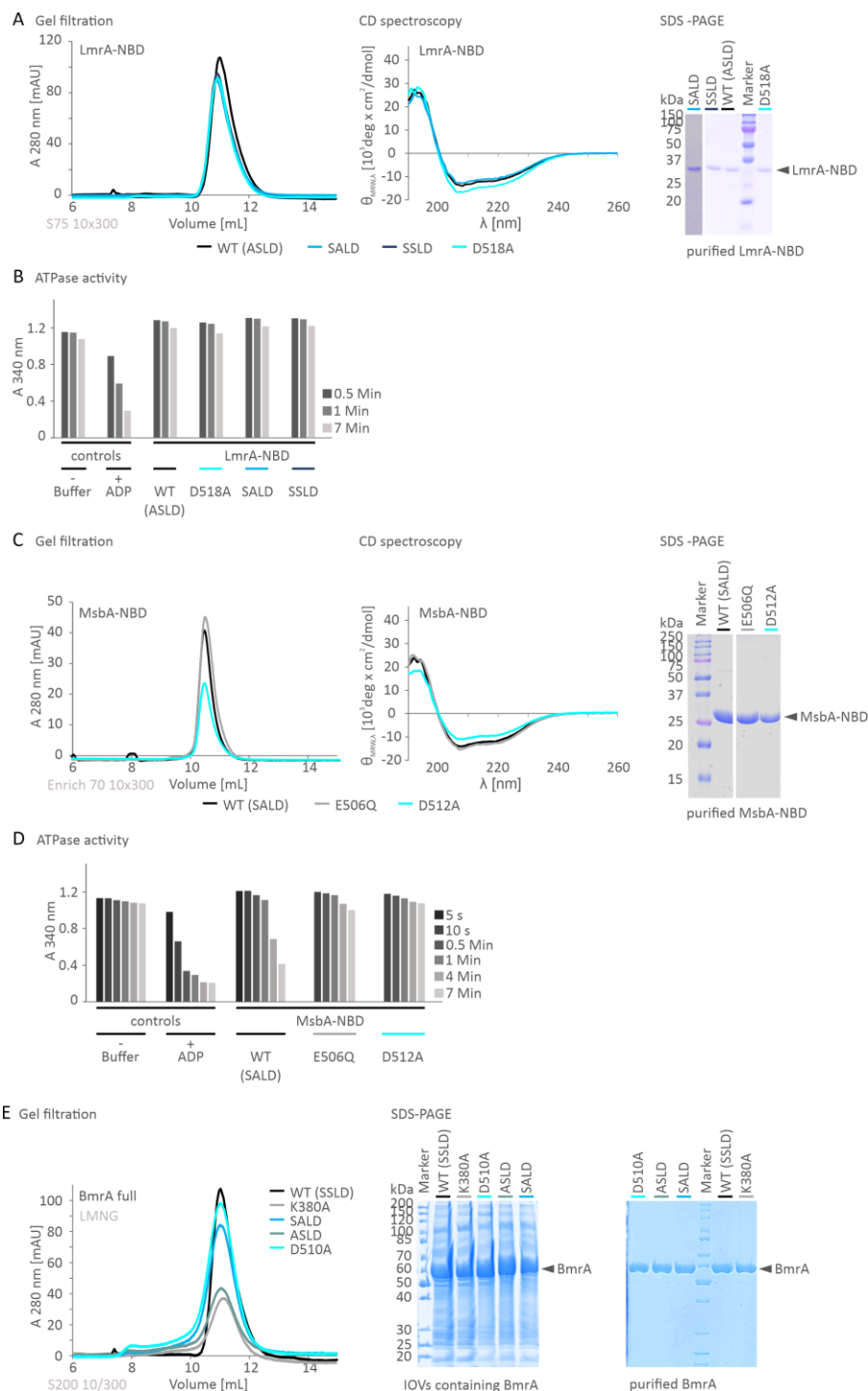
Appendix 28: ATP binding to the D-loop mutant (D518A) of LmrA-NBD

Overlay of ^1H - ^{15}N TROSY HSQC spectra of ^{15}N -labeled LmrA-NBD D518A in the apo (dark turquoise) and ATP-bound state (light turquoise-10 mM ATP).



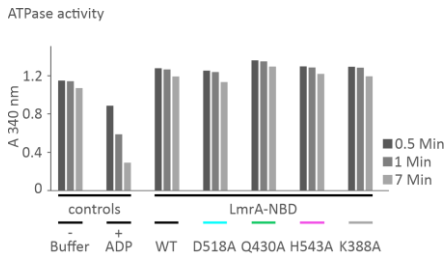
Appendix 29: Spectral differences between WT LmrA-NBD and its D-loop variants (SALD and SSLD) in the ADP-bound state (10 mM ADP)

Overlay of ^1H - ^{15}N TROSY HSQC spectra of ^{15}N -labeled LmrA-NBD WT (blue), SALD LmrA-NBD mutant (light blue) and SSLD LmrA-NBD mutant (dark blue).



Appendix 30: Characterization of WT NBDs and their D-loop variants

A) Structural integrity of WT LmrA-NBD and D-loop variants (SALD - light blue, SS LD - dark blue and D518A - cyan) analyzed by gel filtration, CD spectroscopy and SDS-PAGE (15% gel and stained with Coomassie blue). **B)** Basal ATPase activities of WT LmrA-NBD and variants (D518A - cyan). ATPase activities of LmrA-NBD (~400 μ g) in buffer (50 mM BisTris pH 6.5, 50 mM NaCl) were recorded at 37 °C. As LmrA-NBD shows no ATPase activity, ADP was added as a positive control and buffer was used as a negative control. **C)** Structural integrity of WT MsbA-NBD and variants (E506Q - gray and D512A - cyan) analyzed by gel filtration, CD spectroscopy and SDS-PAGE (15% gel). **D)** Basal ATPase activities of WT MsbA-NBD and variants (E506Q - gray and D512A - cyan). ATPase activities of MsbA-NBD (~400 μ g) in buffer (50 mM BisTris pH 6.5, 50 mM NaCl) were recorded at 37 °C. As positive control, ADP was used and as a negative control buffer without any protein. **E)** Gel filtration of WT full-length BmrA and variants (K380A - gray, SALD - light blue, ASLD - dark cyan and D510A - cyan) in LMNG. (left) SDS PAGE (12% gel) stained with Coomassie blue showing the overexpression of WT full-length BmrA and variants (K380A - gray, SALD - light blue, ASLD - dark cyan and D510A - cyan) in IOVs of *E. coli* C41 (DE3) cells. (middle) SDS-PAGE (12% gel) stained with Coomassie blue showing WT full-length BmrA and variants (K380A - gray, SALD - light blue, ASLD - dark cyan and D510A - cyan) after purification in LMNG. (right) IOV - Inside out vesicles. LMNG - Lauryl maltose neopentyl glycol.



Appendix 31: Basal ATPase activities of WT LmrA-NBD and variants (K388A-gray, D518A-cyan, Q430A-green and H543A-violet). ATPase activities of LmrA-NBD (~400 µg) in buffer (50 mM BisTris pH6.5, 50 mM NaCl) were recorded at 37 °C. As LmrA-NBD shows no ATPase activity, ADP was added as a positive control and buffer was used as a negative control.

3.3. Discovery of a novel communication hinge Linking NBS and TMD in multidrug ABC transporters

Sequences used for the sequence alignment in clustal omega (www.ebi.ac.uk/Tools/msa/clustalo/³¹⁰):

>sp|P97046|349-584_LmrA_*L. lactis*

MERGPQMANRIEGKAVDKTSIKHFVKLIRAAKPRYLFFVIGIVAGIIGTLIQLQVPMVQ
 PLINSFGHGVNGGKVALVIALYIGSAAVSAIAAIVLGIFGESVVKNLRTVWVKMIHLPV
 KYFDEVKTGEMSSRLANDTTQVKNLANSIPQAFTSILLVGSIIFMLQMQRWRLTAMII
 AVPIVMLIMFPIMTFGQKIGWTRQDSLAFQGIASESLSEIRLVKSSNAEKQASKKAEND
 VNALYKIGVKEAVFDGLMSPVMMMLMIFGLLAYGIYLISTGVMSLGTLLGMMMYLMN
 LIGVVPTVATFFTELAKASGSTGRTELLEDEEQEVLHQGDSLDEGKTLSAHHVDFAYDD
 SEQILHDISFEAQPNISIAFAGPSGGGKSTIFSLLEFYQPTAGEITIGGQPIDSVLEN
 WRSQIGFVSQDSAIMAGTIRENLTYGLEGNFTDEDLWQVLDLAFARFVENMPDQLNTEV
 GERGVKISGGQRQLAIARAFLRNPKILMLDEATASLSESESMVQRALDSLMKGRITLV
 IAHRLSTIVDADKIYFIEKGEITGSGKHNELVATHPLYAKYVSEQLTVGQ

>sp|O06967|BmrA_*B. subtilis*

MPTKKQKSKSKLKPFFALVRRNTNPSYGKLAFAALSVVTTLVSLLIPLLTQQLVDGFSMS
 NLSGTQIGLIALVFFVQAGLSAYATYALNYNGQKIISGLRELLWKKLIKLPVSYFDTNAS
 GETVSRVTNDTMVVKELITTHISGFITGIISVIGSLTILFIMNWKLTLLVLVVVPLAALI
 LVPIGRKMFSISRETQDETARFTGLLNQILPEIRLVKASNAEDVEYGRGKMGISLFLKLG
 VREAKVQSLVGPLISLVLMAALVAVIGYGGMQVSSGELTAGALVAFILYLFQIIMPMPGQI
 TFFFTQLQKSIGATERMIEILAEEDTDTGKQIENAHLPQLDRVDFGKPDQLILKEV
 SAVIEAGKVTAIVGPSGGGKTLFLKLLERFYSPTAGTIRLGDEPVDTSLESWREHIGYV
 SQESPLMSGTIRENICYGLERDVTDAEIEKAAEMAYALNFIKELPNQFDTEVGERGIMLS
 GGQRQRIAIARALLRNPSILMLDEATSSLDQSEKSVQQALEVLMEGRITIVIAHRLSTV
 VDADQLLFVEKGEITGRGTHHELMASHGLYRDFAEQQLKMNADLENKAG

>sp|P60752|MSBA_ *E. coli* (strain K12)

MHNDKDLSTWQTFRRLLWPTIAPFKAGLIVAGVALILNAASDTFMLSLLKPLDDGFGKTD
RSVLVWVWMLVIGLMILRGITSYVSSYICISWVSGKVVMTMRRRLFGHMMGMPVSFFDKQS
TGTLLSRITYDSEQVASSSSGALITVVREGASIIGLFIMMFYYSWQLSILIVLAPIVSI
AIRVVSKRFRNISKNMQNTMGQVTTSAEQMLKGHKEVLIFGGQEVETKRFDKVSNRMRLQ
GMKMSVASSISDPIIQLIASLALAFVLYAASFPSVMDSLTAGTITVVFSSMIALMRPLKS
LTVNAQFQRGMAACQTLFTILDSEQEKDEGKRVIERATGDVEFRNVFTTYPGRDVPALR
NINLKIPAGKTVALVGRSGSGKSTIASLITRFYDIDEGEILMDGHDREYTLASLRNQVA
LVSQNVHLFNDTVANNIAYARTEQYSREQIEEAARMAYAMDFINKMDNGLDVTIGENGVL
LSGGQRQRIAIARALLRDSPIILDEATSALDTESEAIQAALDELQKNRTSLVIAHRLS
TIEKADEIVVVEDGVIVERGTHNDLLEHRGVYAQLHKMQFGQ

>sp|Q9HUG8|356-592_MsbA_ *P. aeruginosa*_NBD

LEVRNLSFRYPGTDKQVLDDISFIAEPGQMIALVGRSGSGKSTLANLVPRFYQHNDGKIL
LDGVEVEDYRLRNLRRHIALVTQQVTLFNDSVANNIAYGDLGAPREEIERAAKANA
FIDNLPQGFDETEVGENGVLSSGGQRQRLAIARALLKDAPLLILDEATSALDTESE
ALDEVMKGRITLIVIAHRLSTIEKADLILVMDQGGQIVERGSHAELLAQNGHYARLHAM

>sp|Q99T13|340-575_Sav1866_ *S. aureus*_NBD

IDIDHVSFQYNDNEAPILKDINLSIEKGETVAFVGMSSGGKSTLINLIPRFYDVTSGQIL
IDGHNIKDFLTGSLRNQIGLVQQDNILFSDTVKENILLGRPTATDEEVVEAKMANAHDF
IMNLPQGYDTEVGERGVKLSGGQKQRLSIARIFLNNPPILILDEATSALDLESESIQEA
LDVLSKDRITLIVIAHRLSTITHADKIVVIENGHIVETGTHRELIKQGGAYEHLYSI

>tr|O32748|341-576_HorA_ *L. brevis*_NBD

LQMNHVVSFYDQHHPILSGVSFTEAPNSVIAFAGPSGGKSTISSLIERFYEPNEGSITI
GNTNITDIQLADWRQQIGLVGQDAAIMSGTIRYNLTYPGHFSDEQLWHVLEMAYATQF
VQKMPRGLDTEVGERGVKLSGGQKQRLAIARAFLRNPKILMLDEATASLDSESEMMVQKA
LDQLMANRITLIVIAHRLSTITNADEIYFIENGRVTGQGGTHQQLVKTTPLYREYVKN

>sp|P08716|468-703_HemB_ *E. coli*_NBD

ITFRNIRFRYKPDSPVILDNINLSIKQGEVIGIVGRSGSGKSTLTKLIQRFYIPENGQVL
IDGHDLALADPNWLRQVGVVLQDNVLLNRSIIDNISLANPGMSVEKVIYAAKLAGAHDF
ISELREGYNTIVGEEQGAGLSGGQRQRIAIARALVNNPKILIFDEATSALDYESEHVIMRN
MhkICKGRtViiiAhRLStVKNADRIIVMEK GKIVEQGKHkELLSEPEsLYsLYQ

>sp|Q03518|TAP1_ *Homo sapiens*

MAELLASAGSACSWDFPRAPPSFPPPAASRGGLGGTRSFRRPHRGAESPRPGRDRDGVVRP
MASSRCPAPRGCRCPLGASLAWLGTVLLLLADWVLLRTALPRIFSLLVPTALPLLRVWAV
GLSRWAVLWLGACGVLRA TVGSKSENAGA QGWLAALKPLAAALGLALPGLALFRELI SWG
APGSADSTRLLHWGSHPTAFVVS YAAALPAAALWHKLGSLWVPGGQGGSGNPVRRLLGCL
GSETRRLSLFLVLVSSLGEMAI PFFTGR L TDWILQDGSADTFTRNLTLMSILTIA SAV
LEFVGDGIYNN TMGHVHSHLQGEVFGAVLRQETEFFQ NQTGNIMSRVTE DTSTLSDSLS
ENLSLFLWYLV RGLCLLGIMLWGSVSLTMVTLITLPLLLPKKVGK WYQLLEVQVRESL
AKSSQVAIEALSAMPTVRSFANE EGEAQKFREKLQEIKTLNQKEAVAYAVNSWTT SISGM
LLKVGILYIGGQLVTSGAVSSGNLVTFVLYQMFTQAVEVLLSIYPRVQKAVGSSEKIFE
YLDRTPRCPPSGLLTPHL EGLVQFQDVSFAYPNRPDVLVLQGLTFTLRPGEVTALVGP N
GSGKSTVAALLQNLYQPTGGQLLLDGKPLQYEHRYLHRQVA AVGQEPQVFGRSLQENIA
YGLTQKPTMEEITAAAVKSGAHSFISGLPQGYDTEVDEAGS QLSGGQRQAVALARALIRK
PCVLILDDATSALDANSQLQVEQLLYESPERYSRSVLLITQHLSLVEQADHILFLEGGAI
REGGTHQQLM EKKGCYWAMVQAPADAPE

>sp|Q03519|468-686_TAP2_ *Homo sapiens*_NBD2

VKFQDVSFAYPNRPDRPV LKGLTFTLRPGEVTALVGPNGSGKSTVAALLQNLYQPTGGQV
LLDEKPI SQYEH CYLHSQVSVGQEPVLFSGSVRNNIAYGLQSCEDDKVMAAAQAAHADD
FIQEMEHGIYTDVGEKGSQ LAAGQKQRLAIARALVRDPRVLILDEATSALDVQCEQALQD
WNSRGDRTVLVIAHRLQTVQRAHQILVLQEGKLQKLAQL

>sp|P13569|423-646_CFTR_Homo sapiens_NBD1

NGDDSLFFSNFSLGTPVLKDINFKIERGQLLAVAGSTGAGKTSLLMVIMGELEPSEGKI
KHSGRISFCSQFSWIMPGTIKENIIFGVSYDEYRYSVIKACQLEEDISKFAEKDNIVLG
EGGITLSGGQRARISLARAVYKDADLYLLDSPFGYLDVLTEKEIFESCVCKLMANKTRIL
VTSKMEHLKKADKILILHEGSSYFYGTFSSELQNLQPDFSSKLMG

>sp|P13569|1210-1443_CFTR_Homo sapiens_NBD2

MTVKDLTAKYTEGGNAILENISFSISPGQRVGLLGRTGSGKSTLLSAFLRLLNTEGEIQI
DGVSWDSITLQQWRKAFGVIPQKVIFSGTFRKNLDPYEQWSDQEIWKVADEVGLRSVIE
QFPGLDFVLVDGGCVLSHGKQLMCLARVLSKAKILLDEPSAHLDPVITYQIIRRTLK
QAFADCTVILCEHRIEAMLECCQFLVIEENKVRQYDSIQKLLNERSLFRQAISP

>sp|P08183|392-628_P-gp_Homo sapiens_NBD1

LEFRNVHFSYPSRKEVKILKGLNLKVQSGQTVALVGNSSGCGKSTTVQLMQRLYDPTEGMV
SVDGQDIRTINVRFLREIIGVVVSQEPVLFATTIAENIRYGRENVMTDEIEKAVKEANAYD
FIMKLPKFDLTVGERGAQLSGGQKQRIAIARALVRNPKILLDEATSALDTESEAVVQV
ALDKARKGRTTIVIAHRLSTVRNADVIAGFDDGVIVEKGNHDELMKEKGIYFKLVTM

>1035-1273_P-gp_Homo sapiens-NBD2

VTFGEVVFNYPTRPDIPVLQGLSLEVKKGQTLALVGSSGCGKSTVVQLLERFYDPLAGKV
LLDGKEIKRLNVQWLRHLGIVSQEPILFDCSIAENIAYGDNSRVVSQEEIVRAAKEANI
HAFIESLPNKYSTKVGDKGTQLSGGQKQRIAIARALVRQPHILLDEATSALDTESEKVV
QEALDKAREGRTCIVIAHRLSTIQNADLIVVFQNGRVKEHGTHQQLLAQKGIYFSMVSV

>sp|P33527|644-868_MRP1_Homo sapiens_NBD1

ITVRNATFTWARSDPPTLNGITFSIPEGALVAVVGQVCGKSSLLSALLAEMDKVEGHVA
IKGSVAYVPQQAWIQNDSLRENILFGCQLEEPYRSVIQACALLPDLEILPSGDRTEIGE
KGVNLSGGQKQRVSLARAVYSNADIYLFDDPLSAVDAHVGKHIFENVIGPKGMLKNKTRI
LVTHSMSYLPQVDVIVMSGGKISEMGSYQELLARDGAFAEFLRT

>sp|P33527|1293-1527_MRP1_ *Homo sapiens*_NBD2

VEFRNYCLRYREDLDFVLRHINVTINGGEKVGIVGRTGAGKSSLTLGLFRINESAEGEII

IDGINIAKIGLHDLRFKITIIPQDPVLFSGSLRMNLDPFQYSDEEVWTSLELAHLKDFV

SALPDKLDHECAEGGENLSVGQRQLVCLARALLRRTKILVLDEATAAVDLETDDLIQSTI

RTQFEDCTVLTIAHRLNTIMDYTRVIVLDKGEIQEYGAPSDLLQQRGLFYMAKD

**ABC exporter type I _ (ABC transporter type IV fold) used for weblogo
(<http://weblogo.threepiusone.com/create.cgi>^{316,317}):**

>sp|P08716|468-703_HemB_*E. coli*_NBD

ITFRNIRFRYKPDSPVILDNINLSIKQGEVIGVGRSGSGKSTLTKLIQRFYIPENGQVL
IDGHDLALADPNWLRQVGVVLQDNVLLNRSIIDNISLANPGMSVEKVIYAAKLAGAHDF
ISELREGYNTIVGEEQGAGLSGGQRQRIAIARALVNNPKILFDEATSALDYESEHVIMRN
MHKICKGRTVIIIHRLSTVKNADRIIVMEKGKIVEQGHKHELLSEPELSYLYQ

>sp|P08183|392-628_P-gp_*Homo sapiens*_NBD1

LEFRNVHFSYPSRKEVKILKGLNLKVQSGQTVALVGNISGCGKSTTVQLMQRLYDPTGEMV
SVDGQDIRTINVRLREIIGVVSQEPVLFATTIAENIRYGRENTMDEIEKAVKEANAYD
FIMKLPKFDLTVGERGAQLSGGQKQRIAIARALVRNPKILLDEATSALDTESEAVVQV
ALDKARKGRTTIVIAHRLSTVRNADVIAGFDDGVIVEKGNHDELMKEKGIYFKLVMT

>sp|P21448|389-625_P-gp-Chinese hamster-NBD1

LEFKNIHFSYPSRKDVQILKGLNLKVQSGQTVALVGNISGCGKSTTVQLLQRLYDPTGEMV
SIDGQDIRTINVRYLREIIGVVSQEPVLFATTIAENIRYGRENTMDEIEKAVKEANAYD
FIMKLPKFDLTVGERGAQLSGGQKQRIAIARALVRNPKILLDEATSALDTESEAVVQA
ALDKAREGRTTIVIAHRLSTVRNADIAGFDGGVIVEQGNHEELMREKGIYFKLVMT

>sp|P21447|388-624_P-gp_*Mus musculus*_NBD1

LEFKNIHFSYPSRKEVQILKGLNLKVQSGQTVALVGNISGCGKSTTVQLMQRLYDPLDGMV
SIDGQDIRTINVRYLREIIGVVSQEPVLFATTIAENIRYGREDVTMDEIEKAVKEANAYD
FIMKLPKFDLTVGERGAQLSGGQKQRIAIARALVRNPKILLDEATSALDTESEAVVQA
ALDKAREGRTTIVIAHRLSTVRNADVIAGFDGGVIVEQGNHDELMREKGIYFKLVMT

>sp|P21449|391-627_P-gy_Chinese hamster_NBD1

LEFKNVHFSYPSRSGIKILKGLNLKVQSGQTVALVGKSGCGKSTTVQLLQRLYDPTGEMV
SIDGQDIRTINVRYLREIIGVVSQEPVLFATTIAENIRYGRENTMDEIEKAVKEANAYD
FIMKLPKFDLTVGERGAQLSGGQKQRIAIARALVRNPKILLDEATSALDTESEAVVQA
ALDKAREGRTTIVIAHRLSTVRNADVIAGFDGGVIVEQGNHEELMKEKGIYCRVMM

>sp|P06795|391-627_ABCB1b_ *Mus musculus*_NBD1

LEFKNVHFNYP SRSEVQILKGLNLKVKSGQTVALVGN SGC GKSTTVQLMQRLYDPLEGVV
SIDGQDIRTINVRYLREIIGVVSQEPVLFATTIAENIRYGRE DVTMDEIEKAVKEANAYD
FIMKLP HQFDTLVGERGAQLSGGQKQRIAIARALVRNPKILLLDEATSALDTESEAVVQA
ALDKAREGRTTIVIAHRLSTVRNADVIAGFDGGVIVEQGNHDELMREKGIYFKLVMT

>sp|P43245|391-627_ABCB1_ *Rattus norvegicus*_NBD1

LEFKNVYFNYP SRSEVKILKGLNLKVKSGQTVALVGN SGC GKSTTVQLLQRLYDPIEGEV
SIDGQDIRTINVRYLREIIGVVSQEPVLFATTIAENIRYGRE NVTMDEIEKAVKEANAYD
FIMKLP HKFDTLVGERGAQLSGGQKQRIAIARALVRNPKILLLDEATSALDTESEAVVQA
ALDKAREGRTTIVIAHRLSTVRNADVIAGFDGGVIVEQGNHEELMKEKGIYFKLVMT

>sp|P08183|1035-1273_P-gp_ *Homo sapiens*_NBD2

VTFGEVVFNYPTRPDIPVLQGLSLEVKKGQTLALVGS SGC GKSTVVQLLERFYDPLAGKV
LLDGKEIKRLNVQWLR AHLGIVSQEPILFDCSIAENIAYGDNSRVVSQEEIVRAAKEANI
HAFIESLPNKYSTKVGDKGTQLSGGQKQRIAIARALVRQPHILLLDEATSALDTESEKVV
QEALDKAREGRTCIVIAHRLSTIQNADLIVVFQNGRVKEHGTHQQLLAQKGIYFSMVSV

>sp|P21449|1033-1271_P-gy_ Chinese hamster_ NBD2

VKFNEVVFNYPTRPDIPVLQGLSLEVKKGQTLALVGS SGC GKSTVVQLLERFYDPMAGTV
FLDGKEIKQLNVQWLR AHLGIVSQEPILFDCSIAENIAYGDNSRVVSQDEIERAAKEANI
HQFIESLPDKYNTRVGDKGTQLSGGQKQRIAIARALVRQPHILLLDEATSALDTESEKVV
QEALDKAREGRTCIVIAHRLSTIQNADLIVVIQNGKVKEHGTHQQLLAQKGIYFSMVQA

>sp|P21448|1032-1270_P-gp_ Chinese hamster_ NBD2

VKFNEVVFNYPTRPDIPVLQGLNLEVKKGQTLALVGS SGC GKSTVVQLLERFYDPMAGTV
FLDGKEVNQLNVQWLR AHLGIVSQEPILFDCSIAENIAYGDNSRVVSQDEIERAAKEANI
HQFIESLPDKYNTRVGDKGTQLSGGQKQRIAIARALVRQPHILLLDEATSALDTESEKVV
QEALDKAREGRTCIVIAHRLSTIQNADLIVVIQNGKVKEHGTHQQLLAQKGIYFSMVSV

>sp|P21447|1031-1269_P-gp_Mus musculus_NBD2

VQFSGVVFNYPTRPSIPVLQGLSLEVKKGQTLALVGSSGCGKSTVVQLLERFYDPMAGSV
FLDGKEIKQLNVQWLRAQLGIVSQEPILFDCSIAENIAYGDNSRVVSYEEIVRAAKEANI
HQFIDSLPKYNTRVGDKGTQLSGGQKQRIAIARALVRQPHILLDEATSALDTESEKVV
QEALDKAREGRTCIVIAHRLSTIQNADLIVVIQNGKVKEHGTHQQLLAQKGIYFSMVSV

>sp|P06795|1033-1271_P-gp_Mus musculus_NBD2

VKFNGVQFNYPTRPNIPVLQGLSLEVKKGQTLALVGSSGCGKSTVVQLLERFYDPMAGSV
FLDGKEIKQLNVQWLRAHLGIVSQEPILFDCSIAENIAYGDNSRAVSHEEIVRAAKEANI
HQFIDSLPKYNTRVGDKGTQLSGGQKQRIAIARALVRQPHILLDEATSALDTESEKVV
QEALDKAREGRTCIVIAHRLSTIQNADLIVVIENGKVKEHGTHQQLLAQKGIYFSMVQA

>sp|P97046|349-584_LmrA_L. lactis_NBD

LSAHHVDFAYDDSEQILHDISFEAQPNIIAFAGPSGGGKSTIFSLLERFYQPTAGEITI
GGQPIDSVLENWRSQIGFVSQDSAIMAGTIRENLTYGLEGNFTDEDLWQVLDLAFARF
VENMPDQLNTEVGERGVKISGGQRQLAIARAFLRNPKILMLDEATASLSESESMVQRA
LDSLMLKGRITLVIAHRLSTIVDADKIYFIEKGEITGSGKHNELVATHPLYAKYVSE

>sp|Q9CHL8|349-584_LmrA_L. lactis subsp. lactis (strain IL1403)_NBD

LSARHVDFAVDSEQLRDISFEAQPNIIAFAGPSGGGKSTIFSLLERFYQPTAGEITI
DGQPIDNISLENWRSQIGFVSQDSAIMAGTIRENLTYGLEGDYDDEDLWQVLDLAFARF
VENMPDQLNTEVGERGVKISGGQRQLAIARAFLRNPKILMLDEATASLSESESMVQKA
LDSLMLKGRITLVIAHRLSTIVDADKIYFIEKGQITGSGKHNELVATHPLYAKYVSE

>sp|P60752|342-578_MsbA_E. coli_NBD

VEFRNVFTYTPGRDVPALRNINLKIPAGKTVALVGRSGSGKSTIASLITRFYDIDEGEIL
MDGHDLREYTLASLRNQVALVSQNVHLFNFTVANNIAYARTEQYSREQIEEAARMAYAMD
FINKMDNGLDVTIGENGVLLSGGQRQLAIARALLRDSPIILDEATSALDTESEAIQA
ALDELQKNRTSLVIAHRLSTIEKADEIVVVEDGVIVERGTHNDLLEHRGVYAQLHKM

>sp|Q9HUG8|356-592_MsbA_ *P. aeruginosa*_NBD

LEVRNLSFRYPGTDKQVLDDISFIAEPGQMIALVGRSGSGKSTLANLVPRFYQHNDGKIL
LDGVEVEDYRLRNLRRHIALVTQQVTLFNDSVANNIAYGDLGAPREEIERAAKANA
FIDNLPQGFDEVEGENGVLLSGGQRQLAIARALLKDAPLLILDEATSALDTERHIQA
ALDEVMKGRITLVIAHRLSTIEKADLILVMDQGGQIVERGSHAELLAQNGHYARLHAM

>sp|Q9KQW9|342-578_MsbA_ *V. cholerae* serotype-serO1_NBD

VDVKDVFTFYQGKEKPALSHVSFSIPQGKTVALVGRSGSGKSTIANLFRFYDVDSGSIC
LDGHDVDRDYKLTNLRHFALVSQNVHLFNNTIANNIAYAAEGEYTRQIEQAARQAHA
FIENMPQGLDVTIGENGTSLSGGQRQRVAIARALLRDAPVLILDEATSALDTERAIQA
ALDELQKNKTVLVIAHRLSTIEQADEILVDEGEIIRGRHADLLAQDGAYAQLHRI

>sp|Q5E0F2|342-578_MsbA_ *A. fischeri*_NBD

IKVDNVFTFYPTADGPALRNVSFDLPAGKTIALVGRSGSGKSTIANLFRFYDVDSGEIS
LDGDKIEDYRLPNLRKHFALVSQNVHLFNNTVANNIAYASEGKFRLEIEKAAELAYAS
FINKMDDGFDTMIGENGASLSGGQRQRRIARALLQNAPVLILDEATSALDTESEKAIQS
ALDELQKDKTVLVIAHRLSTIEDADQILVDEGEVVERGNHAELIAHDGAYAQLHRI

>sp|Q65U21|345-581_MsbA_ *M. succiniciproducens*_NBD

VSKDVSFTFYQKQDQPKHLSFDIPHGKTFALVGRSGSGKSTIANLVTRFYDINQGEIL
LDGVNVQDYTLNLRTHCSVVSQQVHLFNNTIANNIAYAAKDKYSREQIIAAKAAHA
FIEPLENGLDVTIGENGASLSGGQRQLAIARALLRDSPVLILDEATSALDTERAIQA
ALEELQKDRITLVIAHRLSTIEKADEILVIDHGEICERGSHEELLALNGAYKQLHKM

>sp|Q6LPK6|345-581_MsbA_ *P. profundum*_NBD

IQVKNVFTFYPTKDTPALRNVSFDLPAGKTLALVGRSGSGKSTIANLLTRFYDIDSGELI
LDGREVKDYQLSNLRDQVAVVSQNVHLFNNTIANNIAYASGDSFSRADIEKAAELAYAM
FIKGMKGLDVTMIGENGVSLSGGQRQLAIARALLRNAPVLILDEATSALDTERAIQS
ALEELQKDRITLVIAHRLSTIEGADQILVDDGEIIRGTHGELIKHDGAYAQLHRI

>sp|Q57R14|342-578_MsbA_*S. choleraesuis*_NBD

LEFRNVFTFTYPGREVPALRNINLKIPAGKTVALVGRSGSGKSTIASLITRFYDIDEGHIL
MDGHDLREYTLASLRNQVALVSQNVHLFNDTVANNIAYARTEEYSREQIEEAARMAYAMD
FINKMDNGLDTIIGENGVLLSGGQRQRIAIARALLRDSPILILDEATSALDTERAIQA
ALDELQKNRTSLVIAHRLSTIEQADEIVVVEDGIIVERGTHSELLAQHGYYAQLHKM

>sp|Q4QP14|347-583_MsbA_*H. influenzae*_NBD

LEFKNVSFAYQGKEELALNNISFSVPAGKTVALVGRSGSGKSTIANLVTRFYDIEQGEIL
LDGVNIQDYRLSNLRENCVVSSQQVHLFNDTIANNIAYAAQDKYSREEIIAAAKAAYALE
FIEKLPQGFDTVIGENGASLSGGQRQLAIARALLRNSPVLILDEATSALDTERAIQS
ALDELKKDRTVIVIAHRLSTIENADEILVIDHGEIRERGNHKALLEQNGAYKQLYSM

>sp|Q6D437|342-578_MsbA_*P. atrosepticum*_NBD

LEFRQVNFAYPARENLALKNINLHIVGKTVALVGRSGSGKSTIASLITRFYDIQSGEIL
LDGHDLREYRLSSLRNQVALVSQNVHLFNDTIANNIAYARNENYSREEIERAAKMAYAMD
FINKMEHGLDTVIGENGVMLSGGQRQRIAIARALLRDSPILILDEATSALDTERAIQA
ALDELQKDRTALVIAHRLSTIEKADEILVVEDGRIIERGNHTALLATNGAYAQLHRM

>sp|O06967|341-576_BmrA_*B. subtilis*_NBD

IQLDRVSFGYKPDQLILKEVSAVIEAGKVTAIVGPSGGGKTTLFKLLERFYSPTAGTIRL
GDEPVDTSLESWREHIGYVSQESPLMSGTIRENICYGLERDVTDAEIEKAAEMAYALNF
IKELPNQFDTEVGERGIMLSGGQRQRIAIARALLRNSPILMLDEATSSLDSSQSEKSVQQA
LEVLMEGRITVIAHRLSTVVDADQLLFVEKGEITGRGTHHELMASHGLYRDFAEQ

>sp|Q03518|563-802_TAP1_*Homo sapiens*_NBD1

VQFQDVSFAYPNRPDVLVLQGLTFTLRPGEVTALVGPNGSGKSTVAALLQNLQPTGGQL
LLDGKPLPQYEHRYLHRQVAAVGQEPQVFRSLQENIAYGLTQKPTMEEITAAVKSGAH
SFISGLPQGYDTEVDEAGSQLSGGQRQAVALARALIRKPCVLILDDATSALDANSQLQVE
QLLYESPERYSRSLITQHLSLVEQADHILFLEGGAIREGGTHQQLMEKKGICYWAMVQA

>sp|P36370|480-719_TAP1_*Rattus norvegicus*_NBD1

VKFQDVSFAYPNHPNVQVLQGLTFTLYPGKVTALVGPNGSGKSTVAALLQNLQPTGGKV
LLDGEPLVQYDHHYLHTQVAAVGQEPLLFGRSFRENIAYGLTRTPTMEEITAVAMESGAH
DFISGFPOGYDTEVGETGNQLSGGQRQAVALARALIRKPRLLILDDATSALDAGNQLRVQ
RLLYESPEWASRTVLLITQQLSLAERAAHILFLKEGSVCEQGTHLQLMERGGCYRSMVEA

>sp|P36370|480-719_TAP2_*Rattus norvegicus*_NBD2

VKFQDVSFAYPNHPNVQVLQGLTFTLYPGKVTALVGPNGSGKSTVAALLQNLQPTGGKV
LLDGEPLVQYDHHYLHTQVAAVGQEPLLFGRSFRENIAYGLTRTPTMEEITAVAMESGAH
DFISGFPOGYDTEVGETGNQLSGGQRQAVALARALIRKPRLLILDDATSALDAGNQLRVQ
RLLYESPEWASRTVLLITQQLSLAERAAHILFLKEGSVCEQGTHLQLMERGGCYRSMVEA

>sp|Q03519|468-686_TAP2_*Homo sapiens*_NBD2

VKFQDVSFAYPNRDRPVLKGLTFTLRPGEVTALVGPNGSGKSTVAALLQNLQPTGGQV
LLDEKPISQYEHCHLSQVSVGQEPVLFSGSVRNNIAYGLQSCEDDKVMAAAQAAHADD
FIQEMEHGIYTDVGEKGSQLAAGQKQRLAIARALVRDPRVLILDEATSALDVQCEQALQD
WNSRGDRTVLVIAHRLQTVQRAHQILVLQEGKLQKLAQL

>sp|P13569|423-646_CFTR_*Homo sapiens*_NBD1

NGDDSLFFSNFLLGTPVLKDINFKIERGQLLAVAGSTGAGKTSLLMVIMGELEPSEGKI
KHSGRISFCSQFSWIMPGTIKENIIFGVSYDEYRYSVIKACQLEEDISKFAEKDNIVLG
EGGITLSGGQRARISLARAVYKDADLYLLDSPFGYLDVLTEKEIFESCCKLMANKTRIL
VTSKMEHLKADKILILHEGSSYFYGTFSSELQNLQPDFSSKLMG

>sp|P13569|1210-1443_CFTR_*Homo sapiens*_NBD2

MTVKDLTAKYTEGGNAILENISFSISPGQRVGLLGRGTSGKSTLLSAFLRLNTEGEIQI
DGVSWDSITLQQWRKAFGVIPQKVFIFSGTFRKNLDPYEQWSDQEIWKVADEVGLRSVIE
QFPGKLDVFLVDGGCVLSHGKQLMCLARSVLSKAKILLDEPSAHLDPVTYQIIRRTLK
QAFADCTVILCEHRIEAMLECCQFLVIEENKVRQYDSIQKLLNERSLFRQAISP

>sp|P33527|644-868_MRP1_ *Homo sapiens*_NBD1

ITVRNATFTWARSDPPTLNGITFSIPEGALVAVVGQVCGKSSLLSALLAEMDKVEGHVA
IKGSVAYVPQQAWIQNDSLRENILFGCQLEEPYYRSVIQACALLPDLEILPSGDRTEIGE
KGVNLSGGQKQRVSLARAVYSNADIYLFDDPLSAVDAHVGKHIFENVIGPKGMLKNKTRI
LVTHSMSYLPQVDVIVMSGGKISEMGSYQELLARDGAFAEFLRT

>sp|P33527|1293-1527_MRP1_ *Homo sapiens*_NBD2

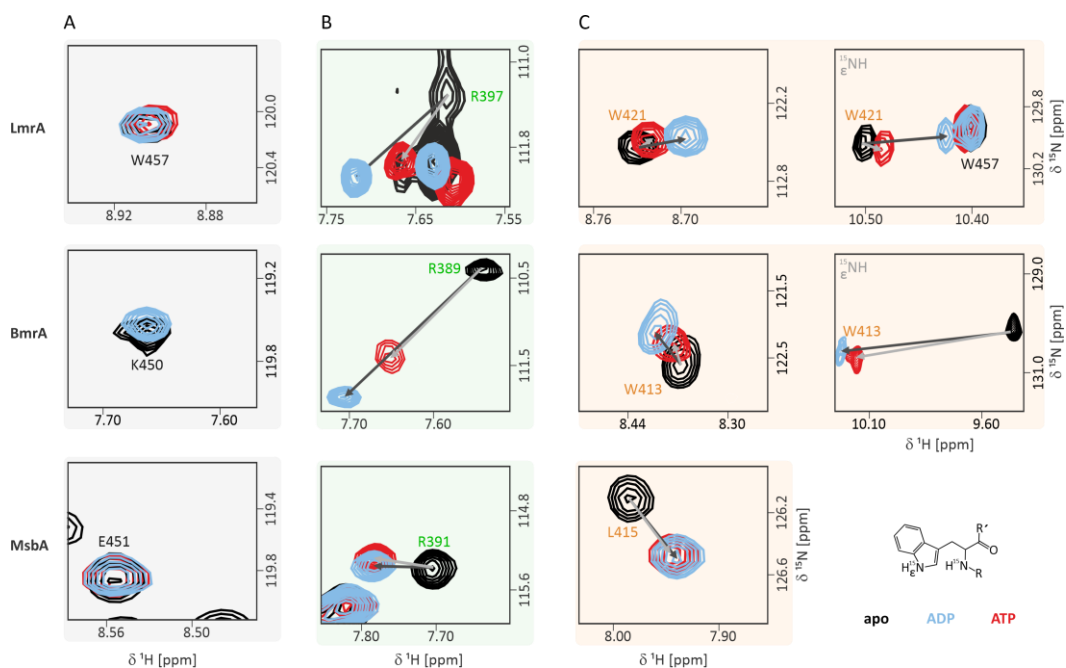
VEFRNYCLRYREDLDFVLRHINVTINGGEKVGIVGRTGAGKSSLTGLFRINESAEGEII
IDGINIAKIGLHDLRFKTIIPQDPVLFSGSLRMNLDPFSQYSDEEVWTSLELAHLKDFV
SALPKLDHECAEGGENLSVGQRQLVCLARALLRKTILVLDEATAAVDLETDDLIQSTI
RTQFEDCTVLTIAHRLNTIMDYTRVIVLDKGEIQEYGAPSDLLQQRGLFY SMAK

>sp|Q99T13|340-575_Sav1866_ *S. aureus*_NBD

IDIDHVSFQYNDNEAPILKDINLSIEKGETVAFVGMSSGGKSTLINLIPRFYDVTSGQIL
IDGHNIKDFLTGSLRNQIGLVQQDNILFSDTVKENILLGRPTATDEEVVEAAKMANAHDF
IMNLPQGYDTEVGERGVKLSGGQKQRLSIARIFLNNPPILILDEATSALDLESESIIQEA
LDVLSKDRRTLIVAHRLSTITHADKIVVIENGHIVETGTHRELIAKQGAYEHLYSI

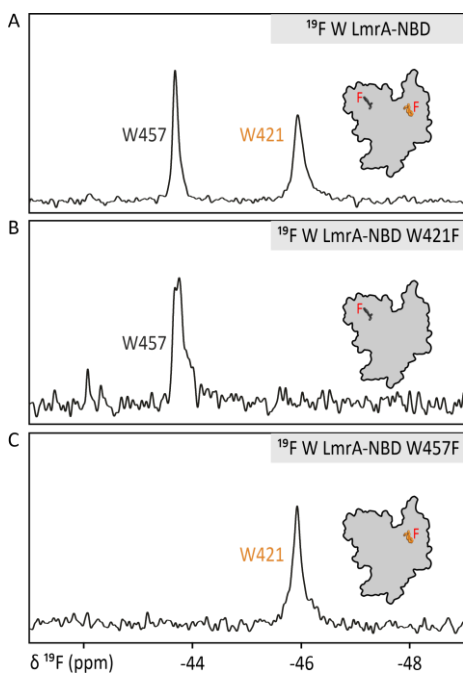
>tr|O32748|341-576_HorA_ *L. brevis*_NBD

LQMNHVSFSYDQHHPILSGVSFTAEPNSVIAFAGPSGGGKSTISSLIERFYEPNEGSITI
GNTNITDIQLADWRQQIGLVGQDAAIMSGTIRYNLTYPGHFSDEQLWHVLEMAYATQF
VQKMPRGLDTEVGERGVKVSQQQRQLAIARAFLRNPKILMLDEATASLDSESEMMVQKA
LDQLMANRTTLVIAHRLSTITNADEIYFIENGRVTGQGTHQQLVKTTPLYREYVKN



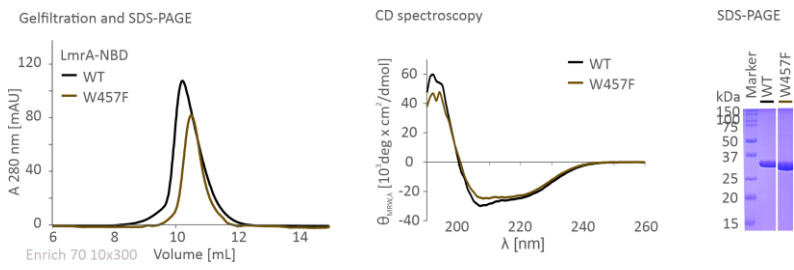
Appendix 32: Identification of an allosterically affected region within the NBD with ^{15}N solution NMR

A) Solution NMR ^1H - ^{15}N TROSY HSQC resonances of LmrA-NBD, BmrA-NBD and MsbA-NBD for a control residue (gray) unaffected by nucleotide addition. The ATP-bound state was not recorded yet for the residue K450 (BmrA) and hence no peak is shown. **B)** Effects of nucleotide binding to the conserved arginine residue (green) in LmrA, BmrA and MsbA. **C)** Effects of nucleotide binding on the residue structurally opposing the conserved arginine residue, W421 in LmrA, W413 in BmrA and L415 in MsbA. For the two Trp residues, both backbone and sidechain amide chemical shift changes are shown. In the ATP-bound state no NH resonance was observed for the W413 sidechain. Blue - 10 mM ADP. Red - 10 mM ATP (Figure 39).

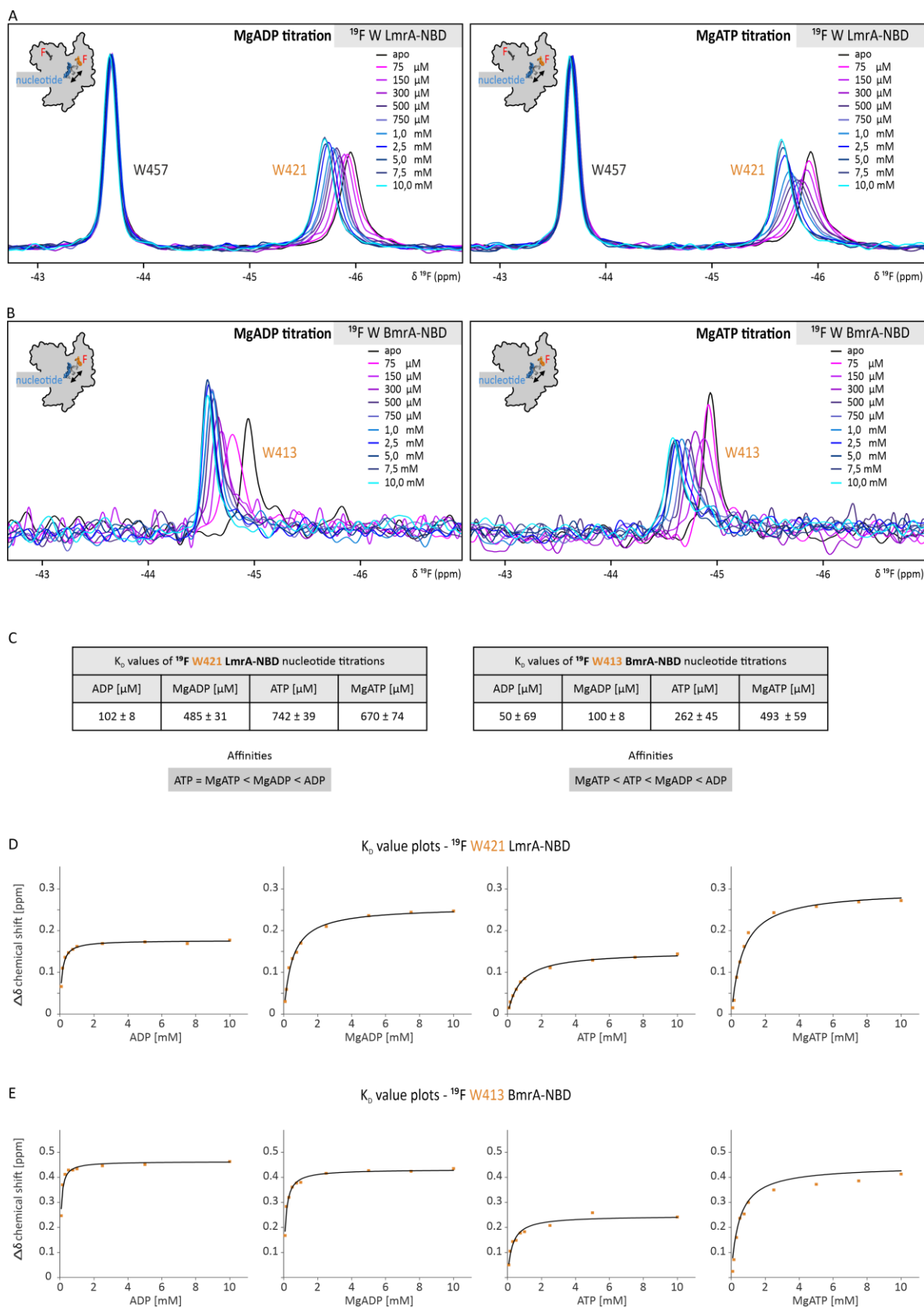


Appendix 33: Assignment of 5- ^{19}F -Trp LmrA-NBD WT spectra

A) ^{19}F NMR spectrum of 5- ^{19}F -Trp-labeled LmrA-NBD WT. **B)** ^{19}F NMR spectrum of 5- ^{19}F -Trp-labeled LmrA-NBD W421F. **C)** ^{19}F NMR spectrum of 5- ^{19}F -Trp-labeled LmrA-NBD W457F. Spectra were recorded in buffer 50 mM BisTris pH 6.5, 50 mM NaCl at 298 K and referenced to BTFA (Material and methods 12.9. 1D ^{19}F - NMR).

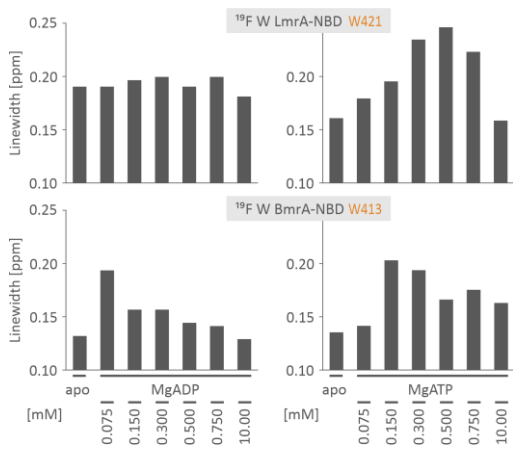
**Appendix 34: Structural integrity of LmrA-NBD constructs**

Comparison of LmrA-NBD W457F (brown) and WT (black) by SEC, CD spectroscopy and SDS-PAGE.



Appendix 35: ¹⁹F NMR on LmrA and BmrA confirms involvement of W421/W413 in nucleotide “sensing”⁴⁰⁸

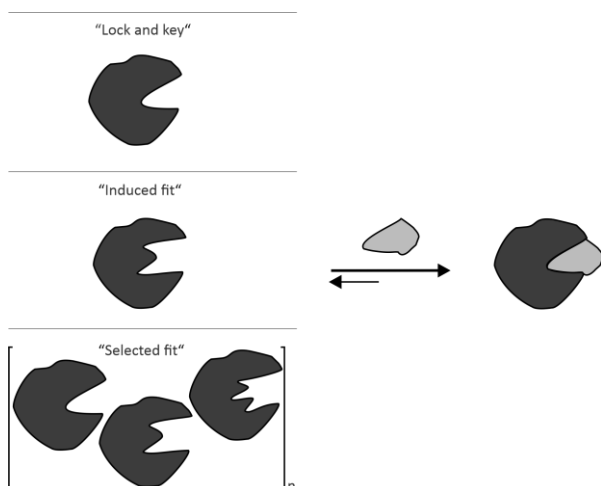
A) ¹⁹F solution NMR spectra of 5-¹⁹F-Trp-labeled LmrA-NBD with two native tryptophan residues (W421 and W457). Titration with MgADP or MgATP shows that only W421 “senses” nucleotide binding. **B)** ¹⁹F solution NMR spectra of 5-¹⁹F-Trp-labeled BmrA-NBD with one native tryptophan residue (W413). Its position corresponds to W421 from LmrA-NBD. Titration with MgADP or MgATP shows that residue W413 “senses” nucleotide binding. Walker A helix is represented in gray and the within the schematic NBDs (A, B). **C, D)** Based on the chemical shift perturbations for residue W421 (LmrA-NBD) and W413 (BmrA-NBD) in A and B, the respective K_D values were determined.



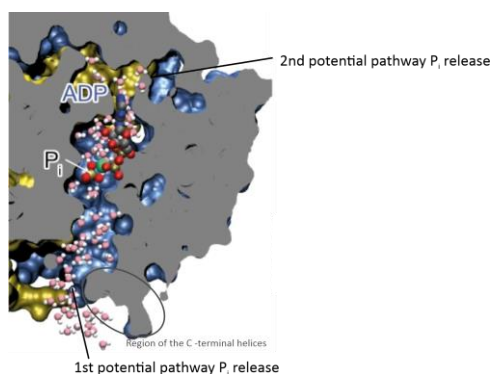
Appendix 36: Linewidth analysis of the ^{19}F resonances of the 5- ^{19}F -Trp LmrA-NBD W421 and 5- ^{19}F -Trp BmrA-NBD W413 in the apo state, MgADP titration and MgATP titration, respectively.

4. CHAPTER IV: DISCUSSION

4.1. Differences in NBD dynamics of the ABC transporter LmrA induced by nucleotide binding

**Appendix 37: Models of protein-ligand (un)binding**

"Lock and key" model⁴⁰⁹: Both protein and ligand are rigid and their binding interfaces are complementary. Simplest form of the "Induced fit" model⁴¹⁰: A conformational change is induced at the ligand binding center of a protein by binding the ligand. In the presence of the ligand the binding center, with one conformation in the apo state, adapts to the ligand, leading to another conformation of the binding center. "Selective fit" model⁴⁰⁹: The binding site is inherently flexible and adopts multiple conformations in the apo state. When the ligand binds the preferred conformation, favorable interactions between ligand and protein are stabilized.



Appendix 38: Molecular dynamic snapshot of the heterodimeric ABC transporter, TmrAB in the outward-facing occluded conformation with MgATP-V_i (PDB ID: 6RAK) from Hoffmann et al., representing two potential pathways to release inorganic phosphate after ATP hydrolysis (modified from Hofmann et al., 2019²⁰²)

One pathway through hydrated channels from the nucleotide binding site towards the C-terminal helices (1) and another towards the coupling helices (2).

5. LIST OF FIGURES

| | |
|--|-----|
| Figure 1: Classification of the seven drug efflux pumps involved in bacterial multidrug resistance | 3 |
| Figure 2: Core domain organization of ABC transporters | 4 |
| Figure 3: Different proposals for the classification of ABC transporters based on their architecture and function | 5 |
| Figure 4: Proposal for a classification of ABC transporter based on the TMD folds | 6 |
| Figure 5: Inter- and intradomain organization of ABC transporter nucleotide binding domains | 12 |
| Figure 6: Cartoon summarizing the two main ABC transporter-catalytic cycle models | 19 |
| Figure 7: Potential transport mechanisms for type I ABC exporters | 23 |
| Figure 8: Protein dynamics by PET-FCS measurements | 56 |
| Figure 9: NH correlations seen in a ^1H - ^{15}N HSQC spectra | 68 |
| Figure 10: Protein characterization/ Structural integrity of LmrA-NBD WT (~28.9 kDa), MsbA-NBD WT (~29.1 kDa) and BmrA-NBD WT (~28.6 kDa) | 72 |
| Figure 11: Affinity of ADP and ATP for ^{15}N -LmrA-NBD determined by ^1H - ^{15}N TROSY HSQC NMR titration experiments | 73 |
| Figure 12: Backbone chemical shift assignment of LmrA-NBD in the ADP-bound state | 74 |
| Figure 13: 2D ^1H - ^{15}N TROSY HSQC spectrum of MsbA-NBD | 75 |
| Figure 14: Backbone chemical shift assignment of BmrA-NBD in the ADP-bound state | 76 |
| Figure 15: Effects of ADP binding to isolated ABC transporter NBDs | 77 |
| Figure 16: Conserved motifs sense nucleotide binding and can distinguish between ATP and ADP | 78 |
| Figure 17: Effect of nucleotide binding to the isolated ABC transporter LmrA-NBD | 80 |
| Figure 18: H/D exchange for LmrA-NBD in the apo and ADP-bound state | 83 |
| Figure 19: Backbone dynamics of LmrA-NBD in the apo and ADP-bound state determined via $\{^1\text{H}\}$, ^{15}N hetNOE measurements | 86 |
| Figure 20: Differences in backbone dynamics on the ps – ns timescale of LmrA-NBD WT between apo and ADP-bound states | 88 |
| Figure 21: PET-FCS reporter positions within the NBDs of LmrA, MsbA and BmrA | 89 |
| Figure 22: PET-FCS analysis of nucleotide binding within the NBD of MsbA | 91 |
| Figure 23: Characterization of WT LmrA-NBD and its variants | 93 |
| Figure 24: Spectral differences between WT LmrA-NBD and the the D-loop mutant (D518) in the ADP-bound state (10 mM ADP) | 93 |
| Figure 25: Spectral differences between WT LmrA-NBD and the the Q-loop mutant (Q430A) in the ADP-bound state (10 mM ADP) | 94 |
| Figure 26: Spectral differences between WT LmrA-NBD and the the H-loop mutant (H543A) in the ADP-bound state (10 mM ADP) | 94 |
| Figure 27: Nucleotide binding ability and affinity is maintained upon mutating the D-, Q- or H-loop residues in LmrA-NBD | 96 |
| Figure 28: Chemical shift differences between LmrA-NBD WT and the D-loop (D518A), Q-loop (Q430A) or H-loop (H543A) mutants in the ADP-bound state | 98 |
| Figure 29: Nucleotide binding and mutation of conserved motifs affect residues within the coupling helix groove | 100 |
| Figure 30: Crosstalk between the conserved D-, Q- and H-loop motifs | 101 |
| Figure 31: Effect of nucleotide addition to the NH resonances of residues within the conserved D-loop and Q-loop motifs | 102 |
| Figure 32: Backbone dynamics of LmrA-NBD WT and the D-, Q- and H-loop variants in the ADP-bound state | 103 |

| | |
|---|-----|
| Figure 33: Backbone dynamics of LmrA-NBD WT and the D-, Q- and H-loop variants in the ADP-bound state | 105 |
| Figure 34: Differences in backbone dynamics between LmrA-NBD WT and its D-, Q- or H-loop mutant | 108 |
| Figure 35: Differences in backbone dynamics caused by mutations in D-, Q- or H-loop | 109 |
| Figure 36: Structural integrity of the D-loop variants of LmrA-NBD, MsbA-NBD and full-length BmrA..... | 110 |
| Figure 37: Molecular crosstalk within the NBD is connected to the D-loop | 112 |
| Figure 38: Sequence alignment and sequence logo of the NBDs of different type I ABC exporters..... | 114 |
| Figure 39: 2D ¹ H- ¹⁵ N TROSY HSQC solution NMR experiments reveal “sensing” of nucleotide binding for residues at the C-terminal end of the Walker A motif helix | 115 |
| Figure 40: ¹⁹ F NMR on LmrA and BmrA confirms involvement of W421/W413 in nucleotide sensing..... | 116 |
| Figure 41: Characterization of full-length BmrA WT and “communication hinge” mutants | 118 |
| Figure 42: Characterization of LmrA-NBD WT and its mutations in the “communication hinge” .. | 119 |
| Figure 43: Role of conserved residue R389 in the NBD of BmrA on ATPase activity and substrate transport..... | 120 |
| Figure 44: Schematic illustration of NBD dynamics obtained from techniques used in this thesis ... for LmrA-NBD and MsbA-NBD, focusing on relative motions of α-helical and catalytic subdomain | 122 |
| Figure 45: Schematic representation of relative movements of the catalytic and the α-helical NBD subdomains. | 124 |
| Figure 46: Residues in the coupling helix groove affected by nucleotide binding..... | 126 |
| Figure 47: C-terminal helices of NBDs of type I ABC exporters (type IV fold)..... | 131 |
| Figure 48: C-terminal helices and C-terminal extensions of NBDs of ABC transporters..... | 133 |
| Figure 49: Coupling helix groove residues affected by mutation of D-, Q- or H-loop in the NBD of LmrA | 138 |
| Figure 50: Potential communication pathways from the nucleotide binding site (NBS) to the TMDs in type I ABC exporters..... | 145 |
| Figure 51: Polar interactions of a tyrosine at the C-terminus of the Walker A helix may mediate allosteric crosstalk within type I ABC exporter (type IV fold) | 148 |
| Figure 52: Potential connection between the C-terminal end of the Walker A helix and the opposing α-helix with the TMD across different ABC transporter architectures .. | 150 |

| | |
|---|-----|
| Appendix 1: Sequence alignment (www.ebi.ac.uk/Tools/msa/clustalo/) of type I ABC exporters (type IV according to a new classification system), LmrA from <i>L. lactis</i> , BmrA from <i>B. subtilis</i> , MsbA from <i>E. coli</i> and human P-glycoprotein (P-gp/MDR1/ABCB1) | 153 |
| Appendix 2: Crystal structure of the NBD of Sav1866 (PDB ID: 2HYD), highlighting two subdomains and the structural diverse region | 154 |
| Appendix 3: Bacterial expression vectors pET11a and pET23a+ | 160 |
| Appendix 4: DNA and protein sequence of LmrA-NBD WT with N-term HisTEV tag (Genscript) .. | 160 |
| Appendix 5: DNA and protein sequence of LmrA-NBD WT with N-term HisTEV tag (Entelechon) | 161 |
| Appendix 6: DNA and protein sequence of MsbA-NBD WT cloned from <i>E. coli</i> BL21-Gold (DE3) with N-terminal HisTEV tag..... | 162 |
| Appendix 7: DNA and protein sequence of full-length MsbA WT cloned from of <i>E. coli</i> BL21-Gold (DE3) with N-terminal HisTEV tag..... | 163 |
| Appendix 8: DNA and protein sequence of full-length BmrA WT with C-terminal His ₆ tag..... | 164 |
| Appendix 9: DNA and protein sequence of BmrA-NBD WT with N-terminal HisTEV tag..... | 165 |
| Appendix 10: DNA and protein sequence of full-length BmrA with N-terminal HisTEV tag..... | 166 |
| Appendix 11: Effect of ADP binding to the isolated ABC transporter NBD of MsbA..... | 167 |
| Appendix 12: Effect of ADP binding to the isolated ABC transporter NBD of BmrA..... | 167 |
| Appendix 13: Effect of ATP binding to the isolated ABC transporter NBD of LmrA..... | 169 |
| Appendix 14: Effect of MgADP binding to the isolated ABC transporter NBD of LmrA..... | 169 |
| Appendix 15: Effect of MgATP binding to the isolated ABC transporter NBD of LmrA..... | 170 |
| Appendix 16: Effect of nucleotide binding with magnesium to the isolated ABC transporter LmrA-NBD | 171 |
| Appendix 17: Bar graph representation of the amino acid residue numbers (total number of peaks) of ¹ H- ¹⁵ N TROSY HSQC spectra of WT LmrA-NBD, MsbA-NBD and BmrA-NBD with and without ligand..... | 172 |
| Appendix 18: Characterization of protein constructs used in PET-FCS..... | 172 |
| Appendix 19: Spectral differences between WT LmrA-NBD and the Walker A motif mutant (K388A) in the ADP-bound state (10 mM ADP) | 173 |
| Appendix 20: Spectral differences between LmrA-NBD Walker A motif mutant (K388A)..... in the apo, ADP-bound state (10 mM ADP) and ATP-bound state (10 mM ATP) ... | 173 |
| Appendix 21: ADP binding to the H-loop mutant (H543A) of LmrA-NBD..... | 174 |
| Appendix 22: ATP binding to the H-loop mutant (H543A) of LmrA-NBD | 174 |
| Appendix 23: NH resonances of the D-loop residues A515-L517 “sense” nucleotide binding | 175 |
| Appendix 24: ADP binding to the Q-loop mutant (Q430A) of LmrA-NBD | 175 |
| Appendix 25: ATP binding to the Q-loop mutant (Q430A) of LmrA-NBD | 176 |
| Appendix 26: Effect of ADP binding to the isolated ABC transporter NBD of LmrA | 176 |
| Appendix 27: ADP binding to the D-loop mutant (D518A) of LmrA-NBD..... | 177 |
| Appendix 28: ATP binding to the D-loop mutant (D518A) of LmrA-NBD | 177 |
| Appendix 29: Spectral differences between WT LmrA-NBD and its D-loop variants (SALD and SSLD) in the ADP-bound state (10 mM ADP) | 178 |
| Appendix 30: Characterization of WT NBDs and their D-loop variants | 179 |
| Appendix 31: Basal ATPase activities of WT LmrA-NBD and variants (K388A-gray, D518A-cyan, Q430A-green and H543A-violet) | 180 |
| Appendix 32: Identification of an allosterically affected region within the NBD with ¹⁵ N solution NMR..... | 193 |
| Appendix 33: Assignment of 5- ¹⁹ F-Trp LmrA-NBD WT spectra | 193 |
| Appendix 34: Structural integrity of LmrA-NBD constructs | 194 |
| Appendix 35: ¹⁹ F NMR on LmrA and BmrA confirms involvement of W421/W413 in nucleotide “sensing” | 195 |

| | |
|--|------------|
| Appendix 36: Linewidth analysis of the ^{19}F resonances of the 5-^{19}F-Trp LmrA-NBD W421 and 5-^{19}F-Trp BmrA-NBD W413 in the apo state, MgADP titration and MgATP titration, respectively..... | 196 |
| Appendix 37: Models of protein-ligand (un)binding..... | 197 |
| Appendix 38: Molecular dynamic snapshot of the heterodimeric ABC transporter, TmrAB in the outward-facing occluded conformation with MgATP-V_i (PDB ID: 6RAK) from Hoffmann et al., representing two potential pathways to release inorganic phosphate after ATP hydrolysis | 197 |

6. LIST OF TABLES

| | |
|--|----|
| Table 1: Human ABC transporters involved in lipid transport | 8 |
| Table 2: Examples of drugs transported by LmrA, BmrA, MsbA and P-gp | 10 |
| Table 3: Consensus sequence, subdomain localization and function of conserved motifs in the NBDs listed according to their occurrence in the subdomains/ interface between the subdomains (β-subdomain, RecA-like subdomain and α-helical subdomain) | 13 |
| Table 4: Models of the catalytic cycle of an ABC transporter in four steps | 20 |
| Table 5: Chemicals from other suppliers than Carl Roth GmbH & Co KG, Karlsruhe | 33 |
| Table 6: Chemicals used for isotope labeling of proteins for NMR studies | 33 |
| Table 7: List of E. coli strains used for protein expression and cloning | 34 |
| Table 8: Oligonucleotides/ Primers used for Quik Change mutagenesis in LmrA | 34 |
| Table 9: Primers for cloning of MsbA from E. coli BL21-Gold (DE3) into the pET11a vector via Gibson assembly | 35 |
| Table 10: Oligonucleotides/ Primers used for Quik Change mutagenesis in MsbA | 35 |
| Table 11: Oligonucleotides/Primers used for Quik Change mutagenesis in BmrA | 35 |
| Table 12: Kapa HiFi HotStart PCR reaction conditions and DpnI digestion mix composition | 36 |
| Table 13: Composition of the isothermal ligation reaction mix for Gibson assembly | 37 |
| Table 14: Composition of 10x TAE buffer for agarose gel electrophoresis | 37 |
| Table 15: Sequencing primers | 37 |
| Table 16: Plasmids encoding the L. lactis ABC transporter LmrA or LmrA variants | 38 |
| Table 17: Plasmids encoding the E. coli ABC transporter MsbA or MsbA variants | 39 |
| Table 18: Plasmids encoding the B. subtilis ABC transporter BmrA or BmrA variants | 40 |
| Table 19: Plasmid used for production of TEV protease | 41 |
| Table 20: LmrA ABC transporter protein from L. lactis and variants | 42 |
| Table 21: MsbA ABC transporter protein from E. coli and variants | 43 |
| Table 22: BmrA ABC transporter protein from B. subtilis and variants | 44 |
| Table 23: TEV-protease used for purification | 45 |
| Table 24: Composition of protein expression media and additives | 45 |
| Table 25: Defined medium for selective isotope labeling of amino acids | 46 |
| Table 26: Expression media used to produce unlabeled and isotope labeled LmrA, MsbA and BmrA | 46 |
| Table 27: Composition of solutions for the preparation of competent cells | 47 |
| Table 28: Buffer compositions for LmrA-NBD, MsbA-NBD or BmrA-NBD protein purification | 49 |
| Table 29: Buffer composition for full-length MsbA and BmrA IOV preparation and protein purification | 50 |
| Table 30: Buffer compositions for BmrA IOV preparation and membrane protein purification | 51 |
| Table 31: Buffer compositions for TEV protease purification | 52 |
| Table 32: Composition of the stacking and running gel to perform 4 gels for SDS-PAGE | 53 |
| Table 33: Buffers to perform SDS-PAGE | 54 |
| Table 34: ATPase activity assay protocol 1 performed in [REDACTED] laboratory | 57 |
| Table 35: ATPase activity assay protocol performed in [REDACTED] laboratory, Lyon | 58 |
| Table 36: Fluorescence drug transport assay protocol for the substrate Hoechst 33342 or Doxorubicin performed in [REDACTED] laboratory, Lyon. | 59 |
| Table 37: LmrA-NBD samples used for backbone chemical shift assignment experiments in the ADP-bound state (10 mM ADP) | 61 |
| Table 38: NMR parameters for LmrA-NBD and MsbA-NBD measurements used for NMR titration experiments (ADP, ATP and addition of magnesium) | 62 |
| Table 39: NMR parameters for LmrA-NBD NMR experiments to analyze backbone dynamics | 63 |

| | |
|--|------------|
| Table 40: NMR parameters for MsbA-NBD WT used for backbone chemical shift assignment experiments in the ADP-bound state (10 mM ADP) and to measure the apo state | 64 |
| Table 41: NMR parameters for BmrA-NBD WT used for backbone chemical shift assignment experiments in the ADP-bound state (10 mM ADP) and to measure the apo state | 65 |
| Table 42: NMR parameters for LmrA-NBD 1D ¹⁹F NMR experiments | 66 |
| Table 43: NMR parameters for BmrA 1D ¹⁹F NMR experiments | 66 |
| Table 44: Concentrations used for titrations of ADP, ATP and addition of magnesium for ¹H-¹⁵N HSQC or ¹H-¹⁵N TROSY HSQC experiments | 69 |
| Table 45: Concentrations used for titrations of (Mg)ADP, (Mg)ATP and magnesium addition for 1D ¹⁹F NMR experiments | 70 |
| | |
| Appendix table 1: Structures of E-Q mutants in NBDs of ABC transporters | 154 |
| Appendix table 2: Structures of E-Q mutants in full-length ABC transporters | 155 |
| Appendix table 3: Available full-length structures of the type I ABC exporters (type IV according to a new classification system) MsbA and BmrA | 157 |
| Appendix table 4: Comparison of reported K_D values for different ABC transporters for ADP and ATP | 168 |

URHEBERSCHAFTSERKLÄRUNG

Ich, Dania Rose-Sperling, versichere, dass ich die vorliegende Dissertation mit dem Titel „Structure and dynamics of multidrug resistance ABC transporters“ selbst verfasst, nicht andere als die in ihr angegebenen Quellen oder Hilfsmittel benutzt, alle vollständig oder sinngemäß übernommenen Zitate als solche gekennzeichnet sowie die Dissertation in der vorliegenden oder einer ähnlichen Form noch bei keiner anderen in- oder ausländischen Hochschule anlässlich eines Promotionsgesuchs oder zu anderen Prüfungszwecken eingereicht habe.

References

- (1) Heijne, G. von (2007) The membrane protein universe: what's out there and why bother?, *Journal of internal medicine* 261, 543–557. DOI: 10.1111/j.1365-2796.2007.01792.x.
- (2) Yin, H., and Flynn, A. D. (2016) Drugging Membrane Protein Interactions, *Annual review of biomedical engineering* 18, 51–76 published online Feb 5, 2016. DOI: 10.1146/annurev-bioeng-092115-025322.
- (3) (Mai 2022) RCSB Protein Data Bank (PDB). <https://www.rcsb.org/>.
- (4) (Mai 2022) Electron Microscopy Data Bank (EMDB). <https://www.emdataresource.org/>.
- (5) (Mai 2022) Membrane Proteins of Known 3D Structure (mpstruc). <https://blanco.biomol.uci.edu/mpstruc/>.
- (6) Hong, M., Zhang, Y., and Hu, F. (2012) Membrane protein structure and dynamics from NMR spectroscopy, *Annual review of physical chemistry* 63, 1–24 published online Nov 28, 2011. DOI: 10.1146/annurev-physchem-032511-143731.
- (7) Bolhuis, H., van Veen, H. W., Poolman, B., Driessen, A. J., and Konings, W. N. (1997) Mechanisms of multidrug transporters, *FEMS microbiology reviews* 21, 55–84. DOI: 10.1111/j.1574-6976.1997.tb00345.x.
- (8) Assaraf, Y. G., Brozovic, A., Gonçalves, A. C., Jurkovicova, D., Linē, A., Machuqueiro, M., Saponara, S., Sarmiento-Ribeiro, A. B., Xavier, C. P. R., and Vasconcelos, M. H. (2019) The multi-factorial nature of clinical multidrug resistance in cancer, *Drug resistance updates : reviews and commentaries in antimicrobial and anticancer chemotherapy* 46, 100645 published online Sep 17, 2019. DOI: 10.1016/j.drup.2019.100645.
- (9) Juliano, R. L., and Ling, V. (1976) A surface glycoprotein modulating drug permeability in Chinese hamster ovary cell mutants, *Biochimica et Biophysica Acta (BBA) - Biomembranes* 455, 152–162. DOI: 10.1016/0005-2736(76)90160-7.
- (10) Shukla, S., Ohnuma, S., and Ambudkar, S. V. (2011) Improving cancer chemotherapy with modulators of ABC drug transporters, *Current Drug Targets* 12, 621–630. DOI: 10.2174/138945011795378540.
- (11) El-Awady, R., Saleh, E., Hashim, A., Soliman, N., Dallah, A., Elrasheed, A., and Elakraa, G. (2016) The Role of Eukaryotic and Prokaryotic ABC Transporter Family in Failure of Chemotherapy, *Frontiers in pharmacology* 7, 535 published online Jan 10, 2017. DOI: 10.3389/fphar.2016.00535.
- (12) Spratt, B. G. (1994) Resistance to antibiotics mediated by target alterations, *Science (New York, N.Y.)* 264, 388–393. DOI: 10.1126/science.8153626.
- (13) Rasmussen, B. A., and Bush, K. (1997) Carbapenem-hydrolyzing beta-lactamases, *Antimicrobial agents and chemotherapy* 41, 223–232. DOI: 10.1128/AAC.41.2.223.
- (14) Chevereau, M., Daniels, P. J., Davies, J., and LeGoffic, F. (1974) Aminoglycoside resistance in bacteria mediated by gentamicin acetyltransferase II, an enzyme modifying the 2'-amino group of aminoglycoside antibiotics, *Biochemistry* 13, 598–603. DOI: 10.1021/bi00700a030.
- (15) Alton, N. K., and Vapnek, D. (1979) Nucleotide sequence analysis of the chloramphenicol resistance transposon Tn9, *Nature* 282, 864–869. DOI: 10.1038/282864a0.
- (16) Munita, J. M., and Arias, C. A. (2016) Mechanisms of Antibiotic Resistance, *Microbiology spectrum* 4. DOI: 10.1128/microbiolspec.VMBF-0016-2015.
- (17) Jarlier, V., and Nikaido, H. (1994) Mycobacterial cell wall: structure and role in natural resistance to antibiotics, *FEMS microbiology letters* 123, 11–18. DOI: 10.1111/j.1574-6968.1994.tb07194.x.

- (18) Fernández, L., and Hancock, R. E. W. (2012) Adaptive and mutational resistance: role of porins and efflux pumps in drug resistance, *Clinical Microbiology Reviews* 25, 661–681. DOI: 10.1128/CMR.00043-12.
- (19) Saier, M. H., Paulsen, I. T., Sliwinski, M. K., Pao, S. S., Skurray, R. A., and Nikaido, H. (1998) Evolutionary origins of multidrug and drug-specific efflux pumps in bacteria, *FASEB journal : official publication of the Federation of American Societies for Experimental Biology* 12, 265–274. DOI: 10.1096/fasebj.12.3.265.
- (20) Hassan, K. A., Jackson, S. M., Penesyan, A., Patching, S. G., Tetu, S. G., Eijkelkamp, B. A., Brown, M. H., Henderson, P. J. F., and Paulsen, I. T. (2013) Transcriptomic and biochemical analyses identify a family of chlorhexidine efflux proteins, *Proceedings of the National Academy of Sciences of the United States of America* 110, 20254–20259 published online Nov 25, 2013. DOI: 10.1073/pnas.1317052110.
- (21) Hassan, K. A., Liu, Q., Henderson, P. J. F., and Paulsen, I. T. (2015) Homologs of the *Acinetobacter baumannii* Acel transporter represent a new family of bacterial multidrug efflux systems, *mBio* 6 published online Feb 10, 2015. DOI: 10.1128/mBio.01982-14.
- (22) Chitsaz, M., and Brown, M. H. (2017) The role played by drug efflux pumps in bacterial multidrug resistance, *Essays in biochemistry* 61, 127–139 published online Mar 3, 2017. DOI: 10.1042/EBC20160064.
- (23) Du, D., Wang-Kan, X., Neuberger, A., van Veen, H. W., Pos, K. M., Piddock, L. J. V., and Luisi, B. F. (2018) Multidrug efflux pumps: structure, function and regulation, *Nat Rev Microbiol* 16, 523–539. DOI: 10.1038/s41579-018-0048-6.
- (24) Locher, K. P. (2016) Mechanistic diversity in ATP-binding cassette (ABC) transporters, *Nature structural & molecular biology* 23, 487–493. DOI: 10.1038/nsmb.3216.
- (25) van Veen, H. W., and Konings, W. N. (1998) The ABC family of multidrug transporters in microorganisms, *Biochimica et Biophysica Acta (BBA) - Bioenergetics* 1365, 31–36. DOI: 10.1016/S0005-2728(98)00039-5.
- (26) Orelle, C., Mathieu, K., and Jault, J.-M. (2019) Multidrug ABC transporters in bacteria, *Research in microbiology* 170, 381–391 published online Jun 25, 2019. DOI: 10.1016/j.resmic.2019.06.001.
- (27) Pao, S. S., Paulsen, I. T., and Saier, M. H. (1998) Major facilitator superfamily, *Microbiology and Molecular Biology Reviews* 62, 1–34. DOI: 10.1128/MMBR.62.1.1-34.1998.
- (28) Quistgaard, E. M., Martinez Molledo, M., and Löw, C. (2017) Structure determination of a major facilitator peptide transporter: Inward facing PepTSt from *Streptococcus thermophilus* crystallized in space group P3121, *PloS one* 12, e0173126 published online Mar 6, 2017. DOI: 10.1371/journal.pone.0173126.
- (29) Brown, M. H., Paulsen, I. T., and Skurray, R. A. (1999) The multidrug efflux protein NorM is a prototype of a new family of transporters, *Molecular microbiology* 31, 394–395. DOI: 10.1046/j.1365-2958.1999.01162.x.
- (30) Paulsen, I. T., Skurray, R. A., Tam, R., Saier, M. H., Turner, R. J., Weiner, J. H., Goldberg, E. B., and Grinius, L. L. (1996) The SMR family: a novel family of multidrug efflux proteins involved with the efflux of lipophilic drugs, *Molecular microbiology* 19, 1167–1175. DOI: 10.1111/j.1365-2958.1996.tb02462.x.
- (31) Tseng, T. T., Gratwick, K. S., Kollman, J., Park, D., Nies, D. H., Goffeau, A., and Saier, M. H. (1999) The RND permease superfamily: an ancient, ubiquitous and diverse family that includes human disease and development proteins, *Journal of molecular microbiology and biotechnology* 1, 107–125.
- (32) Nikaido, H. (2018) RND transporters in the living world, *Research in microbiology* 169, 363–371 published online Mar 22, 2018. DOI: 10.1016/j.resmic.2018.03.001.

- (33) Delmar, J. A., and Yu, E. W. (2016) The AbgT family: A novel class of antimetabolite transporters, *Protein science : a publication of the Protein Society* 25, 322–337 published online Nov 3, 2015. DOI: 10.1002/pro.2820.
- (34) Dawson, R. J. P., and Locher, K. P. (2006) Structure of a bacterial multidrug ABC transporter, *Nature* 443, 180–185 published online Aug 30, 2006. DOI: 10.1038/nature05155.
- (35) Heng, J., Zhao, Y., Liu, M., Liu, Y., Fan, J., Wang, X., Zhao, Y., and Zhang, X. C. (2015) Substrate-bound structure of the E. coli multidrug resistance transporter MdfA, *Cell Research* 25, 1060–1073 published online Aug 4, 2015. DOI: 10.1038/cr.2015.94.
- (36) He, X., Szewczyk, P., Karyakin, A., Evin, M., Hong, W.-X., Zhang, Q., and Chang, G. (2010) Structure of a cation-bound multidrug and toxic compound extrusion transporter, *Nature* 467, 991–994 published online Sep 22, 2010. DOI: 10.1038/nature09408.
- (37) Shcherbakov, A. A., Hisao, G., Mandala, V. S., Thomas, N. E., Soltani, M., Salter, E. A., Davis, J. H., Henzler-Wildman, K. A., and Hong, M. (2021) Structure and dynamics of the drug-bound bacterial transporter EmrE in lipid bilayers, *Nature Communications* 12, 172 published online Jan 8, 2021. DOI: 10.1038/s41467-020-20468-7.
- (38) Su, C.-C., Bolla, J. R., Kumar, N., Radhakrishnan, A., Long, F., Delmar, J. A., Chou, T.-H., Rajashankar, K. R., Shafer, W. M., and Yu, E. W. (2015) Structure and function of Neisseria gonorrhoeae MtrF illuminates a class of antimetabolite efflux pumps, *Cell reports* 11, 61–70 published online Mar 26, 2015. DOI: 10.1016/j.celrep.2015.03.003.
- (39) Murakami, S., Nakashima, R., Yamashita, E., Matsumoto, T., and Yamaguchi, A. (2006) Crystal structures of a multidrug transporter reveal a functionally rotating mechanism, *Nature* 443, 173–179 published online Aug 16, 2006. DOI: 10.1038/nature05076.
- (40) Mikolosko, J., Bobyk, K., Zgurskaya, H. I., and Ghosh, P. (2006) Conformational flexibility in the multidrug efflux system protein AcrA, *Structure (London, England : 1993)* 14, 577–587. DOI: 10.1016/j.str.2005.11.015.
- (41) Bavro, V. N., Pietras, Z., Furnham, N., Pérez-Cano, L., Fernández-Recio, J., Pei, X. Y., Misra, R., and Luisi, B. (2008) Assembly and channel opening in a bacterial drug efflux machine, *Molecular Cell* 30, 114–121. DOI: 10.1016/j.molcel.2008.02.015.
- (42) Wu, C.-P., Ohnuma, S., and Ambudkar, S. V. (2011) Discovering natural product modulators to overcome multidrug resistance in cancer chemotherapy, *Current pharmaceutical biotechnology* 12, 609–620. DOI: 10.2174/138920111795163887.
- (43) Kunjachan, S., Rychlik, B., Storm, G., Kiessling, F., and Lammers, T. (2013) Multidrug resistance: Physiological principles and nanomedical solutions, *Advanced drug delivery reviews* 65, 1852–1865 published online Oct 10, 2013. DOI: 10.1016/j.addr.2013.09.018.
- (44) Krogstad, D. J., Gluzman, I. Y., Kyle, D. E., Oduola, A. M., Martin, S. K., Milhous, W. K., and Schlesinger, P. H. (1987) Efflux of chloroquine from Plasmodium falciparum: mechanism of chloroquine resistance, *Science (New York, N.Y.)* 238, 1283–1285. DOI: 10.1126/science.3317830.
- (45) Perea, S., López-Ribot, J. L., Kirkpatrick, W. R., McAtee, R. K., Santillán, R. A., Martínez, M., Calabrese, D., Sanglard, D., and Patterson, T. F. (2001) Prevalence of molecular mechanisms of resistance to azole antifungal agents in Candida albicans strains displaying high-level fluconazole resistance isolated from human immunodeficiency virus-infected patients, *Antimicrobial agents and chemotherapy* 45, 2676–2684. DOI: 10.1128/AAC.45.10.2676-2684.2001.
- (46) Gat, O., Mendelson, I., Chitlaru, T., Ariel, N., Altboum, Z., Levy, H., Weiss, S., Grosfeld, H., Cohen, S., and Shafferman, A. (2005) The solute-binding component of a putative Mn(II) ABC transporter (MntA) is a novel Bacillus anthracis virulence determinant, *Molecular microbiology* 58, 533–551. DOI: 10.1111/j.1365-2958.2005.04848.x.

- (47) Jones, P. M., and George, A. M. (2005) Multidrug resistance in parasites: ABC transporters, P-glycoproteins and molecular modelling, *International journal for parasitology* 35, 555–566. DOI: 10.1016/j.ijpara.2005.01.012.
- (48) McDevitt, C. A., Ogunniyi, A. D., Valkov, E., Lawrence, M. C., Kobe, B., McEwan, A. G., and Paton, J. C. (2011) A molecular mechanism for bacterial susceptibility to zinc, *PLoS pathogens* 7, e1002357 published online Nov 3, 2011. DOI: 10.1371/journal.ppat.1002357.
- (49) Manzano, J. I., García-Hernández, R., Castanys, S., and Gamarro, F. (2013) A new ABC half-transporter in *Leishmania major* is involved in resistance to antimony, *Antimicrobial agents and chemotherapy* 57, 3719–3730 published online May 28, 2013. DOI: 10.1128/AAC.00211-13.
- (50) Remy, L., Carrière, M., Derré-Bobillot, A., Martini, C., Sanguinetti, M., and Borezée-Durant, E. (2013) The *Staphylococcus aureus* Opp1 ABC transporter imports nickel and cobalt in zinc-depleted conditions and contributes to virulence, *Molecular microbiology* 87, 730–743 published online Dec 23, 2012. DOI: 10.1111/mmi.12126.
- (51) Lewinson, O., and Livnat-Levanon, N. (2017) Mechanism of Action of ABC Importers: Conservation, Divergence, and Physiological Adaptations, *Journal of molecular biology* 429, 606–619 published online Jan 16, 2017. DOI: 10.1016/j.jmb.2017.01.010.
- (52) Cole, S. P., Bhardwaj, G., Gerlach, J. H., Mackie, J. E., Grant, C. E., Almquist, K. C., Stewart, A. J., Kurz, E. U., Duncan, A. M., and Deeley, R. G. (1992) Overexpression of a transporter gene in a multidrug-resistant human lung cancer cell line, *Science (New York, N.Y.)* 258, 1650–1654. DOI: 10.1126/science.1360704.
- (53) Doyle, L. A., Yang, W., Abruzzo, L. V., Krogmann, T., Gao, Y., Rishi, A. K., and Ross, D. D. (1998) A multidrug resistance transporter from human MCF-7 breast cancer cells, *Proceedings of the National Academy of Sciences of the United States of America* 95, 15665–15670. DOI: 10.1073/pnas.95.26.15665.
- (54) Gottesman, M. M., Fojo, T., and Bates, S. E. (2002) Multidrug resistance in cancer: role of ATP-dependent transporters, *Nature reviews. Cancer* 2, 48–58. DOI: 10.1038/nrc706.
- (55) Thomas Efferth, Maen Zeino, and Manfred Volm (2015) Modulation of P-Glycoprotein-Mediated Multidrug Resistance by Synthetic and Phytochemical Small Molecules, Monoclonal Antibodies, and Therapeutic Nucleic Acids. in *Resistance to Targeted ABC Transporters in Cancer*, Springer, Cham.
- (56) Kadioglu, O., Saeed, M. E. M., Munder, M., Spuller, A., Greten, H. J., and Efferth, T. (2020) Effect of ABC transporter expression and mutational status on survival rates of cancer patients, *Biomedicine & pharmacotherapy = Biomedecine & pharmacotherapie* 131, 110718 published online Sep 12, 2020. DOI: 10.1016/j.biopha.2020.110718.
- (57) I. Holland, S. Cole, K. Kuchler, and C. Higgins (2003) ABC proteins : from bacteria to man, *undefined*.
- (58) George, A. M., Ed. (2016) ABC Transporters - 40 Years On, Springer International Publishing AG, Cham.
- (59) Ames, G. F., Mimura, C. S., Holbrook, S. R., and Shyamala, V. (1992) Traffic ATPases: a superfamily of transport proteins operating from *Escherichia coli* to humans, *Advances in enzymology and related areas of molecular biology* 65, 1–47. DOI: 10.1002/9780470123119.ch1.
- (60) Higgins, C. F. (1992) ABC transporters: from microorganisms to man, *Annual review of cell biology* 8, 67–113. DOI: 10.1146/annurev.cb.08.110192.000435.
- (61) Dassa, E., and Bouige, P. (2001) The ABC of ABCs: a phylogenetic and functional classification of ABC systems in living organisms, *Research in microbiology* 152, 211–229. DOI: 10.1016/S0923-2508(01)01194-9.

- (62) Møller, S. G., Kunkel, T., and Chua, N. H. (2001) A plastidic ABC protein involved in intercompartmental communication of light signaling, *Genes & development* 15, 90–103. DOI: 10.1101/gad.850101.
- (63) Higgins, C. F. (2001) ABC transporters: physiology, structure and mechanism – an overview, *Research in microbiology* 152, 205–210. DOI: 10.1016/s0923-2508(01)01193-7.
- (64) Ambudkar, S. V., Kimchi-Sarfaty, C., Sauna, Z. E., and Gottesman, M. M. (2003) P-glycoprotein: from genomics to mechanism, *Oncogene* 22, 7468–7485. DOI: 10.1038/sj.onc.1206948.
- (65) Holland, I. B., Cole, S. P. C., Kuchler, K., and Higgins, C. F. (2003) ABC Proteins. From Bacteria to Man, Elsevier.
- (66) Schmidt, K. L., Peterson, N. D., Kustus, R. J., Wissel, M. C., Graham, B., Phillips, G. J., and Weiss, D. S. (2004) A predicted ABC transporter, FtsEX, is needed for cell division in *Escherichia coli*, *Journal of bacteriology* 186, 785–793. DOI: 10.1128/JB.186.3.785-793.2004.
- (67) Rea, P. A. (2007) Plant ATP-binding cassette transporters, *Annual review of plant biology* 58, 347–375. DOI: 10.1146/annurev.arplant.57.032905.105406.
- (68) Davidson, A. L., Dassa, E., Orelle, C., and Chen, J. (2008) Structure, function, and evolution of bacterial ATP-binding cassette systems, *Microbiology and Molecular Biology Reviews* 72, 317–64, table of contents. DOI: 10.1128/MMBR.00031-07.
- (69) Paytubi, S., Wang, X., Lam, Y. W., Izquierdo, L., Hunter, M. J., Jan, E., Hundal, H. S., and Proud, C. G. (2009) ABC50 promotes translation initiation in mammalian cells, *The Journal of Biological Chemistry* 284, 24061–24073 published online Jul 1, 2009. DOI: 10.1074/jbc.M109.031625.
- (70) Lewis, V. G., Ween, M. P., and McDevitt, C. A. (2012) The role of ATP-binding cassette transporters in bacterial pathogenicity, *Protoplasma* 249, 919–942 published online Jan 13, 2012. DOI: 10.1007/s00709-011-0360-8.
- (71) Lewinson, O., and Livnat-Levanon, N. (2017) Mechanism of Action of ABC Importers: Conservation, Divergence, and Physiological Adaptations, *Journal of molecular biology* 429, 606–619 published online Jan 16, 2017. DOI: 10.1016/j.jmb.2017.01.010.
- (72) Theodoulou, F. L., and Kerr, I. D. (2015) ABC transporter research: going strong 40 years on, *Biochemical Society transactions* 43, 1033–1040 published online Oct 9, 2015. DOI: 10.1042/BST20150139.
- (73) (2017) Solid-state NMR studies of the ABC transporter BmrA in its lipid environment.
- (74) Oldham, M. L., Khare, D., Quioco, F. A., Davidson, A. L., and Chen, J. (2007) Crystal structure of a catalytic intermediate of the maltose transporter, *Nature* 450, 515–521. DOI: 10.1038/nature06264.
- (75) Korkhov, V. M., Mireku, S. A., and Locher, K. P. (2012) Structure of AMP-PNP-bound vitamin B12 transporter BtuCD-F, *Nature* 490, 367–372 published online Sep 23, 2012. DOI: 10.1038/nature11442.
- (76) Xu, K., Zhang, M., Zhao, Q., Yu, F., Guo, H., Wang, C., He, F., Ding, J., and Zhang, P. (2013) Crystal structure of a folate energy-coupling factor transporter from *Lactobacillus brevis*, *Nature* 497, 268–271 published online Apr 14, 2013. DOI: 10.1038/nature12046.
- (77) Lee, J.-Y., Kinch, L. N., Borek, D. M., Wang, J., Wang, J., Urbatsch, I. L., Xie, X.-S., Grishin, N. V., Cohen, J. C., Otwinowski, Z., Hobbs, H. H., and Rosenbaum, D. M. (2016) Crystal structure of the human sterol transporter ABCG5/ABCG8, *Nature* 533, 561–564 published online May 4, 2016. DOI: 10.1038/nature17666.
- (78) Luo, Q., Yang, X., Yu, S., Shi, H., Wang, K., Le Xiao, Zhu, G., Sun, C., Li, T., Li, D., Zhang, X., Zhou, M., and Huang, Y. (2017) Structural basis for lipopolysaccharide extraction by ABC transporter

- LptB2FG, *Nature structural & molecular biology* 24, 469–474 published online Apr 10, 2017. DOI: 10.1038/nsmb.3399.
- (79) Crow, A., Greene, N. P., Kaplan, E., and Koronakis, V. (2017) Structure and mechanotransmission mechanism of the MacB ABC transporter superfamily, *Proceedings of the National Academy of Sciences of the United States of America* 114, 12572–12577 published online Nov 6, 2017. DOI: 10.1073/pnas.1712153114.
- (80) Beek, J. ter, Guskov, A., and Slotboom, D. J. (2014) Structural diversity of ABC transporters, *The Journal of general physiology* 143, 419–435 published online Mar 17, 2014. DOI: 10.1085/jgp.201411164.
- (81) Greene, N. P., Kaplan, E., Crow, A., and Koronakis, V. (2018) Antibiotic Resistance Mediated by the MacB ABC Transporter Family: A Structural and Functional Perspective, *Frontiers in microbiology* 9, 950 published online May 28, 2018. DOI: 10.3389/fmicb.2018.00950.
- (82) Thomas, C., Aller, S. G., Beis, K., Carpenter, E. P., Chang, G., Chen, L., Dassa, E., Dean, M., van Duong Hoa, F., Ekiert, D., Ford, R., Gaudet, R., Gong, X., Holland, I. B., Huang, Y., Kahne, D. K., Kato, H., Koronakis, V., Koth, C. M., Lee, Y., Lewinson, O., Lill, R., Martinoia, E., Murakami, S., Pinkett, H. W., Poolman, B., Rosenbaum, D., Sarkadi, B., Schmitt, L., Schneider, E., Shi, Y., Shyng, S.-L., Slotboom, D. J., Tajkhorshid, E., Tieleman, D. P., Ueda, K., Váradi, A., Wen, P.-C., Yan, N., Zhang, P., Zheng, H., Zimmer, J., and Tampé, R. (2020) Structural and functional diversity calls for a new classification of ABC transporters, *FEBS letters* 594, 3767–3775 published online Oct 26, 2020. DOI: 10.1002/1873-3468.13935.
- (83) Locher, K. P., Lee, A. T., and Rees, D. C. (2002) The E. coli BtuCD structure: a framework for ABC transporter architecture and mechanism, *Science (New York, N.Y.)* 296, 1091–1098. DOI: 10.1126/science.1071142.
- (84) Wang, T., Fu, G., Pan, X., Wu, J., Gong, X., Wang, J., and Shi, Y. (2013) Structure of a bacterial energy-coupling factor transporter, *Nature* 497, 272–276 published online Apr 14, 2013. DOI: 10.1038/nature12045.
- (85) Dong, H., Zhang, Z., Tang, X., Paterson, N. G., and Dong, C. (2017) Structural and functional insights into the lipopolysaccharide ABC transporter LptB2FG, *Nature Communications* 8, 222 published online Aug 9, 2017. DOI: 10.1038/s41467-017-00273-5.
- (86) Fitzpatrick, A. W. P., Llabrés, S., Neuberger, A., Blaza, J. N., Bai, X.-C., Okada, U., Murakami, S., van Veen, H. W., Zachariae, U., Scheres, S. H. W., Luisi, B. F., and Du, D. (2017) Structure of the MacAB-TolC ABC-type tripartite multidrug efflux pump, *Nature microbiology* 2, 17070 published online May 15, 2017. DOI: 10.1038/nmicrobiol.2017.70.
- (87) Okada, U., Yamashita, E., Neuberger, A., Morimoto, M., van Veen, H. W., and Murakami, S. (2017) Crystal structure of tripartite-type ABC transporter MacB from *Acinetobacter baumannii*, *Nature Communications* 8, 1336 published online Nov 6, 2017. DOI: 10.1038/s41467-017-01399-2.
- (88) Yang, H.-B., Hou, W.-T., Cheng, M.-T., Jiang, Y.-L., Chen, Y., and Zhou, C.-Z. (2018) Structure of a MacAB-like efflux pump from *Streptococcus pneumoniae*, *Nature Communications* 9, 196 published online Jan 15, 2018. DOI: 10.1038/s41467-017-02741-4.
- (89) Nöll, A., Thomas, C., Herbring, V., Zollmann, T., Barth, K., Mehdipour, A. R., Tomasiak, T. M., Brüchert, S., Joseph, B., Abele, R., Oliéric, V., Wang, M., Diederichs, K., Hummer, G., Stroud, R. M., Pos, K. M., and Tampé, R. (2017) Crystal structure and mechanistic basis of a functional homolog of the antigen transporter TAP, *Proceedings of the National Academy of Sciences of the United States of America* 114, E438–E447 published online Jan 9, 2017. DOI: 10.1073/pnas.1620009114.
- (90) Hohl, M., Hürlimann, L. M., Böhm, S., Schöppe, J., Grütter, M. G., Bordignon, E., and Seeger, M. A. (2014) Structural basis for allosteric cross-talk between the asymmetric nucleotide binding sites of

- a heterodimeric ABC exporter, *Proceedings of the National Academy of Sciences of the United States of America* **111**, 11025–11030 published online Jul 16, 2014. DOI: 10.1073/pnas.1400485111.
- (91) Mi, W., Li, Y., Yoon, S. H., Ernst, R. K., Walz, T., and Liao, M. (2017) Structural basis of MsbA-mediated lipopolysaccharide transport, *Nature* **549**, 233–237 published online Sep 6, 2017. DOI: 10.1038/nature23649.
- (92) Li, J., Jaimes, K. F., and Aller, S. G. (2014) Refined structures of mouse P-glycoprotein, *Protein science : a publication of the Protein Society* **23**, 34–46 published online Nov 15, 2013. DOI: 10.1002/pro.2387.
- (93) Chaptal, V., Zampieri, V., Wiseman, B., Orelle, C., Martin, J., Nguyen, K.-A., Gobet, A., Di Cesare, M., Magnard, S., Javed, W., Eid, J., Kilburg, A., Peuchmaur, M., Marcoux, J., Monticelli, L., Hogbom, M., Schoehn, G., Jault, J.-M., Boumendjel, A., and Falson, P. (2022) Substrate-bound and substrate-free outward-facing structures of a multidrug ABC exporter, *Science Advances* **8**, eabg9215 published online Jan 26, 2022. DOI: 10.1126/sciadv.abg9215.
- (94) Bi, Y., Mann, E., Whitfield, C., and Zimmer, J. (2018) Architecture of a channel-forming O-antigen polysaccharide ABC transporter, *Nature* **553**, 361–365 published online Jan 10, 2018. DOI: 10.1038/nature25190.
- (95) Chen, L., Hou, W.-T., Fan, T., Liu, B., Pan, T., Li, Y.-H., Jiang, Y.-L., Wen, W., Chen, Z.-P., Sun, L., Zhou, C.-Z., and Chen, Y. (2020) Cryo-electron Microscopy Structure and Transport Mechanism of a Wall Teichoic Acid ABC Transporter, *mBio* **11** published online Mar 17, 2020. DOI: 10.1128/mBio.02749-19.
- (96) Manolaridis, I., Jackson, S. M., Taylor, N. M. I., Kowal, J., Stahlberg, H., and Locher, K. P. (2018) Cryo-EM structures of a human ABCG2 mutant trapped in ATP-bound and substrate-bound states, *Nature* **563**, 426–430 published online Nov 7, 2018. DOI: 10.1038/s41586-018-0680-3.
- (97) Qian, H., Zhao, X., Cao, P., Lei, J., Yan, N., and Gong, X. (2017) Structure of the Human Lipid Exporter ABCA1, *Cell* **169**, 1228–1239.e10 published online Jun 8, 2017. DOI: 10.1016/j.cell.2017.05.020.
- (98) Barthelme, D., Dinkelaker, S., Albers, S.-V., Londei, P., Ermler, U., and Tampé, R. (2011) Ribosome recycling depends on a mechanistic link between the FeS cluster domain and a conformational switch of the twin-ATPase ABCE1, *Proceedings of the National Academy of Sciences of the United States of America* **108**, 3228–3233 published online Feb 3, 2011. DOI: 10.1073/pnas.1015953108.
- (99) Boël, G., Smith, P. C., Ning, W., Englander, M. T., Chen, B., Hashem, Y., Testa, A. J., Fischer, J. J., Wieden, H.-J., Frank, J., Gonzalez, R. L., and Hunt, J. F. (2014) The ABC-F protein EttA gates ribosome entry into the translation elongation cycle, *Nature structural & molecular biology* **21**, 143–151 published online Jan 5, 2014. DOI: 10.1038/nsmb.2740.
- (100) Pasello, M., Giudice, A. M., and Scotlandi, K. (2020) The ABC subfamily A transporters: Multifaceted players with incipient potentialities in cancer, *Seminars in Cancer Biology* **60**, 57–71 published online Oct 9, 2019. DOI: 10.1016/j.semcancer.2019.10.004.
- (101) Bryan, J., Muñoz, A., Zhang, X., Düfer, M., Drews, G., Krippeit-Drews, P., and Aguilar-Bryan, L. (2007) ABCC8 and ABCC9: ABC transporters that regulate K⁺ channels, *Pflugers Archiv : European journal of physiology* **453**, 703–718 published online Aug 8, 2006. DOI: 10.1007/s00424-006-0116-z.
- (102) Tarr, P. T., Tarling, E. J., Bojanic, D. D., Edwards, P. A., and Baldán, A. (2009) Emerging new paradigms for ABCG transporters, *Biochimica et biophysica acta* **1791**, 584–593 published online Jan 22, 2009. DOI: 10.1016/j.bbailip.2009.01.007.
- (103) Tusnády, G. E., Sarkadi, B., Simon, I., and Váradi, A. (2006) Membrane topology of human ABC proteins, *FEBS letters* **580**, 1017–1022 published online Dec 1, 2005. DOI: 10.1016/j.febslet.2005.11.040.

- (104) Vasiliou, V., Vasiliou, K., and Nebert, D. W. (2009) Human ATP-binding cassette (ABC) transporter family, *Human genomics* 3, 281–290. DOI: 10.1186/1479-7364-3-3-281.
- (105) Tarling, E. J., Aguiar Vallim, T. Q. de, and Edwards, P. A. (2013) Role of ABC transporters in lipid transport and human disease, *Trends in endocrinology and metabolism: TEM* 24, 342–350 published online Feb 14, 2013. DOI: 10.1016/j.tem.2013.01.006.
- (106) Neumann, J., Rose-Sperling, D., and Hellmich, U. A. (2017) Diverse relations between ABC transporters and lipids: An overview, *Biochimica et Biophysica Acta (BBA) - Biomembranes* 1859, 605–618 published online Sep 29, 2016. DOI: 10.1016/j.bbamem.2016.09.023.
- (107) Berge, K. E., Tian, H., Graf, G. A., Yu, L., Grishin, N. V., Schultz, J., Kwiterovich, P., Shan, B., Barnes, R., and Hobbs, H. H. (2000) Accumulation of dietary cholesterol in sitosterolemia caused by mutations in adjacent ABC transporters, *Science (New York, N.Y.)* 290, 1771–1775. DOI: 10.1126/science.290.5497.1771.
- (108) Allikmets, R., Singh, N., Sun, H., Shroyer, N. F., Hutchinson, A., Chidambaram, A., Gerrard, B., Baird, L., Stauffer, D., Peiffer, A., Rattner, A., Smallwood, P., Li, Y., Anderson, K. L., Lewis, R. A., Nathans, J., Leppert, M., Dean, M., and Lupski, J. R. (1997) A photoreceptor cell-specific ATP-binding transporter gene (ABCR) is mutated in recessive Stargardt macular dystrophy, *Nature genetics* 15, 236–246. DOI: 10.1038/ng0397-236.
- (109) Fitzgerald, M. L., Mujawar, Z., and Tamehiro, N. (2010) ABC transporters, atherosclerosis and inflammation, *Atherosclerosis* 211, 361–370 published online Jan 21, 2010. DOI: 10.1016/j.atherosclerosis.2010.01.011.
- (110) Adamska, A., and Falasca, M. (2018) ATP-binding cassette transporters in progression and clinical outcome of pancreatic cancer: What is the way forward?, *World journal of gastroenterology* 24, 3222–3238. DOI: 10.3748/wjg.v24.i29.3222.
- (111) Cordon-Cardo, C., O'Brien, J. P., Casals, D., Rittman-Grauer, L., Biedler, J. L., Melamed, M. R., and Bertino, J. R. (1989) Multidrug-resistance gene (P-glycoprotein) is expressed by endothelial cells at blood-brain barrier sites, *Proceedings of the National Academy of Sciences of the United States of America* 86, 695–698. DOI: 10.1073/pnas.86.2.695.
- (112) Thiebaut, F., Tsuruo, T., Hamada, H., Gottesman, M. M., Pastan, I., and Willingham, M. C. (1989) Immunohistochemical localization in normal tissues of different epitopes in the multidrug transport protein P170: evidence for localization in brain capillaries and crossreactivity of one antibody with a muscle protein, *The journal of histochemistry and cytochemistry: official journal of the Histochemistry Society* 37, 159–164. DOI: 10.1177/37.2.2463300.
- (113) Hoffmeyer, S., Burk, O., Richter, O. von, Arnold, H. P., Brockmöller, J., Johne, A., Cascorbi, I., Gerloff, T., Roots, I., Eichelbaum, M., and Brinkmann, U. (2000) Functional polymorphisms of the human multidrug-resistance gene: multiple sequence variations and correlation of one allele with P-glycoprotein expression and activity in vivo, *Proceedings of the National Academy of Sciences* 97, 3473–3478. DOI: 10.1073/pnas.97.7.3473.
- (114) Juliano, R. L., and Ling, V. (1976) A surface glycoprotein modulating drug permeability in Chinese hamster ovary cell mutants, *Biochimica et Biophysica Acta (BBA) - Biomembranes* 455, 152–162. DOI: 10.1016/0005-2736(76)90160-7.
- (115) Cordon-Cardo, C., O'Brien, J. P., Boccia, J., Casals, D., Bertino, J. R., and Melamed, M. R. (1990) Expression of the multidrug resistance gene product (P-glycoprotein) in human normal and tumor tissues, *The journal of histochemistry and cytochemistry: official journal of the Histochemistry Society* 38, 1277–1287. DOI: 10.1177/38.9.1974900.
- (116) Chen, C., Chin, J. E., Ueda, K., Clark, D. P., Pastan, I., Gottesman, M. M., and Roninson, I. B. (1986) Internal duplication and homology with bacterial transport proteins in the mdr1 (P-

- glycoprotein) gene from multidrug-resistant human cells, *Cell* 47, 381–389. DOI: 10.1016/0092-8674(86)90595-7.
- (117) Szakács, G., Paterson, J. K., Ludwig, J. A., Booth-Genthe, C., and Gottesman, M. M. (2006) Targeting multidrug resistance in cancer, *Nature reviews. Drug discovery* 5, 219–234. DOI: 10.1038/nrd1984.
- (118) Leslie, E. M., Deeley, R. G., and Cole, S. P. C. (2005) Multidrug resistance proteins: role of P-glycoprotein, MRP1, MRP2, and BCRP (ABCG2) in tissue defense, *Toxicology and applied pharmacology* 204, 216–237. DOI: 10.1016/j.taap.2004.10.012.
- (119) Obradovic, T., Dobson, G. G., Shingaki, T., Kungu, T., and Hidalgo, I. J. (2007) Assessment of the first and second generation antihistamines brain penetration and role of P-glycoprotein, *Pharmaceutical research* 24, 318–327 published online Dec 19, 2006. DOI: 10.1007/s11095-006-9149-4.
- (120) Hrycyna, C. A., Ramachandra, M., Ambudkar, S. V., Ko, Y. H., Pedersen, P. L., Pastan, I., and Gottesman, M. M. (1998) Mechanism of action of human P-glycoprotein ATPase activity. Photochemical cleavage during a catalytic transition state using orthovanadate reveals cross-talk between the two ATP sites, *The Journal of Biological Chemistry* 273, 16631–16634. DOI: 10.1074/jbc.273.27.16631.
- (121) van Veen, H. W., Venema, K., Bolhuis, H., Oussenko, I., Kok, J., Poolman, B., Driessen, A. J., and Konings, W. N. (1996) Multidrug resistance mediated by a bacterial homolog of the human multidrug transporter MDR1, *Proceedings of the National Academy of Sciences of the United States of America* 93, 10668–10672. DOI: 10.1073/pnas.93.20.10668.
- (122) van Veen, H. W., Callaghan, R., Soceneantu, L., Sardini, A., Konings, W. N., and Higgins, C. F. (1998) A bacterial antibiotic-resistance gene that complements the human multidrug-resistance P-glycoprotein gene, *Nature* 391, 291–295. DOI: 10.1038/34669.
- (123) Bolhuis, H., van Veen, H. W., Molenaar, D., Poolman, B., Driessen, A. J., and Konings, W. N. (1996) Multidrug resistance in *Lactococcus lactis*: evidence for ATP-dependent drug extrusion from the inner leaflet of the cytoplasmic membrane, *The EMBO journal* 15, 4239–4245.
- (124) Huijbregts, R. P., Kroon, A. I. de, and Kruijff, B. de (2000) Topology and transport of membrane lipids in bacteria, *Biochimica et Biophysica Acta (BBA) - Reviews on Biomembranes* 1469, 43–61. DOI: 10.1016/S0304-4157(99)00014-3.
- (125) Zhou, Z., White, K. A., Polissi, A., Georgopoulos, C., and Raetz, C. R. (1998) Function of *Escherichia coli* MsbA, an essential ABC family transporter, in lipid A and phospholipid biosynthesis, *The Journal of Biological Chemistry* 273, 12466–12475. DOI: 10.1074/jbc.273.20.12466.
- (126) Doerrler, W. T., Reedy, M. C., and Raetz, C. R. (2001) An *Escherichia coli* mutant defective in lipid export, *The Journal of Biological Chemistry* 276, 11461–11464 published online Feb 22, 2001. DOI: 10.1074/jbc.C100091200.
- (127) Reuter, G., Janvilisri, T., Venter, H., Shahi, S., Balakrishnan, L., and van Veen, H. W. (2003) The ATP binding cassette multidrug transporter LmrA and lipid transporter MsbA have overlapping substrate specificities, *The Journal of Biological Chemistry* 278, 35193–35198 published online Jul 2, 2003. DOI: 10.1074/jbc.M306226200.
- (128) Woebking, B., Reuter, G., Shilling, R. A., Velamakanni, S., Shahi, S., Venter, H., Balakrishnan, L., and van Veen, H. W. (2005) Drug-lipid A interactions on the *Escherichia coli* ABC transporter MsbA, *Journal of bacteriology* 187, 6363–6369. DOI: 10.1128/JB.187.18.6363-6369.2005.
- (129) Margolles, A., Putman, M., van Veen, H. W., and Konings, W. N. (1999) The purified and functionally reconstituted multidrug transporter LmrA of *Lactococcus lactis* mediates the transbilayer

- movement of specific fluorescent phospholipids, *Biochemistry* 38, 16298–16306. DOI: 10.1021/bi990855s.
- (130) Dalmas, O., Do Cao, M.-A., Lugo, M. R., Sharom, F. J., Di Pietro, A., and Jault, J.-M. (2005) Time-resolved fluorescence resonance energy transfer shows that the bacterial multidrug ABC half-transporter BmrA functions as a homodimer, *Biochemistry* 44, 4312–4321. DOI: 10.1021/bi0482809.
- (131) Eckford, P. D. W., and Sharom, F. J. (2008) Functional characterization of Escherichia coli MsbA: interaction with nucleotides and substrates, *The Journal of Biological Chemistry* 283, 12840–12850 published online Mar 15, 2008. DOI: 10.1074/jbc.M708274200.
- (132) Siarheyeva, A., and Sharom, F. J. (2009) The ABC transporter MsbA interacts with lipid A and amphipathic drugs at different sites, *The Biochemical journal* 419, 317–328. DOI: 10.1042/BJ20081364.
- (133) van Veen, H. W., Margolles, A., Müller, M., Higgins, C. F., and Konings, W. N. (2000) The homodimeric ATP-binding cassette transporter LmrA mediates multidrug transport by an alternating two-site (two-cylinder engine) mechanism, *The EMBO journal* 19, 2503–2514. DOI: 10.1093/emboj/19.11.2503.
- (134) Ravaud, S., Do Cao, M.-A., Jidenko, M., Ebel, C., Le Maire, M., Jault, J.-M., Di Pietro, A., Haser, R., and Aghajari, N. (2006) The ABC transporter BmrA from Bacillus subtilis is a functional dimer when in a detergent-solubilized state, *The Biochemical journal* 395, 345–353. DOI: 10.1042/BJ20051719.
- (135) Ward, A., Reyes, C. L., Yu, J., Roth, C. B., and Chang, G. (2007) Flexibility in the ABC transporter MsbA: Alternating access with a twist, *Proceedings of the National Academy of Sciences of the United States of America* 104, 19005–19010 published online Nov 16, 2007. DOI: 10.1073/pnas.0709388104.
- (136) Putman, M., van Veen, H. W., Degener, J. E., and Konings, W. N. (2000) Antibiotic resistance: era of the multidrug pump, *Molecular microbiology* 36, 772–773. DOI: 10.1046/j.1365-2958.2000.01871.x.
- (137) Steinfels, E., Orelle, C., Fantino, J.-R., Dalmas, O., Rigaud, J.-L., Denizot, F., Di Pietro, A., and Jault, J.-M. (2004) Characterization of YvcC (BmrA), a multidrug ABC transporter constitutively expressed in Bacillus subtilis, *Biochemistry* 43, 7491–7502. DOI: 10.1021/bi0362018.
- (138) Krügel, H., Licht, A., Biedermann, G., Petzold, A., Lassak, J., Hupfer, Y., Schlott, B., Hertweck, C., Platzer, M., Brantl, S., and Saluz, H.-P. (2010) Cervimycin C resistance in Bacillus subtilis is due to a promoter up-mutation and increased mRNA stability of the constitutive ABC-transporter gene bmrA, *FEMS microbiology letters* 313, 155–163 published online Nov 15, 2010. DOI: 10.1111/j.1574-6968.2010.02143.x.
- (139) Yusa, K., and Tsuruo, T. (1989) Reversal mechanism of multidrug resistance by verapamil: direct binding of verapamil to P-glycoprotein on specific sites and transport of verapamil outward across the plasma membrane of K562/ADM cells, *Cancer research* 49, 5002–5006.
- (140) Tamai, I., and Safa, A. R. (1991) Azidopine noncompetitively interacts with vinblastine and cyclosporin A binding to P-glycoprotein in multidrug resistant cells, *The Journal of Biological Chemistry* 266, 16796–16800.
- (141) Naito, M., Tsuge, H., Kuroko, C., Koyama, T., Tomida, A., Tatsuta, T., Heike, Y., and Tsuruo, T. (1993) Enhancement of cellular accumulation of cyclosporine by anti-P-glycoprotein monoclonal antibody MRK-16 and synergistic modulation of multidrug resistance, *Journal of the National Cancer Institute* 85, 311–316. DOI: 10.1093/jnci/85.4.311.
- (142) Saeki, T., Ueda, K., Tanigawara, Y., Hori, R., and Komano, T. (1993) Human P-glycoprotein transports cyclosporin A and FK506, *The Journal of Biological Chemistry* 268, 6077–6080.

- (143) Germann, U. A. (1996) P-glycoprotein—A mediator of multidrug resistance in tumour cells, *European journal of cancer (Oxford, England : 1990)* 32, 927–944. DOI: 10.1016/0959-8049(96)00057-3.
- (144) Shapiro, A. B., and Ling, V. (1997) Positively cooperative sites for drug transport by P-glycoprotein with distinct drug specificities, *European journal of biochemistry* 250, 130–137. DOI: 10.1111/j.1432-1033.1997.00130.x.
- (145) Schinkel, A. H., and Jonker, J. W. (2003) Mammalian drug efflux transporters of the ATP binding cassette (ABC) family: an overview, *Advanced drug delivery reviews* 55, 3–29. DOI: 10.1016/S0169-409X(02)00169-2.
- (146) Wang, R. C., Chen, X., Parissenti, A. M., Joy, A. A., Tuszynski, J., Brindley, D. N., and Wang, Z. (2017) Sensitivity of docetaxel-resistant MCF-7 breast cancer cells to microtubule-destabilizing agents including vinca alkaloids and colchicine-site binding agents, *PLoS one* 12, e0182400 published online Aug 7, 2017. DOI: 10.1371/journal.pone.0182400.
- (147) Martino, E., Casamassima, G., Castiglione, S., Cellupica, E., Pantalone, S., Papagni, F., Rui, M., Siciliano, A. M., and Collina, S. (2018) Vinca alkaloids and analogues as anti-cancer agents: Looking back, peering ahead, *Bioorganic & medicinal chemistry letters* 28, 2816–2826 published online Jun 25, 2018. DOI: 10.1016/j.bmcl.2018.06.044.
- (148) Aller, S. G., Yu, J., Ward, A., Weng, Y., Chittaboina, S., Zhuo, R., Harrell, P. M., Trinh, Y. T., Zhang, Q., Urbatsch, I. L., and Chang, G. (2009) Structure of P-glycoprotein reveals a molecular basis for poly-specific drug binding, *Science (New York, N.Y.)* 323, 1718–1722. DOI: 10.1126/science.1168750.
- (149) Thonghin, N., Collins, R. F., Barbieri, A., Shafi, T., Siebert, A., and Ford, R. C. (2018) Novel features in the structure of P-glycoprotein (ABCB1) in the post-hydrolytic state as determined at 7.9 Å resolution, *BMC structural biology* 18, 17 published online Dec 13, 2018. DOI: 10.1186/s12900-018-0098-z.
- (150) Smriti, Zou, P., and Mchaourab, H. S. (2009) Mapping daunorubicin-binding Sites in the ATP-binding cassette transporter MsbA using site-specific quenching by spin labels, *The Journal of Biological Chemistry* 284, 13904–13913 published online Mar 11, 2009. DOI: 10.1074/jbc.M900837200.
- (151) Davidson, A. L., and Chen, J. (2004) ATP-binding cassette transporters in bacteria, *Annual review of biochemistry* 73, 241–268. DOI: 10.1146/annurev.biochem.73.011303.073626.
- (152) Oldham, M. L., and Chen, J. (2011) Snapshots of the maltose transporter during ATP hydrolysis, *Proceedings of the National Academy of Sciences of the United States of America* 108, 15152–15156 published online Aug 8, 2011. DOI: 10.1073/pnas.1108858108.
- (153) Thomas, C., and Tampé, R. (2020) Structural and Mechanistic Principles of ABC Transporters, *Annual review of biochemistry* 89, 605–636. DOI: 10.1146/annurev-biochem-011520-105201.
- (154) Schmitt, L., Benabdelhak, H., Blight, M. A., Holland, I., and Stubbs, M. T. (2003) Crystal Structure of the Nucleotide-binding Domain of the ABC-transporter Haemolysin B: Identification of a Variable Region Within ABC Helical Domains, *Journal of molecular biology* 330, 333–342. DOI: 10.1016/S0022-2836(03)00592-8.
- (155) Szöllősi, D., Rose-Sperling, D., Hellmich, U. A., and Stockner, T. (2018) Comparison of mechanistic transport cycle models of ABC exporters, *Biochimica et Biophysica Acta (BBA) - Biomembranes* 1860, 818–832 published online Oct 31, 2017. DOI: 10.1016/j.bbamem.2017.10.028.
- (156) Hung, L. W., Wang, I. X., Nikaido, K., Liu, P. Q., Ames, G. F., and Kim, S. H. (1998) Crystal structure of the ATP-binding subunit of an ABC transporter, *Nature* 396, 703–707. DOI: 10.1038/25393.
- (157) Ambudkar, S. V., Kim, I.-W., Di Xia, and Sauna, Z. E. (2006) The A-loop, a novel conserved aromatic acid subdomain upstream of the Walker A motif in ABC transporters, is critical for ATP

- binding, *FEBS letters* 580, 1049–1055 published online Dec 22, 2005. DOI: 10.1016/j.febslet.2005.12.051.
- (158) Urbatsch, I. L., Gimi, K., Wilke-Mounts, S., and Senior, A. E. (2000) Investigation of the role of glutamine-471 and glutamine-1114 in the two catalytic sites of P-glycoprotein, *Biochemistry* 39, 11921–11927. DOI: 10.1021/bi001220s.
- (159) Ambudkar, S. V., Kim, I.-W., and Sauna, Z. E. (2006) The power of the pump: mechanisms of action of P-glycoprotein (ABCB1), *European journal of pharmaceutical sciences : official journal of the European Federation for Pharmaceutical Sciences* 27, 392–400 published online Dec 13, 2005. DOI: 10.1016/j.ejps.2005.10.010.
- (160) Zolnerciks, J. K., Wooding, C., and Linton, K. J. (2007) Evidence for a Sav1866-like architecture for the human multidrug transporter P-glycoprotein, *FASEB journal : official publication of the Federation of American Societies for Experimental Biology* 21, 3937–3948 published online Jul 12, 2007. DOI: 10.1096/fj.07-8610com.
- (161) Zolnerciks, J. K., Akkaya, B. G., Snippe, M., Chiba, P., Seelig, A., and Linton, K. J. (2014) The Q loops of the human multidrug resistance transporter ABCB1 are necessary to couple drug binding to the ATP catalytic cycle, *FASEB journal : official publication of the Federation of American Societies for Experimental Biology* 28, 4335–4346 published online Jul 11, 2014. DOI: 10.1096/fj.13-245639.
- (162) Loo, T. W., and Clarke, D. M. (2017) Attachment of a 'molecular spring' restores drug-stimulated ATPase activity to P-glycoprotein lacking both Q loop glutamines, *Biochemical and biophysical research communications* 483, 366–370 published online Dec 23, 2016. DOI: 10.1016/j.bbrc.2016.12.137.
- (163) Kim, Y., and Chen, J. (2018) Molecular structure of human P-glycoprotein in the ATP-bound, outward-facing conformation, *Science (New York, N.Y.)* 359, 915–919 published online Jan 25, 2018. DOI: 10.1126/science.aar7389.
- (164) Walker, J. E., Saraste, M., Runswick, M. J., and Gay, N. J. (1982) Distantly related sequences in the alpha- and beta-subunits of ATP synthase, myosin, kinases and other ATP-requiring enzymes and a common nucleotide binding fold, *The EMBO journal* 1, 945–951.
- (165) Geourjon, C., Orelle, C., Steinfels, E., Blanchet, C., Deléage, G., Di Pietro, A., and Jault, J.-M. (2001) A common mechanism for ATP hydrolysis in ABC transporter and helicase superfamilies, *Trends in Biochemical Sciences* 26, 539–544. DOI: 10.1016/S0968-0004(01)01907-7.
- (166) Leipe, D. D., Wolf, Y. I., Koonin, E. V., and Aravind, L. (2002) Classification and evolution of P-loop GTPases and related ATPases, *Journal of molecular biology* 317, 41–72. DOI: 10.1006/jmbi.2001.5378.
- (167) Verdon, G., Albers, S. V., Dijkstra, B. W., Driessen, A. J., and Thunnissen, A.-M. W. (2003) Crystal Structures of the ATPase Subunit of the Glucose ABC Transporter from *Sulfolobus solfataricus*: Nucleotide-free and Nucleotide-bound Conformations, *Journal of molecular biology* 330, 343–358. DOI: 10.1016/S0022-2836(03)00575-8.
- (168) Hopfner, K.-P., Karcher, A., Shin, D. S., Craig, L., Arthur, L., Carney, J. P., and Tainer, J. A. (2000) Structural Biology of Rad50 ATPase, *Cell* 101, 789–800. DOI: 10.1016/s0092-8674(00)80890-9.
- (169) Smith, P. C., Karpowich, N., Millen, L., Moody, J. E., Rosen, J., Thomas, P. J., and Hunt, J. F. (2002) ATP Binding to the Motor Domain from an ABC Transporter Drives Formation of a Nucleotide Sandwich Dimer, *Molecular Cell* 10, 139–149. DOI: 10.1016/s1097-2765(02)00576-2.
- (170) Chen, J., Lu, G., Lin, J., Davidson, A. L., and Quioco, F. A. (2003) A tweezers-like motion of the ATP-binding cassette dimer in an ABC transport cycle, *Molecular Cell* 12, 651–661. DOI: 10.1016/j.molcel.2003.08.004.

- (171) Zaitseva, J., Jenewein, S., Jumpertz, T., Holland, I. B., and Schmitt, L. (2005) H662 is the linchpin of ATP hydrolysis in the nucleotide-binding domain of the ABC transporter HlyB, *The EMBO journal* 24, 1901–1910 published online May 12, 2005. DOI: 10.1038/sj.emboj.7600657.
- (172) Procko, E., Ferrin-O'Connell, I., Ng, S.-L., and Gaudet, R. (2006) Distinct structural and functional properties of the ATPase sites in an asymmetric ABC transporter, *Molecular Cell* 24, 51–62. DOI: 10.1016/j.molcel.2006.07.034.
- (173) Jones, P. M., and George, A. M. (2012) Role of the D-loops in allosteric control of ATP hydrolysis in an ABC transporter, *The journal of physical chemistry. A* 116, 3004–3013 published online Mar 13, 2012. DOI: 10.1021/jp211139s.
- (174) Grossmann, N., Vakkasoglu, A. S., Hulpke, S., Abele, R., Gaudet, R., and Tampé, R. (2014) Mechanistic determinants of the directionality and energetics of active export by a heterodimeric ABC transporter, *Nature Communications* 5, 5419 published online Nov 7, 2014. DOI: 10.1038/ncomms6419.
- (175) Oswald, C., Holland, I. B., and Schmitt, L. (2006) The motor domains of ABC-transporters. What can structures tell us?, *Naunyn-Schmiedeberg's archives of pharmacology* 372, 385–399 published online Mar 16, 2006. DOI: 10.1007/s00210-005-0031-4.
- (176) Schmitt, L. (2002) Structure and mechanism of ABC transporters, *Current opinion in structural biology* 12, 754–760. DOI: 10.1016/S0959-440X(02)00399-8.
- (177) Oancea, G., O'Mara, M. L., Bennett, W. F. D., Tieleman, D. P., Abele, R., and Tampé, R. (2009) Structural arrangement of the transmission interface in the antigen ABC transport complex TAP, *Proceedings of the National Academy of Sciences of the United States of America* 106, 5551–5556 published online Mar 18, 2009. DOI: 10.1073/pnas.0811260106.
- (178) Becker, J.-P., van Bambeke, F., Tulkens, P. M., and Prévost, M. (2010) Dynamics and structural changes induced by ATP binding in SAV1866, a bacterial ABC exporter, *The journal of physical chemistry. B* 114, 15948–15957 published online Nov 11, 2010. DOI: 10.1021/jp1038392.
- (179) Damas, J. M., Oliveira, A. S. F., Baptista, A. M., and Soares, C. M. (2011) Structural consequences of ATP hydrolysis on the ABC transporter NBD dimer: molecular dynamics studies of HlyB, *Protein science : a publication of the Protein Society* 20, 1220–1230. DOI: 10.1002/pro.650.
- (180) Kluth, M., Stindt, J., Dröge, C., Linnemann, D., Kubitz, R., and Schmitt, L. (2015) A mutation within the extended X loop abolished substrate-induced ATPase activity of the human liver ATP-binding cassette (ABC) transporter MDR3, *Journal of Biological Chemistry* 290, 4896–4907 published online Dec 22, 2014. DOI: 10.1074/jbc.M114.588566.
- (181) Xu, Y., Seelig, A., and Bernèche, S. (2017) Unidirectional Transport Mechanism in an ATP Dependent Exporter, *ACS Central Science* 3, 250–258 published online Mar 7, 2017. DOI: 10.1021/acscentsci.7b00068.
- (182) Lacabanne, D., Orelle, C., Lecoq, L., Kunert, B., Chuilon, C., Wiegand, T., Ravaud, S., Jault, J.-M., Meier, B. H., and Böckmann, A. (2019) Flexible-to-rigid transition is central for substrate transport in the ABC transporter BmrA from *Bacillus subtilis*, *Communications Biology* 2, 149 published online Apr 29, 2019. DOI: 10.1038/s42003-019-0390-x.
- (183) Shintre, C. A., Pike, A. C. W., Li, Q., Kim, J.-I., Barr, A. J., Goubin, S., Shrestha, L., Yang, J., Berridge, G., Ross, J., Stansfeld, P. J., Sansom, M. S. P., Edwards, A. M., Bountra, C., Marsden, B. D., Delft, F. von, Bullock, A. N., Gileadi, O., Burgess-Brown, N. A., and Carpenter, E. P. (2013) Structures of ABCB10, a human ATP-binding cassette transporter in apo- and nucleotide-bound states, *Proceedings of the National Academy of Sciences of the United States of America* 110, 9710–9715 published online May 28, 2013. DOI: 10.1073/pnas.1217042110.

- (184) Kodan, A., Yamaguchi, T., Nakatsu, T., Matsuoka, K., Kimura, Y., Ueda, K., and Kato, H. (2019) Inward- and outward-facing X-ray crystal structures of homodimeric P-glycoprotein CmABCB1, *Nature Communications* 10, 88 published online Jan 8, 2019. DOI: 10.1038/s41467-018-08007-x.
- (185) Dalmás, O., Orelle, C., Foucher, A.-E., Geourjon, C., Crouzy, S., Di Pietro, A., and Jault, J.-M. (2005) The Q-loop disengages from the first intracellular loop during the catalytic cycle of the multidrug ABC transporter BmrA, *The Journal of Biological Chemistry* 280, 36857–36864 published online Aug 17, 2005. DOI: 10.1074/jbc.M503266200.
- (186) Jin, M. S., Oldham, M. L., Zhang, Q., and Chen, J. (2012) Crystal structure of the multidrug transporter P-glycoprotein from *Caenorhabditis elegans*, *Nature* 490, 566–569 published online Sep 23, 2012. DOI: 10.1038/nature11448.
- (187) Saraste, M., Sibbald, P. R., and Wittinghofer, A. (1990) The P-loop — a common motif in ATP- and GTP-binding proteins, *Trends in Biochemical Sciences* 15, 430–434. DOI: 10.1016/0968-0004(90)90281-F.
- (188) Diederichs, K., Diez, J., Grellner, G., Müller, C., Breed, J., Schnell, C., Vonrhein, C., Boos, W., and Welte, W. (2000) Crystal structure of MalK, the ATPase subunit of the trehalose/maltose ABC transporter of the archaeon *Thermococcus litoralis*, *The EMBO journal* 19, 5951–5961. DOI: 10.1093/emboj/19.22.5951.
- (189) Zaitseva, J., Oswald, C., Jumpertz, T., Jenewein, S., Wiedenmann, A., Holland, I. B., and Schmitt, L. (2006) A structural analysis of asymmetry required for catalytic activity of an ABC-ATPase domain dimer, *The EMBO journal* 25, 3432–3443 published online Jul 6, 2006. DOI: 10.1038/sj.emboj.7601208.
- (190) Gaudet, R., and Wiley, D. C. (2001) Structure of the ABC ATPase domain of human TAP1, the transporter associated with antigen processing, *The EMBO journal* 20, 4964–4972. DOI: 10.1093/emboj/20.17.4964.
- (191) Dawson, R. J. P., and Locher, K. P. (2007) Structure of the multidrug ABC transporter Sav1866 from *Staphylococcus aureus* in complex with AMP-PNP, *FEBS letters* 581, 935–938 published online Feb 7, 2007. DOI: 10.1016/j.febslet.2007.01.073.
- (192) Matte, A., and Delbaere, L. T. J. (2005) ATP-binding Motifs. in *Encyclopedia of life sciences*. (John Wiley & Sons, L., Ed.), John Wiley & Sons, London, New York.
- (193) Azzaria, M., Schurr, E., and Gros, P. (1989) Discrete mutations introduced in the predicted nucleotide-binding sites of the *mdr1* gene abolish its ability to confer multidrug resistance, *Molecular and Cellular Biology* 9, 5289–5297. DOI: 10.1128/mcb.9.12.5289-5297.1989.
- (194) Hellmich, U. A., Haase, W., Velamakanni, S., van Veen, H. W., and Glaubitz, C. (2008) Caught in the Act: ATP hydrolysis of an ABC-multidrug transporter followed by real-time magic angle spinning NMR, *FEBS letters* 582, 3557–3562 published online Sep 24, 2008. DOI: 10.1016/j.febslet.2008.09.033.
- (195) Orelle, C., Gubellini, F., Durand, A., Marco, S., Lévy, D., Gros, P., Di Pietro, A., and Jault, J.-M. (2008) Conformational change induced by ATP binding in the multidrug ATP-binding cassette transporter BmrA, *Biochemistry* 47, 2404–2412 published online Jan 24, 2008. DOI: 10.1021/bi702303s.
- (196) Amann, T., Schell, S., Kühner, P., Winkler, M., Schwanstecher, M., Russ, U., and Quast, U. (2010) Substitution of the Walker A lysine by arginine in the nucleotide-binding domains of sulphonylurea receptor SUR2B: effects on ligand binding and channel activity, *Naunyn-Schmiedeberg's archives of pharmacology* 381, 507–516 published online Mar 30, 2010. DOI: 10.1007/s00210-010-0510-0.
- (197) Bukowska, M. A., Hohl, M., Geertsma, E. R., Hürlimann, L. M., Grütter, M. G., and Seeger, M. A. (2015) A Transporter Motor Taken Apart: Flexibility in the Nucleotide Binding Domains of a

- Heterodimeric ABC Exporter, *Biochemistry* 54, 3086–3099 published online May 7, 2015. DOI: 10.1021/acs.biochem.5b00188.
- (198) Chène, P. (2002) ATPases as drug targets: learning from their structure, *Nature reviews. Drug discovery* 1, 665–673. DOI: 10.1038/nrd894.
- (199) Story, R. M., and Steitz, T. A. (1992) Structure of the recA protein-ADP complex, *Nature* 355, 374–376. DOI: 10.1038/355374a0.
- (200) Muneyuki, E., Noji, H., Amano, T., Masaike, T., and Yoshida, M. (2000) FOF1-ATP synthase: general structural features of ‘ATP-engine’ and a problem on free energy transduction, *Biochimica et Biophysica Acta (BBA) - Bioenergetics* 1458, 467–481. DOI: 10.1016/s0005-2728(00)00095-5.
- (201) Esser, L., Zhou, F., Pluchino, K. M., Shiloach, J., Ma, J., Tang, W., Gutierrez, C., Zhang, A., Shukla, S., Madigan, J. P., Zhou, T., Kwong, P. D., Ambudkar, S. V., Gottesman, M. M., and Di Xia (2017) Structures of the Multidrug Transporter P-glycoprotein Reveal Asymmetric ATP Binding and the Mechanism of Polyspecificity, *The Journal of Biological Chemistry* 292, 446–461 published online Nov 18, 2016. DOI: 10.1074/jbc.M116.755884.
- (202) Hofmann, S., Janulienė, D., Mehdipour, A. R., Thomas, C., Stefan, E., Brüchert, S., Kuhn, B. T., Geertsma, E. R., Hummer, G., Tampé, R., and Moeller, A. (2019) Conformation space of a heterodimeric ABC exporter under turnover conditions, *Nature* 571, 580–583 published online Jul 17, 2019. DOI: 10.1038/s41586-019-1391-0.
- (203) Chi, X., Fan, Q., Zhang, Y., Liang, K., Wan, L., Zhou, Q., and Li, Y. (2020) Structural mechanism of phospholipids translocation by MlaFEDB complex, *Cell Research* 30, 1127–1135 published online Sep 3, 2020. DOI: 10.1038/s41422-020-00404-6.
- (204) Sharma, S., and Davidson, A. L. (2000) Vanadate-induced trapping of nucleotides by purified maltose transport complex requires ATP hydrolysis, *Journal of bacteriology* 182, 6570–6576. DOI: 10.1128/JB.182.23.6570-6576.2000.
- (205) Russell, P. L., and Sharom, F. J. (2006) Conformational and functional characterization of trapped complexes of the P-glycoprotein multidrug transporter, *The Biochemical journal* 399, 315–323. DOI: 10.1042/BJ20060015.
- (206) Zutz, A., Hoffmann, J., Hellmich, U. A., Glaubitz, C., Ludwig, B., Brutschy, B., and Tampé, R. (2011) Asymmetric ATP hydrolysis cycle of the heterodimeric multidrug ABC transport complex TmrAB from *Thermus thermophilus*, *Journal of Biological Chemistry* 286, 7104–7115 published online Dec 29, 2010. DOI: 10.1074/jbc.M110.201178.
- (207) Pan, X., Zhang, Q., Qu, S., Huang, S., Wang, H., and Mei, H. (2016) Allosteric effects of ATP binding on the nucleotide-binding domain of a heterodimeric ATP-binding cassette transporter, *Integrative biology : quantitative biosciences from nano to macro* 8, 1158–1169. DOI: 10.1039/c6ib00136j.
- (208) Oloo, E. O., Fung, E. Y., and Tieleman, D. P. (2006) The dynamics of the MgATP-driven closure of MalK, the energy-transducing subunit of the maltose ABC transporter, *Journal of Biological Chemistry* 281, 28397–28407 published online Jul 28, 2006. DOI: 10.1074/jbc.M513614200.
- (209) Wang, J., Grishin, N., Kinch, L., Cohen, J. C., Hobbs, H. H., and Xie, X.-S. (2011) Sequences in the nonconsensus nucleotide-binding domain of ABCG5/ABCG8 required for sterol transport, *Journal of Biological Chemistry* 286, 7308–7314 published online Jan 5, 2011. DOI: 10.1074/jbc.M110.210880.
- (210) Hürlimann, L. M., Hohl, M., and Seeger, M. A. (2017) Split tasks of asymmetric nucleotide-binding sites in the heterodimeric ABC exporter EfrCD, *The FEBS Journal* 284, 1672–1687 published online Apr 18, 2017. DOI: 10.1111/febs.14065.
- (211) Schultz, K. M., Merten, J. A., and Klug, C. S. (2011) Effects of the L511P and D512G Mutations on the *Escherichia coli* ABC Transporter MsbA, *Biochemistry* 50, 2594–2602. DOI: 10.1021/bi1018418.

- (212) Polissi, A., and Georgopoulos, C. (1996) Mutational analysis and properties of the *msbA* gene of *Escherichia coli*, coding for an essential ABC family transporter, *Molecular microbiology* 20, 1221–1233. DOI: 10.1111/j.1365-2958.1996.tb02642.x.
- (213) Schultz, K. M., Merten, J. A., and Klug, C. S. (2011) Characterization of the E506Q and H537A dysfunctional mutants in the *E. coli* ABC transporter *MsbA*, *Biochemistry* 50, 3599–3608 published online Apr 13, 2011. DOI: 10.1021/bi101666p.
- (214) Oldham, M. L., and Chen, J. (2011) Crystal structure of the maltose transporter in a pretranslocation intermediate state, *Science (New York, N.Y.)* 332, 1202–1205 published online May 12, 2011. DOI: 10.1126/science.1200767.
- (215) Shyamala, V., Baichwal, V., Beall, E., and Ames, G. F. (1991) Structure-function analysis of the histidine permease and comparison with cystic fibrosis mutations, *The Journal of Biological Chemistry* 266, 18714–18719.
- (216) Nikaido, K., and Ames, G. F. (1999) One intact ATP-binding subunit is sufficient to support ATP hydrolysis and translocation in an ABC transporter, the histidine permease, *The Journal of Biological Chemistry* 274, 26727–26735. DOI: 10.1074/jbc.274.38.26727.
- (217) Davidson, A. L., and Sharma, S. (1997) Mutation of a single MalK subunit severely impairs maltose transport activity in *Escherichia coli*, *Journal of bacteriology* 179, 5458–5464. DOI: 10.1128/jb.179.17.5458-5464.1997.
- (218) Karpowich, N., Martsinkevich, O., Millen, L., Yuan, Y.-R., Dai, P. L., MacVey, K., Thomas, P. J., and Hunt, J. F. (2001) Crystal Structures of the MJ1267 ATP Binding Cassette Reveal an Induced-Fit Effect at the ATPase Active Site of an ABC Transporter, *Structure (London, England : 1993)* 9, 571–586. DOI: 10.1016/S0969-2126(01)00617-7.
- (219) Campbell, J. D., Deol, S. S., Ashcroft, F. M., Kerr, I. D., and Sansom, M. S. P. (2004) Nucleotide-dependent conformational changes in HisP: molecular dynamics simulations of an ABC transporter nucleotide-binding domain, *Biophysical Journal* 87, 3703–3715 published online Sep 17, 2004. DOI: 10.1529/biophysj.104.046870.
- (220) Jones, P. M., and George, A. M. (2007) Nucleotide-dependent allostery within the ABC transporter ATP-binding cassette: a computational study of the MJ0796 dimer, *The Journal of Biological Chemistry* 282, 22793–22803 published online May 7, 2007. DOI: 10.1074/jbc.M700809200.
- (221) Jones, P. M., and George, A. M. (1999) Subunit interactions in ABC transporters: towards a functional architecture, *FEMS microbiology letters* 179, 187–202. DOI: 10.1111/j.1574-6968.1999.tb08727.x.
- (222) Shalaeva, D. N., Cherepanov, D. A., Galperin, M. Y., and Mulkidjanian, A. Y. (2018) Comparative analysis of active sites in P-loop nucleoside triphosphatases suggests an ancestral activation mechanism, *bioRxiv*, 439992. DOI: 10.1101/439992.
- (223) Higgins, C. F., and Linton, K. J. (2004) The ATP switch model for ABC transporters, *Nature structural & molecular biology* 11, 918–926. DOI: 10.1038/nsmb836.
- (224) Janas, E., Hofacker, M., Chen, M., Gompf, S., van der Does, C., and Tampé, R. (2003) The ATP hydrolysis cycle of the nucleotide-binding domain of the mitochondrial ATP-binding cassette transporter Mdl1p, *The Journal of Biological Chemistry* 278, 26862–26869 published online May 13, 2003. DOI: 10.1074/jbc.M301227200.
- (225) van der Does, C., and Tampé, R. (2004) How do ABC transporters drive transport?, *Biological chemistry* 385, 927–933. DOI: 10.1515/BC.2004.121.

- (226) Jones, P. M., and George, A. M. (2009) Opening of the ADP-bound active site in the ABC transporter ATPase dimer: evidence for a constant contact, alternating sites model for the catalytic cycle, *Proteins* 75, 387–396. DOI: 10.1002/prot.22250.
- (227) Senior, A. E., al-Shawi, M. K., and Urbatsch, I. L. (1995) The catalytic cycle of P-glycoprotein, *FEBS letters* 377, 285–289. DOI: 10.1016/0014-5793(95)01345-8.
- (228) Sauna, Z. E., and Ambudkar, S. V. (2007) About a switch: how P-glycoprotein (ABCB1) harnesses the energy of ATP binding and hydrolysis to do mechanical work, *Molecular cancer therapeutics* 6, 13–23. DOI: 10.1158/1535-7163.MCT-06-0155.
- (229) Sauna, Z. E., Kim, I.-W., Nandigama, K., Kopp, S., Chiba, P., and Ambudkar, S. V. (2007) Catalytic cycle of ATP hydrolysis by P-glycoprotein: evidence for formation of the E.S reaction intermediate with ATP-gamma-S, a nonhydrolyzable analogue of ATP, *Biochemistry* 46, 13787–13799 published online Nov 8, 2007. DOI: 10.1021/bi701385t.
- (230) Sjarheyeva, A., Liu, R., and Sharom, F. J. (2010) Characterization of an asymmetric occluded state of P-glycoprotein with two bound nucleotides: implications for catalysis, *The Journal of Biological Chemistry* 285, 7575–7586 published online Jan 8, 2010. DOI: 10.1074/jbc.M109.047290.
- (231) Jones, P. M., O'Mara, M. L., and George, A. M. (2009) ABC transporters: a riddle wrapped in a mystery inside an enigma, *Trends in Biochemical Sciences* 34, 520–531 published online Sep 11, 2009. DOI: 10.1016/j.tibs.2009.06.004.
- (232) Albe, K. R., Butler, M. H., and Wright, B. E. (1990) Cellular concentrations of enzymes and their substrates, *Journal of Theoretical Biology* 143, 163–195. DOI: 10.1016/S0022-5193(05)80266-8.
- (233) Stefan, E., Hofmann, S., and Tampé, R. (2020) A single power stroke by ATP binding drives substrate translocation in a heterodimeric ABC transporter, *eLife* 9 published online Apr 21, 2020. DOI: 10.7554/eLife.55943.
- (234) Jardetzky, O. (1966) Simple allosteric model for membrane pumps, *Nature* 211, 969–970. DOI: 10.1038/211969a0.
- (235) Rees, D. C., Johnson, E., and Lewinson, O. (2009) ABC transporters: the power to change, *Nature reviews. Molecular cell biology* 10, 218–227. DOI: 10.1038/nrm2646.
- (236) Clay, A. T., and Sharom, F. J. (2013) Lipid bilayer properties control membrane partitioning, binding, and transport of p-glycoprotein substrates, *Biochemistry* 52, 343–354 published online Jan 4, 2013. DOI: 10.1021/bi301532c.
- (237) Higgins, C. F., and Gottesman, M. M. (1992) Is the multidrug transporter a flippase?, *Trends in Biochemical Sciences* 17, 18–21. DOI: 10.1016/0968-0004(92)90419-A.
- (238) Eytan, G. D., Regev, R., Oren, G., and Assaraf, Y. G. (1996) The role of passive transbilayer drug movement in multidrug resistance and its modulation, *The Journal of Biological Chemistry* 271, 12897–12902. DOI: 10.1074/jbc.271.22.12897.
- (239) Ambudkar, S. V., Lelong, I. H., Zhang, J., Cardarelli, C. O., Gottesman, M. M., and Pastan, I. (1992) Partial purification and reconstitution of the human multidrug-resistance pump: characterization of the drug-stimulatable ATP hydrolysis, *Proceedings of the National Academy of Sciences of the United States of America* 89, 8472–8476. DOI: 10.1073/pnas.89.18.8472.
- (240) Sarkadi, B., Müller, M., Homolya, L., Holló, Z., Seprödi, J., Germann, U. A., Gottesman, M. M., Price, E. M., and Boucher, R. C. (1994) Interaction of bioactive hydrophobic peptides with the human multidrug transporter, *FASEB journal : official publication of the Federation of American Societies for Experimental Biology* 8, 766–770. DOI: 10.1096/fasebj.8.10.7914178.
- (241) Urbatsch, I. L., al-Shawi, M. K., and Senior, A. E. (1994) Characterization of the ATPase activity of purified Chinese hamster P-glycoprotein, *Biochemistry* 33, 7069–7076. DOI: 10.1021/bi00189a008.

- (242) Senior, A. E., al-Shawi, M. K., and Urbatsch, I. L. (1995) ATP hydrolysis by multidrug-resistance protein from Chinese hamster ovary cells, *Journal of bioenergetics and biomembranes* 27, 31–36. DOI: 10.1007/BF02110328.
- (243) Loo, T. W., and Clarke, D. M. (1997) Drug-stimulated ATPase activity of human P-glycoprotein requires movement between transmembrane segments 6 and 12, *The Journal of Biological Chemistry* 272, 20986–20989. DOI: 10.1074/jbc.272.34.20986.
- (244) Ford, R. C., and Beis, K. (2019) Learning the ABCs one at a time: structure and mechanism of ABC transporters, *Biochemical Society transactions* 47, 23–36 published online Jan 9, 2019. DOI: 10.1042/BST20180147.
- (245) Choudhury, H. G., Tong, Z., Mathavan, I., Li, Y., Iwata, S., Zirah, S., Rebuffat, S., van Veen, H. W., and Beis, K. (2014) Structure of an antibacterial peptide ATP-binding cassette transporter in a novel outward occluded state, *Proceedings of the National Academy of Sciences of the United States of America* 111, 9145–9150 published online Jun 11, 2014. DOI: 10.1073/pnas.1320506111.
- (246) Lin, D. Y., Huang, S., and Chen, J. (2015) Crystal structures of a polypeptide processing and secretion transporter, *Nature* 523, 425–430. DOI: 10.1038/nature14623.
- (247) Bountra, K., Hagelueken, G., Choudhury, H. G., Corradi, V., El Omari, K., Wagner, A., Mathavan, I., Zirah, S., Yuan Wahlgren, W., Tieleman, D. P., Schiemann, O., Rebuffat, S., and Beis, K. (2017) Structural basis for antibacterial peptide self-immunity by the bacterial ABC transporter McjD, *The EMBO journal* 36, 3062–3079 published online Sep 1, 2017. DOI: 10.15252/embj.201797278.
- (248) Husada, F., Bountra, K., Tassis, K., Boer, M. de, Romano, M., Rebuffat, S., Beis, K., and Cordes, T. (2018) Conformational dynamics of the ABC transporter McjD seen by single-molecule FRET, *The EMBO journal* 37 published online Sep 20, 2018. DOI: 10.15252/embj.2018100056.
- (249) Moeller, A., Lee, S. C., Tao, H., Speir, J. A., Chang, G., Urbatsch, I. L., Potter, C. S., Carragher, B., and Zhang, Q. (2015) Distinct conformational spectrum of homologous multidrug ABC transporters, *Structure (London, England : 1993)* 23, 450–460 published online Feb 5, 2015. DOI: 10.1016/j.str.2014.12.013.
- (250) Romano, M., Fusco, G., Choudhury, H. G., Mehmood, S., Robinson, C. V., Zirah, S., Hegemann, J. D., Lescop, E., Marahiel, M. A., Rebuffat, S., Simone, A. de, and Beis, K. (2018) Structural Basis for Natural Product Selection and Export by Bacterial ABC Transporters, *ACS chemical biology* 13, 1598–1609 published online May 18, 2018. DOI: 10.1021/acscchembio.8b00226.
- (251) Angiulli, G., Dhupar, H. S., Suzuki, H., Wason, I. S., van Duong Hoa, F., and Walz, T. (2020) New approach for membrane protein reconstitution into peptidiscs and basis for their adaptability to different proteins, *eLife* 9 published online Mar 3, 2020. DOI: 10.7554/eLife.53530.
- (252) Perez, C., Gerber, S., Boilevin, J., Bucher, M., Darbre, T., Aebi, M., Reymond, J.-L., and Locher, K. P. (2015) Structure and mechanism of an active lipid-linked oligosaccharide flippase, *Nature* 524, 433–438 published online Aug 12, 2015. DOI: 10.1038/nature14953.
- (253) Johnson, Z. L., and Chen, J. (2018) ATP Binding Enables Substrate Release from Multidrug Resistance Protein 1, *Cell* 172, 81–89.e10 published online Dec 28, 2017. DOI: 10.1016/j.cell.2017.12.005.
- (254) Hellmich, U. A., Lyubenova, S., Kaltenborn, E., Doshi, R., van Veen, H. W., Prisner, T. F., and Glaubitz, C. (2012) Probing the ATP hydrolysis cycle of the ABC multidrug transporter LmrA by pulsed EPR spectroscopy, *Journal of the American Chemical Society* 134, 5857–5862 published online Mar 21, 2012. DOI: 10.1021/ja211007t.
- (255) Bordignon, E., Seeger, M. A., Galazzo, L., and Meier, G. (2020) From in vitro towards in situ: structure-based investigation of ABC exporters by electron paramagnetic resonance spectroscopy, *FEBS letters* 594, 3839–3856 published online Dec 1, 2020. DOI: 10.1002/1873-3468.14004.

- (256) Galazzo, L., Meier, G., Timachi, M. H., Hutter, C. A. J., Seeger, M. A., and Bordignon, E. (2020) Spin-labeled nanobodies as protein conformational reporters for electron paramagnetic resonance in cellular membranes, *PNAS* *117*, 2441–2448 published online Jan 21, 2020. DOI: 10.1073/pnas.1913737117.
- (257) Buchaklian, A. H., Funk, A. L., and Klug, C. S. (2004) Resting state conformation of the MsbA homodimer as studied by site-directed spin labeling, *Biochemistry* *43*, 8600–8606. DOI: 10.1021/bi0497751.
- (258) Buchaklian, A. H., and Klug, C. S. (2005) Characterization of the Walker A motif of MsbA using site-directed spin labeling electron paramagnetic resonance spectroscopy, *Biochemistry* *44*, 5503–5509. DOI: 10.1021/bi047568v.
- (259) Dong, J., Yang, G., and Mchaourab, H. S. (2005) Structural basis of energy transduction in the transport cycle of MsbA, *Science (New York, N.Y.)* *308*, 1023–1028. DOI: 10.1126/science.1106592.
- (260) Buchaklian, A. H., and Klug, C. S. (2006) Characterization of the LSGGQ and H motifs from the Escherichia coli lipid A transporter MsbA, *Biochemistry* *45*, 12539–12546. DOI: 10.1021/bi060830a.
- (261) Borbat, P. P., Surendhran, K., Bortolus, M., Zou, P., Freed, J. H., and Mchaourab, H. S. (2007) Conformational motion of the ABC transporter MsbA induced by ATP hydrolysis, *PLoS Biology* *5*, e271. DOI: 10.1371/journal.pbio.0050271.
- (262) Westfahl, K. M., Merten, J. A., Buchaklian, A. H., and Klug, C. S. (2008) Functionally important ATP binding and hydrolysis sites in Escherichia coli MsbA, *Biochemistry* *47*, 13878–13886. DOI: 10.1021/bi801745u.
- (263) Zou, P., Bortolus, M., and Mchaourab, H. S. (2009) Conformational cycle of the ABC transporter MsbA in liposomes: detailed analysis using double electron-electron resonance spectroscopy, *Journal of molecular biology* *393*, 586–597 published online Aug 26, 2009. DOI: 10.1016/j.jmb.2009.08.050.
- (264) Mishra, S., Verhalen, B., Stein, R. A., Wen, P.-C., Tajkhorshid, E., and Mchaourab, H. S. (2014) Conformational dynamics of the nucleotide binding domains and the power stroke of a heterodimeric ABC transporter, *eLife* *3*, e02740 published online May 16, 2014. DOI: 10.7554/eLife.02740.
- (265) Do Cao, M.-A., Crouzy, S., Kim, M., Becchi, M., Cafiso, D. S., Di Pietro, A., and Jault, J.-M. (2009) Probing the conformation of the resting state of a bacterial multidrug ABC transporter, BmrA, by a site-directed spin labeling approach, *Protein Science* *18*, 1507–1520. DOI: 10.1002/pro.141.
- (266) Wiegand, T., Lacabanne, D., Keller, K., Cadalbert, R., Lecoq, L., Yulikov, M., Terradot, L., Jeschke, G., Meier, B. H., and Böckmann, A. (2017) Solid-state NMR and EPR Spectroscopy of Mn²⁺ - Substituted ATP-Fueled Protein Engines, *Angewandte Chemie (International ed. in English)* *56*, 3369–3373 published online Feb 13, 2017. DOI: 10.1002/anie.201610551.
- (267) Wiegand, T. (2020) A solid-state NMR tool box for the investigation of ATP-fueled protein engines, *Progress in nuclear magnetic resonance spectroscopy* *117*, 1–32 published online Feb 27, 2020. DOI: 10.1016/j.pnmrs.2020.02.001.
- (268) Zoghbi, M. E., and Altenberg, G. A. (2018) Luminescence resonance energy transfer spectroscopy of ATP-binding cassette proteins, *Biochimica et Biophysica Acta (BBA) - Biomembranes* *1860*, 854–867 published online Aug 8, 2017. DOI: 10.1016/j.bbamem.2017.08.005.
- (269) Cooper, R. S., and Altenberg, G. A. (2013) Association/dissociation of the nucleotide-binding domains of the ATP-binding cassette protein MsbA measured during continuous hydrolysis, *Journal of Biological Chemistry* *288*, 20785–20796 published online May 30, 2013. DOI: 10.1074/jbc.M113.477976.
- (270) Zoghbi, M. E., Cooper, R. S., and Altenberg, G. A. (2016) The Lipid Bilayer Modulates the Structure and Function of an ATP-binding Cassette Exporter, *Journal of Biological Chemistry* *291*, 4453–4461. DOI: 10.1074/jbc.M115.698498.

- (271) Liu, Y., Liu, Y., He, L., Zhao, Y., and Zhang, X. C. (2018) Single-molecule fluorescence studies on the conformational change of the ABC transporter MsbA, *Biophys Rep* 4, 153–165. DOI: 10.1007/s41048-018-0057-z.
- (272) Dalmas, O., Do Cao, M.-A., Lugo, M. R., Sharom, F. J., Di Pietro, A., and Jault, J.-M. (2005) Time-resolved fluorescence resonance energy transfer shows that the bacterial multidrug ABC half-transporter BmrA functions as a homodimer, *Biochemistry* 44, 4312–4321. DOI: 10.1021/bi0482809.
- (273) Mason, A. J., Siarheyeva, A., Haase, W., Lorch, M., van Veen, H., and Glaubitz, C. (2004) Amino acid type selective isotope labelling of the multidrug ABC transporter LmrA for solid-state NMR studies, *FEBS letters* 568, 117–121. DOI: 10.1016/j.febslet.2004.05.016.
- (274) Kunert, B., Gardiennet, C., Lacabanne, D., Calles-Garcia, D., Falson, P., Jault, J.-M., Meier, B. H., Penin, F., and Böckmann, A. (2014) Efficient and stable reconstitution of the ABC transporter BmrA for solid-state NMR studies, *Front. Mol. Biosci.* 1, 5 published online Jun 12, 2014. DOI: 10.3389/fmolb.2014.00005.
- (275) Hellmich, U. A., Mönkemeyer, L., Velamakanni, S., van Veen, H. W., and Glaubitz, C. (2015) Effects of nucleotide binding to LmrA: A combined MAS-NMR and solution NMR study, *Biochimica et biophysica acta* 1848, 3158–3165 published online Oct 9, 2015. DOI: 10.1016/j.bbamem.2015.10.003.
- (276) Kaur, H., Lakatos-Karoly, A., Vogel, R., Nöll, A., Tampé, R., and Glaubitz, C. (2016) Coupled ATPase-adenylate kinase activity in ABC transporters, *Nature Communications* 7, 13864 published online Dec 22, 2016. DOI: 10.1038/ncomms13864.
- (277) Siarheyeva, A., Lopez, J. J., Lehner, I., Hellmich, U. A., van Veen, H. W., and Glaubitz, C. (2007) Probing the molecular dynamics of the ABC multidrug transporter LmrA by deuterium solid-state nuclear magnetic resonance, *Biochemistry* 46, 3075–3083 published online Feb 16, 2007. DOI: 10.1021/bi062109a.
- (278) Kaur, H., Abreu, B., Akhmetzyanov, D., Lakatos-Karoly, A., Soares, C. M., Prisner, T., and Glaubitz, C. (2018) Unexplored Nucleotide Binding Modes for the ABC Exporter MsbA, *J. Am. Chem. Soc.* 140, 14112–14125 published online Oct 22, 2018. DOI: 10.1021/jacs.8b06739.
- (279) Hellmich, U. A., Duchardt-Ferner, E., Glaubitz, C., and Wöhnert, J. (2012) Backbone NMR resonance assignments of the nucleotide binding domain of the ABC multidrug transporter LmrA from *Lactococcus lactis* in its ADP-bound state, *Biomolecular NMR assignments* 6, 69–73 published online Jul 23, 2011. DOI: 10.1007/s12104-011-9327-0.
- (280) Kaur, H., Lakatos, A., Spadaccini, R., Vogel, R., Hoffmann, C., Becker-Baldus, J., Ouari, O., Tordo, P., Mchaourab, H., and Glaubitz, C. (2015) The ABC exporter MsbA probed by solid state NMR – challenges and opportunities, *Biological chemistry* 396, 1135–1149. DOI: 10.1515/hsz-2015-0119.
- (281) Spadaccini, R., Kaur, H., Becker-Baldus, J., and Glaubitz, C. (2018) The effect of drug binding on specific sites in transmembrane helices 4 and 6 of the ABC exporter MsbA studied by DNP-enhanced solid-state NMR, *Biochimica et Biophysica Acta (BBA) - Biomembranes* 1860, 833–840. DOI: 10.1016/j.bbamem.2017.10.017.
- (282) Doshi, R., Ali, A., Shi, W., Freeman, E. V., Fagg, L. A., and van Veen, H. W. (2013) Molecular disruption of the power stroke in the ATP-binding cassette transport protein MsbA, *Journal of Biological Chemistry* 288, 6801–6813 published online Jan 10, 2013. DOI: 10.1074/jbc.M112.430074.
- (283) Marcoux, J., Wang, S. C., Politis, A., Reading, E., Ma, J., Biggin, P. C., Zhou, M., Tao, H., Zhang, Q., Chang, G., Morgner, N., and Robinson, C. V. (2013) Mass spectrometry reveals synergistic effects of nucleotides, lipids, and drugs binding to a multidrug resistance efflux pump, *PNAS* 110, 9704–9709 published online May 20, 2013. DOI: 10.1073/pnas.1303888110.

- (284) Mehmood, S., Domene, C., Forest, E., and Jault, J.-M. (2012) Dynamics of a bacterial multidrug ABC transporter in the inward- and outward-facing conformations, *Proceedings of the National Academy of Sciences* 109, 10832–10836 published online Jun 18, 2012. DOI: 10.1073/pnas.1204067109.
- (285) Miroux, B., and Walker, J. E. (1996) Over-production of proteins in Escherichia coli: mutant hosts that allow synthesis of some membrane proteins and globular proteins at high levels, *Journal of molecular biology* 260, 289–298. DOI: 10.1006/jmbi.1996.0399.
- (286) Gibson, D. G., Young, L., Chuang, R.-Y., Venter, J. C., Hutchison, C. A., and Smith, H. O. (2009) Enzymatic assembly of DNA molecules up to several hundred kilobases, *Nature methods* 6, 343–345 published online Apr 12, 2009. DOI: 10.1038/nmeth.1318.
- (287) Artimo, P., Jonnalagedda, M., Arnold, K., Baratin, D., Csardi, G., Castro, E. de, Duvaud, S., Flegel, V., Fortier, A., Gasteiger, E., Grosdidier, A., Hernandez, C., Ioannidis, V., Kuznetsov, D., Liechti, R., Moretti, S., Mostaguir, K., Redaschi, N., Rossier, G., Xenarios, I., and Stockinger, H. (2012) ExPASy: SIB bioinformatics resource portal, *Nucleic Acids Research* 40, W597-603 published online May 31, 2012. DOI: 10.1093/nar/gks400.
- (288) Steinfels, E., Orelle, C., Dalmas, O., Penin, F., Miroux, B., Di Pietro, A., and Jault, J.-M. (2002) Highly efficient over-production in E. coli of YvcC, a multidrug-like ATP-binding cassette transporter from Bacillus subtilis, *Biochimica et Biophysica Acta (BBA) - Biomembranes* 1565, 1–5. DOI: 10.1016/s0005-2736(02)00515-1.
- (289) Orelle, C., Dalmas, O., Gros, P., Di Pietro, A., and Jault, J.-M. (2003) The conserved glutamate residue adjacent to the Walker-B motif is the catalytic base for ATP hydrolysis in the ATP-binding cassette transporter BmrA, *The Journal of Biological Chemistry* 278, 47002–47008 published online Sep 10, 2003. DOI: 10.1074/jbc.M308268200.
- (290) Mathieu, K., Javed, W., Vallet, S., Lesterlin, C., Candusso, M.-P., Ding, F., Xu, X. N., Ebel, C., Jault, J.-M., and Orelle, C. (2019) Functionality of membrane proteins overexpressed and purified from E. coli is highly dependent upon the strain, *Scientific reports* 9, 2654 published online Feb 25, 2019. DOI: 10.1038/s41598-019-39382-0.
- (291) LOWRY, O. H., ROSEBROUGH, N. J., FARR, A. L., and RANDALL, R. J. (1951) Protein measurement with the Folin phenol reagent, *The Journal of Biological Chemistry* 193, 265–275.
- (292) Micsonai, A., Wien, F., Kernya, L., Lee, Y.-H., Goto, Y., Réfrégiers, M., and Kardos, J. (2015) Accurate secondary structure prediction and fold recognition for circular dichroism spectroscopy, *Proceedings of the National Academy of Sciences of the United States of America* 112, E3095-103 published online Jun 2, 2015. DOI: 10.1073/pnas.1500851112.
- (293) Micsonai, A., Wien, F., Bulyáki, É., Kun, J., Moussong, É., Lee, Y.-H., Goto, Y., Réfrégiers, M., and Kardos, J. (2018) BeStSel: a web server for accurate protein secondary structure prediction and fold recognition from the circular dichroism spectra, *Nucleic Acids Research* 46, W315-W322. DOI: 10.1093/nar/gky497.
- (294) Ries, J., Schwarze, S., Johnson, C. M., and Neuweiler, H. (2014) Microsecond folding and domain motions of a spider silk protein structural switch, *Journal of the American Chemical Society* 136, 17136–17144 published online Nov 25, 2014. DOI: 10.1021/ja508760a.
- (295) Sauer, M., and Neuweiler, H. (2014) PET-FCS: probing rapid structural fluctuations of proteins and nucleic acids by single-molecule fluorescence quenching, *Methods in molecular biology (Clifton, N.J.)* 1076, 597–615. DOI: 10.1007/978-1-62703-649-8_27.
- (296) Keller, R. L. J. (2004) CANTINA verlag.

- (297) Salzmann, M., Pervushin, K., Wider, G., Senn, H., and Wüthrich, K. (1998) TROSY in triple-resonance experiments: new perspectives for sequential NMR assignment of large proteins, *Proceedings of the National Academy of Sciences* *95*, 13585–13590. DOI: 10.1073/pnas.95.23.13585.
- (298) Pérez Carrillo, V. H., Rose-Sperling, D., Tran, M. A., Wiedemann, C., and Hellmich, U. A. (2022) Backbone NMR assignment of the nucleotide binding domain of the *Bacillus subtilis* ABC multidrug transporter BmrA in the post-hydrolysis state, *Biomol NMR Assign* *16*, 81–86 published online Jan 5, 2022. DOI: 10.1007/s12104-021-10063-2.
- (299) Mulder, F. A., Schipper, D., Bott, R., and Boelens, R. (1999) Altered flexibility in the substrate-binding site of related native and engineered high-alkaline *Bacillus subtilis*ins, *Journal of molecular biology* *292*, 111–123. DOI: 10.1006/jmbi.1999.3034.
- (300) Williamson, M. P. (2013) Using chemical shift perturbation to characterise ligand binding, *Progress in Nuclear Magnetic Resonance Spectroscopy* *73*, 1–16 published online Mar 21, 2013. DOI: 10.1016/j.pnmrs.2013.02.001.
- (301) Carlomagno, T. (2005) Ligand-target interactions: what can we learn from NMR?, *Annual review of biophysics and biomolecular structure* *34*, 245–266. DOI: 10.1146/annurev.biophys.34.040204.144419.
- (302) Mörs, K., Hellmich, U. A., Basting, D., Marchand, P., Wurm, J. P., Haase, W., and Glaubitz, C. (2013) A lipid-dependent link between activity and oligomerization state of the *M. tuberculosis* SMR protein TBsmr, *Biochimica et biophysica acta* *1828*, 561–567 published online Oct 24, 2012. DOI: 10.1016/j.bbamem.2012.10.020.
- (303) (2016) Structure of the nucleotide binding domain of an ABC transporter MsbA from *Acinetobacter baumannii*.
- (304) Halavaty, A. S., Minasov, G., Dubrovskaya, I., Kiryukhina, O., Grimshaw, S., and Anderson, W. F. (2015) 1.73 Å resolution crystal structure of the ABC-ATPase domain (residues 357–609) of lipid A transport protein (msbA) from *Francisella tularensis* subsp. *tularensis* SCHU S4 in complex with ADP.
- (305) Steffel, L. R., Cashman, T. J., Reutershan, M. H., and Linton, B. R. (2007) Deuterium Exchange as an Indicator of Hydrogen Bond Donors and Acceptors, *J. Am. Chem. Soc.* *129*, 12956–12957 published online Oct 4, 2007. DOI: 10.1021/ja076185s.
- (306) Farrow, N. A., Muhandiram, R., Singer, A. U., Pascal, S. M., Kay, C. M., Gish, G., Shoelson, S. E., Pawson, T., Forman-Kay, J. D., and Kay, L. E. (1994) Backbone Dynamics of a Free and a Phosphopeptide-Complexed Src Homology 2 Domain Studied by ¹⁵N NMR Relaxation, *Biochemistry* *33*, 5984–6003. DOI: 10.1021/bi00185a040.
- (307) Sturlese, M., Manta, B., Bertarello, A., Bonilla, M., Lelli, M., Zambelli, B., Grunberg, K., Mammi, S., Comini, M. A., and Bellanda, M. (2018) The lineage-specific, intrinsically disordered N-terminal extension of monothiol glutaredoxin 1 from trypanosomes contains a regulatory region, *Scientific reports* *8*. DOI: 10.1038/s41598-018-31817-4.
- (308) Orelle, C., Alvarez, F. J. D., Oldham, M. L., Orelle, A., Wiley, T. E., Chen, J., and Davidson, A. L. (2010) Dynamics of α -helical subdomain rotation in the intact maltose ATP-binding cassette transporter, *Proceedings of the National Academy of Sciences* *107*, 20293–20298. DOI: 10.1073/pnas.1006544107.
- (309) Jones, P. M., and George, A. M. (2015) The Nucleotide-Free State of the Multidrug Resistance ABC Transporter LmrA: Sulfhydryl Cross-Linking Supports a Constant Contact, Head-to-Tail Configuration of the Nucleotide-Binding Domains, *PLoS one* *10*, e0131505 published online Jun 29, 2015. DOI: 10.1371/journal.pone.0131505.

- (310) Madeira, F., Pearce, M., Tivey, A. R. N., Basutkar, P., Lee, J., Edbali, O., Madhusoodanan, N., Kolesnikov, A., and Lopez, R. (2022) Search and sequence analysis tools services from EMBL-EBI in 2022, *Nucleic Acids Research published online* Apr 12, 2022. DOI: 10.1093/nar/gkac240.
- (311) Johnson, Z. L., and Chen, J. (2017) Structural Basis of Substrate Recognition by the Multidrug Resistance Protein MRP1, *Cell* 168, 1075-1085.e9 published online Feb 23, 2017. DOI: 10.1016/j.cell.2017.01.041.
- (312) Alam, A., Küng, R., Kowal, J., McLeod, R. A., Tremp, N., Broude, E. V., Roninson, I. B., Stahlberg, H., and Locher, K. P. (2018) Structure of a zosuquidar and UIC2-bound human-mouse chimeric ABCB1, *Proceedings of the National Academy of Sciences of the United States of America* 115, E1973-E1982 published online Feb 13, 2018. DOI: 10.1073/pnas.1717044115.
- (313) Ho, H., Miu, A., Alexander, M. K., Garcia, N. K., Oh, A., Zilberleyb, I., Reichelt, M., Austin, C. D., Tam, C., Shriver, S., Hu, H., Labadie, S. S., Liang, J., Wang, L., Wang, J., Lu, Y., Purkey, H. E., Quinn, J., Franke, Y., Clark, K., Beresini, M. H., Tan, M.-W., Sellers, B. D., Maurer, T., Koehler, M. F. T., Wecksler, A. T., Kiefer, J. R., Verma, V., Xu, Y., Nishiyama, M., Payandeh, J., and Koth, C. M. (2018) Structural basis for dual-mode inhibition of the ABC transporter MsbA, *Nature* 557, 196–201. DOI: 10.1038/s41586-018-0083-5.
- (314) Hutter, C. A. J., Timachi, M. H., Hürlimann, L. M., Zimmermann, I., Egloff, P., Göddeke, H., Kucher, S., Štefanić, S., Karttunen, M., Schäfer, L. V., Bordignon, E., and Seeger, M. A. (2019) The extracellular gate shapes the energy profile of an ABC exporter, *Nature Communications* 10, 2260 published online May 21, 2019. DOI: 10.1038/s41467-019-09892-6.
- (315) Nosol, K., Romane, K., Irobalieva, R. N., Alam, A., Kowal, J., Fujita, N., and Locher, K. P. (2020) Cryo-EM structures reveal distinct mechanisms of inhibition of the human multidrug transporter ABCB1, *Proceedings of the National Academy of Sciences of the United States of America* 117, 26245–26253 published online Oct 5, 2020. DOI: 10.1073/pnas.2010264117.
- (316) Schneider, T. D., and Stephens, R. M. (1990) Sequence logos: a new way to display consensus sequences, *Nucleic Acids Res* 18, 6097–6100. DOI: 10.1093/nar/18.20.6097.
- (317) Crooks, G. E., Hon, G., Chandonia, J.-M., and Brenner, S. E. (2004) WebLogo: a sequence logo generator, *Genome Res.* 14, 1188–1190. DOI: 10.1101/gr.849004.
- (318) Waqas Javed (2020) Study of the conformational states of bacterial multidrug ABC transporter BmrA. PhD thesis, University of Grenoble.
- (319) Wang, C., Karpowich, N., Hunt, J. F., Rance, M., and Palmer, A. G. (2004) Dynamics of ATP-binding cassette contribute to allosteric control, nucleotide binding and energy transduction in ABC transporters, *Journal of molecular biology* 342, 525–537. DOI: 10.1016/j.jmb.2004.07.001.
- (320) Verhalen, B., Dastvan, R., Thangapandian, S., Peskova, Y., Koteiche, H. A., Nakamoto, R. K., Tajkhorshid, E., and Mchaourab, H. S. (2017) Energy transduction and alternating access of the mammalian ABC transporter P-glycoprotein, *Nature* 543, 738–741 published online Mar 13, 2017. DOI: 10.1038/nature21414.
- (321) Zou, P., and Mchaourab, H. S. (2009) Alternating access of the putative substrate-binding chamber in the ABC transporter MsbA, *Journal of molecular biology* 393, 574–585 published online Aug 26, 2009. DOI: 10.1016/j.jmb.2009.08.051.
- (322) Dastvan, R., Mishra, S., Peskova, Y. B., Nakamoto, R. K., and Mchaourab, H. S. (2019) Mechanism of allosteric modulation of P-glycoprotein by transport substrates and inhibitors, *Science (New York, N.Y.)* 364, 689–692. DOI: 10.1126/science.aav9406.
- (323) Javed, W., Vallet, S., Clement, M.-P., Le Roy, A., Moulin, M., Härtlein, M., Breyton, C., Burlet-Schiltz, O., Marcoux, J., Orelle, C., Ebel, C., Martel, A., and Jault, J.-M. (2022) Structural Insights into

- the Catalytic Cycle of a Bacterial Multidrug ABC Efflux Pump, *Journal of molecular biology* 434, 167541 published online Mar 12, 2022. DOI: 10.1016/j.jmb.2022.167541.
- (324) Collauto, A., Mishra, S., Litvinov, A., Mchaourab, H. S., and Goldfarb, D. (2017) Direct Spectroscopic Detection of ATP Turnover Reveals Mechanistic Divergence of ABC Exporters, *Structure (London, England : 1993)* 25, 1264-1274.e3 published online Jul 14, 2017. DOI: 10.1016/j.str.2017.06.014.
- (325) Khare, D., Oldham, M. L., Orelle, C., Davidson, A. L., and Chen, J. (2009) Alternating access in maltose transporter mediated by rigid-body rotations, *Molecular Cell* 33, 528–536. DOI: 10.1016/j.molcel.2009.01.035.
- (326) Wen, P.-C., and Tajkhorshid, E. (2008) Dimer opening of the nucleotide binding domains of ABC transporters after ATP hydrolysis, *Biophysical Journal* 95, 5100–5110 published online Sep 12, 2008. DOI: 10.1529/biophysj.108.139444.
- (327) Yuan, Y. R., Blecker, S., Martsinkevich, O., Millen, L., Thomas, P. J., and Hunt, J. F. (2001) The crystal structure of the MJ0796 ATP-binding cassette. Implications for the structural consequences of ATP hydrolysis in the active site of an ABC transporter, *The Journal of Biological Chemistry* 276, 32313–32321 published online Jun 11, 2001. DOI: 10.1074/jbc.M100758200.
- (328) Jones, P. M., and George, A. M. (2017) How Intrinsic Dynamics Mediates the Allosteric Mechanism in the ABC Transporter Nucleotide Binding Domain Dimer, *Journal of chemical theory and computation* 13, 1712–1722 published online Mar 29, 2017. DOI: 10.1021/acs.jctc.6b00839.
- (329) George, A. M., and Jones, P. M. (2013) An asymmetric post-hydrolysis state of the ABC transporter ATPase dimer, *PLoS one* 8, e59854 published online Apr 3, 2013. DOI: 10.1371/journal.pone.0059854.
- (330) Wang, C., and Palmer, A. G. (2003) Solution NMR methods for quantitative identification of chemical exchange in ¹⁵N-labeled proteins, *Magn. Reson. Chem.* 41, 866–876. DOI: 10.1002/mrc.1262.
- (331) Wang, C., Rance, M., and Palmer, A. G. (2003) Mapping chemical exchange in proteins with MW 50 kD, *J. Am. Chem. Soc.* 125, 8968–8969. DOI: 10.1021/ja035139z.
- (332) Mourez, M., Hofnung, M., and Dassa, E. (1997) Subunit interactions in ABC transporters: a conserved sequence in hydrophobic membrane proteins of periplasmic permeases defines an important site of interaction with the ATPase subunits, *The EMBO journal* 16, 3066–3077. DOI: 10.1093/emboj/16.11.3066.
- (333) Hunke, S., Mourez, M., Jehanno, M., Dassa, E., and Schneider, E. (2000) ATP modulates subunit-subunit interactions in an ATP-binding cassette transporter (MalFGK2) determined by site-directed chemical cross-linking, *The Journal of Biological Chemistry* 275, 15526–15534. DOI: 10.1074/jbc.275.20.15526.
- (334) Jones, P. M., and George, A. M. (2002) Mechanism of ABC transporters: a molecular dynamics simulation of a well characterized nucleotide-binding subunit, *Proceedings of the National Academy of Sciences* 99, 12639–12644 published online Sep 17, 2002. DOI: 10.1073/pnas.152439599.
- (335) Hollenstein, K., Dawson, R. J. P., and Locher, K. P. (2007) Structure and mechanism of ABC transporter proteins, *Current opinion in structural biology* 17, 412–418 published online Aug 27, 2007. DOI: 10.1016/j.sbi.2007.07.003.
- (336) Oldham, M. L., Davidson, A. L., and Chen, J. (2008) Structural insights into ABC transporter mechanism, *Current opinion in structural biology* 18, 726–733 published online Nov 5, 2008. DOI: 10.1016/j.sbi.2008.09.007.

- (337) Caffalette, C. A., Corey, R. A., Sansom, M. S. P., Stansfeld, P. J., and Zimmer, J. (2019) A lipid gating mechanism for the channel-forming O antigen ABC transporter, *Nature Communications* 10, 824 published online Feb 18, 2019. DOI: 10.1038/s41467-019-08646-8.
- (338) Currier, S. J., Kane, S. E., Willingham, M. C., Cardarelli, C. O., Pastan, I., and Gottesman, M. M. (1992) Identification of residues in the first cytoplasmic loop of P-glycoprotein involved in the function of chimeric human MDR1-MDR2 transporters, *The Journal of Biological Chemistry* 267, 25153–25159.
- (339) Cotten, J. F., Ostedgaard, L. S., Carson, M. R., and Welsh, M. J. (1996) Effect of cystic fibrosis-associated mutations in the fourth intracellular loop of cystic fibrosis transmembrane conductance regulator, *The Journal of Biological Chemistry* 271, 21279–21284. DOI: 10.1074/jbc.271.35.21279.
- (340) Loo, T. W., and Clarke, D. M. (2016) P-glycoprotein ATPase activity requires lipids to activate a switch at the first transmission interface, *Biochemical and biophysical research communications* 472, 379–383 published online Mar 2, 2016. DOI: 10.1016/j.bbrc.2016.02.124.
- (341) Ford, R. C., Thonghin, N., Collins, R. F., Barbieri, A., Shafi, T., and Siebert, A. (2018) Structure of P-glycoprotein(ABCB1) in the post-hydrolytic state.
- (342) Tsai, C. J., Kumar, S., Ma, B., and Nussinov, R. (1999) Folding funnels, binding funnels, and protein function, *Protein science : a publication of the Protein Society* 8, 1181–1190. DOI: 10.1110/ps.8.6.1181.
- (343) Kurashima-Ito, K., Ikeya, T., Senbongi, H., Tochio, H., Mikawa, T., Shibata, T., and Ito, Y. (2006) Heteronuclear multidimensional NMR and homology modelling studies of the C-terminal nucleotide-binding domain of the human mitochondrial ABC transporter ABCB6, *Journal of biomolecular NMR* 35, 53–71 published online Jun 8, 2006. DOI: 10.1007/s10858-006-9000-6.
- (344) Moody, J. E., Millen, L., Binns, D., Hunt, J. F., and Thomas, P. J. (2002) Cooperative, ATP-dependent Association of the Nucleotide Binding Cassettes during the Catalytic Cycle of ATP-binding Cassette Transporters, *Journal of Biological Chemistry* 277, 21111–21114. DOI: 10.1074/jbc.C200228200.
- (345) Yuan, Y.-R., Martsinkevich, O., and Hunt, J. F. (2003) Structural characterization of an MJ1267 ATP-binding cassette crystal with a complex pattern of twinning caused by promiscuous fiber packing, *Acta crystallographica. Section D, Biological crystallography* 59, 225–238 published online Jan 23, 2003. DOI: 10.1107/s0907444902018954.
- (346) Chen, J., Sharma, S., Quijcho, F. A., and Davidson, A. L. (2001) Trapping the transition state of an ATP-binding cassette transporter: evidence for a concerted mechanism of maltose transport, *Proceedings of the National Academy of Sciences* 98, 1525–1530 published online Feb 6, 2001. DOI: 10.1073/pnas.041542498.
- (347) Vergani, P., Lockless, S. W., Nairn, A. C., and Gadsby, D. C. (2005) CFTR channel opening by ATP-driven tight dimerization of its nucleotide-binding domains, *Nature* 433, 876–880. DOI: 10.1038/nature03313.
- (348) Wishart, D. S., and Sykes, B. D. (1994) The ¹³C chemical-shift index: a simple method for the identification of protein secondary structure using ¹³C chemical-shift data, *Journal of biomolecular NMR* 4, 171–180. DOI: 10.1007/BF00175245.
- (349) Simpson, B. W., Pahil, K. S., Owens, T. W., Lundstedt, E. A., Davis, R. M., Kahne, D., and Ruiz, N. (2019) Combining Mutations That Inhibit Two Distinct Steps of the ATP Hydrolysis Cycle Restores Wild-Type Function in the Lipopolysaccharide Transporter and Shows that ATP Binding Triggers Transport, *mBio* 10 published online Aug 20, 2019. DOI: 10.1128/mBio.01931-19.
- (350) Thélot, F. A., Zhang, W., Song, K., Xu, C., Huang, J., and Liao, M. (2021) Distinct allosteric mechanisms of first-generation MsbA inhibitors, *Science (New York, N.Y.)* 374, 580–585 published online Sep 23, 2021. DOI: 10.1126/science.abi9009.

- (351) Kodan, A., Yamaguchi, T., Nakatsu, T., Sakiyama, K., Hipolito, C. J., Fujioka, A., Hirokane, R., Ikeguchi, K., Watanabe, B., Hiratake, J., Kimura, Y., Suga, H., Ueda, K., and Kato, H. (2014) Structural basis for gating mechanisms of a eukaryotic P-glycoprotein homolog, *Proceedings of the National Academy of Sciences* *111*, 4049–4054 published online Mar 3, 2014. DOI: 10.1073/pnas.1321562111.
- (352) Liu, F., Zhang, Z., Csanády, L., Gadsby, D. C., and Chen, J. (2017) Molecular Structure of the Human CFTR Ion Channel, *Cell* *169*, 85–95.e8. DOI: 10.1016/j.cell.2017.02.024.
- (353) Li, J., Jaimes, K. F., and Aller, S. G. (2014) Refined structures of mouse P-glycoprotein, *Protein Science* *23*, 34–46 published online Nov 15, 2013. DOI: 10.1002/pro.2387.
- (354) Szewczyk, P., Tao, H., McGrath, A. P., Villaluz, M., Rees, S. D., Lee, S. C., Doshi, R., Urbatsch, I. L., Zhang, Q., and Chang, G. (2015) Snapshots of ligand entry, malleable binding and induced helical movement in P-glycoprotein, *Acta crystallographica. Section D, Biological crystallography* *71*, 732–741 published online Feb 26, 2015. DOI: 10.1107/S1399004715000978.
- (355) Alam, A., Küng, R., Kowal, J., McLeod, R. A., Tremp, N., Broude, E. V., Roninson, I. B., Stahlberg, H., and Locher, K. P. (2018) Structure of a zosuquidar and UIC2-bound human-mouse chimeric ABCB1, *Proceedings of the National Academy of Sciences* *115*, E1973–E1982 published online Feb 13, 2018. DOI: 10.1073/pnas.1717044115.
- (356) Lee, J. Y., Yang, J. G., Zhitnitsky, D., Lewinson, O., and Rees, D. C. (2014) Structural basis for heavy metal detoxification by an Atm1-type ABC exporter, *Science (New York, N.Y.)* *343*, 1133–1136. DOI: 10.1126/science.1246489.
- (357) Arnold, F. M., Weber, M. S., Gonda, I., Gallenito, M. J., Adenau, S., Egloff, P., Zimmermann, I., Hutter, C. A. J., Hürlimann, L. M., Peters, E. E., Piel, J., Meloni, G., Medalia, O., and Seeger, M. A. (2020) The ABC exporter IrtAB imports and reduces mycobacterial siderophores, *Nature* *580*, 413–417 published online Mar 25, 2020. DOI: 10.1038/s41586-020-2136-9.
- (358) Henderson, R. (2004) Realizing the potential of electron cryo-microscopy, *Quarterly reviews of biophysics* *37*, 3–13. DOI: 10.1017/s0033583504003920.
- (359) Cheng, Y. (2018) Single-particle cryo-EM-How did it get here and where will it go, *Science (New York, N.Y.)* *361*, 876–880. DOI: 10.1126/science.aat4346.
- (360) Frank, J. (2018) New Opportunities Created by Single-Particle Cryo-EM: The Mapping of Conformational Space, *Biochemistry* *57*, 888 published online Jan 25, 2018. DOI: 10.1021/acs.biochem.8b00064.
- (361) Frank, G. A., Shukla, S., Rao, P., Borgnia, M. J., Bartesaghi, A., Merk, A., Mobin, A., Esser, L., Earl, L. A., Gottesman, M. M., Di Xia, Ambudkar, S. V., and Subramaniam, S. (2016) Cryo-EM Analysis of the Conformational Landscape of Human P-glycoprotein (ABCB1) During its Catalytic Cycle, *Molecular pharmacology* *90*, 35–41 published online May 11, 2016. DOI: 10.1124/mol.116.104190.
- (362) Kadaba, N. S., Kaiser, J. T., Johnson, E., Lee, A., and Rees, D. C. (2008) The high-affinity E. coli methionine ABC transporter: structure and allosteric regulation, *Science (New York, N.Y.)* *321*, 250–253. DOI: 10.1126/science.1157987.
- (363) Gerber, S., Comellas-Bigler, M., Goetz, B. A., and Locher, K. P. (2008) Structural basis of trans-inhibition in a molybdate/tungstate ABC transporter, *Science (New York, N.Y.)* *321*, 246–250 published online May 29, 2008. DOI: 10.1126/science.1156213.
- (364) Hvorup, R. N., Goetz, B. A., Niederer, M., Hollenstein, K., Perozo, E., and Locher, K. P. (2007) Asymmetry in the structure of the ABC transporter-binding protein complex BtuCD-BtuF, *Science (New York, N.Y.)* *317*, 1387–1390 published online Aug 2, 2007. DOI: 10.1126/science.1145950.
- (365) Korkhov, V. M., Mireku, S. A., Hvorup, R. N., and Locher, K. P. (2012) Asymmetric states of vitamin B₁₂ transporter BtuCD are not discriminated by its cognate substrate binding protein BtuF, *FEBS letters* *586*, 972–976 published online Mar 8, 2012. DOI: 10.1016/j.febslet.2012.02.042.

- (366) Swier, L. J. Y. M., Guskov, A., and Slotboom, D. J. (2016) Structural insight in the toppling mechanism of an energy-coupling factor transporter, *Nature Communications* 7, 11072 published online Mar 30, 2016. DOI: 10.1038/ncomms11072.
- (367) Orlando, B. J., and Liao, M. (2020) ABCG2 transports anticancer drugs via a closed-to-open switch, *Nature Communications* 11, 2264 published online May 8, 2020. DOI: 10.1038/s41467-020-16155-2.
- (368) Manolaridis, I., Jackson, S. M., Taylor, N. M. I., Kowal, J., Stahlberg, H., and Locher, K. P. (2018) Cryo-EM structures of a human ABCG2 mutant trapped in ATP-bound and substrate-bound states, *Nature* 563, 426–430 published online Nov 7, 2018. DOI: 10.1038/s41586-018-0680-3.
- (369) Tang, X., Chang, S., Luo, Q., Zhang, Z., Qiao, W., Xu, C., Zhang, C., Niu, Y., Yang, W., Wang, T., Zhang, Z., Zhu, X., Wei, X., Dong, C., Zhang, X., and Dong, H. (2019) Cryo-EM structures of lipopolysaccharide transporter LptB2FGC in lipopolysaccharide or AMP-PNP-bound states reveal its transport mechanism, *Nature Communications* 10, 4175 published online Sep 13, 2019. DOI: 10.1038/s41467-019-11977-1.
- (370) Mittal, A., Böhm, S., Grütter, M. G., Bordignon, E., and Seeger, M. A. (2012) Asymmetry in the homodimeric ABC transporter MsbA recognized by a DARPin, *The Journal of Biological Chemistry* 287, 20395–20406 published online Apr 20, 2012. DOI: 10.1074/jbc.M112.359794.
- (371) Liu, Y., Liu, Y., He, L., Zhao, Y., and Zhang, X. C. (2018) Single-molecule fluorescence studies on the conformational change of the ABC transporter MsbA, *Biophys Rep* 4, 153–165. DOI: 10.1007/s41048-018-0057-z.
- (372) Lerner-Marmarosh, N., Gimi, K., Urbatsch, I. L., Gros, P., and Senior, A. E. (1999) Large scale purification of detergent-soluble P-glycoprotein from *Pichia pastoris* cells and characterization of nucleotide binding properties of wild-type, Walker A, and Walker B mutant proteins, *The Journal of Biological Chemistry* 274, 34711–34718. DOI: 10.1074/jbc.274.49.34711.
- (373) Padayatti, P. S., Lee, S. C., Stanfield, R. L., Wen, P.-C., Tajkhorshid, E., Wilson, I. A., and Zhang, Q. (2019) Structural Insights into the Lipid A Transport Pathway in MsbA, *Structure* 27, 1114-1123.e3. DOI: 10.1016/j.str.2019.04.007.
- (374) Yaginuma, H., Kawai, S., Tabata, K. V., Tomiyama, K., Kakizuka, A., Komatsuzaki, T., Noji, H., and Imamura, H. (2014) Diversity in ATP concentrations in a single bacterial cell population revealed by quantitative single-cell imaging, *Scientific reports* 4, 6522 published online Oct 6, 2014. DOI: 10.1038/srep06522.
- (375) Qu, Q., Chu, J. W. K., and Sharom, F. J. (2003) Transition state P-glycoprotein binds drugs and modulators with unchanged affinity, suggesting a concerted transport mechanism, *Biochemistry* 42, 1345–1353. DOI: 10.1021/bi0267745.
- (376) Mannering, D. E., Sharma, S., and Davidson, A. L. (2001) Demonstration of conformational changes associated with activation of the maltose transport complex, *The Journal of Biological Chemistry* 276, 12362–12368 published online Jan 9, 2001. DOI: 10.1074/jbc.M011686200.
- (377) Vakkasoglu, A. S., Srikant, S., and Gaudet, R. (2017) D-helix influences dimerization of the ATP-binding cassette (ABC) transporter associated with antigen processing 1 (TAP1) nucleotide-binding domain, *PloS one* 12, e0178238 published online May 23, 2017. DOI: 10.1371/journal.pone.0178238.
- (378) Walter, C., Wilken, S., and Schneider, E. (1992) Characterization of side-directed mutations in conserved domains of MalK, a bacterial member of the ATP-binding cassette (ABC) family, *FEBS letters* 303, 41–44. DOI: 10.1016/0014-5793(92)80473-T.
- (379) Bliss, J. M., Garon, C. F., and Silver, R. P. (1996) Polysialic acid export in *Escherichia coli* K1: the role of KpsT, the ATP-binding component of an ABC transporter, in chain translocation, *Glycobiology* 6, 445–452. DOI: 10.1093/glycob/6.4.445.

- (380) Benabdelhak, H., Schmitt, L., Horn, C., Jumel, K., Blight, M. A., and Holland, I. B. (2005) Positive co-operative activity and dimerization of the isolated ABC ATPase domain of HlyB from *Escherichia coli*, *The Biochemical journal* **386**, 489–495. DOI: 10.1042/BJ20041282.
- (381) Perria, C. L., Rajamanickam, V., Lapinski, P. E., and Raghavan, M. (2006) Catalytic Site Modifications of TAP1 and TAP2 and Their Functional Consequences, *The Journal of Biological Chemistry* **281**, 39839–39851 published online Oct 26, 2006. DOI: 10.1074/jbc.M605492200.
- (382) Hofacker, M., Gompf, S., Zutz, A., Presenti, C., Haase, W., van der Does, C., Model, K., and Tampé, R. (2007) Structural and Functional Fingerprint of the Mitochondrial ATP-binding Cassette Transporter Mdl1 from *Saccharomyces cerevisiae*, *The Journal of Biological Chemistry* **282**, 3951–3961 published online Dec 6, 2006. DOI: 10.1074/jbc.M609899200.
- (383) Hanekop, N., Zaitseva, J., Jenewein, S., Holland, I. B., and Schmitt, L. (2006) Molecular insights into the mechanism of ATP-hydrolysis by the NBD of the ABC-transporter HlyB, *FEBS letters* **580**, 1036–1041 published online Nov 21, 2005. DOI: 10.1016/j.febslet.2005.11.012.
- (384) Qin, L., Zheng, J., Grant, C. E., Jia, Z., Cole, S. P. C., and Deeley, R. G. (2008) Residues responsible for the asymmetric function of the nucleotide binding domains of multidrug resistance protein 1, *Biochemistry* **47**, 13952–13965. DOI: 10.1021/bi801532g.
- (385) Gao, M., Cui, H. R., Loe, D. W., Grant, C. E., Almquist, K. C., Cole, S. P., and Deeley, R. G. (2000) Comparison of the functional characteristics of the nucleotide binding domains of multidrug resistance protein 1, *The Journal of Biological Chemistry* **275**, 13098–13108. DOI: 10.1074/jbc.275.17.13098.
- (386) Matsuo, M., Kioka, N., Amachi, T., and Ueda, K. (1999) ATP binding properties of the nucleotide-binding folds of SUR1, *The Journal of Biological Chemistry* **274**, 37479–37482. DOI: 10.1074/jbc.274.52.37479.
- (387) Nagata, K., Nishitani, M., Matsuo, M., Kioka, N., Amachi, T., and Ueda, K. (2000) Nonequivalent nucleotide trapping in the two nucleotide binding folds of the human multidrug resistance protein MRP1, *The Journal of Biological Chemistry* **275**, 17626–17630. DOI: 10.1074/jbc.M000792200.
- (388) Jackson, S. M., Manolaridis, I., Kowal, J., Zechner, M., Taylor, N. M. I., Bause, M., Bauer, S., Bartholomaeus, R., Bernhardt, G., Koenig, B., Buschauer, A., Stahlberg, H., Altmann, K.-H., and Locher, K. P. (2018) Structural basis of small-molecule inhibition of human multidrug transporter ABCG2, *Nature structural & molecular biology* **25**, 333–340 published online Apr 2, 2018. DOI: 10.1038/s41594-018-0049-1.
- (389) Loria, J. P., Rance, M., and Palmer, A. G. (1999) A Relaxation-Compensated Carr–Purcell–Meiboom–Gill Sequence for Characterizing Chemical Exchange by NMR Spectroscopy, *J. Am. Chem. Soc.* **121**, 2331–2332. DOI: 10.1021/ja983961a.
- (390) Mulder, F. A., Mittermaier, A., Hon, B., Dahlquist, F. W., and Kay, L. E. (2001) Studying excited states of proteins by NMR spectroscopy, *Nat Struct Mol Biol* **8**, 932–935. DOI: 10.1038/nsb1101-932.
- (391) Kay, L. E., Nicholson, L. K., Delaglio, F., Bax, A., and Torchia, D. (1992) Pulse sequences for removal of the effects of cross correlation between dipolar and chemical-shift anisotropy relaxation mechanisms on the measurement of heteronuclear T1 and T2 values in proteins, *Journal of Magnetic Resonance (1969)* **97**, 359–375. DOI: 10.1016/0022-2364(92)90320-7.
- (392) Kneuttinger, A. C., Straub, K., Bittner, P., Simeth, N. A., Bruckmann, A., Busch, F., Rajendran, C., Hupfeld, E., Wysocki, V. H., Horinek, D., König, B., Merkl, R., and Sterner, R. (2019) Light Regulation of Enzyme Allostery through Photo-responsive Unnatural Amino Acids, *Cell chemical biology* **26**, 1501-1514.e9 published online Sep 5, 2019. DOI: 10.1016/j.chembiol.2019.08.006.

- (393) Zoghbi, M. E., Fuson, K. L., Sutton, R. B., and Altenberg, G. A. (2012) Kinetics of the association/dissociation cycle of an ATP-binding cassette nucleotide-binding domain, *Journal of Biological Chemistry* 287, 4157–4164 published online Dec 9, 2011. DOI: 10.1074/jbc.M111.318378.
- (394) Tomblin, G., Bartholomew, L. A., Urbatsch, I. L., and Senior, A. E. (2004) Combined mutation of catalytic glutamate residues in the two nucleotide binding domains of P-glycoprotein generates a conformation that binds ATP and ADP tightly, *Journal of Biological Chemistry* 279, 31212–31220 published online May 24, 2004. DOI: 10.1074/jbc.M404689200.
- (395) Tomblin, G., Bartholomew, L. A., Tyndall, G. A., Gimi, K., Urbatsch, I. L., and Senior, A. E. (2004) Properties of P-glycoprotein with mutations in the "catalytic carboxylate" glutamate residues, *Journal of Biological Chemistry* 279, 46518–46526 published online Aug 23, 2004. DOI: 10.1074/jbc.M408052200.
- (396) Fan, C., Kaiser, J. T., and Rees, D. C. (2020) A structural framework for unidirectional transport by a bacterial ABC exporter, *PNAS* 117, 19228–19236 published online Jul 23, 2020. DOI: 10.1073/pnas.2006526117.
- (397) Zhang, Z., Liu, F., and Chen, J. (2017) Conformational Changes of CFTR upon Phosphorylation and ATP Binding, *Cell* 170, 483–491.e8 published online Jul 20, 2017. DOI: 10.1016/j.cell.2017.06.041.
- (398) Liu, F., Lee, J., and Chen, J. (2021) Molecular structures of the eukaryotic retinal importer ABCA4, *eLife* 10 published online Feb 19, 2021. DOI: 10.7554/eLife.63524.
- (399) Kehlenbeck, D.-M., Traore, D. A. K., Josts, I., Sander, S., Moulin, M., Haertlein, M., Prevost, S., Forsyth, V. T., and Tidow, H. (2021) Cryo-EM structure of MsbA in saposin-lipid nanoparticles (Salipro) provides insights into nucleotide coordination, *The FEBS Journal* published online Dec 17, 2021. DOI: 10.1111/febs.16327.
- (400) Verma, V. A., Wang, L., Labadie, S. S., Liang, J., Sellers, B. D., Wang, J., Dong, L., Wang, Q., Zhang, S., Xu, Z., Zhang, Y., Niu, Y., Wang, X., Wai, J., Koehler, M. F. T., Hu, H., Alexander, M. K., Nishiyama, M., Miu, A., Xu, Y., Pang, J., Katakam, A. K., Reichelt, M., Austin, C. D., Ho, H., Payandeh, J., and Koth, C. M. (2022) Discovery of Inhibitors of the Lipopolysaccharide Transporter MsbA: From a Screening Hit to Potent Wild-Type Gram-Negative Activity, *Journal of medicinal chemistry* 65, 4085–4120 published online Feb 20, 2022. DOI: 10.1021/acs.jmedchem.1c01909.
- (401) Chen, C.-A., and Cowan, J. A. (2003) Characterization of the Soluble Domain of the ABC7 Type Transporter Atm1, *The Journal of Biological Chemistry* 278, 52681–52688 published online Sep 26, 2003. DOI: 10.1074/jbc.M306472200.
- (402) Ramaen, O., Masscheleyn, S., Duffieux, F., Pamard, O., Oberkamp, M., Lallemand, J.-Y., Stoven, V., and Jacquet, E. (2003) Biochemical characterization and NMR studies of the nucleotide-binding domain 1 of multidrug-resistance-associated protein 1: evidence for interaction between ATP and Trp653, *The Biochemical journal* 376, 749–756. DOI: 10.1042/BJ20030998.
- (403) Buyse, F., Hou, Y., Vigano, C., Zhao, Q., Ruyschaert, J.-M., and Chang, X. (2006) Replacement of the positively charged Walker A lysine residue with a hydrophobic leucine residue and conformational alterations caused by this mutation in MRP1 impair ATP binding and hydrolysis, *The Biochemical journal* 397, 121–130. DOI: 10.1042/BJ20051363.
- (404) Qu, Q., Russell, P. L., and Sharom, F. J. (2003) Stoichiometry and affinity of nucleotide binding to P-glycoprotein during the catalytic cycle, *Biochemistry* 42, 1170–1177. DOI: 10.1021/bi026555j.
- (405) Liu, R., Siemiarzuk, A., and Sharom, F. J. (2000) Intrinsic fluorescence of the P-glycoprotein multidrug transporter: sensitivity of tryptophan residues to binding of drugs and nucleotides, *Biochemistry* 39, 14927–14938. DOI: 10.1021/bi0018786.
- (406) Dayan, G., Baubichon-Cortay, H., Jault, J. M., Cortay, J. C., Deléage, G., and Di Pietro, A. (1996) Recombinant N-terminal nucleotide-binding domain from mouse P-glycoprotein. Overexpression,

purification, and role of cysteine 430, *The Journal of Biological Chemistry* 271, 11652–11658. DOI: 10.1074/jbc.271.20.11652.

(407) Baubichon-Cortay, H., Baggetto, L. G., Dayan, G., and Di Pietro, A. (1994) Overexpression and purification of the carboxyl-terminal nucleotide-binding domain from mouse P-glycoprotein. Strategic location of a tryptophan residue, *Journal of Biological Chemistry* 269, 22983–22989. DOI: 10.1016/s0021-9258(17)31607-1.

(408) Rose-Sperling, D., Tran, M. A., Lauth, L. M., Goretzki, B., and Hellmich, U. A. (2019) 19F NMR as a versatile tool to study membrane protein structure and dynamics, *Biological chemistry* 400, 1277–1288. DOI: 10.1515/hsz-2018-0473.

(409) James, L. C., and Tawfik, D. S. (2003) Conformational diversity and protein evolution – a 60-year-old hypothesis revisited, *Trends in Biochemical Sciences* 28, 361–368. DOI: 10.1016/S0968-0004(03)00135-X.

(410) Koshland, D. E. (1958) Application of a Theory of Enzyme Specificity to Protein Synthesis, *Proceedings of the National Academy of Sciences* 44, 98–104. DOI: 10.1073/pnas.44.2.98.

CURRICULUM VITAE

Dania Rose-Sperling, M. Sc. Chemistry

dania.rose-sperling@gmx.de

Tel: + 49 176 82119141

Address: Maurerstr. 32a

07749 Jena

Research Interests

Conformational dynamics of ABC-exporters, Multi Drug Resistance, NMR spectroscopy, consequences of nucleotide binding and hydrolysis

Research Experience and Education

- MAI 2019 PhD internship (Assistant Prof. ██████████)
 Research topic: "Molecular insides into a multi-drug resistance related protein/ ABC transporters by protein crystallography"
 Faculty of Science and Engineering, University of Groningen, Netherlands
- SEP – DEC 2018 PhD Internship (Prof. Dr. ██████ and Dr. ██████)
 Research topic: "Functional analysis of a multi-drug resistance related protein/ ABC transporters"
 Molecular Microbiology and Structural Biochemistry, French National Centre for Scientific Research, Lyon, France
- SINCE 2016 PhD Student (Prof. Dr. ██████████)
 Research topic: "Conformational dynamics of ABC exporters" Membrane biochemistry, University of Mainz (2015-2020)/Jena (2021), Germany
- SEP – APR 2016 Scientific Research Assistant (Prof. Dr. ██████████)
- MAY – AUG 2015 Scientific Research Assistant (Prof. Dr. ██████████)
 Research topic: "Clusterin-regulation of brain receptor signalling pathways"
 Biochemistry, University of Mainz, Germany
- SEP 2013 – SEP 2014 Paul Flechsig Institute of Brain Research, Leipzig, Germany
Master thesis: "Influence of Cholesterol, 27-OH-Cholesterol and Statins on Gene Expression of Neuronal Cells"
- OCT 2011 – SEP 2014 Master of Science in Chemistry (final grade: very good)
 Leipzig University, Germany
- APR – MAY 2013 Helmholtz-Zentrum Dresden-Rossendorf e.V., Germany
 Research topic: "Synthesis of a potential CB2 receptor ligand for use in Positron Emission Tomography"
- JUL – AUG 2012 Internship, Universidade Nova de Lisboa, Lisbon, Portugal
 Research topic: "Characterization of peptides from enzymatic hydrolysis of *Catostylus tagi* umbrella"
- SEP 2011 – AUG 2012 ERASMUS Fellowship at Universidade Nova de Lisboa, Lisbon, Portugal
- JUL – AUG 2011 Center for Biotechnology and Biomedicine, Leipzig University, Germany
 Research topic: "Deamidation of tau protein"

| | |
|---------------------|---|
| MAY – AUG 2011 | Employed at Amedes MVZ for laboratory diagnostics, microbiology and human genetics, Halle/ Leipzig GmbH (microbiological and medical-biochemical applications, pathogenic assays) |
| MAR – MAY 2011 | Center for Biotechnology and Biomedicine, Leipzig University, Germany Bachelor thesis: “Analysis of phosphorylated proteins” |
| OCT 2008 – SEP 2011 | <u>Bachelor of Science in Chemistry</u> , Leipzig University, Germany |
| JUL 2007 | A level (German Abitur, allowing entrance to study at university) |
| JUL – AUG 2006 | Internship at SCHOTT Lithotec AG, Jena, Germany |
| 2001 – 2003 | Employment in the Science Center IMAGINATA, Jena, Germany |

Awards and Scholarships

| | |
|-------------|--|
| 2020 | Conference participation grant from Hans Böckler Foundation |
| 2019 | Conference organization grant from Hans Böckler Foundation, Mainz, Germany |
| 2018 | Hans Böckler PhD internship Fellowship, Lyon, France |
| 2018 | FEBS Fellowship, ABC meeting, Innsbruck, Austria |
| 2017 – 2021 | Hans Böckler PhD Fellowship, Mainz University, Germany |
| 2016 | Poster Award, ABC meeting, Innsbruck, Austria |
| 2015 | Hans Böckler PhD Fellowship, Bremen University, Germany (declined) |
| 2011/12 | Erasmus Fellowship, Universidade Nova de Lisboa, Portugal |

Publications

Rose-Sperling D, Anh Tran M, Lauth LM, Goretzki B, Hellmich UA; (2018) ^{19}F NMR as a versatile tool to study membrane protein structure and dynamics. *Biol. Chem.*, 400(10):1277-1288.

Szöllösi D, Rose-Sperling D, Hellmich UA, Stockner T; (2017) Comparison of mechanistic transport cycle models of ABC exporters. *Biochim. Biophys. Acta Biomembranes*, 1860(4):818-832.

Neumann J, Rose-Sperling D, Hellmich UA; (2016) Diverse relations between ABC transporters and lipids: An overview. *Biochim. Biophys. Acta Biomembranes*, 1859(4):605-618.

Supervised student projects

██████████; (2019) Structural and functional investigation of ABC exporters. Bachelor thesis.

██████████; (2019) Spectroscopic analysis of point mutations in the nucleotide binding domain. Internship.

██████████; (2017-2018) Structure and dynamics of ABC transporter: LmrA and MsbA. ERASMUS student-Bachelor thesis.

██████████; (2017) Structure and dynamics of a parasitic ABC transporter. DAAD RISE Internship.

██████████ (2017) Spectroscopic analysis of the structural effects of point mutations in the nucleotide binding domain of an ABC transporter. Internship.

██████████; (2016) Biophysical studies of the nucleotide binding domain of an ABC exporter. Bachelor thesis.

██████████; (2015-2016) Influence of the conserved D-loop on structure and dynamics of the motor domain of an ABC transporter. Bachelor thesis.

Conference contributions

| | |
|------------------|---|
| 14 FEB 2021 | PhD presentation, Hans Böckler Foundation (<u>oral presentation</u>) |
| 1 -7 MAR 2020 | ATP-Binding Cassette (ABC) Proteins: From Multidrug Resistance to Genetic Diseases, Innsbruck, Austria (<u>oral presentation, poster</u>) |
| 22 AUG 2019 | 11 th BMRZ Symposia, Bad Homburg, Germany |
| 1 APR 2019 | 4 th Life Science Meeting Mainz, Germany (fundraising, organizer, chair, <u>poster</u>) |
| 30 NOV 2018 | ABC of membrane transport meeting, Paris, France |
| 24 APR 2018 | 3 rd Life Science Mainz Symposium (BioChem), Mainz, Germany (<u>poster</u>) |
| 16 MAR 2018 | 3 rd Interdisciplinary Symposium, Mainz, Germany |
| 11 – 13 MAR 2018 | 11 th Transport Colloquium, Rauischholzhausen, Germany (<u>oral presentation, poster</u>) |
| 6 – 12 MAR 2018 | ATP-Binding Cassette (ABC) Proteins: From Multidrug Resistance to Genetic Diseases, Innsbruck, Austria (<u>oral presentation, poster</u>) |
| 11 OCT 2017 | 2 nd BioChem Symposium, Mainz, Germany (<u>oral presentation, poster</u>) |
| 4 – 6 OCT 2017 | New Horizons in Membrane Transport and Communication, Frankfurt am Main, Germany (<u>poster</u>) |
| 25 – 30 JUN 2017 | Gordon Research Conference: Mechanism of Membrane Transport, New London, USA (<u>poster</u>) |
| 24 – 25 JUN 2017 | Gordon Research Seminar: Mechanism of Membrane Transport, New London, USA (<u>poster</u>) |
| 10 APR 2017 | 1 st BioChem Symposium, Mainz, Germany (<u>poster</u>) |
| 7 MAR 2017 | 2 nd Interdisciplinary Symposium, Mainz, Germany |
| 12 APR 2016 | 1 st Interdisciplinary Symposium, Mainz, Germany (<u>oral presentation</u>) |
| 5 – 11 MAR 2016 | ATP-Binding Cassette (ABC) Proteins: From Multidrug Resistance to Genetic Diseases, Innsbruck, Austria (<u>oral presentation, poster</u>) |
| 7 – 10 SEP 2015 | GDCh FGMR Meeting, Darmstadt, Germany |
| 24 – 27 MAR 2015 | International meeting of the German Society for Cell Biology, Cologne, Germany |

Certificates

| | |
|---------------------|---|
| SEP 2019 | Certificate of GMP, GLP, GCP and pharmacovigilance course, Pharmaakademie, Frankfurt, Germany |
| DEC 2014 – APR 2015 | Three Certificates TÜV Rhineland (Quality representative, quality management and internal auditor), Comcave Collage, Leipzig, Germany |
| 18 JUL 2014 | Certificate for research animal handling and animal welfare, Leipzig University, Herzzentrum, Germany |

Extracurricular Activities

- Member and representative of the Hans-Böckler-foundation City Mainz (2018-2020)
Interviewing and writing references for applicants and foundation members, documenting meetings
- Supervising national and international students (2015-2020)
- Member in the students association for chemistry and mineralogy Leipzig (2008/2009)
Student representative in faculty committees and student parliament; coaching of first-year chemistry students; organizer of chemistry student retreats; fundraising for welfare projects and discussion rounds
- Organizer of four symposia in Mainz (BioChemSymposium/ Life Science Mainz Meeting; 2017-2019)
- Leipzig University Sports Programme: Coaching Dance to fellow students (2011)
- Member at "Cradle to Cradle", a sustainability project (2014), active member of junior Society for Biochemistry and Molecular Biology (GBM) Mainz (2017-2019), member of the junior Society for Chemistry Mainz (JCF-Jungchemikerforum, GDCh) (2016-2019), member of JUNQ Journal (2017-2018)
- Au pair in Madrid, Spain (SEP 07 – JUN 08)